iPN

université paris — sud
INSTITUT DE PHYSIQUE NUCLEAIRE
B.P. N° 1 ~ 91406 - ORSAY ~ TEL. 941.51.10
laboratoire associé à l'IN2P3

THESE

présentée

AU CENTRE D'ORSAY

UNIVERSITÉ PARIS-SUD

pour obtenir

LE GRADE DE DOCTEUR ES – SCIENCES

par

Axel Valter BERG

Sujet : Contribution à l'étude de la structure nucléaire par la mesure des probabilités de transition.

DEUXIEME PARTIE

Soutenue le 13/2/1976.

UNIV.
LEIDEN
BIBL.

ORSAY
Série A, n°
N° d'ordre :
1591

THÈSE

PRESENTEE

AU CENTRE D'ORSAY

UNIVERSITÉ PARIS-SUD

POUR OBTENIR

LE GRADE DE DOCTEUR ES SCIENCES

PAR

Axel Valter BERG

Sujet : Contribution à l'étude de la structure nucléaire par la mesure des probabilités de transition.

Soutenues le 13/2/1976 **devant la Commission d'examen**

MM.me N. MARTY Président.

MM. M. RIOU
R. FOUCHER
J. YOCCOZ
A. KNIPPER
} Examinateurs.

D E U X I E M E P A R T I E

Digitized by the Internet Archive
in 2026

https://archive.org/details/IA41548109_0007

DEUXIEME PARTIE

LISTE DES ARTICLES PUBLIES SE RAPPORTANT AUX TRAVAUX PRESENTES DANS LA THESE.

---

pages

1) Some E2 rates in ^{211}At,
G. Astner and V. Berg, Physica Scripta 5 (1972) 55 — 63

2) Charge effective du proton $h_{9/2}$ dans le polonium-210
V. Berg, C. Bourgeois, et N. Perrin,
C.R. Acad. Sc. 276 B (1973) 761. — 69

3) Transition rates in ^{161}Dy, V. Berg and S.G. Malmskog,
Nucl. Phys. A 135 (1969) 401 — 73

4) E2 and M1 transition probabilities in ^{193}Au and ^{195}Au.
B. Fogelberg, A. Bäcklin, V. Berg and S.G. Malmskog.
Nucl. Phys. A 153 (1970) 301. — 85

5) E2 and M1 transition probabilities in odd-mass Hg nuclei,
A. Bäcklin, B. Fogelberg, V. Berg and S.G. Malmskog,
Nucl. Phys. A 138 (1969) 429. — 95

6) Mesures de vies moyennes d'états excités dans les lanthanes 135 et 133, V. Berg. J. Letessier, C. Bourgeois et R. Foucher.
Journal de Physique 33 (1972) 829 — 105

7) A study of the 190 keV transition in ^{141}La, V. Berg, A. Höglund and B. Fogelberg, Nucl. Phys. A 155 (1970) 297. — 113

8) The decay of the 79.5 keV level in ^{134}I, V. Berg and A. Höglund
Nucl. Phys. A 175 (1971) 495. — 121

9) The level structure in ^{193}Ir,
V. Berg, S.G. Malmskog and A. Bäcklin
Nucl. Phys. A 143 (1970) 177 — 127

10) The low energy level structure of ^{191}Ir,
S.G. Malmskog, V. Berg, A. Bäcklin and G. Hedin,
Nucl. Phys. A 143 (1970) 160 — 143

11) E2 and M1 transition probabilities between low-energy states in ^{189}Ir, A. Bäcklin, G. Hedin, V. Berg and S.G. Malmskog, Nucl. Phys. A 181 (1972) 76. — 155

12) Absolute transition rates in ^{188}Ir.
S.G. Malmskog and V. Berg, Nucl. Phys. A 139 (1969) 17 — 169

13) The decay of ^{187}Pt : Comparaison of the levels of ^{187}Ir with those of heavier odd mass iridium isotopes, C. Sebille-Schück, M. Finger, F. Foucher, J.P. Husson, J. Jastrzebski, V. Berg, S.G. Malmskog, G. Astner, B.R. Erdal, P. Patzelt and P. Siffert, Nucl. Phys. A 212 (1973) 45 — 175

14) Negative parity states in odd-mass Ir and Au nuclei,
A. Bäcklin, V. Berg and S.G. Malmskog, Nucl. Phys. A 156 (1970) 647. 195

15) On the low energy band structure in ^{187}Os, S.G. Malmskog, V. Berg, B. Fogelberg and A. Bäcklin, Nucl. Phys. A 166 (1971) 573. 211

16) Transition probabilities in ^{189}Os,
S.G. Malmskog, V. Berg and A. Bäcklin,
Nucl. Phys. A 153 (1970) 316 225

17) Quasi-prolate and quasi-oblate bands in soft ^{189}Au,
V. Berg, R. Foucher and A. Höglund,
Nucl. Phys. A 244 (1975) 462 239

18) Some features of odd Au nuclei revealed by half-life measurements,
V. Berg, C. Bourgeois and R. Foucher,
Journal de Physique 36 (1975) 325. 255

19) Coexistence de forme dans le noyau ^{187}Au,
M.A. Deleplanque, C. Gerschel, M. Ishihara, et N. Perrin,
V. Berg, C. Bourgeois, M.G. Desthuilliers, J.P. Husson
P. Kilcher et J. Letessier, Journal de Phys. Lett. 36 (1975) 205. 261

R E F E R E N C E I

SOME E2 RATES IN $^{211}_{85}At_{126}$

G. Astner[1] and V. Berg[2]

([1]) Research Institute for Physics, Stockholm, Sweden

([2]) Institute of Physics, University of Stockholm, Stockholm, Sweden.

Physica Scripta. Vol. 5, 55–57, 1972

Some $E2$ Rates in $^{211}_{85}At_{126}$

G. Astner*[1] and V. Berg*,**[2]

[1]Research Institute for Physics, Stockholm, Sweden

[2]Institute of Physics, University of Stockholm, Stockholm, Sweden

Received March 8, 1972

Abstract

Some E2 rates in $^{211}_{85}At_{126}$. G. Astner (Research Institute for Physics, Stockholm Sweden) and V. Berg (Institute of Physics, University of Stockholm, Stockholm, Sweden).
Physica Scripta (Sweden) 5, 55–57, 1972.

The half-life of a 3/2⁻ level at 1 116 keV excitation energy in ^{211}At has been measured to be 0.57±0.04 nsec, using the delayed-coincidence technique. From a high-resolution study of parts of the conversion-electron spectrum it is shown that the depopulating transitions have the following multipolarities: 169 keV ($E2+(13\pm2)\%$ $M1$), 250 keV ($E2$) and 442 keV ($E2$). The reduced $E2$ transition probabilities are compared with theoretical predictions. The $M1$ rate corresponds to 1/6 400 Weisskopf units, in accordance with the interpretation of the two involved levels as essentially pure $\pi(h_{9/2}^3)$ states.

1. Introduction

In a recent paper by Bergström et al. [1] it was shown that a group of levels in $^{211}_{85}At_{126}$ could be identified as essentially pure members of the $\pi(h_{9/2}^3)$ configuration. Not only did the experimental energies agree well with those predicted for a pure configuration but also three $E2$ rates for transitions between high-spin states ($j_i \geq 15/2$) were compatible with this assumption. If this holds true even for the low-spin ($j \leq 7/2$) members of the $\pi(h_{9/2}^3)$ configuration observed in the electron-capture decay of ^{211}Rn [2] (cf. Fig. 1), it is easy to see that the half-life of the 3/2⁻ level at 1 116 keV should be about 1 nsec. We thus decided to measure this half-life and to improve the multipolarity assignments of ref. [2] by more detailed conversion-electron measurements in order to get precise transition probabilities.

2. Experimental procedures and results

2.1. *The half-life of the 3/2⁻ 1 116.2 keV level*

Sources of ^{211}Rn were produced at the ISOLDE facility as described in ref. [2]. This measurement was performed by studying delayed gamma–electron coincidences. Both electrons and gamma rays were detected with fast plastic scintillators (Ne 111) mounted on XP1020 photo-multipliers. A long lens magnetic spectrometer with a momentum resolution of 3% and a transmission of about 5% [3, 4] selected the electrons and an ORTEC fast-slow coincidence unit recorded the delay between the feeding and depopulating radiations. The spectrometer was focused on the 442.2 K electrons and the window of the gamma channel was set to accept part of the Compton distributions from the 1 538.8 and 1 362.9 keV gamma rays. The threshold of this channel was set high in order to improve the time resolution and to avoid coincidences with the 674.1 keV ground state transition. A delayed coincidence spectrum is shown in Fig. 2. For comparison, prompt curves were recorded with a ^{124}Sb source using unchanged settings. The spectra were analysed according to the momentum and convolution methods [5, 6]. The half-life obtained was

$$T_{1/2}\ (1\ 116.2\ \text{keV level}) = 0.57 \pm 0.04\ \text{ns}$$

The same result was found when the 250.2 K or 168.7 K electrons were focused with the spectrometer.

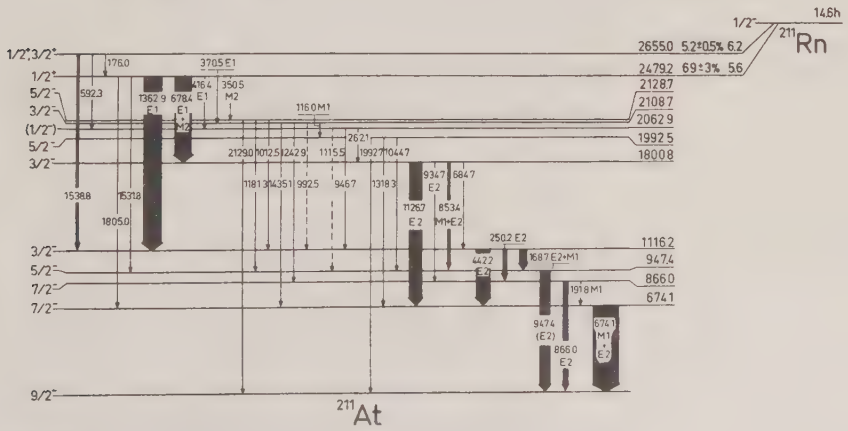

Fig. 1. The decay scheme of ^{211}Rn according to ref. [2].

* The ISOLDE Collaboration, CERN, Geneva, Switzerland.
** Present address: Institute de Physique Nucléaire, 91 Orsay, France.

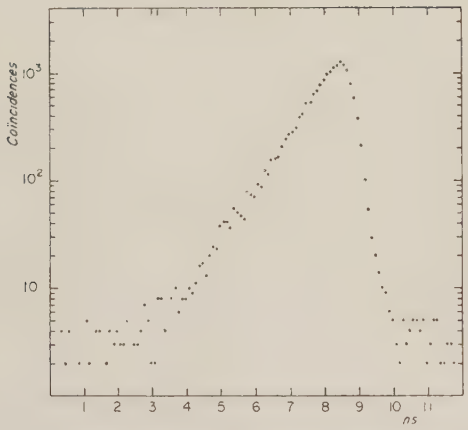

Fig. 2. Delayed coincidences defining the half-life of the 1 116.2 keV level. The time to pulse-height converter was started by the *K* electrons from the 442.2 keV transition which de-excites the level, and was stopped by Compton events between 800 and 1 100 keV from the feeding 1 538.8 and 1 362.9 keV gamma rays.

2.2. *Conversion electron spectroscopy*

The double-focusing beta spectrometer [7] utilized in the preceding paper [2] was used also here, but at higher resolution. Figs. 3 and 4 show the two regions covered at 0.35% momentum resolution. These contain the 169 keV *LMN* lines and the 250 keV *KLM* lines. The results are summarized in Table I. They represent a significant improvement upon those of ref. [2]. As pointed out in ref. [2], the 250 *K* and 169 L_{III} lines coincide to within 0.1 keV, and hence cannot be resolved. Using the normalization against gamma rays from ref. [2], the total *L* conversion coefficient of the 250 keV transition is deduced to be 0.105 ± 0.024. The experimental L_I+L_{II}/L_{III} intensity ratio is 3.5 ± 1.9. A comparison with the theoretical values of ref. [8] (*L* conversion coefficients = 0.135 (*M*1), 0.100 (*E*2), others widely off; $L_I+L_{II}/L_{III}=167$ (*M*1), 2.6 (*E*2)) shows that these values are only compatible with an almost pure *E*2 multipolarity. As the comparison with theory in ref. [2] strongly suggests that this transition proceeds between states with spin and parity 3/2⁻ and 7/2⁻, respectively, the 169 *L*–250 *K* complex is analysed on the assumption that the 250 keV transition has pure *E*2 character. The value obtained for the *M*1/*E*2 mixing ratio of the 169 keV transition is a weighted average deduced from the K and L absolute conversion coefficients and the K/L and L_I+L_{II}/L_{III} ratios.

Table II summarizes intensities, multipolarities, and partial half-lives for the transitions depopulating the 1 116 keV level. Also reduced transition probabilities and effective $h_{9/2}$ proton charges, for the two transitions between levels assigned as essentially $\pi(h_{9/2}^3)$ (cf. refs. [1, 2]), are given.

Table I. *Conversion electron lines*

Energy[a] (keV)	Relative intensity[b]	Assignment
151.8	4.6 ±0.2	169 L_I+L_{II}
154.4	3.2 ±0.2	169 L_{III}+250 *K*
164.7	1.4 ±0.2	169 *M*
165.8	0.5 ±0.2	262 *K*
167.6	0.5 ±0.1	169 *N*
174.1	0.43±0.10	192 L_I
233.1	1.1 ±0.2	250 L_{II}
235.8	0.31±0.16	250 L_{III}
245.8	Weak	250 *M*
(273.8)	<0.15	370 *K*

[a] Error typically 0.3 keV.
[b] Normalization as in ref. [2].

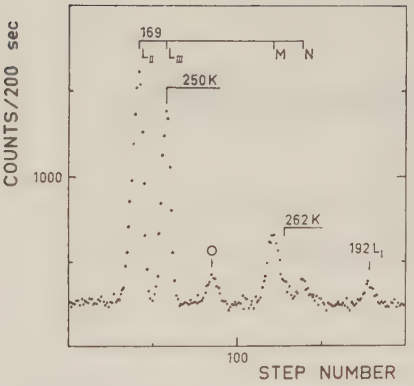

Fig. 3. The conversion electron spectrum from 145 to 180 keV measured at 0.35% momentum resolution. The line indicated ○ comes from the decay of ^{207}Po.

3. Discussion

3.1. *The 169 and 250 keV E2 transitions*

As demonstrated in refs. [1, 2], the three levels at 1 116 keV (3/2⁻), 947 keV (5/2⁻) and 866 keV (7/2⁻) can be identified as emanating essentially from the $\pi(h_{9/2}^3)$ configuration. If this were perfectly true, the *E*2 rates would be completely determined by the $\pi(h_{9/2})$ effective charge. Assuming pure configurations, effective charges have been worked out using Racah algebra as in ref. [1]. The results for e_{eff}/e, 2.04 ± 0.10 and 2.06 ± 0.11 clearly deviate from the value 1.53 ± 0.04 for the $\pi(h_{9/2})$ orbital, as deduced [9] from the quadrupole moment of the ^{209}Bi ground state and two transition rates in ^{210}Po. There is no reason, however, to connect this deviation with any break-down of the 'additivity' of the effective charge, as discussed in ref. [9]. Such effects are expected [10] to be of the order A^{-1} (A = mass number). Rather, the deviation should be taken as evidence for configuration mixing. As is well-known (see e.g. ref. [11]), the P_2 part of the residual interaction causes admixtures that interfere constructively to enhance *E*2 transitions. Clearly the possibilities for admixtures are much larger for the low-spin states involved here, than for the high-spin states ($j_1 \geq 15/2$) studied in ref. [1], where no deviation from additivity was observed.

3.2. *The 442 keV E2 transition*

The 442 keV transition proceeds between two levels whose configurations to first order (cf. ref. [2]) are $\pi(h_{9/2}^3)_{3/2}$ and ^{210}Po

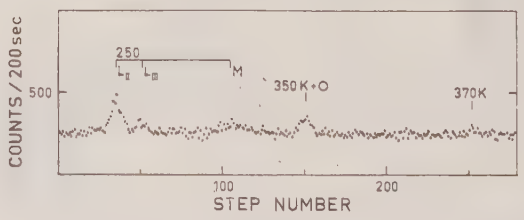

Fig. 4. The conversion electron spectrum from 230 to 280 keV measured at 0.35% momentum resolution. ○ indicates contamination from the decay of ^{207}Po (cf. ref. [2]).

Table II

Transition energy (keV)	Gamma[a] intensity	K conversion-electron intensity	Total intensity	Multi-polarity	$T_{1/2}^{(part.)}$(ns)	$B(E2)_{exp}/e^2(fm^4)$	$B(E2)_{th}/e^2_{eff}(fm^4)$	e_{eff}/e
168.7	14.9±0.8	7.2±0.7	31 ±2	$E2+(13\pm2)\%\,M1$	4.4/30	920±90	220	2.04±0.10
250.2	13.3±0.7	1.4±0.3[b]	16.4±1.9	$E2$	4.3	135±14	32	2.06±0.11
442.2	51 ±3	1.5[c]	53 ±3	$(E2)$	1.12	34±2	—	

[a] I_γ (674) = 100.
[b] Total L conversion intensity. $I(L_I+L_{II})/I(L_{III}) = 3.5\pm1.9$ (cf. text).
[c] Used for normalization, assuming pure $E2$ multipolarity (cf. ref. [2]).

(g.s.)$\otimes\pi(f_{7/2})$, respectively (the latter notation is used to allow for pairing correlations). Hence an $E2$ transition, that can only change one particle, is forbidden in this approximation. This is in accordance with the observed hindrance of 2.5 compared to the Weisskopf estimate [12]. Which particular admixtures that cause the transition to proceed, is not clear to us. The most likely candidates seem to be either a $\pi[(h_{9/2}{}^2 f_{7/2}]_{3/2}$ admixture into the initial state, adding the very fast $(h_{9/2}{}^2)_2 \rightarrow (h_{9/2}{}^2)_0$, or a $\pi(h_{9/2}{}^3)_{7/2}$ admixture in the final state.

3.3. *The 169 keV M1 transition*

The $M1$ component, only 13 %, of the 169 keV transition, is highly retarded. From a comparison with the Weisskopf estimate [12], one infers a hidrance factor of 6 400. For pure $\pi(h_{9/2}{}^3)$ states the $M1$ transition would be completely forbidden. This is a special case of a general rule [13] stating that *within a j^n configuration M1 transitions are completely forbidden.* This can be understood as follows: The $M1$ operator is proportional to $\sum_i g_i \vec{j}_i$ where $\vec{j}_i$ is the total angular momentum of the ith nucleon and g_i its gyromagnetic factor. With all g_i equal the sum becomes $g\sum_i \vec{j}_i = g\vec{J}_{tot}$. This operator can only connect states with the same total $\vec{J}$. Corresponding, but not so strong, retardations have been observed in ^{19}O $(\nu(d_{5/2}{}^3))$ [14] and ^{51}V $(\pi(f_{7/2}{}^3))$ [15]. The large hindrance cannot be taken as any measure of the purity of the wave-functions, however. The admixtures which most likely occur, $\pi(h_{9/2}{}^2 f_{7/2})$, only add 1-forbidden $M1$ transitions.

4. Conclusion

The moral to be learnt from this work is an old one. A model that describes energy levels beautifully (in our case the assumption of pure $\pi(h_{9/2}{}^3)$ states) may fail severely (here with a factor of about 2) when applied to transition rates. The 169 keV $M1$ transition, forbidden within the $\pi(h_{9/2}{}^3)$ configuration, is indeed highly retarded, compared to the single-particle estimate.

References

1. Bergström, I., Fant, B., Herrlander, C. J., Thieberger, P., Wikström, K. and Astner, G., Phys. Letters **32B**, 476 (1970).
2. Astner G., Physica Scripta **5**, 31 (1972).
3. Gerholm, T. R. and Lindskog, J., Arkiv Fysik **24**, 171 (1963).
4. Malmskog, S. G., Arkiv Fysik **35**, 255 (1967).
5. Olsen, B. and Boström, L , Nucl. Instr. and Meth. **44**, 65 (1966).
6. Sundström, T., Nucl. Instr. and Meth. **16**, 153 (1967).
7. Arbman, E. and Svartholm, N., Arkiv Fysik **10**, 1 (1955).
8. Hager, R. S. and Seltzer, E. C., Nuclear Data **A4**, 1 (1968).
9. Astner, G., Bergström, I., Blomqvist, J., Fant, B. and Wikström, K., Nucl. Phys., *A 182*, 219 (1972).
10. Mottelson, B., Nikko Summer School Lectures 1967, NORDITA publ. No. 288.
11. Bès, D. R. and Sorensen, R. A., *in* Advances in Nuclear Physics, vol. 2 (ed. M. Baranger and E. Vogt). Plenum Press, New York, 1969.
12. Wapstra, A. H., Nijjh, G. J. and van Lieshout, R., Nuclear Spectroscopy Tables. North-Holland Publ. Co., Amsterdam, 1959.
13. de-Shalit, A. and Talmi, I., Nuclear Shell Theory, p. 409. Academic Press, New York, 1963.
14. Zimmerman, W., Jr, Phys. Rev. **114**, 837 (1959).
15. Lederer, C. M., Hollander, J. M. and Perlman, I., Table of Isotopes. Wiley, New York, 1967.

Research Institute for Physics
P.O. Box
S-104 05 Stockholm 50, Sweden

Institute of Physics
University of Stockholm
Vanadisvägen 9
S-113 46 Stockholm, Sweden

R E F E R E N C E 2

CHARGE EFFECTIVE DU PROTON $H_{9/2}$ DANS LE POLONIUM - 210.

Note(*) de MM. Valter BERG, Christian BOURGEOIS, et Nils PERRIN, présentée par M. Francis PERRIN.

PHYSIQUE NUCLÉAIRE. — *Charge effective du proton $h_{9/2}$ dans le polonium-210.* Note (*) de MM. **Valter Berg, Christian Bourgeois** et **Nils Perrin**, présentée par M. Francis Perrin.

Pour évaluer la charge effective du proton $h_{9/2}$ dans ^{210}Po, nous avons mesuré les vies moyennes des niveaux 4^+ à 1426,7 keV et 6^+ à 1473,2 keV. Nos résultats $T_{1/2}(4^+) = (1{,}53 \pm 0{,}08)$ ns et $T_{1/2}(6^+) = (43{,}0 \pm 1{,}5)$ ns donnent respectivement pour valeur de la charge effective $(1{,}72 \pm 0{,}05)\,e$ et $(1{,}67 \pm 0{,}04)\,e$, ce qui est supérieur de 10 % à la charge effective du proton $h_{9/2}$ évaluée dans ^{209}Bi.

Introduction. — Pour un nucléon célibataire lié à un cœur sphérique, il apparaît une force qui tend à polariser le cœur. La probabilité de transition du nucléon d'un état vers un autre n'est plus alors seulement le résultat de son mouvement mais aussi de la polarisation du cœur. Cet effet peut être exprimé par une modification de l'opérateur de particule en un opérateur effectif. Une question importante est celle de l'additivité du moment magnétique effectif et de la charge effective : chaque particule (trou) ajoutée à une orbitale apporte une quantité donnée de moment magnétique ou de charge, indépendamment du nombre de particules déjà présentes dans cette orbitale.

Maier et coll. ([2]) ont mesuré les facteurs g autour de ^{208}Pb et considèrent que l'additivité des moments magnétiques est bien établie. Astner et coll. ([1]) ont calculé les charges effectives dans ^{210}Po et ^{211}At en comparant les valeurs théoriques et expérimentales des probabilités de transitions réduites B (E 2) entre les états $(h_{9/2})^2$ et $(h_{9/2})^3$. Leurs résultats sont en bon accord avec la valeur de la charge effective du proton célibataire dans la couche $h_{9/2}$ de ^{209}Bi soit $e_{\text{eff}} = (1{,}50 \pm 0{,}06)\,e$. Cependant il existe dans ^{210}Po une charge effective, évaluée à partir de la transition $6^+ \to 4^+$, qui donne un résultat trop élevé : $e_{\text{eff}} = (1{,}78 \pm 0{,}12)\,e$. C'est pour vérifier cette irrégularité que nous avons remesuré les vies moyennes des niveaux 6^+ et 4^+ de ^{210}Po [([3]), ([4])].

Préparation de la source. — Les sources d'astate sont obtenues en irradiant des cibles de bismuth avec des particules α de 37 MeV. ^{210}At est séparé au séparateur électromagnétique et recueilli sur un support d'argent de 5 μ d'épaisseur. Un spectre d'électrons entre 10 et 350 keV d'énergie (*fig.* 1) effectué à l'aide d'un spectromètre magnétique confirme la pureté des sources.

Mesures. — La vie moyenne du niveau 4^+ a été mesuré par des coïncidences retardées électrons-électrons réalisées avec un spectromètre à doubles lentilles de type Gerholm [([3]) à ([6])]. Nous avons choisi les électrons L de la transition de 46,5 keV d'un côté et les électrons L de la transition de 245,3 keV de l'autre (détectés au travers du support d'argent). Une courbe de coïncidence promptes de référence a été réalisée avec une source de ^{212}Pb. La courbe de coïncidences retardées a été analysée en

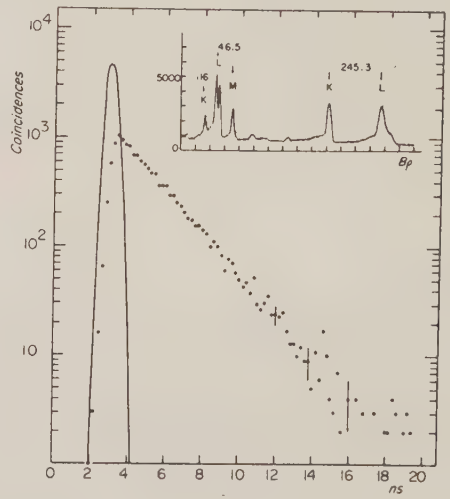

Fig. 1. — $T_{1/2} = (1{,}53 \pm 0{,}08)$ ns pour le niveau 4^+ à 1426,7 keV de ^{210}Po.
Courbe de coïncidences retardées : les électrons 46,5 L et 245,3 L de ^{210}Po sont sélectionnés pour les coïncidences après une préaccélération de 10 kV.
Courbe de coïncidences promptes de référence : les électrons 238,6 L de ^{212}Pb sont préaccélérés par 15 kV pour apparaître dans la fenêtre choisie pour les électrons 245,3 L de ^{210}Po.
Le spectre d'électrons de ^{210}Po inséré a été réalisé avec un lentille du spectromètre Gerholm.

utilisant la méthode des produits de convolution et la méthode des moments ([7]) (*fig.* 1). On a trouvé

$$T_{1/2}\,(4^+;\ \text{niveau 1426,7 keV de } ^{210}\text{Po}) = (1{,}53 \pm 0{,}08)\ \text{ns}.$$

La vie moyenne du niveau 6^+ a été mesurée par des coïncidences retardées entre les électrons L de la transition de 46,5 keV et les rayonnements X de ^{210}Po détectés à l'aide d'un scintillateur plastique Pilot B (5 % Pb). Une courbe de coïncidences promptes de référence a été réalisée avec la cascade e-γ d'une source de ^{60}Co. L'analyse de la courbe des coïncidences retardées (*fig.* 2) donne

$$T_{1/2}\,(6^+;\ \text{niveau 1473,2 keV de } ^{210}\text{Po}) = (13{,}0 \pm 1{,}5)\ \text{ns}.$$

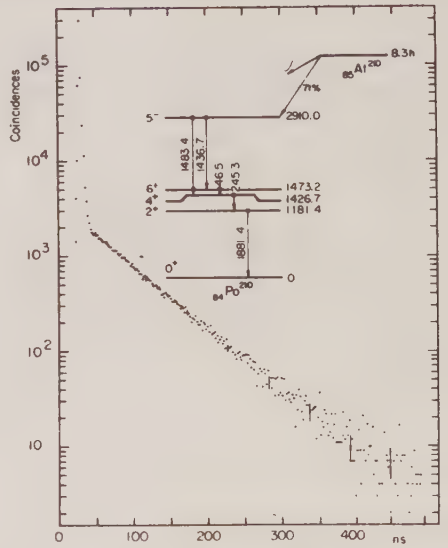

Fig. 2. — $T_{1/2} = (43{,}0 \pm 1{,}5)$ ns pour le niveau 6^+ à 1473,2 keV de ^{210}Po.

Discussion. — La colonne 5 du tableau donne les valeurs des charges effectives calculées à l'aide de la mesure du moment quadrupolaire pour ^{209}Bi ([10]) et à l'aide des probabilités de transitions E 2 expérimentales, utilisant les fonctions d'ondes de Kuo et Herling ([11]), pour ^{210}Po.

Tableau

Noyau	État initial	État final	E_γ (keV)	e_{eff}/e	e_{eff}/e (Notre travail)
^{209}Bi	$h_{9/2}$	$h_{9/2}$	–	$1{,}50 \pm 0{,}06$	–
^{210}Po	$(h^2_{9/2})_{6^+}$	$(h^1_{9/2} f^1_{5/2})_{6^+}$	83,7	$1{,}53 \pm 0{,}06$	–
^{210}Po	$(h^2_{9/2})_{6^+}$	$(h^1_{9/2} f^1_{5/2})_{4^+}$	46,5	$1{,}78 \pm 0{,}12$	$1{,}67 \pm 0{,}04$
^{210}Po	$(h^2_{9/2})_{4^+}$	$(h^1_{9/2} f^1_{5/2})_{4^+}$	245,3	$1{,}59 \pm 0{,}09$	$1{,}72 \pm 0{,}05$

La colonne 6 donne les valeurs obtenues en introduisant dans les calculs de Astner et coll. ([1]) les vies moyennes mesurées dans ce travail; on note que la charge effective déduite de la transition $6^+ \to 4^+$ a diminué tandis que celle évaluée à partir de la transition $4^+ \to 2^+$ a augmenté. Ces deux valeurs se sont rapprochées l'une de l'autre mais elles sont nettement plus élevées que la charge effective du proton $h_{9/2}$ de ^{209}Bi. Une explication

possible serait que l'on doit modifier les mélanges dans les fonctions d'ondes utilisées. Ainsi pour la transition $6^+ \to 4^+$ la composante la plus importante [après $(h_{9/2})^2\, 4^+$] est $(h_{9/2}, f_{5/2})_{4^+}$; son amplitude doit passer de 0,045 à 0,2 pour abaisser e_{eff}/e à 1,53, ce qui paraît improbable.

Conclusion. — Nous trouvons que les charges effectives calculées à partir des vies moyennes des niveaux 6^+ et 4^+ dans ^{210}Po sont de 10 % plus grandes que celles obtenues pour le proton célibataire de ^{209}Bi; dans ce cas, la règle d'additivité ne semble pas respectée.

Le professeur Ingmar Bergström nous a proposé ce travail et le docteur Jan Blomquist nous a fait part de ses commentaires. M. Jacques Obert a effectué la séparation isotopique des sources de ^{210}At.

(*) Séance du 16 avril 1973.
([1]) G. Astner, I. Bergström, J. Blomquist, B. Fant et K. Wikström, *Nucl. Phys.*, A, 182, 1972, p. 219.
([2]) K. H. Maier, K. Nakai, J. R. Leigh, R. M. Diamond et F. S. Stephens, *Nucl. Phys.*, A, 183, 1972, p. 289.
([3]) T. R. Gerholm et J. Lindskog, *Ark. Fys.* 24,, 1963, p. 171.
([4]) S. G. Malmskog, *Ark. Fys.*, 35, 1967, p. 255.
([5]) V. Berg, J. Letessier, C. Bourgeois et R. Foucher, *J. Phys.*, 33, 1972, p. 829.
([6]) B. L. Ader et N. N. Perrin, *Nucl. Phys.*, A, 197, 1972, p. 593.
([7]) L. Bostrom et B. Olsen, *Nucl. Instr. Meth.*, 44, 1966, p. 65.
([8]) A. W. Sunyar, *Phys. Rev.*, 98, 1955, p. 653.
([9]) E. G. Funk Jr, H. J. Prask, F. Schima, J. Mc Nulty et J. W. Mihelich, *Phys. Rev.*, 129, 1963, p. 757.
([10]) G. Eisele, I. Koniordos, G. Müller et R. Winkler, *Phys. Lett.*, 28 B, 1968, p. 256.
([11]) T. T. S. Kuo et G. H. Herling, Naval Research Laboratory, Memorandum Report 2258, 1971.

Institut de Physique Nucléaire,
B. P. n° 1,
91406 *Orsay.*

REFERENCE 3

TRANSITION RATES IN ^{161}Dy

V. BERG AND S. G. MALMSKOG

AB Atomenergi, Studsvik, Nyköping, Sweden

and

Department of Physics, University of Stockholm, Sweden

1.E.1:
3.A

Nuclear Physics A135 (1969) 401—418; © *North-Holland Publishing Co., Amsterdam*
Not to be reproduced by photoprint or microfilm without written permission from the publisher

TRANSITION RATES IN ^{161}Dy

V. BERG and S. G. MALMSKOG

AB Atomenergi, Studsvik, Nyköping, Sweden
and
Department of Physics, University of Stockholm, Sweden

Received 9 June 1969

Abstract: The decay of ^{161}Tb has been studied using a high-resolution Ge(Li) detector. Five new transitions were observed and fitted into the earlier proposed decay scheme. The half-life of the 131.8 keV level in ^{161}Dy was determined in a delayed-coincidence measurement to be 145 ± 15 psec. The low level scheme in ^{161}Dy is discussed within a quasiparticle model allowing for Coriolis mixing. Special attention is given to the strongly retarded, *K*-allowed 131.8 keV E1 transition with a retardation factor $F_W > 1.5 \times 10^8$.

E RADIOACTIVITY ^{161}Tb [from ^{160}Gd(n, γ)^{161}Gd(β^-)]; measured E_γ, I_γ, β, cece-delay. ^{161}Dy levels deduced $T_{\frac{1}{2}}$, $B(L)$. Ge(Li) detector.

1. Introduction

Over a period of several years, we have systematically studied transition rates in deformed nuclei [1]). The main aim has been to see whether or not these transition rates can be reasonably well accounted for within the existing theories. Such a comparison with predictions was also made by Bès [2]) when he tried to account for the experimental results for transitions in ^{161}Dy given by Hansen *et al.* [3]). Since that time, several accurate measurements on the low level structure in ^{161}Dy have been reported [4, 5]). One of the striking results from earlier investigations is the large intensity ratio for E1 transitions from the 131.8 keV level to members of the ground state rotational band. From a measurement of the half-life of this level, absolute transition probabilities are obtained which can be compared with different predictions to see whether this unusually large ratio can be explained.

During our investigation, the earlier reported weak high-energy gamma-ray spectrum observed by Funke *et al.* [6]) was also studied with a high-resolution Ge(Li) detector. Five new transitions were observed; all of them could be fitted into the earlier proposed decay scheme.

2. Experimental procedure

2.1. SOURCE PREPARATION

Samples of Gd_2O_3 enriched to 96 % in ^{160}Gd were irradiated in a flux density of 2×10^{14} thermal neutrons/cm^2 · sec in the R2 reactor at Studsvik. The time of irradiation was approximately 10 h for the sample used for gamma-ray spectroscopy and 10 d for the sample used for the half-life determinations. During the irradiation, ^{160}Gd is transformed into ^{161}Gd, which, with a half-life of only 3 min, decays to ^{161}Tb. The Tb activity obtained was extracted from the remaining bulk of inactive Gd_2O_3 and at the same time separated from contaminating rare-earth activities through ion exchange techniques. Among the contaminants were identified ^{159}Gd, ^{165}Dy and ^{169}Yb. Of these activities the half-life measurement of the 131.8 keV level in ^{161}Dy could have been endangered by the interference from the 130 psec 58 keV level in ^{159}Tb.

After the ion-exchange process, the $TbCl_3$-solution intended for gamma-ray spectroscopy was evaporated to dryness on an aluminium backing. As the half-life measurement required sources in the form of a very thin and uniform active layer, the $TbCl_3$ was for this purpose electroplated onto a thin aluminium foil.

2.2. GAMMA-RAY MEASUREMENTS

The spectrum of gamma rays emitted following the decay of ^{161}Tb was measured with a 1.5 cm^3 Ge(Li) detector. The pulses were amplified with a cooled FET preamplifier, a Tennelec TC 200 main amplifier and a Tennelec TC 250 bias amplifier and stored in a 4096-channel Nuclear Data analyser.

To protect the detector from the intense flow of beta particles and from low-energy gamma rays and to enhance the high-energy part of the gamma-ray spectrum, the detector was shielded in one measurement with 1 mm of lead and 2 mm of cadmium. Another measurement with a shielding of only 0.5 mm of cadmium was later performed to make it possible to normalize the intensities of the low-energy to the high-energy peaks in the gamma spectrum. These measurements were reproduced after a 10 d interval to check that the decrease in gamma-ray intensity agreed with the known decay rate of ^{161}Tb. Gamma rays emitted by a longer-lived activity were then observed and identified as due to the decay of ^{160}Tb. As the gamma-ray spectrum of this nucleus is well known, the presence of these gamma lines did not cause any difficulty. On the contrary, these gamma rays served as excellent calibration points, owing to the fact that their energies and intensities have been very accurately measured. Further energy and relative efficiency calibrations were accomplished using a set of absolute calibrated sources obtained from IAEA, Vienna.

The gamma-ray spectrum presented in figs. 2–3 was obtained with the lead and cadmium shielding; it is due only to the decay of ^{161}Tb. The subtraction of the ^{160}Tb contribution was relatively easy, as a pure ^{160}Tb spectrum was registered with unchanged geometry and electronic settings. Figs. 2 and 3 show some earlier unobserved gamma rays with energies 315.1, 341.2, 348.2, 425.8 and 506.7 keV. Observed gamma-ray energies and relative intensities in the decay of ^{161}Tb are presented in table 1.

2.3. HALF-LIFE MEASUREMENTS

Half-life measurements were carried out with a long-lens electron-electron coincidence spectrometer, which has been described earlier [7, 8]).

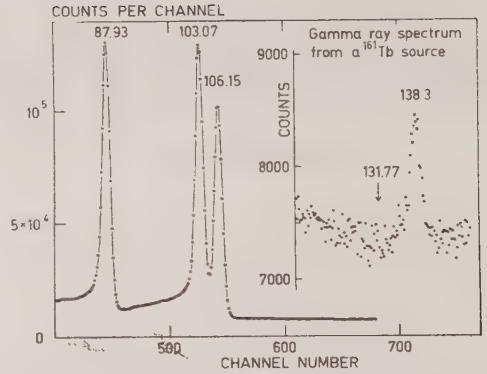

Fig. 1. Low-energy gamma-ray spectrum observed in the decay of ^{161}Tb.

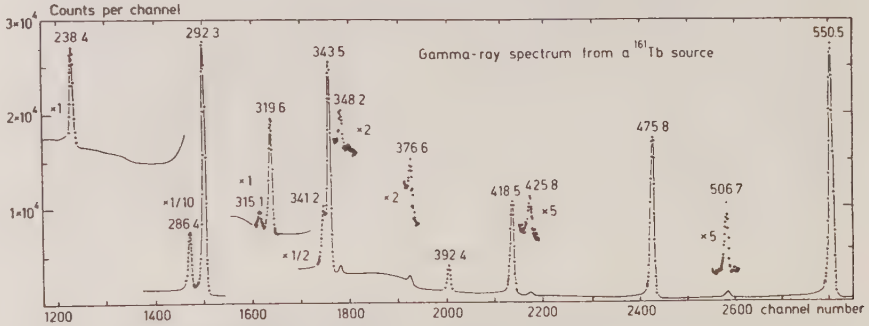

Fig. 2. High-energy gamma-ray spectrum observed in the decay of ^{161}Tb.

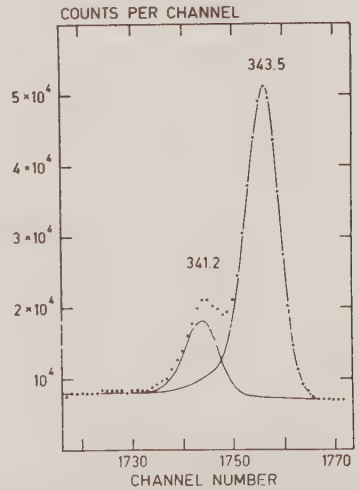

Fig. 3. The 341.2–343.5 keV gamma transition doublet in the decay of ^{161}Tb.

The 131.8 keV level is de-excited by five transitions with the following energies: 131.8, 106.2, 87.9, 57.2 and 28.7 keV, while the main feeding is via a 450 keV β-branch. As the 57.2 keV transition is by far the strongest (more than 95 % of the de-excitation goes through it), it appeared judicious to base the measurements on conversion electrons from this transition. As the 57.2 L electrons and the N electrons originating from the intense 48.9 keV transition have very similar energy

Table 1

γ-ray energies and intensities observed in the decay of ^{161}Tb

Transition energy (keV)	Relative γ-ray intensity	
	present work	ref. [6])
74.6±0.1	100	100
87.9±0.1	2.1 ±0.2	2.0 ±0.2
103.1±0.1	1.2 ±0.1	1.1 ±0.2
106.2±0.1	0.90 ±0.08	0.7 ±0.1
131.8±0.1	<0.002	<0.01
138.3±0.1	0.011±0.002	≈0.02
238.4±0.1	0.019±0.003	0.05±0.02
286.4±0.1	0.125±0.013	0.22±0.02
292.3±0.1	0.65 ±0.07	0.78±0.08
315.1±0.2	0.004±0.001	
319.6±0.1	0.032±0.004	0.04±0.01
341.2±0.1	0.035±0.004	
343.5±0.1	0.138±0.014	0.23±0.03
348.2±0.2	0.004±0.001	
376.6±0.2	0.005±0.001	≈0.01
392.4±0.1	0.022±0.003	0.02±0.01
418.5±0.1	0.086±0.008	0.10±0.01
425.8±0.2	0.003±0.001	
475.8±0.1	0.190±0.019	0.23±0.03
506.7±0.2	0.008±0.001	
550.5±0.1	0.400±0.040	0.45±0.05

and the energy resolution of the spectrometer is not good enough to completely separate these different electron groups, it was found necessary to focus the spectrometer lens on the 57.2 M electron line in order to obtain an undisturbed time spectrum. The only other contribution then possible could come from the 106.2 K conversion electrons. As they also depopulate the 131.8 keV level, their interference is only constructive.

With one lens fixed in this way, the second lens was adjusted to transmit the K conversion electrons from the nearly prompt 238.6 keV transition appearing in the decay of ^{212}Pb. Then 30 min measurements were successively carried out alternately with ^{212}Pb and ^{161}Tb sources registering coincidences in the β-238.6 K and $\beta \rightarrow$ 57.2 M cascades, where the ^{212}Pb coincidences were used to define the zero

TABLE 2

Experimental data and hindrance factors for gamma transitions in ^{161}Dy

Level (keV)	$T_{\frac{1}{2}}$ (exp) of level (nsec)	Transition energy (keV)	Initial state $IK^{\pi}(Nn_zA)$	Final state $IK^{\pi}(Nn_zA)$	Multipolarity	Relative N_γ [a])	Relative N_e [b])	$T_{\frac{1}{2}\gamma}$ (exp) (sec)	B(M1) ↓ B(E2) ↓ or B(E1) ↓ [c])	Error %	F_W [d])	F_N [e])
131.77	0.145±0.015	131.77	$\frac{5}{2}\frac{3}{2}^-(521)$	$\frac{5}{2}\frac{3}{2}^+(642)$	E1	< 0.002		> 1.5 E−5 [f])	< 1.3 E−10	−	> 1.5 E+8	> 2.5 E+4
		106.15	$\frac{5}{2}\frac{3}{2}^-(521)$	$\frac{5}{2}\frac{5}{2}^-(523)$	M1	0.53	1.6	5.7 E−8	5.8E − 4	15	3.0 E+3	16
					E2	0.36		8.4 E−8	5.0 E − 2	15	1.1 E−1	7.8 E−5
		87.93	$\frac{5}{2}\frac{3}{2}^-(521)$	$\frac{7}{2}\frac{5}{2}^+(642)$	E1	2.0	0.9	1.5 E−8	4.3 E − 7	20	4.5 E+4	19
		57.20	$\frac{5}{2}\frac{3}{2}^-(521)$	$\frac{3}{2}\frac{3}{2}^-(521)$	M1	15.5	184	2.0 E−9	1.1 E − 1	12	17	interband
					E2	0.53		5.6 E−8	1.67	20	3.2 E−3	transition
		28.72	$\frac{5}{2}\frac{3}{2}^-(521)$	$\frac{7}{2}\frac{5}{2}^-(523)$	M1	0.18	2.8	1.7 E−7	9.8 E − 3	25	1.8 E+2	2.3
74.58	3.34 ±0.18	74.58	$\frac{3}{2}\frac{3}{2}^-(521)$	$\frac{5}{2}\frac{5}{2}^+(642)$	E1	10.0	6.5	3.0 E−8	3.5 E − 7	10	5.5 E+4	33
		48.92	$\frac{3}{2}\frac{3}{2}^-(521)$	$\frac{5}{2}\frac{5}{2}^-(523)$	M1	16.1	58	1.9 E−8	1.8 E − 2	10	1.0 E+2	1.8
					E2	0.06		5.0 E−6	4.0 E − 2	30	1.3 E−1	9.6 E−5

[a]) Ref. [4]).
[b]) Total conversion coefficient from ref. [5]).
[c]) In units of $(e\hbar/2Mc)^2$, e^2b^2 and e^2b, respectively.
[d]) Calculated according to ref. [11]) using a statistical factor of 1.
[e]) Calculated according to ref. [13]) with $\delta = 0.3$, $\mu = 0.45$, $\kappa = 0.05$, $g_s = g_s$ (free) and $g_R = 0.25$.
[f]) 1.5 E−5 stands for 1.5×10^{-5} and so on.

time. The automatic spectrometer operation described in ref. [8]) proved very useful, and more than 40 spectra were registered. The analysis of these spectra was performed by the centroid shift method as well as by the convolution method [9]); both gave $T_{\frac{1}{2}} = 0.145 \pm 0.015$ nsec for the 131.8 keV level in ^{161}Dy. No earlier value has been reported.

A determination of the half-life of the 74.6 keV level was also performed registering coincidences between the 48.9 L and 57.2 M conversion electrons. A typical time spectrum is shown in fig. 4. From the slope of such curves, we obtain an average value 3.34±0.18 nsec for the half life of the 74.6 keV level in ^{161}Dy. This is in agreement with earlier reported values [10]).

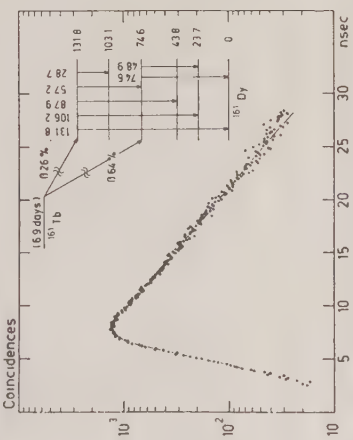

Fig. 4. Delayed coincidence curve taken between the 48.9 L and 57.2 M conversion electrons giving a half-life of 3.34±0.18 nsec for the 74.6 keV level in ^{161}Dy.

3. Discussion

3.1. THE LOW-ENERGY LEVEL STRUCTURE

Our half-life determination for the 131.8 keV level in ^{161}Dy with the gamma intensities and multipolarity assignments of refs. [4,5]) give three M1, two E2 and two E1 absolute transition probabilities for transitions de-exciting the 131.8 keV level. All the experimental information needed to deduce these is given in table 2. The corresponding reduced transition probabilities given in column 10 are obtained from the following relations:

$$B(\mathrm{M1})\downarrow = 3.94 \times 10^{-5}/T_{\frac{1}{2}\gamma}(\mathrm{M1})E_\gamma^3,$$
$$B(\mathrm{E2})\downarrow = 56.4/T_{\frac{1}{2}\gamma}(\mathrm{E2})E_\gamma^5,$$
$$B(\mathrm{E1})\downarrow = 4.37 \times 10^{-9}/T_{\frac{1}{2}\gamma}(\mathrm{E1})E_\gamma^3,$$

where the partial half-life $T_{\frac{1}{2}\gamma}$ is in sec, E_γ in keV, $B(\mathrm{E}\lambda)$ in units of e^2b^λ and $B(\mathrm{M1})$ in units of $(e\hbar/2Mc)^2$.

It is common to compare experimental results with theoretical predictions by giving the hindrance factor F (theoretical transition probability/corresponding experimental

transition probability). Column 12 shows the hindrance factors obtained using the single-particle Weisskopf estimate [11]). We see that the E2 transition within the $\frac{3}{2}^-(521)$ rotational band is enhanced 310 times, which is roughly 30 times faster than the E2 transitions between members of the $\frac{3}{2}^-(521)$ and $\frac{5}{2}^-(523)$ rotational bands. The M1 transitions are hindered between 17 and 3000 times, the fastest being the 57.2 keV interband M1 transition. The E1 transitions are generally strongly retarded and the transitions between members of the $\frac{3}{2}^-(521)$ and $\frac{5}{2}^+(642)$ rotational bands are no exceptions; they have hindrance factors between four and six times 10^4, while the unusually slow 131.8 keV E1 transition is hindered more than 1.5×10^8 times. None of these values is, however, outside the extreme value known from the systematics of transition probabilities in deformed nuclei [12]).

Better theoretical predictions of the transition rates in deformed nuclei are known to be obtained using the deformed potential single-particle model formulated by Nilsson [13]). According to this model, the reduced M1, E2 and E1 transition probabilities can be written

$$B(\mathrm{M1}) = 5.907\times10^{-2}[\langle I_i K_i 1, K_f - K_i | I_f K_f\rangle + b_{\mathrm{M1}}(-1)^{I_f+K_f}\langle I_i K_i 1, -K_f - K_i | I_f, -K_f\rangle]^2 G_{\mathrm{M1}}^2, \quad (1)$$

$$B(\mathrm{E2}) = 4.028\times10^{-5}A^{\frac{2}{3}}[\langle I_i K_i 2, K_f - K_i | I_f K_f\rangle + b_{\mathrm{E2}}(-1)^{I_f+K_f}\langle I_i K_i 2, -K_f - K_i | I_f, -K_f\rangle]^2 G_{\mathrm{E2}}^2, \quad (2)$$

$$B(\mathrm{E1}) = 2.414\times10^{-3}A^{\frac{1}{3}}\left(1-\frac{Z}{A}\right)^2\{\langle I_i K_i 1, K_f - K_i | I_f K_f\rangle + b_{\mathrm{E1}}(-1)^{I_f+K_f}\langle I_i K_i 1, -K_f - K_i | I_f, -K_f\rangle]^2 G_{\mathrm{E1}}^2, \quad (3)$$

where $B(\mathrm{M1})$ is in units of $(e\hbar/2Mc)^2$, $B(\mathrm{E2})$ in $e^2\mathrm{b}^2$ and $B(\mathrm{E1})$ in e^2b. The quantities b and G depend on the wave functions of the initial and final states of the transition and are defined by eqs. (35) and (36) in ref. [13]). The result from a comparison with this model is given in table 2, column 13, where the hindrance factor F_{N} is given.

For a more sophisticated prediction, the effect of pairing correlations should also be taken into account. To do this, we have to specify a single-particle level scheme appropriate for the studied nucleus. We have done this in a semi-empirical way; the single-particle states are determined so that a BCS blocking calculation with $G = 0.18$ MeV roughly reproduces the lowest-lying states in ^{161}Dy and higher lying states as expected from systematics in neighbouring nuclei. The resulting semi-empirical single-particle level scheme is shown in fig. 5. The transition matrix elements in this quasiparticle model are a factor $P_\pm$ times the matrix element used before. The new hindrance factor is then $F_{\mathrm{QM}} = P_\pm^2 F_{\mathrm{N}}$, where $P_\pm = (U_i U_f \pm V_i V_f)R$. Plus or minus signs are used in magnetic and electric transitions, respectively. The parameters U and V are defined through $U^2+V^2=1$, $V^2 = \frac{1}{2}(1-(\varepsilon-\lambda)/\mathrm{E})$ and $\mathrm{E} = \sqrt{(\varepsilon-\lambda)^2+\Delta^2}$ [ref. [14])]. The parameters used in the calculation of the $P_\pm$ factors of interest in this work are given in fig. 5; the results are summarized in table 3. The accuracy of

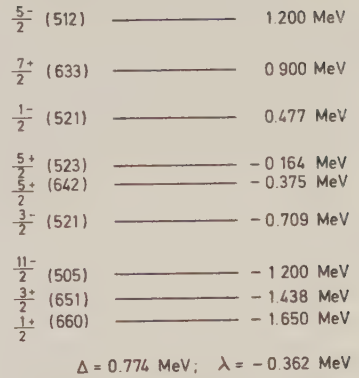

Fig. 5. Semi-empirical single-particle level scheme of ^{161}Dy used for the calculation of the pairing factors $P_\pm = (U_i U_f \pm V_i V_f)R$.

TABLE 3

Pairing factors for Nilsson orbitals of interest in the present work

Transition	P_-	P_+
$\frac{3}{2}^-(521)-\frac{5}{2}^+(642)$	−0.20	0.98
$\frac{5}{2}^-(523)-\frac{5}{2}^+(642)$	0.13	0.99
$\frac{3}{2}^-(521)-\frac{5}{2}^-(523)$	−0.084	0.94
$\frac{3}{2}^+(651)-\frac{3}{2}^-(521)$	−0.63	0.97
$\frac{3}{2}^+(651)-\frac{5}{2}^+(642)$	−0.46	0.89
$\frac{3}{2}^+(651)-\frac{5}{2}^-(523)$	−0.34	0.82
$\frac{1}{2}^-(521)-\frac{3}{2}^-(521)$	0.20	0.81
$\frac{1}{2}^-(521)-\frac{5}{2}^+(642)$	0.39	0.91

the model calculation of the P-factors is believed to be better than 20 %. As can be seen from table 3, especially dramatic effects can only be expected for electric multipole transitions for which reductions in the transition probabilities of several orders of magnitude can be obtained.

Further contributions to the transition rates are also given via non-adiabatic effects, of which the Coriolis mixing of particle states is the best studied. Significant contributions from β- and γ-vibrational bands as well as from the octupole bands may also be obtained in some cases. A detailed discussion of the observed transition rates of different multipolarities in ^{161}Dy is given below.

3.2. THE E2 TRANSITION RATES WITHIN BANDS

From the E2 part of the interband 57.2 keV transition, we obtain a value for the collective electric quadrupole strength for the excited $\frac{3}{2}^-(521)$ rotational band in ^{161}Dy. From the experimental data given in table 2, we get a reduced E2 transition probability $B(\mathrm{E2}, \frac{5}{2}\frac{3}{2} \rightarrow \frac{3}{2}\frac{3}{2}) = (1.67\pm0.33)e^2\mathrm{b}^2$, where the main contributions to

the error come from the uncertainty in the E2 part of the 57.2 keV transition taken as (3.0±0.5) % from ref. [4]) and from the measured half-life of the 131.8 keV level. Using the collective-model relationship

$$B(\mathrm{E2}, I_i K \rightarrow I_f K) = \frac{5}{16\pi} Q^2 \langle I_i K 20 | I_f K \rangle^2,$$

we obtain an electric quadrupole moment $Q_{75} = 7.0 \pm 0.7$ b or an equivalent deformation parameter $\delta = 0.28 \pm 0.02$.

Several earlier investigators have measured the intrinsic quadrupole moment for the $\frac{5}{2}^+(642)$ ground state in ^{161}Dy by Coulomb excitation [15,16]) or from a study of the hyperfine splitting patterns by the Mössbauer technique [17]). The latter method has also been used to deduce the ratio of quadrupole moments for the 75 keV $\frac{3}{2}^-(521)$ excited state and the ground state in ^{161}Dy [refs. [18–21])]. These earlier results are shown in table 4. Using $Q_0 = 7.1 \pm 0.2$ b and $Q_{75}/Q_0 = 1.00 \pm 0.05$ as average values from table 4, we obtain $Q_{75} = 7.1 \pm 0.4$ b, which compares very favourably with our measured value for Q_{75}. It is also interesting to note that several investigations [19,21]) show that $Q_{26}/Q_0 = 1.00 \pm 0.04$, therefore all the low-lying bands in ^{161}Dy have the same deformation.

TABLE 4

Measurements of Q_{75} and μ_{75} in ^{161}Dy

Method [a])	Q_{75}/Q_0	μ_{75}/μ_0	Q_0	μ_0	Ref.
ME	1.07±0.09	0.852±0.012			[18])
ME	1.00±0.07	0.840±0.024			[19])
ME	0.86±0.07	0.840±0.048			[20])
ME	1.04±0.07	0.828±0.012			[21])
CE			7.3±0.1		[15])
CE			7.0±0.2		[16])
AB			6.6±1.1	−(0.47 ±0.09)	[17])
AB				−(0.473±0.012)	[28])

[a]) ME – Mössbauer effect, CE – Coulomb excitation and AB – atomic-beam-resonance measurement.

3.3. THE E2 TRANSITION RATES WITH $|\Delta K| = 1$

The systematics of E2, $|\Delta K| = 1$ transitions [12]) shows that these are generally strongly enhanced as compared with the Nilsson-model predictions. This is also the case for the two measured E2 transition rates between members of the $\frac{3}{2}^-(521)$ and $\frac{5}{2}^-(523)$ rotational bands in ^{161}Dy. The transitions are enhanced 1.3×10^4 and 1.0×10^4 times, respectively. This enhancement is usually understood when Coriolis mixing between the two bands is considered, which gives rise to collective contributions to the interband E2 transition rates. Taking this Coriolis mixing into account, the reduced interband E2 transition probability defined by eq. (2) can in a first approximation be written

$$B(\mathrm{E2}, I_i \tfrac{3}{2} \rightarrow I_f \tfrac{5}{2}) = 1.18 \times 10^{-3} [P_-(\tfrac{3}{2} \rightarrow \tfrac{5}{2}) G_{\mathrm{E2}}(\tfrac{3}{2} \rightarrow \tfrac{5}{2}) \langle I_i \tfrac{3}{2} 21 | I_f \tfrac{5}{2} \rangle + C(I_f \tfrac{3}{2} \tfrac{5}{2}) G_{\mathrm{E2}}^{\mathrm{coll}} \langle I_i \tfrac{3}{2} 20 | I_f \tfrac{3}{2} \rangle + C(I_i \tfrac{5}{2} \tfrac{3}{2}) G_{\mathrm{E2}}^{\mathrm{coll}} \langle I_i \tfrac{5}{2} 20 | I_f \tfrac{5}{2} \rangle]^2. \quad (4)$$

The diagonal contribution to the E2 matrix element $G_{\mathrm{E2}}^{\mathrm{coll}}$ is given by

$$G_{\mathrm{E2}}^{\mathrm{coll}} = \frac{Q_0}{2\beta^2}, \quad (5)$$

where $\beta = \sqrt{\hbar/Mw_0}$ and $\hbar w_0 \approx 41\, A^{-\frac{1}{3}}$ MeV, which for ^{161}Dy gives $2\beta^2 = 0.108$. The amplitude of the state $I_v K_C$ being Coriolis admixed into the $I_v K_m$ member of the main band is $C(I_v K_C K_m)$. In the perturbation approximation, these amplitudes are given by

$$C(I_v K_C K_m) = -E^* \frac{P_+ \langle K_C | j_\pm | K_m \rangle \sqrt{(I_v - K_<)(I_v + K_< + 1)}}{E(I_v K_m) - E(I_v K_C)}, \quad (6)$$

$K_<$ being the smaller of K_C and K_m; E^* is the non-diagonal equivalent to $\hbar^2/2J$ and the denominator gives the energy difference between the two levels being admixed. When predicted values of $P_-(\frac{3}{2}^- \rightarrow \frac{5}{2}^-) \times G_{\mathrm{E2}}(\frac{3}{2}^- \rightarrow \frac{5}{2}^-)$ and $E^* P_+ \langle \frac{3}{2} | j_- | \frac{5}{2} \rangle G_{\mathrm{E2}}^{\mathrm{coll}}$ were put into eqs. (4)–(6) it became clear that the first single-particle term in eq. (4) was at least two orders of magnitude smaller than the second largest term and could therefore be neglected; thus in this approximation the $B(\mathrm{E2})$ transition rate is only dependent on one parameter, namely $E^* P_+ \langle \frac{3}{2} | j_- | \frac{5}{2} \rangle G_{\mathrm{E2}}^{\mathrm{coll}}$, which could then be evaluated. As a mean value from the two interband E2 transitions, we obtain

$$E^* P_+ \langle \tfrac{3}{2} | j_- | \tfrac{5}{2} \rangle G_{\mathrm{E2}}^{\mathrm{coll}} = \pm(430 \pm 75). \quad (7)$$

To estimate the value of the Coriolis coupling matrix element $\langle \frac{3}{2} | j_- | \frac{5}{2} \rangle$, we can use the reasonable values $E^* \approx \hbar^2/2J = 11$ keV, $Q_0 = 7.1 \pm 0.4$ b and $P_+ = 0.97$, which gives $\langle \frac{3}{2} | j_- | \frac{5}{2} \rangle = \pm 0.60 \pm 0.10$. This value can now be compared with the predictions of the Nilsson model, which with the parameters $\mu = 0.45$ and $\kappa = 0.05$ gives $\langle \frac{3}{2} | j_- | \frac{5}{2} \rangle = 1.11$ and 0.89 for the two deformation parameters $\delta = 0.2$ and 0.3, respectively. Recently Hansen *et al.* [29]) have deduced the Coriolis coupling strength $A_K = E^* P_+ \langle \frac{3}{2} | j_- | \frac{5}{2} \rangle$ in ^{161}Dy from β, E.C. and γ-ray transition ratios and conclude that all data are consistent with $A_K \approx 5$ keV (±25 %) in agreement with our value $A_K = 6.5 \pm 1.0$ keV.

3.4. THE M1 TRANSITION RATES WITHIN BANDS

The magnetic properties within a rotational band with $K \neq \frac{1}{2}$ are, according to the Nilsson model, described by the two gyromagnetic ratios g_K and g_R. A measurement of an intraband $B(\mathrm{M1})$ value and a magnetic moment is then enough to de-

termine both g_K and g_R separately. The following expressions are valid:

$$B(\mathrm{M1}, I_i K \to I_f K) = \frac{3}{4\pi} K^2 \langle I_i K 10 | I_f K \rangle^2 (g_K - g_R)^2, \tag{8}$$

$$\mu = \frac{K^2}{I+1}(g_K - g_R) + I g_R . \tag{9}$$

The choice between a positive or a negative sign for $(g_K - g_R)$ from eq. (8) is usually obvious as only one of the solutions is physically relevant. From the measurements of μ_0 and μ_{75}/μ_0 given in table 4, we use as an average value $\mu_{75} = -(0.397 \pm 0.011)$ which, together with our measured $B(\mathrm{M1}, \frac{5}{2}\frac{3}{2}^- \to \frac{3}{2}\frac{3}{2}^-) = (0.110 \pm 0.013)\ (e\hbar/2Mc)^2$, gives $g_K = -(0.62 \pm 0.09)$ and $g_R = 0.25 \pm 0.04$ for the $\frac{3}{2}^-(521)$ band. The same band is also the ground state band in ^{155}Gd and ^{157}Gd and the gyromagnetic ratios in these nuclei have been derived by Boehm *et al.* [22]) as $g_K = -0.484 \pm 0.012$ and -0.533 ± 0.014 with $g_R = 0.323 \pm 0.017$ and 0.261 ± 0.019 for the two Gd nuclei, respectively. The theoretical prediction for g_K is roughly a factor of 1.4 too high. This discrepancy is usually taken care of by introducing an effective gyromagnetic ratio g_s which is smaller than the one obtained for a free nucleon. Agreement with theory is obtained for the $\frac{3}{2}^-(521)$ particle state in the three nuclei mentioned for a g_s(eff) value between 0.6–0.7. This is in accordance with results obtained for other deformed nuclei.

In a recent letter, Hagemann and Tveter [23]) have pointed out that the ground state rotational band in ^{161}Dy has an unusually low value of $g_R = 0.11 \pm 0.02$, which is in line with the recent theoretical predictions [24,25]). No experimental evidence for such a low g_R value is, however, found for the excited bands in ^{161}Dy.

3.5. THE M1 TRANSITION RATES WITH $|\Delta K| = 1$

From our measurements, we determine three absolute M1 transition probabilities with $|\Delta K| = 1$, two of which de-excite the $\frac{5}{2}\frac{3}{2}^-(521)$ particle state at 131.8 keV, feeding the $\frac{5}{2}$ and $\frac{7}{2}$ members of the $\frac{5}{2}^-(523)$ band, respectively. According to the adiabatic model, the ratio of the reduced gamma-ray intensities of these transitions is

$$B(\mathrm{M1}, \tfrac{5}{2}\tfrac{3}{2} \to \tfrac{7}{2}\tfrac{5}{2})/B(\mathrm{M1}, \tfrac{5}{2}\tfrac{3}{2} \to \tfrac{5}{2}\tfrac{5}{2}) = [\langle \tfrac{5}{2}\tfrac{3}{2}11 | \tfrac{7}{2}\tfrac{5}{2}\rangle / \langle \tfrac{5}{2}\tfrac{3}{2}11 | \tfrac{5}{2}\tfrac{5}{2}\rangle]^2 \approx 2.50,$$

which should be compared with the experimental ratio [4]) of 18.6 ± 6.6. Although the Coriolis coupling is usually not expected to have a dominating influence on K-allowed M1 transition rates, intensity differences as observed in this case may be explained from such a mixing of states. To first order, the reduced M1 transition probability can be written in this case as

$$B(\mathrm{M1}, I_i \tfrac{3}{2} \to I_f \tfrac{5}{2}) = 5.91 \times 10^{-2} [P_+(\tfrac{3}{2} \to \tfrac{5}{2}) G_{\mathrm{M1}}(\tfrac{3}{2} \to \tfrac{5}{2}) (I_i \tfrac{3}{2} 11 | I_f \tfrac{5}{2}) + C(I_f \tfrac{3}{2}\tfrac{5}{2}) G_{\mathrm{M1}}(\tfrac{3}{2} \to \tfrac{3}{2}) (I_i \tfrac{3}{2} 10 | I_f \tfrac{3}{2}) + C(I_i \tfrac{5}{2}\tfrac{3}{2}) G_{\mathrm{M1}}(\tfrac{5}{2} \to \tfrac{5}{2}) (I_i \tfrac{5}{2} 10 | I_f \tfrac{5}{2})]^2. \tag{10}$$

TABLE 5

E1 transition rates in ^{161}Dy

	Experimental value	Comparison with different predictions[a])		
		F_N[b])	F_{QM}[c])	F_{PC}[d])
$B(\mathrm{E1}, \frac{5}{2}\frac{3}{2}^- \to \frac{5}{2}\frac{5}{2}^+)$	(3.5±0.4) E−7	33 ±4	1.3 ±0.2	1.01	0.98
$B(\mathrm{E1}, \frac{5}{2}\frac{3}{2}^- \to \frac{5}{2}\frac{3}{2}^+)$	(4.3±0.9) E−7	19 ±4	0.79±0.17	0.94	1.08
$B(\mathrm{E1}, \frac{7}{2}\frac{5}{2}^- \to \frac{7}{2}\frac{5}{2}^+)$	(1.6±0.3) E−6	0.86±0.16	(1.5 ±0.3) E−2	1.06	1.01
$B(\mathrm{E1}, \frac{7}{2}\frac{5}{2}^- \to \frac{5}{2}\frac{5}{2}^+)$	(1.7±0.3) E−6	0.43±0.08	(7.6 ±1.4) E−3	0.54	0.94
$B(\mathrm{E1}, \frac{5}{2}\frac{5}{2}^- \to \frac{5}{2}\frac{5}{2}^+)$	(2.6±0.7) E−6	0.93±0.25	(1.6 ±0.4) E−2	1.08	1.01
$B(\mathrm{E1}, \frac{5}{2}\frac{3}{2}^- \to \frac{5}{2}\frac{5}{2}^+)$	< 1.3 E−10	> 2.5 E+4	> 4.4 E+2	> 40[e])	> 45[e])
$G_{\mathrm{E1}}(\frac{3}{2}^- \to \frac{5}{2}^+)$	5.03 E−2				
$P_-(\frac{3}{2}^- \to \frac{5}{2}^+) G_{\mathrm{E1}}(\frac{3}{2}^- \to \frac{5}{2}^+)$	−2.72 E−2	−1.02 E−3	−(8.6±2.5) E−3		−(8.4±0.6) E−3
$G_{\mathrm{E1}}(\frac{5}{2}^- \to \frac{5}{2}^+)$					
$P_-(\frac{5}{2}^- \to \frac{5}{2}^+) G_{\mathrm{E1}}(\frac{5}{2}^- \to \frac{5}{2}^+)$		−3.62 E−3	−(2.9±0.3) E−2		−(2.7±0.1) E−2
$E^* P_+ \langle \frac{3}{2}^- \| J_- \| \frac{5}{2}^- \rangle$			6.5[e])		9.7[f])

[a]) Only experimental errors are considered.
[b]) Calculated from predictions of the Nilsson model [13]) with $\delta = 0.3$, $\kappa = 0.05$ and $\mu = 0.45$.
[c]) Calculated in the quasiparticle formalism where $F_{QM} = P_-^2 F_N$. The relevant P_- values are given in table 3.
[d]) Calculated in the quasiparticle model with the inclusion of Coriolis coupling. The $P_- G_{E1}$ values were obtained from a least-squares fit to the first five B(E1) values in this table for two values of $E^* P_+ \langle \frac{3}{2}^- | J_- | \frac{5}{2}^- \rangle$. (See subsect. 3.6.)
[e]) Experimental value from intraband E2 transitions. (See subsect. 3.3.).
[f]) Theoretical value from the Nilsson model with $\delta = 0.3$, $\kappa = 0.05$ and $\mu = 0.45$.
[g]) See discussion in the text.

This expression and our three measured values of $B(\mathrm{M1}, I_i\,\frac{3}{2} \rightarrow I_f\,\frac{5}{2})$ were used in a least-squares fit to determine the asymptotically forbidden quantities $P_+(\frac{3}{2} \rightarrow \frac{5}{2})$ $G_{\mathrm{M1}}(\frac{3}{2} \rightarrow \frac{5}{2})$ and $E^*P_+ \langle \frac{3}{2} \,|\, j_- \,|\, \frac{5}{2} \rangle$ introduced via the mixing amplitudes [eq. (6)]. This fit was performed with Nilsson wave functions for several sets of the parameters g_s(eff) [= 100, 80, 60, 40 % of g_s (free)], g_R[= 0.20, 0.25 and 0.30] and δ[= 0.2 and 0.3] used in the evaluation of the diagonal quantities $G_{\mathrm{M1}}(\frac{3}{2} \rightarrow \frac{3}{2})$ and $G_{\mathrm{M1}}(\frac{5}{2} \rightarrow \frac{5}{2})$. The quantity $P_+(\frac{3}{2} \rightarrow \frac{5}{2})G_{\mathrm{M1}}(\frac{3}{2} \rightarrow \frac{5}{2})$ became $\pm 0.42 \pm 0.14$ almost independently of g_s, g_R and δ. From the pairing-correlation calculation, we find that $P_+(\frac{3}{2} \rightarrow \frac{5}{2}) = 0.94$, thus giving $G_{\mathrm{M1}}(\frac{3}{2} \rightarrow \frac{5}{2}) = \pm(0.45 \pm 0.15)$. This value can be compared with the predictions of the Nilsson model. Agreement is obtained for the reasonable parameters g_s(eff) $= (0.7 \pm 0.1) g_s$(free), $g_R = 0.25 \pm 0.05$ and $\delta = 0.25 \pm 0.05$.

The value of $E^*P_+ \langle \frac{3}{2} \,|\, j_- \,|\, \frac{5}{2} \rangle$ determined from this fit is uncertain and rather dependent on the choice of parameters. As an average, we get $E^*P_+ \langle \frac{3}{2} \,|\, j_- \,|\, \frac{5}{2} \rangle = \pm(4 \pm 3)$, which compares favourably with the more accurate value of 6.5 ± 1.0 obtained from the interband E2 transition rates. It should be remarked that in all the reasonably good fits, $P_+(\frac{3}{2} \rightarrow \frac{5}{2})G_{\mathrm{M1}}(\frac{3}{2} \rightarrow \frac{5}{2})$ and $E^*P_+ \langle \frac{3}{2} \,|\, j_- \,|\, \frac{5}{2} \rangle$ have the same signs in agreement with predictions.

3.6. THE E1 TRANSITION RATES

At present, three absolute E1 transition probabilities and one upper limit have been measured in ^{161}Dy. These transitions connect the $\frac{3}{2}^-(521)$ or $\frac{5}{2}^-(523)$ bands with the $\frac{5}{2}^+(642)$ ground state band. The reasonable assumption that the electric quadrupole moment in the $\frac{5}{2}^-(523)$ band is the same as in the ground state band will furthermore give the strength for the two E1 transitions from the $\frac{7}{2}\,\frac{5}{2}^-(523)$ state at 103.0 keV. All the experimental information on E1 transition rates in ^{161}Dy has been compiled in table 5. When these values are compared with the Nilsson predictions through the F_N factor, we see that transitions with $|\Delta K| = 1$ are hindered, while the $|\Delta K| = 0$ transitions agree reasonably well with predictions. This fact, which was already pointed out by Vergnes [26]), has been further supported in later works [1]). The most remarkable feature is shown by the $\frac{5}{2}\,\frac{3}{2}^-(521) \rightarrow \frac{5}{2}\,\frac{5}{2}^+(642)$ transition with a F_N value of more than 2.5 E+4, which probably makes it the most hindered K-allowed E1 transition observed. The transition between the $\frac{5}{2}\,\frac{3}{2}^-(521) \rightarrow \frac{7}{2}\,\frac{5}{2}^+(642)$ levels, however, shows a normal strength which indicates that some particular cancellation effect takes place for this specially retarded case.

Switching on the pairing correlations generally leads to a reduction in the transition rates between different single-particle orbitals, while the relative transition rates to different band members are unaffected. The comparison with predictions from this quasiparticle description is given in table 5 through $F_{QM} = P_-^2 F_N$, where the appropriate pairing factors P_- are given in table 3. As can be seen in table 5, the general agreement with experiments after the inclusion of pairing can scarcely be regarded as superior to the predictions of the pure adiabatic model.

TABLE 6

Comparison with predictions from the Nilsson model for E1 transition rates

	Fitted value	Predicted value from the Nilsson model [13])			
		$\delta = 0.3$, $\kappa = 0.05$, $\mu = 0.45$	$\delta = 0.2$, $\kappa = 0.05$, $\mu = 0.45$	$\delta = 0.3$, $\kappa = 0.06$, $\mu = 0.45$	$\delta = 0.3$, $\kappa = 0.05$, $\mu = 0.70$
$G_{\mathrm{E1}}(\frac{3}{2}^- \rightarrow \frac{5}{2}^+)$	(4.3 ± 1.3) E−2	5.0 E−2	3.9 E−2	4.6 E−2	6.0 E−2
$G_{\mathrm{E1}}(\frac{5}{2}^- \rightarrow \frac{5}{2}^+)$	$-(2.2 \pm 0.2)$ E−1	−2.7 E−2	−2.5 E−2	−2.7 E−2	−3.2 E−2

TABLE 7

Predicted and experimental gamma-ray intensity ratios

Transition energy (keV)	Initial state $IK^{\pi}(Nn_z\Lambda)$	Final state	Multipolarity	Predicted ratio	Experimental gamma-ray transition ratio [a])
475.8	$\frac{9}{2}\frac{9}{2}^{+}(651)$	$\frac{9}{2}\frac{9}{2}^{-}(521)$	E1	2.2	2.21±0.32
418.5		$\frac{7}{2}\frac{9}{2}^{-}(521)$	E1		
376.6	$\frac{5}{2}\frac{1}{2}^{-}(521)$	$\frac{9}{2}\frac{9}{2}^{-}(521)$	M1	0.24	0.16±0.04
319.6		$\frac{7}{2}\frac{9}{2}^{-}(521)$	M1		
376.6	$\frac{9}{2}\frac{1}{2}^{-}(521)$	$\frac{9}{2}\frac{9}{2}^{-}(521)$	M1	0.55	0.26±0.07
238.4		$\frac{7}{2}\frac{9}{2}^{-}(521)$	M1		
343.5	$\frac{11}{2}\frac{1}{2}^{-}(521)$	$\frac{9}{2}\frac{9}{2}^{-}(521)$	M1	1.2	1.10±0.16
286.4		$\frac{5}{2}\frac{9}{2}^{-}(521)$	M1		
425.8	$\frac{9}{2}\frac{1}{2}^{-}(521)$	$\frac{9}{2}\frac{9}{2}^{-}(523)$	M1	*K*-forbidden	0.75±0.30
348.2		$\frac{7}{2}\frac{9}{2}^{-}(523)$	M1		

[a]) E2 content disregarded, which as a first approximation is justified from the fact that M1 is allowed but E2 hindered.

To be able to improve the predictions, we are thus forced to include non-adiabatic effects and/or quasiparticle interactions. For low-lying states, the most important non-adiabatic effect comes from the Coriolis coupling [14]), which in the present case will mix the $\frac{3}{2}^{-}(521)$ and $\frac{5}{2}^{-}(523)$ bands. To first order, the reduced E1 transition probability in ^{161}Dy can be written

$$B(\mathrm{E1}, I_i\tfrac{3}{2}^{-} \to I_f\tfrac{5}{2}^{+}) = 4.57\times10^{-3}\{(I_i\tfrac{3}{2}11|I_f\tfrac{5}{2})P_{-}(\tfrac{3}{2}^{-} \to \tfrac{5}{2}^{+})G_{\mathrm{E1}}(\tfrac{3}{2}^{-} \to \tfrac{5}{2}^{+}) + C(I_i\tfrac{5}{2}\tfrac{3}{2})(I_i\tfrac{5}{2}10|I_f\tfrac{5}{2})P_{-}(\tfrac{5}{2}^{-} \to \tfrac{5}{2}^{+})G_{\mathrm{E1}}(\tfrac{5}{2}^{-} \to \tfrac{5}{2}^{+})\}^2, \quad (11)$$

with a similar expression for the E1 transitions between the $\frac{5}{2}^{-}(523)$ and $\frac{5}{2}^{+}(642)$ rotational bands. Eq. (6) gives $C(I_i\,\frac{5}{2}\,\frac{3}{2})$. Using the experimental value of $E^{*}P_{+}$ $\langle\frac{3}{2}|j_{-}|\frac{5}{2}\rangle = 6.5$ (from subsect. 3.3), the five known $B(\mathrm{E1})$ values in ^{161}Dy were used in equations of type (11) in a least-squares fit to determine the parameters $P_{-}(\frac{3}{2}^{-} \to \frac{5}{2}^{+})G_{\mathrm{E1}}(\frac{3}{2}^{-} \to \frac{5}{2}^{+})$ and $P_{-}(\frac{5}{2} \to \frac{5}{2}^{+})G_{\mathrm{E1}}(\frac{5}{2}^{-} \to \frac{5}{2}^{+})$. For comparison, a similar fit was also performed for the predicted value of $E^{*}P_{+}\langle\frac{3}{2}|j_{-}|\frac{5}{2}\rangle = 9.7$. The result is given in the last two columns in table 5 with the fitted values of the two parameters including their errors. As a consistency check, these fitted parameters were used to predict the value of $B(\mathrm{E1}, \frac{5}{2}\frac{3}{2}^{-} \to \frac{5}{2}\frac{5}{2}^{+})$, which then was the difference

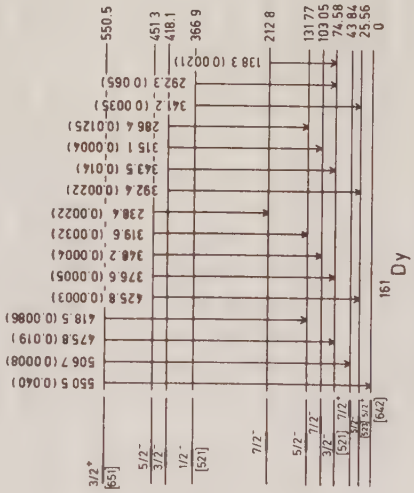

Fig. 6. Level scheme of ^{161}Dy.

of two roughly equal terms. The F_{PC} values given in this case is when the nominal value of the parameters were inserted, but it should be observed that small changes of these nominal values changes the given F_{PC} value drastically. A complete cancellation of the $B(\mathrm{E1}\ \frac{5}{2}\frac{3}{2}^{-} \to \frac{5}{2}\frac{5}{2}^{+})$ value is thus obtained for $P_{-}(\frac{5}{2}^{-} \to \frac{5}{2}^{+})G_{\mathrm{E1}}(\frac{5}{2}^{-} \to \frac{5}{2}^{+})/P_{-}(\frac{3}{2}^{-} \to \frac{5}{2}^{+})G_{\mathrm{E1}}(\frac{3}{2}^{-} \to \frac{5}{2}^{+})G_{\mathrm{E1}} = 4.5$ as compared with the corresponding fitted ratio 3.4±1.1. The unusually low value of $B(\mathrm{E1}, \frac{5}{2}\frac{3}{2}^{-} \to \frac{5}{2}\frac{5}{2}^{+})$ can thus be completely explained through the Coriolis mixing, and the two fitted parameters are consistent with all the presently known E1 transition rates in ^{161}Dy.

Using our calculated values for $P_-(\frac{3}{2}^- \rightarrow \frac{5}{2}^+) = -0.20$ and $P_-(\frac{5}{2}^- \rightarrow \frac{5}{2}^+) = 0.13$ (see table 3), we get $G_{E1}(\frac{3}{2}^- \rightarrow \frac{5}{2}^+) = (4.3 \pm 1.3)\text{E}-2$ and $G_{E1}(\frac{5}{2}^- \rightarrow \frac{5}{2}^+) = -(2.2 \pm 0.2)\text{E}-1$, which are quantities that can be directly calculated within the Nilsson model. Results from the comparison are given in table 6. The sign and the magnitude of the $G_{E1}(\frac{3}{2}^- \rightarrow \frac{5}{2}^+)$ factor are in excellent agreement with predictions, while for $G_{E1}(\frac{5}{2}^- \rightarrow \frac{5}{2}^+)$ the predicted values are a factor of eight too low. This disagreement is, however, not astonishing when considering that only small particle matrix elements are involved in E1 transitions, and thus admixtures may play an important role. It has, for instance, been pointed out by Monsonego and Piepenbring [27]) that in particular $\Delta K = 0$, E1 transition rates are sensitive to admixture from octupole vibrations. Such contributions will not change the formalism used but will only adjust the internal structure of the matrix elements. It will thus be justified to regard the fitted P_-G parameters as effective quasiparticle matrix elements whose magnitude can only be calculated taking all relevant contributions into account.

3.7. TRANSITIONS FROM HIGHER-LYING BANDS

From their gamma-ray spectra observed with a Ge(Li) detector, Funke *et al.* [6]) reported a number of higher-energy gamma rays in the decay of ^{161}Tb. These transitions were interpreted as de-exciting members of the expected $\frac{1}{2}^-(521)$ and $\frac{3}{2}^+(651)$ rotational bands (see fig. 6). From our measurements with better energy resolution and higher statistical accuracy, another five previously unreported transitions have been observed. These can all be placed within the decay scheme previously proposed. From our more accurate energy determinations, we have been forced to change the place of an observed 238.4 keV transition now de-exciting the 451.3 keV level, thus giving a reasonable feed to the proposed 212.8 keV level decaying mainly with an observed 138.3 keV transition. The observed energies and intensities of gamma-ray transitions in the decay of ^{161}Tb are given in table 1 with the corresponding values reported by Funke *et al.* [6]).

According to the adiabatic model, the gamma-ray intensity $I_\gamma = \text{const.} \cdot B(\lambda)E_\gamma^{2\lambda+1}$, where $B(\lambda)$ is the reduced transition probability [eqs. (1)–(3)]. Different predicted transition ratios and our experimental values are given in table 7. According to assignments given in fig. 6, three of the observed M1 transitions are K-forbidden. Their existence is explained through the Coriolis mixing mainly between the $\frac{3}{2}^-(521)$ and $\frac{5}{2}^-(523)$ bands. It is further worth noting that no E1 transition is observed between the $\frac{3}{2}^+(651)$ and $\frac{5}{2}^-(523)$ bands, while the E1 transitions to the $\frac{3}{2}^-(521)$ band is clearly observed. Partly this is due to the relatively larger pairing factor in the latter case (see table 3).

We are indebted to Dr. Sven Wahlborn for help with the BCS calculation to obtain the pairing factors.

References

1) S. G. Malmskog, dissertation, Stockholm (1967)
2) D. R. Bès, Nucl. Phys. **6** (1958) 645

3) P. G. Hansen, O. Nathan, O. B. Nielsen and R. K. Sheline, Nucl. Phys. **6** (1958) 630
4) R. T. Brockmeier and J. D. Rogers, Nucl. Phys. **67** (1965) 428
5) R. L. Graham, J. S. Geiger and G. T. Ewan, Bull. Am. Phys. Soc. **6** (1961) 72
6) L. Funke, H. Graber, K.-H. Kaun, J. Römer, H. Sodan and J. Frána, Nucl. Phys. **84** (1966) 443
7) T. R. Gerholm and J. Lindskog, Ark. Fys. **24** (1963) 171
8) S. G. Malmskog, Ark. Fys. **35** (1967) 255
9) B. Olsen and L. Boström, Nucl. Instr. **44** (1966) 65
10) W. Meiling and F. Stary, Nucl. Phys. **74** (1965) 113
11) A. H. Wapstra, G. J. Nijgh and R. van Lieshout, Nuclear spectroscopy tables (North-Holland Publ. Co., Amsterdam, 1959)
12) K. E. G. Löbner and S. G. Malmskog, Nucl. Phys. **80** (1966) 505
13) S. G. Nilsson, Mat. Fys. Medd. Dan. Vid. Selsk. **29**, No. 16 (1955)
14) O. Nathan and S. G. Nilsson, in Alpha-, beta- and gamma-ray spectroscopy, ed. by K. Siegbahn (North-Holland Publ. Co., Amsterdam, 1965) chap. 10
15) B. Elbek, K. O. Nielsen and M. C. Olesen, Phys. Rev. **108** (1957) 406
16) E. M. Bernstein and R. Graetzer, Phys. Rev. **119** (1960) 1321
17) W. Ebenhöh, V. J. Ehlers and J. Ferch, Z. Phys. **200** (1967) 84
18) W. Henning, D. Heunemann, W. Weber, P. Kienle and H. J. Körner, Z. Phys. **207** (1967) 505
19) G. Crecelius and D. Quitmann, Proc. Conf. on hyperfine structure and nuclear radiations, Pacific-Graove, Clif., August 25–30, 1967 (North-Holland Publ. Co., Amsterdam, 1968) p. 172
20) G. J. Bowden, St. P. Bunbury and J. H. Williams, Proc. Phys. Soc. **91** (1967) 612
21) B. Khurgin, S. Ofer and M. Rakavy, Nucl. Phys. **A110** (1968) 577
22) F. Boehm, G. Goldring, G. B. Hagemann, G. D. Symons and A. Tveter, Phys. Lett. **22** (1966) 627
23) G. B. Hagemann and A. Tveter, Phys. Lett. **26B** (1968) 136
24) O. Prior, F. Boehm and S. G. Nilsson, Nucl. Phys. **A110** (1968) 257
25) A. Z. Hrynkiewicz and S. Ogaza, Institute of Nuclear Physics, Krakov, Poland (JFJK 466/PL)
26) M. N. Vergnes, Nucl. Phys. **39** (1962) 273
27) G. Monsonego and R. Piepenbring, Nucl. Phys. **78** (1966) 265
28) E. Munck, Thesis, Darmstadt 1967, quoted in ref. [19])
29) P. G. Hansen, O. B. Nielsen and G. Sidenius, Int. Conf. on nuclear structure (Tokyo 1967) paper 4, 136

R E F E R E N C E 4

E2 AND M1 TRANSITION PROBABILITIES IN ^{193}Au AND ^{195}Au

B. FOGELBERG and A. BÄCKLIN

Institute of Physics, Uppsala University and The Swedish Research Concil's Laboratory, Studsvik, Nyköping, Sweden,

V. BERG and S. G. MALMSKOG

AB Atomenergi, Studsvik, Nyköping, Sweden and Institute of Physics, University of Stockholm, Sweden

1.E.4 *Nuclear Physics* A153 (1970) 301—315; © *North-Holland Publishing Co., Amsterdam*
Not to be reproduced by photoprint or microfilm without written permission from the publisher

E2 AND M1 TRANSITION PROBABILITIES IN ^{193}Au AND ^{195}Au

B. FOGELBERG and A. BÄCKLIN

Institute of Physics, Uppsala University and the Swedish Research Council's Laboratory, Studsvik, Nyköping, Sweden

V. BERG and S. G. MALMSKOG

AB Atomenergi, Studsvik, Nyköping, Sweden and Institute of Physics, University of Stockholm, Sweden

Received 14 May 1970

Abstract: High-resolution conversion electron- and γ-ray spectroscopy has been made on the transitions depopulating the three lowest excited states in ^{193}Au and ^{195}Au. The half-lives of these levels have been measured with the delayed coincidence method. The multipole assignments are for the transitions in ^{193}Au: 38.22 keV M1+(17.7±1.0) % E2, 219.75 keV E2, 257.97 keV M1+(21±7) % E2 and for ^{195}Au: 61.44 keV M1+(16.6±1.0) % E2, 180.32 keV M1+< 3 % E2, 200.38 keV E2, 261.74 keV M1+(21.5±4.0) % E2. The obtained half-lives are for ^{193}Au: 38.22 keV level (3.81±0.18) ns, 224.84 keV level < 0.03 ns, 257.97 keV level (45±20) ps and for ^{195}Au: 61.44 keV level (3.0±0.2)ns, 241.72 keV level < 0.03 ns, 261.79 keV level (54±10) ps. A systematic compilation of absolute E2 and M1 transition rates in odd-mass Au nuclei is given and compared to the predictions of the pairing-plus-quadrupole force model and the core-excitation model.

E RADIOACTIVITY ^{193}Hg, ^{195}Hg[from Pb(p, 3pxn)]. measured E_γ, I_γ, E_{ce}, I_{ce}, cece-γce-delay. ^{193,195}Au deduced levels, γ-mixing, γ-branching, $T_{\frac{1}{2}}$, $B(\lambda)$. Isotope separated sources.

1. Introduction

Considerable interest has been focused on the low-lying levels of odd-mass gold isotopes, in particular ^{197}Au, which is the experimentally best studied case. Information on the low-energy levels in this nucleus has been gathered from both radioactive decay see e.g. refs.[1-3]) and Coulomb excitation [4, 5]). Theoretical calculations to explain the data have been made either in terms of the pairing-plus-quadrupole force model [6-9]), or in terms of the core-excitation model [10-12]). It turns out, that the gross low-energy level structure of ^{197}Au (i.e. spins, parities and level order) can be reproduced satisfactorily in either model, while no model is capable to account for all transition rates.

It is of interest to make similar model tests for other odd-mass gold isotopes. In ^{193}Au and ^{195}Au the low-energy level energies, spins and parities can be considered to be known, and the aim of the present work has been to determine the absolute transition rates between the lowest states in these nuclei. To do this, we have performed gamma spectroscopy, high-resolution conversion-electron spectroscopy, electron-electron and electron-gamma delayed coincidence measurements.

The systematic behaviour of the resulting E2 and M1 transition probabilities has been studied and compared to the models mentioned above. Experimental data on ^{197}Au [refs. [1-5,13])] and ^{199}Au [ref. [14])] have been included in the systematics.

2. Conversion-electron and γ-ray measurements

Isotope separated ^{193}Hg and ^{195}Hg sources, prepared by spallation of lead with 600 MeV protons, were obtained from the ISOLDE collaboration at CERN [15]). The ion beams in the mass-separator were stopped on a 0.8 mg/cm^2 Ni foil. Typical irradiation times were of the order of 10-20 h and the transport time from Geneva to Studsvik amounted to about the same time.

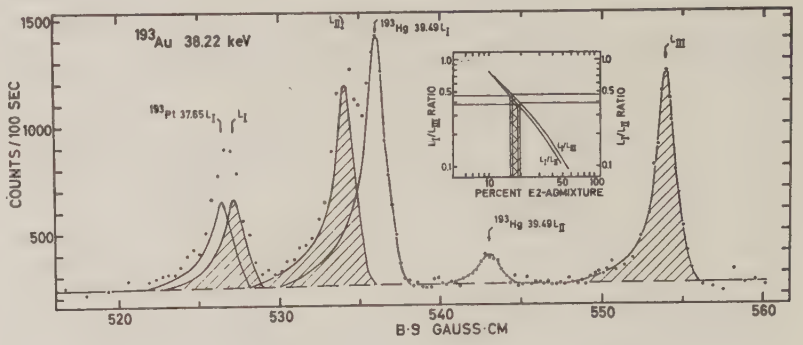

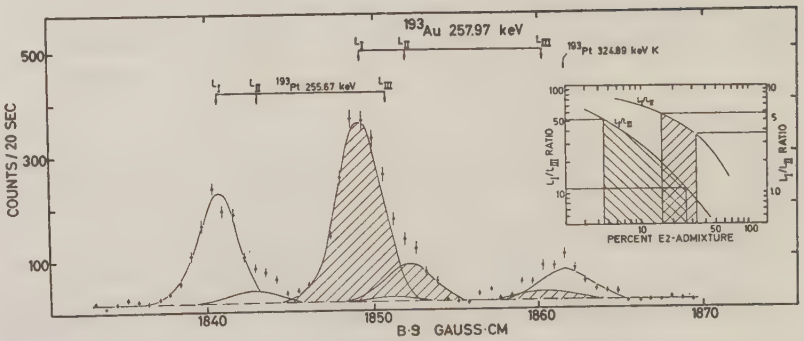

Fig. 1. Conversion electron lines observed in the $\pi\sqrt{2}$ spectrometer from the decay of ^{193,193m}Hg. The hatched lines, representing transitions in ^{193}Au, could be resolved from transitions in ^{193}Pt by the use of relative intensities from ref. [17]). The inset shows theoretical L-subshell ratios as functions of the E2 admixture, with the experimental values indicated.

Internal conversion electron lines from the decays of ^{193,193m}Hg and ^{195,195m}Hg were measured with a $\pi\sqrt{2}$ β-spectrometer [16]) using a momentum resolution of about 0.2 %.

The levels of the gold nuclei are fed in different amounts from the isomeric and ground states of mercury, which gives rise to complicated time dependences of the transition intensities. Thus some care had to be exercised in the measurements and in the analysis of the data. Effects due to the different half-lives in the feeding were minimized by measuring conversion lines from transitions depopulating the same levels with the smallest possible time interval.

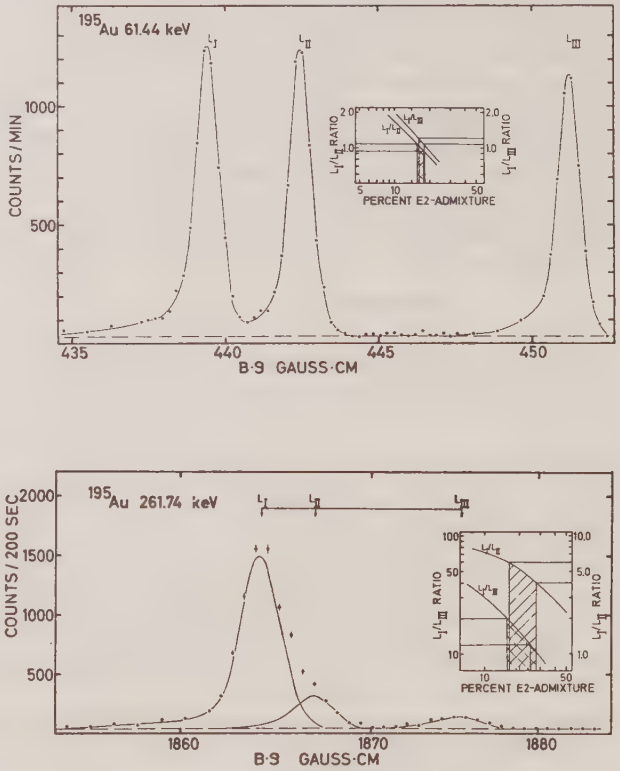

Fig. 2. Conversion electron lines from transitions in ^{195}Au following the decay of ^{195,195m}Hg, as measured with the $\pi\sqrt{2}$ β-spectrometer. The insets show L-subshell ratios as functions of the E2 admixture.

In ^{193}Au the daughter-activity caused some trouble, as a few conversion electron and γ-ray lines in ^{193}Au and ^{193}Pt are too close to be resolved by the present instruments. The conversion electron spectrum of ^{193}Au has, however, recently been measured with high resolution by Svahn *et al.* [17]. It was thus possible to subtract contributions from lines in ^{193}Pt with rather good accuracy by the use of relative conversion electron intensities from ref. [17]).

The K-line of the 117.99±0.02 keV [ref. [17])] transition in ^{193}Pt was used as energy standard in the measurement of the ^{193}Au spectrum. Energy calibration of the ^{195}Au transitions was made by comparison with the L_{III} line of the 122.78±0.03 keV transition [18]) in ^{195}Hg. Some of the measured conversion lines are shown in figs. 1 and 2.

TABLE 1

Relative intensities and multipole admixtures of transitions from low-lying levels in ^{193,195}Au

Nucleus	Level energy (keV)	Transition energy (keV)	Relative [a]) gamma-intensity	Relative [a]) electron-intensity	Multipole assignment
^{193}Au	38.22±0.02	38.22±0.02		L_I: 42±4 L_{II}: 97.5±9 L_{III}: 100	M1+(17.7±1.0) % E2 from L-subshell ratios
	224.84±0.05	186.62±0.05	100	K: 100	
	224.84±0.05	224.84	< 5.2	K: < 3.2	
	257.97±0.03	219.75±0.05	5.72±0.30	K: 14.0±1.5 L_I: 2.35±0.3 L_{II}: 6.7 ±0.7 L_{III}: 5.1 ±0.6	E2 from L-subshell ratios
	257.97±0.03	257.97±0.05	100	L_I: 100 L_{II}: 22±4 L_{III}: $4.7^{+4.7}_{-3.0}$	M1+(21±7) % E2 from L-subshell ratios
^{195}Au	61.44±0.03	61.44±0.03		L_I: 100 L_{II}: 99±6 L_{III}: 87±4	M1+(16.6±1.0) % E2 from L-subshell ratios
	241.72±0.06	180.32±0.04	100	K: 100 L_I: 15.5±0.7 L_{II}: $1.95^{+0.45}_{-0.25}$ L_{III}: 0.22±0.16	M1+ < 3 % E2 from L-subshell ratios
	241.72±0.06	241.56±0.15	3.65±0.30	K: < 1.6	
	261.79±0.05	200.38±0.04	2.43±0.10	L_I: 0.29±0.12 L_{II}: 0.64±0.20 L_{III}: 0.45±0.20	E2 from L-subshell ratios
	261.79±0.05	261.74±0.06	100	K: 100 L_I: 14.7±1.2 L_{II}: 2.95±0.80 L_{III}: 0.95±0.20	M1+(21.5±4.0) % E2 from L-subshell ratios

[a]) Intensities of transitions depopulating different levels are not comparable in this table.

To deduce absolute transition probabilities it was essential to measure a few γ-ray branching ratios. This was done with a 1.5 cm^3 Ge(Li) detector with a 1.2 keV energy resolution at 122 keV.

The results of the conversion electron and γ-ray measurements are found in table 1.

3. Half-life measurements

The half-life measurements reported below have been carried out using a long lens electron-electron coincidence spectrometer described in detail earlier [19,20]. The same sources as in the conversion electron and γ-ray measurements have been used.

3.1. THE 38.2 keV LEVEL IN ^{193}Au

The main feeding to this level is via a 187 keV transition in the ^{193}Hg (6h) decay and a 220 keV transition in the ^{193m}Hg(10 h) decay. The coincidence relation between these two transitions and the 38 L c.e. line has been used to determine the half-life of the 38 keV level.

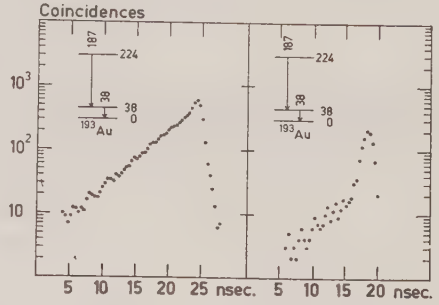

Fig. 3. Left-hand side. The observed decay curve obtained from the registration of 38L-187K coincidences. From the slope the half-life of the 38.2 keV level in ^{193}Au was determined to 3.81 ± 0.18 nsec. Right-hand side. The time distribution observed after a source decay time of 24 hours showing that the prompt part comes from cascades in ^{193}Pt.

In one experiment the 187 K and 38 L c.e. lines were focused in each lens spectrometer and the delayed coincidence distribution was registered in a multichannel analyser. An observed spectrum is shown in the left-hand side of fig. 3. Besides the delayed form a small prompt peak is observed. The origin of the prompt coincidences was determined by following the ^{193}Hg source over several half-lives. The right-hand side of fig. 3 gives the observed distribution after 24 hours decay. The prompt peak showed a decay rate of approximately 16 hours demonstrating that the corresponding prompt cascades take place in ^{193}Pt. The prompt contributions are obtained from the 37.7 L $\rightarrow$ 186.2 K, 37.7 L $\rightarrow$ 187.8 K, 37.7 L $\rightarrow$ 117.9 L and 99.9 K $\rightarrow$ 117.9 L cascades introducing the half-lives of the 114.2, 187.8 and 232.2 keV levels in ^{193}Pt. From a parallel study of the half-lives of excited states in ^{193}Pt [ref. [21])] none of these levels have been found to have a half-life longer than 0.3 nsec. From the slope of the observed decay curves (fig. 3a) the half-life of the 38.2 keV level in ^{193}Au was determined to be (3.81 ± 0.18) nsec.

A second measurement was performed using the 220 K $\rightarrow$ 38 L cascade. Although this case is cleaner, with only a weak contaminant from the 155.7 L $\rightarrow$ 37.7 L cascade

in ^{193}Pt, the relatively weak intensity of the 220 K line caused the statistics to be inferior in this measurement. The result obtained was, however, in good agreement with the one mentioned above.

One earlier measurement of this half-life has been reported by Jastrzebski and Kilcher [22]) giving $T_{\frac{1}{2}}(38.2 \text{ keV}) = 4.2 \pm 0.6$ nsec.

3.2. THE 224.8 keV LEVEL IN ^{193}Au

This level is only fed via γ-rays $>$ 500 keV in the decay of ^{193g}Hg(6 h). The depopulation takes place mainly through a 187 keV transition. Due to the transport time between Geneva and Studsvik, measurements could never start before 15 hours after irradiation, which in this case causes the ^{193}Au(16 h) activity to build up appreciably. This is especially unfavourable here, as the ^{193}Au decay introduces a very strong 186.2 keV transition [17]), which fortunately seems to have only weak γ-ray feeding.

Therefore the experiment was set up to record coincidences between the 187 K c.e. line and γ-rays above 300 keV detected in a 2.5×2.5 cm^2 cylindrical Naton 136 plastic scintillator. As the observed time distribution appeared to be prompt, a shift measurement was performed using the $\beta\gamma$ cascade in ^{60}Co as a time reference. Measurements were made in long sequences where alternatively ^{193}Hg and ^{60}Co sources were used. Every individual measurement was limited to 15 min to reduce spurious shifts due to instabilities in the electronic system. A total of 45 runs were made. The data were analysed according to the first momentum method [23]). Although a small shift was observed between certain successive measurements the systematic error introduced due to the difference in shape of the Compton distribution in the γ-ray detection channel may well account for this effect. We therefore prefer to give only an upper limit of the half-life for the 224.8 keV level in ^{193}Au as $<$ 30 psec. No earlier measurement has been reported.

3.3. THE 258.0 keV LEVEL IN ^{193}Au

The main de-excitation of the ^{193m}Au(3.9 sec.) isomer is via a 32 keV E3 transition to the 258 keV level. The half-life measurement of the latter was done by registering the time distribution between the 32 L and 258 K c.e. lines focused in each lens spectrometer. With these energy settings a small contribution from the 37.7 L $\rightarrow$ 186.2 L cascade in ^{193}Pt could be expected. To determine its strength the coincidence rate was followed in time. The correction for this disturbing effect was then found to be small.

As the coincidence distribution showed an approximately prompt shape a centroid shift measurement was performed using the delayed coincidence curve from the β-94.7 K cascade in the decay of ^{165}Dy(2.4 h) to determine the prompt reference time. To be able to perform the two measurements with the same energy settings, the ^{193}Hg source was put at a high voltage of 21 keV relative to the spectrometer. The measurements were made in sequence alternatively on the ^{193}Hg and ^{165}Dy sources, each individual run being 15 min long. The registered decay curves were analysed according

to the momentum method [23]). After correcting the obtained centroid shifts for the half-life of the 94.7 keV level in ^{165}Ho (18 psec) and the change in transit time of the electrons through the spectrometer due to the pre-acceleration ($\approx$ 40 psec) we obtain a half-life of 45$\pm$20 psec. for the 258 keV level in ^{193}Au. No earlier measurement has been reported.

3.4. THE 61.4 keV LEVEL IN ^{195}Au

This level is fed by two transitions around 200 keV and several transitions around one MeV. As some disturbances might occur from the strong 57 keV E3 transition we have chosen to record coincidences between the 61 L c.e. line and γ-rays above 400 keV knowing that the 57 keV transition is isolated from such transitions by the 318 keV isomeric level. A ^{60}Co source was used to get a prompt reference spectrum.

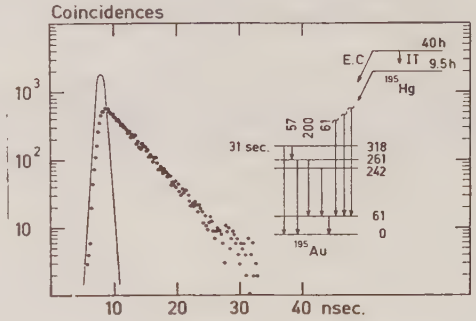

Fig. 4. The decay curve obtained by registering coincidences between 61 L conversion line and gamma rays > 400 keV in ^{195}Au. The full line shows the corresponding prompt distribution. From the slope we obtain a half-life for the 61.4 keV level in ^{195}Au of 3.0$\pm$0.2 nsec.

The typical delayed and corresponding prompt curves obtained are shown in fig. 4. The half-life of the 61.4 keV level in ^{195}Au was determined from the slope of the delayed curve as 3.0$\pm$0.2 nsec. Fair agreement with the average value 2.8$\pm$0.3 nsec given in ref. [25]) is obtained.

3.5. THE 241.7 keV LEVEL IN ^{195}Au

This level is fed in the decay of ^{195g}Hg(9.5 h) mainly via three transitions with energies greater than 600 keV and partly via direct electron capture. A delayed coincidence measurement was performed between the deexciting 180 K c.e. line and the feeding γ-rays using the centroid shift method in a very similar way to that described in subsect. 3.2. No systematic shift was observed. From the statistical uncertainty we can set an upper limit for the half-life of the 241.7 keV level in ^{195}Au as < 30 psec. No earlier measurement has been reported.

3.6. THE 261.8 keV LEVEL IN ^{195}Au

The main deexcitation of the 318.6 keV isomeric level (31 sec), proceeds by a 57 keV E2 transition to the 261.8 keV level. The half-life of the latter was determined by observing the time distribution between the 57 L and 262 K c.e. lines focused in each spectrometer. A small contribution was also obtained from the 57 L -200 L cascade defining the same half-life. A centroid shift measurement similar to the one described in subsect. 3.3 was performed using the ^{165}Dy source with 3.5 kV pre-acceleration as a prompt reference. An example of a prompt and a delayed spectrum is shown in fig. 5. All observed curves were analysed according to the momentum method [23]). The inset of fig. 5 shows the value of the first momentum from a consecutive series of

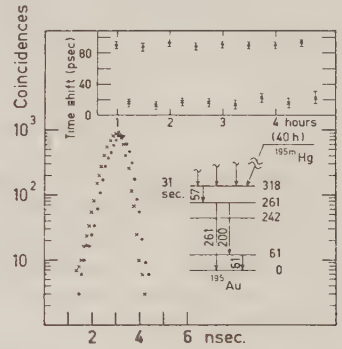

Fig. 5. A pair of delayed (points) and prompt (crosses) time distributions obtained by focusing the two lenses on the 57L and 261K conversion electron lines in ^{195}Au. The prompt curve was taken with a ^{165}Dy source +3.5 kV pre-acceleration. A series of curves was taken alternatively with ^{195}Hg and ^{165}Dy sources and a momentum analysis was performed, the results of which is shown in the upper part. From the analysis we obtain a half-life of 54$\pm$10 psec for the 261.8 keV level in ^{195}Au.

prompt and delayed coincidence curves given in a relative time scale. After correction for the half-life of the 94.7 keV level in ^{165}Ho(18 psec) the average difference between the first momenta from the prompt and delayed curves is equal to the meanlife of the intermediate 261.8 keV level.

The individual pair of runs were also analysed using the convolution method [24]). Besides the decay constant for the investigated level this method also gives an indication of any spurious shifts which can influence the result from the first momentum method. No such shifts exceeding the statistical errors were, however, observed. As an average from the above methods of analysis we obtained a half-life for the 261.8 keV level in ^{195}Au of 54$\pm$10 psec. In an earlier report [26]) this half-life is given as less than 200 psec.

4. Results

The experimental results are given in tables 1 and 2. Relative intensities of transitions de-exciting different levels are not given, as the levels are fed in different proportions

(which were not of interest in the present work) from the ground and isomeric states of the corresponding mercury isotopes. Therefore we give relative intensities only for transitions going from the same level. All multipolarity assignments are based on L-subshell ratios, using internal conversion coefficients from the work of Hager and Seltzer [27]).

In table 2 are given the experimental reduced transition probabilities calculated from the formulae:

$$B(\mathrm{E2})\downarrow = \frac{0.563pf}{(1+\alpha_T)T_{\frac{1}{2}}E^5}\, e^2\cdot \mathrm{b}^2, \qquad (1)$$

$$B(\mathrm{M1})\downarrow = \frac{3.94\cdot 10^{-7}(100-p)f}{(1+\alpha_T)T_{\frac{1}{2}}E^3}\, \mu_N^2, \qquad (2)$$

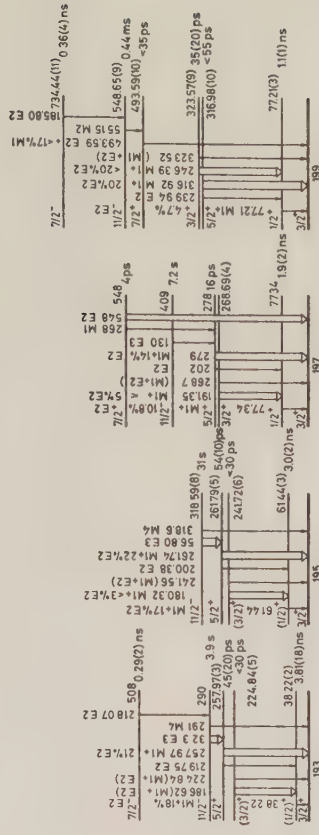

Fig. 6. Partial level schemes of odd-mass Au isotopes. Level half-lives and multipole admixtures for ^{193}Au and ^{195}Au are given as measured in the present work, except for the isomers, whose data have been taken from ref. [34]). Data on ^{197}Au have been compiled from refs. [1,2,4,5,13,34]), and on ^{199}Au data are taken from ref. [14]). A wide arrow indicates that this transition strongly dominates the depopulation of the level.

where p denotes the E2 percentage, f the fraction of decays of the level proceeding through the transition, α_T the total conversion coefficient, $T_{\frac{1}{2}}$ the level half-life in sec and E the transition energy in keV.

Partial level schemes of ^{193}Au and ^{195}Au are shown in fig. 6, which for comparison also includes the lowest levels of ^{197}Au and ^{199}Au.

5. Discussion

In the following, the experimental results on the depopulation of the three lowest excited states in ^{193,195}Au are compared with theoretical predictions. For the sake of completeness we have also included relevant data from previous experiments on ^{197}Au, refs. [1,2,4,5,13]) and ^{199}Au, refs. [3,14]).

TABLE 2

Detailed properties of E2 and M1 transitions in ^{193}Au and ^{195}Au

Nucleus	Level energy (keV)	$T_{\frac{1}{2}}$ level (ns)	Initial spin I_i	Final spin I_f	Transition (keV)	Branching %	E2 %	α_{tot} [a])	B(M1) $10^{-2}\mu_N^2$	F_w [b])	B(E2) (10^{-50} $e^2\cdot$cm^4)	$\frac{B(\mathrm{E2})_{exp}}{B(\mathrm{E2})_{s.p.}}$ [c])
^{193}Au	38.22	3.81±0.18	$\frac{3}{2}$	$\frac{1}{2}$	38.22	100	17.7±1.1	104	0.147±0.010	2300±160	30.8±2.5	23 ±2
	224.84	< 0.03	$\frac{3}{2}$	$\frac{1}{2}$	186.62	> 95	0 [d])	1.30	> 9	< 19		
	224.84		$\frac{3}{2}$	$\frac{3}{2}$	224.84	< 5						
	257.97	(4.5±2.0)×10^{-2}	$\frac{5}{2}$	$\frac{1}{2}$	219.75	4.8±0.3	100	0.274			9.8±4.5	15 ±7
	257.97		$\frac{5}{2}$	$\frac{3}{2}$	257.97	95.2	21 ±7	0.448	2.6 ±1.2	78±35	15 ±7	80 ±40
^{195}Au	61.44	3.0±0.2	$\frac{1}{2}$	$\frac{3}{2}$	61.44	100	16.6±1.0	12.5	0.339±0.025	990±100	26.4±2.0	19.8±1.5
	241.72	< 0.03	$\frac{3}{2}$	$\frac{1}{2}$	180.32	97.6	< 3	1.44	> 9	< 19	≧ 6 [e])	≧8.5 [e])
	241.72		$\frac{3}{2}$	$\frac{3}{2}$	241.56	2.4±0.3						
	261.79	(5.4±1.0)×10^{-2}	$\frac{5}{2}$	$\frac{1}{2}$	200.38	2.3±0.1	100	0.374			5.3±1.2	8.3±1.9
	261.79		$\frac{5}{2}$	$\frac{3}{2}$	261.74	97.7	21.5±4.0	0.434	2.2 ±0.6	92± 26	13 ±4	68 ±21

[a]) Conversion coefficients are taken from the work of Hager and Seltzer [27]).

[b]) Calculated as if all transitions were l-allowed from the formula (1) $B(\mathrm{M1})_{s.p.} = \frac{3}{4\pi}\cdot\frac{2l(l+1)}{(2l+1)(2I_1+1)}(g_s-g_l)^2\mu_N^2$ using $g_s = 5.59$, $g_l = 1$.

[c]) $B(\mathrm{E2})_{s.p.} = 5.93\cdot 10^{-6}A^{\frac{4}{3}}S$, where S is the statistical factor [33]).

[d]) Assumed to be zero in the calculations. The corresponding transitions in ^{195}Au and ^{197}Au contain less than 3 % and less than 5 % E2 [ref. [13])].

[e]) From the upper limits of E2 percentage and half-life.

Regarding the level energies, there is a general slight increase for the three lowest excited levels with increasing mass-number. The excited $\frac{3}{2}^+$ state rises faster than the $\frac{5}{2}^+$ state finally leading to a change in order of the $\frac{3}{2}^+$ and $\frac{5}{2}^+$ levels between ^{197}Au and ^{199}Au (cf. fig. 6). The level energies as calculated in the pairing-plus-quadrupole model [6]) agree reasonably with experiment.

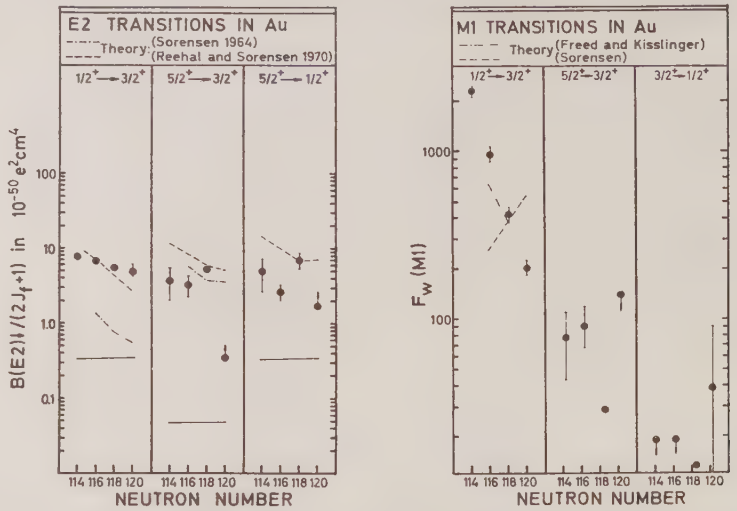

Fig. 7. Experimental E2 transition probabilities and M1 retardation factors for transitions in odd-mass gold isotopes. The values for ^{193}Au and ^{195}Au have been determined from the present experiment, for ^{199}Au from ref. [14]) and for ^{197}Au we have taken the $\frac{1}{2}^+$ level half-life from ref. [2]), B(E2)↓ and B(M1)↓ from ref. [5]), modified by using multipole assignments of M1+(10.8±0.3) % E2 for the 77.34 keV transition and M1+ < 5 % E2 for the 191.35 keV transition, the latter figures from ref. [13]). The E2 transition rates calculated in the pairing-plus-quadrupole model are shown with broken lines, and the single-particle estimate [8]) with full lines. No errors are given in ref. [5]) for B(M1; $\frac{5}{2}^+ \to \frac{3}{2}^+$) and B(M1; $\frac{3}{2}^+ \to \frac{1}{2}^+$), and these points are shown without error bars. Theoretically calculated B(M1) values are indicated with broken lines.

TABLE 3

Experimental E2 transition rates compared with the core-excitation model

Neutron number	B(E2)↓ in Pt [a,b]) $2^+ \to 0^+$	B(E2)↓ in Au [b]) $\frac{1}{2}^+ \to \frac{3}{2}^+$	B(E2)↓ in Au [b]) $\frac{5}{2}^+ \to \frac{3}{2}^+$
114	46.5±3.6	30.8±2.5	15±7
116	39.0±4.0	26.4±2.0	13±4
118	25.3±2.5	22.0±2.5	21 [c])
120	30.0±3.0	$19.4^{+4.5}_{-2.9}$ [d])	≲ 1.4 [e])

[a]) Data on B(E2) values in Pt taken from ref. [32]).
[b]) All B(E2) values in $10^{-2}\, e^2 \cdot b^2$.
[c]) See caption to fig. 7. [d]) From ref. [3]). [e]) From ref. [14]).

TABLE 4

Experimental M1 transition probabilities in Au compared with the core-excitation model predictions. The unit is $10^{-4}\mu_N$

Mass number		193			195		197			199		
	g_c A/Z	exp.	case I	case II	exp.	case I	case II	exp.	case I	case II	exp.	case I	case II
$B(M1; 2\frac{1}{2} \rightarrow 0\frac{3}{2})$	1.5	14.7±1.0	44± 22	(14.7±1.0) [a])	33.9±2.5	63± 20	(33.9±2.5) [a])	75.3±9.0	55.8	(75.3±9.0) [a])	160± 17	430	(160±17) [a])
	1.0		27± 14			38± 13			33.7			275	
	0.5		10± 5			14± 5			12.4			95	
$B(M1; 2\frac{5}{2} \rightarrow 0\frac{3}{2})$	1.5	260±120	21± 10	6.8±3.5	220±60	29± 10	16± 6	700 [b])	26.0	3.5± 0.4	> 130	200	75± 8
	1.0		13± 6			18± 6			15.6			124	
	0.5		5± 2			7± 2			5.8			44	
$B(M1; 2\frac{3}{2} \rightarrow 2\frac{1}{2})$	1.5	> 900	1000±500	104±60	> 900	950±320	270±90	1300 [b])	930	1720±220	430±250	720	50± 5
	1.0		360±180			350±110			340			220	
	0.5		47± 23			43± 14			42			small	

[a]) This value has been used for a simultaneous determination of $(g_c - g_p)$ and A^2 from the magnetic moment and ^{195}Au: $\mu = 0.146 \pm 0.007$ [ref. [30])], ^{197}Au: $\mu = 0.1439$ [ref. [11])] and ^{199}Au: $\mu = 0.2673$ [ref. [31])], all expressed ^{197}Au: 2.13×10^{-2} and 0.70, ^{199}Au: 0.62 and 0.19. Errors in the calculated transition probabilities are mainly text for further details.

[b]) See caption to fig. 7.

$B(M1; 2\frac{1}{2} \rightarrow 0\frac{3}{2})$. The following values of magnetic moments were used: ^{193}Au: $\mu = 0.140 \pm 0.007$ [ref. [29])], in μ_N. The derived values of $(1 - A^2)$ and $(g_c - g_p)$ are: ^{193}Au: 6.6×10^{-2} and 0.176, ^{195}Au: 5.93×10^{-2} and 0.282e due to the uncertainty of the magnetic moments and are assumed to be negligible for ^{197}Au and ^{199}Au. Se,

5.1. E2 TRANSITIONS

In fig. 7 the experimental reduced E2 transition probabilities are compared with theoretical values calculated within the pairing-plus-quadrupole force model. Two such calculations have been performed. Sorensen [8]) has calculated $B(E2)$ values using the wave functions of ref. [6]), which consist of zero- and one-phonon components. Recently Reehal and Sorensen have calculated $B(E2)$ values using wave functions that also include two-phonon components [28]). Inspecting fig. 7 we find for the $\frac{1}{2}^+ \rightarrow \frac{3}{2}^+$ transition that the two-phonon calculations [28]) reproduce the experimental data much better than the one-phonon calculations [8]). For the $\frac{5}{2}^+ \rightarrow \frac{3}{2}^+$ transitions no significant improvement is obtained by including two phonons. The two-phonon calculations carried out for the $\frac{5}{2}^+ \rightarrow \frac{3}{2}^+$ transition do not agree better than about a factor of four with the experimental data.

In the calculations of ref. [6]) the strength of the quadrupole coupling is fitted using the 2^+ level of the adjacent even nucleus. The generally rather good agreement between theory and experiment indicates, according to Sorensen [6]), that the properties of the phonons of an odd-mass nucleus, and of its even neighbour, are the same. This is also assumed in the core-excitation model [10]), in which these excitations are assumed to be identical. In this latter model, the E2 transition rates from the members of the core-particle level multiplet to the ground state, are predicted to be equal to the rate from the 2^+ state in the doubly even core nucleus. In table 3 we compare $B(E2)$ values from the $\frac{5}{2}^+$ and $\frac{1}{2}^+$ state in odd-mass gold nuclei with $B(E2; 2^+ \rightarrow 0^+)$ of the corresponding platinum cores. The striking similarity of the figures in the case of ^{197}Au is not reproduced for the other gold isotopes and therefore we conclude that the core-excitation model in the sense that only small admixtures are considered is not generally applicable to the Au nuclei.

5.2. M1 TRANSITIONS

The experimental values of M1 transition probabilities in odd-mass Au nuclei are plotted versus the neutron number in fig. 7. Theoretical calculations for the $\frac{1}{2}^+ \rightarrow \frac{3}{2}^+$ transitions have been made by Sorensen [7]) in the pairing-plus-quadrupole force model [6]) and by Freed and Kisslinger [9]), who in addition also consider admixtures of higher seniority configurations, which are demonstrated to cause M1 rates of the same order of magnitude as in the pairing-plus-quadrupole model. The latter calculations are seen to fairly well reproduce both the magnitude and the trend of the experimental M1 transition probabilities, while Sorensen's values show the wrong trend.

Values of $B(M1)$ for the $\frac{1}{2}^+ \rightarrow \frac{3}{2}^+$ transition can also be calculated in the core-excitation model of de-Shalit [10]). From the general expression given in ref. [10]) we derive:

$$B(M1; 2\tfrac{1}{2} \rightarrow 0\tfrac{3}{2}) = \frac{3}{4\pi} 3(1 - A^2)(g_c - g_p)^2, \quad (3)$$

$$B(M1; 2\tfrac{5}{2} \rightarrow 0\tfrac{3}{2}) = \frac{3}{4\pi} \tfrac{7}{5}(1 - A^2)(g_c - g_p)^2, \quad (4)$$

$$B(M1; 2\tfrac{3}{2} \rightarrow 2\tfrac{1}{2}) = \frac{3}{4\pi} \tfrac{3}{2} A^2 (g_c - g_p)^2, \quad (5)$$

where all $B(M1)$ values are expressed in μ_N^2. The quantity A is the mixing amplitude of the $\frac{3}{2}^+$ states. In ref. [10]) the following formula for the magnetic moment expressed in μ_N is also given:

$$\mu_{\frac{3}{2}} = \tfrac{3}{2}g_p + \tfrac{6}{5}(1-A^2)(g_c - g_p). \quad (6)$$

Inserting the Schmidt value 0.084 for the particle g-factor g_p we may calculate A^2 and g_c from experiment. In table 4 we compare experimental M1 rates with values calculated from formulae (3)-(6) above. Two approaches have been used in the calculations, shown as case I and II in the table. Case I gives the $B(M1)$ values obtained from a determination of A^2 from experimental values of magnetic moments [11,29-31]), and using three values of g_c; $1.5Z/A$, $1.0Z/A$ and $0.5Z/A$. In case II are given the corresponding $B(M1)$ values when both A^2 and $(g_c - g_p)$ are determined from measured magnetic moments and from the experimental value of $B(M1; 2\frac{1}{2} \rightarrow 0\frac{3}{2})$. From table 4 it is evident that the core-excitation model hardly can explain all the measured M1 transition probabilities, although a reasonable fit can be obtained for the $\frac{1}{2}^+ \rightarrow \frac{3}{2}^+$ and $\frac{3}{2}^+ \rightarrow \frac{1}{2}^+$ transitions, especially in the case of ^{197}Au.

We are indebted to the Nuclear Chemistry Group at CERN, in particular to A. Kjelberg and R. Mohr, for providing us with mass-separated sources. We are also indebted to B. S. Reehal and R. A. Sorensen for communicating their results prior to publication.

References

1) J. Brunner, J. Halter and P. Sherrer, Helv. Phys. Acta **31** (1958) 335
2) J. Jastrzebski, H. Abou-Leila and N. N. Perrin, Nucl. Phys. **70** (1965) 392
3) A. Bäcklin and S. G. Malmskog, Ark. Fys. **34** (1967) 59
4) M. Martin, P. Marmier and J. de Boer, Helv. Phys. Acta **31** (1958) 435
5) F. McGowan, private communication
6) L. S. Kisslinger and R. A. Sorensen, Rev. Mod. Phys. **35** (1963) 853
7) R. A. Sorensen, Phys. Rev. **132** (1963) 2270
8) R. A. Sorensen, Phys. Rev. **133** (1964) B281
9) N. Freed and L. S. Kisslinger, Nucl. Phys. **A116** (1968) 401
10) A. de-Shalit, Phys. Rev. **122** (1961) 1530
11) A. de-Shalit, Phys. Lett. **15** (1965) 170
12) G. Alaga and G. Ialongo, Nucl. Phys. **A97** (1967) 600
13) B. Fogelberg and A. Bäcklin, to be published
14) A. Bäcklin, B. Fogelberg and S. G. Malmskog, Nucl. Phys. **A103** (1967) 337
15) A. Kjelberg and G. Rudstam (ed.), CERN yellow report 70-3 (1970)
16) A. Bäcklin, Nucl. Instr. **57** (1967) 261
17) B. Svahn, A. Johansson, B. Nyman, G. Malmsten and H. Petterson, Z. Phys. **210** (1968) 466
18) A. Bäcklin, B. Fogelberg, V. Berg and S. G. Malmskog, Nucl. Phys. **A138** (1969) 429
19) T. R. Gerholm and J. Lindskog, Ark. Fys. **24** (1963) 171
20) S. G. Malmskog, Ark. Fys. **35** (1967) 255
21) V. Berg, A. Höglund and S. G. Malmskog, to be published
22) J. Jastrzebski and P. Kilcher, Compt. Rend. **254** (1962) 411
23) T. Sundstrom, Nucl. Instr. **16** (1962) 153
24) B. Olsen and L. Broström, Nucl. Instr. **44** (1966) 153

25) A. Marelius, P. Sparrman and T. Sundström, Table of nuclear lifetimes in hyperfine structure and nuclear radiations, eds. E. Matthias and D. A. Shirley, (North-Holland, Amsterdam, 1968) appendix D, p. 1043
26) P. Reyes-Suter and T. Suter, Ark. Fys. **20** (1961) 415
27) R. S. Hager and E. C. Seltzer, Internal conversion tables, Part 1, Nucl. Data **A4** (1968) 1-2
28) B. S. Reehal and R. A. Sorensen, to be published
29) I. Lindgren, Table of nuclear spins and moments, in Alpha-, beta- and gamma-ray spectroscopy, ed. K. Siegbahn (North-Holland, Amsterdam, 1965)
30) Yau Wa Chan, W. B. Ewbank, W. A. Nierenberg and H. A. Shugart, Phys. Rev. **137** (1965) B1129
31) P. A. Vanden Bout *et al.*, Phys. Rev. **158** (1967) 1078
32) P. H. Stelson and L. Grodzins, Nucl. Data **A1** (1965) 21
33) S. A. Moszkowski, Theory of multipole radiation, in Alpha-, beta- and gamma-ray spectroscopy, ed. K. Siegbahn (North-Holland, Amsterdam, 1965)
34) C. M. Lederer, J. M. Hollander and I. Perlman, Table of isotopes, sixth ed. (Wiley and Sons, Inc., New York, London, Sydney)

R E F E R E N C E 5

E2 AND M1 TRANSITION PROBABILITIES IN ODD-MASS Hg NUCLEI

A. BÄCKLIN and B. FOGELBERG
Institute of Physics, Uppsala University and
The Swedish Research Councils Laboratory, Studsvik, Nyköping, Sweden

V. BERG AND S. G. MALMSKOG

AB Atomenergi, Studsvik, Nyköping, Sweden and
Institute of Physics, University of Stockholm, Sweden

1.E.4

Nuclear Physics **A138** (1969) 429—441; © *North-Holland Publishing Co., Amsterdam*

Not to be reproduced by photoprint or microfilm without written permission from the publisher

E2 AND M1 TRANSITION PROBABILITIES IN ODD-MASS Hg NUCLEI

A. BÄCKLIN and B. FOGELBERG

Institute of Physics, Uppsala University and
The Swedish Research Councils Laboratory, Studsvik, Nyköping, Sweden

V. BERG and S. G. MALMSKOG

AB Atomenergi, Studsvik, Nyköping, Sweden and
Institute of Physics, University of Stockholm, Sweden

Received 8 September 1969

Abstract: L- and M-subshell ratios have been measured for the 39.45 keV transition in ^{193}Hg and the 37.13 and 16.2 keV transitions in ^{195}Hg yielding 0.38 ± 0.12, < 0.02 and 0.08 ± 0.03 % E2, respectively. The half-lives of the 39.49 keV level in ^{193}Hg, and the 53.34 and 37.13 keV levels in ^{195}Hg have been measured with the delayed coincidence method yielding values of 0.63 ± 0.03, 0.72 ± 0.03 and < 0.05 nsec respectively. A systematic compilation of reduced E2 and M1 transition probabilities in odd mass Pt, Hg and Pb nuclei is given and compared to theoretical predictions.

1. Introduction

The three lowest levels in the odd-neutron isotopes of Hg, Pt and Pb have $I^\pi = \frac{1}{2}^-$, $\frac{3}{2}^-$ and $\frac{5}{2}^-$. This is in qualitative agreement with the shell model, which predicts the $p_{\frac{1}{2}}$, $p_{\frac{3}{2}}$ and $f_{\frac{5}{2}}$ orbitals to be the last occupied in the shell closed at $N = 126$. These states have also been theoretically investigated by Kisslinger and Sorensen within the frame of the pairing plus quadrupole force model [1]). For the Hg and Pt nuclei these authors find for some of the states fairly strong quadrupole vibration components, which should give rise to E2 transitions enhanced over the single-particle rate. Calculations by Sorensen [2]) using the wave functions of ref. [1]) predict E2 transition rates in these nuclei with enhancement factors varying several orders of magnitude; up to 15 times the single-particle estimate.

Experimental values of E2 transition rates are sparse for odd neutron nuclei in this mass region. Some data exist for the $\frac{5}{2}^- \to \frac{1}{2}^-$ transitions for which the agreement between experiment and theory [2]) is found to be reasonable [3,4]). For the $\frac{5}{2}^- \rightleftarrows \frac{3}{2}^-$ and $\frac{3}{2}^- \rightleftarrows \frac{1}{2}^-$ transitions, however, data on B(E2) values are given in literature only for ^{199}Hg and ^{207}Pb. To improve this situation, we have undertaken a study of the E2 transition rates from the $\frac{5}{2}^-$ state in ^{193}Hg and the $\frac{3}{2}^-$ and $\frac{5}{2}^-$ states in ^{195}Hg. The half-lives of these levels were studied earlier by Reyes-Suter and Suter [5]). In ^{195}Hg, however, the half-life was measured in such a way that it could not be assigned

to a definite level. We have, therefore, performed new measurements of the half-lives of the levels mentioned.

Regarding the multipolarity mixing ratios of the transitions, no data exist to our knowledge on the $\frac{5}{2}^- \to \frac{3}{2}^-$ transition in ^{193}Hg. Measurements of L and M subshell ratios in ^{195}Hg have been made by Jung and Svedberg [6]), who report only upper limits for the E2 admixtures. In the present work we report determinations of E2/M1 mixing ratios in ^{193}Hg and ^{195}Hg from measurements of L and M subshell ratios.

2. Conversion electron measurements

Conversion electrons from the decays of ^{193m}Hg and ^{195m}Hg were measured using a 50 cm $\pi\sqrt{2}$ beta spectrometer [7,8]) operated at a momentum resolution of ≈ 0.2 %. The GM tube detector had a window of 0.55 mg/cm^2 aluminized Melinex-foil with a cut-off energy of about 16 keV electron energy. As some of the conversion lines of interest had much lower energy than this, a special source arrangement was constructed in which a suitable high voltage could be applied to the source, thus giving the electrons a pre-acceleration. The influence of the high voltage on the transmission properties of the spectrometer was found to be negligible.

The sources were obtained from the ISOLDE [9]) experiment at CERN. A target of liquid lead was bombarded by 600 MeV protons from the proton synchrotron giving a large number of mainly neutron-deficient isotopes. After isotope separation, the mercury isotopes were collected on a 0.9 mg/cm^2 nickel foil, which served as backing in the internal conversion electron measurements. The source thickness was small enough to allow the measurement of 12 keV electron lines without serious broadening of the lines. Typical irradiation times were of the order of 20 hours, and typical transport time from Geneva to Studsvik was 12 hours.

The L-shell conversion lines of the 39.5 keV transition in ^{193}Hg nearly coincide with the corresponding lines of the intense 38.2 keV transition in the daughter ^{193}Au. The line half-width in this energy region was about 135 eV, which was sufficient to clearly resolve the two line groups, as is evident from fig. 1. No other conversion lines from the decay chain ^{193}Hg $\to$ ^{193}Au $\to$ ^{193}Pt were found to disturb the L-subshell lines of the 39.5 keV transition. The results concerning the 39.5 keV transition are found in table 1. All multipole assignments and total intensities in this work are based on the internal conversion coefficients calculated by Hager and Seltzer [10]).

The levels of ^{195m}Hg are shown in fig. 2. The M-group of the 16.2 keV transition was measured with 15 keV pre-acceleration which made only a small correction for window absorption necessary. No pre-acceleration was needed for measuring the other conversion lines in the decay, but the 37.1 keV L_1 line was also included in the same run as the 16.2 keV M-lines for normalization purposes.

The evaluation of the M-subshell ratios of the 16.2 keV transition met some difficulties as higher LNN Auger lines are expected in this region of the spectrum. The relative intensities in the LNN group in Hg and Au are not known in this case. In

fig. 2 of ref.[11]) a recording of L Auger lines in Pb is shown. We assume the Au and Hg L Auger groups to be similar to this group, implying that a weak Auger line with a position corresponding to the energy expected for the $L_{II}N_{IV}N_{V}$ line is the only one

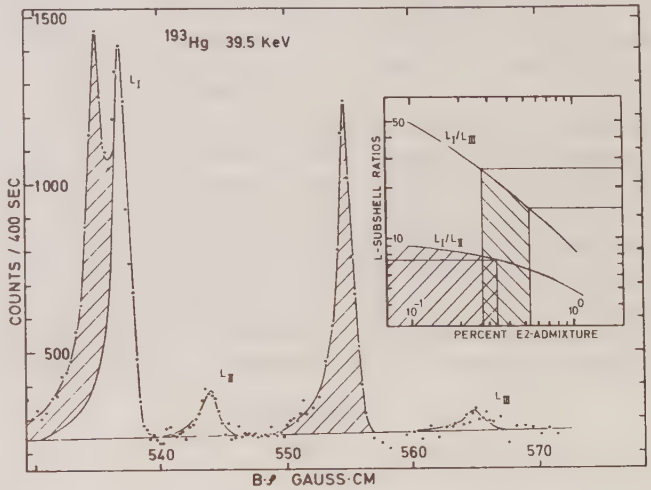

Fig. 1. L-lines of the 39.5 keV transition in ^{193}Hg. All points have been corrected for the decay of ^{193m}Hg. The shadowed lines belong to the 38.2 keV transition in ^{193}Au. In the inset, the L-subshell ratios are shown as a function of the E2 admixture.

TABLE 1

Energy and relative intensities of the L lines of the 39.49 keV transition in ^{193}Hg as obtained in the present work

Transition energy [a]) (keV)	Shell	Relative intensity	Multipole assignment
39.49±0.03	L_I	100	M1+(0.38±0.12) % E2
	L_{II}	11.6±1.2	from L-subshell ratios
	L_{III}	5.1±1.3	

[a]) The energy was determined by comparison with the well-known [27]) energies of conversion electrons emitted in the decay of the daughter activity ^{193}Au.

which gives a noticeable contribution in comparison with the 16.2 keV M-lines. The intensity and position of the same Auger line in Hg can be estimated by using the figure of ref. [11]) and fig. 1 in the work by Jung and Svedberg [6]). The obtained intensity and position agree well with the experimental points as is shown in fig. 3 in the present work. In this figure, the "best fit" intensity of the same Auger line in Au is

also indicated. The fortunate circumstance that the Auger lines do not coincide with the calculated positions for the 16.2 keV M_{II} and M_{III} lines (cf. fig. 3) makes it possible to determine the E2 admixture in the 16.2 keV transition with some certainty. The estimated uncertainty in the background due to the presence of the L Auger lines have been included in the errors given in table 2. Fig. 4 shows the L-lines of the 53.3 keV transition.

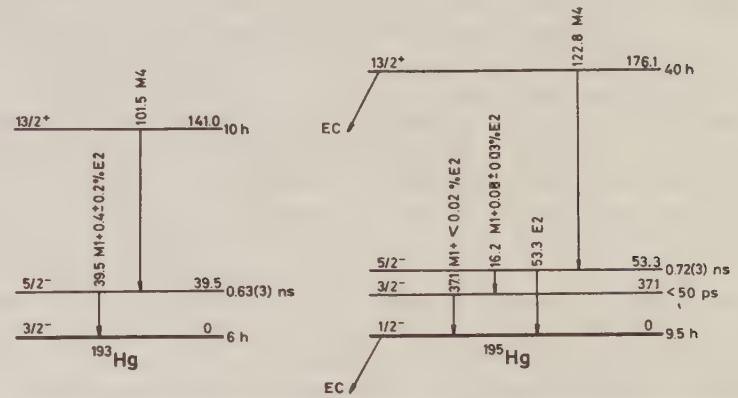

Fig. 2. Level schemes of ^{193}Hg and ^{195}Hg with the experimental data from the present work included.

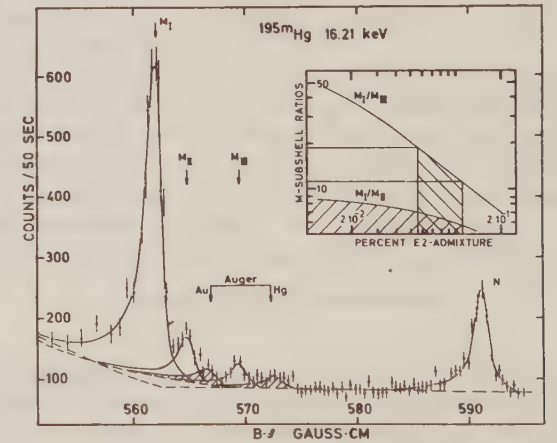

Fig. 3. M-lines of the 16.21 keV transition in ^{195}Hg. 15 kV preacceleration of the electrons has been used. The two different dashed backgrounds to the left of the figure show two ways of extrapolating the rather smooth structure of the higher LXX and LXY Auger line-group. Further details concerning the contribution from Auger lines are given in the text. M-subshell ratios as a function of the E2-admixture are shown in the inset. Conversion coefficients are taken from ref. [10]). The arrows indicate the expected positions for the 16.21 keV M-lines.

The distance between the K and L_{III} lines of the 122.78 keV isomeric transition is more than 70 % in momentum units, and by measuring the lines in the same magnetization cycle and using the accurately known difference in the electron binding energies, a rather accurate value of the transition energy could be determined.

The experimental findings in ^{195}Hg are summarized in table 2 below. For comparison, the results of Jung and Svedberg [6]) were included in the table. The two experiments agree fairly well.

Fig. 4. L_{II} and L_{III} lines of the 53.3 keV crossover transition in ^{195}Hg. The rise of the background to the right in the figure is caused by the L_I line of 56.7 keV E3 transition of the daughter activity ^{195m}Au. The points are corrected for decay.

3. Half-life measurements

The half-life measurements reported below have all been carried out using a long lens electron-electron coincidence spectrometer described earlier [12, 13]). The same sources as for the internal conversion measurements were used.

3.1. THE 39.5 keV LEVEL IN ^{193}Hg

The 101.5L and 39.5L conversion lines were focused in each spectrometer and the corresponding delayed coincidence time distribution was registered. Some disturbing coincidences could possibly be expected to come from the tail of the 187K-38.2L cascade in ^{193}Au as the 187K line was degraded in passing through the source backing. This cascade would have introduced a 4 nsec half-life into the registered decay curve but no such component was observed.

To obtain a prompt reference curve, we used the $\beta \rightarrow$ 94.7K cascade in the decay of ^{165}Dy. To be able to use the same energy setting in both the prompt and delayed

TABLE 2

Properties of conversion lines in ^{195}Hg

Transition energy (keV)	Shell	Intensity in % per isomeric decay [a])		Total transition intensity [b]) present work	Multipole assignment	
		present work	Jung *et al.* [6])		present work	Jung *et al.* [6])
16.21±0.06 [c])	M_I	15.4	21 ±5	99 ±15	M1+(0.08±0.03) % E2 from M-subshell ratios	M1(+E2)
	M_{II}	2.19±0.45	2.8 ±0.7			
	M_{III}	1.1±0.30	0.70±0.35			
	N	6.7 ±1.1	5.5 ±1.4			
37.13±0.05	L_I	69.0	69.0	100	M1+<0.02 % E2 from L-subshell ratios	M1(+< 0.01 % E2)
	L_{II}	7.7 ±0.8	6.3 ±1.4			
	L_{III}	$0.66^{+0.20}_{-0.15}$	< 0.75			
53.34±0.03	L_I	< 0.14	< 0.19	1.1± 0.20	E2 from L-subshell ratios	E2
	L_{II}	0.49±0.09	0.62±0.28			
	L_{III}	0.48±0.09	0.55±0.28			
122.78±0.03	K	8.7 ±1.4	6.2 ±0.7	112 ±15	M4+< 0.5 % E5 from L-subshell ratios	M4
	L_I	24.0 ±1.1	21.0 ±2.1			
	L_{II}	5.6 ±0.7				
	L_{III}	58.0	44.5 ±4.2			

[a]) The errors given for the intensity of each individual line are the estimated uncertainties when the line is compared with the most intense line belonging to the same transition. The estimated errors when comparing lines belonging to different transitions are given in the column labelled "Total transition intensity".

[b]) The total intensities have been calculated by using the conversion coefficients of Hager and Seltzer [10]). These conversion coefficients have also been used in assigning multipolarities, with the exception of the 122.78 keV transition where the ICC's of Sliv and Band [20]) were used, as ref. [10]) lacks multipolarities higher than 4.

[c]) Difference between 53.34 and 37.13 keV.

coincidence measurements, 14 keV of high tension was added to the ^{193}Hg source. A pair of observed time distributions is shown in fig. 5. The data were analysed using both the momentum [14]) and convolution [15]) methods. Good agreement between the different methods was obtained, and, as a mean value of the half-life for the 39.5 keV level, we adopt 0.63 ± 0.03 nsec. One earlier measurement of this half-life given as 0.8 ± 0.1 nsec is reported in the literature [5]). These authors used a previously recorded energy-shape calibration curve to obtain an average prompt shape which they used together with the inherently, statistically less accurate second and third order momentum methods [14]). Moreover, as their time resolution was not as good as ours, the discrepancy between the results is not unreasonable.

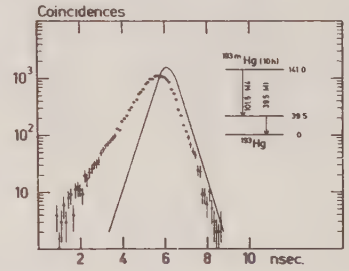

Fig. 5. Delayed time distribution obtained by registering coincidences between the 101.5L and 39.5L conversion electrons in the decay of ^{193m}Hg giving a half-life of 0.63 ± 0.03 nsec for the 39.5 keV level in ^{193}Hg.

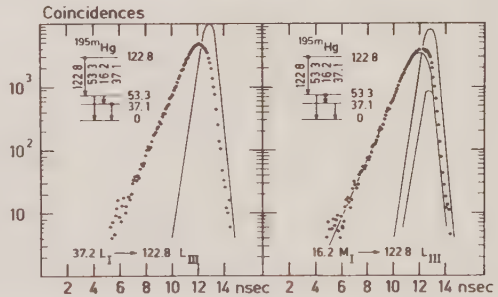

Fig. 6. Left part: Delayed time distribution from coincidences between the 122.8L_{III} and 37.1L conversion electron lines. From the analysis (see text) we obtain a half-life of < 50 psec for the 37.1 keV level in ^{195}Hg.

Right part: Delayed time distribution from coincidences between the 122.8L_{III} and 16.2M conversion electron lines. After correction for a small prompt contribution from the LMN(LNN)Auger → 122.8L_{III} cascade we obtain a half-life of 0.72 ± 0.03 nsec for the 53.3 keV level in ^{195}Hg.

3.2. THE 53.3 keV LEVEL IN ^{195}Hg

Delayed coincidence time distributions have been recorded focusing the 123L_{III} conversion electrons in the decay of ^{195m}Hg in one spectrometer while the other

spectrometer registered either the 16M or the 37L_I conversion lines. According to the decay scheme of ^{195m}Hg, fig. 2, these two measurements should contain information on the half-lives of the 37.1 and 53.3 keV levels in ^{195}Hg. Examples of the time distributions obtained are shown in fig. 6. At first sight, these curves are very similar in shape, indicating that the half-lives of the two levels are very different, the one for the 53.3 keV level being the longest. In the measurement of the 123L_{III}-16M cascade there is a definite prompt contribution from the 123L_{III} electrons in coincidence with the LMN(LNN) Auger electrons accompanying the conversion process and being partly accepted in the 16M channel. From the electron intensity measurements with the double focusing spectrometer reported above, this contribution was estimated and its contribution subtracted as is shown by the full drawn line in the right-hand part of fig. 6. The form and exact position of the prompt distribution used was obtained from measurements of the β-238.6K cascade in the decay of ^{212}Pb. To be able to use the same energy settings in both measurements, the 123L_{III} line was made to coincide energetically with a slightly degraded 238.6K line by accelerating the 123L_{III} electrons in a 22 keV electrostatic field. The corrected decay curves were analysed with the momentum [14]) and convolution [15]) methods with the following results

1st momentum method $= 9.26 \pm 0.09$ † channels,
2nd momentum method $= 9.11 \pm 0.18$ channels,
3rd momentum method $= 8.98 \pm 0.32$ channels,
convolution method $= 9.25 \pm 0.08$ channels,

where the errors are of a purely statistical nature. The general agreement between the different methods of analysis is obvious. From these measurements, we obtain a half-life for the 53.3 keV level in ^{195}Hg of 0.72 ± 0.03 nsec. The increase in error also takes the time calibration into account.

3.3. THE 37.1 keV LEVEL IN ^{195}Hg

In the case of the 123L_{III}-37.1L coincidence measurement, no disturbing coincidence rates are expected. An observed time distribution together with an associated prompt curve is shown in the left hand part of fig. 6. Within experimental errors, this curve appears to be identical with the corrected curve from the 123L_{III}-16M measurement. An analysis similar to the one described above was also performed in this case. The form and position of the observed decay curve is consistent with a half-life of 0.73 ± 0.03 nsec. This value is, however, a function of the half-lives of both the 53.3 and 37.1 keV levels. That it almost coincides with the value obtained for the 53.5 keV level indicates that the half-life of the 37.1 keV level is much shorter. To get a limit for the half-life of the 37.1 keV level, use was made of the fact that the observed first moment of the composite decay curve $= 9.40 \pm 0.10$ channels is proportional to the sum of the mean lives of the two levels involved [14]). Subtracting the moment cor-

† Corrected for a 10 psec shift due to the finite acceleration distance and for a spurious constant shift of 0.27 channels as detected by the convolution method [15]).

TABLE 3

Properties of E2 and M1 transitions in odd mass Hg, Pt and Pb nuclei

Nucleus	Level energy (keV)	$T_{\frac{1}{2}}$ level (nsec)	Spin I_i	Spin I_f	Transition (keV)	Branching %	E2 multipolarity %	α_{tot} [a]	B(M1) $\mu_N^2 \times 10^2$	F_W [b]	B(E2) 10^{-50} (e^2 cm^4)	$\frac{B(E2)\ [c]}{B(E2)_{s.p.}}$
^{193}Hg	39.5	0.63 ± 0.03 [d]	$\frac{5}{2}^-$	$\frac{3}{2}^-$	39.5	100	0.38 ± 0.12 [d]	24.6	4.0 ± 0.2	35 ± 2	15 ± 8	74 ± 40
^{195}Hg	53.3	0.72 ± 0.03 [d]	$\frac{5}{2}^-$	$\frac{3}{2}^-$	16.2	99	0.08 ± 0.03 [d]	363	3.7 ± 0.2	38 ± 2	16 ± 6	80 ± 30
				$\frac{1}{2}^-$	53.3	1.1 ± 0.2 [d]	100	101			1.9 ± 0.4	2.8 ± 0.5
	37.1	< 0.05 [d]	$\frac{3}{2}^-$	$\frac{1}{2}^-$	37.1	100	< 0.02	27	> 55	< 2	(≲ 7) [e]	(≲ 10) [e]
^{197}Hg	133.9	7.0 ± 0.2 [f]	$\frac{5}{2}^-$	$\frac{1}{2}^-$	133.9	100	100	1.7			6.9 ± 0.2	9.6 ± 0.3
^{199}Hg	208.2	(66 ± 6)·10^{-3} [g]	$\frac{5}{2}^+$	$\frac{5}{2}^-$	49.8	16 [h]	0.19 ± 0.06 [h]	11.5	6.2 ± 0.6	34 ± 3	6.6 ± 2.0	21 ± 6
				$\frac{3}{2}^-$	208.2	84 [h]	11 ± 3	0.95	2.9 ± 0.3	41 ± 4	10 ± 3	14 ± 4
	158.4	2.4 ± 0.1 [i]	$\frac{3}{2}^+$	$\frac{1}{2}^-$	158.4	100	100	0.92			12.4 ± 0.5	16.8 ± 0.7
^{193}Pt	14.3	2.2 [j]	$\frac{5}{2}^-$	$\frac{3}{2}^-$	12.6	100	0.02 ± 0.01 [k]	160	5.6	25	10 ± 5	50 ± 25
			$\frac{3}{2}^-$	$\frac{1}{2}^-$	14.3	< 3 [i]	100	≈1.7 · 10^4			< 7	< 10
^{195}Pt	98.8	0.17 ± 0.02 [m]	$\frac{3}{2}^-$	$\frac{1}{2}^-$	98.8	100	1.9 ± 0.5 [n]	8.5	1.9 ± 0.2	98 ± 12	7 ± 2	10 ± 2.5
^{197}Pt	52.9	18.5 ± 1.5 [o]	($\frac{5}{2}^-$)	($\frac{1}{2}^-$)	52.9	100	100	97			6.6 ± 0.8	9 ± 1
^{203}Pb	126.4	75 ± 3 [p]	($\frac{1}{2}^-$)	($\frac{5}{2}^-$)	126.4	100	100	2.38			0.69 ± 0.03	0.30 ± 0.01
^{207}Pb	569.6	0.128 ± 0.005 [i]	$\frac{5}{2}^-$	$\frac{1}{2}^-$	569.6	100	100	0.0215			0.72 ± 0.03	0.96 ± 0.04
	897.3		$\frac{1}{2}^-$	$\frac{3}{2}^-$	897.3						1.6 ± 0.8 [q]	1.0 ± 0.5

[a]) Obtained from the experimental value of the E2/M1 mixing ratio and the theoretical values of Hager and Seltzer [10]).

[b]) $F_W = B(M1)_{s.p.}/B(M1)_{exp}$. $B(M1)_{s.p.}$ was calculated as if the transitions were l-allowed from the formula [18])

$$B(M1)_{s.p.} = \frac{3}{4\pi}\frac{2l(l+1)}{(2I+1)(2I_i+1)}(g_s-g_l)^2\mu_N^2 \text{ inserting } g_s = -3.83,\ g_l = 0.$$

[c]) $B(E2)_{s.p.}$ is the Weisskopf estimate [16]) $B(E2)_{s.p.} = 5.93 \cdot 10^{-6}A^{\frac{4}{3}}S$, where S is the statistic factor [21]).

[d]) Present work. [e]) Values calculated with the upper limits for the half-life and the E2 percentage.

[f]) Ref. [22]). [g]) Ref. [23]). [h]) Ref. [24]). [i]) Average of values given in ref. [25]). [j]) Ref. [26]). [k]) Ref. [27]).

[l]) Estimated from fig. 6 of ref. [27]). [m]) Ref. [28]). [n]) From average of L-subshell ratios given in ref. [29]).

[o]) Ref. [4]). [p]) Ref. [3]). [q]) Ref. [30]).

responding to the 53.3 keV level and taking the extreme limits, we obtain τ(37.1 keV) < 0.33 channels. If we take twice this value as an upper limit, we obtain $T_{\frac{1}{2}}$(37.1 keV) < 50 psec. †

One previous measurement has been reported on the half-lives of excited levels in ^{195}Hg [ref. [5])]. This group found a half-life of 0.79 ± 0.07 nsec when measuring coincidences between the 123L and 37.1L electrons, but were not able to assign this half-life to a definite level. They made no attempts to measure coincidence from the 122.8L-16.2M cascade mainly because of the low detection efficiency of the 16.2M line. In our case, we used 22 keV of pre-acceleration on the ^{195m}Hg source which, together with our thin mass-separated sources, seems to have increased our detection efficiency of the 16.2M line by at least a factor of 10, as compared with the value indicated in fig. 3 of ref. [5]).

4. Discussion

In table 3 a compilation is given of the data on E2 and M1 transition rates in odd mass Pt, Hg and Pb isotopes as obtained from the present work and from literature. Values of B(E2) and B(M1) were calculated from the formulas

$$B(E2)\downarrow = \frac{0.563pf}{(1+\alpha_{tot})T_{\frac{1}{2}}E^5}\,10^{-48}\,e^2\cdot\text{cm}^4,$$

$$B(M1)\downarrow = \frac{3.94\cdot 10^{-7}(100-p)f}{(1+\alpha_{tot})T_{\frac{1}{2}}E^3}\,\mu_N^2,$$

where $T_{\frac{1}{2}}$ is the half-life of the level, p is the E2 percentage of the transition, f is the fraction of decays proceeding through the transition and α_{tot} is the total conversion coefficient; E is given in keV.

4.1. E2 TRANSITIONS

The systematic behaviour of the experimental B(E2) values is shown in fig. 7 together with the theoretical predictions of the pairing plus quadrupole force model [2]). All transition probabilities are given in units of the single-particle estimate [16]). The gross structure follows the pattern expected on general grounds with small B(E2) values for Pb and larger values as one moves away from the region of closed shells. It is, however, seen that the model predictions [2]) do not reproduce the experimental data very well. The smallest deviations are found for the $\frac{5}{2}^- \rightleftarrows \frac{1}{2}^-$ transitions, which, on the other hand, are found to have a dependence on the neutron number that is opposite the predicted.

† We also tried to measure the half-life of the 37.1 keV level directly from the 16.2M-37.1L cascade but the backing material of the source was unfortunately too thick to allow a sufficient number of 37.1L electrons to penetrate the backing to obtain a reasonable statistical accuracy.

The collective character is clearly demonstrated for the $\frac{5}{2}^- \rightleftarrows \frac{3}{2}^-$ and to some extent also for the $\frac{3}{2}^- \rightleftarrows \frac{1}{2}^-$ transitions of the most neutron deficient nuclei. This effect is even more pronounced if the pairing factors of the single-particle transitions are considered. For $N = 115$ these have values between 0.1 and 0.4 [ref. [17])]. For the $\frac{5}{2}^- \rightleftarrows \frac{3}{2}^-$ transitions in ^{193}Hg, ^{195}Hg and ^{193}Pt, the B(E2) value for a pure phonon transition as obtained from the B(E2) value of the $N+1$ doubly even nucleus seems to be a better estimate than what is obtained from the wave functions of Kisslinger and Sorensen [1]).

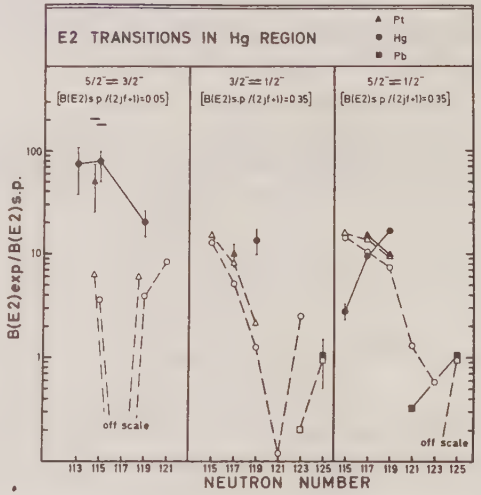

Fig. 7. Experimental (solid symbols) and predicted [2]) (hollow symbols) enhancement factors for E2 transitions in odd mass Pt, Hg and Pb nuclei as given in table 3. The horizontal bars give the enhancement factors expected for a pure phonon transition.

An attempt to modify these to fit the B(E2) values of ^{195}Hg showed that this cannot be done with only minor adjustments of the amplitudes of the components, but at least one of the $\frac{5}{2}^-$ or $\frac{3}{2}^-$ states must be assumed to be predominantly a phonon state. (No quantitative calculations are, however, possible without further information, e.g. on quadrupole moments.)

4.2. M1 TRANSITIONS

The retardation factors relative the single-particle estimates are shown in fig. 8. The $\frac{5}{2}^- \rightleftarrows \frac{3}{2}^-$ transitions are l-forbidden in terms of the shell model ($f_{\frac{5}{2}} \rightleftarrows p_{\frac{3}{2}}$) and should accordingly show large values of F_W. The introduction of phonon admixtures according to Kisslinger and Sorensen [1]) should relax this forbiddenness. Sorensen [18]) has carried out the calculations for neutron-rich Hg nuclei, using the wave functions

of ref. [1]), but, as seen from fig. 8, the experimental transition rates are considerably larger than obtained with the fairly small phonon admixtures of ref. [1]). An extension of this treatment of l-forbidden M1 transitions has recently been made by Freed and Kisslinger [19]), who in addition to phonon admixtures, also consider admixtures of higher seniority configurations due to short-range correlations. For $\frac{5}{2}^- \rightarrow \frac{3}{2}^-$ transitions in Hg nuclei, the latter type of admixture is found to have a predominantly influence on the M1 transition probability, and a good agreement is obtained with experiment as shown in fig. 8.

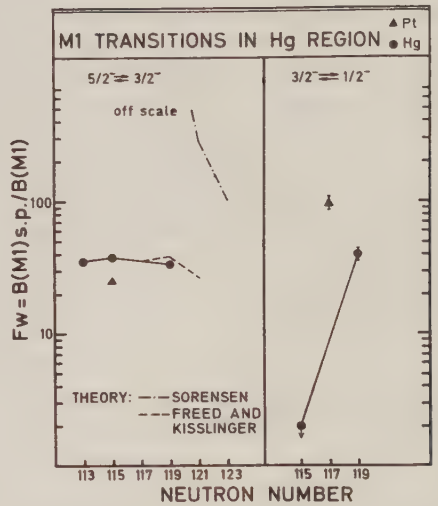

Fig. 8. Experimental (points) and theoretical (dashed lines) retardation factors for M1 transitions in Hg and Pt nuclei as given in table 3.

We want to express our gratitude to Dr. A. Kjelberg and the Nuclear Chemistry group at CERN for providing the sources. We are also indebted to Mr. I. Pettersson for spending so many dark hours on the roads between Studsvik and the Stockholm airport when bringing us the sources.

References

1) L. S. Kisslinger and R. A. Sorensen, Rev. Mod. Phys. **35** (1963) 853
2) R. A. Sorensen, Phys. Rev. **133** (1964) B281
3) I. Bergström, C. J. Herrlander, P. Thieberger and J. Uhler, Ark. Fys. **10** (1961) 93
4) S. G. Malmskog, Ark. Fys. **34** (1967) 195
5) P. Reyes-Suter and T. Suter, Ark. Fys. **20** (1961) 415
6) B. Jung and J. Svedberg, Ark. Fys. **19** (1961) 447
7) G. Bäckström, A. Bäcklin, N. E. Holmberg and K. E. Bergkvist, Nucl. Instr. **16** (1962) 199

8) A. Bäck[illegible] Nucl. Instr. **57** (1967) 261
9) P. G. Hansen *et al.*, Phys. Lett. **28B** (1969) 415
10) R. S. Hager and E. C. Seltzer, Nucl. Data **A4** (1968) No. 1 and 2
11) R. Stockendal, Ark. Fys. **17** (1960) 553
12) T. R. Gerholm and J. Lindskog, Ark. Fys. **24** (1963) 171
13) S. G. Malmskog, Ark. Fys. **35** (1967) 255
14) T. Sundström, Nucl. Instr. **16** (1967) 153
15) B. Olsen and L. Boström, Nucl. Instr. **44** (1966) 65
16) A. H. Wapstra, G. J. Nijgh and R. van Lieshout, Nuclear spectroscopy tables (North-Holland Publ. Co., Amsterdam, 1959)
17) S. Wahlborn and I. Martinsson, Ark. Fys. **31** (1966) 355
18) R. A. Sorensen, Phys. Rev. **132** (1963) 2270
19) N. Freed and L. A. Kisslinger, Nucl. Phys. **A116** (1968) 401
20) L. A. Sliv and I. M. Band, α-, β- and γ-ray spectroscopy, ed. K. Siegbahn (North-Holland Publ. Co., Amsterdam, 1965)
21) S. Moszkowski, α-, β- and γ-ray spectroscopy, ed. K. Siegbahn (North-Holland Publ. Co., Amsterdam, 1965)
22) T. Suter, P. Reyes-Suter and T. R. Gerholm, Ark. Fys. **20** (1961) 183
23) J. Lindskog, T. Sundström, J. O. Lindström and P. Sparrman, Ark. Fys. **24** (1963) 161
24) G. Bäckström, O. Bergman and J. Burde, Nucl. Phys. **7** (1958) 263
25) A. Marelius, P. Sparrman and T. Sundström, HF interactions and nuclear transitions, ed. E. Matthias and D. Shirley
26) S. G. Malmskog, to be published
27) B. Svahn, A. Johansson, B. Nyman, G. Malmsten and H. Petterson, Z. Phys. **210** (1968) 466
28) J. R. Harris, G. M. Rothberg and N. Benczer-Koller, Phys. Rev. **138** (1965) B554
29) Nuclear Data Sheets, (National Academy of Sciences, Washington DC)
30) O. Nathan, Nucl. Phys. **30** (1962) 332

R E F E R E N C E 6

MESURES DE VIES MOYENNES D'ETATS EXCITES DANS LES LANTHANES 135 ET 133

V. BERG, J. LETESSIER, C. BOURGEOIS et R. FOUCHER
Institut de Physique Nucléaire, Orsay

Classification :
Physics Abstracts
12.17, 12.20

MESURES DE VIES MOYENNES D'ÉTATS EXCITÉS DANS LES LANTHANES 135 ET 133

V. BERG, J. LETESSIER, C. BOURGEOIS et R. FOUCHER
Institut de Physique Nucléaire, Orsay

(*Reçu le 28 avril 1972*)

Résumé. — Dans le cadre d'une étude systématique des noyaux de transition, les périodes des niveaux de 119,4 et 206,4 keV du ^{135}La ont été mesurées égales à 3,9 $\pm$ 0,1 et 0,48 $\pm$ 0,03 ns respectivement. Des valeurs limites ont été obtenues pour les périodes des niveaux de 265,3 keV, 299,8 keV du ^{135}La (< 0,12 ns) et du niveau de 97,2 keV du ^{133}La (< 0,10 ns). Les mesures ont été effectuées par des coïncidences retardées e-γ ou e-e, la sélection en énergie des électrons étant assurée par un double spectromètre Gerholm. Les probabilités de transition partielles déduites de ces mesures sont comparées aux prévisions théoriques, en particulier à celles d'un modèle unifié avec un couplage intermédiaire entre la particule et les vibrations de la surface du cœur.

Abstract. — In the frame of a systematic study of transitional nuclei, the half-lives of the 119.4 keV and 206.4 keV levels in ^{135}La have been measured and are found to be 3.9 $\pm$ 0.1 and 0.48 $\pm$ 0.03 ns respectively. Limits have been obtained for the levels at 265.3 keV and 299.8 keV of ^{135}La (< 0.12 ns) and for the 97.2 keV level of ^{133}La (< 0.10 ns). The measurements have been made with delayed e-γ and e-e coincidences, the electrons being selected by a double lens Gerholm spectrometer. The partial transition probabilities calculated from the measurements are compared with theoretical predictions, in particular with those of a unified model with intermediate coupling between a single odd particle and the surface vibrations of the core.

1. **Introduction.** — Cette étude se situe dans le cadre d'une étude systématique des noyaux de transition.

Les noyaux de lanthane 135 et 133 sont situés dans une région intermédiaire entre une région où les noyaux sont sphériques et une région où ils ont une déformation permanente. Le caractère « noyau de transition » ou « mou » des noyaux de cette région est d'autant plus sûr qu'il ressort à la fois des valeurs de B(E2) observées pour les transitions $2_1^+ \rightarrow 0_1^+$ des noyaux pairs-pairs, de l'existence d'états collectifs de basse énergie et des calculs de surfaces d'énergie potentielle, par exemple ceux faits par S. G. Nilsson et coll. [1].

Pour ces noyaux de transition, on s'attend à avoir une assez bonne représentation des caractéristiques nucléaires avec un modèle unifié. En utilisant un tel modèle avec un couplage intermédiaire entre la particule et les vibrations de la surface du cœur, N. Freed et W. Miles [2], ont fait récemment des calculs pour essayer de décrire les noyaux de lanthane. L'accord théorie-expérience pour les lanthanes 139 et 137 étant assez satisfaisant, il était intéressant d'avoir un ensemble de résultats expérimentaux concernant les lanthanes plus déficients en neutrons à comparer avec les prévisions de ce type de modèle. Comme maintenant les schémas de niveaux de basse énergie des ^{135}La, ^{133}La commencent à être bien établis par A. Abdul-Malek et R. A. Naumann [3], C. Gerschel [4] (Fig. 1) ; nous avons essayé de mesurer les vies moyennes des premiers états excités du ^{135}La et du premier état excité du ^{133}La par la méthode des coïncidences retardées e-e et e-γ à l'aide d'un double spectromètre magnétique Gerholm.

Au cours de ce travail, des résultats de mesures des vies moyennes des deux premiers niveaux du ^{135}La et du premier niveau du ^{133}La ont été publiées par Y. Nagai et coll. [5] et R. Babadzhanov et coll. [6] avec d'autres dispositifs expérimentaux ; leurs résultats ne sont pas cohérents.

Dans cet exposé nous donnons successivement la méthode de préparation des sources, une description succincte du dispositif expérimental utilisé et les résultats obtenus. Ensuite nous comparons les probabilités de transition partielles issues de nos mesures aux prévisions théoriques pour un modèle en couche sphérique, puis pour le modèle à couplage fort de S. G. Nilsson [7] en considérant le carré moyen de la déformation pour vérifier qu'il n'apparaît encore aucune déformation permanente dans ces lanthanes et enfin pour le modèle à couplage intermédiaire entre la particule et les vibrations de la surface du cœur de D. C. Choudhury et T. F. O'Dwyer [8].

2. **Préparation de la source.** — Pour produire les ^{133,135}Ce, nous irradions le La métal au synchrocyclotron d'Orsay :

^{139}La(p 95 MeV, 7 n)^{133}Ce et

^{139}La(p 87 MeV, 5 n)^{135}Ce .

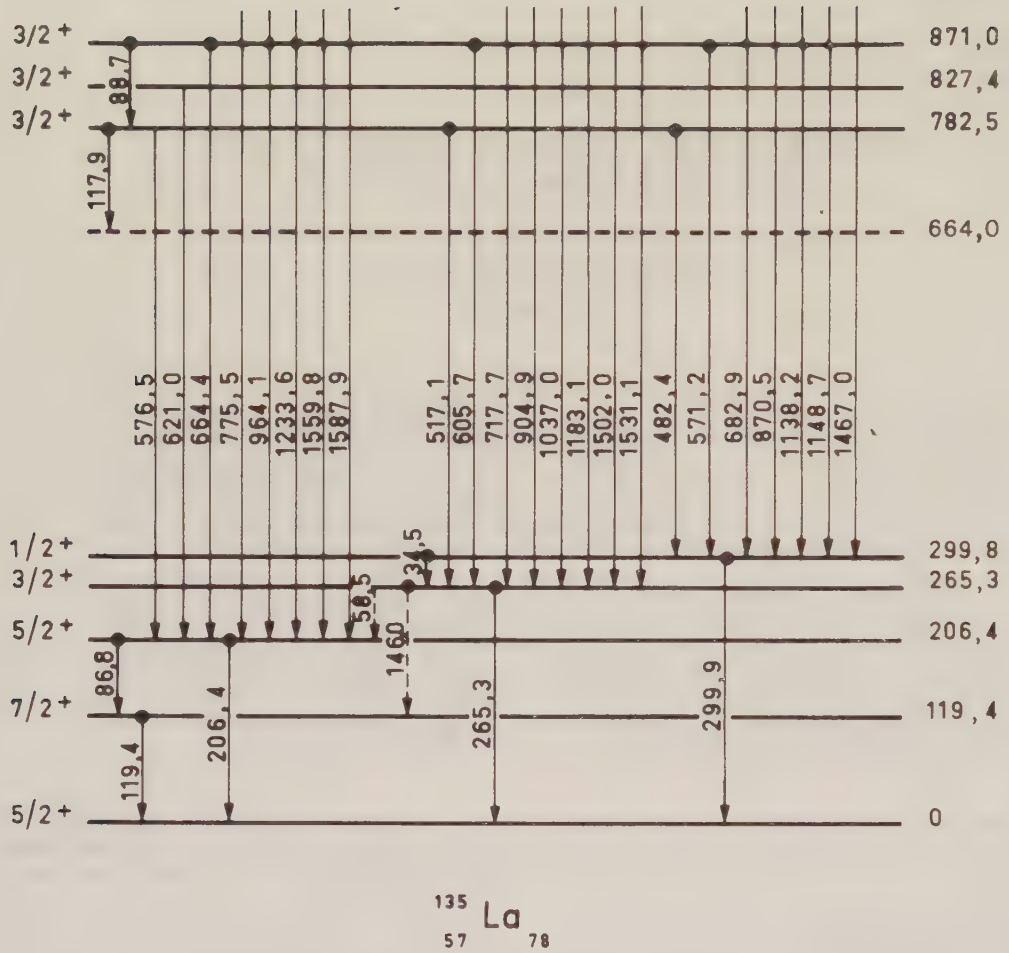

FIG. 1*a*. — Schéma de niveaux partiel extrait du schéma de niveaux proposé par A. Abdul-Malek et R. A. Naumann [3]. (Nos mesures sont en faveur de ce schéma et semblent infirmer l'autre solution proposée par les auteurs quant à la position de la transition de 34,5 keV.)

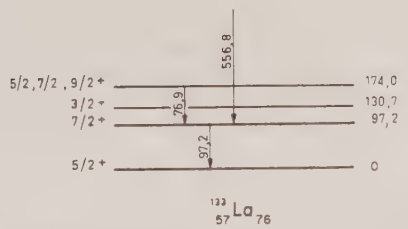

FIG. 1*b*. — Schéma de niveaux partiel extrait du schéma de niveaux proposé par C. Gerschel [4].

Des sources isotopiquement pures sont obtenues au séparateur électromagnétique d'isotopes de l'institut ; les ions Ce sont collectés sur des feuilles d'aluminium de 10 μ : ainsi les électrons de basse énergie peuvent traverser le support, ce qui permet les coïncidences e-e.

3. **Dispositif expérimental.** — Les mesures ont été effectuées par une méthode de coïncidences retardées e-e ou e-γ.

3.1. MESURES PAR COÏNCIDENCES e-e. — La discrimination des électrons est faite par un double spectromètre Gerholm [9] dont la résolution en impulsion a été prise égale à 3 % pour ces mesures. Pour faciliter les mesures, en particulier en ce qui concerne la comparaison des courbes retardées avec les courbes promptes, les électrons peuvent être accélérés par une tension variable de 0 à 20 kV. Les détecteurs utilisés sont des scintillateurs plastiques SPP RADIOTECHNIQUE, coniques couplés à des photomultiplicateurs 56 DVP par l'intermédiaire de guides de lumière. L'électronique associée aux détecteurs comprend : pour les coïncidences rapides, des discriminateurs à fraction constante d'amplitude SAIP 7043 et un convertisseur temps-

amplitude ORTEC 437 ; pour les coïncidences lentes un système classique ORTEC (Fig. 2).

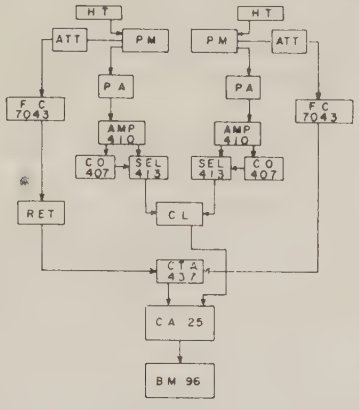

FIG. 2. — Schéma synoptique du dispositif expérimental.

3.2 MESURES PAR COÏNCIDENCES e-γ. — Les rayonnements γ sont détectés par leur effet Compton dans un scintillateur plastique, SPP, cylindrique, placé à 15 mm de la source. Par ailleurs, l'ensemble utilisé est identique à celui décrit précédemment.

4. **Mesures.** — Nous avons mesuré les périodes des niveaux de 119,4 et 206,4 keV du ^{135}La et pu donner des valeurs limites pour les périodes des niveaux de 265,3 et 299,8 keV du ^{135}La et du niveau de 97,2 keV du ^{133}La (Fig. 1). Chaque fois que c'était possible, nous avons fait les mesures à partir de coïncidences retardées e-e, car nous sélectionnons ainsi beaucoup mieux les transitions qui alimentent et désexcitent le niveau qui nous intéresse et nous nous affranchissons des fonds parasites inévitables et sources d'erreur qui existent dans les spectres γ. Les courbes de coïncidences retardées sont analysées par un programme utilisant la méthode des produits de convolution et la méthode du déplacement du centre de gravité (moment d'ordre 1) affinée par le calcul des moments d'ordre 2 et 3 [10].

4.1 NIVEAU DE 119,4 keV. — On a observé les coïncidences entre les électrons K des raies de 86,8 keV qui alimente le niveau et de 119,4 keV qui le désexcite. Pour obtenir une courbe rapide dans les mêmes conditions à partir d'une source de ^{144}Ce(β-e$_k$ (133 keV)), nous devons appliquer une tension d'accélération de 10 keV aux électrons issus de la source de La.

L'analyse de la courbe retardée obtenue (Fig. 3) nous donne :

$$T_{1/2} = (3{,}9 \pm 0{,}1)\ \text{ns}\ .$$

Les mesures de Y. Nagai et coll. [5] et de R. Babadzhanov et coll. [6] donnent pour ce niveau 4,1 $\pm$ 0,1 ns et 1,54 $\pm$ 0,15 ns respectivement.

Dans nos conditions de mesure, nous ne pouvons pas éliminer complètement les coïncidences parasites

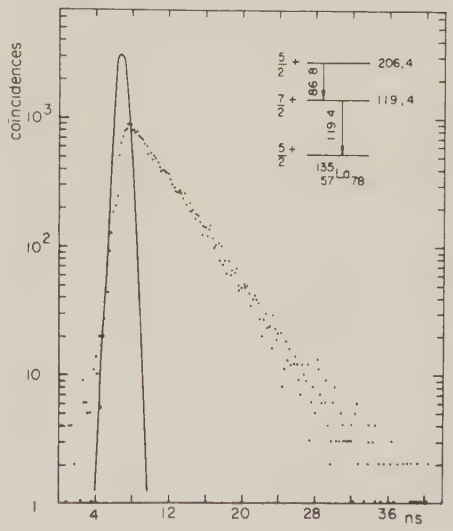

FIG. 3. — $T_{1/2}$ = (3,9 $\pm$ 0,1) ns pour le niveau de 119,4 keV du ^{135}La.

entre les électrons K de la transition de 88,7 keV et de la transition de 117,9 keV. Toutefois, elles sont négligeables, l'intensité de la raie de 117,9 keV en coïncidence avec la transition de 88,7 keV étant faible [3] devant l'intensité de la raie de 119,4 keV en coïncidence avec la raie de 86,8 keV.

Pour les autres niveaux du ^{135}La, la mesure en coïncidence e-e n'était pas possible. En effet, pour les niveaux 206,4 et 299,8 keV, aucune des transitions intenses, qui alimentent directement le niveau, n'est suffisamment convertie ; pour le niveau de 265,3 keV la transition de 34,5 keV, seule transition intéressante, donne des électrons de conversion dont l'énergie est très voisine de celle des électrons Auger.

4.2 NIVEAU DE 206,4 keV. — Les coïncidences sont observées entre les électrons Compton de 200 à 500 keV des rayonnements γ qui alimentent le niveau et les électrons K de la raie de 206,4 keV. La courbe rapide est obtenue avec une source de ^{60}Co(β-γ) dans les mêmes conditions expérimentales.

L'analyse de la courbe retardée (Fig. 4) donne :

$$T_{1/2} = (0{,}48 \pm 0{,}03)\ \text{ns}\ .$$

La mesure de Y. Nagai et coll. [5] donne pour ce niveau

$$T_{1/2} = (0{,}59 \pm 0{,}04)\ \text{ns}\ .$$

4.3 NIVEAUX DE 265,3 ET 299,8 keV. — Pour ces mesures, les conditions sont identiques à celles énoncées au paragraphe précédent, mais avec les électrons K des raies de 265,3 et 299,8 keV. Dans les deux cas, une comparaison avec des courbes rapides obtenues avec une source de ^{60}Co dans les mêmes conditions expérimentales nous permet seulement de donner une valeur limite : $T_{1/2} \leqslant 0{,}12$ ns.

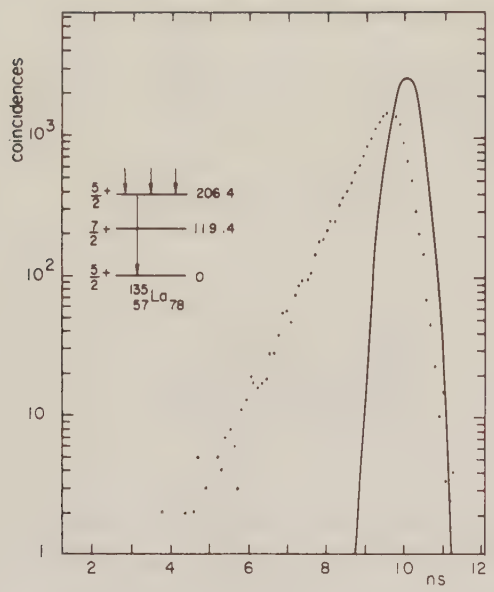

FIG. 4. — $T_{1/2} = (0{,}48 \pm 0{,}03)$ ns pour le niveau de 206,4 keV du ^{135}La.

4.4 NIVEAU DE 97,2 keV DU ^{133}La. — Nous avons observé les coïncidences entre les électrons L de la raie de 76,9 keV et les électrons K de la raie de 97,2 keV avec une accélération de 20 kV. La comparaison de la courbe de coïncidences retardées avec une courbe rapide obtenue avec une source de ^{144}Ce dans les mêmes conditions nous permet de donner une limite de la période de ce niveau :

$$T_{1/2} \leqslant 0{,}1 \text{ ns} .$$

5. **Calcul des facteurs d'interdiction.** — Les probabilités de transition partielles P_{exp} M1 et E2 pour les transitions de 119,4, 206,4 et 86,8 keV sont calculées à partir des périodes que nous avons mesurées, des intensités relatives mesurées par A. Abdul-Malek et coll. [3], des rapports de mélange donnés par Y. Nagai et coll. [5] et des coefficients de conversion calculés en utilisant les tables de R. S. Hager et E. G. Seltzer [11].

Nous avons comparé les résultats obtenus avec les calculs théoriques suivants :

1) A partir du modèle à particule indépendante dans un potentiel moyen sphérique (S. A. Moszhowski [12]) avec un facteur statistique $S = 1$.

2) A partir du modèle unifié avec un couplage fort (S. G. Nilsson [7]) en supposant une petite déformation permanente du noyau, $\varepsilon = 0{,}15$. Les fonctions d'onde utilisées sont celles calculées par R. Piepenbring [13] avec le programme de I. L. Lamm [14] pour les paramètres donnés par C. Gustafson et coll. [15].

3) A partir du modèle unifié avec un couplage intermédiaire entre la particule et les vibrations de la surface du cœur (D. C. Choudhury et T. F. O'Dwyer [8]) avec les fonctions d'onde données par N. Freed et W. Miles [2] qui sont de la forme suivante :

$$| \Psi_I > = \sum_{N,R} [a \mid d_{5/2}, NR >_I + b \mid g_{7/2}, NR >_I]$$

N est le nombre de phonons limité à 2,
R est le spin du phonon considéré,
I est le spin de l'état.

Dans ce calcul, quatre paramètres interviennent : la force de couplage, l'énergie d'excitation du phonon, la déformabilité de la surface nucléaire et la distance en énergie des niveaux $d_{5/2}$ et $g_{7/2}$. Ces paramètres sont ajustés à partir de résultats expérimentaux (*).

Pour ces trois cas, nous avons calculé les facteurs d'interdiction $F = \dfrac{\text{Probabilité théorique}}{P_{exp}}$. Les valeurs obtenues sont données dans les colonnes 8, 9 et 10 du tableau I. Nous portons également dans ce tableau les valeurs obtenues précédemment par d'autres auteurs sur les premiers états excités du ^{139}La d'une part et du ^{137}La d'autre part.

6. **Discussion.** — 6.1 MODÈLE DES COUCHES SPHÉRIQUES. — Dans ce modèle, les deux premiers états des La sont décrits comme les états de particule $d_{5/2}$ et $g_{7/2}$ ce qui conduit à une transition M1 7/2 → 5/2 interdite l ($\Delta l = 2$). En fait, on s'attend à trouver seulement un retard appréciable de la transition M1 par rapport à une transition M1 7/2 → 5/2 supposée sans interdiction l. C'est effectivement ce qu'on a observé (colonne 8 du tableau). Le caractère de particule indépendante est donc qualitativement valable. Peut-on maintenant interpréter quantitativement les résultats avec un modèle à couplage fort en supposant une déformation moyenne ou avec un modèle à couplage intermédiaire entre la particule et les vibrations de la surface du cœur ?

Les surfaces d'énergie potentielle calculées à partir du programme de Nilsson et Ragnarsson [1] montrent que plus les lanthanes deviennent déficients en neutrons plus ils tendent à devenir mous ; cette tendance existe également dans les noyaux pairs-pairs voisins (Ce et Ba). Il est donc probable qu'un modèle du type modèle unifié à couplage intermédiaire soit plus représentatif des noyaux de La de cette région qu'un modèle à couplage fort (sauf si pour un état donné la déformation du noyau était particulièrement grande et stable). Il faut regarder jusqu'à quel point un modèle à couplage fort tel que celui de Nilsson permettrait d'interpréter les résultats expérimentaux. Par ailleurs, il est intéressant de voir si l'accord théorie-expérience

(*) Pour tous les détails concernant ce modèle nous renvoyons à la référence [8] dans laquelle les calculs sont très clairement exposés.

TABLEAU I

A	E_{niveau}	$E_{transition}$	$T_{1/2}$	Transition	Nature	P_{exp}	F_M	F_C	$F_N(a)$	$F_N(b)$
139	166	166	1,47 ns	$5/2^+ \rightarrow 7/2^+$	M1	$3,74 \times 10^8$	352	0,27	4,6	
					E2 (*c*)		> 4,4	> 193		
137	10	10	89 ns	$5/2^+ \rightarrow 7/2^+$	M1	$5,7 \times 10^4$	507	0,77	6,1	
135	119,4	119,4	3,9 ns	$7/2^+ \rightarrow 5/2^+$	M1	$1,04 \times 10^8$	475	1,12	3,9	0,039
					E2	$4,33 \times 10^6$	0,288	0,62	0,094	20
					(4 %)					
	206,4	206,4	0,48 ns	$5/2^+ \rightarrow 5/2^+$	M1	$9,02 \times 10^8$	283		7,1	
					E2	$7,83 \times 10^7$	0,246		$2,3 \times 10^{-4}$	
					(8 %)					
		86,8	0,48 ns	$5/2^+ \rightarrow 7/2^+$	M1	$7,45 \times 10^7$	254		0,275	2,6
					E2	$3,19 \times 10^7$	$7,9 \times 10^{-3}$		$2,5 \times 10^{-5}$	$1,0 \times 10^{-5}$
					(30 %)					

$$F_x = \frac{P_{théorique}}{P_{expérimentale}}$$

x = *M* S. A. Moszkowski
x = *C* D. C. Choudhury et T. F. O'Dwyer
x = *N* S. G. Nilsson.

a) en attribuant l'état $5/2^+$ [413] au niveau fondamental, l'état $7/2^+$ [404] au niveau de 119,4 keV, l'état $5/2^+$ [402] au niveau de 206,4 keV du ^{135}La et les états $5/2^+$ [413] et $7/2^+$ [404] aux niveaux considérés dans les lanthanes 137 et 139,

b) en attribuant l'état 7/2 $5/2^+$ [413] au niveau de 119,4 keV,

c) ce résultat est pris dans la table des isotopes C. M. Lederer, J. M. Hollander, I. Perlman.

s'améliore pour des noyaux de lanthane de plus en plus déficients en neutrons ce qui correspondrait à l'apparition d'une déformation permanente à basse énergie.

6.2 MODÈLE DE NILSSON. — Les valeurs de la déformation ε sont identifiées aux valeurs des paramètres β_{rms} tirés des B(E2) des transitions $2_1^+ \rightarrow 0_1^+$ (K. Kumar et M. Baranger [16] et [17]) des noyaux pairs-pairs voisins. Ces valeurs variant de 0,10 à 0,17 dans la région nous avons utilisé pour tous nos calculs : $\varepsilon = 0,15$.

On voit dans la colonne 10 que l'accord théorie-expérience est satisfaisant pour les transitions M1. Les résultats concernant les transitions E2 montrent qu'elles ont un caractère collectif, mais que le $7/2^+$ n'est quand même pas un niveau rotationnel : il semble bien que le noyau de ^{135}La ne présente encore aucune déformation permanente.

6.3 MODÈLE A COUPLAGE INTERMÉDIAIRE. — On voit dans la colonne 9 du tableau I que l'accord théorie-expérience est très satisfaisant en ce qui concerne les transitions M1 entre le premier état excité et le fondamental. Ce résultat n'est pas surprenant puisque la transition M1 entre les composantes principales $| d_{5/2}\, 0\, 0 >_{5/2}$ et $| g_{7/2}\, 0\, 0 >_{7/2}$ des fonctions d'onde qui décrivent les états considérés est interdite et que seules les petites composantes des fonctions d'onde contribuent à ces transitions M1.

Pour la partie E2 de la transition de 119,4 keV du ^{135}La, nous avons également un accord très satisfaisant ; par contre, pour la transition partielle E2 dans le ^{139}La, comme on pouvait s'y attendre étant donné le caractère semi-magique de ce noyau, l'accord est moins bon que pour un modèle en couche sphérique.

Dans ce modèle, l'interaction résiduelle à courte portée entre les nucléons est négligée, et les états $d_{3/2}$ et $s_{1/2}$ ne sont pas considérés alors que les calculs faits par L. S. Kisslinger et R. A. Sorensen [18] montrent que les composantes $| d_{3/2},\ 12 >$ et $| s_{1/2},\ 12 >$ ne sont pas toujours négligeables devant les composantes $| d_{5/2},\ 12 >$ et $| g_{7/2},\ 12 >$.

Toutefois, nous avons un bon accord théorie-expérience, car l'essentiel des phénomènes négligés est inclus par l'intermédiaire du processus utilisé pour l'ajustement des paramètres. Malheureusement ce calcul [8] n'a été effectué que pour le couplage des particules $d_{5/2}$ et $g_{7/2}$ avec le cœur ; aussi il ne peut pas prévoir tous les états vus expérimentalement.

6.3 CAS DU ^{133}La. — Pour la période du niveau $7/2^+$ de 97,2 keV du ^{133}La, nous attendions une valeur de l'ordre de 4 ns par comparaison avec les périodes du 1er niveau excité $7/2^+$ ou $5/2^+$ dans les autres isotopes du La. La valeur trouvée $T_{1/2} \leqslant 0,1$ ns semble indiquer que le niveau $7/2^+$ de 97,2 keV n'est pas analogue au niveau $7/2^+$ observé dans les autres Lanthanes. Ce problème est actuellement étudié en collaboration avec M^{me} C. Gerschel et fera l'objet d'une publication ultérieure.

7. **Conclusion.** — Nos conclusions peuvent se résumer ainsi :

1) Il semble bien qu'on ne voit apparaître aucune déformation permanente dans le ^{135}La, ce qui est en accord avec les prévisions des surfaces potentielles calculées avec le programme de Nilsson, mais toutefois que les probabilités de transition M1 entre les états de particules sont assez bien prévues à l'aide de ce modèle.

2) Bien que le modèle de R. C. Choudhury et T. F. O'Dwyer soit très approximatif, nous avons

montré qu'il rendait bien compte des probabilités de transitions M1 et E2 de 119,4 keV dans le ^{135}La et il serait intéressant de voir dans quelle mesure il continue à bien représenter les noyaux encore plus déficients en neutrons.

Remerciements. — Nous remercions très sincèrement l'équipe du séparateur d'isotopes, en particulier MM. A. Ferro, J. Fournet et J. Obert, pour leur concours dévoué lors de la réalisation des sources.

Nous remercions également très vivement l'équipe d'électronique, en particulier MM. G. Corbe, G. Landois, et A. Richard, qui ont assuré avec compétence la mise au point délicate de l'électronique rapide.

Bibliographie

[1] Nilsson (S. G.), Tsang (C. F.), Sobiczewski (A.), Szymanski (Z.), Wycech (S.), Gustafson (C.), Lamm (I. L.), Möller (P.), Nilsson (B.), *Nucl. Phys.*, 1969, **A 131**, 1.
Ragnarsson (I.), *Proceedings*, Leysin, 1970, 847.
[2] Freed (N.) et Miles (W.), *Nuovo cimento*, 1969, **LXB**, 301.
[3] Abdul-Malek (A.) et Naumann (R. A.), *Phys. Rev.*, 1968, **166**, 1194.
[4] Gerschel (C.), *Nucl. Phys.*, 1968, **A 108**, 337.
[5] Nagai (Y.), Akiba (M.) et Hisatake (K.), *J. Phys. Soc. Japan*, 1970, **29**, 790.
[6] Babadzhanov (R.), Morozov (V. A.), Muminov (T. M.), Razov (V. J.), Khalikalov (A. B.), J INR/P6, 1970, 5200.
[7] Nilsson (S. G.), *Mat. Fys. Medd. Dan. Vid. Selsk.*, 1955, **29**, 16.
[8] Choudhury (D. C.) et O'Dwyer (T. F.), *Nucl. Phys.*, 1967, **A 93**, 300.
[9] Gerholm (T. R.) et Lindskog (J.), *Ark Fys.*, 1963, **24**, 171.
Malmskog (S. G.), *Ark. Fys.*, 1967, **35**, 255.
[10] Olsen (B.) et Brostrom (L.), *Nucl. Inst.*, 1966, **44**, 153.
[11] Hager (R. S.) et Seltzer (E. G.), Int. Conv. Tables, Cal. Inst. of Tech., Pasadena, 1967.
[12] Moszkowski (S. A.) α, β and γ spectroscopy, ed. K. Siegbahn, North Holland, Amsterdam, 1965, Ch. 15.
[13] Piepenbring (R.), Communication privée.
[14] Lamm (I. L.), *Nucl. Phys.*, 1969, **A 125**, 504.
[15] Gustafson (C.), Lamm (I. L.), Nilsson (B.), Nilsson (S. G.), *Ark. Fys.*, 1967, **36**, 613.
[16] Kumar (K.) et Baranger (M.), *Nucl. Phys.*, 1968, **A 122**, 273.
[17] Kumar (K.), *Proceedings*, Leysin, 1970, 779.
[18] Kisslinger (L. S.) et Sorensen (R. A.), *Rev. Mod. Phys.*, 1963, **35**, 853.

R E F E R E N C E 7

A STUDY OF THE 190 keV TRANSITION IN ^{141}La

V. BERG and A. HOGLUND

Institute of Physics, University of Stockholm and AB Atomenergi, Studsvik, Nyköping, Sweden,

B. FOGELBERG

Institute of Physics, Uppsala University, and The Swedish Research Council's Laboratory, Studsvik,

Nyköping, Sweden

3.A

Nuclear Physics A155 (1970) 297—305; © *North-Holland Publishing Co., Amsterdam*

Not to be reproduced by photoprint or microfilm without written permission from the publisher

A STUDY OF THE 190 keV TRANSITION IN ^{141}La

V. BERG and Å. HÖGLUND

Institute of Physics, University of Stockholm and AB Atomenergi, Studsvik, Nyköping, Sweden

B. FOGELBERG

Institute of Physics, Uppsala University, and The Swedish Research Council's Laboratory, Studsvik, Nyköping, Sweden

Received 5 May 1970

Abstract: The γ-ray spectrum from the decay of 18 min ^{141}Ba has been studied. Seventeen transitions were found below 900 keV, with energies and (intensities) as follows: 112.9±0.2(3.0), 163.1±0.3 (1.0), 165.7±0.4(0.7), 180.5±0.2(0.9), 190.3±0.1(100), 276.9±0.1(52.2), 304.2±0.1(55.8), 343.6±0.1(30.8), 364.4±0.6(1.6), 389.7±0.2(2.8), 457.7±0.2(10.4), 462.3±0.2(10.5), 467.3±0.1 (11.4), 625.1±0.2(6.1), 647.9±0.2(10.7), 739.1±0.3(8.7) and 876.5±0.3(6.7). The K- and L-shell conversion coefficients have been measured for the 190.3 keV transition, yielding a multipolarity of M1+ <8% E2. Half-life measurements using a delayed coincidence technique have given the following results: $T_{\frac{1}{2}}$ (190 keV level) = $1.27^{+0.06}_{-0.10}$ ns, $T_{\frac{1}{2}}$ (304 keV level) <200 ps, $T_{\frac{1}{2}}$ (467 keV level) <120 ps. A level scheme of ^{141}La has been constructed, and the spin-parity assignments of the ground state and first excited state are discussed in terms of the shell model.

E RADIOACTIVITY ^{141}Ba[from ^{232}U(n, f)]; measured E_γ, I_γ, E_{ce}, I_{ce}, α_K, βce-delay. ^{141}La deduced levels, partial $T_{\frac{1}{2}}$, γ-multipolarity.

1. Introduction

The decay properties of fission-produced ^{141}Ba were first studied in detail by Fritze and Kennett [1]) in 1962. Thanks to a new method they had succeeded in obtaining ^{141}Ba sources free from ^{142}Ba. Single γ-ray measurements, $\gamma\gamma$ and $\beta\gamma$ coincidence experiments, using NaI(Tl) and plastic scintillators, permitted them to construct a level scheme for ^{141}La. Later Alväger *et al.* [2]) measured the γ-ray spectrum following the decay of ^{141}Ba using Ge(Li) detectors in on-line studies of mass-separated xenon fission products. More accurate energy assignments led them to propose a tentative decay scheme, meant to be tested in future coincidence experiments. The two level schemes are rather alike, the most important difference being that Alväger *et al.* propose a new level at 100.9 keV.

The present work deals with the low-energy spectrum of ^{14}La and is specially directed on the 190 keV ground state transition. It includes γ-ray, internal conversion and half-life measurements connected with this particular transition.

2. Experimental procedure

2.1. SOURCE PREPARATION

Sources for all the experiments were obtained from the on-line mass separator of fission fragments at Studsvik [3]).

2.2. GAMMA-RAY SPECTROSCOPY

The γ-ray spectrum below 900 keV following the decay of 18 min ^{141}Ba was investigated with a 2.3 cm^3 Ge(Li) detector, giving a resolution of 2.3 keV (FWHM) at 662 keV, and was recorded and analysed with a PDP-9 computer. The sources, collected during 15 min, were left to decay for 5 min before measurements were started. In this way the short lived precursors of barium in the 141 mass chain, i.e.

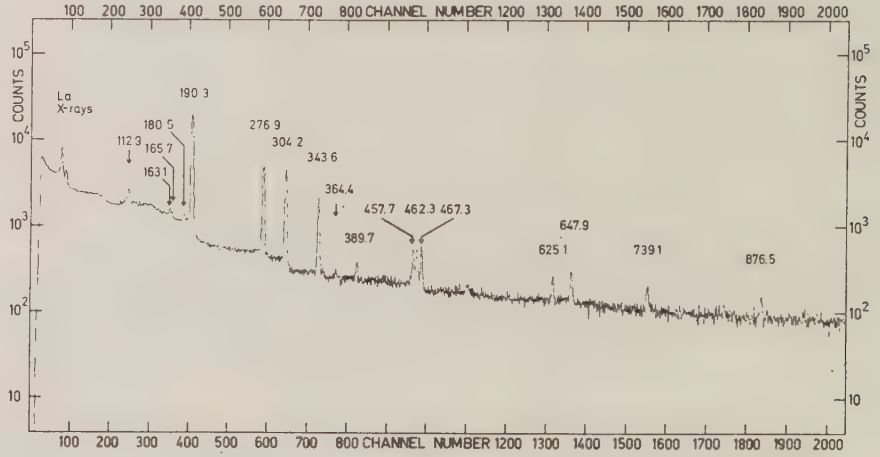

Fig. 1. Gamma-ray spectrum below 900 keV following the decay of ^{141}Ba.

2 s Xe and 24 s Cs [ref. [4])], had time to disintegrate. In order to check the identity of the γ-lines, two consecutive measurements, each lasting about 30 min were performed with the same source. Energy and intensity calibrations were made using standard sources from IAEA, Vienna. Fig. 1 shows one spectrum and table 1 gives the energies and intensities of the gamma rays together with the corresponding results of earlier measurements. The two transitions at 89.7 and 100.9 keV, which should define the new level proposed by ref. [2]), did not appear with expected strength and we conclude that the 100.9 keV level does not exist. Twelve transitions could be arranged to fit in a level scheme (fig. 2), which is similar to the one constructed by Fritze and Kennett as a result of coincidence experiments. The 112.9 keV transition could not be placed in the scheme. A further study of this transition was made in the half-life experiments.

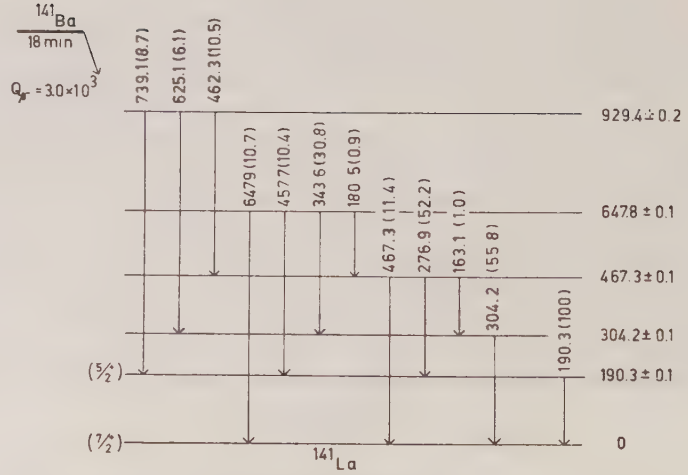

Fig. 2. Low-energy levels in ^{141}La.

TABLE 1

Energies and intensities of γ-rays below 900 keV in the decay of ^{141}Ba

Fritze and Kennett [1])		Alväger *et al.* [2])		Present work	
energy (keV)	intensity	energy (keV)	intensity	energy (keV)	intensity
		89.7±2.0	2.3±1.2		<0.4
		100.9±1.5	6.4±3.2		<0.6
		113.4±1.5	2.5±1.3	112.9±0.2	3.0±1.0
				163.1±0.3	1.0±0.2
				165.7±0.4	0.7±0.2
				180.5±0.2	0.9±0.2
193±6	100	190.4±1.5	100 ±15	190.3±0.1	100 ±5
276±8	50	277.2±1.5	49.0±15	276.9±0.1	52.2±4.0
307±9	60	304.7±1.5	55.1±8.3	304.2±0.1	55.8±5.0
348±10	20	344.3±1.5	28.1±5.6	343.6±0.1	30.8±3.0
				364.4±0.6	1.6±0.5
				389.7±0.2	2.8±0.5
		460	34.1±6.8	457.7±0.2	10.4±1.5
460±14	30			462.3±0.2	10.5±1.5
		468.2±1.5	17.8±3.6	467.3±0.1	11.4±1.5
				625.1±0.2	6.1±1.1
640±19	20	647.7±1.5	21.1±4.2	647.9±0.2	10.7±1.6
730±22	7			739.1±0.3	8.7±1.5
860±26	6			876.5±0.3	6.7±1.2

2.3. INTERNAL CONVERSION ELECTRON MEASUREMENTS

A double focussing, iron-yoke β-spectrometer of the Siegbahn-Svartholm type [5]) was used to record the K- and L-lines of the 190 keV transition in ^{141}La. The activity was collected on a rather thick Al backing, which was transported to the β-spectrometer by means of a rabbit system. Measurements could be started less than one minute after the end of the mass separation.

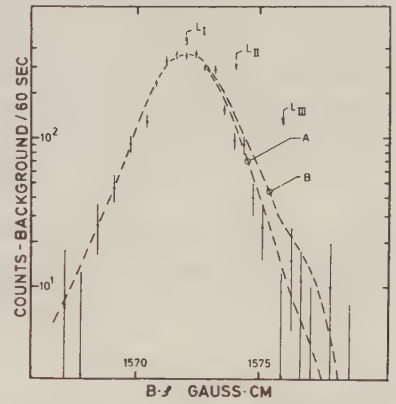

Fig. 3. Semilogarithmic plot of the L-line of the 190 keV transition in ^{141}La. Experimental points are shown together with constructed line profiles for a) a pure M1, and b) a M1+5 % E2 transition. The shape of a single conversion line is known from the K-line of the 190 keV transition. Arrows indicate the calculated positions of lines from the different L-subshells.

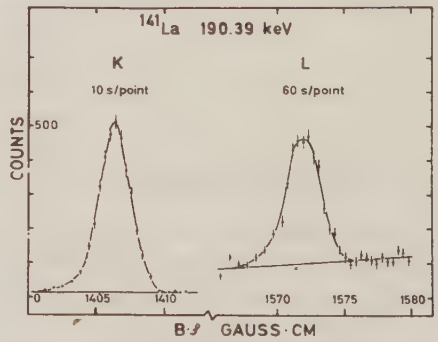

Fig. 4. Conversion electron lines of the 190 keV transition. The points have been corrected for decay, which gives rise to the slope of the background at the L-line.

A resolution of 0.2 % FWHM was employed and the precision in measuring and regulating the magnetic field of the spectrometer was better than one part in 10^4. By use of the known difference in electron binding energies it was possible to determine the transition energy from the K to L distance. The small relative energy separation

gave rise, in this case, to a rather large error. The value obtained was 190.39±0.20 keV, which agrees well with the γ-ray measurement.

The K-shell conversion coefficient was measured by a comparison method, i.e. the K-conversion line of the 190 keV transition and the K-line of the isomeric transition emitted in the decay of ^{137m}Ba were measured under equivalent conditions. A carefully calibrated Ge(Li) detector was then used to record the corresponding γ-rays. From the measured intensities, conversion coefficients were calculated and compared with the value given for the ^{137m}Ba line in ref. [4]) and with the theoretical values of Hager and Seltzer [6]). A multipolarity of M1 or E2 was established in this way.

To determine possible admixtures of these multipolarities a special run of the K and L lines was performed, as the K/L ratio is rather sensitive to the E2 part of a mixed transition. The resolution was not sufficient to separate the L-group into distinct lines. The distance between the L_I and L_{III} lines is, however, larger than the employed resolution of 0.2 % and the general structure of the L-group can thus give some indications on the L sub-shell ratios. Fig. 3 shows the experimental L-line together with constructed L-group profiles for two different multipole admixtures. The upper limit of 8 % E2 given by the K/L ratio is confirmed by this study of the L-group.

TABLE 2

Results of the internal conversion electron measurements on the 190 keV transition in ^{141}La

Transition energy (keV)	Shell	Relative intensity	Conversion coefficient × 10^2 exp.	theory [a]) M1	theory [a]) E2	Multipole assignment
190.39±0.20	K	100	16.9 ±1.5	15.6	16.2	M1+<8 % E2 from K/L-ratio and L-line structure
	L	12.3±1.2	2.08±0.3	2.06	3.95	

[a]) Theoretical values of conversion coefficients are taken from the work of Hager and Seltzer [6]).

The experimental findings are summarized in table 2 below. Fig. 4 shows the K- and L-lines of the 190 keV transition in ^{141}La.

2.4. HALF-LIFE MEASUREMENTS

A magnetic coincidence spectrometer earlier described in refs. [7,8]) was used for the half-life measurements. In order to increase the coincidence rate, one of the lenses was replaced by a 3 mm × 20 mm ∅ cylindrical plastic scintillator mounted on a 56 DVP photomultiplier and placed 2.5 cm from the source.

The mass-141 ions were collected on 10 mg/cm^2 Al foils during periods of approximately 20 min, and the experiments were started about 5 min after the separation in order to avoid the short-lived precursors of barium. The decay of the ingrowing 3.9 h ^{141}La could not interfere with the measurements, as 98 % of the β-decay feeds the ground state and the remaining 2 % a high-energy transition in 33 d ^{141}Ce [ref. [4])].

From ref. [1]) we know that the 190.3 keV level is fed by a strong β-branch and the experiment was arranged to measure beta-electron coincidences. The spectrometer lens, giving 3 % momentum resolution, was set to select the 190.3 K-electrons, while the windows in the scintillator channel admitted pulses within a rather wide energy range (600–1000 keV). The time resolution is not much affected by this arrangement, because the time spread due to difference in rise time is small when the pulses are high. The delayed time distribution in fig. 5 is the results of one of our measurements.

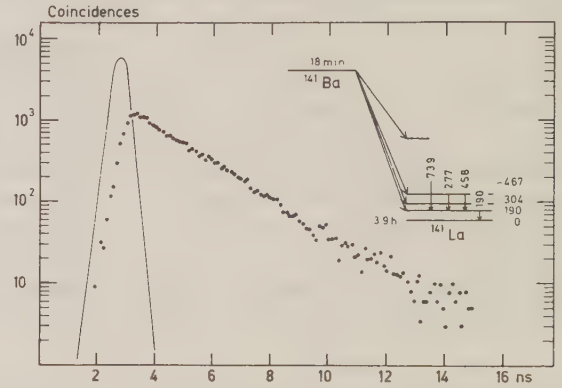

Fig. 5. Delayed coincidence curve taken between 0.6–1.0 MeV β-particles and 190 K conversion electrons. The prompt comparison curve was obtained with a ^{60}Co source. The half-life of the 190 keV level in ^{141}La was found to be $1.27^{+0.06}_{-0.10}$ ns.

The prompt curve is due to a ^{60}Co source, measured with identical settings. Beta particles of the same energy as 190.3 K were then transferred by the spectrometer lens, while Compton events due to the strong ^{60}Co γ-rays were recorded with the scintillator. To avoid unduly high counting rate, a 2 mm thick shield of aluminium protected the scintillator from β-particles. The prompt spectrum gave the time resolution and was used in this case for the analysis of the delayed curve according to the convolution method [9]). The time shift measured is not quite significative of the 190.4 keV level, as the β-particles recorded in the scintillator channel come from different branches and contributions owing to the lifetimes of higher levels are added. The constant slope of the delayed curve shows that such contributions are small. To form an estimate of one of them, the half-life of the 467 keV level was measured. The scintillator channel was then kept unchanged while the spectrometer was focused on the 277 K electrons. Before and after the measurements ^{60}Co spectra were recorded. The shape of the time distributions and the centroid shifts set the following limit, in which also the influence of βγ coincidences has been taken into consideration:

$$T_{\frac{1}{2}}(467 \text{ keV level}) < 120 \text{ ps}.$$

It is worth noting that, with the method used, this limit also includes contributions from higher levels. With the use of the above result and available decay data, corrections to the β-190 K time shift were estimated. They proved to be small and were included in the errors. As result we obtained

$$T_{\frac{1}{2}}(190.3 \text{ keV level}) = 1.27^{+0.06}_{-0.10} \text{ ns}.$$

The half-lives of the 304 keV level and of the level which is depopulated by the 112.9 keV transition were measured using the same technique. In both cases a half-life <0.2 ns was found.

3. Calculations and discussion

The results of the internal conversion and half-life measurements make it possible to calculate the partial M1 and E2 half-lives of the 190.3 keV transition. In table 3 these quantities are given together with the hindrance factor F_W, which compares the transition rates with the single-particle or Weisskopf estimate [10]).

TABLE 3

Experimental information on the 190 keV transition in ^{141}La

Level (keV)	$T_{\frac{1}{2}}$ (exp) level (sec)	Transition energy (keV)	Multi-polarity	Relative N_γ	Relative N_e	$T_{\frac{1}{2}\gamma}$(exp.) (sec)	$F_W = \frac{T_{\frac{1}{2}}(\text{exp.})}{T_{\frac{1}{2}}W}$
190.3	$(1.27^{-0.06}_{+0.10}) \times 10^{-9}$	190.3	M1	>92	20	$(1.40 < T_{\frac{1}{2}} < 1.73) \times 10^{-9}$	$415 < F_W < 524$
			E2	< 8		$> 1.7 \times 10^{-8}$	> 0.33

The ground state spin of ^{141}La has not been measured but information about it might be obtained from systematics. The La isotopes follow the usual trend of nuclei with odd proton number over 50 where the $g_{\frac{7}{2}}$ and $d_{\frac{5}{2}}$ orbits are filled in. As long as the neutron number is sufficiently far from 82 to permit slow vibrations, the $d_{\frac{5}{2}}$ state is suppressed compared with $g_{\frac{7}{2}}$ and even appears as ground state. When more neutrons are added, the phonon interaction gets weaker, the level order changes, and the distance due to almost pure quasiparticle states appears, when the neutron shell is filled. In La the change of ground state from $\frac{5}{2}$ to $\frac{7}{2}$ takes place, when the neutron number goes from 78 to 80. In ^{137}La the $\frac{5}{2}$ level is at 10 keV, and in ^{139}La, with 99 % pure quasiproton wave functions [11]), it is 166 keV over the $\frac{7}{2}$ ground state. When the neutron number exceeds 82, the neutron-proton quadrupole interaction is expected to regain its influence on the particle states. However, we do not expect to find the levels interchanged in ^{141}La, as it has only two neutrons outside the closed neutron shell, and we consequently assume the ground state assignment to be $\frac{7}{2}^+$. This seems to be supported by the log ft values 7.6 and 7.2 of the once forbidden β-transitions

from ^{141}La to the $\frac{9}{2}^-$ and $\frac{7}{2}^-$ levels in ^{141}Ce [ref. [4])]. The β-decay of 18 min ^{141}Ba with expected ground state $f_{\frac{7}{2}}$, seems to contradict the proposed assignment, as only a weak branch feeds the ^{141}La ground state, while in contrast the population of the 190.3 keV level is strong [1]). However, it might be supposed that ^{141}Ba, like ^{143}Ce [ref. [12])], which also has 85 neutrons, has a $\frac{3}{2}^-$ ground state. A $\frac{5}{2}^+$ assignment to the 190.3 keV level could then account for the β-branch intensities. It would also explain the hindrance of ≈ 500 (table 3) of the 190.3 keV M1 transition. According to the pure shell-model $d_{\frac{5}{2}}$–$g_{\frac{7}{2}}$ M1 transitions are strictly forbidden ($\Delta l = 2$, $\Delta j = 1$), but

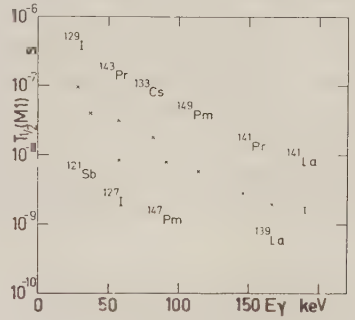

Fig. 6. Partial half-lives of $d_{\frac{5}{2}}$ to $g_{\frac{7}{2}}$ M1 transitions expressed as functions of the transition energies.

admixtures of higher seniority states and of phonons in the wave functions remove the forbiddenness [13]) partly. The corresponding transitions in ^{137}La and ^{139}La are retarded by factors of ≈ 400 and ≈ 600. The ^{141}La value falls in between. In figure 6 the M1 partial half-lives of known $d_{\frac{5}{2}}$–$g_{\frac{7}{2}}$ transitions are plotted as functions of the transition energy. The ^{141}La value is also indicated and fits nicely into the trend.

From a systematic point of view plausible spin assignments for the ground state and first excited state of ^{141}La could consequently be $\frac{7}{2}^+$ and $\frac{5}{2}^+$. If they are adopted, we are faced with the problem of explaining why the level spacing between the states exceeds the quasiparticle distance. It seems also necessary to reject $\frac{7}{2}^-$ as ground state assignment of the ^{141}Ba nucleus.

We want to express our gratitude to the Mass Separator Group at Studsvik for providing the sources and to Mr. Björn Rydberg for running the PDP computer.

References

1) K. Fritze and T. J. Kennett, Phys. Rev. **127** (1962) 1262
2) T. Alväger *et al.*, Phys. Rev. **167** (1968) 1105
3) S. Borg *et al.*, to be published
4) C. M. Lederer, J. M. Hollander and I. Perlman, Table of isotopes, sixth ed. (Wiley, New York, 1967)

5) A. Bäcklin, Nucl. Instr. **57** (1967) 261
6) R. S. Hager and E. C. Seltzer, Nucl. Data, **A4** (1968) 1 and 2
7) T. R. Gerholm and J. Lindskog, Ark. Fys. **24** (1963) 171
8) S. G. Malmskog, Ark. Fys. **35** (1967) 255
9) B. Olsen and L. Broström, Nucl. Instr. **44** (1966) 65
10) A. H. Wapstra, G. J. Nijgh and R. van Lieshout, Nuclear spectroscopy tables (North-Holland, Amsterdam, 1959)
11) L. S. Kisslinger and R. A. Sorensen, Rev. Mod. Phys. **35** (1963) 853
12) I. Maleh, Phys. Rev. **138** (1965) B766
13) N. Freed and L. S. Kisslinger, Nucl. Phys. **A116** (1968) 401

R E F E R E N C E 8

THE DECAY OF THE 79,5 keV LEVEL IN ^{134}I

V. BERG and A. HOGLUND
Institute of Physics, University of Stockholm
and
AB Atomenergi, Studvik, Nyköping, Sweden

1.E.4:3.A *Nuclear Physics* A175 (1971) 495—500; © *North-Holland Publishing Co., Amsterdam*
Not to be reproduced by photoprint or microfilm without written permission from the publisher

THE DECAY OF THE 79.5 keV LEVEL IN ^{134}I

V. BERG and A. HÖGLUND
Institute of Physics, University of Stockholm
and
AB Atomenergi, Studsvik, Nyköping, Sweden

Received 24 May 1971

Abstract: The decay of ^{134}Te has been investigated using a Ge(Li) detector and a double-lens coincidence spectrometer. Four new transitions were found. The half-lives of the lowest excited levels in ^{134}I were measured with the following results:

$T_{\frac{1}{2}}$(79.5 keV level) = 1.62±0.10 ns,
$T_{\frac{1}{2}}$(181.1 keV level) < 100 ps,
$T_{\frac{1}{2}}$(210.8 keV level) < 150 ps.

A comparison with theory confirms that the ^{134}I ground state configuration is predominantly $(g_{\frac{7}{2}}, d_{\frac{5}{2}})$.

E RADIOACTIVITY ^{134}Te [from ^{235}U(n, f)]; measured E_γ, I_γ, γce delay. ^{134}I deduced B(M1), B(E2), $T_{\frac{1}{2}}$. Ge(Li) detector.

1. Introduction

The two lowest levels in odd-mass iodine nuclei are mostly ascribed to the $d_{\frac{5}{2}}$ and $g_{\frac{7}{2}}$ proton states. The M1 transitions connecting them are *l*-forbidden and their appearance is explained by higher-seniority states in the wave functions and by phonon-particle coupling [1]). Retardation factors of about 60, 70, 150 and 200 measured in ^{125}I, ^{127}I, ^{129}I and ^{131}I [refs. [1–3])] support this interpretation, the hindrance becoming stronger as the neutron number approaches 82 and the vibrational contribution decreases.

In odd iodine nuclei the M1 transitions from the first excited state seem to be faster, which suggests a different mode of decay. The hindrance factor is only 30 in ^{132}I and the transition is supposed to take place between the 3^+ and 4^+ members of a $(g_{\frac{7}{2}}, d_{\frac{5}{2}})$ multiplet [4]). As similar features may be expected in ^{134}I it seemed interesting to determine absolute transition rates for the 79.5 keV ground state transition in this nucleus and to make a comparison with theory.

2. Experimental procedure

2.1. SOURCE PREPARATION

Sources were obtained from the on-line isotope separator of uranium fission fragments, which has been built in communication with the R2-0 reactor at Studsvik [ref. [5])]. The mass-134 ions were collected during periods of approximately 15 min on 1 mm thick aluminium backings, and measurements could be started 2 min after the separation. At that time the source contained as active substance 42 min ^{134}Te admixed with the 53 min daughter ^{134}I.

2.2. GAMMA-RAY SPECTROSCOPY

In order to get an estimate of the iodine content, γ-ray spectra were recorded using a 3 cm^3 Ge(Li) detector giving 2.3 keV resolution at 662 keV. It was found that, at the end of the separation, about 10 % of the activity came from ^{134}I. Earlier unobserved γ-rays following the decay of ^{134}Te appeared in the spectra. Their energies and intensities [normalized to the scale of ref. [6])] were

131.3±0.3 keV	(1.0±0.3),
259.8±0.6 keV	(1.2±0.5),
635.9±0.5 keV	(6.0±1.5),
925.2±0.5 keV	(4.5±1.0).

They all fit in the level scheme for ^{134}I, which was proposed in ref. [6]). Their placement is indicated in the decay scheme of fig. 1. The 259.8 and 925.2 keV transitions give further evidence for the suggested level at 1106.0 keV.

2.3. HALF-LIFE MEASUREMENTS

The half-life measurements were made with a Gerholm double-lens coincidence spectrometer [7, 8]), which in these experiments was modified to record electron-γ coincidences. Only one lens was used, and for the other was substituted a 2 cm × 2 cm

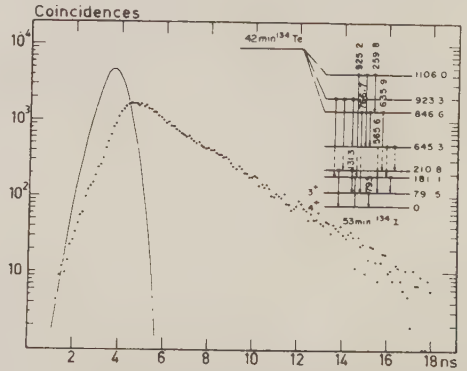

Fig. 1. Decay curve of the 79.5 keV excited state of ^{134}I obtained from a measurement of coincidences between the 766.7 and 565.6 keV γ-rays and 79.5 K electrons. The slope corresponds to a half-life of 1.62±0.10 ns. The prompt time resolution curve was recorded with unchanged settings using a ^{60}Co source.

cylindrical plastic scintillator mounted on a 56 AVP photomultiplier. The detector was placed inside the unused lens, 2 cm from the source.

The presence of ^{134}I in the source could not seriously impair the experiments, as the decay to stable ^{134}Xe does not give birth to strong electron lines, which coincide with the lines involved in the measurements. The iodine influence was also limited by a frequent change to fresh sources.

The 79.5 keV level in ^{134}I is predominantly fed by the 766.7 keV and 565.6 keV γ-rays, as the 101.4 keV transition [ref. [6]) and fig. 1] and the above mentioned 131.3 keV transition are in comparison very weak. The scintillator channel was set to admit Compton events from the two high-energy γ-rays within a region of 320–560 keV and the spectrometer lens was focused on the 79.5 K-electrons. The aluminium backing turned towards the scintillator, was thick enough to hinder the passage of β-particles from the ^{134}Te decay, and β-electron coincidences, which could have added lifetimes from upper levels, were thus excluded. The contribution from β-γ coincidences was estimated by focusing the lens on the β-continuum beside the electron line. The result of one measurement is shown in fig. 1 where the prompt spectrum, which gives the time resolution, was obtained with a ^{60}Co source using unchanged settings. From the slopes of several delayed curves we obtained

$$T_{\frac{1}{2}}(79.5\ \text{keV level}) = 1.62 \pm 0.10\ \text{ns}.$$

Attempts were also made to measure the half-lives of the 181.1 and 210.8 keV levels using the same technique, and the following limits could be set:

$$T_{\frac{1}{2}}(181.1\ \text{keV level}) < 100\ \text{ps},$$
$$T_{\frac{1}{2}}(210.8\ \text{keV level}) < 150\ \text{ps}.$$

2.4. CALCULATIONS

The measured half-life of the 79.5 keV level, together with the internal-conversion data of ref. [6]), makes it possible to calculate absolute transition probabilities according to the following relations

$$B(\text{M1}) = \frac{3.94 \times 10^{-5}}{T_{\frac{1}{2}\gamma}(\text{M1})E^3},$$

$$B(\text{E2}) = \frac{56.4}{T_{\frac{1}{2}\gamma}(\text{E2})E^5},$$

where the partial half-life, $T_{\frac{1}{2}\gamma}$ is in s, E in keV, B(M1) in units of $(e\hbar/2M_0c)^2$ and B(E2) in units of $e^2 \cdot \text{b}^2$. The information needed for the calculation is shown in table 1, which gives the resulting values of B(M1) and B(E2) and also the hindrance factor $F_W = T_{\frac{1}{2}\text{exp}}/T_{\frac{1}{2}W}$, which compares the experimental transition rate with the single-particle or Weisskopf estimate.

TABLE 1

A summary of experimental information on the 79.5 keV transition

$T_{\frac{1}{2}}$ exp level (ns)	Transition (keV)	Multipolarity	Relative N_γ	Relative N_e	$T_{\frac{1}{2}\gamma}$ exp (ns)	F_W	B(M1) $\left(\frac{e\hbar}{2M_0c}\right)^2$	B(E2) $(e^2 \cdot \text{b}^2)$
1.62±0.10	79.5	M1	98±2	152 [a])	4.2±0.3	93	$(1.9 \pm 0.1) \cdot 10^{-2}$	
		E2	< 4		> 99	$> 2 \cdot 10^{-2}$		$> 1.8 \cdot 10^{-1}$

[a]) From ref. [6]).

3. Comparison with transition probabilities obtained from pure multiplet configurations

It has been shown [9]) that the ground state of an odd nucleus may often be interpreted as a simple combination of the ground state configurations of the neighbouring odd-mass nuclei which have the same odd-neutron or odd-proton number as the odd system. If no low-lying particle excitations are found in the odd-mass nuclei, it is expected that the relatively weak neutron-proton interaction which appears in the odd system, will give rise to low-energy states which all belong to the same configurations [10]) and only differ in their total angular momentum. Reduced transition probabilities for M1 and E2 transitions between such multiplet states in spherical nuclei, can be calculated according to the following formulas from ref. [11])

$$B(\text{M1}) = (2J'+1)[\sqrt{2j_1+1}\,W(j_1 J' j_1 J; j_2 L)\langle j_1 \| t(\text{M1}) \| j_1 \rangle + (-1)^{J+J'}\sqrt{2j_2+1}\,W(j_2 J' j_2 J; j_1 L)\langle j_2 \| t(\text{M1}) \| j_2 \rangle]^2, \quad (1)$$

with j_1 and j_2 being the proton and neutron spins and J and J' the initial and final total spins. The W are Racah coefficients and the diagonal single-particle elements are given by

$$\langle j \| t(\text{M1}) \| j \rangle = e\left(\frac{\hbar}{2M_0c}\right)\sqrt{\frac{3}{\pi}}\,(\tfrac{1}{4})\sqrt{j(j+1)} \times \{(g_l+g_s)+(g_l-g_s)[4l(l+1)-3][4j(j+1)]^{-1}\};$$

B(E2) is calculated with eq. (1) using the matrix element

$$\langle j \| t(\text{E2}) \| j \rangle = e_2(nlj|r^2|nlj)\sqrt{\frac{5}{\pi}}\,(\tfrac{1}{4})[4j(j+1)-3][4j(j+1)(2j-1)(2j+3)]^{-\frac{1}{2}}.$$

If a harmonic-oscillator potential is used the radial factor can be written

$$(nl|r^2|nl)_{\text{h.o.p.}} = b_0^2(2n+l-\tfrac{1}{2}),$$

where $b_0 = \sqrt{\hbar/M_0\omega}$ is the oscillator length.

The ^{134}I nucleus is expected to be spherical, as it has only 3 protons outside the closed 50 shell and a single hole in the 82 neutron shell. The ground state of the

corresponding odd-mass systems ^{133}I and ^{137}Ba give reason to anticipate a rather unmixed ground state configuration in ^{134}I. According to the calculations of Kisslinger and Sorensen [12]) the $g_{\frac{7}{2}}$ state in ^{133}I is a pure quasiparticle state to at least 95 %, and the $d_{\frac{5}{2}}$ state in ^{137}Ba is pure to 99 %, so it seems probable that the ground state of ^{134}I will be chiefly $(g_{\frac{7}{2}}, d_{\frac{5}{2}})$. This is supported by the Brennan-Bernsteins 3rd rule, which is applicable to particle-hole states. It predicts for this configuration the ground state spin to be 4^+, which is in fact the probable spin of ^{134}I, as found from the decay of ^{134}Te [ref. [6])] and the β-decay to ^{134}Xe [ref. [13])]. But the $(g_{\frac{7}{2}}, d_{\frac{5}{2}})$ configuration is certainly not pure. In ^{133}I the $d_{\frac{5}{2}}$ state is at 312 keV [ref. [14])], and the $s_{\frac{1}{2}}$ state in ^{137}Ba is at 281 keV [ref. [3])]. Groups like $(d_{\frac{5}{2}}, d_{\frac{5}{2}})$ and $(g_{\frac{7}{2}}, s_{\frac{1}{2}})$ can also couple to 4^+ and take part in the ground state. For this reason calculations of transition rates for all groups mentioned were made. The three protons outside the closed shell were then presumed to couple to a state with seniority 1. In order to obtain as good B(M1) values as possible from eq. (1), we have used effective gyromagnetic ratios calculated for the $g_{\frac{7}{2}}$ proton and for the $d_{\frac{5}{2}}$ neutron from the measured magnetic dipole moments in ^{133}I and ^{137}Ba [ref. [15])]. The g-values for the $d_{\frac{5}{2}}$ proton and the $s_{\frac{1}{2}}$ neutron have not been derived from experimental data, as the corresponding magnetic dipole values, measured for instance in ^{127}I and ^{129}Xe include considerable phonon admixtures. The values were instead determined from the $d_{\frac{5}{2}}$ and $s_{\frac{1}{2}}$ quasiparticle dipole moments given for ^{133}I and ^{137}Ba by ref. [12]).

A comparison with adjacent even- and odd-A nuclei leads to the conclusion that the vibrational admixtures should be small, so that we can represent their contribution by effective charges. In the calculations of B(E2), the oscillator length b_0 was estimated as $0.226 \cdot 10^{-12}$ cm and the effective charges as $e_p = 2e$ and $e_n = e$. The result of the calculations are presented in table 2.

TABLE 2

A comparison of theoretical and experimental transition probabilities

Configuration	Total spin initial	Total spin final	B(M1) theor. $(e\hbar/2M_0c)^2$	B(E2) theor. $(e^2 \cdot b^2)$
$(g_{\frac{7}{2}}, d_{\frac{5}{2}})$	3^+	4^+	$1.7 \cdot 10^{-2}$	$5.8 \cdot 10^{-3}$
$(d_{\frac{5}{2}}, d_{\frac{5}{2}})$	3^+	4^+	$1.8 \cdot 10^{-1}$	$1.6 \cdot 10^{-3}$
$(g_{\frac{7}{2}}, s_{\frac{1}{2}})$	3^+	4^+	$8.3 \cdot 10^{-1}$	$3.2 \cdot 10^{-3}$
Experiment			$(1.9 \pm 0.1) \cdot 10^{-2}$	$< 1.8 \cdot 10^{-1}$

The experimental B(E2) value does not select any of the groups but agrees with all. The B(M1) value behaves very differently. It agrees very closely with that calculated for the $(g_{\frac{7}{2}}, d_{\frac{5}{2}})$ configuration, while, compared with the transition rates obtained for the other two groups, it is 10 and 40 times too small. This state of things proves to be rather unaffected by reasonable changes of the gyromagnetic ratios for the $d_{\frac{5}{2}}$ proton and $s_{\frac{1}{2}}$ neutron. The 79.5 keV M1 transition is, according to table 1 retarded

by a factor 93, and in the calculation made for the $(g_{\frac{7}{2}}, d_{\frac{5}{2}})$ group, a low value of B(M1) comes out because the proton and neutron contributions in eq. 1 partly cancel. In contrast they add and give rise to a higher transition rate in the corresponding calculations for the $(g_{\frac{7}{2}}, s_{\frac{1}{2}})$ group.

The M1 transition rates in table 2 column 3 suggest that the ground state of ^{134}I is mainly built on the $(g_{\frac{7}{2}}, d_{\frac{5}{2}})$ configuration. The calculation for this group was based on the most accurate g-value. Taking into account the more uncertain B(M1) values determined for the other two groups, we find that admixtures of about 25 % of $(d_{\frac{5}{2}}, d_{\frac{5}{2}})$ or of 10 % of $(g_{\frac{7}{2}}, s_{\frac{1}{2}})$ are allowed by the experimental value. It is probable that both groups are present, which would indicate that at least 75 % of the ground state is $(g_{\frac{7}{2}}, d_{\frac{5}{2}})$. A similar analysis of the 49.72 keV M1 transition in ^{132}I shows that the admixtures might be more important than in ^{134}I.

We want to express our gratitude to Dr. S. Wahlborn for valuable comments on the manuscript and to the separator group at Studsvik for providing the sources.

References

1) N. Freed and L. S. Kisslinger, Nucl. Phys. **A116** (1968) 401
2) Å. Höglund, S. G. Malmskog and F. Munnich, private communication
3) C. M. Lederer, J. M. Hollander and I. Perlman, Table of isotopes, sixth ed. (Wiley, New York, 1967)
4) K. Fransson and C. E. Bemis, Jr., Nucl. Phys. **78** (1966) 207
5) S. Borg *et al.*, to be published
6) V. Berg, K. Fransson and C. E. Bemis, Ark. Fys. **37** (1968) 203
7) T. R. Gerholm and J. Lindskog, Ark. Fys. **24** (1963) 171
8) S. G. Malmskog, Ark. Fys. **35** (1968) 255
9) M. H. Brennan and A. M. Bernstein, Phys. Rev. **120** (1960) 927
10) A. de-Shalit and J. D. Walecka, Nucl. Phys. **22** (1961) 184
11) S. Wahlborn and I. Martinson, Ark. Fys. **31** (1966) 355
12) L. S. Kisslinger and R. A. Sorensen, Rev. Mod. Phys. **35** (1963) 853
13) N. R. Johnson *et al.*, Phys. Rev. **122** (1961) 1546
14) B. Parsa, G. E. Gordon and W. B. Walters, Nucl. Phys. **A110** (1968) 674
15) I. Lindgren, Table of nuclear spins and moments in Alpha-, beta- and gamma-ray spectroscopy, vol. 2, ed. K. Siegbahn (North-Holland, Amsterdam, 1965) p. 1621

R E F E R E N C E 9

THE LEVEL STRUCTURE IN ^{193}Ir

V. BERG AND S.G. MALMSKOG
Institute of Physics, University of Stockholm
and
AB Atomenergi, Studsvik, Nyköping, Sweden
and
A. BÄCKLIN
The Swedish Research Council's Laboratory, Studsvik, Nyköping, Sweden

1.E.1:
3.A

Nuclear Physics **A143** (1970) 177—201; © *North-Holland Publishing Co., Amsterdam*
Not to be reproduced by photoprint or microfilm without written permission from the publisher

THE LEVEL STRUCTURE IN ^{193}Ir

V. BERG and S. G. MALMSKOG
Institute of Physics, University of Stockholm
and
AB Atomenergi, Studsvik, Nyköping, Sweden

and

A. BÄCKLIN
The Swedish Research Councils' Laboratory, Studsvik, Nyköping, Sweden

Received 11 November 1969

Abstract: The decay of ^{193}Os has been studied using Ge(Li) detectors and a 50 cm $\pi\sqrt{2}$ spectrometer. Multipolarities and E2/M1 mixing ratios have been determined for 23 transitions. Half-life measurements applying the delayed coincidence technique have given the following mean lives: τ(138.97 keV level) = 108±15 ps and τ(180.17 keV level) = 80^{+11}_{-21} ps. The M1 and E2 transition probabilities obtained are discussed in terms of the core excitation model and the Nilsson model.

E | RADIOACTIVITY ^{193}Os [from ^{192}Os(n,γ)]; measured E_γ, I_γ, E_{ce}, I_{ce}, cece-delay; deduced log ft. ^{193}Ir deduced levels, $T_{\frac{1}{2}}$, J, π, cc, multipolarities, γ-mixing ratios, B(M1), B(E2). Enriched target, Ge(Li) detector.

1. Introduction

It is well known that the deformation of nuclei gradually becomes smaller as one moves along the line of stability from the rare-earth region to the Pt and Au nuclei, which are believed to be essentially spherical. In odd-mass Ir nuclei the lowest part of the level scheme shows a similar structure to that at odd-mass Au levels, but the levels may also be ordered into rotational bands. In general more specific information on the character of the states may be obtained from transition probabilities.

In this paper, which is the first in a series on odd-mass Ir nuclei, we report on a study of ^{193}Ir from the decay of ^{193}Os. The main interest has been to determine experimentally E2 and M1 transition probabilities between low-lying levels. Half-lives have been measured by the delayed coincidence method and E2/M1 mixing ratios have been obtained from measurements of L-subshell ratios. We have also studied the gamma-ray spectrum with Ge(Li) detectors. The results are discussed in terms of the Nilsson model [1]) and de-Shalit's core excitation model [2]).

When this work was initiated several years ago the information available on the decay of ^{193}Os → ^{193}Ir was rather sparse [3,4]). Recently the results of several investigations on this decay have been published [5–11]).

2. Experimental procedure and results

2.1. GAMMA-RAY SPECTROSCOPY

The gamma-ray spectrum following the decay of ^{193}Os was studied using lithium-drifted germanium detectors of various sizes. One detector with a 1.5 cm^3 sensitive volume and an energy resolution of 1.2 keV FWHM at 122 keV was used to measure the low-energy spectrum and some interesting doublet lines. Two other detectors with 2.4 cm^3 and 24 cm^3 active volumes and resolutions of 3.2 and 3.5 keV respectively at 662 keV were employed for the study of high-energy gamma rays. In order to avoid pile-up effects due to low-energy gamma-ray contributions, they were shielded by 4 mm of lead. Energy and intensity calibration was performed by measuring a set of absolute calibrated standard sources obtained from IAEA, Vienna.

Sources for gamma-ray spectroscopy were obtained by irradiating small amounts (≈ 1 mg) of osmium metal powder †, enriched to 98.7 % in ^{192}Os in the R2 reactor at Studsvik. The samples were exposed to a neutron flux density of 2×10^{14} neutrons · cm^{-2} · sec^{-1} during a period of approximately one hour.

TABLE 1

Energies and relative intensities of gamma rays in the decay of ^{193}Os

Transition energy (keV)	Relative γ-ray intensity	Transition energy (keV)	Relative γ-ray intensity
41.18±0.07	< 0.01 [a])	387.48±0.12	29.0 ±2.0
65.87±0.06	0.06 [a])	414.0 ±0.3	0.11 ±0.03
73.10±0.04	50 [a])	418.16±0.20	1.6 ±0.2
96.90±0.05	2.5 [a])	420.07±0.20	3.7 ±0.4
98.77±0.06	0.4 [a])	440.90±0.20	2.2 ±0.2
107.10±0.04	12.8 ±0.7	460.56±0.12	100.0 ±6.0
138.97±0.04	100.0 ±6.0	484.22±0.15	4.8 ±0.5
142.26±0.06	1.4 ±0.2	515.2 ±0.2	0.40 ±0.06
154.68±0.10	0.63±0.07	525.3 ±0.2	0.40 ±0.06
180.15±0.06	4.5 ±0.5	532.3 ±0.2	2.2 ±0.2
181.89±0.06	4.7 ±0.5	557.41±0.15	39.1 ±5.0
219.18±0.08	6.6 ±0.6	559.22±0.15	15.5 ±2.0
234.60±0.12	1.2 ±0.1	573.4 ±0.2	0.54 ±0.06
251.66±0.08	5.4 ±0.4	598.6 ±0.4	0.02 ±0.01
280.50±0.08	33.0 ±1.7	639.3 ±0.2	0.21 ±0.03
288.98±0.15	4.0 ±0.3	667.0 ±0.4	0.03 ±0.01
298.71±0.15	4.8 ±0.3	695.3 ±0.2	0.09 ±0.02
321.63±0.10	35.0 ±2.0	710.0 ±0.4	0.04 ±0.02
333.0 ±0.3	0.04±0.02	712.1 ±0.2	0.50 ±0.05
350.2 ±0.3	0.16±0.05	735.5 ±0.4	0.030±0.006
357.8 ±0.3	0.30±0.18	777.4 ±0.4	0.06 ±0.02
361.92±0.12	6.4 ±0.4	784.2 ±0.4	0.02 ±0.01
377.60±0.20	1.7 ±0.2	848.9 ±0.4	0.12 ±0.02
379.0 ±0.5	0.20±0.08	874.2 ±0.3	0.58 ±0.06
		891.0 ±0.4	0.080±0.012

[a]) Evaluated from internal conversion intensities and the theoretical conversion coefficients by Hager and Seltzer [16]).

† Obtained from Oak Ridge National Laboratory, Tennessee.

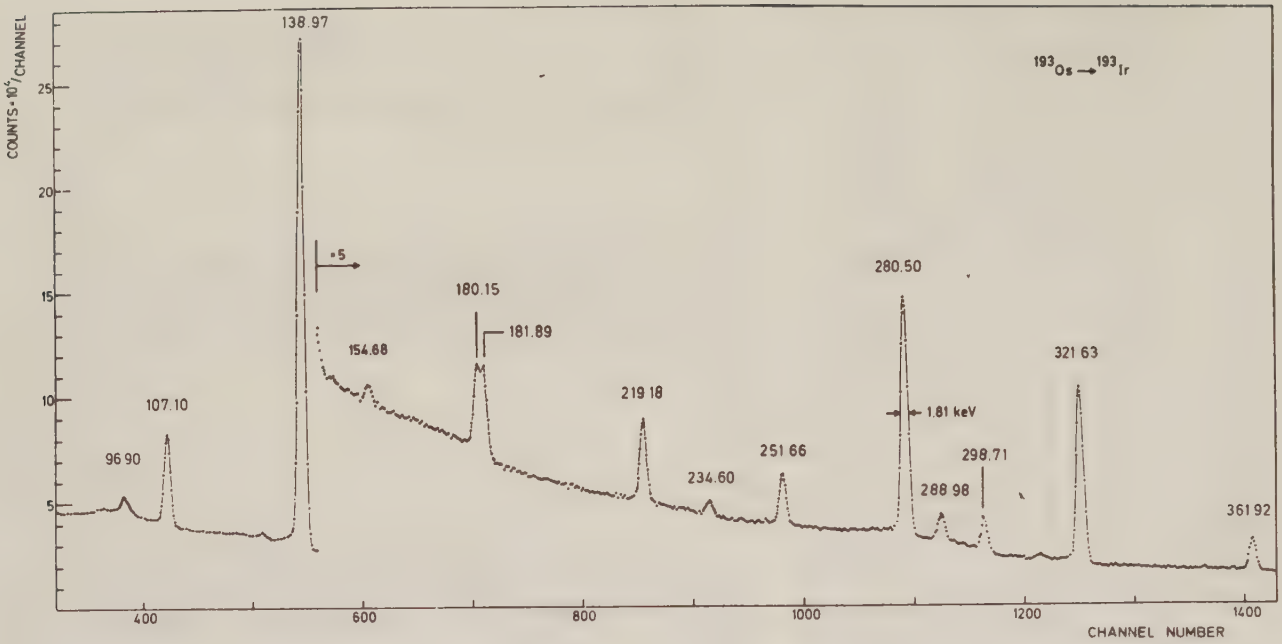

Fig. 1. Gamma-ray spectrum from the decay of ^{193}Os obtained with a 1.5 cm^3 Ge(Li) detector.

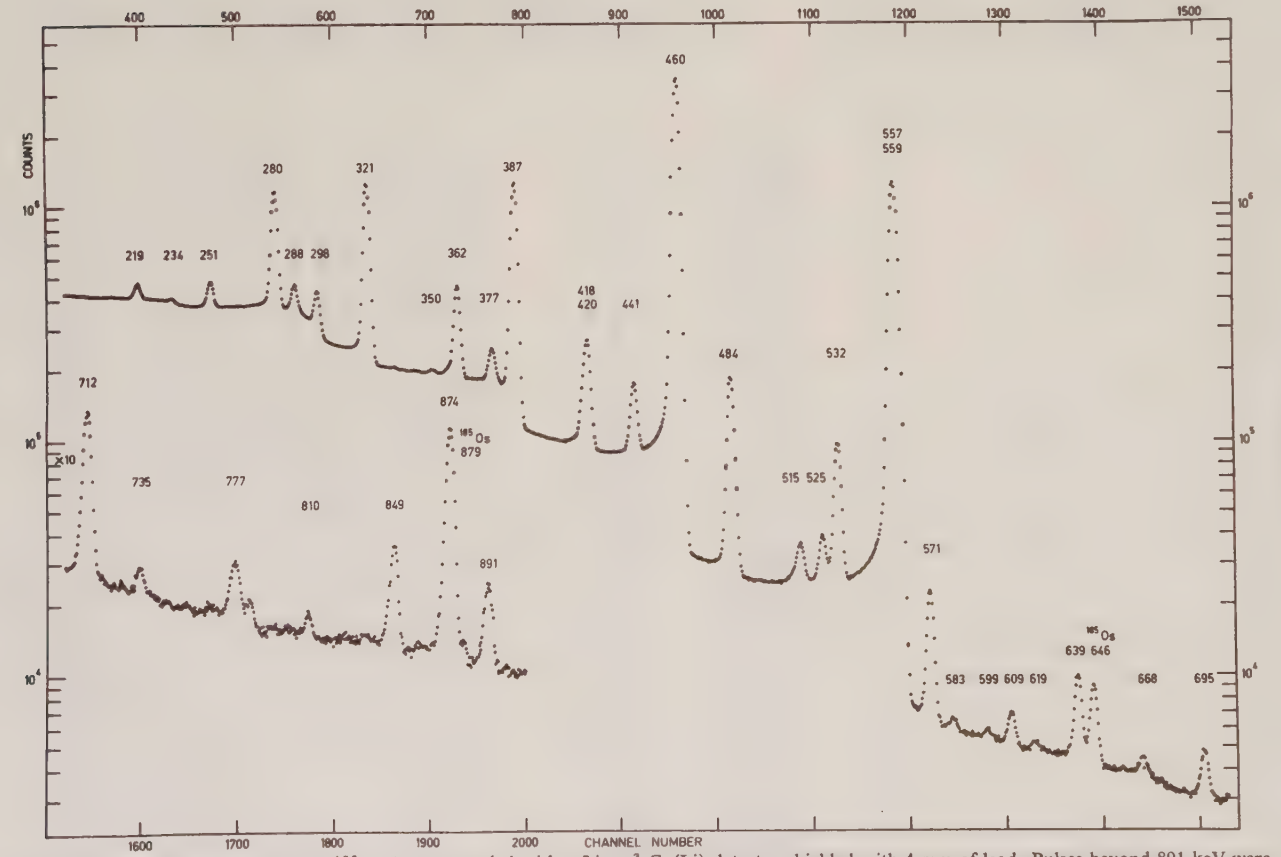

Fig. 2. Gamma-ray spectrum of the ^{193}Os decay recorded with a 24 cm^3 Ge(Li) detector shielded with 4 mm of lead. Pulses beyond 891 keV were due to ^{60}Co background activity.

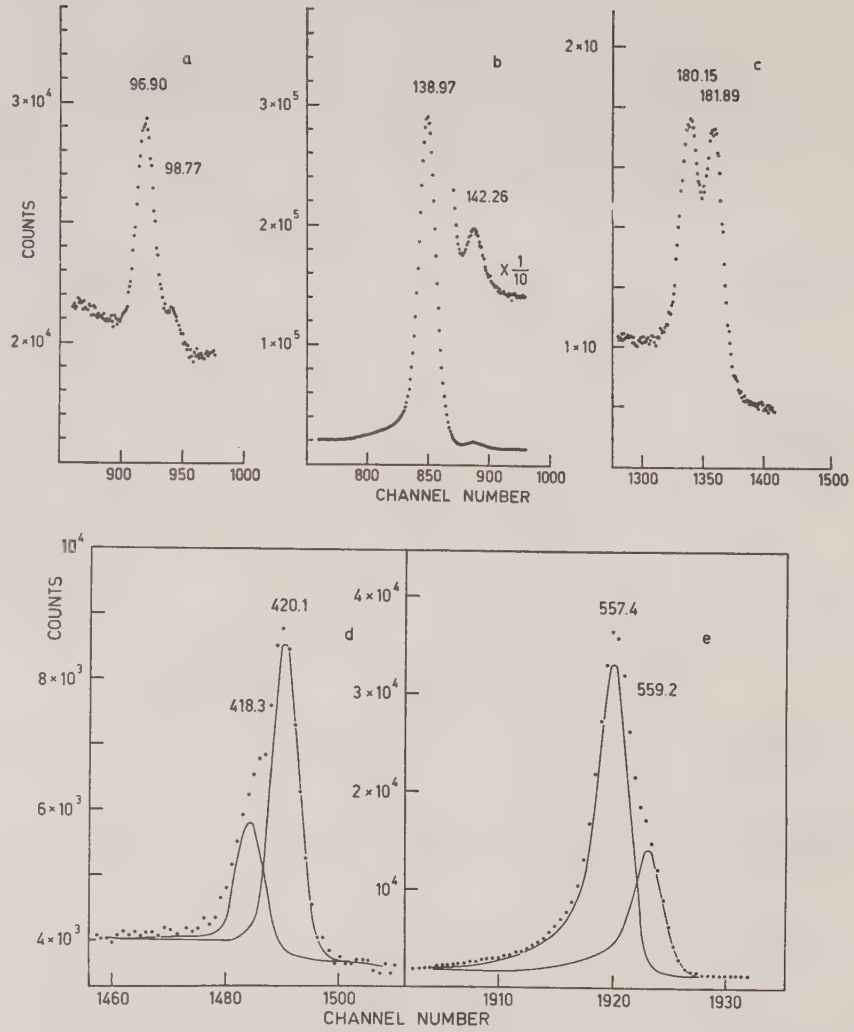

Fig. 3. Doublet gamma lines in the ^{193}Os decay recorded with a 1.5 cm^3 Ge(Li) detector (cf. text).

Preliminary measurements revealed strong iodine contamination, which was eliminated in the following way. The irradiated osmium metal was dissolved in nitric acid. Air was sparged into the solution and the volatile OsO_4 formed was carried by the air stream to a sample tube, cooled with ice and containing 6N NaOH. The solution was mixed with an equal part of phosphate buffer solution and diluted with water.

From this bath the osmium was electroplated on a Ni foil cathode at a current of a few mA for about 2 hours. During this process the bromide ions migrated to the anode. The purified osmium metal was used as a source for gamma-ray spectroscopy. The results of the measurements are presented in figs. 1-3 and in table 1. Fig. 2 shows a spectrum obtained with the 24 cm^3 detector. The gamma lines at 609 and 810 keV seen in this spectrum decayed faster than the iridium lines. Their identity has not been established.

Our data confirm earlier suggested doublet structures. Examples are shown in fig. 3. The two lines in fig. 3c were first resolved by Alexander and Ryde in a bent crystal spectrometer measurement [7]). The gamma rays in figs. 3a, 3b and 3d have been reported by Johns *et al.* [8]) and the lines in fig. 3e were found in a resonance scattering experiment by Metzger [12]).

2.2. INTERNAL CONVERSION ELECTRON SPECTROSCOPY

The internal conversion electron spectrum of ^{193}Os was measured with the 50 cm iron yoke double focusing beta spectrometer at Studsvik [14]). The baffles were adjusted to give an energy resolution of 0.2-0.4 % FWHM. The electrons were detected using a GM counter with a 0.6 mg/cm^2 mylar window, which transmitted the measured electrons without observable energy or intensity loss.

The sources were prepared similarly to the gamma-ray sources. The ^{192}Os was electroplated on thin aluminium strips over an area of 0.2 cm × 3 cm and the strips

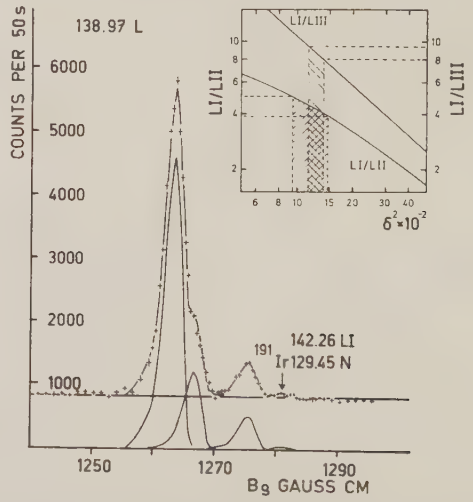

Fig. 4. Examples of internal conversion electron lines in ^{193}Ir. All points have been corrected for decay. In the insets theoretical values of sub-shell ratios [16]) are expressed as functions of the E2/M1 mixing ratio. The horizontal lines indicate limits of experimental values (cf. text and tables 2 and 3).

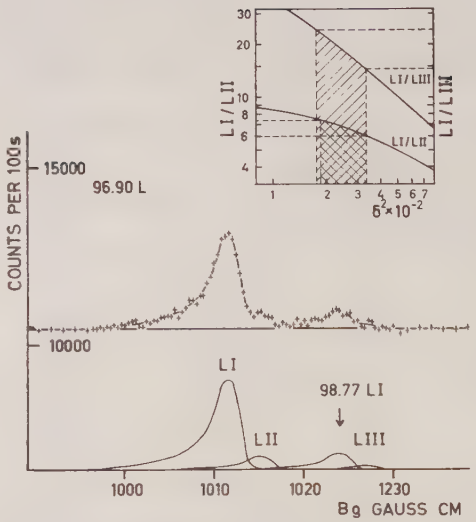

Fig. 5. (See caption fig. 4.)

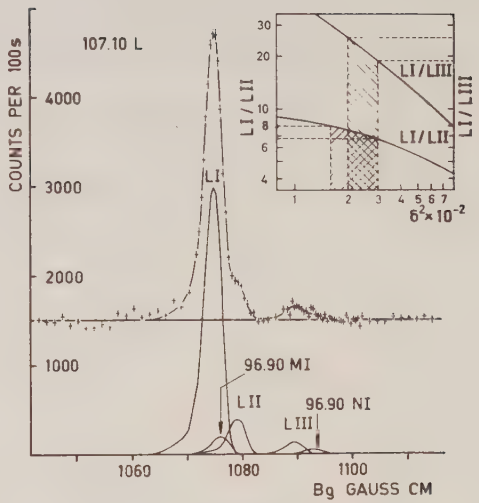

Fig. 6. (See caption fig. 4.)

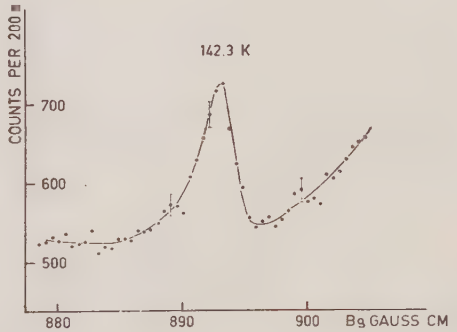

Fig. 7. (See caption fig. 4.)

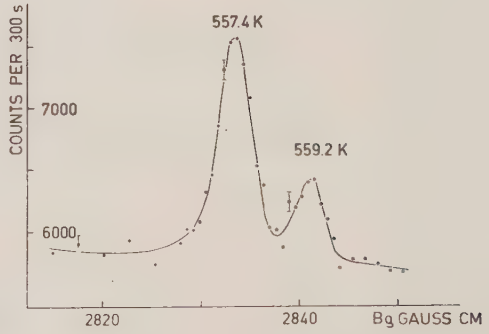

Fig. 8. (See caption fig. 4.)

were then irradiated for 15 to 20 hours at a neutron density flux of 2×10^{14} neutrons · cm^{-2} · sec^{-1}. The 100.104 L_{II} line in ^{182}W and the 661.595 K-line in ^{137}Ba were used for the energy calibration. Complicated line structures were analysed with a computer programme [15]). Examples of internal conversion groups are shown in figs. 4-8.

The results of the measurements are summed up in tables 2 and 3. The experimental K-conversion coefficients have been calculated using the gamma intensities in table 1 and the K-conversion electron intensities in table 2. They are compared with the theo-

TABLE 2
Internal conversion data of transitions in ^{193}Ir

Transition energy (keV)	Shell	Relative electron intensity	Error % [a]	K-conversion coefficients experiment	theory E1	theory E2	theory M1	Assignment
41.18±0.07	L_I	< 0.3						
65.87±0.06	L_{III}	0.7	30					
73.10±0.04	ΣL	302	8					M1+(29±2) % E2 [b]
96.90±0.05	ΣL	2.7	10					M1+(2.3±0.6) %E2 [b]
98.77±0.06	ΣL	0.4	20					M1
107.10±0.04	K	50	20	3.9 ±0.9	0.174	0.71	4.40	M1+(2.2±0.4) %E2 [b]
	ΣL	11.7	8					
138.97±0.04	K	180	5	1.8 ±0.3	0.143	0.42	2.07	M1+(11±1) %E2 [b]
	ΣL	36.0	5					
142.26±0.06	K	2.7	15	1.9 ±0.4	0.133	0.40	1.86	M1+< 25 % E2
180.15±0.06	K	3.6	15	0.80 ±0.15	0.072	0.22	0.95	M1+(35±12) %E2 [b]
	ΣL	0.8	25					
181.89±0.06	K	4.4	8	0.94 ±0.11	0.071	0.22	0.94	M1+< 16 % E2
	ΣL	0.7	18					
219.18±0.08	K	0.8	12	0.12 ±0.02	0.045	0.14	0.56	E2
251.66±0.08	K	2.0	10	0.37 ±0.05	0.032	0.094	0.38	M1+(4±^{17}) % E2
280.50±0.08	K	8.4	6	0.25 ±0.02	0.024	0.068	0.27	M1+(10±10) % E2
	ΣL	1.5	10					
288.98±0.15	K	0.28	25	0.070±0.018	0.023	0.066	0.26	E2+ < 10 % M1
298.71±0.15	K	0.35	25	0.073±0.018	0.021	0.062	0.26	E2
321.63±0.10	K	6.10	6	0.17 ±0.02	0.018	0.050	0.20	M1+(20±13) % E2
	ΣL	0.96	12					
	M_I	0.20	25					
361.92±0.12	K	1.06	12	0.17 ±0.03	0.014	0.038	0.14	M1
377.60±0.20	K	0.21	25	0.11 ±0.03	0.012	0.034	0.13	M1+(20±$^{30}_{20}$) % E2
387.48±0.12	K	3.64	8	0.13 ±0.01	0.012	0.032	0.12	M1+ < 6 % E2
	ΣL	0.65	15					
420.07±0.20	K	0.37	20	0.100±0.023	0.010	0.027	0.097	M1+ < 29 % E2
440.90±0.20	K	0.18	30	0.082±0.027	0.009	0.024	0.086	M1+(6±$^{44}_{6}$) % E2
460.56±0.12	K	6.28	5	0.063±0.007	0.008	0.021	0.076	M1+(24±13) % E2
	ΣL	0.95	12					
484.22±0.15	K	0.28	25	0.058±0.015	0.007	0.019	0.066	M1+(17±$^{32}_{17}$) % E2
557.41±0.15	K	1.57	15	0.040±0.007	0.005	0.014	0.047	M1+(21±21) % E2
559.22±0.15	K	0.60	20	0.039±0.009	0.005	0.014	0.046	M1+(22±$^{28}_{22}$) % E2

[a]) The errors are standard deviations.

[b]) From L subshell ratios. See table 3.

retical values given by Hager and Seltzer [16]) in fig. 9, which shows that most transitions have essentially M1 multipolarity. Exceptions are the E2 transitions at 219, 289 and 298 keV.

Special care was taken in the measurement of the 139 L group, as from its subshell ratios, together with theoretical conversion coefficients [16]), the normalization constant (used for coordination of gamma-ray and electron line intensities) was calculated. A graph of the 139 L lines is presented in fig. 4. The weak lines appearing on the high-energy side of 139 L_{III} are due to 142 L_I and to the N lines of the 129 keV transition

TABLE 3
L-subshell data for some transitions in ^{193}Ir

Transition energy (keV)	Shell	Relative electron intensity	Conversion electron ratios	E2/M1 mixing ratio adopted value
73.10±0.04	ΣL	302±24	L_I/L_{II} = 0.70±0.07 L_I/L_{III} = 0.79±0.08 L_{II}/L_{III} = 1.13±0.12	0.41 ±0.03
96.90±0.05	ΣL	2.7 ±0.3	L_I/L_{II} = 6.7±0.7 L_I/L_{III} = 19.4±4.8	0.024±0.006
107.10±0.04	ΣL	11.7 ±0.9	L_I/L_{II} = 7.4±0.6 L_I/L_{III} = 22.1±3.3	0.023±0.004
138.97±0.04	ΣL	36.0 ±1.8	L_I/L_{II} = 4.4±0.6 L_I/L_{III} = 8.7±0.7 L_{II}/L_{III} = 2.0±0.3	0.125±0.015
180.15±0.06	K	3.6 ±0.6	K/L_{II} = 16.3±5.0	0.55±$^{0.36}_{0.18}$
	L_I+L_{II}	0.66±0.15	L_I/L_{II} = 2.0±0.7	

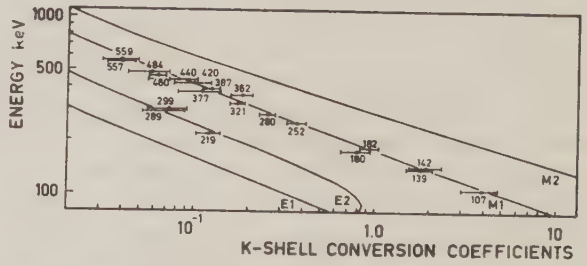

Fig. 9. Experimental and theoretical [16]) K-conversion coefficients of transitions in ^{193}Ir (cf. text and table 2).

in ^{191}Ir. In evaluating the intensity of the 139 L_{II} line it was necessary to take into account that it contained the 129 M lines in ^{191}Ir. To get an estimate of the contribution due to these lines, the strength of the 129 K line was measured. It was found that the correction due to ^{191}Ir content never exceeded 10 % of the total 139 L_{II} intensity. Even if the uncertainty mentioned here is not taken into consideration, the L_{II} line is the one in the 139 L group impaired by the largest errors, as it is not resolved from the L_I line. Using smaller current steps and longer time intervals, 139 L_{III} was recorded in a special run. The mixing ratio was obtained from the L_I/L_{III}, L_{II}/L_{III} and L_I/L_{II} ratios and is given in table 3. The analysis of the 97 L group (fig. 5) revealed an electron line corresponding to the 98.77 keV gamma ray seen in fig. 3a.

The determination of line intensities in the 107 L group was impeded by the presence of the M and N lines from the 97 keV transition. These lines were subtracted from the 107 L group in the computer analysis assuming an L/M ratio for the 97 keV transition of 4.4 [ref. [16]] and an L/N ratio of 19. The two K lines corresponding to

the gamma-ray doublet at 180 keV appeared well separated and the low-energy component seemed approximately 1.5 times stronger than its companion. However, with the aid of ref. [16]) we found that 40 % of the line identified as 180 K was due to the 107 M lines. Similarly the 107 N lines partly coincided with 182 K. The decomposition of the line group was made assuming a 107 M/N ratio equal to the L/M ratio.

2.3. LIFETIME MEASUREMENTS

The half-life of the two levels at 139 keV and 180 keV have been measured. The experiments were carried out using a Gerholm type electron-electron coincidence spectrometer [17,18]). The reliability and stability of the total equipment were tested before and after the main experiments by performing self-comparison measurements using the β-238 K electron cascade following the decay of ^{212}Pb. This cascade is prompt and the 238 K line rises very isolated on the corresponding β-continuum. The shifting of the on-line position from one lens to the other was achieved by applying 15 keV to the source. In this way all further changes of spectrometer and electronic settings were avoided. A series of about 20 fifteen-minute measurements, performed with and without high tension on the source and analysed by the centroid shift method, gave evidence that the electronic instability was negligible and that no systematic shift disturbed the experiment.

The source was prepared by electrodeposition of irradiated osmium metal on a 0.8 mg/cm^2 nickel foil. The active layer formed a circular spot 3 mm in diameter on the backing. The nickel foil was thin enough to let all electrons measured in the experiment pass without disturbing intensity loss, but care was taken to turn the source in such a way that the most energetic particles in a cascade had to penetrate the backing.

In the measurement of the 139 keV level one spectrometer lens was focused on the K electrons of the 321 keV transition which feeds this level, while the other lens was set to admit the L electrons of the de-exciting 139 keV transition. The prompt $\beta \rightarrow$ 238 K cascade from ^{212}Pb was used as time reference. In order to have the 139 L electrons accepted in the same lens as the 238 K electrons, a preaccelerating voltage of 22.5 keV was applied to the osmium source. With this arrangement the spectrometer and electronic settings had to be kept fixed when shifting from one source to the other. With the aid of the automatic operation of the spectrometer [18]) some 20 successive time spectra with alternatively ^{212}Pb and ^{193}Os sources were recorded. Each spectrum was measured during 30 minutes.

The analysis of the half-life measurements was made by the centroid shift method. It was then observed that the resolution of the prompt curve had remained at 500 ps during the whole series of measurements. The result of the analysis gave an observed time shift of 104 ± 5 ps.

This value has to be corrected for disturbing shifts. As ^{193}Os decays by β-emission, the spectrometer, when focusing a certain conversion line (for instance the 321 K line), necessarily admits that part of the β-distribution which has the same energy as the line

(in the following referred to as 321 K β). The coincidences measured come mainly from the 321 K $\rightarrow$ 139 L and the 321 K $\beta \rightarrow$ 139 L cascades, the last cascade mixing in lifetimes of all levels which decay via the 139 keV transition. Other coincidences arise from the 139 L$\beta \rightarrow$ 321 K cascades. Here the main part is due to the 139 L betas in the branch feeding the 460 keV level but, as before, 139 L betas in higher-level branches mix in the lifetimes of these and intermediate levels. In connection with this it is worth noticing that in 321 K and 321 K $\beta \rightarrow$ 139 L coincidences the 139 L electrons succeed, while in 139 L $\beta \rightarrow$ 321 K coincidences the 139 L betas precede, their cascade partners. This causes partial cancellation of contributions coming from the upper levels. This is favourable as the mean lives of these levels are not all well determined. An analysis based on decay-property data has been performed. The shapes of the different β-branches have been calculated supposing the β-decay to be allowed and the β-intensity has been normalized so that the sum of all branches is in agreement with the line to the beta ratio measured in the electron spectrum. The result of the analysis is expressed by the following equation:

$$0.894(\tau 139)+0.025(\tau 460)+0.023(\tau 557) = (104\pm 5)-(6\pm 1)\ \text{psec},$$

in which the parentheses stand for the mean lives of the corresponding levels. The analysis showed that the contributions from the 695 keV and 712 keV levels totally cancelled, while the time shifts due to the 460 keV and 557 keV levels appeared with very small coefficients. The correction on the right-hand side of the equation is due to the time difference that appears between 139 L and 321 K electrons when moving in the preaccelerating field.

Using appropriate mean lives from table 4 we obtain the value

$$\tau(139\ \text{keV}) = (108\pm 15)\ \text{psec},$$

where the error is calculated to cover the uncertainties in the analysis as well as those associated with the mean life assignments of the upper levels. Results from earlier investigations are given in table 4.

The half-life of the 180 keV level was obtained in almost the same way. In the experiment the time delay in the 280 keV-107 keV cascade was measured. The prompt β-electron coincidences in the decay of ^{212}Pb to ^{212}Bi were once more used to define zero time. With a tension of 18 kV applied to the osmium source the 280 K electrons were accelerated to the same energy as the 238 L electrons in ^{212}Bi. One lens was adjusted to accept the 280 K and the 238 L electrons and the other lens was focused on the 107 L_I line. When the Pb source was measured, this lens admitted a narrow portion of the β-continuum. As above, the sources were shifted every half-hour and 30 successive measurements were performed.

The centroid shift analysis of the resulting time spectra gave a time shift of (74 ± 5) psec. This is chiefly due to the 280 K $\rightarrow$ 107 L cascade. Only few direct coincidences of the type 280 K $\beta \rightarrow$ 107 L occur, as there is not much β-feeding to the 180 keV level, but the β-branches to upper levels provide indirect coincidences of this kind and

TABLE 4
Summary of recent mean-life measurements for excited levels in ^{193}Ir

Level (keV)	73.1	139.0	180.2	362.0	460.6	557.4	559.2	712.3	Ref.
Mean lives	ns	ps	ps	ps	ps	ps	ps	ps	
		108 ± 15	(80^{+11}_{-21})						a)
		127 ± 13	≤ 50	≤ 130	27 ± 7	≤ 300		≤ 160	ref. [10])
	9.1 ± 0.3	107 ± 16	112 ± 40		20 ± 13	≤ 67	≤ 280		ref. [19])

a) Present investigation.

mix in other lifetimes in the result. The coincidences 107 L $\beta \rightarrow$ 280 K come mainly from the strong beta branch which populates the 460 keV level, but contributions from the β-branches to higher levels have also to be taken into account. As before, one observes that the 107 L succeed but the 107 L β precede in the cascades. This implies that the contributions from higher levels may come out with different signs in the analysis and a certain cancellation will take place. An extra correction has to be made to this measurement because of the 97 M electrons which coincide in energy with the 107 L_I peak. The number of coincidences owing to the 97 M line can be calculated, as the intensity of the 97 L group has been measured (table 3) and the number of M electrons compared to L electrons is given in the tables of ref. [16]). A correction of (7 ± 1) psec has been applied to the result in order to compensate for the difference in time of flight of the 107 L and 280 K electrons which occurs during the pre-acceleration.

The result of an analysis built on our decay data is given by the following equation

$$0.81(\tau\,180)+0.05(\tau\,360)+0.11(\tau\,460)+0.05(\tau\,557)$$
$$+0.02(\tau\,712) = (74\pm5)-(7\pm1)\ \text{psec}.$$

Using appropriate mean lives from table 4 we obtain

$$\tau(180\ \text{keV}) = (80^{+11}_{-21})\ \text{psec}.$$

Results from earlier investigations are given in table 4.

The present information on absolute transition probabilities for the low-energy levels in ^{193}Ir is presented in table 5.

3. Level scheme of ^{193}Ir

By combining the transition energies of tables 1 and 2 the level scheme in fig. 10 was constructed. The levels at 73, 139, 180, 362, 461, 557 and 712 keV are common with all recently published works [5, 6, 8, 9, 11]). The spins of the 73, 139 and 460 keV levels were confirmed by angular correlations by Gustavsson *et al.* [5]) as $\frac{1}{2}$, $\frac{5}{2}$, and $\frac{3}{2}$, respectively. The M1+E2 multipolarity of the 107 and 180 keV transitions suggests $\frac{1}{2}^+$ or $\frac{3}{2}^+$ for the 180 keV level. Avida *et al.* [9]) find from their angular correlations a spin of $\frac{3}{2}$. The spin of the 362 keV level has been suggested to be $\frac{1}{2}$ [ref. [8])], $\frac{3}{2}$ [ref. [9])], $\frac{5}{2}$ [ref. [11])] and $\frac{7}{2}$ [ref. [5])]. Our multipolarity data immediately exclude the $\frac{7}{2}$ but do not allow us to decide between the other alternatives. The pure E2 multipolarity of the transition to the $\frac{1}{2}^+$ state seems to indicate $\frac{5}{2}$, but it is then difficult to understand the missing transition to the 139 keV $\frac{5}{2}^+$ level. From angular correlations Avida *et al.* [9]) find the spin to be $\frac{3}{2}$. If this is true, the M1 transitions both to the $\frac{1}{2}$ and $\frac{5}{2}$ states are strongly retarded, the hindrance factor relative to the Weisskopf estimate [20]) F_W being $\gtrsim 10^3$ for both transitions. The weak 358 keV transition in table 1 may indicate that the $\frac{7}{2}^+$ state observed at 358 keV in Coulomb excitation [13]) is also populated in the decay of ^{193}Os. The expected transition to the 139 keV state is masked by the strong 219 keV transition. From their modes of de-excitation the 557 keV state is found to be $\frac{3}{2}^+$ and the 712 keV state $\frac{1}{2}^+$, $\frac{3}{2}^+$ or $\frac{5}{2}^+$. In addition to these states we find states defined by 3 or 4 de-exciting transitions at 559, 695 and 874 keV. The probability of finding so many unlocated transitions combine by accident is small. The decay modes of these states imply the spin assignments indicated in fig. 10. These states are among the many states suggested by Johns *et al.* [8]). In a recent publication the work of the McMaster group has been improved and extended [21]). The present level scheme is in good agreement with the main part of the scheme of ref. [21]), although we tentatively suggest alternative positions of some transitions as follows.

Almost all transitions given in table 1 have been placed in the level scheme. The exceptions are, in addition to half a dozen weak transitions of fairly high energy, the medium strong E2 transitions of 219.18 and 298.71 keV, and the M1 transitions at 142.26 and 440.90 keV. Available coincidence data [6, 8, 9, 11, 21]) indicate these transitions to be coincident with each other but with no other transition of comparable intensity. Our energy data show good agreement between the sum of the 142+298 keV energies and the 441 keV energy and our intensity data are compatible with $I_{\text{total}}(219) = I_{\text{total}}(298)+I_{\text{total}}(441)$ and $I_{\text{total}}(298) = I_{\text{total}}(142)$. Thus these fairly strong transitions seem to form a level sub-system that is weakly or not at all connected with the rest of the levels. Johns *et al.* [8, 21]) suggest that the sub-system is connected to the ground state according to fig. 11. Some (although weak) support for this is obtained from the two weak transitions making up the 667 keV level as indicated in the figure.

We find, however, that this scheme leads to rather large difficulties concerning the depopulation of the states. The log *ft* value of the 660 keV level implies a spin of $\frac{7}{2}^+$ or less and the level should therefore have a reasonable probability of decaying with M1 transitions to lower levels with spin $\frac{5}{2}^+$ or less. No such lines are observed; assuming the 219 keV E2 transition to be as fast as 100 s.p.u. we obtain retardation factors for the expected M1 transitions of 10^4-10^5.

Even when rearranging the subsystem to more favourable configurations from this point of view we obtain retardation factors larger than 10^4 for the transitions from

TABLE 5

Absolute transition probabilities in ^{193}Ir

Level in keV	$T_{\frac{1}{2}}$(exp) of level in nsec	Transition energy in keV	Initial state $IK^{\pi}[Nn_z\Lambda]$	Final state $IK^{\pi}[Nn_z\Lambda]$	Multipolarity	Relative N_γ	Relative N_e	$T_{\frac{1}{2}\gamma}$(exp) (sec)	B(M1)↓ in $\left(\frac{e\hbar}{2Mc}\right)^2$ units	B(E2)↓ in $e^2 \cdot b^2$ units	Q_0	F_W [a]
73.1	6.3 ±0.2	73.1	$\frac{1}{2}\frac{1}{2}^+(400)$	$\frac{3}{2}\frac{3}{2}^+(402)$	M1	35	406	8.07E- 8	(1.26±0.12)E-3			1400
					E2	15		1.88E- 7		(1.45±0.14)E-1		4.64E-2
139.0	0.075±0.010	139.0	$\frac{5}{2}\frac{3}{2}^+(402)$	$\frac{3}{2}\frac{3}{2}^+(402)$	M1	89	234	2.84E-10	(5.2 ±0.7)E-2			33.8
					E2	11		2.29E- 9		(4.8±0.7)E-1	3.7±0.3	1.41E-2
		65.9		$\frac{1}{2}\frac{1}{2}^+(400)$	E2	0.07	2	3.61E- 7		(1.26±0.36)E-1		5.32E-2
180.2	$0.055\pm^{0.008}_{0.014}$	107.1	$\frac{3}{2}\frac{1}{2}^+(400)$	$\frac{1}{2}\frac{1}{2}^+(400)$	M1	12.5	66	3.85E-10	(8.5 ±1.4)E-2			21.0
					E2	0.3		1.61E- 8		(2.5 ±0.6)E-1	3.5±0.5	2.68E-2
		180.2		$\frac{3}{2}\frac{3}{2}^+(402)$	M1	3.4	4.6	1.42E- 9	(4.9 ±0.9)E-3			368
					E2	1.0		4.84E- 9		(6.2 ±1.5)E-2		1.09E-1
		41.2		$\frac{5}{2}\frac{3}{2}^+(402)$	M1	< 0.03	< 0.3	>1.6E- 7	<3.5 E-3			> 495
					E2	< 0.003		>1.6E- 6		<3.0E-1		> 2.2E-2
357.8	0.015 [b]	177.7	$\frac{7}{2}\frac{3}{2}^+(402)$	$\frac{3}{2}\frac{1}{2}^+(400)$	E2	< 0.15	< 0.08	>8.6 E-11		<3.7		>1.8E-3
		218.8		$\frac{5}{2}\frac{3}{2}^+(402)$	M1 [c]	0.22	0.16	5.86E-11	(6.5 ±1.8)E-2			27.2
					E2 [c]	0.06		2.15E-10		(3.4 ±0.5)E-1	4.0	1.29E-2
		357.8		$\frac{3}{2}\frac{3}{2}^+(402)$	E2	0.30	0.02	4.30E-11		(2.29±0.33)E-1 [b]	4.0	3.00E-2
362.0	0.016 [b]	181.9	$\frac{5}{2}\frac{1}{2}^+(400)$	$\frac{3}{2}\frac{1}{2}^+(400)$	M1	4.70	5.45	7.69E-11	(8.5 ±1.7)E-2			20.6
					E2	0.12		3.02E- 9		(9.1 ±1.1)E-2	4.0	7.16E-2
		222.9		$\frac{5}{2}\frac{3}{2}^+(402)$	M1	< 0.2		>1.8E- 9	<1.9 E-3			>880
					E2	< 0.2		>1.8E- 9		< 5.7E-2		>1.1 E-1
		289.0		$\frac{1}{2}\frac{1}{2}^+(400)$	E2	4.0	0.43	9.00E-11		(3.18±0.38)E-1 [b]	4.0	2.17E-2
		361.9		$\frac{3}{2}\frac{3}{2}^+(402)$	M1	6.4	1.13	5.64E-11	(1.48±0.29)E-2			120
					E2	< 0.6		>6.0 E-10		< 1.5E-2		>4.4 E-1

[a]) Hindrance factor relative to the Weisskopf estimate with statistical factor equal to one [20]).
[b]) Calculated using $Q_0 = 4.0\pm0.4$.
[c]) From ref. [13]).

the uppermost levels. Such large factors are only associated with K-forbiddenness in the region of a well developed static deformation. The levels of the subsystem do not, however, seem to form the well-behaved rotational band that one would expect in such a case. Furthermore, considering feeding strengths and level spins, these do not seem compatible with the assumption of rotational bands with large differences in K-quantum number.

We therefore suggest that the subsystem may feed the 80.19 keV $\frac{11}{2}^-$ isomeric level. This has not been experimentally verified, but we have not been able to find any strong arguments to contradict it.

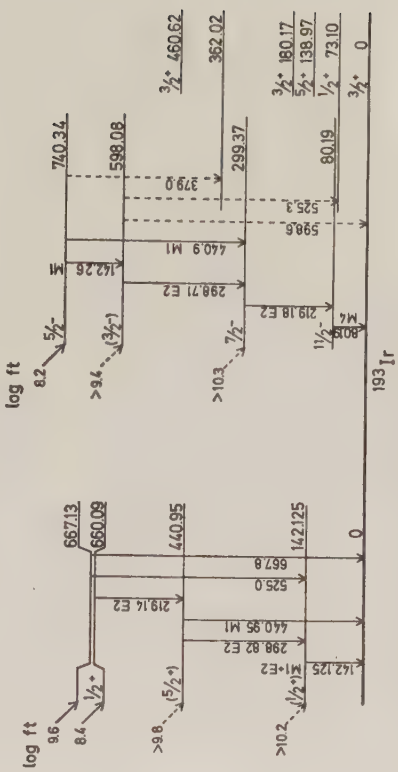

Fig. 11. Possible positions of the 142, 219, 298, 441 keV transitions in ^{193}Ir. a) according to Price *et al.* [21]), b) suggested in present work.

In fig. 11 we have indicated a possible level order. To some extent it is supported by the two weak transitions fitting to lower-lying levels as shown in the figure. Almost all other possible E1 transitions expected to the low-lying positive parity states are masked by strong transitions fitting elsewhere in the scheme. Admittedly the experimental support for this suggestion of level scheme is weak and further experimental work is needed to clarify this puzzling problem, which also exists for ^{191}Ir and ^{189}Ir [ref. [22])]. The intention here has been to point out a possible similarity with the odd-mass Au nuclei, where a $\frac{7}{2}^-$ state is observed about 200 keV above the $\frac{11}{2}^-$ state [refs. [23,26])].

4. Discussion

The Ir nuclei are intermediate between, on the one hand, Re and Os nuclei, which exhibit well developed rotational bands, and Pt and Au nuclei, which do not show

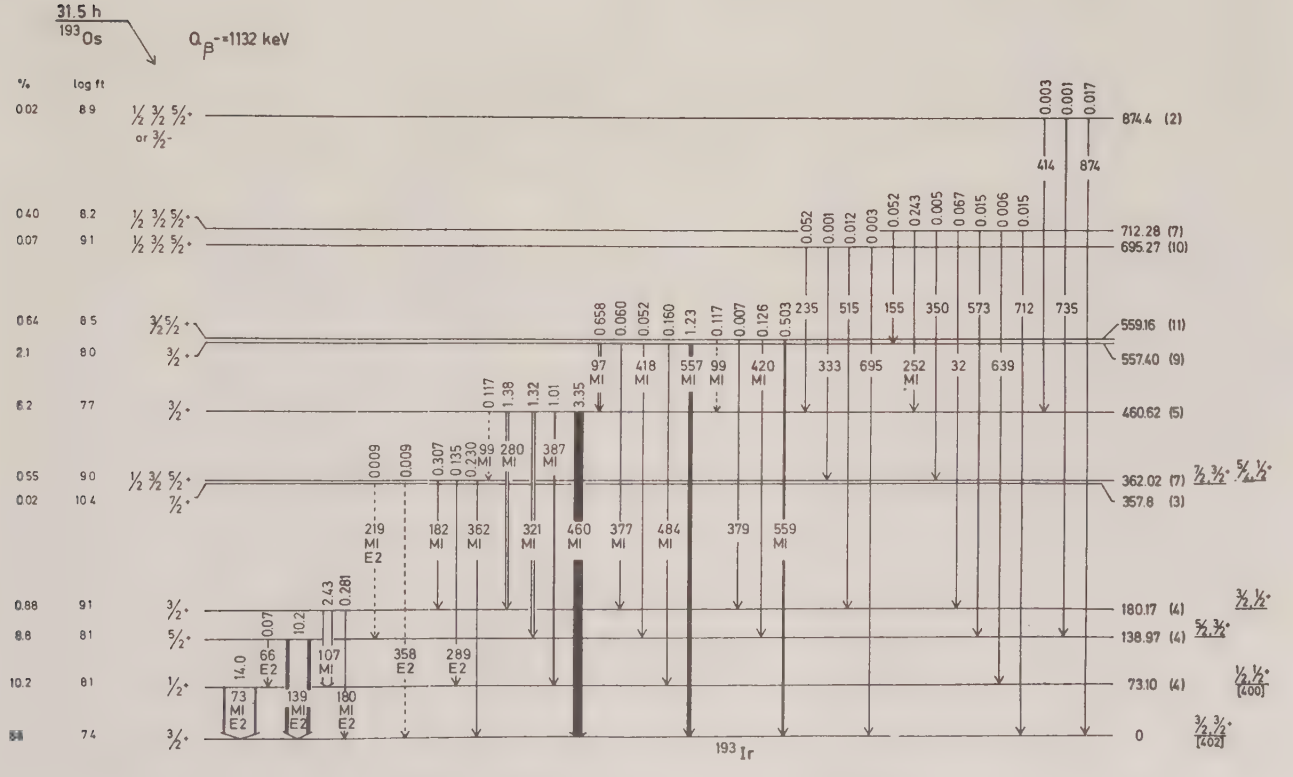

Fig. 10. Decay scheme of ^{193}Os. Intensities are given in per cent of ^{193}Os decays assuming that 68 % feed the ^{193}Ir ground state [8]).

this level structure. It is therefore justified to compare the experimental data with predictions of models for both spherical and deformed nuclei.

4.1. COMPARISON WITH THE CORE EXCITATION MODEL

The core excitation model of de-Shalit [2]) has been found to work fairly well for odd-mass nuclei [24-26]). In a recent work Avida *et al.* [10]) have compared transition rates in ^{193}Ir with predictions of the core excitation model. Since more information on the transition rates than were available to Avida *et al.* has been available in the present work, it is of interest to make a new comparison with the core excitation model. The three first excited states of fig. 10 together with the $\frac{7}{2}^+$ level at 358 keV, observed in Coulomb excitation [13]), are treated as the quartet of states obtained by coupling the $\frac{3}{2}^+$ particle ground state to a 2^+ excitation of the core. As a first check of the applicability of the model one may compute the centre of gravity of the quartet = 227 keV. This is in decent agreement with the energies of the 2^+ levels in the neighbouring even nuclei, which are 206 keV for ^{192}Os and 328 keV for ^{194}Pt.

TABLE 6

Comparison between experiment and the core excitation model for B(M1) values (in units of μ_N^2) and magnetic moments

Quantity	Predicted from the core exc. model		Experiments [c])
	[a])	[b])	
$B(M1; \frac{1}{2} \to \frac{3}{2})$	1.3 E-3	1.3 E-3	1.26 (12) E-3 [d])
$B(M1; \frac{3}{2} \to \frac{1}{2})$	6.2 E-2	6.2 E-3	8.5 (14) E-2 [d])
$B(M1; \frac{3}{2} \to \frac{5}{2})$	1.0 E-3	1.0 E-3	4.9 (9) E-3 [d])
$B(M1; \frac{5}{2} \to \frac{3}{2})$	5.9 E-2	5.2 E-2	5.2 (7) E-3 [d])
$B(M1; \frac{7}{2} \to \frac{5}{2})$	3.6 E-2	3.3 E-2	6.5 (18) E-2 [d])
$\mu_{\frac{3}{2}}$	1.589 E-1 [e])	1.589 E-1 [e])	1.589(1) E-1 [e])
$\mu_{\frac{1}{2}}$	4.70 E-1 [f])	4.70 E-1 [f])	4.70 (1) E-1 [f])
$\mu_{\frac{5}{2}}$	0.91	1.30	0.57 (9) [g])

[a]) $g_c = 0.52$, $g_p = 0.10$, $A = 0.995$, $B = 1$ (see text).
[b]) $g_c = 0.52$, $g_p = 0.10$, $A = 0.995$, $B = 0.95$ (see text).
[c]) Error of last digits given in parentheses.
[d]) Present work.
[e]) Ref. [31]). Value used to determine the core excitation model parameters (see text).
[f]) Ref. [30]). Value used to determine the core excitation model parameters (see text).
[g]) $\omega\tau$ from ref. [5]); g calculated with the present value of $T_{\frac{1}{2}}$ for the 139 keV level.

A comparison between the experimental and predicted values of B(M1) is given in table 6. The values given in column 2 were calculated from the formulas given in refs. [2,26]) assuming only the two $\frac{3}{2}^+$ states to mix with mixing amplitude A. The values of the parameters g_c and g_p (the subscripts c and p refer to core and particle respectively) are most sensitive to the value of the magnetic moments $\mu_{\frac{3}{2}}$ and $\mu_{\frac{1}{2}}$ and were accordingly obtained from experimental values of these quantities. The value of A was obtained from a least-squares fit including all quantities depending on A. The calculated values of column 2 agree with experiment in some cases, but deviate for the B(M1) values of the $\frac{3}{2} \to \frac{3}{2}$ and $\frac{7}{2} \to \frac{5}{2}$ transitions and $\mu_{\frac{5}{2}}$. One may try to improve the situation for the quantities connected to the $\frac{5}{2}$ state by mixing it with a small amount of $d_{\frac{5}{2}}$ single-particle wave function. A mixing amplitude $\sqrt{(1-B^2)} = 0.30$ was obtained from the experimental value of $B(M1; \frac{5}{2} \to \frac{3}{2})$. It is, however, seen from table 6 that such an admixture only impairs the fit for $B(M1; \frac{7}{2} \to \frac{5}{2})$ and $\mu_{\frac{5}{2}}$.

In order to account for the large value of $B(M1; \frac{3}{2} \to \frac{3}{2})$ Avida *et al.* [10]) introduced a third component, i.e. the $|2\,\frac{1}{2}; \frac{3}{2}\rangle$ state [†] in the $\frac{3}{2}$ states, which improves the fit for $B(M1; \frac{3}{2} \to \frac{3}{2})$. Assuming the 460 keV level to be predominantly the $|2\,\frac{1}{2}; \frac{3}{2}\rangle$ state, the transition probabilities from this state are also fairly well explained. However, if the 460 keV level is really the $|2\,\frac{1}{2}; \frac{3}{2}\rangle$ state, one may ask why the $s_{\frac{1}{2}}$ state is not observed below that energy. There also remains the badly reproduced value of $\mu_{\frac{3}{2}}$, and it seems likely that for a realistic description of the low-lying states in ^{193}Ir one may have to introduce additional states, e.g. the $|2\,\frac{1}{2}; \frac{5}{2}\rangle$ state.

Also the E2 transition probabilities indicate that it is necessary to mix in more states than were needed in the simple model for ^{197}Au. According to the core excitation model the B(E2) values for the transitions from the multiplet members to the ground state should all have the same value as the $B(E2; 2^+ \to 0^+)$ in the neighbouring even nuclei under the likely assumption that the core excitations in even and odd-mass nuclei are identical [2]). In ^{197}Au this rule works perfectly well except for the $\frac{3}{2} \to \frac{3}{2}$ transition, for which the low value is explained by the mixing of the two $\frac{3}{2}$ states [25]). As is seen in table 5, only $B(E2; \frac{5}{2} \to \frac{3}{2})$ and $B(E2; \frac{7}{2} \to \frac{3}{2})$ have values of the expected magnitude (0.48 and 0.23 $e^2 \cdot b^2$ to be compared to $B(E2; 2^+ \to 0^+) \approx 0.41$ $e^2 \cdot b^2$), while in addition to the $\frac{3}{2} \to \frac{3}{2}$ transition also the $\frac{1}{2} \to \frac{3}{2}$ transition shows a definitely smaller value.

We conclude that, as long as only a limited number of small admixtures are considered, the core excitation model does not work for ^{193}Ir as well as it does for ^{197}Au.

4.2. DISCUSSION WITHIN THE NILSSON MODEL

4.2.1. *Low-lying energy level spectrum.* From the level scheme of ^{193}Ir (fig. 10) it is clear that the low-lying energy levels form rotational-like patterns characteristic of deformed nuclei. Although ^{193}Ir is not expected to be a strongly deformed nucleus, it is still interesting to see whether or not the well developed formalism for such nuclei also holds for ^{193}Ir. The ground state is then identified with the $\frac{3}{2}^+(402)$ Nilsson orbital with rotational levels at 139 and 358 keV, while the expected $\frac{1}{2}^+(400)$ orbital is identified with the 73 keV level with rotational states at 180 and 362 keV. Members of the two rotational bands are expected to be strongly mixed with each other mainly due to Coriolis and vibrational effects. To obtain an idea of the amount of

[†] The state vector is given as $|J_c j_p; J\rangle$, where J_c (the angular momentum of the core excitation) and j_p (the angular momentum of the particle) couple to J.

coupling that exists between the $K = \frac{1}{2}$ and $K = \frac{3}{2}$ bands we have diagonalized the energy matrix $\langle \Psi^I_K | H_{\rm int} + H_{\rm rot} + H_{\rm Cor} | \Psi^{I'}_{K'} \rangle$ where $H_{\rm int}$ and $H_{\rm rot}$ describe the intrinsic and rotational motions and $H_{\rm Cor} = (\hbar^2/2J)(I_+ j_- + I_- j_+)$ takes into account the coupling between these two degrees of freedom. The known experimental energy eigenvalues of this matrix determine the single-particle energies $\varepsilon_{\frac{1}{2}}$ and $\varepsilon_{\frac{3}{2}}$, the rotational parameters $(\hbar^2/2J)_{K=\frac{1}{2}}$ and $(\hbar^2/2J)_{K=\frac{3}{2}}$, the decoupling factor $\langle \Psi_{\frac{3}{2}} | j_+ | \Psi_{-\frac{1}{2}} \rangle$ and the Coriolis matrix element $\langle \Psi_{\frac{3}{2}} | j_- | \Psi_{\frac{1}{2}} \rangle$. As a further result of this diagonalization we obtain the amplitudes for the different components for each nuclear level. The result is given in table 7, where the second column shows the above parameters if no coupling is taken into account. The diagonalization was performed for different values of the Coriolis coupling matrix element. The result is given in the right-hand part of table 7. This shows that only a moderate Coriolis coupling is needed to get a fit to the experimental rotational energies, although it should be stressed that the fit is not very dependent on the coupling strength. In all cases the decoupling parameter a comes out as a small number, which is in accordance with findings in other Ir isotopes [27]). The Nilsson model predicts $a = 0.3$.

TABLE 7

Parameters from a least-squares fit to rotational level energies in ^{193}Ir

Quantity	No coupling	Fit to experimental data
$\langle \psi_{\frac{1}{2}} \| j_- \| \psi_{\frac{3}{2}} \rangle$	0	±0.37
$\langle \psi_{\frac{1}{2}} \| j_+ \| \psi_{-\frac{1}{2}} \rangle$	0.009	0.019
$\varepsilon_{\frac{1}{2}}$ (in keV)	45.77	45.66
$\varepsilon_{\frac{3}{2}}$ (in keV)	−115.65	−115.40
$(\hbar^2/2J)_{K=\frac{1}{2}}$ (in keV)	36.02	35.18
$(\hbar^2/2J)_{K=\frac{3}{2}}$ (in keV)	29.84	30.51

4.2.2. *The* E2 *transition rates.* From the absolute B(E2) values for intraband transitions given in table 5 the deformation δ of the two low-lying bands in ^{193}Ir can be determined from

$$B(\mathrm{E2};\, K+1,\, K \to K,\, K) = \frac{5}{16\pi}\,(K+1,\, K20|KK)^2 Q_0^2\, e^2 \cdot \mathrm{b}^2,$$

$$Q_0 = 0.8\, Z R_0^2 \delta (1 + 0.5\delta), \qquad (1)$$

where Q_0 is in barns and $R_0 = 1.2\, A^{\frac{1}{3}}$ fm. For both bands we get $Q_0 = 4.0 \pm 0.4$ b corresponding to $\delta = 0.13 \pm 0.01$. The E2 strengths within the supposed rotational bands are hardly larger than for vibrational E2 transitions in spherical nuclei and thus the adiabatic approximation is not expected to be strictly fullfilled. The consequence of this is that couplings between bands are of importance.

A possiblity of estimating the magnitude of this mixing is to study the interband E2 transition rates. If single-particle terms are neglected the relevant E2 transition probabilities can be written

$$B(\mathrm{E2},\, IK \to I'K') = 1.34 \times 10^{-3} \sum [C(IXK) C(I'YK')(IX2,\, Y-X | I'Y) G^{\rm coll}_{\rm E2}]^2, \qquad (2)$$

where $C(IXK)$ is the amplitude of the contribution for the state IX being Coriolis mixed into the main K band [28]); X and Y will in this case take on the values $X = Y = \frac{1}{2}$ or $\frac{3}{2}$; $G^{\rm coll}_{\rm E2}$ is the diagonal E2 strength and is given by $G^{\rm coll}_{\rm E2} = Q_0/2\beta^2$ where $2\beta^2 = (2\hbar/M_0\omega_0) = 0.115$ b for ^{193}Ir.

From the diagonalization of the Hamiltonian including the RPC-term $(\hbar^2/2J)(I_+ j_- + I_- j_+)$ the admixtures in the new wave functions can be written [29])

$$C(I\,\tfrac{1}{2}\,\tfrac{3}{2}) = -C(I\,\tfrac{3}{2}\,\tfrac{1}{2}) = \pm\{1 + [R + \sqrt{1+R^2}]^2\}^{-\frac{1}{2}},$$

$$R = \frac{E_{\frac{1}{2}}(I) - E_{\frac{3}{2}}(I)}{2M}. \qquad (3)$$

Here $E_{\frac{1}{2}}(I) - E_{\frac{3}{2}}(I)$ is equal to the energy difference between the two mixing states and

$$M = \langle \tfrac{1}{2} | RPC | \tfrac{3}{2} \rangle = -P_+ E^x \langle \tfrac{1}{2} | j_- | \tfrac{3}{2} \rangle \sqrt{(I-\tfrac{1}{2})(I+\tfrac{3}{2})}. \qquad (4)$$

From eqs. (3)-(4) we see that C is essentially a function of $P_+ E^x \langle \frac{1}{2} | j_- | \frac{3}{2} \rangle$ where $P_+ \approx 1.0$. Using eqs. (2)-(4) we have calculated several interband B(E2) values for different values of this particular parameter. The result is compared with experimental values in table 8. Using the values of κ and μ recommended by Nilsson [1]) we have $\langle \frac{1}{2} | j_- | \frac{3}{2} \rangle = 0.67 \pm 0.02$. For low-lying excitations we expect E^x to be of the same order of magnitude as the rotational parameter $\hbar^2/2J$, which for the Ir isotopes is about 30 keV. This means that we expect a value of 20 keV for the $P_+ E^x \langle \frac{1}{2} | j_- | \frac{3}{2} \rangle$ parameter. It is seen that a much larger effective mixing than expected from theory is needed to explain the observed strong interband E2 transition rates. This is not unexpected since vibrational interactions should also be important in the rather soft Ir nuclei.

TABLE 8

E2 rates for interband transitions in ^{193}Ir

	Experimental data (in $e^2 \cdot \mathrm{b}^2$)	Calculated values from eqs. (2)-(4) [a])		
		$E^x \langle \frac{1}{2} \| j_- \| \frac{3}{2} \rangle = 10$	$E^x \langle \frac{1}{2} \| j_- \| \frac{3}{2} \rangle = 30$	$E^x \langle \frac{1}{2} \| j_- \| \frac{3}{2} \rangle = 90$
B(E2, $\frac{1}{2}\frac{1}{2} \to \frac{3}{2}\frac{3}{2}$)	(1.45±0.14) E-1	0.050 E-1	0.34 E-1	1.2 E-1
B(E2, $\frac{3}{2}\frac{3}{2} \to \frac{1}{2}\frac{1}{2}$)	(1.26±0.36) E-1	0.041 E-1	0.26 E-1	0.71 E-1
B(E2, $\frac{3}{2}\frac{1}{2} \to \frac{3}{2}\frac{3}{2}$)	(6.2 ±1.5) E-2	0.96 E-2	6.5 E-2	18.2 E-2
B(E2, $\frac{5}{2}\frac{1}{2} \to \frac{5}{2}\frac{3}{2}$)	<3.0 E-1	0.13 E-2	0.97 E-2	3.3 E-2
B(E2, $\frac{7}{2}\frac{3}{2} \to \frac{5}{2}\frac{1}{2}$)	< 3.7	2.5 E-3	9.0 E-3	9.2 E-3
B(E2, $\frac{5}{2}\frac{1}{2} \to \frac{5}{2}\frac{3}{2}$)	< 5.7 E-2	0.26 E-2	1.5 E-2	3.2 E-2
B(E2, $\frac{5}{2}\frac{1}{2} \to \frac{3}{2}\frac{3}{2}$)	< 1.5 E-2	0.32 E-2	1.7 E-2	3.7 E-2

[a]) We used $G_{\rm E2}(\frac{1}{2} \to \frac{1}{2}) = G_{\rm E2}(\frac{3}{2} \to \frac{3}{2}) = 30$, corresponding to $Q_0 = 3.5$ b. The quantity $E^x \langle \frac{1}{2} | j_- | \frac{3}{2} \rangle$ is given in keV.

Recently Wagner *et al.* [30]) studied isomer shifts in ^{191}Ir and ^{193}Ir. These authors conclude that their data was not in accordance with the excited core model but could, at least to some extent, be understood within the Nilsson model including appreciable Coriolis mixing.

4.2.3. *The* M1 *transition rates.* From the data given in table 5 we get nine B(M1)

TABLE 9

Magnetic properties in ^{193}Ir

	Experimental data [a]	Calculated values using the fitted parameters given below						
		$E^x\langle\frac{1}{2}\|j_-\|\frac{3}{2}\rangle = 0$	$E^x\langle\frac{1}{2}\|j_-\|\frac{3}{2}\rangle = 10$	$E^x\langle\frac{1}{2}\|j_-\|\frac{3}{2}\rangle = 20$ [c]	$E^x\langle\frac{1}{2}\|j_-\|\frac{3}{2}\rangle = 30$	$E^x\langle\frac{1}{2}\|j_-\|\frac{3}{2}\rangle = 50$	$E^x\langle\frac{1}{2}\|j_-\|\frac{3}{2}\rangle = 20$ [f]	$E^x\langle\frac{1}{2}\|j_-\|\frac{3}{2}\rangle = 10$ [g]
$\mu\ \frac{3}{2}\frac{3}{2}^+(402)$	0.1589±0.0001 [b]	0.156	0.156	0.155	0.155	0.155	0.159	0.162
$\mu\ \frac{5}{2}\frac{3}{2}^+(402)$	0.57 ±0.09 [c]	0.950	0.957	0.971	0.998	0.969		1.31
$\mu\ \frac{1}{2}\frac{1}{2}^+(400)$	0.470 ±0.001 [d]	0.468	0.469	0.469	0.477	0.455	0.477	0.304
B(M1, $\frac{1}{2}\frac{1}{2}\to\frac{3}{2}\frac{3}{2}$)	(1.26±0.12)E-3	1.37E-3	1.26E-3	1.23E-3	1.26E-3	1.27E-3	1.25E-3	1.38E-3
B(M1, $\frac{3}{2}\frac{1}{2}\to\frac{3}{2}\frac{3}{2}$)	(4.9 ±0.9)E-3	0.55E-3	4.25E-3	4.92E-3	8.40E-3	14.8 E-3	5.08E-3	8.8 E-3
B(M1, $\frac{5}{2}\frac{1}{2}\to\frac{3}{2}\frac{3}{2}$)	(1.48±0.29)E-2	0.009E-2	0.61E-2	1.51E-2	3.07E-2	5.68E-2	0.64E-2	0.49E-2
B(M1, $\frac{5}{2}\frac{3}{2}\to\frac{3}{2}\frac{3}{2}$)	(5.2 ±0.7)E-2	4.07E-2	4.17E-2	3.79E-2	3.44E-2	2.46E-2	5.22E-2	9.85E-2
B(M1, $\frac{3}{2}\frac{1}{2}\to\frac{1}{2}\frac{1}{2}$)	(8.5 ±1.4)E-2	7.97E-2	8.10E-2	8.65E-2	7.82E-2	7.03E-2	8.37E-2	31.8 E-2
B(M1, $\frac{5}{2}\frac{1}{2}\to\frac{3}{2}\frac{1}{2}$)	(8.5 ±1.7)E-2	9.86E-2	9.85E-2	7.81E-2	7.82E-2	5.80E-2	8.80E-2	3.06E-2
B(M1, $\frac{7}{2}\frac{3}{2}\to\frac{5}{2}\frac{3}{2}$)	(6.5 ±1.8)E-2	5.49E-2	5.33E-2	4.58E-2	3.94E-2	2.86E-2	6.65E-2	11.9 E-2
$P_+(\frac{1}{2}\to\frac{3}{2})G_{M1}(\frac{1}{2}\to\frac{3}{2})$		−(0.152±0.046)	−(0.309±0.043)	−(0.200±0.063)	−(0.298±0.093)	−(0.446±0.16)	−(0.311±0.012)	−(0.175±0.149)
$G_{M1}(\frac{3}{2}\to\frac{3}{2})$		−(1.61 ±0.25)	−(1.67 ±0.19)	−(1.73 ±0.20)	−(1.84 ±0.25)	−(1.88 ±0.34)	−(1.85 ±0.06)	−(2.53 ±0.63)
$G_{M1}(\frac{5}{2}\to\frac{3}{2})$		2.02 ±0.31	2.02 ±0.24	2.02 ±0.25	2.03 ±0.29	1.92 ±0.39	1.98 ±0.07	2.58 ±0.85
$G_{M1}(\frac{1}{2}\to\frac{1}{2})b_{M1}$		−(0.03 ±0.30)	−(0.04 ±0.022)	0.09 ±0.22	−(0.09 ±0.25)	−(0.16 ±0.31)	0.06 ±0.06	2.00
g_R		0.59 ±0.07	0.58 ±0.06	0.59 ±0.06	0.58 ±0.07	0.53 ±0.09	0.65 ±0.02	0.84 ±0.19
mean square sum		2.65	1.60	1.79	2.59	5.00	0.10	26.7
B(M1, $\frac{3}{2}\frac{1}{2}\to\frac{5}{2}\frac{3}{2}$)	< 3.5E-3	(8.3 ±0.7)E-4	(3.0 ±1.2)E-4	(1.04 ±0.03)E-2	(2.10 ±0.08) E-2	(3.2 ±0.2)E-2	(3.0 ±0.1)E-4	[e] (1.2±1.2)E-3
B(M1, $\frac{5}{2}\frac{1}{2}\to\frac{5}{2}\frac{3}{2}$)	< 1.9E-3	(6.3 ±0.6)E-4	(7.58 ±0.08)E-3	(8.9 ±0.2)E-3	(1.92 ±0.04)E-2	(3.2 ±0.1)E-2	(7.72 ±0.01)E-3	(1.4±0.7)E-3

[a]) B(M1) is given in units of $(e\hbar/2Mc)^2$ and μ in units of $e\hbar/2Mc$.
[b]) From ref. [31]).
[c]) From $(\omega\tau)_{ext} = 0.0060\pm0.0007$ rad given in ref. [5]) and our value $\tau_{139} = 108\pm15$ psec.
[d]) From ref. [30]).
[e]) Equals the predicted value of $\langle\frac{1}{2}|j_-|\frac{3}{2}\rangle = 0.67$ from ref. [1]) together with $E^x \approx \hbar^2/2J = 30$ keV.
[f]) Best fit to the experimental data with $\mu\ \frac{5}{2}\frac{3}{2}^+(402)$ excluded.
[g]) Fit to experimental data when $G_{M1}(\frac{1}{2}\to\frac{1}{2})b_{M1}$ is fixed to 2.0.

values (including two limits). These, together with three measured magnetic moments, can be confronted with the Nilsson model predictions. The experimental data are collected in the left-hand part of table 9. That some of this information is not consistent with the pure Nilsson model is immediately seen, as for instance this model predicts that B(M1; $\frac{5}{2}\frac{1}{2}\to\frac{5}{2}\frac{3}{2}$)/$B$(M1, $\frac{5}{2}\frac{1}{2}\to\frac{3}{2}\frac{3}{2}$) = 6.75 as compared with the experimental value < 0.13.

To see whether better agreement with experiment can be obtained, we have made an analysis with the inclusion of Coriolis coupling. For simplicity we have confined ourselves to a system containing the $\frac{1}{2}^+(400)$ and $\frac{3}{2}^+(402)$ orbitals, although contributions from, for instance, the $\frac{3}{2}^+(411)$ and $\frac{5}{2}^+(402)$ orbitals may be of some importance. With the mentioned simplifications the reduced M1 transition rates can be written

$$B(\mathrm{M1}, IK\to I'K') = 5.91\times10^{-2}\sum_{XY}\{C(IXK)C(I'YK') \times[P_+(X\to Y)G_{M1}(X\to Y)\times(IX1, Y-X|I'Y)+(-1)^{I'+Y} \times(IX1, -Y-X|I', -Y)b_{M1}\delta_{X,\frac{1}{2}}\delta_{Y,\frac{1}{2}}]\}^2, \quad (5)$$

while the magnetic moment for a state (IK) is given by

$$\mu_K(I) = g_R I + \sum_X C(IXK)^2\frac{X^2}{2(I+1)}G_{M1}(X\to X)[1+(-1)^{I+\frac{1}{2}}(2I+1)b_{M1}\delta_{X,\frac{1}{2}}] +\tfrac{1}{2}\frac{I}{I+1}\sum_{X\neq Y}C(IXK)C(IYK)(IX1, Y-X|IY)G_{M1}(X\to Y), \quad (6)$$

where X and Y can take any of the combinations of K and K' (in this case $\frac{1}{2}$ and $\frac{3}{2}$) and $P_+ \approx 1.0$. The quantities G_{M1} are defined by eqs. (36a) and (36b) in ref. [1]). To describe the magnetic properties of the $K = \frac{1}{2}$ and $\frac{3}{2}$ bands we now need the following six parameters, namely $P_+(\frac{1}{2}\to\frac{3}{2})G_{M1}(\frac{1}{2}\to\frac{3}{2})$, $G_{M1}(\frac{3}{2}\to\frac{3}{2})$, $G_{M1}(\frac{1}{2}\to\frac{1}{2})$, $b_{M1}G_{M1}(\frac{1}{2}\to\frac{1}{2})$, g_R and $E^x\langle\frac{1}{2}|j_-|\frac{3}{2}\rangle$. The known experimental data have been used to evaluate the first five of these parameters from a least-squares fit to eqs. (5)-(6) using different values of $E^x\langle\frac{1}{2}|j_-|\frac{3}{2}\rangle$ which through eqs. (3)-(4) determines the mixing amplitudes $C(IXK)$.

The fitted parameters as well as the calculated μ and B(M1) values are given in table 9 for some selected $E^x\langle\frac{1}{2}|j_-|\frac{3}{2}\rangle$ values. As a measure of the goodness of the fit

we have used the mean square sum defined through

$$\sum_N \frac{(T_N - T_{\text{fit}})^2}{\Delta T_N} \frac{1}{N},$$

where $T_N \pm \Delta T_N$ is the experimental value with estimated error, T_{fit} is the corresponding fitted value and N the number of fitted data. Table 9 shows that especially the reduced transition probabilities $B(\text{M1}, \frac{3}{2}\frac{1}{2} \rightarrow \frac{3}{2}\frac{3}{2})$ and $B(\text{M1}, \frac{5}{2}\frac{1}{2} \rightarrow \frac{3}{2}\frac{3}{2})$ are sensitive to admixtures. It is also seen that the fit is improved when Coriolis mixing is taken into account with an optimum around the predicted value of $E^x\langle\frac{1}{2}|j_-|\frac{3}{2}\rangle = 20$ keV. The fitted parameters in each case are given in the lower part of table 9. We can see that $G_{\text{M1}}(\frac{3}{2} \rightarrow \frac{3}{2})$, $G_{\text{M1}}(\frac{1}{2} \rightarrow \frac{1}{2})$ and g_{R} are quite independent of the coupling strength. Using the fitted parameters, predicted values for $B(\text{M1}, \frac{3}{2}\frac{1}{2} \rightarrow \frac{5}{2}\frac{3}{2})$ and $B(\text{M1}, \frac{5}{2}\frac{1}{2} \rightarrow \frac{5}{2}\frac{3}{2})$ are obtained and compared with the experimental limits at the bottom of the table. The only experimental value that significantly deviates from the fitted value is the magnetic moment for the $\frac{5}{2}\frac{3}{2}^+(402)$ state where no improvement is obtained by mixing. A new fit was therefore attempted excluding this particular experimental point. The best fit was again obtained for $E^x\langle\frac{1}{2}|j_-|\frac{3}{2}\rangle = 20$ keV and the result is shown in the right-hand part of table 9. The fit is now in general better. Although the fitted parameters have not changed very much by excluding $\mu\frac{5}{2}\frac{3}{2}^+(402)$ the corresponding errors have been reduced considerably.

It is now interesting to see whether the Nilsson model can account for the fitted parameters. According to a recent calculation [32]) the gyromagnetic ratio g_{R} in ^{191}Ir is 0.56, which is close to the value of $g_{\text{R}} = 0.59 \pm 0.06$ which we get in ^{193}Ir. We have therefore used this comparatively high value of g_{R} in our further calculations. To evaluate the theoretical predictions we have used the parameters $\kappa = 0.05$, $\mu = 0.55$, $\delta = 0.1$ and $g_{\text{s}}(\text{effective}) = 0.6\, g_{\text{s}}(\text{free})$, where we have also investigated the predicted values for 10 % changes in all mentioned parameters. Below are given the obtained nominal values and the worst deviations of these values from the 10 % changes. We get $G_{\text{M1}}(\frac{1}{2} \rightarrow \frac{3}{2}) = -(0.19 \pm 0.05)$, $G_{\text{M1}}(\frac{3}{2} \rightarrow \frac{3}{2}) = -(1.7 \pm 0.3)$, $G_{\text{M1}}(\frac{1}{2} \rightarrow \frac{1}{2}) = 2.2 \pm 0.3$ and $G_{\text{M1}}(\frac{1}{2} \rightarrow \frac{1}{2})b_{\text{M1}} = 3.0 \pm 0.5$. We see from a comparison with the fitted parameters given in table 9 that the signs of all quantities are correctly predicted, and so is the magnitude of the three first parameters; while $G_{\text{M1}}(\frac{1}{2} \rightarrow \frac{1}{2})b_{\text{M1}}$ comes out too low in the fit.

To see whether a reasonable fit can also be obtained for a larger value of $G_{\text{M1}}(\frac{1}{2} \rightarrow \frac{1}{2})$ b_{M1} we have quite arbitrarily set this parameter at 2.0 and made a new fit, the result of which is shown in the last column in table 9. As is seen, the other parameters are not changed very much by fixing this value and we still get a reasonable fit to experimental data. This means that using Nilsson model parameters we are able to predict the magnetic properties of the $\frac{1}{2}^+(400)$ and $\frac{3}{2}^+(402)$ bands in ^{193}Ir at least to within a factor of three.

5. Conclusion

The transition probabilities between the low-lying states in ^{193}Ir agree in general better with the Nilsson model than with the core excitation model. Both models, however, predict a magnetic moment of the 139 keV $\frac{5}{2}^+$ state which is almost twice the experimental value.

References

1) S. G. Nilsson, Mat. Fys. Medd. Dan. Vid. Selsk. **29**, No. 16 (1955)
2) A. de-Shalit, Phys. Rev. **122** (1961) 1530
3) S. V. Nablo *et al.*, Can. J. Phys. **36** (1958) 1409
4) Nuclear Data Sheets 1958, Nat. Academy of Sciences, Washington D.C.
5) S. Gustafsson *et al.*, Ark. Fys. **34** (1967) 169
6) F. C. Perry and E. Smith Murphy Jr., Nucl. Phys. **A99** (1967) 497
7) P. Alexander and H. Ryde, Bull. Am. Phys. Soc. **12** (1967) 597 and private communication
8) M. W. Johns, R. H. Price and N. M. Ahmed, contributions to Int. Conf. on nuclear structure (Sept. 7-13, 1967, Tokyo) Tokyo Univ. Tokyo 1967
9) R. Avida *et al.*, Nucl. Phys. **A114** (1968) 365
10) R. Avida, J. Burde and A. Molchadzki, Nucl. Phys. **A115** (1968) 405
11) Z. Plajner *et al.*, Nucl. Phys. **A121** (1968) 367
12) F. R. Metzger, Phys. Rev. **161** (1967) 1249
13) F. K. McGowan and P. H. Stelson, Phys. Rev. **109** (1958) 901
14) A. Bäcklin, Nucl. Instr. **57** (1967) 261
15) A. Bäcklin, B. Fogelberg, M. Saraceno and G. Hedin, to be published
16) S. Hager and E. C. Seltzer, Nucl. Data **A4** No. 1 and 2 (1968)
17) T. R. Gerholm and J. Lindskog, Ark. Fys. **24** (1963) 171
18) S. G. Malmskog, Ark. Fys. **35** (1967) 255
19) J. Lindskog *et al.*, Nucl. Phys. **A137** (1969) 511
20) A. H. Wapstra, G. J. Nijgh and R. van Lieshout, Nuclear spectroscopy tables (North-Holland Publ. Co., Amsterdam, 1959)
21) R. H. Price *et al.*, Can. J. Phys. **47** (1969) 727
22) A. Bäcklin, S. G. Malmskog and V. Berg, to be published
23) K. H. Frank, Z. Phys. **203** (1967) 71
24) A. de-Shalit, Phys. Lett. **15** (1965) 170
25) A. Braunstein and A. de-Shalit, Phys. Lett. **1** (1962) 264
26) A. Bäcklin, B. Fogelberg and S. G. Malmskog, Nucl. Phys. **A103** (1967) 337
27) P. H. Blichert-Toft, E. G. Funk and J. W. Mihelich, Nucl. Phys. **77** (1966) 513
28) R. T. Brockmeier *et al.*, Nucl. Phys. **63** (1965) 102
29) A. K. Kerman, Mat. Fys. Medd. Dan. Vid. Selsk. **30**, No. 15 (1956)
30) F. Wagner *et al.*, Z. Phys. **207** (1967) 500
31) A. Narath and D. C. Barham, Bull. Am. Phys. Soc. **12** (1967) 314
32) O. Prior, F. Boehm and S. G. Nilsson, Nucl. Phys. **A110** (1968) 257

REFERENCE 10

THE LOW-ENERGY LEVEL STRUCTURE OF ^{191}Ir

S. G. MALMSKOG and V. BERG
AB Atomenergi, Studsvik, Nyköping, Sweden and
Institute of Physics, University of Stockholm, Sweden

A. BÄCKLIN and G. HEDIN
The Swedish Research Councils
Laboratory, Studsvik, Nyköping, Sweden and
Institute of Physics, University of Uppsala, Sweden

1.E.1:
3.A

Nuclear Physics **A143** (1970) 160—176; © *North-Holland Publishing Co., Amsterdam*
Not to be reproduced by photoprint or microfilm without written permission from the publisher

THE LOW-ENERGY LEVEL STRUCTURE OF ^{191}Ir

S. G. MALMSKOG and V. BERG
AB Atomenergi, Studsvik, Nyköping, Sweden and
Institute of Physics, University of Stockholm, Sweden

A. BÄCKLIN and G. HEDIN
The Swedish Research Councils
Laboratory, Studsvik, Nyköping, Sweden and
Institute of Physics, University of Uppsala, Sweden

Received 17 November 1969

Abstract: The decay of ^{191}Pt to ^{191}Ir has been investigated using Ge(Li) detectors and a double focusing beta spectrometer. Thirty-five transitions were observed and most of them were placed in a level scheme. Special attention was given to the low energy level band structure. Several multipolarity mixing ratios were determined from L-subshell ratio measurements. Using the delayed coincidence technique the half-life of the 179.05 keV level was measured to 40 ± 12 psec. The low-level decay properties are discussed in terms of the Nilsson model with the inclusion of Coriolis coupling.

E RADIOACTIVITY ^{191}Pt [from Pb (p, spallation)]; measured E_γ, I_γ, E_{ce}, I_{ce}, cece-delay. ^{191}Ir deduced levels, $T_{\frac{1}{2}}$, J, π, cc, multipolarities, mixing ratios, B(E2), B(M1), Q. Isotope separated sources, Ge(Li) detector.

1. Introduction

Over the last fifteen years it has been common practice to classify nuclei as either having a spherical or a deformed shape. The border line between these two groups is, however, not sharp and in some cases both spherical and deformed states possibly exist in the same nucleus [1,2]). The Os and Ir isotopes belong to a group of nuclei situated between the deformed rare-earth region and the spherical lead region. For some years we have made systematic studies of such transitional nuclei with a special emphasis to investigate the decay properties of the low-lying excited levels [3]).

The present paper is part of this general survey by reporting on the low-level structure of ^{191}Ir. In particular we have devoted our interest to examine the transitions within the proposed low-lying rotational bands [4]) in this nucleus. Here we have measured accurate transition energies and L-subshell conversion ratios to determine multipole mixing ratios. Half-lives of excited levels have been measured with the delayed coincidence technique and γ-ray transition intensities determined from Ge(Li) detector spectra. From this experimental material absolute transition probabilities have been deduced and the result is discussed in terms of the Nilsson model [5]) with the inclusion of Coriolis coupling [6]).

2. Experimental procedure

2.1. SOURCE PREPARATION

The ^{191}Pt activity was obtained as a decay product of ^{191}Hg. This mercury activity was produced from spallation in a molten lead target at 700 °C when bombarded in an external beam of 600 MeV protons from the synchrocyclotron at CERN. The extracted mercury was isotopically separated in the ISOLDE on line mass separator facility [7]) and collected on a 0.9 mg/cm^2 nickel foil, which served as backing in all measurements described below. Typical irradiation times were of the order of 20 h and typical transport times from Geneva to Studsvik were 12 h.

2.2. GAMMA-RAY SPECTROSCOPY

The ^{191}Pt sources were first measured with Ge(Li) spectrometers to decide the purity of the source. An effort was also made to determine more accurately the intensity of the low-energy γ-rays of special interest to this work and to verify the high-energy spectrum recently reported by Schumacher *et al.* [8]).

Two Ge(Li) detectors were used. One detector had a 1.5 cm^3 sensitive volume and an energy resolution of 1.2 keV at 122 keV. This detector was used to measure the low-energy γ-ray spectrum up to 360 keV and some intense doublet lines. A second detector with 24 cm^3 active volume and shielded with 4 mm Pb was used to record the high-energy γ-ray spectrum. All detector units were furnished with cooled FET preamplifiers together with a TC 200 linear amplifier, a Tennelec 250 bias amplifier and a Nuclear Data 4096-channel analyser. Energy and intensity calibration of the system was performed by measuring a set of absolute calibrated standard sources † of ^{57}Co, ^{60}Co, ^{137}Cs, ^{22}Na, ^{54}Mn and ^{88}Y together with the well determined γ-rays from the decay of ^{182}Ta [refs. [9,10])] and ^{187}W [refs. [11,12])]. The γ-ray spectrum from the ^{191}Pt decay was followed for several half-lives in order to assign the observed transitions to the proper decay. Only very weak contaminants could be observed among which the strongest lines in the decay of ^{188}Pt(10.2 d) and ^{189}Ir(13.3d) could be clearly identified, since the decay of these two nuclei is well known to us through parallel studies [3]).

The low- and high-energy γ-ray spectra observed in the decay of ^{191}Pt are shown in fig. 1. The result from the analysis of γ-ray energies and intensities are given in table 1 together with the result of Blichert-Toft *et al.* [4]) and Schumacher *et al.* [8,14]). For comparison we also give the transition energies reported by Harmatz *et al.* [15]) and Marklund *et al.* [16]). The triplet group around 222 keV has been resolved in the Ge(Li) γ-ray spectrum and the result is shown in fig. 2. The conversion electron spectrum also shows that there should be a doublet of lines with energies of 267.99 ± 0.06 and 268.81 ± 0.05 keV. Using these accurate energies and an average shape of the observed γ-ray peaks from the single peaks at 179.05, 219.74, 351.25 and 360.00 keV we have used a computer to unfold the expected peaks at 267.99 and 268.81 keV.

† Obtained from IAEA, Vienna.

145

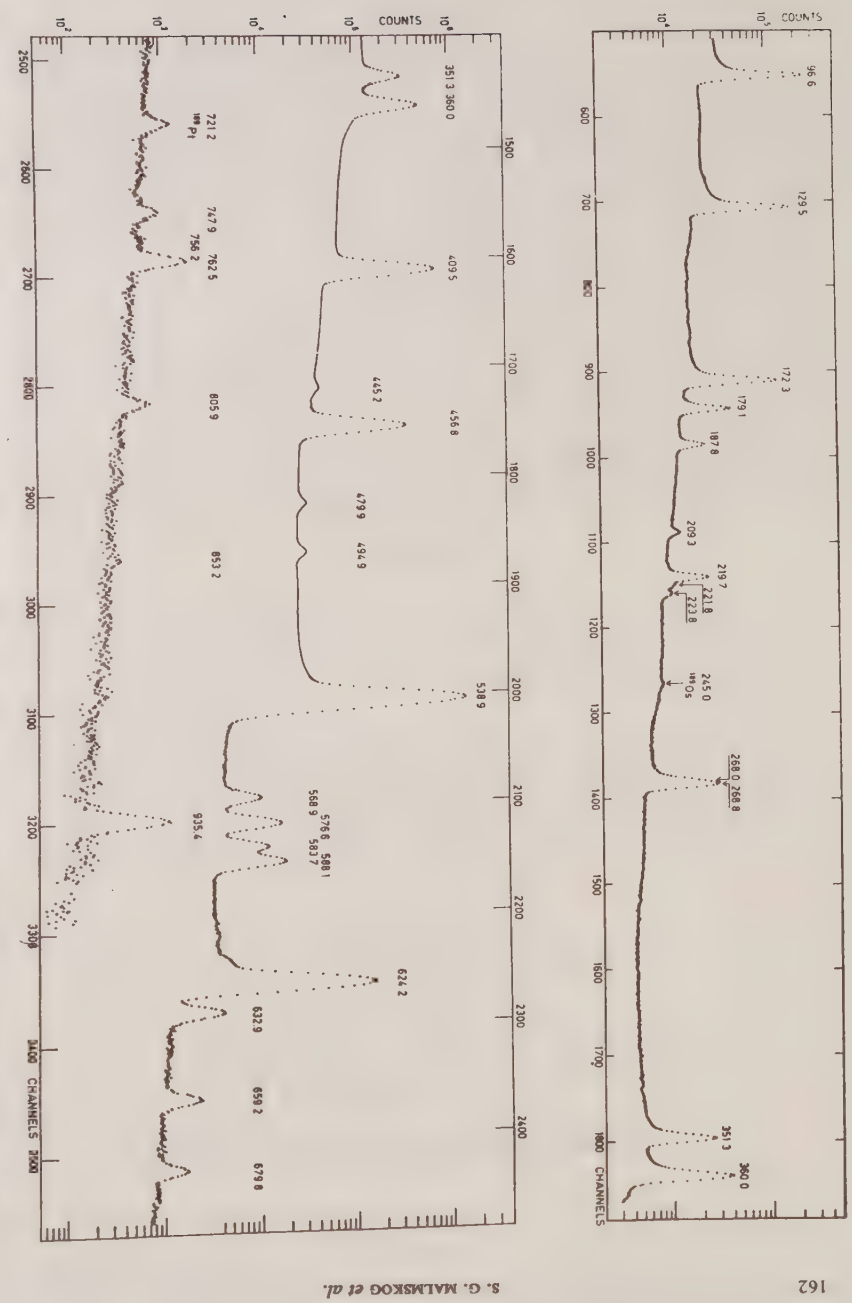

Fig. 1. Gamma-ray spectra in the decay of ^{191}Pt. The upper spectrum was observed with a 1.5 cm^3 Ge(Li) detector while in the lower spectrum a 24 cm^3 Ge(Li) detector shielded with 4 mm Pb was used.

The result is shown in the right-hand part of fig. 2. The intensity ratio obtained between the 268.81 and 267.99 keV transitions is 2.7 ± 0.5 where the error mainly comes from the uncertainty in the exact position and shape of the γ-lines.

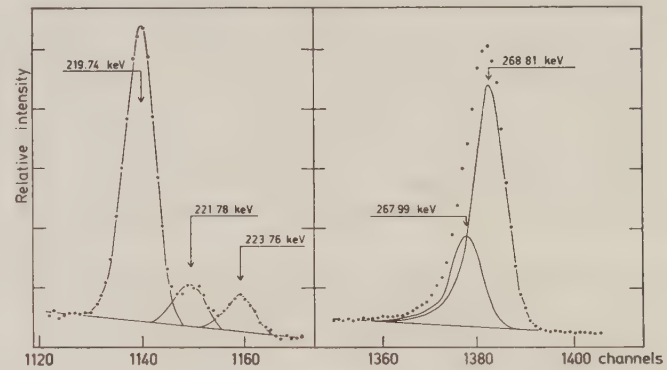

Fig. 2. The triplet group at 222 keV and the doublet group at 268 keV as observed in the 1.5 cm^3 Ge(Li) detector.

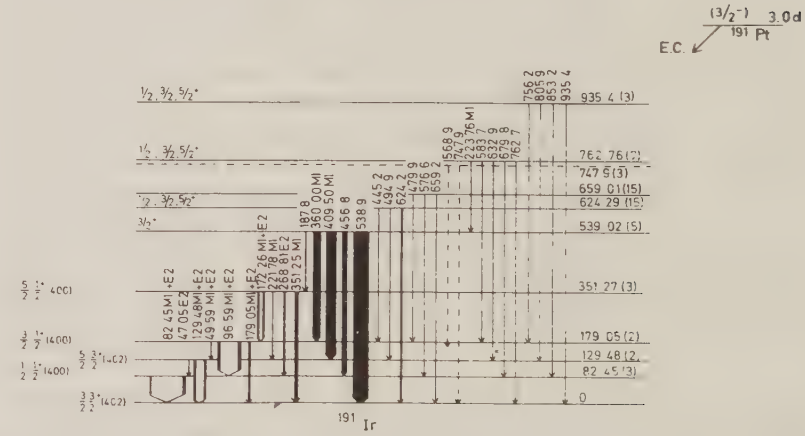

Fig. 3. Levels of ^{191}Ir populated from the decay of ^{191}Pt. The widths of the arrows are approximately proportional to the intensities of the corresponding transitions, the white part indicating the internal conversion intensity. The numbers in parenthesis after the level energies give the error of the last decimal. To the left are shown the interpretation of the lowest levels in the Nilsson scheme.

From the γ-ray and conversion electron measurements (see below) a decay scheme of ^{191}Ir is suggested in fig. 3. Table 2 gives intensity limits for transitions which might exist according to this decay scheme but which are not observed in this work.

TABLE 1

Gamma-ray transition energies and intensities in ^{191}Ir observed in the decay of ^{191}Pt

Energies						Gamma-intensities			
Harmatz *et al.* 1962 ref. [15])	Marklund *et al.* 1962 ref. [16])	Blichert-Toft *et al.* 1966 ref. [4])	Schumacher *et al.* 1966 ref. [14])	Schumacher *et al.* 1967 ref. [8])	Present work 1969	Blichert-Toft *et al.* 1966 ref. [4])	Schumacher *et al.* 1966 ref. [14])	Schumacher *et al.* 1967 ref. [8])	Present work 1969
41.8					41.92±0.02 [a])				
49.5					47.05±0.03 [a])				
82.45	82.33	82	82		49.59±0.03 [b])				
85.2					82.45±0.03 [b])	63.0 ± 7.0	62		
96.5	96.45	96.5	96		96.59±0.03 [b])	38.0 ± 4.0	36		37.9 ±1.9
129.45	129.39	129	129		129.48±0.02 [b])	34.5 ± 4.0	36		37.1 ±1.8
172.3	172.16	172	172		172.26±0.03 [b])	40.0 ± 4.0	42		41.9 ±2.0
179.0	178.90	179	179		179.05±0.03 [b])	11.0 ± 2.0	12.4		12.2 ±0.6
	186.83	} 188	} 187			0.5 ± 0.3	} 4.8		< 0.4
187.75	187.76				187.8 ±0.1	4.4 ± 2.0			5.0 ±0.3
213.8		214			209.3 ±0.1				1.6 ±0.1
219.8	219.71	} 220	220			1.4 ± 0.5		< 0.2	< 0.1
221.9	221.79		222		219.74±0.04 [b])	} 13.0 ± 2.0 { 8	16	10.1 ±1.6	10.9 ±0.6
223.7		223	224		221.78±0.04 [b])	5		1.3 ±0.4	1.7 ±0.2
	227.93				223.76±0.04 [b])	2.1 ± 0.4	< 2	0.9 ±0.3	1.3 ±0.2
268.25								< 0.5	< 0.3
269.1	268.8	} 269	} 269		267.99±0.06 [b])				
272.0					268.81±0.05 [b])	} 30.0 ± 4.0 { 9 21 0.5 }	} 36	} 32.0 ±2.5	} 33.1 ±1.7 [c])
351.5	351.26	351	351						<0.3
360.3	360.0	360	360		351.25±0.05 [b])	41.0 ± 4.0	34	42.0 ±3.1	43.5 ±2.1
409.9	409.58	410	410		360.00±0.05 [b])	80.0 ± 8.0	58	72.0 ±6.0	73.1 ±3.7
				444.9±0.6	409.50±0.05 [b])	100	100	100	100
457.0	456.80	457	457	456.8	445.2 ±0.2			1.2 ±0.2	0.82 ±0.08
			481	480.1±0.4	456.8 ±0.2	42 ± 4	42	42.0 ±1.7	42.4 ±2.0
493.0		} 494	} 495 ~		479.9 ±0.2		1.2	0.82 ±0.09	0.61 ±0.07
495.1				494.9±0.5	494.9 ±0.2	} 0.7 ± 0.3	} 0.8	} 0.81 ±0.08	< 0.2
	501.42	501				0.12± 0.08			0.76 ±0.08
539.5	539.11	539	539	539.0±0.3	538.9 ±0.2	185.0 ±15.0	184	< 0.15	< 0.2
	569.08	570	569	568.8±0.3	568.9 ±0.3	0.9 ± 0.1	0.68	184.5 ±5.5	186.0 ±8.0
	575.60	576	577	576.3±0.3	576.6 ±0.3	1.6 ± 0.2	1.6	0.75 ±0.03	0.68 ±0.04
584.2		584	586	583.5±0.4	583.7 ±0.3	1.0 ± 0.1	2.0	1.62 ±0.07	1.61 ±0 09
588.3	587.89	588		588.0±0.3	588.1 ±0.3	2.0 ± 0.5		1.11 ±0.06	1.37 ±0.10
604.6			(602)				(0.24)	1.89 ±0.07	1.92 ±0.10
624.6	624.06	624	624	623.9±0.3	624.2 ±0.3	21.0 ± 4.0	19.2		
	632.57	633		632.7±0.4	632.9 ±0.5	0.36± 0.05		20.1 ±0.8	20.5 ±1.5
		659	660	658.7±0.7	659.2 ±0.5	0.23± 0.03	0.22	0.38 ±0.02	0.37 ±0.04
		679	678	679.7±0.4	679.8 ±0.5	0.09± 0.07	0.06	0.18 ±0.03	0.20 ±0.04
			750	747.7±0.8	747.9 ±0.5		0.06	0.11 ±0.02	0.11 ±0.03
				756.0±0.9	756.2 ±0.8			0.05 ±0.01	0.045±0.010
		762	764	762.2±0.2	762.7 ±0.4	0.23± 0.08	0.14	0.02 ±0.01	0.015±0.010
			810	805.7±0.7	805.9 ±0.5		0.054	0.18 ±0.03	0.17 ±0.02
				853.0±1.2	853.2 ±1.0			0.054±0.009	0.045±0.010
			940	935.6±0.4	935.4 ±0.4			0.02 ±0.01	0.015±0.010
								0.14 ±0.02	0.16 ±0.02

[a]) Given by the authors in ref. [21]). [b]) From conversion electron measurements, table 3.

[c]) See subsect. 2.2.

TABLE 2

Missing transitions in the ^{191}Ir decay scheme proposed in fig. 3

Initial level (keV)	Final level (keV)	Transition (keV)	Initial I^π	Final I^π	Suggested multipolarity	Gamma ray intensity [a])
935.4	762.8	172.6	$\frac{1}{2}, \frac{3}{2}, \frac{5}{2}$	$\frac{1}{2}, \frac{3}{2}, \frac{5}{2}^+$	M1	< 3.0 [b])
935.4	659.0	276.4	$\frac{1}{2}, \frac{3}{2}, \frac{5}{2}$	—	M1, E2	< 0.1
935.4	624.3	311.1	$\frac{1}{2}, \frac{3}{2}, \frac{5}{2}$	$\frac{1}{2}, \frac{3}{2}, \frac{5}{2}$	M1	< 0.1
935.4	539.0	396.6	$\frac{1}{2}, \frac{3}{2}, \frac{5}{2}^+$	$\frac{3}{2}^+$	M1	<0.3
935.4	351.3	584.3	$\frac{1}{2}, \frac{3}{2}, \frac{5}{2}$	$\frac{5}{2}^+$	M1	< 0.7 [c])
762.8	659.0	103.8	$\frac{1}{2}, \frac{3}{2}, \frac{5}{2}^+$	—	M1, E2	< 0.05
762.8	624.3	138.5	$\frac{1}{2}, \frac{3}{2}, \frac{5}{2}^+$	$\frac{1}{2}, \frac{3}{2}, \frac{5}{2}$	M1	< 0.5 [d])
762.8	351.3	411.5	$\frac{1}{2}, \frac{3}{2}, \frac{5}{2}^+$	$\frac{3}{2}^+$	M1	< 4.0 [e])
659.0	539.0	120.0		$\frac{3}{2}^+$	M1	< 0.07
659.0	351.3	307.7		$\frac{5}{2}^+$	M1	< 0.1
659.0	129.5	529.5		$\frac{5}{2}^+$	M1	< 0.3
624.3	351.3	273.0	$\frac{1}{2}, \frac{3}{2}, \frac{5}{2}$	$\frac{5}{2}^+$	M1	< 0.2
624.3	82.5	541.8	$\frac{1}{2}, \frac{3}{2}, \frac{5}{2}$	$\frac{1}{2}^+$	M1, E2	< 3.0 [f])

[a]) Same intensity scale as in table 1.
[b]) Not resolved from the 172.26 keV line.
[c]) Not resolved from the 583.7 keV line.
[d]) There is an observed line at roughly that energy, but its apparent half-life is much larger than 3 days. Probably a line in the decay of ^{188}Pt.
[e]) Not resolved from the 409.50 keV line.
[f]) Not resolved from the 538.9 keV line.

2.3. ELECTRON SPECTROSCOPY

A special effort was made to investigate the conversion electron spectrum of all transitions in the rotational like low-lying energy region of ^{191}Ir. For this purpose we used the 50 cm $\pi\sqrt{2}$ iron yoke double-focusing β-spectrometer at Studsvik [17,18]). The baffles were adjusted to give an energy resolution of 0.2–0.4 % FWHM. The electrons were detected using a GM-counter with a thin mylar window which transmitted the measured electrons without observable energy and intensity loss.

The active sources, collected in the ISOLDE mass separator on a thin nickel foil, had an extension of about 4 mm and were masked to 2 mm width. To get good statistical accuracy some groups of lines were recorded with up to 1000 sec per point. In all cases each measured point has been corrected for decay relative to a fixed time so that also a comparison of intensity measurements between different groups of lines have been possible. The energy calibration was made against the 100.104 L_{II} line in ^{182}W, the 276.43 K line in ^{133}Cs and the 661.595 K line in ^{137}Ba. Where possible we have tried to accurately determine the L-subshell ratios for the transitions in order to deduce the multipolarity mixing ratios so vital to the following discussion of the low energy level structure in ^{191}Ir. In fig. 4 are shown the resolved groups together with an analysis for the determination of the E2/M1 mixing ratio δ^2. The results from the conversion electron measurements are summarized in table 3 giving transition energies

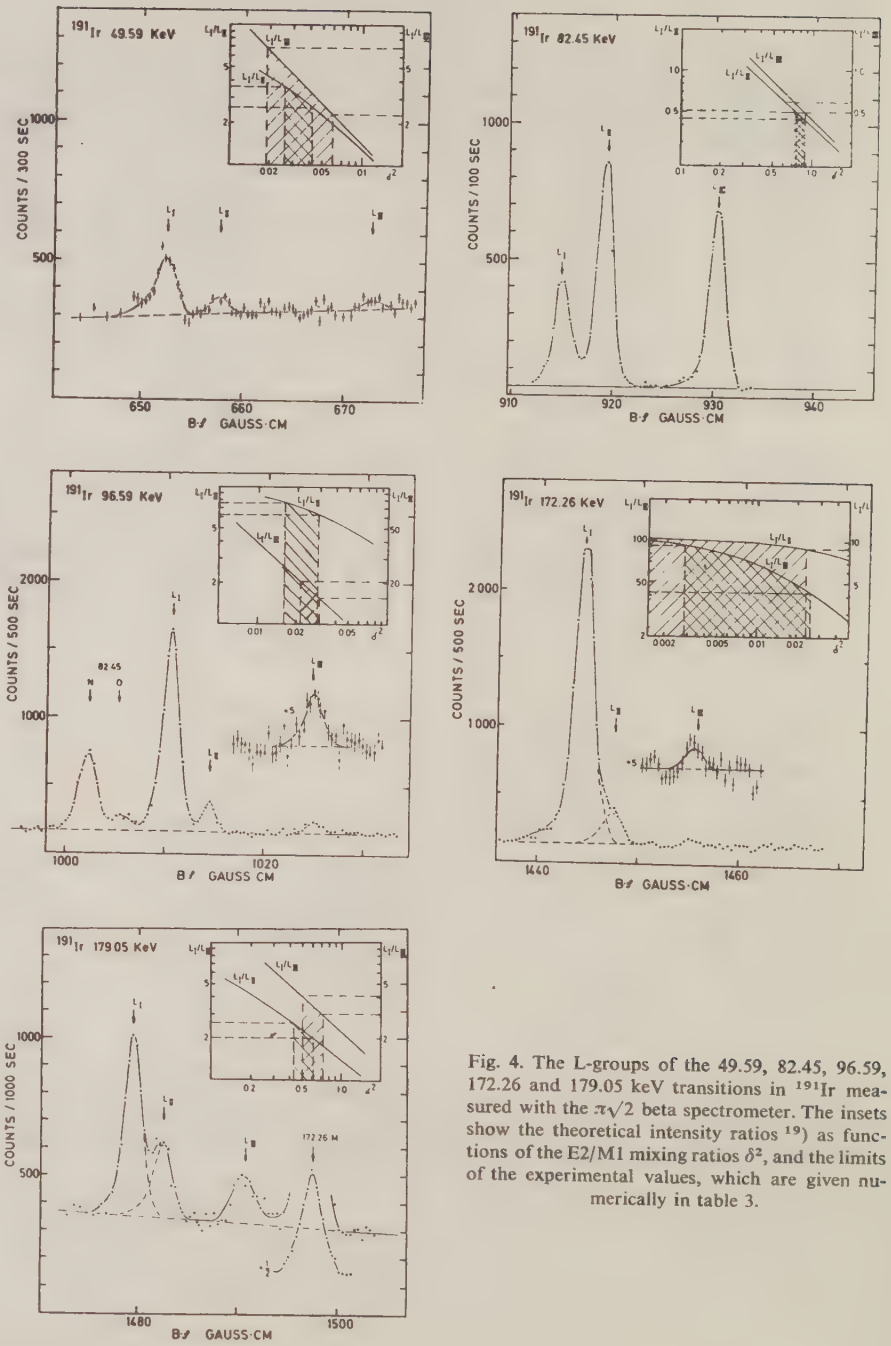

Fig. 4. The L-groups of the 49.59, 82.45, 96.59, 172.26 and 179.05 keV transitions in ^{191}Ir measured with the $\pi\sqrt{2}$ beta spectrometer. The insets show the theoretical intensity ratios [19]) as functions of the E2/M1 mixing ratios δ^2, and the limits of the experimental values, which are given numerically in table 3.

and conversion electron intensities. These data in combination with the γ-ray intensities from table 1 give the conversion coefficients in column 6 of table 3. Normalization was made on the average of the theoretical values [19]) of the K-conversion coefficients of the 129 and 172 keV transitions using the experimental E2/M1 mixing ratios obtained from the L-subshell ratios. The multipolarities given in the last column in table 3 have been obtained from the experimental K-conversion coefficients and L-subshell ratios together with the theoretical calculations of Hager and Seltzer[19]).

2.4. HALF-LIFE MEASUREMENT

Half-lives for some of the low-lying levels in ^{191}Ir have been studied before [20]). We have recently measured the half-life of the 129.45 keV level in the decay of ^{191}Os obtaining 126±11 psec [ref. [21])]. Of the half-lives not measured up to now the one of the 179.05 keV level is of particular interest as it feeds levels in the proposed $K = \frac{1}{2}$ and $K = \frac{3}{2}$ rotational bands.

In the measurement to be presented below we used a long lens electron-electron coincidence spectrometer described in detail earlier [22,23]). The same sources were used as in the conversion electron measurement. To determine the time delay of the 179.05 keV level we observed the time coincidence distribution between 172.26 L and 96.59 L conversion electrons. As the observed spectrum had a prompt shape a centroid shift measurement had to be performed. The prompt reference curve was obtained from the $\beta \rightarrow$ 238.6 K cascade in the decay of ^{212}Pb. To be able to use the same energy settings in the two measurements 11 kV was applied to the ^{212}Pb source in order to pre-accelerate the 238.6 K electrons. Using the automatic operation of the spectrometer [23]) some 50 time spectra were altogether accumulated. These were taken at three different occasions with different sources. All spectra were measured during a 30 min period with alternatively the ^{191}Pt or the ^{212}Pb sample in the measuring position. Before and after each sequence of measurements the energy settings and spectrometer currents were carefully controlled. The stability of the entire equipment was also checked using the self-comparison method [24]) and the ^{212}Pb source. To shift the 238.6 K line between the two spectrometers we used a high tension of 15 kV. After correction for the change in transit time due to the pre-acceleration process no systematic shifts were observed.

All the accumulated data were analysed with the centroid shift method [24]). From the observed centroid shift when studying the 172.26 L → 96.59 L cascade, corrected for the effect of the pre-acceleration, we obtain a half-life of 40±12 psec for the 179.05 keV level in ^{191}Ir.

3. Discussion

3.1. THE DECAY SCHEME

Using the accurate transition energy values obtained from our conversion electron and γ-ray measurements a level scheme of ^{191}Ir has been constructed from energy sum combinations [25]). The level scheme obtained is shown in fig. 3. The major parts

TABLE 3

^{191}Pt → ^{191}Ir Internal conversion data

Transition energy (keV)	Electron intensity K	L_I	L_{II}	L_{III}	K conversion coefficient experiment	theory E1	theory E2	theory M1	Multipolarity
47.05		$\Sigma L = 0.47\pm0.08$ [b])							E2
49.59±0.03		3.7 ±0.5	1.2 ±0.2	0.8 ±0.4					M1+(3.2±0.8)%E2
82.45±0.03		53 ±3	116 ±6	98 ±6					M1+(45±2)%E2
96.59±0.03	(≈260)	43 ±2	6.2 ±0.6	2.4 ±0.3	1.05 [c])	0.0658 [c])	3.45 [c])	0.949 [c])	M1+(2.4±0.4)%E2
129.48±0.03	100 ±5				2.10 [a])	0.170	0.489	2.51	M1+(12.0±1.5)%E2 [b])
(170.55) [d])	< 0.4								
172.26±0.03	63 ±3	8.8 ±0.4	0.90±0.09	0.13±0.05	1.17 [a])	0.0823	0.251	1.11	M1+(1.0$^{+1.5}_{0.7}$)%E2
179.05±0.03	10.3 ±0.8	1.70±0.15	0.75±0.08	0.48±0.07	0.66 ±0.08	0.0747	0.227	0.984	M1+(36±2)%E2
219.74±0.04	2.1 ±0.2				0.151±0.018	0.0447	0.134	0.564	E2, < 10 %M1
221.78±0.04	1.30±0.15				0.59 ±0.09	0.0438	0.131	0.550	M1, < 12 %E2
223.76±0.04	1.10±0.12				0.66 ±0.12	0.0428	0.129	0.537	M1, < 10 %E2
267.99±0.06	1.2 ±0.1				0.104±0.025	0.0273	0.0803	0.325	E2, < 20 %M1
268.81±0.06	2.2 ±0.2				0.072±0.016	0.0271	0.0795	0.322	E2, < 4 %M1
(349) [d])	< 0.1								
351.25±0.07	8.2 ±0.4				0.147±0.015	0.0144	0.0405	0.156	M1, < 20 %E2
360.00±0.07	14.9 ±1.5				0.159±0.020	0.0137	0.0385	0.147	M1, < 8 %E2
409.50±0.08	13.2 ±1.3				0.103±0.012	0.0103	0.0284	0.110	M1, < 15 %E2

[a]) Normalization constant obtained as average of 129K and 172K. [b]) From ref. [21]). [c]) L-shell conversion coefficient.
[d]) Lines suggested in ref. [16]).

of it is very similar to the one recently proposed by Schumacher *et al.* [8]). A few things are, however, worth commenting on.

We did not observe any 186.8 keV transition as suggested in ref. [16]) and if a level at that energy exists at all in ^{191}Ir it is certainly only weakly fed in the decay of ^{191}Pt.

Blichert-Toft *et al.* [4]) have suggested a level at 569.08 keV decaying with a 569.1 keV ground state transition and a 219.8 keV transition to the well established 351.27 keV level. Comparing the transition energies we find an energy discrepancy in this suggested crossover/cascade of 2.0 keV, which is nearly ten times the experimental energy errors. Schumacher *et al.* [8]) suggested that the 219.8 keV transition may feed the 350 keV level observed in Coulomb excitation [26]). This level was, however, found to decay with a strong 350 keV transition which has not been observed in this work. We thus find no evidence for a level around 569 keV in ^{191}Ir.

In a nuclear resonance scattering experiment Langhoff [27]) observed a 590±15 keV transition. He interpreted this transition to come from a level with the same energy and assigned this level as $\frac{5}{2}\,\frac{5}{2}^+$ (402). In recent high-resolution decay works an unassigned 588.1±0.3 keV transition is observed which by Schumacher *et al.* [8]) has been identified with the earlier 590±15 keV line. No other evidence for a level at 588.1 keV has been found by us. No γ-ray feeding to this level has been observed and the expected de-excitations to the $\frac{5}{2}^+$, 129.48 keV and $\frac{3}{2}^+$, 179.05 keV levels have not been observed either.

We tentatively suggest a level at 747.9 keV from the energy sum 568.9+179.0 and the observed 747.9±0.5 keV transition. The probability of obtaining an accidental combination between the few unplaced transitions is fairly small (of the order of 10 %). The expected transitions to the 82.45 and/or 129.48 keV levels have, however, not been observed.

After having completed the level scheme given in fig. 3 there are still two comparatively strong E2 transitions at 219.74 and 267.99 keV that do not combine with the established levels. A $\frac{7}{2}^+$ state has been observed in an early Coulomb excitation experiment [26]) at about 350 keV. Since with very few exceptions, first forbidden unique β-transitions have log $ft \leqq 9.4$, a $\frac{7}{2}^+$ level at 350 keV can be expected to be fed strongly enough in the decay of ^{191}Pt for the depopulating transitions to be observed in the present work (total $I_\gamma \geqq 1.5$ in the units of table 1). It could therefore be possible that the 219.74 keV E2 transition ($I_\gamma = 10.9$ units) is the $\frac{7}{2}^+ \rightarrow \frac{5}{2}^+$ transition. On the other hand, a fairly strong 350 keV transition was found in the Coulomb excitation experiment [26]), which was assigned as the ground state transition from the $\frac{7}{2}^+$ state. Since no such transition was found in the present study (the K-conversion line being weaker than 5 % of the 219.74 K line) the suggested position of the 219.74 keV transition is not likely.

3.2. THE LOW-LYING ENERGY LEVEL SPECTRUM

In a preceding paper [13]) the transition probabilities in the low energy structure in ^{193}Ir was compared to the predictions of the core excitation model [28]) and the Nilsson model including Coriolis coupling [5]). It was found that the Nilsson model reproduces the experimental data better than the core excitation model assuming only small admixtures of a limited number of states in the latter. Since both the level energies and transition probabilities change very little in going from ^{193}Ir to ^{191}Ir we restrict ourselves in the latter case to make a comparison only with the Nilsson model.

The low-energy part of the ^{191}Ir level scheme (fig. 3) clearly shows a rotational like pattern so characteristic for deformed nuclei. The two lowest expected single-particle states are according to the Nilsson model [5]) $\frac{3}{2}^+$ (402) and $\frac{1}{2}^+$ (400). Three members of the first band consists of the ground state and the 129.48 and ≈ 348 keV levels [26]). The $\frac{1}{2}^+$ (400) band head is assigned to the 82.45 keV level with rotational levels at 179.05 and 351.27 keV. Blichert-Toft *et al.* [4]) have suggested that the $\frac{7}{2}^+$ member of the $K = \frac{1}{2}$ is at 569.08 keV. As was discussed in subsect. 3.1 no convincing experimental evidence exists for a level at that energy and even if it existed its decay properties with a 219.74 keV E2 transition to the $\frac{5}{2}^+$ member of the same band and no observable transition to its $\frac{3}{2}^+$ component is not consistent with the simple Nilsson model predictions.

Owing to the expected weak deformation of the ^{191}Ir nucleus and to the closeness of the $K = \frac{1}{2}$ and $\frac{3}{2}$ bands these two are likely to be heavily mixed through Coriolis coupling. An idea of the strength of this coupling can be obtained from the diagonalisation of the energies. We have done this considering only the intrinsic and rotational degrees of freedom including the Coriolis coupling. We then observe that only a moderate Coriolis coupling is needed to get the optimum fit to the experimental rotational energies, but this fit is not very dependent on the coupling strength. In all cases the decoupling parameter comes out as a small number (< 0.1). This seems to be a general feature in many Ir isotopes [3,13]).

3.3. E2 TRANSITION RATES

It is well known that the nature of a level is characterized by the transition strength depopulating the level. Therefore all available data on absolute M1 and E2 transition probabilities for de-excitations within and between members of the $K = \frac{1}{2}$ and $\frac{3}{2}$ bands have been collected in table 4.

From the absolute B(E2) values for intra-band transitions we obtain the quadrupole moment Q_0 and from that the actual stable deformation for the nucleus in a certain particle configuration. For the ground state band we obtain $Q_0 = 3.4 \pm 0.4$ b corresponding to a deformation of $\delta = 0.11 \pm 0.01$. This agrees with the corresponding values found in ^{193}Ir [ref. [13])]. For the $K = \frac{1}{2}$ band in ^{191}Ir we find the slightly higher value $Q_0 = 4.8 \pm 0.7$ b corresponding to $\delta = 0.15 \pm 0.02$. Both values are, however, hardly much larger than can be expected for vibrational E2 transition strengths in spherical nuclei and thus we cannot expect the adiabatic approximation to be strictly fullfilled in ^{191}Ir. The consequence of this is that Coriolis mixing between bands will be important.

TABLE 4

Absolute transition probabilities in ^{191}Ir

Level (keV)	$T_{\frac{1}{2}}$ (exp) of level (nsec)	Transition energy (keV)	Initial state $IK^{\pi}[N, n_z, \Lambda]$	Final state $IK^{\pi}[N, n_z, \Lambda]$	Multi-polarity	Relative N_γ	Relative N_e	$T_{\frac{1}{2}}$ (exp) (sec)	B(M1) in $\left(\frac{e\hbar}{2Mc}\right)^2$	B(E2) in $e^2 \cdot b^2$	Q_0 (b)	F_W [a]
82.5	3.8 ±0.4	82.5	$\frac{1}{2}\frac{1}{2}^+(400)$	$\frac{3}{2}\frac{3}{2}^+(402)$	M1	56	1085	8.1 E-8	(8.8 ±1.0) E-4			2020
					E2	44		1.0 E-7		(1.45±0.16) E-1		4.5 E-2
129.5	0.126±0.011	47.1	$\frac{3}{2}\frac{3}{2}^+(402)$	$\frac{1}{2}\frac{1}{2}^+(400)$	E2	0.008	1.2	6.1 E-6		(4.0 ±0.8) E-2		1.7 E-1
		129.5		$\frac{3}{2}\frac{3}{2}^+(402)$	M1	88	288	5.6 E-10	(3.28±0.31) E-2			54
					E2	12.3		4.0 E-9		(3.9 ±0.7) E-1	3.4±0.4	1.7 E-2
179.1	0.040±0.012	49.5	$\frac{5}{2}\frac{1}{2}^+(400)$	$\frac{5}{2}\frac{3}{2}^+(402)$	M1	0.43	5.3	3.1 E-8	(1.06±0.35) E-2			167
					E2	0.014		9.5 E-7		(2.0 ±0.9) E-1		4.6 E-2
		96.5		$\frac{1}{2}\frac{1}{2}^+(400)$	M1	37.0	265	3.6 E-10	(1.23±0.36) E-1			15
					E2	0.89		1.5 E-8		(4.6 ±1.5) E-1	4.8±0.7	1.5 E-2
		179.1		$\frac{3}{2}\frac{3}{2}^+(402)$	M1	7.9	9.8	1.7 E-9	(4.1 ±1.2) E-3			435
					E2	4.3		3.1 E-9		(9.9 ±3.0) E-2		6.6 E-2
349	0.0136 [b]	219	$\frac{7}{2}\frac{3}{2}^+(402)$	$\frac{5}{2}\frac{3}{2}^+(402)$	M1	94	68	4.1 E-11	(9.2 ±2.0) E-2			20
					E2	15		2.6 E-10		0.43 [b]	4.5	1.6 E-2
		349		$\frac{3}{2}\frac{3}{2}^+(402)$	E2	100	6.2	3.9 E-11		0.29 [b]	4.5	2.3 E-2
351.3	0.0104 [c]	172.3	$\frac{5}{2}\frac{1}{2}^+(400)$	$\frac{3}{2}\frac{1}{2}^+(400)$	M1	41.5	55.8	4.2 E-11	(1.82±0.42) E-1			10
					E2	0.38		4.8 E-9		$(7.7^{+11.5}_{-5.4})$ E-2	$3.7^{+2.1}_{-1.7}$	8.5 E-2
		221.8		$\frac{5}{2}\frac{3}{2}^+(402)$	M1	1.7	1.1	1.1 E-9	(3.3 ±0.8) E-3			54
					E2	0.2		>9.0 E-9		<1.2 E-2		>5.7 E-1
		268.8		$\frac{1}{2}\frac{1}{2}^+(400)$	E2	21	2.8	8.7 E-11		(4.6 ±1.5) E-1 [c]	4.8	1.4 E-2
		351.3		$\frac{3}{2}\frac{3}{2}^+(402)$	M1	43.5	8.3	4.2 E-11	(2.17±0.50) E-2			81
					E2	<8.7		>2.1 E-10		<5.0 E-2		>1.3 E-1

[a]) Hindrance factor relative to the Weisskopf estimate [30]) with the statistical factor equal to one.
[b]) Calculated using $Q_0 = 4.5$ b a value slightly lower than measured by Davis *et al.* [26]).
[c]) Calculated using our measured value $Q_0 = 4.8$ b in the $\frac{1}{2}^+(400)$ band.

A possibility to estimate the effective magnitude of this mixing is to study the interband E2 transition strengths only taking the strong diagonal components into account. As discussed in detail in ref. [13]) the amplitude of these components is only a function of the parameter $\Delta E/2M$ where ΔE is the energy difference between the two states with the same spin that mix and

$$M = -P_+ E^* \langle \tfrac{1}{2}|j_-|\tfrac{3}{2}\rangle \sqrt{(I-\tfrac{1}{2})(I+\tfrac{3}{2})},$$

where the pairing factor $P_+ \approx 1.0$ and $E^* \approx \hbar^2/2J$ for the actual rotational bands e.g. 20 to 30 keV. Using the deformed potential parameters recommended by Nilsson [5]) and $\delta = 0.13 \pm 0.02$ the Nilsson model predicts $\langle \frac{1}{2}|j_-|\frac{3}{2}\rangle = 0.67 \pm 0.02$. In table 5 are shown calculated interband B(E2) values for three different values of the parameter $E^*\langle \frac{1}{2}|j_-|\frac{3}{2}\rangle$. By comparing these with the corresponding experimental quantities we see that generally a much larger effective mixing than expected from theory is needed to explain the observed strong interband E2 transition rates. This is not unexpected since in the probably rather soft ^{191}Ir nucleus contributions from vibrational interactions should also be taken into account.

TABLE 5

E2 rates for interband transitions in ^{191}Ir

Experimental data (in $e^2 \cdot b^2$)		Calculated values [a]) $E^*\langle\frac{1}{2}|j_-|\frac{3}{2}\rangle = 10$	$E^*\langle\frac{1}{2}|j_-|\frac{3}{2}\rangle = 30$	$E^*\langle\frac{1}{2}|j_-|\frac{3}{2}\rangle = 90$
$B(E2, \frac{1}{2}\frac{1}{2} \rightarrow \frac{3}{2}\frac{3}{2})$	(1.45±0.16) E-1	0.083 E-1	0.60 E-1	2.1 E-1
$B(E2, \frac{5}{2}\frac{3}{2} \rightarrow \frac{3}{2}\frac{1}{2})$	(4.0 ±0.8) E-2	0.70 E-2	4.5 E-2	12.0 E-2
$B(E2, \frac{5}{2}\frac{3}{2} \rightarrow \frac{3}{2}\frac{3}{2})$	(9.9 ±3.0) E-2	1.3 E-2	8.5 E-2	24.1 E-2
$B(E2, \frac{5}{2}\frac{1}{2} \rightarrow \frac{3}{2}\frac{1}{2})$	(2.0 ±0.9) E-1	0.42 E-3	4.0 E-3	16.0 E-3
$B(E2, \frac{5}{2}\frac{1}{2} \rightarrow \frac{3}{2}\frac{3}{2})$	< 5.0 E-2	0.23 E-2	1.3 E-2	2.3 E-2
$B(E2, \frac{5}{2}\frac{1}{2} \rightarrow \frac{3}{2}\frac{3}{2})$	< 1.2 E-2	0.52 E-2	3.0 E-2	6.5 E-2

[a]) We used $G_{E2}(\frac{1}{2} \rightarrow \frac{1}{2}) = 40$ and $G_{E2}(\frac{3}{2} \rightarrow \frac{3}{2}) = 30$ corresponding to $Q_0 = 4.6$ and 3.5 b respectively. $E^*\langle\frac{1}{2}|j_-|\frac{3}{2}\rangle$ is given in keV.

3.4. M1 TRANSITION RATES

The relevant data on the magnetic properties in ^{191}Ir have been collected in table 6. They includes nine B(M1) values and two magnetic moments which can now be compared with the predictions of the Nilsson model [5]. That this model in its simplest form has its limitations can be seen from the $B(\mathrm{M1}, \frac{5}{2}\frac{1}{2} \rightarrow \frac{5}{2}\frac{3}{2})/B(\mathrm{M1}, \frac{5}{2}\frac{3}{2} \rightarrow \frac{5}{2}\frac{3}{2})$ branching ratio which is predicted to be 6.75 while experiments give 0.15±0.05. The same quantity is obtained in ^{193}Ir [ref. [13])] as < 0.13.

Hopefully some improvement in the predictions can be obtained by inclusion of various admixtures. For simplicity we have confined ourselves to the Coriolis type of mixing in a system consisting of the $\frac{1}{2}^+$ (400) and $\frac{3}{2}^+$ (402) particle states which are the ones expected to be the most important. The expressions for the relevant reduced M1 transition rates and magnetic moments are given in detail in ref. [13]). In the mentioned approximation the magnetic properties of the $K = \frac{1}{2}$ and $\frac{3}{2}$ bands in ^{191}Ir are determined by the following six parameters, namely

$$P_+(\tfrac{1}{2} \rightarrow \tfrac{3}{2}) G_{M1}(\tfrac{1}{2} \rightarrow \tfrac{3}{2}), \quad G_{M1}(\tfrac{3}{2} \rightarrow \tfrac{3}{2}), \quad G_{M1}(\tfrac{1}{2} \rightarrow \tfrac{1}{2}),$$
$$b_{M1} G_{M1}(\tfrac{1}{2} \rightarrow \tfrac{1}{2}), \quad g_R \text{ and } E^*\langle\tfrac{1}{2}|j_-|\tfrac{3}{2}\rangle \quad [\text{ref. } [13])].$$

The known experimental data in table 6 has through a least-squares fit been used to determine the first five of these parameters for different values of the coupling strength $E^*\langle\frac{1}{2}|j_-|\frac{3}{2}\rangle$. The fitted parameters as well as the calculated μ and B(M1) values are given in the right-hand part of table 6 for some selected values of $E^*\langle\frac{1}{2}|j_-|\frac{3}{2}\rangle$. As is seen especially $B(\mathrm{M1}, \frac{5}{2}\frac{1}{2} \rightarrow \frac{5}{2}\frac{3}{2})$, $B(\mathrm{M1}, \frac{5}{2}\frac{1}{2} \rightarrow \frac{5}{2}\frac{3}{2})$ and $B(\mathrm{M1}, \frac{5}{2}\frac{1}{2} \rightarrow \frac{5}{2}\frac{3}{2})$ are sensitive to admixture. It is also clear that the fit is improved when the Coriolis mixing is taken into account with an optimum around $E^*\langle\frac{1}{2}|j_-|\frac{3}{2}\rangle = 10$ keV. This is slightly less than the predicted value of $E^*\langle\frac{1}{2}|j_-|\frac{3}{2}\rangle = 15$–20 keV.

The fitted parameters are given in the lower part of table 6 and are seen to be rather independent on the coupling strength. They also agree well with the cor-

TABLE 6

Magnetic properties in ^{191}Ir

Experimental data [a])		Calculated B(M1) and μ values using the fitted parameters given below. $E^*\langle\frac{1}{2}|j_-|\frac{3}{2}\rangle = 0$	$= 10$	$= 20$ [d])	$= 30$
$\mu\ \frac{3}{2}\frac{3}{2}^+(402)$	0.14589±0.00003 [b])	0.146	0.146	0.150	0.146
$\mu\ \frac{1}{2}\frac{1}{2}^+(400)$	0.542 ±0.005 [c])	0.542	0.542	0.537	0.541
$B(\mathrm{M1}, \frac{1}{2}\frac{1}{2} \rightarrow \frac{3}{2}\frac{3}{2})$	(8.8 ±1.0) E-4	10.8 E-4	8.6 E-4	9.5 E-4	9.0 E-4
$B(\mathrm{M1}, \frac{3}{2}\frac{1}{2} \rightarrow \frac{3}{2}\frac{3}{2})$	(4.1 ±1.2) E-3	0.43 E-3	1.2 E-3	2.1 E-3	2.0 E-3
$B(\mathrm{M1}, \frac{3}{2}\frac{1}{2} \rightarrow \frac{5}{2}\frac{3}{2})$	(1.06 ±0.35)E-2	0.065 E-2	0.55 E-2	1.6 E-2	3.7 E-2
$B(\mathrm{M1}, \frac{5}{2}\frac{1}{2} \rightarrow \frac{3}{2}\frac{3}{2})$	(2.17 ±0.50)E-2	0.007 E-2	0.70 E-2	1.7 E-2	0.50 E-2
$B(\mathrm{M1}, \frac{5}{2}\frac{1}{2} \rightarrow \frac{5}{2}\frac{3}{2})$	(3.3 ±0.8) E-3	0.49 E-3	4.1 E-3	11.8 E-3	8.1 E-3
$B(\mathrm{M1}, \frac{3}{2}\frac{1}{2} \rightarrow \frac{1}{2}\frac{1}{2})$	(1.23 ±0.36)E-1	1.1 E-1	2.2 E-1	0.58 E-1	0.38 E-1
$B(\mathrm{M1}, \frac{5}{2}\frac{1}{2} \rightarrow \frac{3}{2}\frac{1}{2})$	(1.82 ±0.42)E-1	1.9 E-1	2.2 E-1	1.1 E-1	0.091 E-1
$B(\mathrm{M1}, \frac{5}{2}\frac{3}{2} \rightarrow \frac{3}{2}\frac{3}{2})$	(3.28 ±0.31)E-2	3.5 E-2	3.8 E-2	3.7 E-2	2.6 E-2
$B(\mathrm{M1}, \frac{7}{2}\frac{3}{2} \rightarrow \frac{5}{2}\frac{3}{2})$	(9.2 ±2.0) E-2	4.7 E-2	4.8 E-2	4.8 E-2	4.9 E-2
$P_+(\frac{1}{2} \rightarrow \frac{3}{2}) G_{M1}(\frac{1}{2} \rightarrow \frac{3}{2})$		0.135±0.036	−0.143±0.060	−0.15±0.11	0.43±0.19
$G_{M1}(\frac{3}{2} \rightarrow \frac{3}{2})$		−1.49 ±0.38	−1.62 ±0.19	−1.74±0.23	−1.61±0.32
$G_{M1}(\frac{1}{2} \rightarrow \frac{1}{2})$		2.65 ±1.25	3.18 ±0.54	2.00±0.53	−1.86±0.68
$G_{M1}(\frac{1}{2} \rightarrow \frac{1}{2}) b_{M1}$		−0.29 ±0.33	0.06 ±0.31	−0.44±0.28	−1.56±0.32
g_R		0.54 ±0.11	0.57 ±0.06	0.59±0.07	0.59±0.09
Mean square sum		14.6	3.9	6.5	13.4

[a]) B(M1) is given in units of $(e\hbar/2Mc)^2$ and μ in units of $e\hbar/2Mc$.
[b]) From ref. [31]).
[c]) From ref. [32]).
[d]) Equals the predicted value of $\langle\frac{1}{2}|j_-|\frac{3}{2}\rangle = 0.67$ from ref. [5]) together with $E^* \approx \hbar^2/2J = 30$ keV.

responding parameters obtained from a similar fit to ^{193}Ir data [13]). It is now of interest to see if the Nilsson model can account for the fitted parameter values. The gyromagnetic ratio g_R has recently been calculated in ^{191}Ir [ref. [29])] as 0.56 in excellent agreement with the observed value 0.57 ± 0.06. To calculate the other quantities we have used the following parameters $\kappa = 0.05$, $\mu = 0.55$, $\delta = 0.1$ and g_s (effective) = $0.6\, g_s$ (free) where given errors are the maximum deviation for a 10 % change in these parameters. We get $G_{M1}(\frac{1}{2} \to \frac{3}{2}) = -(0.19 \pm 0.05)$, $G_{M1}(\frac{3}{2} \to \frac{3}{2}) = -(1.7 \pm 0.3)$, $G_{M1}(\frac{1}{2} \to \frac{1}{2}) = 2.2 \pm 0.3$ and $b_{M1} G_{M1}(\frac{1}{2} \to \frac{1}{2}) = 3.0 \pm 0.5$. Reasonable agreement is obtained in all cases except for $b_{M1} G_{M1}(\frac{1}{2} \to \frac{1}{2})$ where experiment indicates a very small value. The same effect is also observed in ^{193}Ir [ref. [13])].

We are indebted to Dr. A. Kjelberg and the Nuclear Chemistry Group at ISOLDE, CERN for providing us with the excellent active sources.

References

1) A. Bäcklin, S. G. Malmskog and H. Solhed, Ark. Fys. **34** (1967) 495
2) A. Bäcklin, B. Fogelberg and S. G. Malmskog, Nucl. Phys. **A96** (1967) 539
3) A. Bäcklin, V. Berg and S. G. Malmskog, to be published 1970
4) P. H. Blichert-Toft, E. G. Funk and J. W. Mihelich, Nucl. Phys. **77** (1966) 513
5) S. G. Nilsson, Mat. Fys. Medd. Dan. Vid. Selsk. **29**, no. 16 (1955)
6) O. Nathan and S. G. Nilsson, Alpha-, beta- and gamma-ray spectroscopy, ed. by K. Siegbahn (North-Holland, Amsterdam 1965)
7) P. G. Hansen *et al.*, Phys. Lett. **28B** (1969) 415
8) M. Schumacher and H. Langhoff, Phys. Rev. **162** (1967) 1153
9) H. Daniel, J. Huefner, Th. Lorenz, O. W. B. Schult and U. Gruber, Nucl. Phys. **56** (1964) 147
10) W. F. Edwards, P. Boehm, J. Rogers and E. J. Seppi, Nucl. Phys. **63** (1965) 97; E. J. Seppi, H. Henrikson, F. Boehm and J. W. M. Du Mond, Nucl. Instr. **16** (1962) 17
11) C. J. Gallagher Jr., W. F. Edwards and G. Manning, Nucl. Phys. **19** (1960) 18
12) J. J. Reidy and M. L. Wiedenbeck, Nucl. Phys. **79** (1966) 193
13) V. Berg, S. G. Malmskog and A. Bäcklin, Nucl. Phys. **A143** (1970) 177
14) M. Schumacher, R. Schöneberg and A. Flammersfeld, Z. Phys. **191** (1966) 343
15) B. Harmatz, T. H. Handley and J. W. Mihelich, Phys. Rev. **128** (1962) 1186
16) I. Marklund, E. Karlsson and K. Korkman, Ark. Fys. **22** (1962) 289
17) G. Bäckström, A. Bäcklin, N. E. Holmberg and K. E. Bergkvist, Nucl. Instr. **16** (1962) 199
18) A. Bäcklin, Nucl. Instr. **57** (1967) 261
19) R. S. Hager and E. C. Seltzer, Nucl. Data **A4**, no. 1 and 2 (1968)
20) A. Marelius, P. Sparrman and T. Sundström, Table of nuclear lifetimes, appendix D in Hyperfine structure and nuclear radiations (Proc. Conf. Pacific Grove Calif Aug. 25–30, 1967) ed. Mattias and D. A. Shirley (North-Holland, Amsterdam, 1968) p. 1043
21) S. G. Malmskog and A. Bäcklin, Ark. Fys. **39** (1969) 411
22) T. R. Gerholm and J. Lindskog, Ark. Fys. **24** (1963) 171
23) S. G. Malmskog, Ark. Fys. **35** (1967) 255
24) T. Sundström, Nucl. Instr. **16** (1962) 153
25) A. Bäcklin, Nucl. Instr. **53** (1967) 177
26) R. H. Davis, A. S. Divatia, D. A. Lind and R. D. Moffat, Phys. Rev. **103** (1956) 1801
27) H. Langhoff, Phys. Rev. **136** (1964) B1590
28) A. de Shalit, Phys. Rev. **122** (1961) 1530
29) O. Prior, F. Boehm and S. G. Nilsson, Nucl. Phys. **A110** (1968) 257
30) A. H. Wapstra, G. J. Nijgh and R. van Lieshout, Nuclear spectroscopy tables (North-Holland, Amsterdam, 1959)
31) A. Narath and D. C. Barham, Bull. Am. Phys. Soc. **12** (1967) 314
32) F. Wagner, G. Kandl, P. Kienle and H. J. Körner, Z. Phys. **207** (1967) 500

R E F E R E N C E 11

E2 AND M1 TRANSITION PROBABILITIES BETWEEN LOW-ENERGY STATES IN ^{189}Ir.

A. BÄCKLIN AND G. HEDIN

The Swedish Research Council's Laboratory, Studsvik, Nyköping, Sweden

V. BERG and S.G. MALMSKOG,

AB Atomenergi, Studsvik, Nyköping, Sweden

and

Institute of Physics, University of Stockholm, Sweden

1.E.4:3.A

Nuclear Physics **A181** (1972) 76—96; © *North-Holland Publishing Co., Amsterdam*

Not to be reproduced by photoprint or microfilm without written permission from the publisher

E2 AND M1 TRANSITION PROBABILITIES BETWEEN LOW-ENERGY STATES IN ^{189}Ir

A. BÄCKLIN and G. HEDIN

The Swedish Research Councils' Laboratory, Studsvik, Nyköping, Sweden

V. BERG and S. G. MALMSKOG †

AB Atomenergi, Studsvik, Nyköping, Sweden
and
Institute of Physics, University of Stockholm, Sweden

Received 1 March 1971
(Revised 28 May 1971, 16 August 1971)

Abstract: Half-lives have been measured for the lowest excited states in ^{189}Ir and the transitions between the states have been studied using high-resolution electron and γ-spectroscopy. The following half-lives were obtained: 94.34 keV, 11.6±0.6 nsec; 113.82 keV, 76±18 psec; 176.53 keV, 22±10 psec; 300.51 keV, < 20 psec. A new transition was found at 62.65 keV. From L subshell ratios the following multipolarity mixtures were obtained: 62.65 keV, M1+(8.5$^{+6}_{-3}$) % E2; 71.69 keV, M2; 82.22 keV, M1+(2.8±0.7) % E2; 94.34 keV, E2+(5.5±1.0) % M1; 113.82 keV, M1+(23±2) % E2; 141.18 keV, M1+(1.5$^{+1.5}_{-0.8}$) % E2; 176.53 keV, M1+(44±3) % E2; 186.70 keV, M1+(21±4) % E2; 203.78 keV, M1+ < 30 % E2; 223.34 keV, E2; 243.50 keV, E2; 258.37 keV, E3; 300.51 keV, E2; 317.65 keV, M1+(23±10) % E2. Reduced E2 and M1 transition probabilities are calculated and compared to the result of a two-band Coriolis coupling calculation. A deformation parameter $\delta = 0.23$ is obtained in ^{189}Ir. This represents a sharp increase from the value $\delta = 0.12$ obtained in ^{191}Ir and ^{193}Ir. The B(E2) and B(M1) values in all odd-A Ir nuclei are presented systematically and compared to current nuclear models.

E | RADIOACTIVITY ^{189}Pt [decay product of ^{189}Hg obtained from Pb(p, 3p xn)]; measured E_γ, I_γ, E_{ce}, I_{ce} cece-delay. ^{189}Ir deduced γ-mixing, γ-branching, $T_{\frac{1}{2}}$, $B(\lambda)$. Isotope separated sources.

1. Introduction

For our understanding of the nuclei in the interesting transitional regions between deformed and spherical equilibrium shapes it is of importance to obtain more systematic experimental data than have been available so far. This paper, which describes a study of the decay of ^{189}Pt → ^{189}Ir, forms part of a systematic investigation of odd-mass Ir nuclei, especially of the E2 and M1 transition probabilities between low-lying states [1–5]).

Several investigations of the decay of ^{189}Pt have earlier been performed [6]). In particular, electron spectroscopy has been carried out by Harmatz *et al.* [7]) and Lewis *et al.* [8]), in which the essential parts of the low-energy structure of the level scheme

† Present address: Institut de Physique Nucléaire, Orsay, France.

have been established, see fig. 1. The γ-ray spectrum has been studied by Fourier *et al.* [9]).

In the present work we have measured the half-lives of three of the lowest excited levels using the delayed-coincidence method. The great complexity of the low-energy conversion electron spectrum required further experimental work in order to deduce reliable values of the E2/M1 mixing ratios of the transitions between the lowest two rotational bands. We have therefore made a re-examination of the L conversion elec-

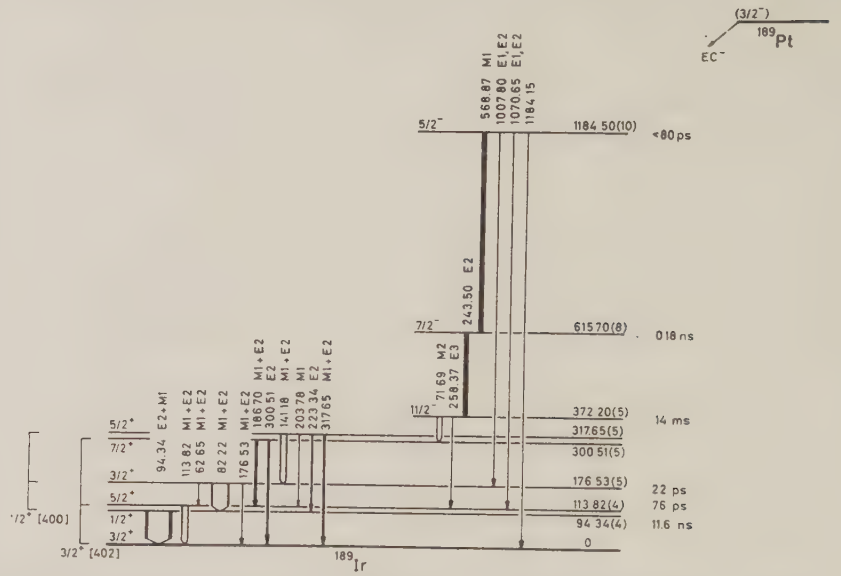

Fig. 1. Low-energy level scheme of ^{189}Ir. The widths of the arrows are proportional to the total intensities of the transitions, the white part indicating the conversion electron intensity. For completeness the negative-parity states reported in ref. [4]) are also shown. The level energies are given in keV, the number in parenthesis giving the error of the last digit.

trons of these transitions using a $\pi\sqrt{2}$ β-spectrometer. Finally, in an attempt to improve on earlier data [9]), we have measured the γ-ray spectrum up to ≈ 0.8 MeV with a Ge(Li) detector. A study of transitions and levels at higher energies will be published later [10]).

2. Experiment

2.1. SOURCES

The ^{189}Pt sources were obtained as a decay product of ^{189}Hg produced in the ISOLDE project [11]), CERN. Molten lead was bombarded with 600 MeV protons and the mercury spallation products were pumped off and mass separated. The ^{189}Hg

was collected on 1 mg/cm² Ni foil, forming excellent sources of negligible thickness for electron spectroscopy. Normally, measurements were started about 15 h after the end of the irradiation when the 10 min ^{189}Hg and 42 min ^{189}Au mother activities had decayed. The $T_{\frac{1}{2}} = 11$ h ^{189}Pt was then the dominating activity for a few days, after which the 13 d ^{189}Ir activity gradually became dominant in the low-energy spectrum.

Several irradiations were made, some of which contained non-negligible amounts of contaminating impurity activities such as 3 d ^{191}Pt, 6+11 h ^{193}Hg and 16 h ^{193}Au. These were however easily detected from their half-lives and characteristic energies [refs. [12–14])].

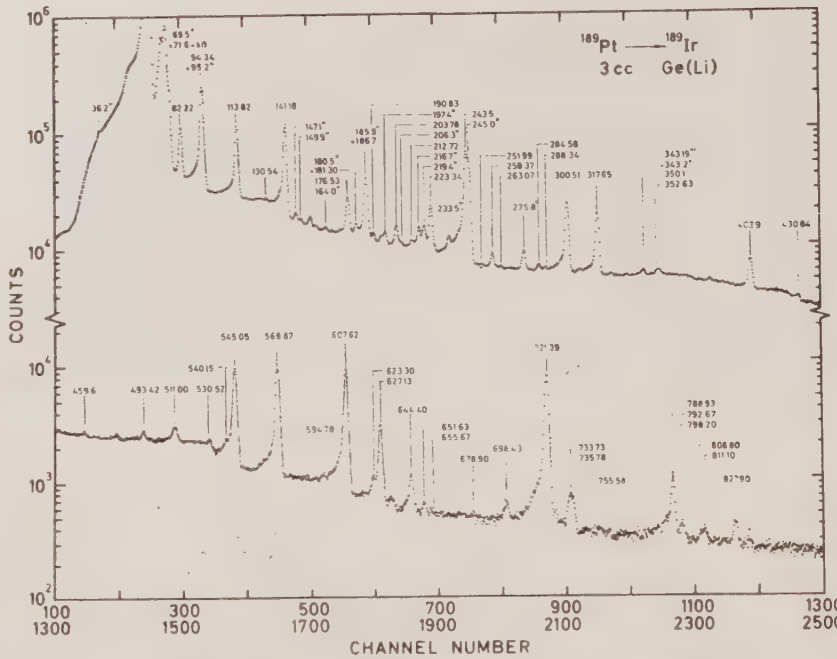

Fig. 2. Low-energy part of the γ-ray spectrum emitted in the decay of 11h ^{189}Pt → ^{189}Ir as registered in a 3 cm³ Ge(Li) detector. Transition energies are given in keV; those indicated by a star belong to the 13 d ^{189}Ir daughter decay.

2.2. THE γ-RAY SPECTRUM

The γ-ray spectrum up to ≈ 0.8 MeV was measured with a Ge(Li) detector system consisting of a 3 cm³ detector, a TC200 amplifier and a ND3300 4k analyser. The resolution of the system was 1.9 keV at 122 keV.

TABLE 1

Energies, intensities conversion coefficients and multipolarities of transitions in ^{189}Ir

ENERGY KEV	ERROR KEV	GAMMA-INTENSITY	ERROR %	ELEC. INTENSITY	I- ERROR %	ALPHA K EXPERIMENT[A]	ERROR %	THEORETICAL CONVERS. COEFFICIENTS F1	E2	M1	MULTIPOLARITY[B]
71.63	0.04										
82.27	0.04	31.20	10.								
94.34	0.04	81.50	7.	87.700	40.	0.1106E 01	41.	0.511E 00	0.829E 00	0.923E 01	M1+0.51±0.6-3.0E2
113.82	0.04	311.0	7.	244.000	8.	0.2771 01	11.	0.337E 00	0.819E 00	0.911E 01	M2
130.54	0.10	5.80	30.					0.235E 00	0.735E 00	0.818E 01	M1+2.8(0.7)E2
141.18	0.04	45.20	10.	97.700	5.	0.196E 01	7.	0.166E 00	0.476E 00	0.534E 01	E2+5.5(1.0)+1
176.53	0.07	10.60	5.	11.200	25.	0.106E 01	25.	0.774E-01	0.235E 00	0.104E 01	M1+5.5(+1.5-0.8)E2
181.30	0.10	1.20	10.					0.722E-01	0.206E 00	0.892E 00	M1+4.4(3.1)E2
186.70	0.06	24.00	10.	15.800	12.	0.698E 00	12.	0.636E-01	0.179E 00	0.833E 00	
190.83	0.10	1.20	25.					0.560E-01	0.156E 00	0.694E 00	M1+4.3(0.8)E2
203.78	0.08	5.20	10.	4.000	30.	0.769E 00	32.	0.485E-01	0.134E 00	0.589E 00	
212.77	0.10	1.10	40.					0.463E-01	0.127E 00	0.562E 00	
223.34	0.10	16.00	7.	1.750	15.	0.109E 00	17.	0.430E-01	0.119E 00	0.519E 00	E2
243.50	0.06	75.20	10.	9.100	7.	0.108E 00	17.	0.348E-01	0.963E-01	0.412E 00	E2
251.94	0.25	0.45	40.					0.320E-01	0.886E-01	0.378E 00	E3 C)
264.37	0.06	3.40	10.	0.720	10.	0.292E 00	14.	0.295E-01	0.817E-01	0.347E 00	
283.07	0.15	0.40	40.					0.268E-01	0.743E-01	0.316E 00	
284.58	0.10	1.70	15.					0.239E-01	0.663E-01	0.282E 00	
288.34	0.10	0.70	15.					0.231E-01	0.640E-01	0.272E 00	
300.51	0.06	40.00	5.	2.370	7.	0.542E-01	9.	0.204E-01	0.564E-01	0.239E 00	E2
317.65	0.06	35.00	5.	4.000	7.	0.171E 00	9.	0.184E-01	0.509E-01	0.215E 00	M1+2.3(1.0)E2
343.20	0.20	2.60	20.	0.600	30.	0.194E 00	39.	0.153E-01	0.423E-01	0.178E 00	M1
351.10	0.25	1.40	20.					0.145E-01	0.400E-01	0.169E 00	
352.63	0.15	1.70	15.					0.144E-01	0.398E-01	0.168E 00	
403.90	0.15	15.20	8.					0.106E-01	0.292E-01	0.123E 00	
410.84	0.15	1.70	20.					0.101E-01	0.279E-01	0.118E 00	
459.66	0.20	0.90	20.					0.788E-02	0.216E-01	0.913E-01	
491.42	0.15	2.50	15.					0.686E-02	0.189E-01	0.797E-01	
530.52	0.35	2.30	30.					0.588E-02	0.161E-01	0.683E-01	
540.15	0.35	4.80	15.					0.567E-02	0.156E-01	0.659E-01	
545.05	0.10	62.00	8.					0.556E-02	0.147E-01	0.623E-01	
568.87	0.07	70.00	7.	2.400	7.	0.509E-02	11.	0.534E-02	0.146E-01	0.618E-01	
594.78	0.15	0.45	25.					0.485E-02	0.133E-01	0.563E-01	M1
607.62	0.10	82.00	10.					0.464E-02	0.127E-01	0.538E-01	
623.30	0.10	4.20	25.					0.447E-02	0.122E-01	0.518E-01	
627.13	0.10	24.00	10.					0.441E-02	0.120E-01	0.509E-01	
640.45	0.40	0.60	10.					0.420E-02	0.114E-01	0.483E-01	
644.40	0.15	4.40	12.					0.415E-02	0.113E-01	0.478E-01	
651.63	0.12	1.04	15.					0.396E-02	0.108E-01	0.457E-01	
655.67	0.15	0.60	20.					0.482E-02	0.988E-02	0.306E-01	
678.90	0.30	0.28	40.					0.356E-02	0.971E-02	0.411E-01	
698.43	0.12	2.32	15.					0.337E-02	0.919E-02	0.389E-01	
721.39	0.10	100.00	10.					0.320E-02	0.872E-02	0.369E-01	
733.73	0.15	3.80	15.					0.312E-02	0.849E-02	0.359E-01	
735.78	0.15	4.00	20.					0.304E-02	0.829E-02	0.350E-01	
788.93	0.25	1.40	20.					0.266E-02	0.726E-02	0.307E-01	
792.67	0.15	13.50	15.					0.264E-02	0.720E-02	0.304E-01	
798.20	0.15	1.74	15.					0.260E-02	0.709E-02	0.300E-01	
808.80	0.30	0.80	20.					0.254E-02	0.693E-02	0.293E-01	
811.10	0.25	1.20	20.					0.252E-02	0.686E-02	0.290E-01	
827.90	0.15	1.70	15.					0.243E-02	0.663E-02	0.280E-01	
835.65	0.30	0.90	20.					0.239E-02	0.652E-02	0.276E-01	

[A]) Powers of ten are given with the notation E sign exponent, i.e. E-01 means 0.1 etc. The theoretical conversion coefficients are from ref. [23]).

[B]) Multipolarities and multipolarity mixtures are obtained from the K-conversion coefficient (α_K) except for the 62.65, 71.69, 82.22, 94.34, 113.82, 141.18, 176.53, 186.70 and 243.50 keV transitions, for which these quantities have been deduced from L subshell ratios and K/L ratios. The parentheses after the admixture percentages indicate the errors. For unsymmetric errors the upper limit is given before the lower limit, i.e. 8.5 (+6.0−3.0) stands for 8.5+6.0−3.0.

[C]) The theoretical K conversion coefficient for one E3 transition is 0.251 [ref. [23])].

The efficiency curve of the system was obtained with the aid of a set of absolutely calibrated standard sources † and the well-known relative intensities in the decay of ^{182}Ta [refs. [15,16])]. Energy calibration was made using the internal conversion data [see subsect. 2.3] below 400 keV. Above that energy the strongest lines were calibrated against the well-known energies of ^{207}Bi [ref. [17])], ^{88}Y [ref. [17])], ^{137}Cs, ^{22}Na and ^{60}Co [ref. [18])].

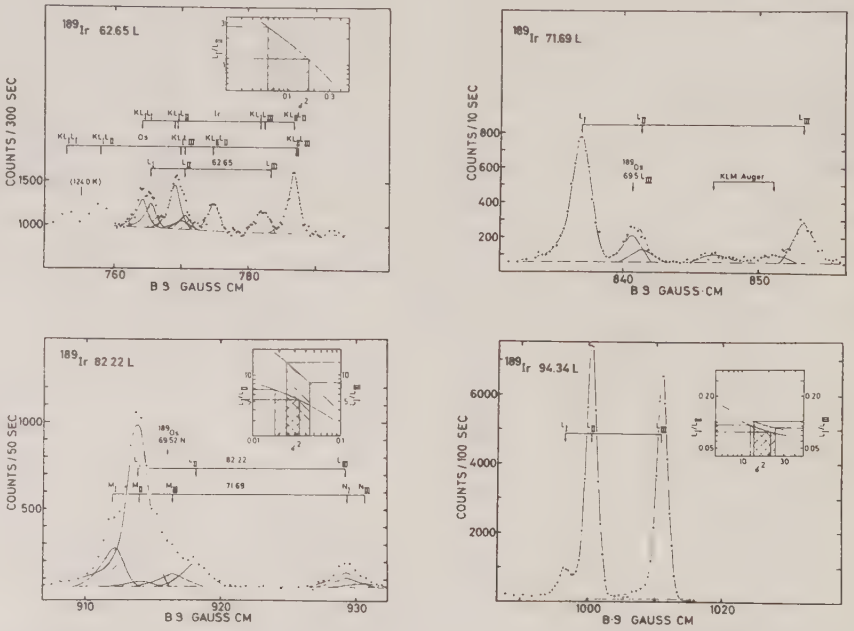

Fig. 3. Internal conversion electron lines in the decay of ^{189}Pt → ^{189}Ir as recorded with a $\pi\sqrt{2}$ β-spectrometer. The points have not been corrected for decay. The insets show theoretical [23]) L subshell ratios as functions of the E2 admixture together with the limits obtained from the corresponding experimental data.

The γ-ray spectrum was recorded several times using different sources. Each time two or three runs were made at intervals of about one day in order to identify the half-lives of the activities. A spectrum is shown in fig. 2.

The data were evaluated with the aid of a curve-fitting program [19]) and the results are given in table 1. The γ-intensities of the earlier known transitions are in fair agreement with the work of Fourrier *et al.* [9]). In addition, several new transitions were observed.

† These were ^{57}Co, ^{22}Na, ^{137}Cs, ^{54}Mn, ^{60}Co and ^{88}Y obtained from IAEA, Vienna.

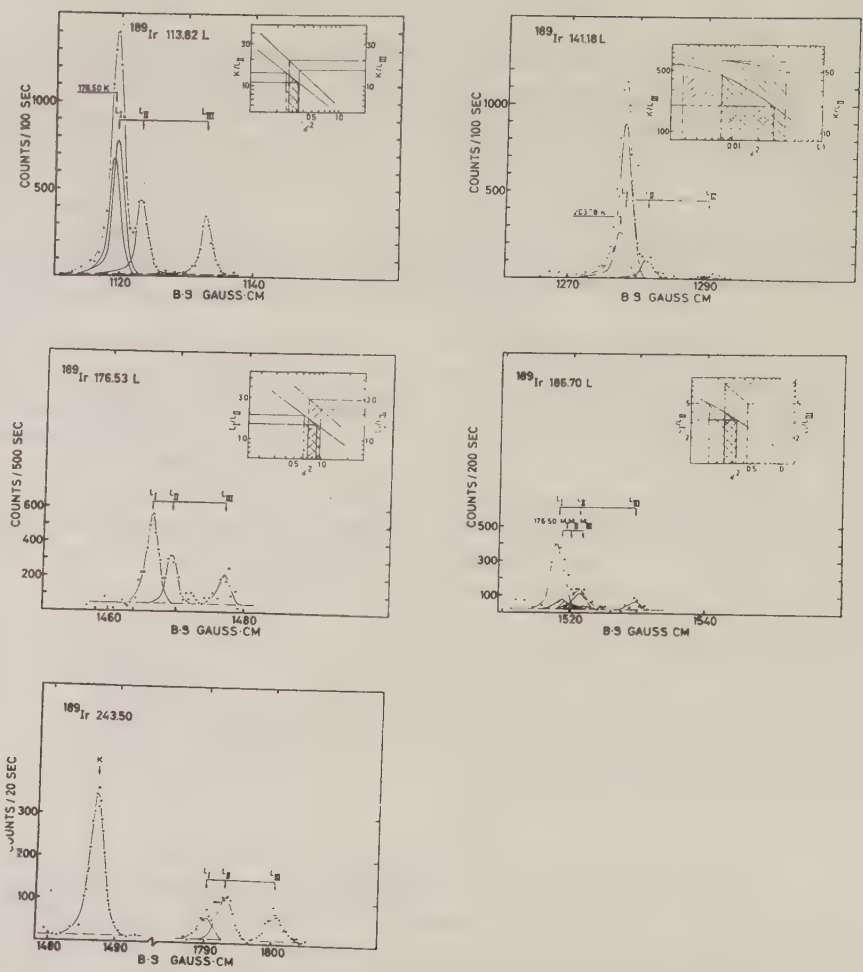

Fig. 4. Internal conversion lines in the decay of ^{189}Pt → ^{189}Ir. For further explanations see caption of fig. 3.

2.3. INTERNAL CONVERSION MEASUREMENTS

Conversion electrons were measured with a 50 cm $\pi\sqrt{2}$ β-spectrometer [20,21]). By masking the sources with a slit of 2 mm width a resolution of 0.2 % was obtained. Several sources were used and most lines studied were measured more than once. The measurements were concentrated on the transitions between and within the two lowest rotational bands, where especially the L subshell ratios were studied in order to obtain as accurate values as possible for the E2/M1 mixing ratios. Figs. 3 and 4 show

TABLE 2

Internal conversion data from the decay ^{189}Pt → ^{189}Ir

Harmatz et.al. [7]		Lewis et.al. [8]		Present work				
Transition energy keV	Election intensity a)	Transition energy keV	Electron intensity a)	Transition energy keV	Error keV	Shell	Electron intensity a)	Error %
				62.65	0.06	L_I	2.90	20
						L_{II}	1.5	40
						L_{III}	< 0.9 [b]	
71.6	40	71.62±0.06	41±5	71.69	0.04	L_I	41	8
	7.9		4.4±2			L_{II}	< 6 [c]	
	12.7		15±4			L_{III}	13.8	10
82.15	56	82.06±0.15	35±13	82.22	0.04	L_I	40	8
	–		< 70			L_{II}	6.7	12
	–		< 26			L_{III}	3.7	25
94.25		94.24±0.07	15±4	94.34	0.04	K	87.7	40
			< 40			L_I	10.6	10
	146		122±26			L_{II}	126	5
	141		109±16			L_{III}	113	5
113.75	74	113.82±0.10	57±5	113.82	0.04	K	86.0	8
	26		26±5 [e]			L_I	12.9 [d]	15
	8.8		8±3			L_{II}	7.0	10
	5.6		7±3			L_{III}	4.9	10
				(124.0)		K	< 2	
141.1	87.7 [f]	141.06±0.06	87.7±10 [f]	141.18	0.04	K	87.7 [f]	5
	17.5		17.5±2 [h]			L_I	13.6 [g]	15
	–		< 2.5			L_{II}	1.53	15
	–		–			L_{III}	0.23	50
176.4	26 [e]	176.3 ±0.3	26±5 [e]	176.53	0.07	K	11.2 [d]	25
	1.4					L_I	1.23	10
			1.5			L_{II}	0.72	10
						L_{III}	0.47	15
181.2	1.5	181.33±0.15	3.6±1.6			K		
186.65	19	186.7 ±0.2	19±5	186.70	0.06	K	15.8 [i]	7
	3.2		5.7±2.6			L_I	2.2	10
	–		< 3			L_{II}	0.54	20
	–		0.37±0.25			L_{III}	0.37	25
						M	0.83	10
190.9	1.15	190.8	2.0			K		
204.0	17.5 [h]	203.7 ±0.4	17.5±2 [h]	203.78	0.08	K	4.0 [g]	30
	0.8		4.1			L_I	0.8	15
	–		–			L_{II}	< 0.25	
	–		–			L_{III}	< 0.2	
223.45	2.3	223.33±0.18	3.5±1.7	223.34	0.10	K	1.75	15
243.6	7.9	243.4 ±0.2	8.2±1.0	243.50	0.06	K	8.1	7
	-					L_I	1.10	25
	5.5		3.8±1.0			L_{II}	2.22	15
	1.35		2.2±0.7			L_{III}	1.51	15
	–	252.0 ±0.5	0.57±0.23			K		
258.3	0.88	258.2 ±0.2	± 3.1	258.37	0.06	K	0.78	10
	–		± 0.10			L_I	0.25	50
	1.03		1.0±0.30			L_{II}	0.98	10
	0.47		0.46±0.16			L_{III}	0.45	12
317.8	6.6	317.6 ±0.2	7.2±0.5	317.65	0.10	K	6.0	7
569.3	3.7	568.8 ±0.4	3.3 ±0.35	568.87	0.05	K	3.5	7
	0.56		0.56			L_I+L_{II}	0.59	10
			<0.16			L_{III}	<0.04	
				Auger		KL_IL_I	4.9	15
				"		KL_IL_{II}	2.9	7
				"		KL_IL_{III}	3.0	15
				"		$KL_{II}L_{II}$	8.9	7
				"		$KL_{II}L_{III}$	3.3	20

some of the L groups measured. Lines corresponding to a new transition were found, since the K L_IL_I and K L_IL_{II} Auger lines showed structure that could be interpreted as the L_I and L_{II} lines of the 62.65 keV transition (cf. fig. 3), which was expected to occur in the level scheme. The resolution of the 62.65 L lines from the interfering Ir and Os Auger lines was facilitated by the known energies [22]) of the latter and by using the intensity ratios of undisturbed Auger lines. Also many other lines had to be resolved from interfering lines. In general this was done in a logarithmic plot using an intensity of the interfering line(s) calculated from theoretical conversion coefficients [ref. [23])] and the measured intensity of other conversion line(s) of the interfering transition, from which also the multipolarity was deduced. The exact positions of these interfering lines were calculated from the measured positions of other conversion lines of the same transition.

The results of the conversion electron measurements are given in tables 1 and 2. Both energies and intensities are generally in good agreement with earlier data [7,8])

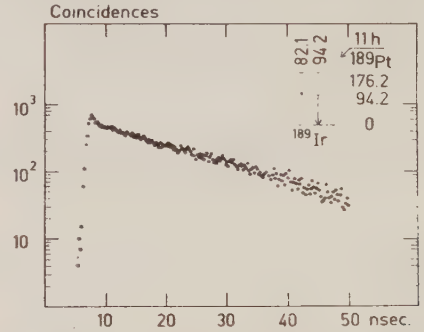

Fig. 5. Delayed coincidence curve taken between the 82.2 L and 94.3 L conversion electron lines giving a half-life of 11.6±0.6 nsec for the 94.3 keV level in ^{189}Ir.

Footnotes to table 2:

[a]) Relative units. Normalization was made setting $I_\gamma = 100$ for the 721.39 keV transition and using the theoretical K conversion coefficient [23]) = 1.94 for the 141.18 keV M1+1.5 % E2 transition.

[b]) The 62.65 L_{III} line is masked by the KL_IL_{III} Auger line. The number gives the upper limit of the intensity.

[c]) The 71.69 L_{II} line is masked by the 69.52 L_{III} line in ^{189}Os.

[d]) The 113.82 L_I line coincides with 176.53 K$_\gamma$, cf. fig. 4. The relative intensities of these lines as obtained in the present work were calculated from the theoretical [23]) L_I/L_{II} and L_I/L_{III} ratios of the 113.82 keV transition for multipolarity M1+23 % E2 as obtained from the experimental K/L_{II} and K/L_{III} ratios.

[e]) Sum of 113.82 L_I and 176.53 K.

[f]) Value used for normalization, see comment [a]).

[g]) The 141.18 L_I line coincides with 203.78 K. The group was resolved in the present work with the aid of the theoretical [23]) L_I/L_{II} and L_{II}/L_{III} ratios of the 141.18 keV transition for a multipolarity mixture M1+1.5 % E2 as obtained from the experimental K/L_{II} and K/L_{III} ratios.

[h]) Sum of 141.18 L_I and 203.78 K.

[i]) The 113.82 M has been subtracted using the theoretical M/L ratio [23]).

when existing. No systematic variation of the electron intensities of ref. [7]) as observed earlier in the decay ^{189}Ir → ^{189}Os [ref. [24])] was found. The accuracy of the intensities of the low-energy lines of special interest in this work has been considerably improved. Most of the mixing ratios were calculated from the L subshell ratios using the theoretical conversion coefficients of Hager and Seltzer [23]). In general the experimental K conversion coefficients (table 1) are consistent with these mixing ratios, the only exception being the 176.53 K coefficient. In this case, however, the conversion intensity is uncertain, since the line coincides almost exactly with the stronger 113.82 L_I line.

2.4. HALF-LIFE MEASUREMENTS

Delayed-coincidence measurements were performed using instrumentation built up around an electron-electron coincidence β-spectrometer described in detail earlier [refs. [25,26])]. The same sources were used as in the measurements described in subsects. 2.2 and 2.3.

The 94.3 keV *level.* The 94.3 keV level is strongly populated by the 82.2 keV transition. For the half-life measurements of the 94.3 keV level we focused the 94.3 L_{II} and 82.2 L_I conversion electron lines in each of the two electron lenses. The delayed time coincidence spectrum was recorded. A result from such a measurement is shown in fig. 5. In table 3 is given a list of possible disturbing coincidence contributions from contaminants in the ^{189}Pt source. All these cascades go via energy levels with half-lives of less than 0.5 nsec or via the 94.2 keV level. These additional cascades are responsible for the small prompt peak observed in fig. 5 but do not influence the slope of the observed decay curve. As an average value we obtain a half-life of 11.6±0.6 nsec for the 94.3 keV level in ^{189}Ir. This value is in good agreement with the values 11±1 nsec reported by Kryukova *et al.* [27]) and with the value 12.5±1.0 nsec reported by Jastrzebski *et al.* [28]).

The 113.8 keV *level.* The half-life of the 113.8 keV level was determined by measuring the delayed-coincidence spectrum between the 113.8 K and 186.7 K conversion electron lines. To get a time zero reference point, coincidences from the β-94.7 K cascade in the decay of ^{165}Dy was also registered using exactly the same energy settings as with the ^{189}Pt source. Since the 94.7 K conversion electrons were slightly degraded in the ^{165}Dy source backing, their energy coincided with the 113.8 K line in ^{189}Ir. Measurements were performed alternatively with the ^{189}Pt and ^{165}Dy sources, each measurement being 15 min long. Such a series of measurements was performed for a continuous period of 10 h. The result was analyzed primarily using the first moment method [29]) although the second and third moments were also calculated for consistency checks. As an average value we obtain a shift of 0.73±0.17 channels. With the used current settings of the lens spectrometers a few contributions from other conversion electron lines were also accepted in the energy channels. The possible candidates are given in table 3. No coincidence contributions are, however, expected from these extra lines. When a correction for the half-life of the 94.7 keV

TABLE 3
Contributions in the energy channels used for half-life measurements of levels in ^{189}Ir

Level under investigation (in keV)	Channel 1		Channel 2		Coincidence contributions
	Main conversion line (^{189}Ir)	Disturbing components (in nucleus)	Main conversion line (^{189}Ir)	Disturbing components (in nucleus)	
94.3	94.3 L_{II}	82.2 MN (^{189}Ir) 95.3 L_I (^{189}Os) 96.7 L_I (^{188}Ir) 98.4 L_I (^{188}Ir)	82.2 L_I	141.1 K (^{189}Ir) 71.6 M (^{189}Ir) 138.3 K (^{189}Os) 147.1 K (^{189}Os) 69.6 MN (^{189}Os) 140.3 K (^{188}Ir)	94.3 L_{II} → 82.2 L_I (^{189}Ir) 94.3 L_{II} → 141.1 K (^{189}Ir) 82.1 MN → 141.1 K (^{189}Ir) 95.3 L_I → 138.3 K (^{189}Os)
113.8	113.8 K	36.2 N (^{189}Os) tail 54.8 L_I (^{188}Ir) 41.9 M (^{188}Ir)	186.6 K	113.8 M (^{189}Ir) 185.9 K (^{189}Os) 188.6 K (^{189}Os) 187.6 K (^{188}Ir)	113.8 K → 186.6 K (^{189}Ir)
176.6	82.2 L_I	71.6 M (^{189}Ir) 141.1 K (^{189}Ir) tail 147.1 K (^{189}Os) 69.6 MN (^{189}Os) tail 140.3 K (^{188}Ir)	141.1 L_I	204.0 K (^{189}Ir) 206.3 K (^{189}Os) tail 147.1 L_I (^{189}Os) 132.8 M (^{188}Ir)	82.2 L_I → 141.1 L_I (^{189}Ir) 69.6 MN → 206.3 K (^{189}Os) 69.6 MN → 147.1 L_I (^{189}Os)
300.5	71.6 L_I	tail 138.3 K (^{189}Os) 69.6 L (^{189}Os) 132.8 K (^{188}Ir)	186.6 L_I	243.6 K (^{189}Ir) 176.4 M (^{189}Ir) 185.9 L_I (^{189}Os) 188.6 L_I (^{189}Os) 187.6 L_I (^{188}Ir)	71.6 L_I → 186.6 L_I (^{189}Ir)

TABLE 4
Absolute transition probabilities in ^{189}Ir

Level in keV	$T_{1/2}$(exp) of level in nsec	Transition energy in keV	Initial state $IK^{\pi}(N,n_z\Lambda)$	Final state	Multipolarity	Relative N_γ [a]	Relative N_e	$T_{1/2\gamma}$ (exp) in sec	B(M1) in $(\frac{e\hbar}{2Mc})^2$	B(E2) in e^2b^2	Q_0 in barns	F_W [b]
94.3	11.6 ± 0.6	94.3	$\frac{1}{2}\frac{1}{2}^+(400)$	$\frac{3}{2}\frac{3}{2}^+(402)$	M1 E2	5.5 94.5	603	1.5 E-6 8.6 E-8	(3.2 ± 0.6) E-5	(8.7 ± 0.5) E-2		5.6 E+3 7.4 E-2
113.8	0.075 ± 0.018	19.5	$\frac{5}{2}\frac{3}{2}^+(402)$	$\frac{1}{2}\frac{1}{2}^+(400)$	E2							
		113.8		$\frac{3}{2}\frac{3}{2}^+(402)$	M1 E2	77 23	402	5.0 E-10 1.6 E-9	(5.4 ± 1.3) E-2	1.8 ± 0.5	7.4 ± 0.8	33 3.5 E-1
176.6	0.022 ± 0.010	62.6	$\frac{3}{2}\frac{1}{2}^+(400)$	$\frac{5}{2}\frac{3}{2}^+(402)$	M1 E2	2.3 0.21	17	9.1 E-9 1.0 E-7	(1.8 ± 0.8) E-2	$0.58^{+0.50}_{-0.36}$		100 1.1 E-2
		82.2		$\frac{1}{2}\frac{1}{2}^+(400)$	M1 E2	70 2.0	815	3.0 E-10 1.1 E-8	0.24 ± 0.11	1.4 ± 0.7	8.3 ± 2.0	7.5 4.7 E-1
		176.5		$\frac{3}{2}\frac{3}{2}^+(402)$	M1 E2	14.2 11.2	24	1.5 E-9 1.9 E-9	(4.8 ± 2.2) E-3	0.18 ± 0.08		367 3.9 E-2
300.4	0.013 [c]	124.0	$\frac{7}{2}\frac{3}{2}^+(402)$	$\frac{3}{2}\frac{1}{2}^+(400)$	E2	<0.25	<0.5	>7.3 E-9		<0.26		>2.5 E-2
		186.7		$\frac{5}{2}\frac{3}{2}^+(402)$	M1 E2	30 7.8	34	6.1 E-11 2.4 E-10	0.10 ± 0.02	1.1 ± 0.2	7.2 ± 0.6	18 6.3 E-3
		300.5		$\frac{3}{2}\frac{3}{2}^+(402)$	E2	62	6	3.0 E-11		0.78 ± 0.17	7.4 ± 0.8 [c]	8.5 E-3
317.7	0.0066 [d]	141.1	$\frac{5}{2}\frac{1}{2}^+(400)$	$\frac{3}{2}\frac{1}{2}^+(400)$	M1 E2	43 0.68	105	3.4 E-11 2.3 E-9	0.42 ± 0.14	$0.48^{+0.41}_{-0.22}$	9.1 ± 3.0	4.3 1.5 E-2
		203.5		$\frac{5}{2}\frac{3}{2}^+(402)$	M1 E2	5.2 <1.2	2.1	2.8 E-10 >1.2 E-9	(1.7 ± 0.5) E-2	<0.14		105 >4.9 E-2
		223.4		$\frac{1}{2}\frac{1}{2}^+(400)$	E2	16	6.4	9.1 E-11		1.1 ± 0.3	7.4 ± 0.8 [d]	5.9 E-3
		317.7		$\frac{3}{2}\frac{3}{2}^+(402)$	M1 E2	27 8	8.8	5.4 E-11 1.8 E-10	(2.3 ± 0.7) E-2	(9.4 ± 4.7) E-2		77 6.7 E-2

[a] Total γ-intensity from each level set equal to 100.
[b] Hindrance factor relative to the Weisskopf estimate.
[c] Calculated using our experimental Q_0 value for the $K = \frac{3}{2}$ band 7.4 ± 0.8 b as compared to our measured value $T_{\frac{1}{2}}$ (300.4 keV) < 20 psec giving $Q_0 > 5.7$ b.
[d] Calculated using $Q_0 = 7.4 \pm 0.8$ b.

level in ^{165}Ho (18 psec) is inserted we obtain a half-life of 76 ± 18 psec for the 113.8 keV level in ^{189}Ir. An analysis was also performed using the convolution method [30]) giving a value consistent with the one given above but with slightly larger errors. No spurious constant shift [30]) was observed from this analysis.

Kryukova *et al.* [26]) report a measurement of the lifetime of the 113.8 keV level where they get $\tau(114) \leqq 0.2 \pm 0.1$ nsec and conclude that the lifetime of this level is less than 0.3 nsec, in agreement with our present result.

The 176.5 keV *level.* The half-life of the 176.5 keV level was obtained by measuring the delayed-coincidence spectrum between the 82.2 L_I and 141.1 L_I conversion electron lines. For the prompt comparison the β-238.6 K cascade in the decay of ^{212}Pb was used. The 141.1 L_I line in ^{189}Ir was brought to energetically coincide with the 238.6 K line by adding 20.5 kV of high voltage to the ^{189}Pt source. Shift measurements on the two sources were performed continuously as described above for a time of 15 h. The resulting time spectra were analysed according to the first moment method [29]) which gave an average shift of 0.26 ± 0.13 channels. With the present energy settings of the spectrometers, small contributions from several close-lying electron lines could be expected. Table 3 gives a survey of all possible candidates. Of these lines coincidence contributions are obtained only from the 69.6 MN → 206.3 K and 69.6 MN → 147.1 L_I cascades, introducing the 1.6 nsec half-life of the 69.6 keV level in ^{189}Os. No coincidences indicating such a long half-life were, however, observed, showing that the influence on the coincidence rate from other activities accepted in our energy channels was negligible. After correction for the time shift due to the acceleration in the 20.5 kV electrostatic field we obtain a half-life of 22 ± 10 psec for the 176.5 keV level in ^{189}Ir. The delayed and prompt time spectra were also analysed using the convolution method [30]) but the calculations did not converge because the delayed and prompt curves were too similar in shape. After 40 iterations the program indicated that the decay constant x of the delayed curve should be larger than 5 channels, corresponding to a half-life of less than 25 psec. It should, however, be pointed out that the fit in this case is rather insensitive to λ and thus the indicated value of λ shows only the consistency between the convolution and moment methods. Kryukova *et al.* [27]) conclude from their measurements that the half-life of the 176.5 keV level is probably very short but, because of some experimental irregularities, they could not set a limit lower than 0.7 nsec.

The 300.5 keV *level.* The 300.5 keV level is strongly fed by a 71.6 keV M2 transition. The main de-excitation takes place by 186.7 and 300.5 keV transitions. For the half-life determination we used the 71.6 L_I → 186.7 L_I cascade. To get a prompt comparison curve we used the β-238.6 K cascade in the decay of ^{212}Pb. By decelerating the 186.7 L_I electrons in a 22 kV electrostatic field they were made to energetically coincide with the slightly degraded 238.6 K electrons. Shift measurements were performed as described above for a total period of 8 h. The result was analyzed using first moments [29]) which all consistently gave a shift for the intermediate level of

0.27 ± 0.16 channels. Although several other conversion lines were also partly accepted within the energy channels used (see table 3) no disturbing coincidence contributions were expected. After correction for the influence from the finite acceleration distance we obtain a half-life of 10 ± 10 psec or < 20 psec for the 300.5 keV level in ^{189}Ir. No earlier value is reported for the half-life of this level.

3. Discussion

The low-energy levels in ^{189}Ir, fig. 1, are well known from earlier work [7,8]). The reduced transition probabilities between these levels as obtained in the present work are given in table 4.

The closest odd-proton neighbours of the Ir nuclei are the Re nuclei, which are clearly deformed, and the Au nuclei, which are little or not at all deformed. It is not evident

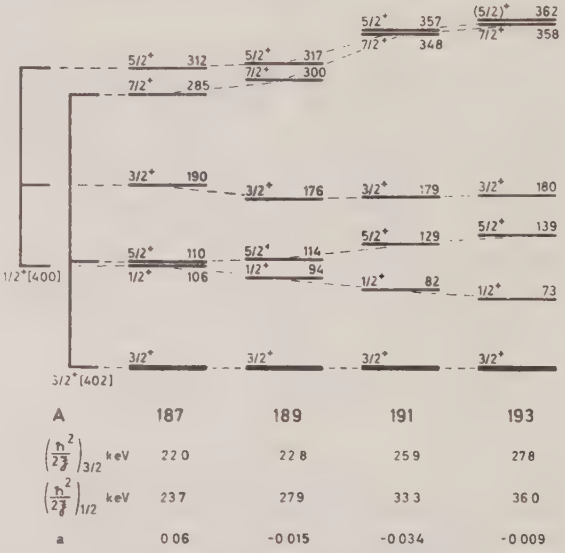

Fig. 6. Low-energy levels in odd-mass Ir nuclei. The rotational level parameters shown are those obtained assuming no Coriolis coupling.

from their level structure whether the Ir nuclei should be classified as deformed or spherical, since the same level sequence is expected for Ir in both cases. For ^{193}Ir and ^{191}Ir attempts have been made to interpret the levels in terms of the $d_{\frac{3}{2}}$ and $s_{\frac{1}{2}}$ shell-model states and the states obtained by coupling one or two quadrupole vibrational phonons to the particle states [31-33]). However, the results are not convincing, and we have earlier discussed these nuclei in terms of the deformed scheme [2,3,34]), which

is supported not only by the grouping of the levels into rotational band-like structures but also by the E2 transition probabilities between the levels [2,3]), see subsect. 3.2.

For ^{189}Ir the deformed scheme also seems applicable. As seen in fig. 6 the five lowest excited states change only little in the odd-A Ir isotopes. It is natural to group the levels into two rotational bands corresponding to the Nilsson orbitals $\frac{3}{2}^+[402]$ and $\frac{1}{2}^+[400]$, which are expected at low energy for a moderately deformed nucleus with $Z = 77$. In the lower part of fig. 6 the parameters of the energy formula [34])

$$E_K(I) = E_K^0 + \left(\frac{\hbar^2}{2J}\right)_K \{I\langle(I+1)+\delta_{K,\frac{1}{2}}a(-1)^{I+\frac{1}{2}}(I+\tfrac{1}{2})\} \qquad (1)$$

are given as calculated from the experimental level energies. For the $K = \frac{3}{2}$ band the $I = \frac{3}{2}$ and $\frac{5}{2}$ states were used. The calculated energy of the $\frac{7}{2}$ state is then about 25 keV lower than the measured value. In order to find out whether this may be explained as an effect of Coriolis coupling between the $K = \frac{3}{2}$ band and the $\frac{1}{2}^+[400]$ band we have performed two-band Coriolis coupling calculations in ^{189}Ir, ^{191}Ir and ^{193}Ir as described in ref. [2]). In all three nuclei the fit to the experimental energies was found not to be significantly improved over the uncoupled case for any value of the coupling matrix element. We therefore conclude that other couplings are of importance for the energies of these states.

Neither is the decoupling parameter a for the $\frac{1}{2}^+[400]$ band influenced very much by the Coriolis coupling. In fig. 6, which gives the parameters for the uncoupled case, it is seen to be close to zero in all the Ir nuclei. The differences between these values and the theoretical value of $a \approx 0.3$ for moderate deformations [34]) are somewhat larger than the uncertainty of the latter value due to uncertainties of the Nilsson-model parameters. This may be due to an admixture of the $\frac{3}{2}^+[K_0-2]$ γ-vibrational band †.

3.1. E2 TRANSITIONS IN ^{189}Ir

From the absolute B(E2) values for the intra-band transitions given in table 4 we can calculate the quadrupole moment Q_0, from which the deformation can be determined [36]). From $B(\mathrm{E2}, \frac{5}{2}\frac{3}{2} \rightarrow \frac{3}{2}\frac{3}{2}) = 1.8 \pm 0.5\ e^2 \cdot \mathrm{b}^2$ we obtain $Q_0 = 7.4 \pm 0.8$ b, giving a deformation parameter $\delta = 0.22 \pm 0.03$. For the $K = \frac{1}{2}$ band we obtain $Q_0 = 8.3 \pm 2.0$ b corresponding to $\delta = 0.24 \pm 0.05$. The values of δ are large enough to definitely classify ^{189}Ir as a deformed nucleus.

It is of interest to investigate in what extent the inter-band E2 transition rates between the $K = \frac{1}{2}$ and $K = \frac{3}{2}$ bands can be explained from Coriolis coupling. We have repeated for ^{189}Ir the same type of coupling calculation as described in ref. [2]) for ^{193}Ir. If the essential mixing between the $K = \frac{1}{2}$ and $\frac{3}{2}$ bands is of the Coriolis type, the amplitudes of these components are a function only of the parameter $\Delta E/2M$ where ΔE is the energy difference between the two states with the same spin that mix,

† This possibility for the corresponding band in ^{191}Ir and ^{193}Ir has recently been discussed by Nørgaard *et al.* [40]).

TABLE 5

E2 rates for inter-band transitions in ^{189}Ir

Experimental data ($e^2 \cdot b^2$)		Calculated B(E2) values [a])		
		$E^*\langle\frac{1}{2}\vert j_-\vert\frac{3}{2}\rangle = 10$	$E^*\langle\frac{1}{2}\vert j_-\vert\frac{3}{2}\rangle = 30$	$E^*\langle\frac{1}{2}\vert j_-\vert\frac{3}{2}\rangle = 90$
B(E2, $\frac{11}{22} \rightarrow \frac{33}{22}$)	(8.7±0.5) E−2	1.2 E−2	8.5 E−2	2.9 E−1
B(E2, $\frac{31}{22} \rightarrow \frac{33}{22}$)	(1.8±0.8) E−1	0.44 E−1	2.9 E−1	8.3 E−1
B(E2, $\frac{31}{22} \rightarrow \frac{53}{22}$)	$(5.8^{+5.0}_{-3.6})$ E−1	0.056 E−1	0.44 E−1	1.5 E−1
B(E2, $\frac{51}{22} \rightarrow \frac{33}{22}$)	(9.4±4.7) E−2	1.3 E−2	7.3 E−2	1.4 E−1
B(E2, $\frac{51}{22} \rightarrow \frac{53}{22}$)	< 1.4 E−1	1.2 E−2	6.8 E−2	1.5 E−1
B(E2, $\frac{73}{22} \rightarrow \frac{31}{22}$)	< 2.6 E−2	1.1 E−2	4.0 E−2	4.1 E−2
B(E2, $\frac{53}{22} \rightarrow \frac{11}{22}$)		1.8 E−2	11.8 E−2	3.2 E−1

[a]) We used $G_{E2}(\frac{1}{2} \rightarrow \frac{1}{2}) = G_{E2}(\frac{3}{2} \rightarrow \frac{3}{2}) = 65$, corresponding to $Q_0 = 7.5$ b.

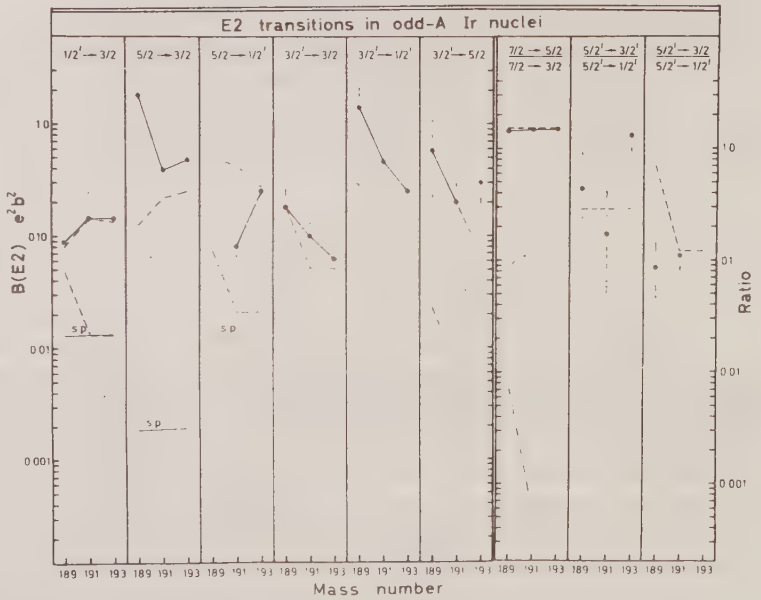

Fig. 7. Reduced E2 transition probabilities and ratios for the lowest positive-parity states in odd-mass Ir nuclei. For the notation the levels have been assumed to form rotational bands, the primed states indicating members of the $K^\pi = \frac{1}{2}^+$ band and the unprimed state indicating members of the $K^\pi = \frac{3}{2}^+$ band (cf. fig. 6). The experimental points are connected with solid lines. The dashed lines indicate for the B(E2) values the results of the Coriolis coupling calculation mentioned in the text. For the ratios these lines indicate the Alaga values. The dot-dash lines are associated with the assumption of a spherical nucleus and show the results of the pairing-plus-quadrupole-force calculations by Reehal and Sorensen [32]).

and

$$M = -P_+ E^* \langle\tfrac{1}{2}\vert j_-\vert\tfrac{3}{2}\rangle \sqrt{(I-\tfrac{1}{2})(I+\tfrac{3}{2})},$$

where the pairing factor $P_+ \approx 1.0$ and $E^* \approx \hbar^2/2J \approx 30$ keV. From the deformed potential parameters recommended by Nilsson [34]) and $\delta = 0.20 \pm 0.05$, the Coriolis matrix element $\langle\frac{1}{2}\vert j_-\vert\frac{3}{2}\rangle$ is predicted to be 0.66 ± 0.15. Several inter-band B(E2) values have been calculated using three different values of the parameter $E^*\langle\frac{1}{2}\vert j_-\vert\frac{3}{2}\rangle$. These are compared with the experimental data in table 5, where it can be seen that the mixing corresponding to the value $E^*\langle\frac{1}{2}\vert j_-\vert\frac{3}{2}\rangle \approx 20$ keV reasonably accounts for the general features of the inter-band E2 transition rates in ^{189}Ir. The only quantity for which a large deviation is observed is B(E2; $\frac{3}{2}\frac{1}{2} \rightarrow \frac{5}{2}\frac{3}{2}$). However, the experimental data on this transition are very uncertain, see subsect. 2.3.

3.2. SYSTEMATICS OF E2 TRANSITION PROBABILITIES IN ODD-MASS Ir NUCLEI

It is interesting to compare the reduced E2 transition probabilities between the low-lying positive-parity states in ^{189}Ir with the corresponding quantities in ^{191}Ir and ^{193}Ir. In fig. 7 we have plotted these quantities as functions of the mass number. The most striking feature is the sharp rise in the B(E2) value of the transitions interpreted as intra-band transitions when the mass number is reduced from 191 to 189. This corresponds to a sharp increase in the deformation δ from 0.12 for ^{193}Ir and ^{191}Ir to 0.23 for ^{189}Ir as the neutron number is reduced from 114 to 112. This rise in deformation is almost as sharp as that observed in Sm and Gd nuclei when the neutron number goes from 88 to 90 [ref. [35])]. In the region around $A = 180$ there are not enough experimental data available on B(E2) values in other odd-proton nuclei, i.e. Re and Au isotopes, to demonstrate a similar strong dependence on the neutron number. Available data in even Pt and Os nuclei [36,37]) indicate a more gradual change of the deformation with the neutron number than for the Ir nuclei, and that the neutron number where the transition between spherical and deformed shape takes place also depends on the charge number.

While the deformed character of ^{189}Ir can hardly be disputed, the situation is less clear for ^{191}Ir and ^{193}Ir. In fig. 7 we have, in addition to the experimental B(E2) values, indicated two sets of theoretically calculated values: the dash-dotted lines give the B(E2) values obtained by Reehal and Sorensen [32]) in the pairing-plus-quadrupole-force model of spherical nuclei including up to two phonons. The dashed lines indicate the B(E2) values calculated in the Nilsson model assuming the Coriolis coupling matrix element $E^*\langle\frac{1}{2}\vert j_-\vert\frac{3}{2}\rangle$ between the $\frac{1}{2}^+[400]$ band and the $\frac{3}{2}^+[402]$ band to have the value ≈ 20 keV (cf. subsect. 3.1).

We see that, although the spherical model amazingly well reproduces the value of B(E2; $\frac{1}{2}\frac{1}{2} \rightarrow \frac{3}{2}\frac{3}{2}$) for all three Ir nuclei, it fails to reproduce most of the other experimental values, including the E2 branching ratios, shown at the right in fig. 7. On the other hand, the values calculated in the deformed model also deviate in general rather much from the experimental points. However, one may point out a few circumstances

TABLE 6
uced M1 transition probabilities and correspondin rameters in

Experimental data [a]	Calculated B(M1) values using the fitted parameters given below					
	$E^*\langle\frac{1}{2}\|j_-\|\frac{3}{2}\rangle = 0$	$E^*\langle\frac{1}{2}\|j_-\|\frac{3}{2}\rangle = 10$	$E^*\langle\frac{1}{2}\|j_-\|\frac{3}{2}\rangle = 15$	$E^*\langle\frac{1}{2}\|j_-\|\frac{3}{2}\rangle = 20$ [b]	$E^*\langle\frac{1}{2}\|j_-\|\frac{3}{2}\rangle = 30$	$E^*\langle\frac{1}{2}\|j_-\|\frac{3}{2}\rangle = 50$
$B(M1, \frac{1}{2}\frac{1}{2} \to \frac{3}{2}\frac{3}{2})$ (3.2 ± 0.6) E-5	3.6 E-5	3.6 E-5	3.3 E-5	3.2 E-5	3.3 E-5	3.3 E-5
$B(M1, \frac{3}{2}\frac{1}{2} \to \frac{3}{2}\frac{3}{2})$ (4.8 ± 2.2) E-3	1.3 E-5	3.3 E-3	4.4 E-3	5.5 E-3	5.6 E-3	6.5 E-3
$B(M1, \frac{3}{2}\frac{1}{2} \to \frac{5}{2}\frac{3}{2})$ (1.8 ± 0.8) E-2	2.1 E-5	7.1 E-3	1.2 E-2	8.1 E-3	7.2 E-3	4.3 E-3
$B(M1, \frac{5}{2}\frac{1}{2} \to \frac{3}{2}\frac{3}{2})$ (2.3 ± 0.7) E-2	2.4 E-6	1.7 E-2	2.7 E-2	2.0 E-2	2.8 E-2	4.6 E-2
$B(M1, \frac{5}{2}\frac{1}{2} \to \frac{5}{2}\frac{3}{2})$ (1.7 ± 0.5) E-2	2.5 E-5	1.7 E-2	2.2 E-2	1.5 E-2	1.7 E-2	1.6 E-2
$B(M1, \frac{3}{2}\frac{1}{2} \to \frac{1}{2}\frac{1}{2})$ (2.4 ± 1.1) E-1	2.4 E-1	2.9 E-1	2.0 E-1	2.7 E-1	2.8 E-1	2.9 E-1
$B(M1, \frac{3}{2}\frac{1}{2} \to \frac{3}{2}\frac{1}{2})$ (4.2 ± 1.4) E-1	4.2 E-1	4.9 E-1	3.4 E-1	6.1 E-1	4.8 E-1	3.7 E-1
$B(M1, \frac{5}{2}\frac{3}{2} \to \frac{3}{2}\frac{3}{2})$ (5.4 ± 1.3) E-2	6.1 E-2	6.5 E-2	6.3 E-2	5.9 E-2	6.0 E-2	5.7 E-2
$B(M1, \frac{7}{2}\frac{3}{2} \to \frac{5}{2}\frac{3}{2})$ (1.0 ± 0.2) E-1	1.3 E-1	8.7 E-2	8.0 E-2	7.6 E-2	7.7 E-2	7.4 E-2
$P_+(\frac{1}{2} \to \frac{3}{2})\, G_{M1}(\frac{1}{2} \to \frac{1}{2})$	-0.025 ± 0.013	-0.35 ± 0.05	-0.37 ± 0.05	-0.59 ± 0.07	-0.81 ± 0.08	-1.13 ± 0.14
$G_{M1}(\frac{3}{2} \to \frac{3}{2})$ [c]	-1.98 ± 0.65	-2.16 ± 0.14	-2.19 ± 0.13	1.75 ± 0.16	1.67 ± 0.14	1.50 ± 0.20
$G_{M1}(\frac{1}{2} \to \frac{1}{2})$	-3.85 ± 2.41	4.22 ± 0.44	3.54 ± 0.35	4.40 ± 0.37	4.15 ± 0.28	3.86 ± 0.37
$G_{M1}(\frac{1}{2} \to \frac{1}{2}) b_{M1}$	0.5 ± 3.4	-0.52 ± 0.41	-0.56 ± 0.27	-1.11 ± 0.26	-0.69 ± 0.18	-0.41 ± 0.21
Mean square sum	12.5	0.63	0.51	0.75	0.59	1.4

[a]) B(M1) is given in units of $(e\hbar/2Mc)^2$.

[b]) Equals the predicted value of $\langle\frac{1}{2}|j_-|\frac{3}{2}\rangle = 0.66 \pm 0.15$ from ref. [4]) together with $E^* \approx \hbar^2/2J = 30$ keV.

[c]) The parameter $G_{M1}(\frac{3}{2} \to \frac{3}{2})$ changes sign between $E^*\langle\frac{1}{2}|j_-|\frac{3}{2}\rangle = 15$ and 20 keV. The reason for this is that there are in fact two solutions to our system of equations that are roughly equally good but they have their optimum fits for slightly different coupling strengths. This means that for $E^*\langle\frac{1}{2}|j_-|\frac{3}{2}\rangle = 10$ and 15 keV a certain combination of signs for $\sqrt{B(M1)}$ gives the best fit while after that another combination is slightly better. Both sets do, however, give better fits than any other combination over the whole range of coupling parameters. So, for instance, the mean square sum for the first sign combination is 1.3 for $E^*\langle\frac{1}{2}|j_-|\frac{3}{2}\rangle = 20$, which is more than ten times better than for an arbitrary combination of signs. This means in practice that we cannot from our data in ^{189}Ir decide which of the two sets of fitted parameters is relevant. This choice can, however, be made on empirical grounds from the earlier studies in ^{191}Ir and ^{193}Ir [refs.[2,3])]. The results are compiled in table 7. In the case of ^{191}Ir and ^{193}Ir the ambiguity was avoided by using experimental information on magnetic moments. From systematics we thus prefer the solution in ^{189}Ir given in table 7 column 4.

that make the deformed model preferable to the spherical model also for ^{191}Ir and ^{193}Ir: (i) the B(E2) values of the transitions corresponding to intra-band transitions are on the average a factor of 3 larger than those corresponding to inter-band transitions; (ii) the E2 branching ratios from the $\frac{7}{2}\frac{3}{2}$ and $\frac{5}{2}\frac{3}{2}$ levels are well reproduced by the Alaga rule, cf. fig. 7, while the spherical-model predictions deviate strongly.

The fact that the experimental B(E2) values of the inter-band transitions all are larger than those obtained from the Coriolis coupling calculations may possibly be explained as due to vibrational modes of excitation, which were neglected in the calculations but are expected to be of importance in this mass region. Calculations in which both Coriolis coupling and coupling to vibrational modes are considered have been performed by Piepenbring and Nopre [38]) for ^{193}Ir. Some improvement over our simple Coriolis coupling calculations is obtained, especially if pairing is also considered, but on the other hand these authors obtain too low values for the intra-band transition probabilities.

3.3. M1 TRANSITIONS IN ^{189}Ir

The presently known data on the M1 transition rates in the proposed $K = \frac{1}{2}$ and $K = \frac{3}{2}$ rotational band system in ^{189}Ir are collected in table 4. To our knowledge no magnetic moments have been measured. This material may be compared with predictions from the Nilsson model [34]). Disregarding admixtures for the moment this model predicts the branching ratio $B(M1; \frac{5}{2}\frac{1}{2} \to \frac{5}{2}\frac{3}{2})/B(M1; \frac{5}{2}\frac{1}{2} \to \frac{3}{2}\frac{3}{2})$ to be 6.75, while in ^{189}Ir we observe 0.74 ± 0.10. It is interesting to see if this discrepancy can be removed by assuming Coriolis mixing between the $\frac{1}{2}^+[400]$ and $\frac{3}{2}^+[402]$ bands. The expressions for the relevant reduced M1 transition rates have been given in detail in ref. [2]). They depend on the following five parameters

$$P_+(\tfrac{1}{2} \to \tfrac{3}{2})G_{M1}(\tfrac{1}{2} \to \tfrac{3}{2}), \quad G_{M1}(\tfrac{3}{2} \to \tfrac{3}{2}), \quad G_{M1}(\tfrac{1}{2} \to \tfrac{1}{2}), \quad b_{M1}G_{M1}(\tfrac{1}{2} \to \tfrac{1}{2}),$$
$$E^*\langle\tfrac{1}{2}\,|j_-|\tfrac{3}{2}\rangle.$$

Our nine experimental B(M1) values (table 6) then give a non-linear, over-determined set of equations from which the first four parameters have been determined through a least-squares fit using several different values of the coupling strength $E^*\langle\frac{1}{2}|j_-|\frac{3}{2}\rangle$. The system of equations was made linear by taking the square root of all experimental B(M1) values and then solving the system of equations for all possible combinations of signs. The parameters as well as the calculated B(M1) values for the sign combination giving the best fit to the experimental data for each value of $E^*\langle\frac{1}{2}|j_-|\frac{3}{2}\rangle$ are given in table 6. Here we can see that most of the inter-band B(M1) values are very sensitive to even a small amount of admixture. From the mean square sum we also see that the total fit to the M1 data is largely improved with the introduction of admixtures with a rather flat minimum of the mean square sum for values of $E^*\langle\frac{1}{2}|j_-|\frac{3}{2}\rangle$ between 10 and 30 keV, which was also found to be compatible with the inter-band E2 transition rates.

3.4. SYSTEMATICS OF M1 TRANSITION PROBABILITIES IN ODD-MASS Ir NUCLEI

Fig. 8 shows the reduced M1 transition probabilities for ^{189,191,193}Ir as functions of the mass number. We note a very large spread of the values and that the values for the intra-band transitions are all larger than for the inter-band transitions. Interesting behaviour is shown by the transition probability between the two band-heads, which drops considerably in going from mass number 191 to 189, where it is as low as $\approx 1.8 \times 10^{-5}$ single-particle units. This trend is further continued in going to ^{187}Ir [ref. [39])].

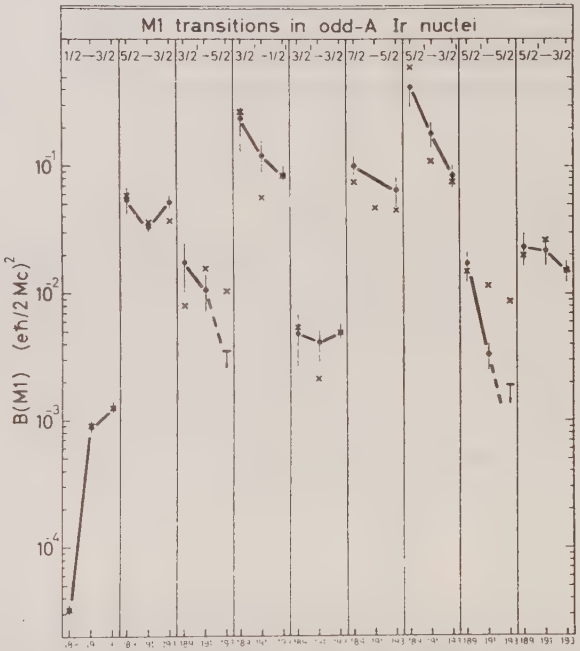

Fig. 8. Reduced M1 transition probabilities between low-lying positive-parity states in odd mass Ir nuclei. For notation, see caption of fig. 7. The experimental points are connected with solid lines. The crosses indicate the results of the Coriolis coupling calculation mentioned in the text.

Fig. 8 also shows the reduced M1 transition probabilities calculated using the parameters given in table 6 for a Coriolis coupling matrix element of $E^*\langle\frac{1}{2}|j_-|\frac{3}{2}\rangle = 20$ keV, which corresponds to the value predicted by the Nilsson model [34]) assuming $E^* = 30$ keV. The agreement with experiment is seen to be good. One may expect a slightly worse fit in ^{191}Ir and ^{193}Ir, where accurately measured magnetic moments were included in the fit.

The fitted values of the parameters may be compared with the values calculated from the Nilsson model. To do this we have used the following model parameters

$\kappa = 0.05$, $\mu = 0.55$, $\delta = 0.20 \pm 0.05$, $g_R = 0.55 \pm 0.05$ † and g_s (effective) $= (0.7 \pm 0.1)$ g_s (free). The results are given in the last column in table 7 showing an excellent agreement for the first three parameters, while the $b_{M1}G_{M1}(\frac{1}{2} \to \frac{1}{2})$ parameter comes out too low for all iridium isotopes. Also the strength of the Coriolis coupling is well accounted for in the model.

TABLE 7

Nilsson-model parameters obtained from fits to experimental magnetic data for iridium nuclei

	$A = 193$	$A = 191$	$A = 189$	Nilsson model [a])
$P_+G_{M1}(\frac{1}{2} \to \frac{3}{2})$	$-(0.309 \pm 0.043)$	$-(0.143 \pm 0.060)$	$-(0.37 \pm 0.05)$	$-(0.28 \pm 0.08)$
$G_{M1}(\frac{3}{2} \to \frac{3}{2})$	$-(1.67 \pm 0.19)$	$-(1.62 \pm 0.19)$	$-(2.19 \pm 0.13)$	$-(1.7 \pm 0.4)$
$G_{M1}(\frac{1}{2} \to \frac{1}{2})$	2.02 ± 0.24	3.18 ± 0.54	3.54 ± 0.35	3.1 ± 0.5
$G_{M1}(\frac{3}{2} \to \frac{1}{2})b_{M1}$	$-(0.04 \pm 0.22)$	0.06 ± 0.31	$-(0.56 \pm 0.27)$	$-(3.5 \pm 0.4)$
$E^*\langle\frac{1}{2}\|j_-\|\frac{3}{2}\rangle$ (keV)	10	10	15	20 ± 5

[a]) Predictions from the Nilsson model [4]) using the parameters $\kappa = 0.05$, $\mu = 0.55$, $\delta = 0.20 \pm 0.05$, $g_R = 0.55 \pm 0.05$ and g_s(effective) $= (0.7 \pm 0.1)g_s$ (free).

4. Conclusion

The transition probabilities between the low-energy positive-parity states in ^{189}Ir are not well predicted in the spherical scheme using the calculations of Sorensen [31]) and Reehal and Sorensen [32]). A considerably better description is offered by the Nilsson model, assuming the states to be members of the $\frac{3}{2}^+[402]$ and $\frac{1}{2}^+[400]$ bands including Coriolis coupling. The intra-band E2 transitions imply a deformation $\delta = 0.23$. For ^{191}Ir and ^{193}Ir the deformations are much smaller, δ being ≈ 0.12 for both, and it is not clear whether these nuclei should be characterized as deformed, although for these nuclei also the deformed model reproduces the E2 transition probabilities better than does the spherical model. The E2 transition rates between the $\frac{3}{2}^+$ and $\frac{1}{2}^+$ bands are well explained by Coriolis coupling between the bands, but vibrational effects may also exist, since the small decoupling parameter of the $\frac{1}{2}^+$ band suggests that it, in addition to the $\frac{1}{2}^+[400]$ component, also contains part of the $K_0 - 2$ γ-vibration based on the $\frac{3}{2}^+[402]$ band. The M1 transition probabilities in all three Ir nuclei are fairly well predicted by the Nilsson model including Coriolis coupling.

The increase in deformation for the Ir nuclei when the neutron number changes from 114 to 112, which has no correspondence in neighbouring even nuclei, in which the deformation changes more slowly, is of the same magnitude as that in Sm and Gd nuclei when the neutron number changes from 88 to 90. This effect may be associated with the $\frac{9}{2}^-[505]$ orbital, which is likely to be occupied by the 57th neutron pair and which is strongly lowered as the deformation decreases, together with the polarizing effect of the odd proton.

† Average value of experimental values for ^{191}Ir [ref. [2])] and ^{193}Ir [ref. [3])].

We are indebted to Fil. lic. B. Fogelberg for valuable assistance in the measurements. The work was supported by the Swedish Atomic Research Council.

References

1) S. G. Malmskog and A. Bäcklin, Ark. Fys. **39** (1969) 411
2) S. G. Malmskog, V. Berg and A. Bäcklin, Nucl. Phys. **A143** (1970) 160
3) V. Berg, S. G. Malmskog and A. Bäcklin, Nucl. Phys. **A143** (1970) 177
4) A. Bäcklin, V. Berg and S. G. Malmskog, Nucl. Phys. **A156** (1970) 647
5) A. Bäcklin, G. Hedin, S. G. Malmskog and V. Berg, Contribution to the Conf. on the properties of nuclei far from the stability line, Leysin, Switzerland, 1970
6) A. Artna, (compiler), Nucl. Data **B1–2** (1966) 85
7) B. Harmatz, T. H. Handley and J. W. Mihelich, Phys. Rev. **128** (1962) 1186
8) H. R. Lewis, Jr., R. A. Naumann, J. M. Prospero and D. Thomas, Phys. Rev. **134** (1964) B322
9) A. Fourrier, J. Jastrzebski, P. Paris, P. Kilcher and J. Treherne, Compt. Rend. **263B** (1966) 509
10) G. Hedin and A. Bäcklin, to be published
11) The ISOLDE collaboration, ed. A. Kjelberg and G. Rudstam, CERN yellow report 70-3, 1970
12) R. J. Hanson, P. G. Hansen, H. L. Nielsen and D. Sorensen, Nucl. Phys. **A115** (1968) 641
13) Z. Planjer, J. Frana, I. Rezanka, A. Spalek and M. Fiser, Z. Phys. **233** (1970) 122
14) A. Bäcklin, B. Fogelberg and S. G. Malmskog, unpublished
15) H. Daniel *et al.*, Nucl. Phys. **56** (1964) 147
16) W. F. Edwards, F. Boehm, J. Rogers and E. J. Seppi, Nucl. Phys. **63** (1965) 97
17) W. W. Black and R. L. Heath, Nucl. Phys. **A90** (1967) 650
18) C. M. Lederer, J. M. Hollander and I. Perlman, Table of isotopes (Wiley, New York, 1967)
19) A. Bäcklin, B. Fogelberg and S. G. Malmskog, Nucl. Phys. **A103** (1967) 337
20) A. Hedgran, K. Siegbahn and N. Svartholm, Proc. Phys. Soc. **A63** (1950) 960
21) A. Bäcklin, Nucl. Instr. **57** (1967) 261
22) O. Hörnfelt, Ark. Fys. **23** (1962) 235
23) R. S. Hager and E. C. Seltzer, Nucl. Data **A4** (1968) 1, 2
24) S. G. Malmskog, V. Berg and A. Bäcklin, Nucl. Phys. **A153** (1970) 316
25) T. R. Gerholm and J. Lindskog, Ark. Fys. **24** (1963) 171
26) S. G. Malmskog, Ark. Fys. **35** (1967) 255
27) L. N. Kryukova, V. O. Kordyukevich and A. A. Sorokin, Bull. Acad. Sci. USSR (phys. ser.) **30** (1966) 1420
28) J. Jastrzebski, H. Abou-Leila and H. H. Perrin, Nucl. Phys. **70** (1965) 392
29) T. Sundström, Nucl. Instr. **16** (1962) 153
30) B. Olsen and L. Boström, Nucl. Instr. **44** (1966) 65
31) L. S. Kisslinger and R. A. Sorensen, Rev. Mod. Phys. **35** (1963) 853;
R. A. Sorensen, Phys. Rev. **133** (1964) B281
32) B. S. Reehal and R. A. Sorensen, Phys. Ref. **C2** (1970) 819
33) R. Avida, J. Burde and A. Molchadzki, Nucl. Phys. **A115** (1968) 405
34) S. G. Nilsson, Mat. Fys. Medd. Dan. Vid. Selsk. **29** (1955) no. 16
35) O. Nathan and S. G. Nilsson, Alpha-, beta- and gamma-spectroscopy, ed. K. Siegbahn (North-Holland, Amsterdam, 1965) ch. 10
36) P. H. Stelson and L. Grodzins, Nucl. Data **A1** (1965) 21
37) S. Malmskog, The ISOLDE collaboration, to be published
38) R. Piepenbring and H. Nopre, Nucl. Phys. **A133** (1969) 113
39) The ISOLDE collaboration, CERN yellow report 70-29, 1970
40) P. N. Nørgaard, K. M. Bisgaard, K. Gregersen and P. Morgen, Nucl. Phys. **A162** (1971) 449

REFERENCE 12

ABSOLUTE TRANSITION RATES IN ^{188}Ir

SVEN G. MALMSKOG

AB Atomenergi, Studsvik, Nyköping, Sweden

and

Valter BERG

DEPARTMENT OF PHYSICS, University of Stockholm, Stockholm, Sweden

1.E.4 *Nuclear Physics* **A139** (1969) 17—23; © *North-Holland Publishing Co., Amsterdam*
Not to be reproduced by photoprint or microfilm without written permission from the publisher

ABSOLUTE TRANSITION RATES IN ^{188}Ir

SVEN G. MALMSKOG
AB Atomenergi, Studsvik, Nyköping, Sweden
and
VALTER BERG
Department of Physics, University of Stockholm, Stockholm, Sweden

Received 25 August 1969

Abstract: Half-lives of several excited levels in ^{188}Ir have been measured using an electron-electron delayed coincidence spectrometer. Active ^{188}Pt sources were prepared from spallation products using the ISOLDE on-line mass separator facility at CERN. The following half-lives were obtained: $T_{\frac{1}{2}}$(54.8 keV level) = 1.93±0.10 nsec; $T_{\frac{1}{2}}$(96.7 keV level) = 1.59±0.12 nsec; $T_{\frac{1}{2}}$(187.6 keV level) = 0.056±0.013 nsec; $T_{\frac{1}{2}}$(195.1 keV level) = 0.051±0.010 nsec; $T_{\frac{1}{2}}$(478.3 keV level) ≤ 0.15 nsec. The 54.8 keV transition was found to have an enhanced E2 transition probability indicating a collective character for this transition.

E RADIOACTIVITY ^{188}Pt [from Pb (p, spallation)]; measured cece-, γce-delay; deduced partial half-lives

1. Introduction

Recently we have studied the low-energy level schemes of odd-A iridium isotopes [1]). Even though they all appear to have rotational bands, the rotational parameters and B(E2) strengths within bands tells us that the stable deformation of these nuclei is very small ($\delta \approx 0.1$). From the interband B(E2) values we also see that these bands are heavily mixed preferably by Coriolis and vibrational band mixing.

When we turn to the doubly odd iridium isotopes we can expect an even more complicated situation in which the rotational bands, built on different combinations of single proton and neutron states, are all mixed together, making a quantitative description rather elaborate. First of all more experimental data regarding the level structure are needed.

Using high resolution electron spectroscopy, Prospero [2]) determined electron energies and intensities for most of the transitions in the decay of ^{188}Pt. For some of the observed transitions multipole assignments were also made. From these data a level scheme of ^{188}Ir was proposed. Recently Hanson *et al.* [3]) increased our knowledge by measuring the gamma-ray spectrum and K-electron capture probabilities in the decay of ^{188}Pt. These two experimental studies give a consistent picture of the decay scheme of ^{188}Ir where also preferred spin and parity assignments have been made. The difficulty, however, arises when the nature of the different levels is questioned. Prospero [2]) proposes that the ground state is a $\langle \frac{3}{2}^+(402)\frac{7}{2}^-(503)\rangle_2$- configuration and Hanson

et al. [3]) suggest a $\langle \frac{1}{2}^-\frac{1}{2}^-(505)\frac{9}{2}^-(505)\rangle_{1+}$ configuration for the strongly fed 478.3 keV level. The nature of the other levels is not known at present.

It is well known that absolute transition strengths usually tell us something about the nature of the levels involved in the transition. Thus strongly enhanced E2 rates, for instance, clearly pick out collective levels. It is the aim of this work to establish as many absolute transition probabilities as possible in ^{188}Ir to see whether the low-lying levels in ^{188}Ir can be interpreted within an extended Nilsson scheme.

2. Experimental procedure

2.1. SOURCE PREPARATION

A molten lead target at 700°C was bombarded in an external beam of 600 MeV protons from the CERN synchro-cyclotron. Mercury extracted from this target was isotope-separated in the ISOLDE on-line mass separator facility [4]). The A = 188 activity chain was collected on a 0.9 mg/cm^2 nickel foil and sent to Studsvik. The active sample was allowed to decay for two weeks and after that period only the ^{188}Pt (10.2 d) activity was observed when measured in a high resolution Ge(Li) counter.

2.2. HALF-LIFE MEASUREMENTS

Half-life measurements were carried out using a long lens electron-electron coincidence spectrometer described earlier [5,6]).

The 54.8 keV *level.* The time distribution from coincidences between the 54.8 $L_{II}+L_{III}$ and 140.3 K conversion electron lines focused in each of the lens spectrometers has been registered. An example of the observed decay curve is shown in fig. 1.

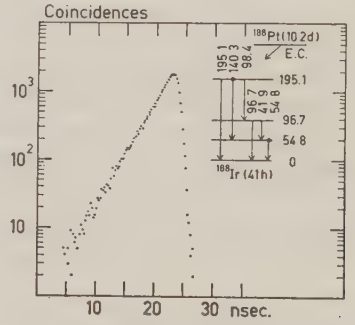

Fig. 1. Delayed time coincidence distribution recorded between the 54.8 $L_{II}+L_{III}$ and 140.3 K conversion electrons giving a half-life of 1.93±0.10 nsec for the 54.8 keV level in ^{188}Ir.

As no disturbing coincidence contributions are expected, the half-life for the 54.8 keV level is directly obtained from the slope of the observed decay curve giving $T_{\frac{1}{2}}$ = 1.93±0.10 nsec.

The 96.7 keV *level.* The half-life of this level has been studied in two ways. In both cases the 41.9 L line was focused in one of the lens spectrometers. To increase the detection efficiency as well as the time resolution, 15 kV was applied to the source. In the first case the 98.4 L line was focused in the second lens and the coincidence distribution from a time to pulse-height converter was recorded. Owing to the comparatively weak intensity of the 98.4 L line the statistical accuracy of this measurement was not very good. A new measurement was therefore made in which the lens in the second channel was replaced by a plastic scintillator set up close to the source. The energy selection was optimised for detection of the 381.6 keV gamma transition. As the 41.9 L channel was free from other electron components, the detection of the 478.3 and 423.6 keV transitions in the second channel did not cause any disturbing coincidence contributions. An example of an observed decay curve in the latter measurements is shown in fig. 2. After correction for random coincidences the half-life of the 96.7 keV level was obtained from the slope of the decay curve as $T_{\frac{1}{2}} = 1.59 \pm 0.12$ nsec.

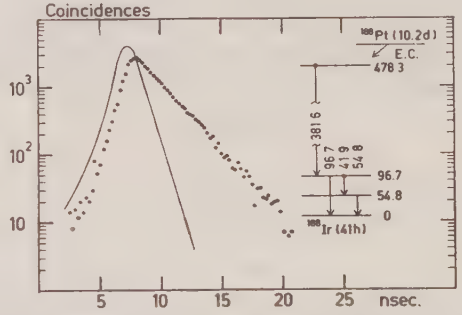

Fig. 2. Observed delayed coincidence curve taken between the 41.9 L conversion electrons and the 381.6 keV gamma transition. The curve drawn in full line is the corresponding prompt decay curve. From the analysis we obtain a half-life of 1.59±0.12 nsec for the 96.7 keV level in ^{188}Ir.

The 187.6 keV *level.* The 187.6 keV level is mainly fed by an EC branch and therefore the only realistic feeding transition to use in the half-life measurement is the KLL Auger electrons. The main de-excitation takes place via a 187.6 keV transition having a K/L ratio of 6.5 [ref. [2])]. Although the intensity of the K-line is much more intense than the L_I line we had to use the latter in our measurement to avoid the difficulty of correcting for the prompt coincidence distribution obtained from the 187.6 K line being in coincidence with the KLL Auger electrons created in the internal conversion process. Because of the comparatively low energy of the KLL Auger electrons we were forced to take the 187.6 L_I line through the supporting nickel foil. The absorption in the foil increased the low-energy tail of the not completely separated 195.1 L_I line giving rise to a false contribution to the KLL Auger → 187.6 L_I distribution. From the slope of the decay curve the half-life of the 187.6 keV level was found to be

less than 200 psec. Therefore a shift measurement was performed using the $\beta \rightarrow$ 94.7 K cascade in the decay of ^{165}Dy as a time reference. To be able to use the same energy settings in the two measurements 11 kV was added to the Dy source. 15 min measurements were taken using the Pt and Dy sources alternatively for a total time of 10 h. The data were analysed according to the centroid shift [7]) and convolution [8]) methods. After correction for the finite acceleration time in the spectrometer, the lifetime of the 94.7 keV level in ^{165}Ho (τ = 18 psec) and the contribution from the KLL Auger → 195.1 L_I cascade (see below), we obtain a half-life for the 187.6 keV level of $T_{\frac{1}{2}} = 56 \pm 13$ psec.

The 195.1 keV *level.* The half-life of this level was measured in a way very similar to the one described for the 187.6 keV level. A shift measurement was performed using the KLL Auger → 195.1 L_I cascade from the ^{188}Pt source and the β-94.7 K cascade from the ^{165}Dy source. The correction for the contribution from the KLL-Auger → 187.6 L_I cascade due to incomplete resolution was less important than in the earlier case. From the data analysis using the centroid shift and convolution methods we obtain a half-life for 195.1 keV level of $T_{\frac{1}{2}} = 51 \pm 10$ psec.

The 478.3 keV *level.* An experiment was set up to measure the KLL-Auger → > 300 keV gamma-ray cascades. No coincidences, however, were observed showing that the Q_{EC} value to the 478.3 keV level in ^{188}Ir is less than the appropriate K-electron binding energy. Instead we focused the LMM Auger group in one lens still detecting > 300 keV gamma rays in a 1.9 × 1.9 cm cylindrical plastic scintillator. To improve the time resolution, 20 kV was added to the ^{188}Pt source. As a prompt comparison cascade we used the β-411.8 keV gamma-ray cascade in the decay of ^{198}Au. The observed shape of the delayed and prompt curves was, however, equal within the statistical errors. Due to the low energy of the LMM Auger electrons combined with a low coincidence rate accurate shift measurements were also difficult to make. From our experimental data we can thus only set an upper limit of less than 150 psec for the half-life of the 478.3 keV level in ^{188}Ir.

3. Discussion

Two earlier measurements of half-lives of excited levels in ^{188}Ir are reported in the literature [9,10]). Jastrzebski *et al.* [9]) determined the half-life of the 54.8 keV to be 2.3±0.2 nsec. From our present knowledge of the ^{188}Ir decay scheme this value is an overestimate of the actual half-life of the 54.8 keV level. The level scheme of ^{188}Ir used in ref. [9]) in analysing the data is obviously wrong. From our delayed coincidence data we can see that the 424 and 42 keV transitions decay with different half-lives and can thus not de-excite the same 478 keV level. We find that the 41.9 keV transition is coincident with and precedes the 54.8 keV transition. On the other hand the 41.9 keV transition is also delayed compared to the 98.4 keV transition and to some gamma rays with energies above 250 keV. All these features are consistent with the decay scheme proposed by Hanson *et al.* [3]) (fig. 3) where the 41.9 keV transition de-excites a 96.7 keV level.

In ref. [9]) the half-life of the 54.8 keV level was measured from a time coincidence spectrum between the conversion electrons from the 54.8 keV transition detected in a thin organic crystal and gamma rays of an energy about 400 keV. Due to the poor electron energy resolution of that detector together with the presently accepted level scheme of ^{188}Ir, the observed decay curve in ref. [9]) is a mixture of contributions from the following cascades:

gamma → 41.9 L ($T_{\frac{1}{2}}$ = 1.59 nsec),

gamma → 54.8 L ($T_{\frac{1}{2}}$ = 1.93 nsec),

gamma → 54.8 L (via the 96.7 keV level giving an effective $T_{\frac{1}{2}} > 2$ nsec),

gamma → KLL-Auger electrons (prompt). The sum of contributions from these cascades gives rise to a decay curve with variable slope, the longest effective component of which is the observed 2.3 nsec. From a 55 L-gamma coincidence measurement Kryukova *et al.* [10]) report a half-life for the 55 keV level of 2.7±0.8 nsec.

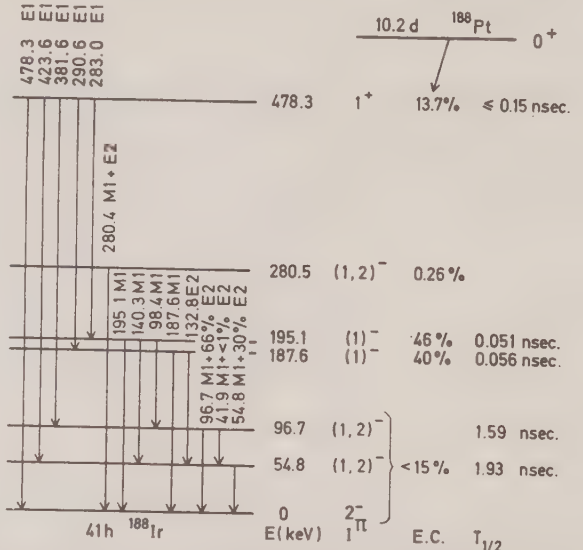

Fig. 3. The accepted level scheme of ^{188}Ir taken from Hanson *et al.* [3]) with the new information from the present work included.

The half-lives of different levels in ^{188}Ir observed in this work, together with the conversion electron data of Prospero [2]) and theoretical conversion coefficients [11]) have been used to determine reduced transition probabilities for many transitions in ^{188}Ir. The relevant data are collected in table 1, where also the hindrance factors as compared to the Weisskopf estimate [12]) are given. A clear difference is then seen to exist between transitions from the 54.8 and 96.7 keV levels. The enhancement of the 54.8 keV E2 part (94 s.p.u.) suggests a collective character for the 54.8 keV transition. With the suggested spins in fig. 3, however, the ground state and 54.8 keV level are

then members of an anomalous band with the lower energy member having the higher spin. This situation can occur, for instance, if both the odd neutron and proton occupy $K = \frac{1}{2}$ single-particle orbitals (e.g. $\frac{1}{2}^-(510)$ or $\frac{1}{2}^-(521)$ and $\frac{1}{2}^+(400)$). The coupling of these two particles will then give rise to both a $K = 0^-$ and $K = 1^-$ band. Through strong Coriolis mixing between these two bands the 2^- member of the $K = 1$ band can be pushed down below the 1^- member of the same band giving rise to a spin sequence such as the one proposed in ^{188}Ir and also accounting for the enhanced transition between the two levels.

TABLE 1

Relevant data to obtain partial half-lives for transitions in ^{188}Ir

Level (keV)	$T_{\frac{1}{2}}$ (level) (nsec)	Transition energy (keV)	Initial state I^π	Final state I^π	Multi-polarity	Relative N_γ [a])	Relative N_e [b])	$T_{\frac{1}{2}\gamma}$(exp) (sec)	F_W [c])
54.8	1.93 ±0.10	54.8	(1, 2)−	(2)−	M1	2.1	87	8.2E− 8 [d])	603
					E2	0.9		1.9E− 7	1.1E−2
96.7	1.56 ±0.12	41.9	(1, 2)−	(1, 2)−	M1	4.0	56	2.9E− 8	95
					E2	< 0.04		> 2.9E− 6	> 4.3E−2
		96.7	(1, 2)−	(2)−	M1	0.67	10	1.7E− 7	6940
					E2	1.33		8.7E− 8	8.4E−2
187.6	0.056±0.013	132.8	(1)−	(1, 2)−	E2	3	4.5	7.4E− 9	3.5E−2
		187.6	(1)−	(2)−	M1	192	198	1.1E−10	33
195.1	0.051±0.010	98.4	(1)−	(1, 2)−	M1	4	27	5.9E− 9	252
		140.3	(1)−	(1, 2)−	M1	22	52	1.1E− 9	132
		195.1	(1)−	(2)−	M1	184	176	1.3E−10	43
478.3	≦ 0.150	283.0	1+	(1)−	E1	11	1	< 2.2E− 9	≦ 2.4E+5
		290.6	1+	(1)−	E1	11	1	≦ 2.2E− 9	≦ 2.7E+5
		381.6	1+	(1, 2)−	E1	70	1	≦ 3.4E−10	≦ 9.3E+4
		423.6	1+	(1, 2)−	E1	44	1	≦ 5.4E−10	≦ 2.0E+5
		478.3	1+	(2)−	E1	19		≦ 1.3E− 9	≦ 6.7E+5

[a]) Using the E2/M1 branching ratios from Prospero [2]) and relative gamma-ray intensities from Hanson *et al.* [3]).
[b]) Using the E2/M1 branching ratios from Prospero [2]) and theoretical conversion coefficients from Hager and Seltzer [10]).
[c]) The hindrance factor $F_W = T_{\frac{1}{2}\gamma}(\text{exp})/T_{\frac{1}{2}\gamma}$ (Weisskopf) where the theoretical estimate is taken from ref. [11]) putting the statistical factor equal to one.
[d]) 8.2E−8 equals $8.2 \cdot 10^{-8}$ and so on.

The E2 transition rates from the 96.7 keV level have values typical of particle or vibrational transitions. Noteworthy is also the strong difference in the M1 transition rates from the 96.7 keV level to the 54.8 keV and ground states respectively.

Another remarkable feature is shown by the 140.3 and 132.8 keV transitions, both populating the 54.8 keV level and de-exciting the 195.1 and 187.6 keV levels respectively. Although these two levels show very similar characteristics (same spin, same $\log ft = 6.6$ and similar half-life) L sub-shell ratios [2]) show that the 140.3 keV tran-

sition is almost pure M1 while both absolute [3]) and relative L-conversion coefficients show that the 132.8 keV transition is of E2 multipolarity. The reason for the strong hindrance of the M1 component of the 132.8 keV transition is not known.

The lack of coincidences between the KLL Auger electrons and gamma rays larger than 300 keV puts an upper limit of 555 keV for the electron capture decay energy of ^{188}Pt. The limit on the half-life of the 478.3 keV level gives hindrance factors for all de-exciting E1 transitions which are normal for K-allowed transitions.

We are indepted to Dr. A. Kjelberg of the Nuclear Chemistry group at CERN for preparing and sending the active ^{188}Pt sources to Studsvik. The interest in this work shown by Prof. Gregers Hansen is also appreciated.

References

1) V. Berg, A. Bäcklin and S. G. Malmskog, to be published
2) J. M. Prospero, Diss., Princeton University (1963)
3) R. J. Hanson *et al.*, Nucl. Phys. **A115** (1968) 641
4) P. G. Hansen *et al.*, Phys. Lett. **28B** (1969) 415
5) T. R. Gerholm and J. Lindskog, Ark. Fys. **24** (1963) 171
6) S. G. Malmskog, Ark. Fys. **35** (1967) 255
7) T. Sundström, Nucl. Instr. **16** (1962) 153
8) B. Olsen and L. Boström, Nucl. Instr. **44** (1966) 65
9) J. Jastrzebski *et al.*, Nucl. Phys. **67** (1965) 271
10) L. N. Kryukova, V. O. Kordyukevich, A. A. Sarokin and N. P. Rudenko, Bull. Akad. Sci. USSR (ser. phys.) **29** (1965) 1091
11) R. S. Hager and E. C. Seltzer, Internal conversion tables, Part 1. K, L. M-shell conversion coefficients 1967 (CALT-63-60).
12) A. H. Wapstra, G. J. Nijgh and R. van Lieshout, Nuclear spectroscopy tables (North-Holland, Amsterdam, 1959)

REFERENCE 13

THE DECAY OF ^{187}Pt : COMPARISON OF THE LEVELS OF ^{187}Ir WITH THOSE OF HEAVIER ODD MASS IRIDIUM ISOTOPES

C. SEBILLE-SCHUCK

Centre de Spectrométrie Nucléaire et de Spectrométrie de Masse, Orsay, France

M. FINGER[+], R. FOUCHER, J.P. HUSSON and J. JASTRZEBSKI[++]

Institut de Physique Nucléaire, Orsay, France

V. BERG[+++] and S.G. MALMSKOG

Institute of Physics, University of Stockholm, Sweden

G. ASTNER[‡], B.R. ERDAL[‡‡] and P. PATZELT[‡‡‡]

CERN, Geneva, Switzerland

and

P. SIFFERT

Centre de Recherches Nucléaires de Strasbourg, France

(The ISOLDE Collaboration)

1.E.1: 3.A

Nuclear Physics **A212** (1973) 45—77; © *North-Holland Publishing Co., Amsterdam*

Not to be reproduced by photoprint or microfilm without written permission from the publisher

THE DECAY OF ^{187}Pt: COMPARISON OF THE LEVELS OF ^{187}Ir WITH THOSE OF HEAVIER ODD MASS IRIDIUM ISOTOPES

C. SÉBILLE-SCHÜCK
Centre de Spectrométrie Nucléaire et de Spectrométrie de Masse, Orsay, France

M. FINGER †, R. FOUCHER, J. P. HUSSON and J. JASTRZEBSKI ††
Institut de Physique Nucléaire, Orsay, France

V. BERG ††† and S. G. MALMSKOG
Institute of Physics, University of Stockholm, Sweden

G. ASTNER ‡, B. R. ERDAL ‡‡ and P. PATZELT ‡‡‡
CERN, Geneva, Switzerland

and

P. SIFFERT
Centre de Recherches Nucléaires de Strasbourg, France

(*The ISOLDE Collaboration*)

Received 13 November 1972
(Revised 7 May 1973)

Abstract: The decay scheme of 2.35 h ^{187}Pt has been investigated using isotopically separated samples produced by the ISOLDE facility at CERN. A total of 20 excited levels in ^{187}Ir have been established. For many of these levels, spin, parity and absolute probabilities of depopulating transitions have been determined. The results indicate that the ^{187}Ir nucleus can be described in terms of a single particle Nilsson model including Coriolis coupling between bands ($\frac{3}{2}^+$[402], $\frac{1}{2}^+$[400]).

E RADIOACTIVITY ^{187}Pt [from Pb (p, 3pxn) Hg → Au → Pt; mass separated]; measured $T_{\frac{1}{2}}$, E_γ, I_γ, E_{ce}, I_{ce}, ICC, $\gamma\gamma$-coin, ce-ce coin, $\gamma\gamma$ delay, γce delay, ce-ce delay. ^{187}Au; measured $T_{\frac{1}{2}}$. ^{187}Ir deduced levels, J, π, $T_{\frac{1}{2}}$, M1/E2 admixtures, B(M1), B(E1), B(E2). Ge(Li), Si(Li), Magnetic spectrometers.

1. Introduction

This report is one of a continuing series of studies [1–5]) made on nuclei in the transitional regions between spherical and deformed nuclei, using ISOLDE [6]) facilities at CERN. These studies were performed in order to obtain a better knowledge of the coupling between collective and individual modes in soft nuclei, mainly in those

† Present address: Joint Institute for Nuclear Research, Dubna, USSR.
†† Present address: Institute for Nuclear Physics, Swierk, Warsaw, Poland.
††† Present address: Institut de Physique Nucléaire, 91406 – Orsay, France.
‡ Present address: Research Institute for Physics, Stockholm, Sweden.
‡‡ Present address: Ames Laboratory USAEC, Iowa State University, Ames, Iowa, USA.
‡‡‡ Present address: Institute for Nuclear Chemistry, University of Marburg, Federal Republic of Germany.

which are in the region of the prolate to oblate shape transition when Z and N vary.

The present paper reports a study of the decay of 2.35 h ^{187}Pt previously poorly investigated [7, 8]), using modern techniques in order to extend the systematics of the level properties in odd-A iridium nuclei [8–19]) into the more neutron deficient region. Some of the preliminary data have been already published [1, 3, 4]). It should be mentioned that a study of the even more neutron deficient ^{185}Pt is in progress as well as of other odd-mass nuclei in this phase transition region.

A rather extensive analysis has been made including electron and γ-ray spectroscopy, γ-γ coincidence measurements and half-life determinations using the delayed coincidence method. From these data a level scheme is proposed for ^{187}Ir which shows clear similarities with the one of ^{189}Ir. The obtained conversion coefficients further give multipole mixing ratios which together with the lifetime data give absolute transition probabilities. Several strong B(E2) values are in favour of a stable deformation of the ^{187}Ir nucleus at least for the positive parity bands. The results are interpreted within the frame of the Bohr and Mottelson [20]) and Nilsson [21, 22]) models taking into account the coupling between the rotation and the intrinsic motion [23]) to first order.

2. Experimental procedure

2.1. SOURCE PREPARATION

The ^{187}Pt sources were obtained as a decay product of ^{187}Hg produced in the ISOLDE facility, CERN [6]), where molten lead was bombarded with 600 MeV protons and the mercury spallation products were pumped off and mass separated. The A = 187 ion beam was collected on a 1 mg/cm^2 aluminium foil. In the case of sources for electron spectroscopy (see below) the beam was shielded down to a spot of 5 mm length and 2 mm width. All sources were normally allowed to decay for half an hour in order to reduce the contamination from ^{187}Au ($T_{\frac{1}{2}}$ = 8.5 min). For the relevant activities we found the following half-lives: 2.35±0.03 h (^{187}Pt) and 8.5±0.7 min (^{187}Au).

2.2. GAMMA-RAY SPECTROSCOPY

Single γ-ray spectra were recorded using different Ge(Li) detectors. The detectors and the electronics used were the same as those described by Finger *et al.* [5]). All the data were evaluated with the aid of curve-fitting computer programs [24, 25]) at CERN and Orsay.

2.3. CONVERSION ELECTRON MEASUREMENTS

Three different spectrometers were used to record parts of the electron spectrum:

(a) A semi-circular permanent magnetic spectrograph with photographic detection and a resolution from 0.08 to 0.25 % was used to measure conversion electron spectra from 20 to 300 keV. Longitudinal shelters were used to detect long-lived activities, and it appeared that the only one present was due to the 11 h ^{187}Ir decay. Accurate positions of lines were observed with an Abbe comparator and energies were calculated with a UNIVAC 1107 computer in Orsay. An internal energy calibration was

made using strong lines from transitions carefully measured with the small Ge(Li) detector. The intensities were analysed with a VASSY microdensitometer and the lines were resolved with a Dupont de Nemours curve resolver. The intensity calibration was made using a ^{239}Np source [26]).

(b) An 18 cm double focusing spectrometer [27]) was used to measure several electron line groups in the energy region 20 to 350 keV with a corresponding momentum resolution from 0.4 to 3%, to get approximately the same transmission. Counts were corrected for decay assuming a 2.35 half-life. In all cases the energy resolution of the spectrograph was superior and the spectrometer data were only used for intensity calibration over a wide energy range.

(c) A Si(Li) detector of 1 cm^2 area, 2 mm thickness and 3 keV energy resolution at 1 MeV was used from 200 to 1200 keV.

2.4. COINCIDENCE MEASUREMENTS

2.4.1. Gamma-gamma coincidences. Two coaxial Ge(Li) detectors of 35 and 25 cm^3 with a 2.4 keV energy resolution at 1330 keV were used for the bidimensional γ-γ coincidence measurements. The coincidence conditions were comparable to those adopted and described in ref. [5]).

The handling of the data was made with the IBM 360/50 computer in Orsay (ARIEL). The digital addresses were first transferred from the tape into a disk memory (IBM 2311). The data were then analysed qualitatively by means of a "Nucart" [28]) map displaying the three-dimensional spectrum in an (x, y) plane, where the z-coordinate (number of counts per each (x, y) channel) was represented by the degree of blackness of a 0.8×0.8 mm^2 square. With the aid of this map the results were also analysed in a quantitative way by choosing digital gates placed over each photo-peak in the x-detector spectrum and having the corresponding y-spectrum plotted in a convenient scale.

2.4.2. Electron-electron coincidences. A double lens Gerholm spectrometer [29, 30]) was used to search for some electron-electron coincidences between the 76.09 L line and the rest of the spectrum.

2.5. HALF-LIFE MEASUREMENTS

Several half-lives of excited states in ^{187}Ir have been measured using the delayed coincidence technique. At an early stage of this investigation, a set-up using two NaI(Tl) scintillators or a Ge(Li) detector in coincidence with a NaI(Tl) scintillator was used [3, 4]). Later, new measurements using an instrumentation built up around the electron-electron coincidence spectrometer mentioned above allowed the search for sub-nanosecond isomers.

3. Results

3.1. TRANSITIONS ENERGIES, INTENSITIES AND MULTIPOLARITIES

A summary of the results from all γ-ray measurements is presented in table 1 where, for completeness, transitions which have only been observed by electron or γ-γ

TABLE 1

Gamma-ray data for the decay of ^{187}Pt

Transition energy (keV)	Gamma-ray intensity	Initial level (keV)	Final level (keV)
76.09±0.03 [a])	[b])	186.2	110.05
79.36±0.05 [a])	[b])	189.54	110.05
83.05±0.05	23 ±2	189.54	106.43
91.47±0.05	8.7±0.9	201.52	110.05
97.53±0.05 [a])	3.2±0.5	486.5	388.6
106.43±0.03	100	106.43	0
110.05±0.03	65 ±6	110.05	0
121.99±0.04	33 ±3	311.65	189.54
159.49±0.08 [a])	4.6±0.8	471.3	311.65
162.4 ±0.15 [a])	1.0±0.5		
166.26±0.15 [a])	0.5±0.2		
174.99±0.05	8.0±0.8	285.04	110.05
186.2 ±0.1 [a,c])	42 ±5	186.2	0
186.9 ±0.1 [a,c])	17 ±5	388.5	201.52
189.61±0.06	10.8±1.0	189.54	0
199.22±0.10	8.5±1.0	388.6	189.54
200.8 ±0.2 [a,d])			
201.5 ±0.2 [a,d])	81.5±8.0	201.52	0
201.8 ±0.2 [a,d])		311.65	110.05
205.19±0.08	9.5±1.0	311.65	106.43
244.8 ±0.2 [a,d])			
245.1 ±0.2 [a,d])	17 ±2	731.5	486.5
247.61±0.08	42 ±4	433.8	186.2
282.10±0.08	27 ±4	388.6	106.43
284.87±0.08	63 ±6	486.5	201.52
		285.0	0
300.3 ±0.1	12.5±1.0		
304.75±0.08	49 ±5	738.6	433.8
311.76±0.10	21 ±2	311.65	0
329.81±0.15	8 ±1		
332.9 ±0.2	2.9±0.6	819.2	486.5
361.3 ±0.1	8.2±1.0	471.3	110.05
376.5 ±0.15	4.1±0.3	819.2	442.9
385.15±0.20	4.6±0.3		
388.8 ±0.2	8 ±1	388.6	0
400.8 ±0.1 [e])	18 ±3		
427.2 ±0.1 [e])	25 ±4	815.8	388.6
480.6 ±0.15	13 ±1	1219.2	738.6
486.6 ±0.15	14 ±1	486.5	0
492.0 ±0.4 [f])	4 ±1		
507.8 ±0.3	15 ±2	819.2	311.65
511.7 ±0.3	≲ 16		
530.0 ±0.3	7.4±1.0	731.5	201.52
536.5 ±0.4	6.3±1.5	1023.0	486.5
622.5 ±0.15	15 ±2		
629.6 ±0.1	31 ±3	819.2	189.54
696.0 ±0.7	10 ±3		
709.2 ±0.1	59 ±5	819.2	110.05
712.6 ±0.3	11.6±1.6	819.2	106.43
732.0 ±0.4	6 ±3		

TABLE 1 (continued)

Transition energy (keV)	Gamma-ray intensity	Initial level (keV)	Final level (keV)
790.2 ±0.4	10 ±3		
792.7 ±0.4	13 ±2		
796.7 ±0.3	10 ±2		
816.5 ±0.4	12 ±2		
819.3 ±0.2	42 ±4	819.2	0
861.1 ±0.4	11 ±2		
891.8 ±0.6	7.5±2.0	1001.8	110.05
895.4 ±0.3	20 ±3	1001.8	106.43
912.7 ±0.3 [f])	20 ±3		
977.9 ±0.4	18 ±7		
1145.5 ±0.3	19 ±4	1255.6	110.05
1149.4 ±0.5	12 ±4	1255.6	106.43
1157.0 ±0.7	13 ±4	1255.6	0
1255.4 ±0.3	27 ±4		
1269.5 ±0.5	11 ±2		

[a]) The energy of this transition has been obtained from electron lines.
[b]) Only electron lines have been observed.
[c]) The K lines of these two transitions have been separated. The corresponding gamma intensities have been deduced from the coincidence measurements.
[d]) The K lines of these transitions have been resolved.
[e]) These transitions are mixed with transitions from ^{187}Ir decay, but have been confirmed by γ-γ coincidences.
[f]) Transitions mixed with those from ^{187}Ir decay.

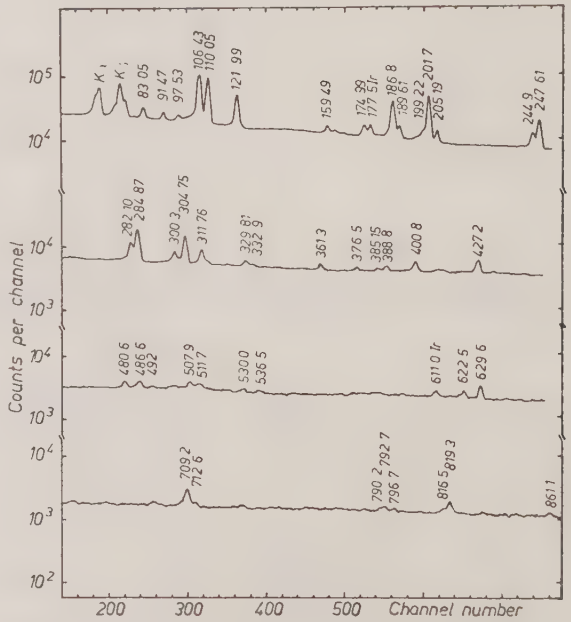

Fig. 1. Gamma-ray spectrum from the decay of ^{187}Pt obtained with a 1 cm^3 Ge(Li) detector.

TABLE 2A

Internal conversion data from the decay of ^{187}Pt obtained with a semi-circular spectrograph

Transition energy (keV)	E_e -	Attribution	I_e -	α_{exp}	α(E1)	α(M2)	α(E3)	Multipolarity
76.09±0.03	62.67	76.08 L_1	19.4± 2.0		0.067	31	4.65	
	63.26	76.08 L_2	8.2± 1.0		0.028	3.25	204	
	64.88	76.09 L_3	10.4± 1.0		0.032	9.1	173	
	72.91	76.09 M_1	5.4± 0.7		0.015	7.6	1.54	M2+(5±2) % E3
	73.17	76.08 M_2	2.6± 0.3		0.0062	0.88	55	
	73.53	76.08 M_3 [c]	3.0± 0.4		0.0072	2.63	46.5	
	75.23	76.1 $N_{1,2}$	1.7± 0.5		0.0053	2.33	15.7	
	75.40	76.1 N_3	1.3± 0.5		0.0018	0.635	14.6	
	75.85	76.1 $N_{4,5}$	0.4± 0.2		0.00019	0.011	1.2	
	76.05	76.1 O	0.6± 0.2		0.00113	0.48	4.5	
					α(M1)	α(E2)	α(E1)	
79.36±0.05	65.95	79.36 L_1	2.2± 0.5	2.2 ±1	1.52	0.145		M1 (E2 < 29%)
					α(M1)	α(E2)		
83.01±0.03	69.60	83.01 L_1	20 ± 2	0.87 ±0.17	1.33	0.146		
	70.18	83.00 L_2	3.3± 0.5	0.14 ±0.04	0.13	3.62		(97±1)%M1
	71.78	83.00 L_3	1.6± 0.5	0.06 ±0.04	0.0135	3.29		
	79.84	83.01 M_1	6.4± 0.7	0.28 ±0.05	0.30	0.037		
	80.15	83.06 M_2	0.8± 0.3	0.035±0.014	0.032	0.85		
	82.35	83.05 N_1	0.9± 0.3	0.04 ±0.016	0.08	0.0106		
91.47±0.05 [a]		L_1	< 0.5	< 0.06	1.01	0.119	0.043	E1
97.53±0.05	21.44	97.55 K	7.3± 1	2.3 ±1	5.65	0.795		
	84.11	97.53 L_1	3.2± 0.5	1.0 ±0.3	0.845	0.105		M1
106.43±0.03	30.32 [b]	106.43 K	50 ±15	0.5 ±0.2	4.37	0.71		E2 (M1 < 1%)
	92.99	106.40 L_1	6.8± 3	0.07 ±0.035	0.65	0.087		
	93.61 [b]	106.43 L_2	123 ±17	1.23 ±0.17	0.063	1.40		
	95.22 [b]	106.43 L_3	98 ±10	0.98 ±0.1 [d]	0.0064	0.98		
	103.54	106.45 M_2	[e]		0.016	0.30		
	103.88	106.43 M_3	24 ± 3	0.24 ±0.03	0.0018	0.25		
	105.89	106.4 $N_{2,3}$	16 ± 2	0.16 ±0.02	0.0047	0.14		
	106.37	106.4 $O_{2,3}$	2.4± 0.5	0.24 ±0.05	0.075	0.024		
110.05±0.04 [a]	33.95 [b]	110.06 K	182 ±30	2.8 ±0.7	3.85	0.66		(70$^{+4}_{-5}$)%M1
	96.63 [b]	110.05 L_1	36 ± 3	0.54 ±0.15	0.575	0.079		
	97.23 [b]	110.05 L_2	27 ± 3	0.4 ±0.07	0.058	0.985		
	98.85	110.06 L_3	[f]		0.0059	0.83		
	106.86	110.04 M_1	8.9± 1.0	0.14 ±0.03	0.13	0.019		
	107.15	110.06 M_2	6.2± 1	0.10 ±0.025	0.014	0.23		
	107.50	110.05 M_3	6.1± 1	0.09 ±0.02	0.0015	0.20		
	109.48	110.0 $N_{1,2}$	4 ± 1	0.045±0.017	0.046	0.07		
	109.95	110.0 O	1.6± 0.5	0.023±0.009	0.067	0.0196		
121.99±0.04 [a]	45.88 [b]	121.99 K	107 ±15	3.3 ±0.7	2.95	0.55		(95±2) % M1
	108.57 [b]	121.99 L_1	17 ± 2	0.5 ±0.1	0.44	0.065		
	109.17	122.00 L_2	2.0± 0.7	0.06 ±0.03	0.043	0.615		
	118.9	122.0 M	3 ± 0.7	0.10 ±0.03	0.11	0.029		
159.49±0.08	83.38	159.49 K	4.7± 0.6	1.0 ±0.4	1.39	0.305		M1
	146.1	159.5 L_1	1.2± 0.4	0.26 ±0.1	0.20	0.036		
162.4 ±0.15	86.37	162.47 K	2.0± 0.5		1.30	0.265		
	148.9	162.3 L_1	0.7± 0.3		0.18	0.032		
166.26±0.15	90.15	166.26 K	1.0± 0.5	2 ±1	1.21	0.275		M1
174.99±0.05	98.9	175.0 K	13 [g]	1.6 ±0.6	1.07	0.245		M1
	161.5	174.9 L_1	0.8± 0.4	0.1 ±0.06	0.15	0.028		
					α(M1)	α(E2)	α(E3)	
186.2 ±0.1	110.08	186.28 K	8 ± 1	0.55 ±0.14 [i]	0.88	0.21	0.58	E3
	173.5	186.3 L_2	30 ± 3	2.0 ±0.5	0.10	0.013	1.57	
	175.0	186.2 L_3	17.5± 2	1.2 ±0.4	0.0012	0.062	0.86	
	183.2	186.1 M_2	10 ± 2	0.7 ±0.25	0.033	0.030	0.46	
	183.7	186.3 M_3	5.3± 1	0.37 ±0.13	0.0003	0.017	0.23	
	185.7	186.2 $N_{2,3}$	4.5± 1	0.31 ±0.12	0.0009	0.010	0.19	
186.9 ±0.1	110.77	186.88 K	9 ± 1	0.17 ±0.04	0.88	0.20		E2
	174.1	186.9 L_2	4.5± 1.5	0.10 ±0.04	0.013	0.094		
	175.8	186.9 L_3	4 ± 1	0.09 ±0.035	0.0012	0.062		
189.61±0.06 [a]	113.5	189.6 K	7 ± 1	0.65 ±0.2	0.85	0.196		M1
					α(M1)	α(M2)	α(E1)	
199.22±0.10 [a]		K	< 0.5	< 0.06	0.225	0.171	0.057	E1

TABLE 2B

Internal conversion data from ^{187}Pt → ^{187}Ir decay (Si(Li) detector)

E_γ	I_e - [a])	α_{exp}	α_{th} (M1)	α_{th} (E2)	α_{th} (E1)	Main multipole component
330 K	1.2 [a])	0.15	0.185	0.047		M1
361 K	2.4	0.29	0.148	0.029		M1
376 K	0.85	0.2	0.131	0.03		M1
385 K	0.72	0.16	0.123	0.033		M1
L	0.25	0.05	0.020	0.011		
388 K	< 0.1	< 0.012	0.12	0.032	0.011	E1
480 K	1.3 [a])	0.087	0.069	0.019		M1
L	0.13	0.011	0.011	0.005		
486 K	< 0.12	< 0.008	0.067	0.019	0.0074	E1
508 K	1.0 [a])	0.06	0.059	0.018		M1
L	0.13	0.0085	0.009	0.004		
512 K	0.37	≧ 0.02	0.058	0.017	0.0063	not E1
530 K	0.36	0.05	0.052	0.015		M1
536 K	0.33	0.052	0.051	0.015		M1
622 K	0.84 [a])	0.05	0.045	0.011		M1
629 K	1.4 [a])	0.045	0.044	0.010		M1
L	0.30	0.01	0.0054	0.0024		
695 K	0.46	0.046	0.029	0.0089		
L	0.07	0.007	0.0042	0.0016		
709 K	1.3 [a])	0.022	0.025	0.0084		M1
L	0.3	0.005	0.0037	0.0012		M1
712 K	0.28	0.024	0.025	0.0084		M1
796 K	0.11	0.01	0.019	0.0068		M1, E2
816 K	< 0.1	< 0.008	0.017	0.0063	0.002	E1, E2
819 K	0.62	0.015	0.017	0.0063		M1
L	0.09	0.002	0.0025	0.0009		
895 K	0.06	0.003	0.015	0.005		E2
1269 K	0.036	0.0032	0.0057	0.0027		E2, M1

[a]) These intensities are 20% precision; for other lines the accuracy is better than 50%.

coincidence measurements have also been included. The low energy part of a γ-ray spectrum taken with the 1 cm^3 Ge(Li) detector is shown in fig. 1. Some photographic films and part of the deduced internal conversion microdensitograms are shown in figs. 2 and 3.

The data obtained from the electron measurements are presented in table 2 together with experimental and theoretical conversion coefficients. We used Hager and Seltzer's [31]) conversion coefficient values for all subshells except for N and O values which have been calculated with the tables of Dragoun [32]). The 106.43 keV transition appeared to be pure E2 (M1 < 1 %) and the 106 L_{III} line was chosen for intensity normalization in table 2. It is to be noticed that the units of tables 1, 2a and 2b are the same.

TABLE 2A (continued)

Transition energy (keV)	E_e -	Attribution	I_e -	α_{exp}	α(E1)	α(M2)	α(E3)	Multipolarity
200.8 ±0.2	124.7	200.8 K	0.9± 0.3	[h])	0.72	0.169		(M1)
201.5 ±0.15	125.4	201.5 K	4.2± 1.0	0.07 [h])	0.72	0.169	0.055	E1
201.8 ±0.15	125.7	201.8 K	5.9± 1	[h])	0.72	0.169		M1
205.19±0.08 [a])	129.1	205.2 K	1.5± 0.4	0.16 ±0.06	0.67	0.16		E2
	192.3	205.1 L_2	0.8± 0.4	0.08 ±0.05	0.009	0.055		
	194.1	205.3 L_3	0.6± 0.3	0.065±0.04	0.00085	0.035		
244.8 ±0.2	168.7	244.8 K	4.7± 1	[h])	0.41	0.10		M1
	231.4	244.5L+245.1L	1.1± 0.3		0.060	0.026		
245.1 ±0.2	169.0	245.1 K	3.4± 1	[h])	0.41	0.10		M1
247.61±0.08 [a])	171.5 [b])	247.6 K	19 ± 2	0.45 ±0.09	0.40	0.099		M1
	234.2	247.6 L_1	3.0± 0.5	0.076±0.02	0.059	0.024		
282.10±0.08 [a])		K	< 0.8	< 0.03	0.283	0.071	0.028	E1
284.87±0.08 [a])	208.8 [b])	284.9 K	17.5± 2	0.27 ±0.05	0.275	0.069		M1
	271.6	285.0 L	3.2± 0.5	0.05 ±0.012	0.045	0.033		
300.3 ±0.1 [a])	224.3	300.4 K	3.8± 0.5	0.3 ±0.07	0.24	0.060		M1
304.75±0.08 [a])	228.5	304.6 K	2.8± 0.5	0.057±0.016	0.23	0.058		E2
	292	305 L	1.3± 0.5	0.027±0.013	0.037	0.026		
311.76±0.10	235.7	311.8 K	5.0± 1	0.24 ±0.07	0.22	0.055		M1

[a]) Energy measured with the small Ge(Li) detector.
[b]) These lines, the energies of which have been calculated from the accurately measured γ-lines, were used for internal energy calibration.
[c]) This line has been corrected for some contribution of the N lines of the 74 keV transition in the ^{187}Ir decay.
[d]) Theoretical value. The electron intensities have been normalized to this value.
[e]) This line is mixed with the K line of the 177 keV transition in ^{187}Ir.
[f]) This line is mixed with the K line of the 175 keV transition.
[g]) This line is mixed with the L_{III} line of the 110 keV transition.
[h]) See discussion in the text (subsect. 3.1).

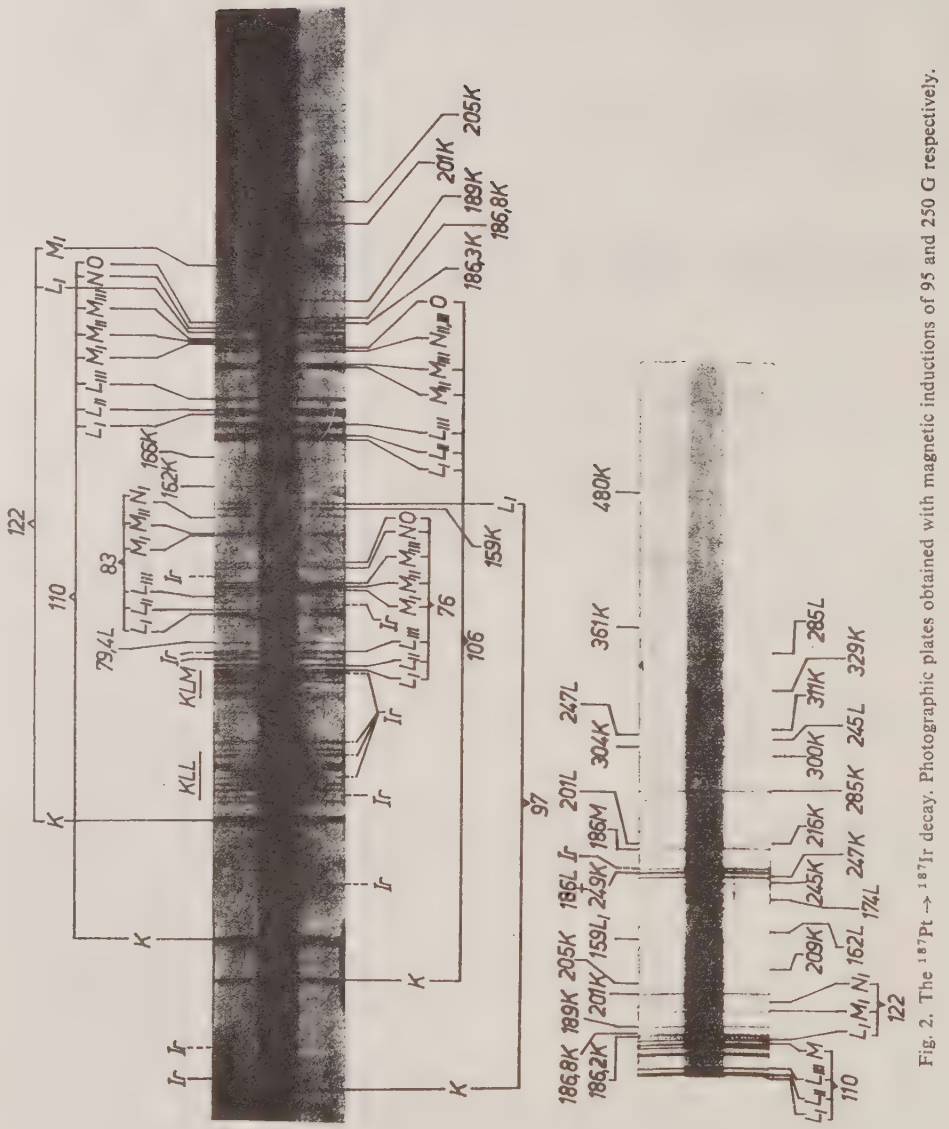

Fig. 2. The $^{187}Pt \rightarrow {}^{187}Ir$ decay. Photographic plates obtained with magnetic inductions of 95 and 250 G respectively.

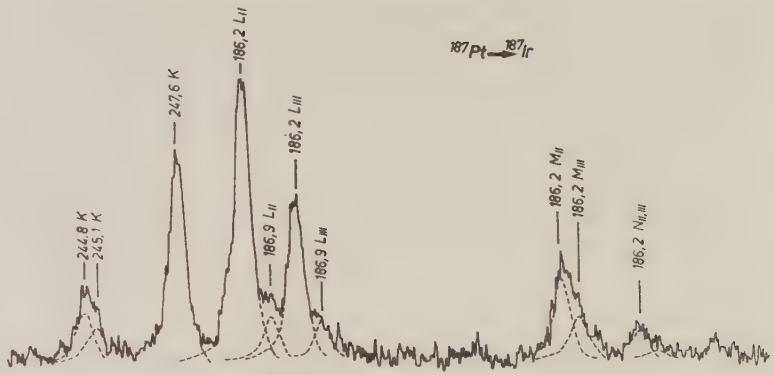

Fig. 3. The $^{187}Pt \rightarrow {}^{187}Ir$ decay. Partial microdensitogram of the photographic plate obtained with 250 G magnetic induction.

We shall now discuss some of the transitions in more detail.

3.1.1. The 76.09 keV transition. In the electron spectrum from the semi-circular spectrograph several lines were observed which fitted as L, M, N and O lines for a 76.09 keV transition (fig. 2). No corresponding γ-ray was, however, observed as its energy closely coincides with the $K_{\beta'2}$ X-rays in iridium. When we tried to deduce the multipolarity of this transition from the L and M subshell ratios, we first found that these were in perfect agreement with those for an E1 multipolarity, namely:

	Exp.	E1	M2	E3
L_I/L_{II}	2.4±0.5	2.38	9.55	0.0228
L_I/L_{III}	1.8±0.4	2.11	3.40	0.0269
M_I/M_{II}	2.1±0.4	2.42	8.64	0.028
M_I/M_{III}	1.8±0.3	2.08	2.93	0.032

With this interpretation an upper limit of a possible M2 content would be 0.05 % from the L subshell ratios and 0.2 % from the M subshell ratios. Assuming the 76.09 keV transition to be pure E1 would however give a corresponding γ-ray intensity of 290 units (in the scale of tables 1 and 2) and it would thus have to be 4.5 times as intense as the iridium $K_{\beta'2}$ X-rays. The following experimental data for K_β X-rays were obtained with intensities in the units of table 1.

	E_γ (keV)	I_γ
$K_{\beta'1}$(Os)	71.2	81
$K_{\beta'1}$(Ir) + $K_{\beta'2}$(Os)	73.4	268
$K_{\beta'2}$(Ir)	75.6	64

After subtraction of the $K_{\beta'2}$(Os) contribution from the 73.4 keV peak, the intensity ratio for iridium is

$$I(K_{\beta'1})/I(K_{\beta'2}) = 248/64 \approx 3.9,$$

which is identical to the theoretically expected ratio [33]). The intensity of the γ-ray from the 76.09 keV transition has thus to be less than the order of the precision of K X-ray intensities and is set to $I_\gamma(76\ \text{keV}) < 10$. This is in complete disagreement with the value of 290 units required from the electron data for a pure E1 transition. Assuming some M2 admixture would of course require a lower γ-ray intensity, but to account for an intensity of < 10 units would need $> 4\,\%$ M2 admixture which is inconsistent with both the L and M subshell data.

We therefore suggest that the 76.09 keV transition has an M2+(5±2 %)E3 multipolarity. This would explain the low intensity (1.5 units would be required) of the corresponding γ-ray.

3.1.2. The 186.2 and 186.9 keV transitions. The K 186.2 and K 186.9 lines are very well separated (fig. 2). The γ-γ coincidence data between the 97.5 and 186.9 keV transitions show that the 186.9 keV transition has a γ-intensity of 53±10 (in table 1 units) which gives E2 multipolarity. If the theoretical coefficient for α_K(E2) is used, a γ-intensity of 42 is obtained for the 186.9 keV transition which leads to 17.5 for the 186.2 keV line.

The L groups for the two 186 keV transitions (fig. 3) were resolved into four lines the intensities of which can only be explained by assuming an E3 multipolarity for the 186.2 transition. The following conversion coefficients are valid:

$$K/L_I/L_{II}/L_{III}/M/N \quad \begin{cases} \text{expt.} & = 0.28/0.1/1/0.6\ /0.5\ /0.15 \\ \text{th. (E3)} & = 0.38/0.083/1/0.58/0.47/0.12. \end{cases}$$

3.1.3. The 201 keV triplet. The broad 201 K electron line could be resolved into three components. The γ-γ coincidence data show that a 201.5 keV component is responsible for the 201 keV ↔ 186 keV coincidence contribution, which gives an intensity of 60±15 for the 201.5 keV transition. This leads to E1 multipolarity. Then, assuming the theoretical α_K(E1) coefficient, the γ-intensity of the 201.5 keV transition is found to be 71 units. As the total observed intensity for the composed γ-line is 82, the total intensity for the 200.8+201.8 keV lines is then about 10 units which is consistent with M1 multipolarity for both transitions.

3.1.4. The 245 keV doublet. A closer inspection of the 245 K electron line showed it to be a doublet which could be resolved into two components of about equal intensities (fig. 3). The total conversion coefficient is that of an M1 transition, so we propose that both are M1 transitions.

3.2. COINCIDENCE MEASUREMENTS

3.2.1. The γ-γ coincidences. A summary of the results is given in table 3 in the form of a classical *x*-*y* table. A part of the two-dimensional spectrum is shown in fig. 4 [Galaxie program [34])].

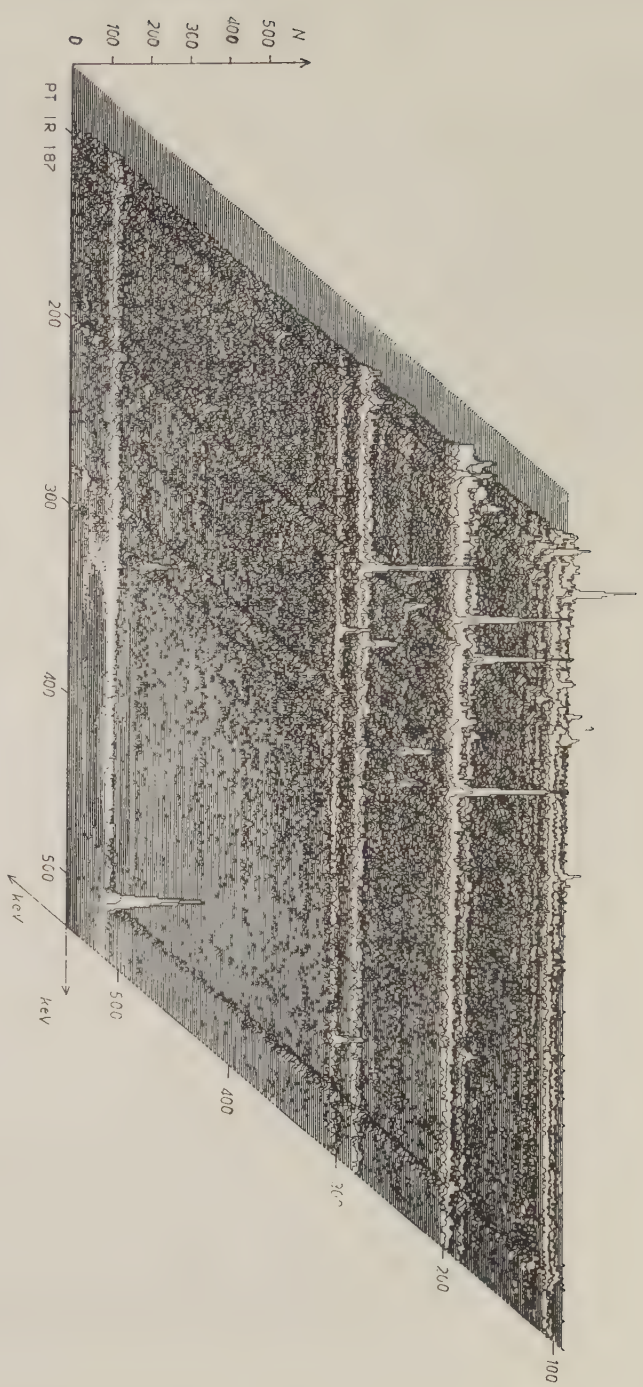

Fig. 4. The $^{187}Pt \longrightarrow {}^{187}Ir$ decay. Partial γ-γ coincidence map.

TABLE 3

Summary of the coincidence data in ^{187}Ir

Y \ X	97	106	110	122	159	162	166	175	186	189	199+201	205	244+245	247	282	285	300	305	312	330	333	361	376	385	389	401	427	481	486	530	536	622	629	709
91			×						×							×																	
97									×		×																						
106				×	×										×																×		
110								×													×											×
122		×			×																												
159				×															×													
162+166																																	
175			×																													
186	×										×		×				○				×						×						
189				×																													×
199+201	×	×							×				×			×											×			×	×		
205					×						×																						
244+245	×																												×				
247							○											×										×					
282	×	×																		○							×				×		
285			×								×		×							○											×		
300													×																				
305							×							×	×	×												×					
312					×																												
330																																	
333									×		×				×	×													×				
361			×																														
376			×																														
385																											×						
389																																	
401																								×									
427									×		×				×																		
481														×				×															
486																				×										×		
507				×			×				×																						
511																																	×
530											×																						
536									×		×																		×				
622																																	
629		×					×			×																							
709			×				×																										
711		×																															

Strong coincidences are shown by × and weak by ○.

3.2.2. The e^--e^- coincidences. The place of the 76.09 keV transition was determined from electron-electron measurements. The 76.09 L electrons were focused in one lens and the other lens was in turn adjusted to admit the different lines of the electron spectrum. The 76.09 keV transition was observed to be in coincidence with the 110.05 keV transition. The coincidence rate of the cascade was followed during 3 half-lives to ensure that the coincidences had taken place in iridium and not in the osmium daughter which has strong lines with similar energies (74.4, 75.1, 112.4, 113.2 keV).

3.3. LEVEL SCHEME

The proposed level scheme is shown in fig. 5. The spin-parity of the ground state is suggested to be $\frac{3}{2}^+$ as a consequence of the observed log ft values to levels in ^{187}Os.

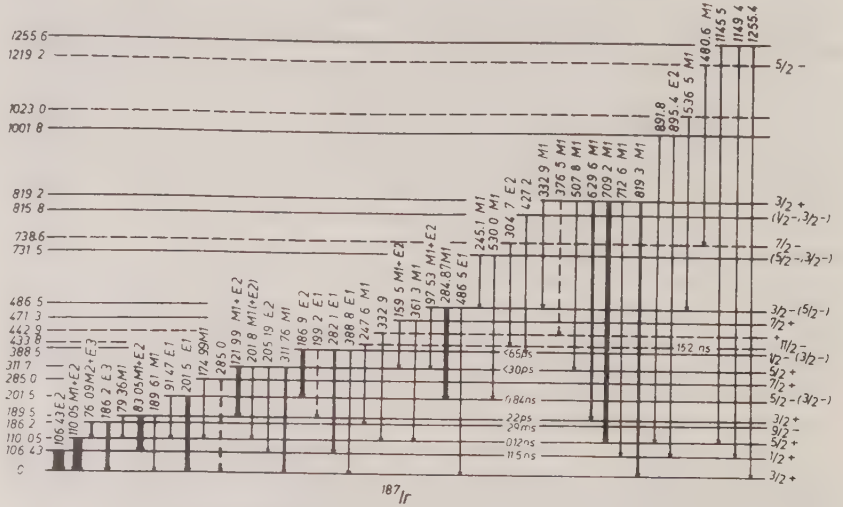

Fig. 5. The proposed level scheme of ^{187}Ir. The energies are given in keV.

3.3.1. The 186.2 keV level. Gritsyna *et al.* [35]), when bombarding an osmium target with protons, observed an isomer of 29 msec in ^{187}Ir with 65 ± 5, 110 ± 5 and 188 ± 5 keV γ-rays. As was indicated in subsect. 3.1, a 76.09 keV M2+E3 transition and a 186.2 keV E3 transition were observed in the present work. From electron-electron measurements, it has been shown (subsect. 3.2.2) that the 76.09 keV transition was in coincidence with the 110.05 keV transition. As a combination of these results, it is proposed that the 76.09 keV transition feeds the 110.05 keV level and that the 186.2 keV transition is the cross-over and does not feed the 110.05 keV level, as proposed by Gritsyna *et al.* [35]). A spin of $\frac{9}{2}$ and negative parity for the 186.2 keV level are consistent with all available experimental data.

3.3.2. The 247.61, 304.75 and 480.6 keV transitions. A group of three intense transitions is not yet placed in the level scheme. A half-life of 152 ± 12 nsec was measured for one of them (247.61 keV M1). As we searched and did not find another transition decaying with the same half-life, the conclusion is that this transition can only feed the ground state or a long-lived isomer. It is proposed that the 247.6 keV transition feeds the 186.2 keV level. Effectively, if the 247.6 keV transition feeds the ground state, it would be very difficult to explain why the corresponding level does not feed other low lying levels. Conversely it is tempting to assume that the 247.6 keV transition comes from a high spin $\frac{11}{2}$ level decaying only to the $\frac{9}{2}$ 186.2 keV level.

The coincidence data show that the three transitions of 247.61, 304.75 and 480.6 keV form a cascade. From the prompt and delayed coincidence data, and the respective intensities of the transitions we propose that these three transitions are placed as shown in fig. 13.

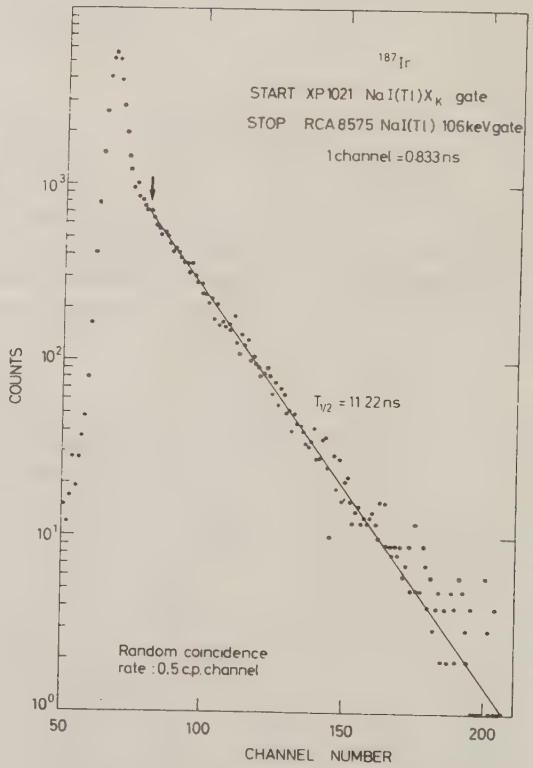

Fig. 6. Half-life determination of the 106.4 keV level.

3.4. HALF-LIFE RESULTS

The 106.43 keV level. The half-life of this level has been measured both with the Na I and the electron-electron set-up with consistent results. In the former case a time-to-pulse-height converter was started by X-rays and stopped by γ-rays from the 106.4 keV transition. An example of an observed decay curve is given in fig. 6. The prompt peak is due to other "prompt" γ-ray distributions (mainly from the strong 110.05 keV transition) is the γ-channel. This was clearly demonstrated when the time distribution between the 83.05 L and 106.43 K lines was registered with the electron spectrometer. Here the energy resolution was good enough to clearly separate out the influence from the strong 110.05 K line. The time distribution then showed a single delayed component but with somewhat less statistical accuracy than in the previous experiment. The half-life of the 106.43 keV level was obtained by determining the slope of the decay curve using a least squares fitting program. As an average value from several runs we obtained

$$T_{\frac{1}{2}}(106.43 \text{ keV level}) = 11.5 \pm 0.3 \text{ nsec}.$$

The 110.05 keV level. The strong 110.05 K line was focused in one lens to measure the half-life of this level. The other lens was focused at the apparently well resolved 201 K line. It later turned out, however, that the 201 K line was actually a triplet. As the 110.05 K channel is very clean, this triplet of lines in the second channel does not disturb our measurements as only the line belonging to the correct coincidence combination was accepted. From a preliminary run it was clear that the observed decay curve had an almost prompt shape. To be able to look at the finer details of this decay curve, it was necessary to have a prompt curve registered under similar conditions as the delayed curve. For this prompt comparison measurement we used the β 238.6 K cascade in the decay of ^{212}Pb. To be able to use the same energy settings in two sets of measurements, the ^{187}Pt electrons were pre-accelerated in a 22 keV electrostatic field. An example of a pair of prompt and delayed time curves obtained in this way is shown in fig. 7. This figure shows that there is a clear change in the shape of the two curves. Several pairs of this kind were registered and all the data were analysed both by the momentum [36]) and convolution [37]) methods. After correction for the change in time of flight of the electrons through the spectrometer due to the pre-acceleration procedure, we obtained an average value of

$$T_{\frac{1}{2}}(110.05 \text{ keV level}) = 120 \pm 15 \text{ psec}.$$

The 189.5 keV level. The de-excitation of the 189.5 keV level occurs mainly through the 83.05 keV transition. Thus the 83.05 L line was focused in one spectrometer while the feeding 122.0 K line was focused in the second lens. Both these channels were comparatively clean from disturbing lines and no interfering cascades are known. This measurement showed that the observed shape of the decay curve was almost identical to the shape of a prompt curve. Therefore we had to make an accurate centroid shift measurement. The only suitable comparison source available was ^{144}Ce

where we could utilize the $\beta \rightarrow$ 133.5 K cascade passing over the 133.5 keV level in ^{144}Pr with a measured half-life of 7.0±0.4 psec [ref. [38])]. In order to be able to use the same energy settings in both the delayed and the comparison measurement we had to refocus the first lens to the 83.05 M line and the ^{187}Pt electrons were pre-accelerated in a 11.5 keV electrostatic field. A special effort was also made to keep the intensity in the two channels constant when changing between the Pt and Ce sources. The automatic operation of the spectrometer was used [30]), and a change between the Pt and Ce sources took place every 15 min to keep the electronic drift to a minimum during the measurement. Several long sets of delayed and prompt decay curves were registered in this way and all the data were analysed with the momentum method [36]). A systematic shift between the delayed and prompt curves was then obtained corresponding to a definite mean life for the 189.5 keV level. After correction for the influence from the pre-acceleration procedure and from the shift introduced by the finite half-life of the 133.5 keV level in ^{144}Pr, an average half-life for the 189.5 keV level was obtained:

$$T_{\frac{1}{2}}(189.5 \text{ keV level}) = 22 \pm 10 \text{ psec}.$$

The 201.5 keV level. In order to measure the half-life of this level the 201 K line was focused in one lens. As this line is comparatively weak and no strong conversion line feeds the actual level, the second channel detected γ-rays above 400 keV in a Naton 136 plastic scintillator placed 2 cm from the source. Several time spectra were

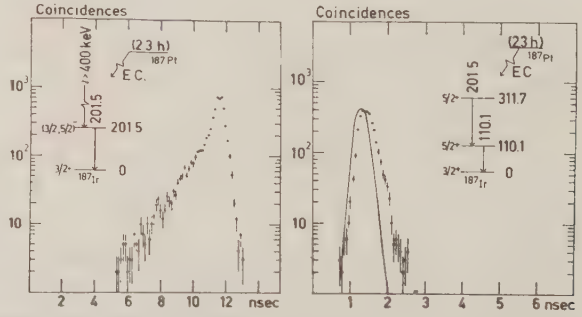

Fig. 7. Typical examples of half-life determinations with the double lens spectrometer.

recorded with these settings at different times and one of them is shown in fig. 7. The composite decay curve is due to the fact that the 201 K line is built up of K lines from three different transitions the two strongest of which de-excite the 201.5 and 311.7 keV levels. The latter of these has been found to have a short half-life (see below) and is thus responsible for the prompt part of the observed decay curve. The delayed part is due to the half-life of the 201.5 keV level. Several such decay curves were analysed by finding the slope in a least-squares fit or, after subtraction of an

appropriate prompt contribution, by the convolution method [37]). As an average result we obtain a value of

$$T_{\frac{1}{2}}(201.5 \text{ keV level}) = 0.84 \pm 0.08 \text{ nsec}.$$

The 311.7 keV level. A set of coincidence measurements were performed on the $\gamma(> 400$ keV$) \rightarrow 122.0$ K cascade using a ^{60}Co source for the comparison measurement. The analysis of the data with the momentum method [36]) gave a centroid shift corresponding to a half-life of 20 ± 10 psec. As spurious shifts of this order of magnitude can be introduced by the difference in shape of the Compton distributions accepted in the γ-channel, we prefer to give an upper limit of

$$T_{\frac{1}{2}}(311.7 \text{ keV level}) < 30 \text{ psec}.$$

The 388.5 keV level. An estimate of the half-life for this level was obtained by analysing coincidence data from the $\gamma(> 400$ keV$) \rightarrow 186.9$ L cascade. The latter line was used as the 186.6 K line was not resolved from the 189.6 K and 122.0 L lines. The 247.6 K line in the 186.6 L channel was of less disturbance as the 247.6 keV transition has been found to have a long delay ($T_{\frac{1}{2}} = 152$ nsec, see below). A ^{60}Co source was again used for comparison. Several sets of delayed and prompt curves were analysed using the momentum method [37]). From the data it was concluded that

$$T_{\frac{1}{2}}(388.5 \text{ keV level}) < 65 \text{ psec}.$$

Delay of the 76.09 keV transition. Several attempts have been made to measure the time distribution between the strong 76.09 L lines and feeding γ-rays. In all cases a single delayed component ($T_{\frac{1}{2}} \approx 11$ nsec) was observed built up on an evenly distributed background. It was tempting at first to assign the observed delayed component to the 76.09 keV transition, but careful intensity measurements showed that the observed coincidence rate was by far too low and that in fact the 11 nsec component could very well originate from the low energy tail of the very strong 106.43 K line known to have an average delay of 11.5 nsec relative to coincident high energy γ-rays. As no prompt peak was observed it is most likely that the 76.09 keV transition was responsible for the high rate of "random" coincidences observed which indicates an average delay of more than 1 μsec for the 76.09 keV transition.

Delay of the 247.6 keV transition. During the early delayed coincidence measurements of the 106.43 keV level, it became apparent that another long lived isomer existed in ^{187}Ir (populated in the ^{187}Pt decay) and which decayed through a roughly 245 keV transition.

A measurement of the transition feeding the delayed 245 keV γ-ray was made by registering all start pulses having the 245 keV transition delayed more than 40 nsec. Only the X-rays and a line at 305 keV appeared in the delayed coincidence spectrum. This fact was used in the actual measurement of the delay of the 245 keV transition where the start pulses of the TPHC were derived from a single channel analyser connected to a Ge(Li) detector with an energy window set on the 245 keV transition.

A NaI detector was used to select the 305 keV transition for the stop signals. As a final average value a half-life of 152 ± 12 nsec was obtained. This value replaces the older result of 140 ± 30 nsec quoted in ref. [1]).

From later single Ge(Li) and conversion electron spectra (see subsect. 3.1) it is now clear that the peaks at 106 and 245 keV in the NaI spectrum are actually a doublet (106.43 and 110.05 keV) and a triplet (244.8, 245.1 and 247.61 keV). In order to determine which transitions are delayed, a new coincidence spectrum measurement was performed using a Ge(Li) stop counter and an X-ray start counter.

In these measurements, the energy resolution (5 keV) was not sufficient to resolve these complex peaks, but the delayed spectrum showed substantially narrower peaks. From the relative position of the peaks it was clear that the two delayed transitions are those with energies of 106.43 and 247.6 keV.

The present data on the transition rates from the low-lying excited states in ^{187}Ir have been collected in table 5. The last column of this table gives a comparison with the Weisskopf estimate [33]).

4. Discussion

4.1. DETERMINATION OF THE MINIMA OF POTENTIAL ENERGY SURFACES

A computer program developed by the Nilsson group was used [39]) to calculate the potential energy surfaces on the basis of a unified oscillator model taking into account pairing and Coulomb energies and with a normalization of the average behavior of the surface to a liquid drop [22, 40–42]).

For each spin, the lower minimum of the potential energy surface was then calculated with respect to quadrupole and hexadecapole deformations ε_2 and ε_4 [see ref. [26])]. It was found that the values of ε_2 and ε_4 minimizing the potential energy surfaces change very little within the different orbitals. The value $\varepsilon_2 = 0.20$ is to be compared with experimental values $\delta_{\text{rms}} = 0.21$ ($K = \frac{3}{2}$) and $\delta_{\text{rms}} = 0.26$ ($K = \frac{1}{2}$) obtained from our B(E2) measurements [see subsect. 4.2.2].

4.2. POSITIVE PARITY STATES

Over the last few years the low energy level structure of several Ir nuclei has been extensively studied [8–17]). Fig. 8 shows the positive parity level systematics for odd-A nuclei from $A = 187$ to $A = 193$. For all masses heavier than $A = 187$ the ground state has been found to have spin and parity of $\frac{3}{2}^+$. It has been shown [43]) that going from ^{191}Ir to ^{189}Ir certain B(E2) values increase drastically. This has been taken as a sign of sudden increase in deformation between these two iridium isotopes. In ^{189}Ir these B(E2) values have been used to deduce a deformation parameter $\delta_{\text{rms}} = 0.23$. As the corresponding transitions in ^{187}Ir also have large B(E2) values, it seems adequate to discuss the low energy level structure of ^{187}Ir in terms of the Nilsson model [refs. [21, 22])].

From the Nilsson diagram, the predicted ground state in Ir($Z = 77$) is $\frac{1}{2}^-$ [505]

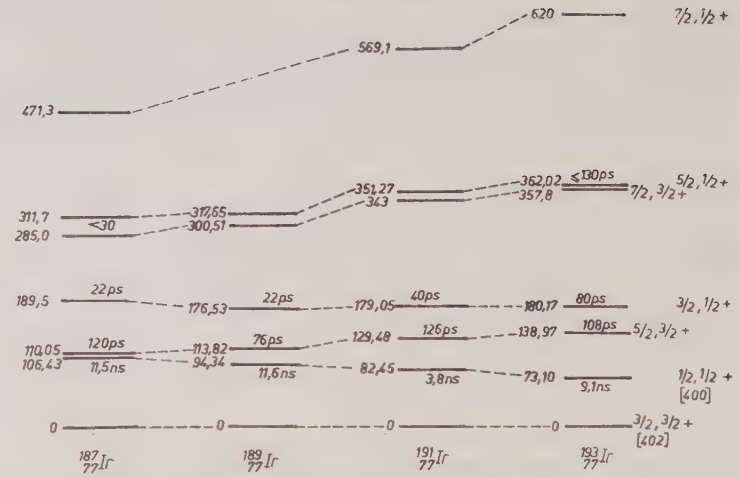

Fig. 8. Systematics of the $\frac{3}{2}^+[402]$ and $\frac{1}{2}^+[400]$ rotational bands in odd-A iridium nuclei.

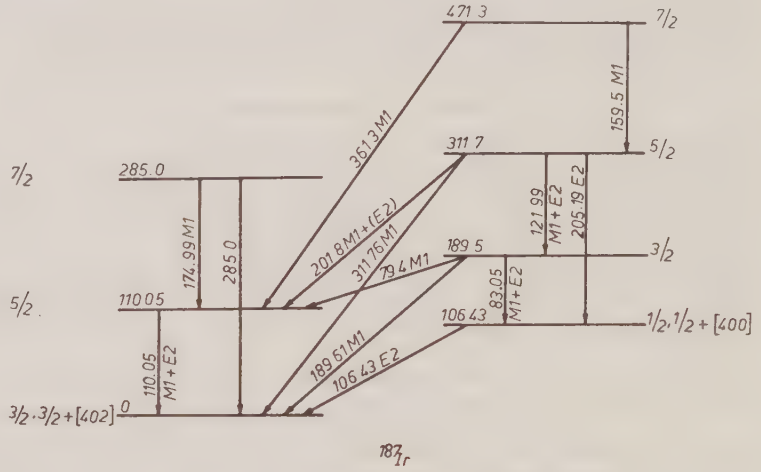

Fig. 9. Low energy positive parity levels.

(it should be the same for heavier odd-A iridium in which the ground state is identified as a $\frac{3}{2}^+[402]$ state). Soloviev [44]) noticed that the interaction with phonons affected weakly the $\frac{9}{2}$ and $\frac{11}{2}$ high K states and more strongly states with lower K. As a consequence he remarked that the states with high K-numbers were not found as ground states of odd-A nuclei when other states with smaller K lay close to these states. It is exactly the situation in all odd-A iridium isotopes where the $\frac{3}{2}^+$ [402] state is expected near the $\frac{11}{2}^-$ [505] state.

4.2.1. Energies. As mentioned above, it is natural to identify the ground state with the $\frac{3}{2}^+[402]$ Nilsson state. As can be seen in fig. 9, natural candidates for the $\frac{5}{2}$ and $\frac{7}{2}$ rotational members also exist. If the energies of the components in this band are fitted by the energy formula

$$E_K(I) = E_K + A[I(I+1)+\delta_{K,\frac{1}{2}}a(-1)^{I+\frac{1}{2}}(I+\tfrac{1}{2})] + B[I(I+1)+\delta_{K,\frac{1}{2}}a(-1)^{I+\frac{1}{2}}(I+\tfrac{1}{2})]^2, \quad (1)$$

one obtains values of 19.1 keV and 0.238 keV for the values of A and B respectively for the $K = \frac{3}{2}$ band in ^{187}Ir. The magnitude and positive sign of B may be due to the fact that there is so strong a Coriolis coupling that eq. (1) is no longer valid.

From its decay characteristics (see below) the first excited state at 106.43 keV is believed to be the intrinsic state $\frac{1}{2}^+[400]$. The corresponding rotational band can be followed up to the $\frac{7}{2}^+$ member. Neglecting for the moment the coupling effects between the $\frac{3}{2}^+[402]$ and $\frac{1}{2}^+[400]$ bands, a fit of the rotational energies in the $\frac{1}{2}^+[400]$ band to eq. (1) gives the parameter values of $A = 26.1$ keV, $B = 0.217$ keV and $a = 0.104$.

In a more detailed calculation, the Coriolis coupling between the $\frac{3}{2}^+[402]$ and $\frac{1}{2}^+[400]$ bands was also taken into account using the method described earlier by Piepenbring and Nopre [12]) and applied by them to other odd mass Ir nuclei closer to stability. The total Hamiltonian $H = H_{\text{int}}+H_{\text{rot}}+H_{\text{Cor}}$ was diagonalized in the basis of the eigenfunctions of H_{int}, the contribution of the rotation independent of I also being included.

TABLE 4

Coriolis interaction in odd-A iridium isotopes

	^{193}Ir	^{191}Ir	^{189}Ir	^{187}Ir
$E_{\exp}\frac{1}{2}$ $\frac{1}{2}+(400)$	73.1	82.5	94.2	106.43
$E_{\exp}\frac{3}{2}$ $\frac{3}{2}+(402)$	139.0	129.5	113.8	110.05
$E_{\exp}\frac{3}{2}$ $\frac{1}{2}+(400)$	180.2	179.0	176.2	189.5
$E_{\exp}\frac{7}{2}$ $\frac{3}{2}+(402)$	357	349.1	300.0	285.0
$E_{\exp}\frac{5}{2}$ $\frac{1}{2}+(400)$	361.9	351.5	317.7	311.6
$E_{\exp}\frac{7}{2}$ $\frac{1}{2}+(400)$		569.1		471.3
$A = \hbar^2/2\mathcal{I}$ keV	31.67	29.38	25.19	24.05
a	−0.0251	−0.0558	−0.0268	+0.069
C^2	0.797	0.850	0.744	0.578
$\varepsilon_{\frac{1}{2}}$	48.5	58.8	74.6	90.1
$\varepsilon_{\frac{3}{2}}$	−104.3	−96.9	−86.0	−84.2
$E_{\text{th}}\frac{7}{2}$ $\frac{3}{2}+(402)$	336.7	311.7	274.3	270.1
$E_{\text{th}}\frac{7}{2}$ $\frac{1}{2}+(400)$	602.0	569	505.1	499.8
α	0.959	0.962	0.976	0.985
β	−0.283	−0.272	−0.219	−0.170
γ	0.921	0.928	0.948	0.963
δ	−0.390	−0.372	−0.318	−0.269

The experimental energies of the levels $|\frac{3}{2}\frac{3}{2}^+\rangle$, $|\frac{1}{2}\frac{1}{2}^+\rangle$, $|\frac{5}{2}\frac{3}{2}^+\rangle$, $|\frac{3}{2}\frac{1}{2}^+\rangle$ and $|\frac{5}{2}\frac{1}{2}^+\rangle$ were then used to invert the eigenvalue problem.

Table 4 gives the results together with those obtained for other odd-A iridium isotopes [12]). It appears that the magnitude of the Coriolis force is about the same in all known odd-A iridium nuclei.

4.2.2. E2 transitions rates. From the measured half-lives and conversion coefficients one can determine several absolute B(E2) values (see table 5). From B(E2) rates within one rotational band it is then possible to calculate the root mean square value of the deformation $\langle\delta\rangle$. This value is independent of the model chosen and is equal to the equilibrium deformation δ for hard and strongly deformed nuclei [45]).

In ^{187}Ir, $B(\mathrm{E2}, \frac{5}{2}\frac{3}{2} \rightarrow \frac{3}{2}\frac{3}{2}) = 1.62\pm0.30\ e^2\cdot\mathrm{b}^2$ gives $Q_0 = 6.9\pm0.6$ b with a deformation parameter $\delta_{\mathrm{rms}} = 0.21\pm0.02$ and $B(\mathrm{E2}, \frac{3}{2}\frac{1}{2} \rightarrow \frac{1}{2}\frac{1}{2}) = 1.5\pm0.7\ e^2\cdot\mathrm{b}^2$ gives $Q = 8.6\pm2.0$ and $\delta_{\mathrm{rms}} = 0.26\pm0.06$. In both cases the large δ_{rms} values and the appearance of rotational bands lead us to assume a stable deformation at least for these positive parity states.

Several interband E2 transition rates were also determined. They are generally larger than expected from a pure single particle model due to admixtures of collective excitations. Such mixing effects can for instance be caused by a Coriolis coupling of the closely lying $K = \frac{1}{2}$ and $\frac{3}{2}$ bands. This particular effect on the transition probabilities was calculated for ^{193}Ir in ref. [15]) and then later transferred to the similar cases in ^{191}Ir and ^{189}Ir in refs. [16, 43]). It was shown [15]) that the amplitudes of the first order admixtures are only a function of the parameter $\Delta E/2M$, where ΔE is the energy difference between the two states with the same spin I that mix, and

$$M = -P_+E^x\langle\tfrac{1}{2}|j_-|\tfrac{3}{2}\rangle\sqrt{(I-\tfrac{1}{2})(I+\tfrac{3}{2})}, \qquad (2)$$

where the pairing factor $P_+ \approx 1.0$ and $E^x \approx \hbar^2/2\mathscr{I}$. As the low energy structure (ΔE, M and δ) is very similar for ^{187}Ir and ^{189}Ir we expect to first order that all corresponding interband B(E2) values in the two nuclei should be similar. A comparison between the two sets is given in table 6, which shows that the E2 rates are indeed very similar. In the right-hand part of the table these B(E2) values have been calculated using three different values of the parameter $E^x\langle\frac{1}{2}|j_-|\frac{3}{2}\rangle$. The experimental values are reasonably well accounted for using $E^x\langle\frac{1}{2}|j_-|\frac{3}{2}\rangle = 25\pm5$ keV. As we expect that $E^x \approx 25$ keV, then $\langle\frac{1}{2}|j_-|\frac{3}{2}\rangle = 1.0\pm0.2$ which should be compared with 0.716 obtained using the deformed potential parameters recommended by Nilsson and $\delta = 0.20$.

In ref. [46]), a systematic plot of all reduced E2 transition probabilities between the low lying positive parity states in odd mass Ir isotopes is given. Of particular interest is the sharp increase in B(E2) for the $\frac{5}{2}\frac{3}{2} \rightarrow \frac{3}{2}\frac{3}{2}$ and $\frac{3}{2}\frac{1}{2} \rightarrow \frac{1}{2}\frac{1}{2}$ intraband transitions going from ^{191}Ir to ^{189}Ir (from neutron number 114 to 112), while the rates of the interband transitions $\frac{1}{2}\frac{1}{2} \rightarrow \frac{3}{2}\frac{3}{2}$ show a tendency to decrease.

TABLE 5

Absolute transition probabilities in ^{187}Ir

Level (keV)	$T_{\frac{1}{2}\,\mathrm{exp}}$ (ns)	Transition energy (keV)	Initial state $IK^\pi(N, n_z\Lambda)$	Final state	Multipolarity	Relative N_γ [a])	Relative N_e	$T_{\frac{1}{2}\,\gamma\mathrm{exp}}$ (s)	B(M1) $((e\hbar/2Mc)^2)$	B(Eλ) $((e\cdot\mathrm{b})^\lambda)$	Q_0 (b)	F_w [b])
106.4	11.5±0.3	106.4	$\frac{1}{2}\frac{1}{2}^+(400)$	$\frac{3}{2}\frac{3}{2}^+(402)$	M1	< 1	362	> 5.3×10^{-6}	< 6.2(−6)			> 2.8(+5)
					E2	100		5.3×10^{-8}		(7.8±0.3) (−2)		8.2(−2)
110.1	0.121±0.013	110.1	$\frac{5}{2}\frac{3}{2}^+(402)$	$\frac{3}{2}\frac{3}{2}^+(402)$	M1	70	432	9.2×10^{-10}	(3.2±0.4) (−2)			55
					E2	30		2.15×10^{-9}		1.62±0.30	6.9±0.6	4.0(−3)
189.3	0.022±0.010	79.4	$\frac{3}{2}\frac{1}{2}^+(400)$	$\frac{5}{2}\frac{3}{2}^+(402)$	M1	2.5	35	8.0×10^{-9}				184
					E2	< 0.9		> 2.2×10^{-8}	$(1.0^{+2.6}_{-0.5})$ (−2)	< 0.82		> 7.8(−3)
		83.1		$\frac{1}{2}\frac{1}{2}^+(400)$	M1	65.0	745	3.1×10^{-10}				7.5
					E2	2.0		1.0×10^{-8}	$(2.2^{+1.9}_{-0.7})$ (−1)	1.5±0.7	8.6±2.0	4.3(−3)
		189.6		$\frac{5}{2}\frac{3}{2}^-(402)$	M1	21.4	27	9.3×10^{-10}				265
					E2	9.1		2.2×10^{-9}	$(6.2^{+5.1}_{-1.9})$ (−2)	(1.1±0.5) (−1)		5.9(−2)
201.5	0.84 ±0.08	91.5	$\frac{5}{2}^-$, $(\frac{3}{2})^-$	$\frac{5}{2}\frac{3}{2}^+(402)$	E1	11	5.6	8.5×10^{-9}		(6.7±0.8) (−7)		3.1(+4)
		201.5		$\frac{3}{2}\frac{3}{2}^+(402)$	E1	89	6.0	1.06×10^{-9}		(5.0±0.6) (−7)		4.2(+4)
311.7	0.006 [c])	122.0	$\frac{5}{2}\frac{1}{2}^+(400)$	$\frac{3}{2}\frac{1}{2}^+(400)$	M1	43.0	159	3.9×10^{-11}				3.1
					E2	< 1.5		> 1.1×10^{-9}	(5.5±1.1) (−1)	< 2.0	< 18.6	> 3.4(−3)
		201.8		$\frac{5}{2}\frac{3}{2}^+(402)$	M1	15 [d])		1.1×10^{-10}	(4.4±1.1) (−2)			40
		205.2		$\frac{1}{2}\frac{1}{2}^+(400)$	E2	13.0	4.1	1.3×10^{-10}		1.2±0.2	7.7±0.7	5.4(−3)
		311.8		$\frac{3}{2}\frac{3}{2}^+(402)$	M1	29.0	7.6	5.6×10^{-11}	(2.3±0.4) (−2)			77
					E2	< 1.5		> 1.1×10^{-9}		< 1.8(−2)		> 3.7(−1)
388.5	< 0.065	186.9	$\frac{1}{2}^-$, $(\frac{3}{2}^-)$	$\frac{5}{2}^-$, $(\frac{3}{2}^-)$	E2	48.7	21.4	< 1.7×10^{-10}		> 1.4		< 4.4(−3)
		199.2		$\frac{3}{2}\frac{1}{2}^+(400)$	E1	9.9	0.7	< 8.1×10^{-10}		6.8(−7)		< 3.1(+4)
		282.1		$\frac{1}{2}\frac{3}{2}^+(400)$	E1	31.8	0.9	< 2.5×10^{-10}		7.8(−7)		< 2.7(+4)
		388.8		$\frac{3}{2}\frac{3}{2}^+(402)$	E1	9.6	0.1	< 8.4×10^{-10}		8.9(−8)		< 2.4(+5)

[a]) Total γ-ray intensity from each level set equal to 100.

[b]) Hindrance factor relative to the Weisskopf estimate [33]) with the statistical factor equal to one.

[c]) Calculated using $Q_0 = (7.7\pm0.7)$ b as compared to our measured value $Q_0 > 3.6$ b as obtained from $T_{\frac{1}{2}}$(311.7 keV level) < 30 ps.

[d]) Due to the triplet structure of the 201 K line the deduced α_K are too uncertain to calculate multipolarity mixing ratios. The given value for N_γ(201.8) was calculated with E1 multipolarity for the 201.5 keV transition and N_γ(200.8) = 0. From systematics the 201.8 keV transition has less than 10% E2 admixture.

TABLE 6

E2 rates ($e^2 \cdot b^2$) for interband transitions in ^{187}Ir

	Experimental		Calculated [a])		
	^{187}Ir	^{189}Ir	$E^x\langle\frac{1}{2}\|j_-\|\frac{3}{2}\rangle = 10$	$E^x\langle\frac{1}{2}\|j_-\|\frac{3}{2}\rangle = 30$	$E^x\langle\frac{1}{2}\|j_-\|\frac{3}{2}\rangle = 90$
$B(\mathrm{E2}, \frac{1}{2}\frac{1}{2} \to \frac{3}{2}\frac{3}{2})$	(7.8±0.3) E-2	(8.7±0.5) E-2	1.2 E-2	8.5 E-2	29.2 E-2
$B(\mathrm{E2}, \frac{3}{2}\frac{1}{2} \to \frac{3}{2}\frac{3}{2})$	(1.0±0.5) E-1	(1.8±0.8) E-1	0.44 E-1	2.9 E-1	3.3 E-1
$B(\mathrm{E2}, \frac{3}{2}\frac{1}{2} \to \frac{5}{2}\frac{3}{2})$	< 8.2 E-1	$(5.8^{+5.0}_{-3.6})$ E-1	0.056 E-1	0.44 E-1	1.5 E-1
$B(\mathrm{E2}, \frac{5}{2}\frac{1}{2} \to \frac{3}{2}\frac{3}{2})$	< 1.8 E-2	(9.4±4.7) E-2	1.3 E-2	7.3 E-2	14.2 E-2
$B(\mathrm{E2}, \frac{5}{2}\frac{1}{2} \to \frac{5}{2}\frac{3}{2})$		< 1.4 E-1	1.2 E-2	6.8 E-2	14.6 E-2
$B(\mathrm{E2}, \frac{5}{2}\frac{3}{2} \to \frac{1}{2}\frac{1}{2})$			1.8 E-2	11.8 E-2	31.7 E-2

[a]) We used $G_{E2}(\frac{1}{2} \to \frac{1}{2}) = G_{E2}(\frac{3}{2} \to \frac{3}{2}) = 65$ corresponding to $Q_0 = 7.7$ b.

These nuclei being on the border between spherical and deformed nuclei, other approaches to account for the E2 transition rates in odd mass Ir nuclei have also been suggested. Recently Reehal and Sorensen [47]) have calculated these transition rates in ^{189}Ir to ^{193}Ir using the pairing-plus-quadrupole force model for spherical nuclei including up to two phonons. Although their prediction for the $s_{\frac{1}{2}} \to d_{\frac{3}{2}}$ transition is remarkably good, they fail completely to predict the sharp rise of the $d_{\frac{3}{2}} \to d_{\frac{3}{2}}$ transition rate, and in calculating B(E2) ratios between $\frac{7}{2} \to \frac{5}{2}$, $\frac{7}{2} \to \frac{3}{2}$, and between $\frac{5}{2} \to \frac{3}{2}$, $\frac{5}{2} \to \frac{1}{2}$ transitions. In this case excellent agreement is obtained with the Alaga rule.

4.2.3. M1 transition rates. From the present measurements several M1 transition rates within the proposed $K = \frac{1}{2}$ and $K = \frac{3}{2}$ rotational band system in ^{187}Ir have been determined (see table 5). To our knowledge no magnetic moment has been measured in this nucleus. The M1 data were compared with the predictions from the Nilsson model [21, 22]). In its simplest form this model predicts that intensity branching ratios of transitions from one level to rotational members in a band should be governed only by geometrical factors independently of the intrinsic structure of the nucleus, and thus be the same for the corresponding ratios in all odd mass Ir isotopes. This prediction can be tested on the $B(\mathrm{M1}, \frac{5}{2}\frac{1}{2} \to \frac{5}{2}\frac{3}{2})/B(\mathrm{M1}, \frac{5}{2}\frac{1}{2} \to \frac{3}{2}\frac{3}{2})$ ratio predicted to be 6.75. The experimental values from ^{187}Ir to ^{193}Ir are plotted in fig. 10, where it is clearly seen that this value is approached when the number of neutrons decreases. The lack of absolute agreement is believed to be due to various admixtures which are more dominant for the more neutron rich nuclei where the deformation is less pronounced and thus the strong coupling Nilsson model less applicable.

As in the case of B(E2) values all B(M1) values were also calculated taking the Coriolis mixing between the $\frac{1}{2}^+[400]$ and $\frac{3}{2}^+[402]$ bands into account. The relevant expressions for the reduced M1 transition probabilities have been given in detail earlier [15]). They depend on the following five parameters:

$$P_+ G_{M1}(\tfrac{1}{2} \to \tfrac{3}{2}),\ G_{M1}(\tfrac{3}{2} \to \tfrac{3}{2}),\ G_{M1}(\tfrac{1}{2} \to \tfrac{1}{2}),\ b_{M1} G_{M1}(\tfrac{1}{2} \to \tfrac{1}{2}),\quad E^x\langle\tfrac{1}{2}|j_-|\tfrac{3}{2}\rangle.$$

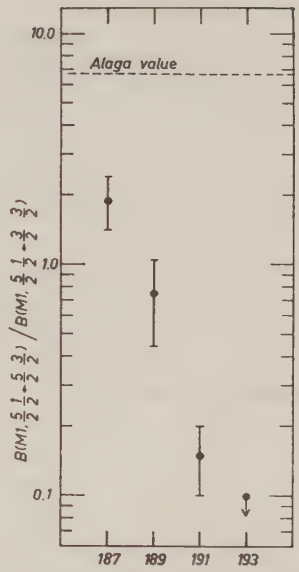

Fig. 10. The experimental $B(\mathrm{M1}, \frac{5}{2}\frac{1}{2} \to \frac{5}{2}\frac{3}{2})/B(\mathrm{M1}, \frac{5}{2}\frac{1}{2} \to \frac{3}{2}\frac{3}{2})$ ratio for some odd-A iridium isotopes.

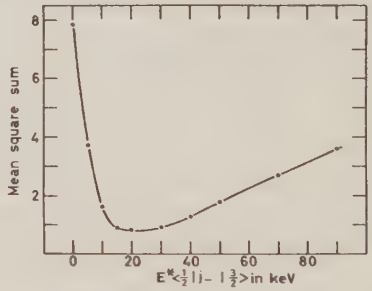

Fig. 11. The mean square sum

$$\frac{(T_N - T_{fit})^2}{\Delta T}\,\frac{1}{N}$$

plotted as a function of the Coriolis parameter $E^x\langle\frac{1}{2}|j_-|\frac{3}{2}\rangle$ for B(M1) transition rates in ^{187}Ir. More details are given in subsect. 4.2.3.

Our eight experimentally determined or deduced B(M1) values give a non-linear, over-estimated set of equations from which the first four parameters have been determined through a least squares fit using several different values of the coupling strength $E^x\langle\frac{1}{2}|j_-|\frac{3}{2}\rangle$. In table 7 are given the fitted parameters as well as the calculated B(M1)

TABLE 7
M1 transition rates in ^{187}Ir

Experimental data [a]		Calculated B(M1) values [b]		Theory [c]			
		$E^x\langle\frac{1}{2}\vert j_-\vert\frac{3}{2}\rangle = 0$	$E^x\langle\frac{1}{2}\vert j_-\vert\frac{3}{2}\rangle = 20$	$E^x\langle\frac{1}{2}\vert j_-\vert\frac{3}{2}\rangle = 0$		$E^x\langle\frac{1}{2}\vert j_-\vert\frac{3}{2}\rangle = 20$	
				$\varepsilon_4 = 0$	$\varepsilon_4 = 0.056$	$\varepsilon_4 = 0$	$\varepsilon_4 = 0.056$
B(M1, $\frac{3}{2}\frac{1}{2} \rightarrow \frac{3}{2}\frac{3}{2}$)	(6.7±3.0) E-3	1.00 E-3	4.66 E-3	1.30 E-3	1.62 E-3	2.59 E-3	3.5 E-4
B(M1, $\frac{3}{2}\frac{1}{2} \rightarrow \frac{5}{2}\frac{3}{2}$)	$(1.2^{+2.6}_{-0.5})$ E-2	1.15 E-3	8.11 E-3	1.95 E-3	2.43 E-3	6.3 E-5	5.9 E-5
B(M1, $\frac{5}{2}\frac{1}{2} \rightarrow \frac{3}{2}\frac{3}{2}$) [d]	(2.3±0.4) E-2	5.18 E-3	3.24 E-2	2.47 E-4	2.70 E-4	3.82 E-3	3.53 E-3
B(M1, $\frac{5}{2}\frac{1}{2} \rightarrow \frac{5}{2}\frac{3}{2}$) [d]	(4.4±1.1) E-2	4.47 E-3	2.76 E-2	1.49 E-3	1.86 E-3		
B(M1, $\frac{3}{2}\frac{1}{2} \rightarrow \frac{1}{2}\frac{1}{2}$)	(2.4±1.0) E-1	5.78 E-1	3.63 E-1	3.98 E-4	5.10 E-4	7.4 E-4	1.0 E-3
B(M1, $\frac{5}{2}\frac{1}{2} \rightarrow \frac{3}{2}\frac{1}{2}$) [d]	(5.5±1.1) E-1	7.15 E-1	5.2 E-1	8.84 E-1	9.07 E-1	7.83 E-1	8.0 E-1
B(M1, $\frac{5}{2}\frac{3}{2} \rightarrow \frac{3}{2}\frac{3}{2}$)	(3.2±0.4) E-2	2.78 E-2	2.82 E-2	2.24 E-2	2.58 E-2	7.65 E-3	9.9 E-3
B(M1, $\frac{1}{2}\frac{1}{2} \rightarrow \frac{3}{2}\frac{3}{2}$)	< 6.2 E-6	5.93 E-4	6.75 E-6	3.26 E-3	4.04 E-3	2.59 E-3	3.19 E-3
$P_+G_{M1}(\frac{1}{2} \rightarrow \frac{3}{2})$		−(0.24±0.13)	−(0.49±0.11)	−(0.28±0.05)	−(0.31±0.05)		
$G_{M1}(\frac{3}{2} \rightarrow \frac{3}{2})$		−(1.41±0.30)	−(1.52±0.15)	−(1.0 ±0.5)	−(1.1 ±0.5)		
$G_{M1}(\frac{5}{2} \rightarrow \frac{3}{2})$		5.5 ±1.9	4.5 ±0.7	3.2 ±0.6	3.2 ±0.6		
$b_{M1}G_{M1}(\frac{1}{2} \rightarrow \frac{1}{2})$		−0.07±2.39	−(0.47±0.59)	−(4.2 ±0.7)	−(4.3 ±0.9)		
Mean square sum		7.85	0.88				

[a]) B(M1) given in units of $(e\hbar/2Mc)^2$.
[b]) Calculated B(M1) values using the fitted parameters given below.
[c]) Predictions from the Nilsson model [22]) using the parameters $\kappa = 0.0620$, $\mu = 0.614$, $\varepsilon_2 = 0.20\pm0.05$.
[d]) These B(M1) values have been deduced using experimental multipolarities and an average value of $Q_0 = 7.7\pm0.7$ b. $g_R = 0.50\pm0.05$ and g_s(effective) $= (0.7\pm0.1)g_s$(free).

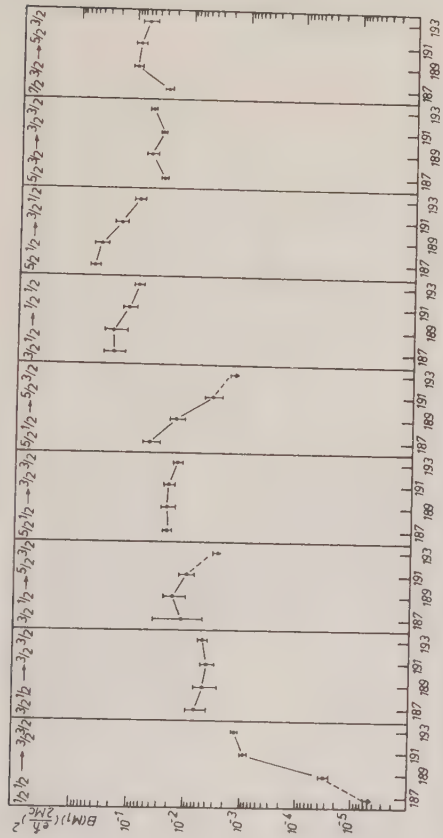

Fig. 12. Reduced M1 transition probabilities between low-lying positive parity states in odd-mass Ir nuclei. The experimental points are connected by solid lines.

values for $E^x\langle\frac{1}{2}|j_-|\frac{3}{2}\rangle = 0$ and 20 keV. In many cases B(M1) is very sensitive to the introduction of a small admixture and then stabilizes with a rather flat optimum for values of $E^x\langle\frac{1}{2}|j_-|\frac{3}{2}\rangle$ between 15 and 25 keV. This is compatible with what was earlier found for the E2 rates. In fig. 11, we have plotted the mean square sum

$$\sum \frac{(T_N - T_{\text{fit}})^2}{\Delta T_N}\frac{1}{N},$$

where $T_N \pm \Delta T_N$ is the experimental value with estimated error, T_{fit} is the corresponding fitted value and N is the number of fitted data, as a function of the Coriolis parameter $E^x\langle\frac{1}{2}|j_-|\frac{3}{2}\rangle$.

As a test of the capabilities of the refined Nilsson model to predict the magnetic properties in Ir nuclei we can now compare the fitted parameters with those calculated from the model. In doing this the following model parameters were used: $\kappa = 0.0620$, $\mu = 0.614$, $\delta = 0.20\pm0.05$, $g_R = 0.50\pm0.05$ and g_s(effective) $= (0.7\pm0.1)\ g_s$(free). The results are given in the lower right part in table 7, showing good agreement for the first three parameters while the $b_{M1}G_{M1}(\frac{1}{2} \rightarrow \frac{1}{2})$ parameter comes out too low as for all other known odd Ir isotopes.

In fig. 12 are shown the reduced M1 transition probabilities for the odd mass Ir isotopes between $A = 187$ and $A = 193$. It is noted that in general all B(M1) values are larger for intra-band transitions than for inter-band transitions. Most of the transition rates are also comparatively insensitive to change in the neutron number. A diverging trend is shown by the M1 component between the two band heads where the transition rate drops considerably with decreasing number of neutrons, reaching the very low limit-value of 6.2×10^{-6} $(e\hbar/2Mc)^2$ in ^{187}Ir. The M1 transition between

the two $I = \frac{5}{2}$ components in the two bands shows the opposite trend explaining the gradual fit in fig. 10 for lower neutron numbers.

It is therefore evident that the strength of the Coriolis force is consistently estimated using different approaches (4.2.1, 4.2.2 and 4.2.3).

The inclusion of only $\frac{1}{2}^+[400]$ and $\frac{3}{2}^+[402]$ orbitals in the discussion of the positive parity states represents, of course, a simplification but should be justified by the phenomenological approach. First the coupling with vibrations was not taken into account. Secondly, if the analysis leading to a deformation $\varepsilon_2 = 0.2$ is essentially correct, $\Delta N = 2$ coupling should be strong [48]) between $\frac{1}{2}^+[400]$ with $\frac{1}{2}^+[660]$ and $\frac{3}{2}^+[402]$ with $\frac{3}{2}^+[651]$ states respectively, quite analogously to ^{233}Pa [refs. [26, 48])] for proton orbitals, and ^{155}Gd, ^{163}Dy and ^{153}Sm where the corresponding neutron orbitals are considered.

4.3. NEGATIVE PARITY STATES

As emphasized by the existence of a great number of E1 transitions, there are a number of negative parity levels which are much more abundant in ^{187}Ir than in heavier odd-A iridium isotopes. This feature seems to be specific to ^{187}Ir and one can try to understand the behaviour of these levels, which form three distinct groups (fig. 13).

4.3.1. Proposed $\frac{1}{2}^-[541]$ band. It is suggested that the levels at 201.5, 388.6 and 486.5 keV are the $\frac{5}{2}^-$, $\frac{1}{2}^-$ and $\frac{3}{2}^-$ rotational components based on the $\frac{1}{2}^-[541]$ particle state. This band has been observed earlier in the odd-mass nuclei ^{161}Ho, $^{167-175}$Tm, ^{171,173}Lu, $^{175-177}$Ta and $^{181-185}$Re, and there is evidence [43]) for the occurrence of the same band in ^{189}Ir. For $\varepsilon_2 = 0.2$, the $\frac{1}{2}^-[541]$ band should have a decoupling parameter $a = 4.7$ [ref. [22])] which, according to eq. (1), would mean that the $\frac{1}{2}^-$ and $\frac{5}{2}^-$ levels almost coincide in energy; but, as is observed in $^{183-187}$Re [ref. [50])] and ^{171}Lu [ref. [51])], the Coriolis coupling with the $\frac{3}{2}^-[532]$ band can explain the unusual position of the levels.

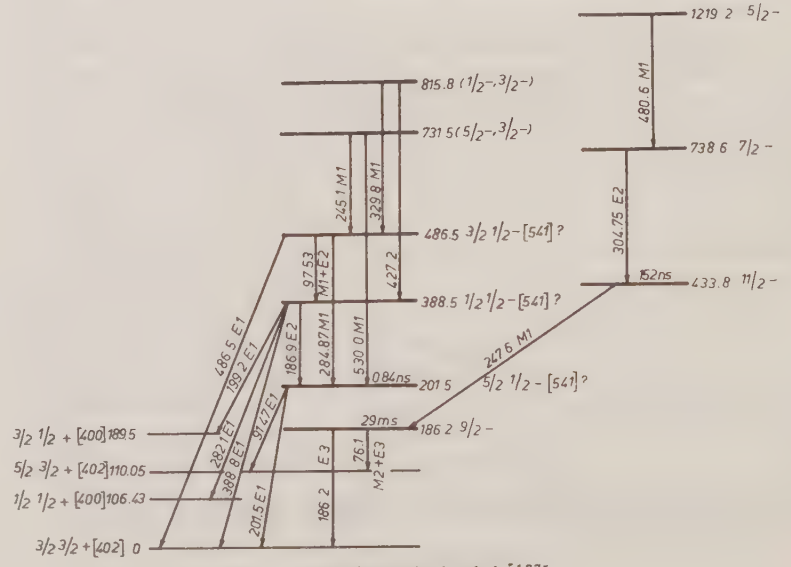

Fig. 13. Negative parity levels in ^{187}Ir.

4.3.2. The $\frac{9}{2}^-$ level at 186.2 keV. One observes that the 186.2 keV E3 transition and the E3 component of the 76.09 keV transition are respectively delayed by a factor of 3 and accelerated by a factor of 1.7 relative to the Weisskopf estimate [33]). Conversely the M2 component of the 76.09 keV transition is hindered by a factor of 10^5.

The $\frac{9}{2}^-$ levels that could appear in this region are the $\frac{9}{2}^-[514]$ intrinsic state and the $\frac{9}{2}\frac{1}{2}^-[541]$ rotational level (pushed below the $I = \frac{1}{2}$ level due to Coriolis interaction as mentioned in 4.3.1).

It is difficult at the present stage of experimental investigation to choose between one of the previously mentioned attributions. The $K = \frac{9}{2}$ hypothesis seems to be favoured by the almost single particle speed of the E3 transitions and a strong delay of the M2 component of the 76 keV transition [see systematics presented in ref. [52])]. However the delay of the M2 component might be also explained by the I-forbiddenness [the $K = \frac{3}{2}$ level originates from the $d_{\frac{3}{2}}$ orbit and $K = \frac{1}{2}$ from the $h_{\frac{11}{2}}$ orbit, ref. [53])].

4.3.3. Levels connected with the 433.8 keV $\frac{11}{2}^-$ level. The only $\frac{11}{2}^-$ particle state expected in this region is $\frac{11}{2}^-[505]$ which should have about the same deformation as the ground state and appears very rigid in Nilsson's calculations with $\kappa_p = 0.0620$, $\mu_p = 0.614$, $\kappa_n = 0.0636$ and $\mu_n = 0.393$ [ref. [26])]. The 738.6 and 1219.2 keV levels seem to form a system practically only connected with the $\frac{11}{2}^-$ level.

The suggestion of a spherical shape has been made for the low-lying $\frac{11}{2}^-$ state in heavier odd-A iridium and gold isotopes [19]). Another possibility of a triaxial shape for the similar $\frac{11}{2}^-$ levels in ^{191}Ir and ^{193}Ir was suggested by Price *et al.* [54]). It might also be possible that the 433.8, 738.6 and 1219.2 keV form a strongly perturbed rotational band. A shape transition or K-forbiddenness (if the $\frac{9}{2}^-$ state is $K = \frac{1}{2}$) can therefore be responsible for the delay of the 247 keV M1 transition.

5. Conclusion

From the present study of the ^{187}Ir low energy level scheme, it seems that those levels can be described in a consistent way, mainly in terms of the Bohr and Mottelson and Nilsson models including Coriolis coupling between bands, at least for the positive parity states. It is likely that coupling with vibrations, as well as $\Delta N = 2$ coupling, could still improve the agreement between the theoretical predictions and the experimental data. The nature of negative parity levels is not yet completely understood and needs further studies.

We thank the direction of CERN, the Institut de Physique Nucléaire, Orsay, and the Laboratoire de Chimie Nucléaire, Strasbourg, for continuous support during the preparation of this work. The assistance of the many members of the ISOLDE collaboration in the different phases of this work is sincerely appreciated. Two of us (M.F. and J.J.) thank the Joliot-Curie Foundation and Institut de Physique Nucléaire for financial support. Professor S. G. Nilsson and Doctor R. Piepenbring are gratefully acknowledged for fruitful discussions.

References

1) P. G. Hansen *et al.*, Phys. Lett. **28B** (1969) 415
2) R. Foucher *et al.*, Proc. Int. Conf. on properties of nuclear states, Montréal, 1969, p. 682
3) M. Finger *et al.*, CERN report 70-20 (1970)
4) B. R. Erdal *et al.*, Leysin Conf., CERN report 70-30 (1970) p. 1045
5) M. Finger *et al.*, Nucl. Phys. **A188** (1972) 369
6) ISOLDE collaboration, CERN report 70-3 (1970), ed. A. Kjelberg and G. Rudstam
7) E. P. Grigorev, B. S. Dzhelepov, V. Zvolska, A. V. Zolotavin, T. V. Molysheva, B. A. Khotin and J. Adam, Izv. Akad. Nauk SSSR (ser. fiz.) **25** (1962) 120
8) Nucl. Data **1** (1966), ed. W. B. Ewbank
9) J. Lindskog, K.-G. Välivaara, Z. Awwad, S.-E. Hägglund, A. Marelius and J. Phil, Nucl. Phys. **A137** (1969) 511
10) C. R. Cothern *et al.*, Phys. Rev. **182** (1969) 1286
11) R. H. Price, M. W. Johns, N. M. Ahmed and E. E. Habib, Can. J. Phys. **47** (1969) 727
12) R. Piepenbring and H. Nopre, Nucl. Phys. **A133** (1969) 113
13) F. R. Metzger, Phys. Rev. **C2** (1970) 2024
14) R. Avida, I. Ben Zvi, P. Gilad, M. B. Goldberg, G. Goldring, K. H. Speidel and A. Sprinzak, Nucl. Phys. **A147** (1970) 200
15) V. Berg, S. C. Malmskog and A. Bäcklin, Nucl. Phys. **A143** (1970) 177
16) S. G. Malmskog, V. Berg, A. Bäcklin and G. Hedin, Nucl. Phys. **A143** (1970) 160
17) A. Bäcklin, V. Berg and S. G. Malmskog, Nucl. Phys. **A156** (1970) 647
18) P. Nørgaard, K. M. Bisgård, K. Gregersen and P. Morgen, Nucl. Phys. **A162** (1971) 449
19) A. Bäcklin, G. Hedin and S. G. Malmskog, Nucl. Phys. **A169** (1971) 122
20) A. Bohr and B. Mottelson, Mat. Fys. Medd. Dan. Vid. Selsk. **27**, no. 16 (1953)
21) S. G. Nilsson, Mat. Fys. Medd. Dan. Vid. Selsk. **29**, no. 16 (1955)
22) S. G. Nilsson *et al.*, Nucl. Phys. **A131** (1969) 1
23) A. K. Kerman, Mat. Fys. Medd. Dan. Vid. Selsk **30**, no. 15 (1956)
24) G. Astner, Program LABSPEC (unpublished)
25) J. T. Routti and S. G. Prussin, Nucl. Instr. **72** (1969) 125
26) C. Sébille-Schück, thèse, Orsay, 1972
27) E. Arbman and N. Svartholm, Ark. Fys. **10** (1955) 1
28) R. Jezequel and R. Sellem, Nucart Program, Orsay (1969)
29) T. R. Gerholm and J. Lindskog, Ark. Fys. **24** (1963) 171
30) S. G. Malmskog, Ark. Fys. **35** (1967) 255
31) R. S. Hager and E. C. Seltzer, Nucl. Data **A4**, nos. 1 and 2 (1968)
32) Dragoun *et al.*, MPIH *V.S.* (1969)
33) A. A. Wapstra, G. J. Nijgh and R. van Lieshout, Nuclear spectroscopy tables (North-Holland, Amsterdam, 1959)
34) R. Jory, Galaxie program, Orsay (1971)
35) V. T. Gritsyna, A. D. Klyucharev and V. V. Remaev, Sov. J. Nucl. Phys. **4** (1966) 678
36) T. Sundström, Nucl. Instr. **16** (1962) 153
37) B. Olsen and L. Boström, Nucl. Instr. **44** (1966) 65
38) J. Burde, M. Rakavy and G. Engler, Phys. Rev. **128** (1962) 325
39) H. Ohlson, IPN, Orsay, internal report, 1971

40) C. Gustafson *et al.*, Ark. Fys. **36** (1967) 613
41) I. L. Lamm, Nucl. Phys. **A125** (1969) 504
42) V. M. Strutinsky, Nucl. Phys. **A95** (1967) 420
43) A. Bäcklin, G. Hedin, S. G. Malmskog and V. Berg, to be published
44) V. G. Soloviev and P. Vogel, Nucl. Phys. **A92** (1967) 449
45) K. Kumar, Phys. Rev. Lett. **26** (1971) 269
46) A. Bäcklin *et al.*, Leysin Conf. CERN report 70-30 vol. 2 (1970) p. 960; Colloquium on transitional nuclei, IPN Orsay (1971) p. 167
47) B. S. Reehal and R. A. Sorensen, Phys. Rev. **C2** (1970) 819
48) M. E. Bunker and C. W. Reich, Rev. Mod. Phys. **43** (1971) 348
49) R. Piepenbring, Colloquium Lyon (1970)
50) M. T. Lu and W. P. Alford, Phys. Rev. **C3** (1971) 1243
51) R. Piepenbring, Contribution to 21st Annual National Conf. of Acad. Sci. USSR on nuclear spectroscopy and structure of the atomic nucleus, Moscow, January 1971
52) K. E. G. Löbner, Phys. Lett. **26B** (1968) 369
53) F. S. Stephens, Proc. 5th Summer School, Rudziska, Poland, 1972, to be published, and private communication
54) R. H. Price, D. G. Burke and M. W. Johns, Nucl. Phys. **A176** (1971) 338

R E F E R E N C E 14

NEGATIVE PARITY STATES IN ODD-MASS Ir AND Au NUCLEI

A. BÄCKLIN

The Swedish Research Council's Laboratory, Nyköping, Studsvik, Sweden

and

V. BERG and S.G. MALMSKOG

AB Atomenergi, Studsvik, Nyköping, Sweden

and

Institute of Physics, University of Stockholm, Sweden

1.E.1:
3.A

Nuclear Physics **A156** (1970) 647–672; © *North-Holland Publishing Co., Amsterdam*
Not to be reproduced by photoprint or microfilm without written permission from the publisher

NEGATIVE PARITY STATES IN ODD-MASS Ir AND Au NUCLEI

A. BÄCKLIN

The Swedish Research Councils' Laboratory, Nyköping, Studsvik, Sweden

and

V. BERG and S. G. MALMSKOG

AB Atomenergi, Studsvik, Nyköping, Sweden

and

Institute of Physics, University of Stockholm, Sweden

Received 8 April 1970

Abstract: The decays of ^{193}Os → ^{193}Ir, ^{191}Pt → ^{191}Ir, ^{189}Pt → ^{189}Ir and ^{193}Hg → ^{193}Au have been studied in γ–γ coincidences, internal conversion and electron-electron delayed coincidences. New levels with the following spin-parity assignments and half-lives are proposed: ^{193}Ir: 299.45±0.09 keV, $I^\pi = \frac{7}{2}^-$, $T_{\frac{1}{2}} = 0.19 \pm 0.03$ ns; 598.26±0.15 keV, $I^\pi = \frac{9}{2}^-$; 740.46±0.15 keV, $I^\pi = \frac{5}{2}^-$. ^{191}Ir: 391.14±0.05 keV, $I^\pi = \frac{7}{2}^-$, $T_{\frac{1}{2}} = 0.24 \pm 0.02$ ns; 659.06±0.08 keV, $I^\pi = \frac{3}{2}^-$, $T_{\frac{1}{2}} < 0.12$ ns. ^{189}Ir: 615.70±0.08 keV, $I^\pi = \frac{7}{2}^-$, $T_{\frac{1}{2}} = 0.18 \pm 0.02$ ns; 1184.54±0.11 keV, $I^\pi = \frac{5}{2}^-$, $T_{\frac{1}{2}} < 0.08$ ns. The 508 keV $\frac{7}{2}^-$ level in ^{193}Au was found to have $T_{\frac{1}{2}} = 0.29 \pm 0.02$ ns. In each nucleus these negative parity states and the $\frac{11}{2}^-$ isomeric state are strongly connected with E2 and M1 transitions and only weakly connected to the low-lying positive parity states. The B(E2) values are close to the values of $B(\mathrm{E2}; 2^+ \rightarrow 0^+)$ in the neighbouring even nuclei. We propose these negative parity level systems to be associated with an essentially spherical shape of the nuclei in contrast to the low-lying positive parity states (including the ground state) of these nuclei, which in Ir are likely to be deformed states.

E RADIOACTIVITY ^{193}Os [from ^{192}Os(n, γ)], $^{191, 189}$Pt, ^{193}Hg [from Pb (p, spallation)]; measured E_{ce}, I_{ce}, $\gamma\gamma$-coin, cece-, γce-delay; deduced log ft. ^{193}Au, $^{193, 191, 189}$Ir deduced levels, J, π, $T_{\frac{1}{2}}$, γ-multipolarity.

1. Introduction

Odd-mass Ir nuclei show an interesting feature in that a small number of transitions of strong or medium intensity are present, which do not seem to energetically combine with other transitions. In the decay of ^{193}Os to ^{193}Ir this applies for the 142.26 keV M1 transition and the 219.18 and 298.71 keV E2 transitions [1–6]), each being about 0.2 % per decay. In the decay of ^{191}Pt to ^{191}Ir the two E2 transitions at 219.74 and 267.99 keV, each about 0.7 % per decay, do not fit into the earlier proposed level scheme [7]). In the decay of ^{189}Pt to ^{189}Ir this applies to the strong (≈ 4 % per decay) 243.50 keV E2 and 568.87 M1 transitions [8]).

Various positions in the level schemes, either as directly feeding the ground state or one of the lowest excited positive parity levels have been suggested for these transitions [1–5, 9–13]). For example, the three transitions mentioned in ^{193}Ir have been

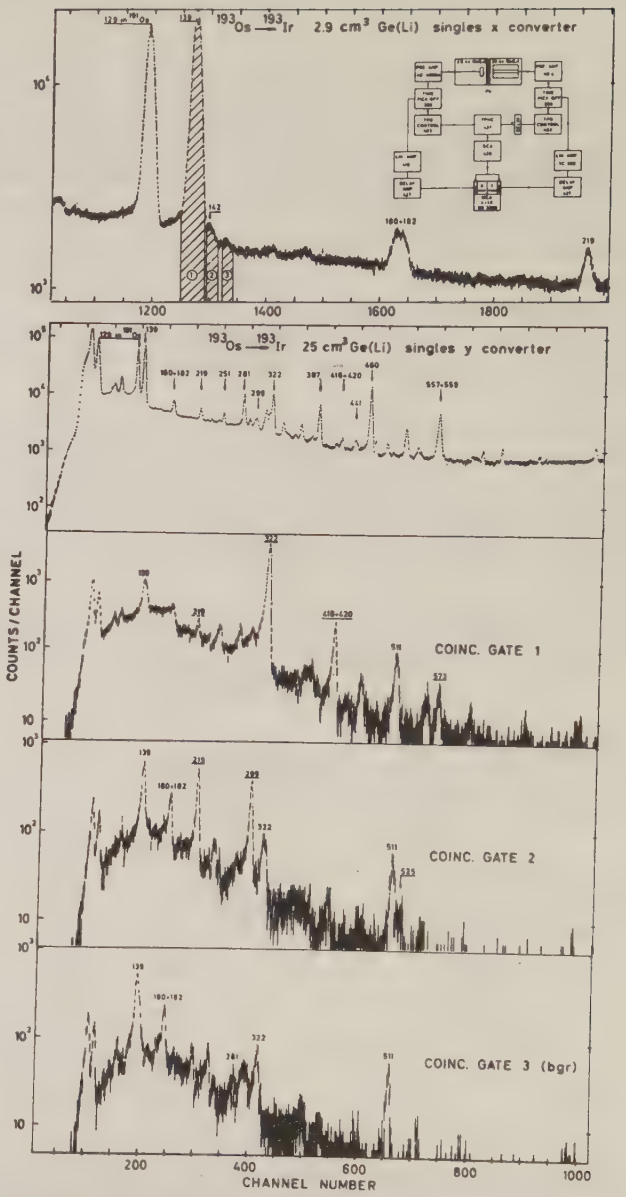

Fig. 1. Coincidence measurements in the decay ^{193}Os → ^{193}Ir. The experimental arrangement is shown in the inset. The uppermost spectrum shows a single spectrum as recorded with the 2.9 cm³ detector. The hatched areas indicate the regions accepted by the three gates. The three lowest spectra show the corresponding coincidence spectra obtained in the 25 cm³ detector. The energies (in keV) are underlined for the coincident lines. From a comparison between the spectrum coincident with the energy region accepted in gate 2 and those accepted in gate 1 (139 keV line) and gate 3 (background) it is clearly seen that the 142 keV line is coincident with the 219, 299 and 525 keV lines. The second spectrum from top shows a corresponding singles spectrum in the 25 cm³ detector for comparison. The contents n in each channel is plotted as a vertical bar with a height corresponding to $2\sqrt{n}$.

proposed to form a cascade to the ground state [2,4,5]). However, since this leads to features of the level scheme that are difficult to understand, we recently suggested that this cascade instead populates the $\frac{11}{2}^-$ isomeric state [6]).

The purpose of the present paper is to show experimentally that in all three Ir nuclei the transitions mentioned form a cascade leading to the $\frac{11}{2}^-$ isomeric state, thereby defining a $\frac{7}{2}^-$, a $\frac{3}{2}^-$ and/or a $\frac{5}{2}^-$ state in each nucleus. Using prompt and delayed coincidence techniques the relative order of the transitions has been established and half-lives of the $\frac{7}{2}^-$ states have been measured. In addition, the half-life of the earlier known [14]) $\frac{7}{2}^-$ state in ^{193}Au has been measured. Finally, the nature of these $\frac{7}{2}^-$ states is discussed within the framework of models for both spherical and deformed nuclei.

2. Experimental equipment and sources

Several different instruments were used in the present work. Conversion electrons were measured with a $\pi\sqrt{2}$ β-spectrometer [15,16]). The momentum resolution was adjusted to 0.2 % FWHM.

Gamma-gamma coincidences were measured with an arrangement similar to that of ref. [17]). A 25 cm^3 Ge(Li) detector was operated in coincidence with either a 2.9 cm^3 planar Ge(Li) detector or a 30 cm^3 coaxial Ge(Li) detector. The arrangement is shown schematically in fig. 1. A time-resolution of about 15 nsec FWHM was obtained with a ^{60}Co source. The window of the single-channel analyser following the TPHC was adjusted to a width corresponding to about 50 nsec, which was sufficient to give a high coincidence efficiency in all cases investigated. The multichannel analyser was wired so that four 1024 spectra could be recorded, each being coincident with pulses in an energy interval set by a digital gate system.

The half-life measurements were performed using the delayed coincidence method. The basic instrument was a long lens, electron-electron coincidence spectrometer [refs. [18,19])]. In some cases when we wanted to detect γ-rays, one lens was replaced by a cylindrical 2.5 × 2.5 cm^3 Naton 136 plastic scintillator placed 1 cm from the source. All measurements were carried out in the same general manner. The investigated source and a "prompt source" were measured alternatively using the automatic operation of the spectrometer [19]). By applying a high tension to the appropriate source such shift measurements were always carried out without having to change the energy settings between measurements of the delayed and prompt reference curves. Each sequence of measurements was usually run for 5 to 10 h. The data were analysed by the centroid shift method [20]) where also second and third order moments were calculated for consistence checks. In several cases an apparent difference between the slope of the delayed and prompt curves was observed and here an analysis with the convolution method [21]) was also performed.

All sources except ^{193}Os were obtained from the ISOLDE project [22]), CERN, as decay products of neutron deficient Hg isotopes produced by bombarding lead with

600 MeV protons. The Hg nucleides were mass separated and driven into 0.8 mg/cm^2 Ni foils, thus forming very thin sources excellent for electron spectroscopy. The sources had an extension of about 4 mm and were therefore masked with a 2 mm slit in order to obtain a sufficient resolution in the electron spectroscopy measurements. The sources were transported to Studsvik rapidly enough to allow measurements to be started about 15 h after the end of the irradiation.

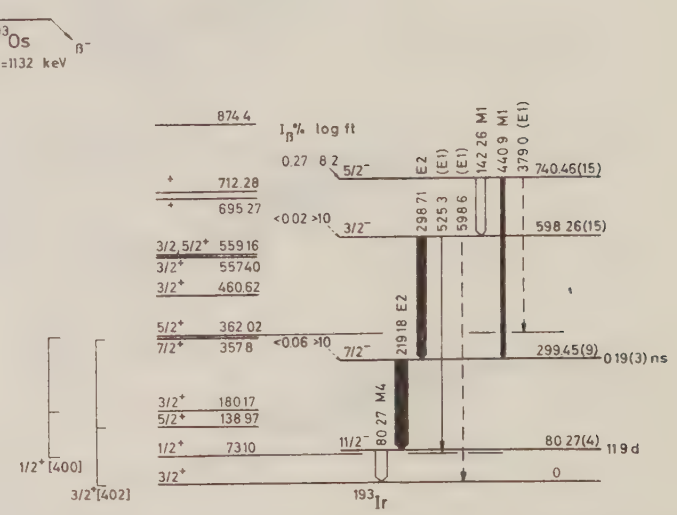

Fig. 2. Partial level scheme of ^{193}Ir as obtained in the present work (for complete scheme regarding the positive parity states, see refs. [4–6])). Energies are given in keV, number in parentheses denotes error in last digit. The widths of the arrows are approximately proportional to the intensities, the white part indicating the part of the transition proceeding by internal conversion. The positions of the transitions indicated by the dashed lines have not been verified by coincidence experiments but are suggested from energy combinations. Multipolarities given in parentheses have not been experimentally verified but are deduced from the position in the level scheme of the transition.

The ^{193}Os sources for the conversion electron and half-life measurements were made by irradiating Os metal enriched to 98.7 % in ^{192}Os † in a flux density of 2 × 10^{14} neutrons/cm^2 · sec in the R2 reactor at Studsvik. The active material was electroplated on 1 mg/cm^2 Ni-foil using the method described in ref. [6]). The source for the $\pi\sqrt{2}$ spectrometer had the dimensions 2 × 30 mm and a thickness of about 50 μg/cm^2, while the source for the double lens coincidence spectrometer covered a circular spot with a diameter of 5 mm and a thickness of the order of 0.5 mg/cm^2.

The sources for the γ–γ coincidences were made by 10 min activations of about 1 mg enriched ^{192}Os in a flux density of 10^{13} neutrons/cm^2 · sec.

† Purchased from Oak Ridge National Laboratory, Tennessee, USA.

3. Experiments

3.1. THE ^{193}Ir NUCLEUS

The task of the present work was to obtain experimental evidence for the level scheme of fig. 2, which was suggested in an earlier paper [6]) on intuitive grounds.

It has earlier been experimentally verified [23]) that the $\frac{11}{2}^-$ isomeric level at 80 keV in ^{193}Ir is fed from ^{193}Os. As the ground state spin of ^{193}Os is $\frac{3}{2}$ it has been suggested [ref. [23])] that this feeding takes place from a 17 min isomeric state in ^{193}Os. We propose, however, that this $\frac{11}{2}^-$ level is also fed from the ^{193}Os ground state via several levels in ^{193}Ir of lower spin, which are connected by the 142, 219 and 299 keV transitions.

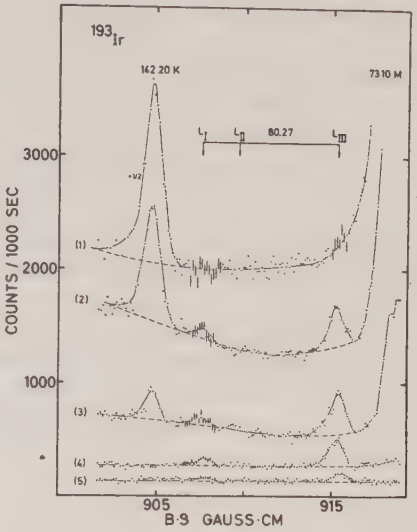

Fig. 3. L-conversion electrons of the 80.27 keV M4 and 142.26 keV M1 transitions in ^{193}Ir recorded at the following time intervals after source preparation: (1) 14, (2) 75, (3) 130, (4) 269 and (5) 698. The times are given in hours and refer to the 80.27 L_{III} line. For clarity the points in spectrum (1) have been multiplied by 0.5 and spectrum (4) has been rised 100 counts.

In order to show this we first studied the intensity of the 80 keV isomeric transition, i.e. the 80L conversion lines, as a function of time. After a 24 h irradiation the proposed [23]) 17 min activity was allowed to decay for 3 h. The possible ^{193m}Ir activity formed during this decay was removed with a good efficiency in the preparation procedure for the conversion electron sources [6]). Using the $\pi\sqrt{2}$ spectrometer the 80L group was scanned together with the K-lines of the 139 and 142 keV transitions five times during a period of 4 weeks. The spectra are shown in fig. 3, and from the intensity values plotted as a function of time in fig. 4 the growth and decay of the 80L_{III} line are clearly seen. The curve is calculated assuming no ^{193m}Ir activity present at the time immediately after the separation. The half-lives of ^{193}Os and ^{193m}Ir were taken as 31 h and 11.9 d, respectively [24]). Normalization was made at the average of the experimental values. As can be seen, the calculated curve agrees decently with the experimental points; from the latter we obtain the half-lives 28±3 h and 12±2 d. From the first measurement, which only gave a limit for the 80L_{III} intensity, one can

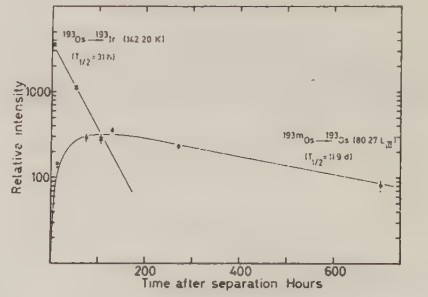

Fig. 4. Time-dependence of the L_{III} line of the 80.27 keV M4 transition and the 142.26 keV line in ^{193}Ir. The experimental points are seen to be well fitted by curves calculated with the half-lives from literature [24]) of 31 h and 11.9 d, respectively, which shows that the isomeric transition is fed in the 31 h decay.

TABLE 1

Relative intensities of conversion lines in the decay of ^{193}Os → ^{193}Ir

Transition energy (keV)	Shell	Electron intensity [a])	Error %	Gamma intensity [a])	Error %	Total intensity [a])	Error %	Multipolarity
138.97	K	180	6	100		334	6	M1+11 % E2
142.26	K	3.8	8	1.4	15	6.6	10	M1+< 15 % E2
	L_I	0.53	10					
	L_{II}	< 0.13						
	L_{III}	< 0.16						
219.18 [b])	K	0.80	12	6.6	10	8.3	10	E2
298.71 [b])	K	0.35	25	4.8	6	5.3	6	E2
440.56 [b])	K	0.18	30	2.2	10	2.2	10	M1
80.27±0.04 [c])	L_I	0.087	12					M4 (L_I/L_{III})exp = 0.24±0.02
	L_{II}	< 0.02						(L_I/L_{III})theory = 0.23
	L_{III}	0.36	6					

[a]) Intensities are given in the units of table 1 in ref. [6]). The total intensities were calculated from the most accurate value of the electron- and γ-ray intensities and the theoretical conversion coefficients [43]).

[b]) All data for the 219.18, 298.71 and 440.56 keV transitions are from ref. [6]).

[c]) The intensities of the L-lines of the 80 keV isomeric transition are averages of 4 measurements performed at 4 different times and corrected for decay to the time of maximum activity 113 h after separation.

see that at most 20 % of the maximum ^{193m}Ir activity could have remained after the separation. We conclude that the 80 keV isomeric level is populated in the 31 h decay.

Since no direct feeding can take place we expect to find transitions feeding the isomeric state with an intensity corresponding to that of the isomeric transition. The conversion electron intensities are given in table 1. The intensities of the 80L lines are the average of the values corrected for decay to the time of maximum activity (113 h after the separation time). The intensity ratio of the 142K and 139K lines was found to be 35 % larger than in ref. [6]), where the low value is probably due to the thicker source used giving a large sloping background from the 73M line. In table 2 are given the

TABLE 2

Comparison of relative intensities of transitions connected to the 80.27 keV isomeric level in ^{193}Ir

Transitions and combinations of transitions (keV)	Total intensity [a])	Total intensity [b])
219.18	8.3±1.0	0.25±0.03
298.71+440.90	7.7±0.6	0.23±0.02
142.26+440.90−525.3	8.4±0.8	0.25±0.02
80.27		0.23±0.02

[a]) In units of table 1 in ref. [6]) ($I_\gamma(139) = 100$). The total intensities of the 219, 299, 441 and 525 keV transitions are calculated from ref. [6]).

[b]) Percent per ^{193}Os decay assuming a β-feeding of the ground state of 68 % [ref. [6])]. The isomeric activity $\lambda_2 N_2(t)$ was assumed to follow the formula

$$\lambda_2 N_2(t) = N_1(0)\,\frac{\lambda_1\lambda_2}{\lambda_2-\lambda_1}\,(e^{-\lambda_1 t}-e^{-\lambda_2 t}),$$

where t is the time after the separation, λ is a decay constant and $N_1(0)$ is the number of ^{193}Os nuclei at $t = 0$ that decay via the isomeric transition. Values of λ_1 and λ_2 were obtained from the half-lives $(T_{\frac{1}{2}})_1 = 31$ h and $(T_{\frac{1}{2}})_2 = 11.9$ d [ref. [24])].

experimental values of the total intensities of the transitions and combinations of transitions that according to the level scheme of fig. 2 should be equal. Since the time dependence of the 80 keV isomeric transition is more complicated than for the other transitions its intensity cannot be directly compared with the other intensities. One may however for both decays calculate the fraction of ^{193}Os nuclei present after the separation that decays through each transition. These values are given in column 3 of table 2. It is seen that the number of ^{193}Os nuclei decaying via the 80 keV isomeric level agrees very well with the number of nuclei decaying via e.g. the 219 keV transition and we take this fact as evidence that the subsystem formed by the 142, 219, 299 and 441 keV transitions leads to the isomeric state as shown in fig. 2.

The next step in this investigation was to establish the order of the transitions forming the subsystem. Since a level de-excited by an E2 transition of either 219 or 299 keV could be expected to have a measurable half-life, an attempt to establish the order of the two E2 transitions was made by measuring delayed coincidences using the double

lens spectrometer mentioned in sect. 2 above. The time delay between these two transitions was determined by focusing the 219K and 299K c.e. lines in one spectrometer each and registering the corresponding time delay distribution. A prompt time curve was also recorded with unchanged spectrometer settings using the β–238K cascade from a ^{212}Pb source. To be able to use the same energy channels a 5 kV pre-accelerating potential was applied to the ^{212}Pb source. An example of an observed pair of delayed and prompt decay curves is shown in fig. 5c. The random coincidence rate in the delayed spectrum is due to the fact that the observed K-lines are comparatively small compared to underlying β^- continuum background. This random rate was subtracted from the observed decay curve together with the weak contributions from the β–219K, β–299K, β–234L and β–155L cascades all accepted by our chosen energy

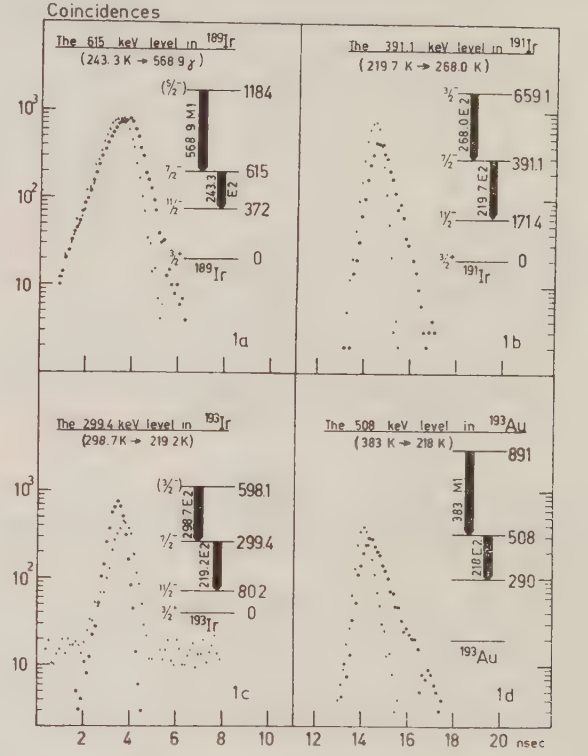

Fig. 5. Delayed coincidence measurements performed on the cascades specifically shown in the figure. From the analysis the following results were obtained: $T_{\frac{1}{2}} = 0.18\pm0.02$ nsec (615 keV level in ^{189}Ir) $T_{\frac{1}{2}} = 0.24\pm0.02$ nsec (391 keV level in ^{191}Ir), $T_{\frac{1}{2}} = 0.19\pm0.03$ nsec (299 keV level in ^{193}Ir) and $T_{\frac{1}{2}} = 0.29\pm0.02$ nsec (508 keV level in ^{193}Au).

settings. The final delayed curves together with the corresponding prompt distributions were analysed both by the momentum [20]) and convolution [21]) methods. Excellent internal consistency was obtained clearly showing that the 219.2 keV transition is delayed relative to the 298.7 keV transition. If we make the reasonable assumption that no so far unrevealed low-energy transition exists that may feed the isomeric state, the experimental result necessarily defines a level at 299.45 keV according to fig. 2. From the above measurements this level is found to have a half-life of 0.19 ± 0.03 nsec (assuming as is shown below that the 299 keV transition immediately precedes the 219 keV transition).

Unfortunately it was technically impossible to define also the order of the 142 and 299 keV transitions by delayed coincidences. Evidence that the 299 keV transition immediately precedes the 219 keV transition is given from the fact that two transitions not fitted between the positive parity levels [6]) energetically fit between the suggested 598 keV level and low-lying positive parity levels. No such transitions could be found from a possible 442 keV defined level by reversing the order of the 142 and 299 keV transitions. In order to establish more definitely the 598 keV level a coincidence experiment was performed with two Ge(Li) detectors (fig. 1). Gates were set at the 139 and 142 keV lines and the neighbouring background as detected in the 2.9 cm^3 detector, which had a good enough resolution to separate these lines, and the coincident spectrum was measured with a 25 cm^3 coaxial detector. The detectors were placed as close together as possible, and a weak source giving only a few percent dead-time in the big detector was placed between the detectors. The coincident spectra resulting after a 50 h run are shown in fig. 1 together with a singles spectrum. The coincidence results are summarized in table 3. The clear evidence for coincidences between the

TABLE 3

Gamma-gamma coincidences in ^{193}Ir

Transition (keV) [a])	Gate energy (keV) [b])	
	139	142
219.18		×
298.71		×
321.63	×	
418.16	×	
420.07	×	
525.3		×
573.4	×	

[a]) From ref. [6]).
[b]) A cross denotes significant coincidence effect.

142 and 525 keV transitions supports the level scheme of fig. 2. The fact that no coincidences could be observed between the 142 and 598 keV transitions may be explained by the weakness of the latter transition, its intensity being only ten percent of that of the 525 keV transition [6]).

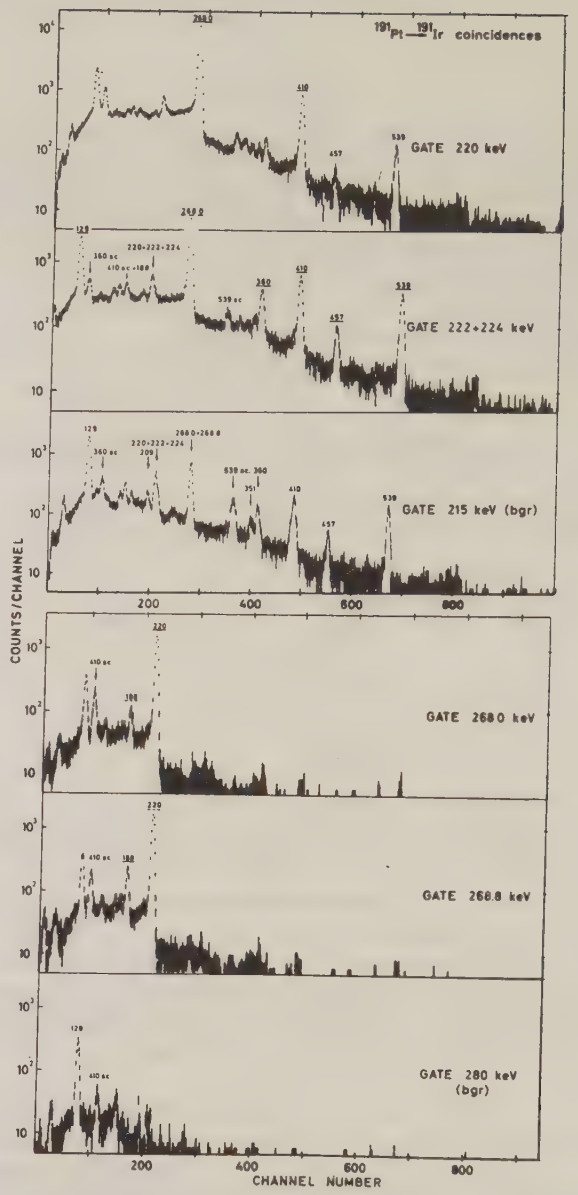

Fig. 6. Coincidence measurements in the decay of ^{191}Pt → ^{191}Ir. The upper three spectra show the lines coincident with different parts of the complex peak 220+222+224 keV. The 220 keV line is seen to be strongly coincident with the 268.0 keV line and to some extent also with the 410 keV line. The 222+224 keV lines are coincident with the 129, 360, 410, 457 and 539 keV lines (underlined) and to some extent also with the 268 keV line (contamination from the 220 keV line in the gate). This result is in agreement with the level scheme of ref. [7]). Due to difficulties in the photo-reproduction the horizontal scale of the 222+224 spectrum has been somewhat distorted. The peaks denoted with sc. are due to Compton scattering. The lowest three spectra show the lines coincident with the close doublet 268.0+268.8 keV. The 220 keV line is seen to be coincident with the 268.0 keV line in agreement with the above result. See also note added in proof.

Energetically it is also possible to fit the 418.16 keV transition [6]) from the 598 keV level to the 180 keV level. The coincidence spectra show that this transition is not coincident with the 142 keV transition.

The multipolarities of the connecting transitions imply a negative parity of all the new states in fig. 2. The spin values indicated can be considered as rather definite; increasing all values with one unit, which is also possible in view of the multipolarities indicated, would imply a second forbidden beta transition to the 740 keV level with a log *ft* of 8.2, which is anomalously low.

3.2. THE ^{191}Ir NUCLEUS

The two E2 transitions at 219.74 and 267.99 keV observed in the decay of ^{191}Pt can not be placed in the level scheme of ^{191}Ir on the basis of energy combinations [7]) although various positions using less accurate energy values have been suggested for these transitions [9–12]). In order to clear up this situation a coincidence experiment was performed with two Ge(Li) detectors with volumes 25 cm^3 and 30 cm^3, respectively. The γ-spectra coincident with the 220 and 268 keV γ-lines are seen in fig. 6. Since both these lines are complex, the 220 keV line not being resolved from the weaker 222 and 224 keV lines [7]) and the 268 keV line almost coinciding with the stronger 269 keV line, gates were also set at the parts of the complex lines corresponding to these contaminating lines. Gates were also set at the background close to the lines according to fig. 6. All gates had the same width. It is clearly seen that the 219.7 keV transition is coincident with the 268.0 keV transition. The coincidence results are summarized in table 4. A puzzling result concerns the 410 keV transition. This

TABLE 4

Gamma-gamma coincidences in ^{191}Ir

Transition energy (keV) [a])	Gate energy (keV) [b])			
	220	222+224	268.0	268.8
129.48		×		
187.8		×	(×)	×
219.74			×	(×)
267.99	× [c])	} (×)		
268.81				
360.00		×		
409.50	× [d])	×		
456.8		×		
538.8		×		

[a]) From ref. [7]).
[b]) A cross denotes strong coincidences, a parenthesis indicates weaker coincidences due to line close in energy to the gate energy.
[c]) The position of the line corresponds to the 267.99 keV line rather than the 268.81 keV line. If the latter were the coincident line one would also observe strongly the 172 and 351 keV transitions, which are not observed, fig. 6.
[d]) See subsect. 3.2.

strong transition de-excites together with the other strong transitions of 360, 457 and 539 keV the 539 keV level [7]). Fig. 6 shows fairly strong coincidences between the 220 keV line and the 410 keV line, while no such coincidences are found for the other 3 transitions from the 539 keV level. We must accordingly propose tentatively that the 410 keV transition is a close (within $\approx$ 0.5 keV) doublet with the weaker component feeding the 220 keV transition (no significant coincidences were observed between the 268 keV line and the 410 keV line) [†].

The coincidence results for the 219.74 and 267.99 keV transitions indicate that these transitions form a cascade feeding either the ground state or the 4.9 sec $\frac{11}{2}^-$ state at 171.40 keV [refs. [24,25])].

In order to find out which alternative should be preferred a search was made for the 42 keV isomeric transition in ^{191}Ir with the aim to see if its intensity matches the γ-cascade. A six day old mass-separated source of ^{191}Pt from the ISOLDE experiment [22]) was used and the expected energy range was scanned with the $\pi\sqrt{2}$ β-spectrometer. The L_{II} and L_{III} lines were observed and their intensities were compared to that of the 129.48 keV K-line. The intensity data are given in table 5 together with the

TABLE 5

Internal conversion lines associated with the $\frac{11}{2}^-$ isomeric level in ^{191}Ir

Transition energy (keV)	Multi-polarity	Electron shell	Relative electron intensity I_e [a])	Relative total intensity of transition I_{tot} [b])
41.92 [c])	E3	L_{II}	5.0±1.0	15.3±3.0
		L_{III}	5.9±1.0	
129.48 [d])	M1+E2	K	100	
219.74 [d])	E2	K	2.1±0.2 [d])	19.6±2.0
267.99 [d])	E2	K	1.2±0.1 [d])	17.0±1.5

[a]) Normalized to 100 for the 129.48 keV K-line.
[b]) Obtained from the relative electron intensities and the theoretical conversion coefficients [43]) using the relation $I_{tot} = I_e(1+\alpha_{tot})\alpha^{-1}$, where α is the theoretical conversion coefficient for the particular line measured.
[c]) Value taken from ref. [25]). The energy found in the present work using the 129.48 keV line as calibration is 41.93±0.03 keV which is slightly less accurate than that of ref. [25]).
[d]) From ref. [7]).

earlier observed [7]) intensities of the 219.74 and 267.99 keV lines. It is seen that the total intensities of the 219.74, 267.99 and 41.92 keV transitions are equal within the errors. Since the $\frac{11}{2}^-$ state is not likely to be fed directly from the ground state of ^{191}Pt, which is believed to have spin and parity $\frac{3}{2}^-$, refs. [10–12,24]), it is very likely that the three transitions form a cascade. However, the possibility still exists that the $\frac{11}{2}^-$ isomer is fed not as suggested above but directly from a long lived isomer in ^{191}Pt. Isomers with $T_{\frac{1}{2}} = 4.4$ d and 4.1 d and a probable spin $\frac{13}{2}^+$ have been found in ^{193}Pt [ref. [26])] and ^{195}Pt [ref. [24])], and it is likely that such a state with a possible

[†] See note added in proof.

long half-life exists also in ^{191}Pt, and furthermore, it could well be fairly strongly populated via high-spin parents from the spallation process in the ISOLDE target. We therefore followed the decay of the isomer and found it to have a half-life of 3.1 ± 0.5 d, which very well agrees with the half-life 2.9 ± 0.2 d we found for the ^{191}Pt ground state decay. The latter value is in good agreement with the accepted value 3.0 d [ref. [24])]. Still the small possibility exists that the possible Pt isomer and the ground state have very similar half-lives. However, the isomeric transition was observed by Harmatz *et al.* [9]) to have almost the same intensity relative e.g. the 129 keV transition as in the present work. In the work of Harmatz *et al.* [9]) the ^{191}Pt activity was made by (p, n) reactions on Ir with 22 MeV protons and it seems very unlikely that the relative yield of an eventual isomeric state in ^{191}Pt would be the same in such a reaction as in a spallation reaction on Pb using 600 MeV protons. We therefore conclude that the 220 and 268 keV lines form a cascade feeding the $\frac{11}{2}^-$ isomeric state, thereby defining two new odd-parity states in ^{191}Ir. The upper of these states has an energy of 659.06 keV. Further support for that level is obtained from the fact that a level at that energy defined by three weak transitions to the lowest positive parity levels (but with unknown spin and parity) has been found in earlier work [7,11,12]).

In order to establish the order between the 220 and 268 keV transitions and to measure the half-life of the intermediate level, a delayed coincidence experiment was performed. The K-conversion electrons from the 220 and 268 keV transitions were focused in one lens spectrometer each and the delayed coincidence spectrum was registered. A prompt reference curve was obtained from the β-238.6K cascade in the decay of ^{212}Pb. To be able to use the same energy settings in both measurements 5 kV was applied to the ^{191}Pt source. About 50 sets of shift measurements were performed each lasting 15 min. The sum of spectra from such a set of runs is given in fig. 5b showing the different slopes of the delayed and prompt curves. We find that the 220 keV line is delayed relative to the 268 keV line, thereby defining a level at 391.14 keV.

Although the 268K c.e. line as seen in the lens spectrometer is known to be a doublet, little interference in the coincidence spectrum is expected as the unresolved 268.8 keV component, to our knowledge, is not coincident with anything in the 219.7K channel. The decay time of the coincidence rate was also followed for 6 d and shown to be approximately 3 d. All coincidence data were analysed both by the momentum and convolution methods. Consistent results were obtained. After a small correction (< 5 psec) for the difference of transit time of the 219.7K and 268.0K conversion electrons due to the 5 kV acceleration field we obtain a half-life of 0.24 ± 0.02 nsec for the 391.1 keV level in ^{191}Ir.

Attempts were also made to determine the half-life of the 659.1 keV level mainly fed in the EC decay of ^{191}Pt. One spectrometer was focused at the de-exciting 268.0K c.e. line while the feeding KLL Auger electrons were detected in the other lens. Unfortunately we were not able to avoid the nearly twice as strong contribution from the prompt KLL 268.8K cascade proceeding over the 351.3 keV level in ^{191}Ir. Another

prompt contribution was obtained between the K c.e. lines and its own KLL Auger line created in the internal conversion process. The corresponding prompt distribution was obtained using the β-94.7K cascade from a ^{165}Dy source supplied with 10 kV pre-acceleration potential. From the momentum analysis no apparent centroid shift was observed and from the experimental uncertainties we are thus only able to set an upper limit for the half-life of the 659.1 keV level in ^{191}Ir of < 120 psec.

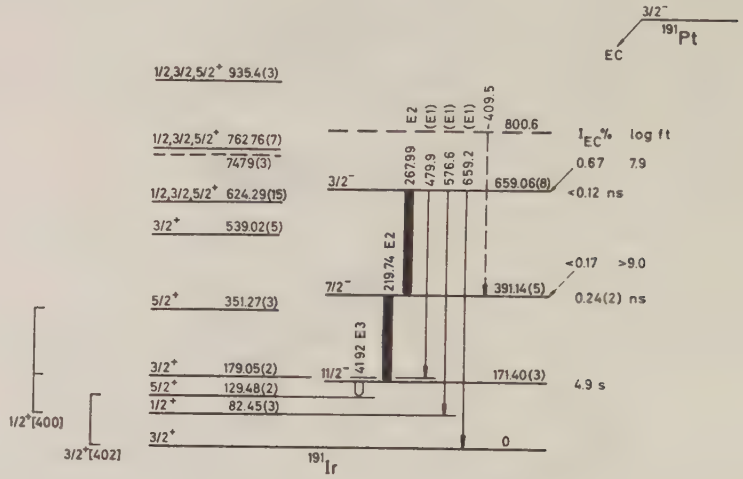

Fig. 7. Partial level scheme of ^{191}Ir obtained in the present work (for a complete scheme of the positive parity levels see ref.[7])). The log *ft* value was calculated assuming 50 % feeding to the ground state and a decay energy of 1.0 MeV [ref. [46])]. For further explanations see caption of fig. 2. See also the note added in proof.

The levels in ^{191}Ir of interest in the present work are shown in fig. 7. The spins of the levels are uniquely defined from the E2 multipolarity of the 220 and 268 keV transitions and the fact that the 659 keV level decays to the low-lying low-spin positive parity levels.

3.3. THE ^{189}Ir NUCLEUS

The 243.50 keV E2 transition and the 568.87 M1 transition have the same total intensity and are too strong to feed any of the known positive parity levels [8]). A 14 msec isomeric state has been identified at 372 keV [ref. [27])]. From the de-exciting M2 and E3 transitions it is clear that it is the $\frac{11}{2}^-$ state [refs. [9,13])]. As is seen in table 6 the summed intensities of the two isomeric transitions approximately equals the intensities of the 243 and 569 keV transitions, which suggests that the two latter transitions form a cascade feeding the $\frac{11}{2}^-$ state, see fig. 8. Support for this was obtained from a γ–γ coincidence experiment. A gate was set at the 243 keV line detected in a 2.9 cm^3

TABLE 6

Intensities of transitions associated with the $\frac{11}{2}^-$ isomeric level in ^{189}Ir

Transition energy (keV) [a])	Multi-polarity	Electron shell	Relative electron intensity [a])	Relative total transition intensity [b])
71.69	M2	L_I	47 ±4	170 ±14
258.37	E3	K	0.89±0.09	12.9± 1.3
71.69+258.37			Intensity sum	183 ±15
243.50	E2	K	9.2 ±0.7	203 ±14
568.87	M1	K	4.0 ±0.3	184 ±13

[a]) Experimental data from ref. [8]). [b]) See comment [b]) of table 5.

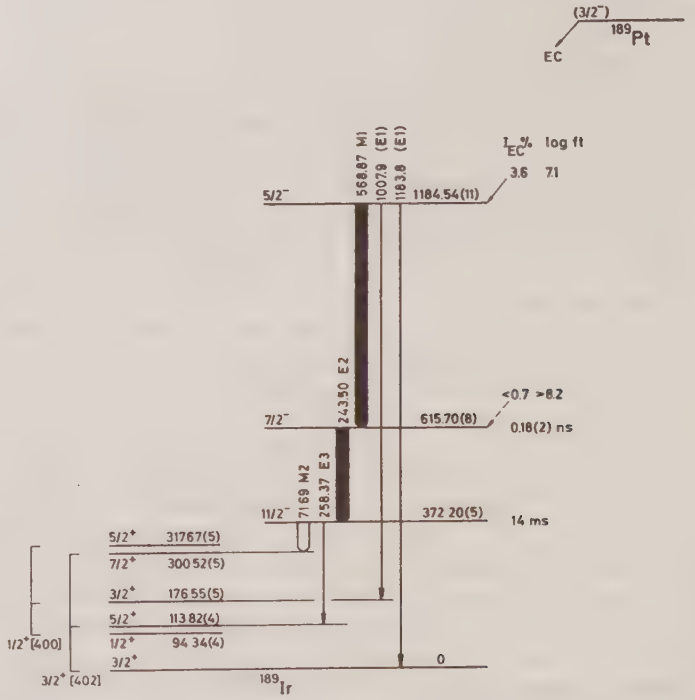

Fig. 8. Partial level scheme of ^{189}Ir obtained in present work (for a complete scheme of the positive parity levels see ref. [8])). The log *ft* value was calculated assuming 50 % feeding to the ground state and a decay energy of 2.0 MeV [ref. [46])]. For further explanations see caption of fig. 2.

Ge(Li) detector. The coincident spectrum detected in a 30 cm^3 detector, fig. 9, clearly shows strong coincidences with the 569 keV line but with no other line. Further sup-

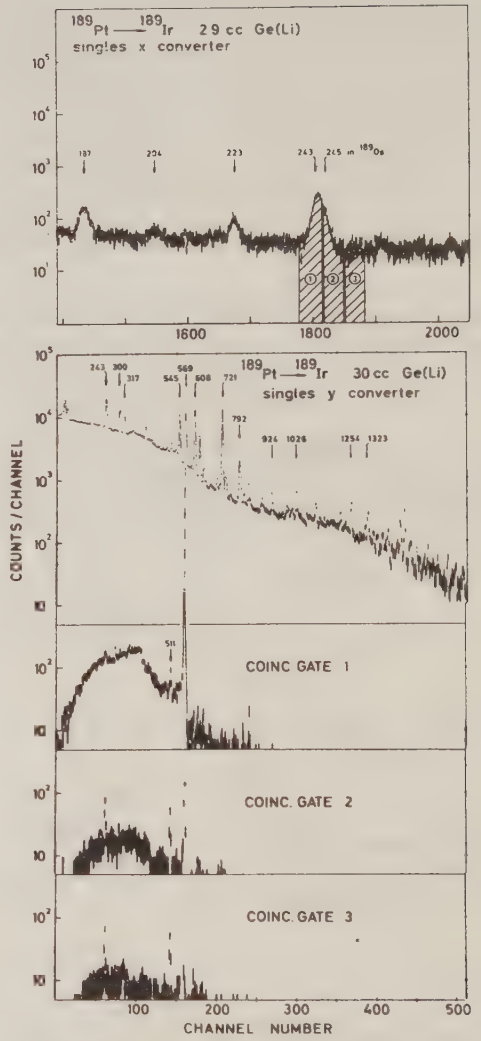

Fig. 9. Result of γ-γ coincidence measurement in ^{189}Ir using the experimental arrangement shown in fig. 1. The 30 cm^3 detector was shielded by 1 mm Pb. The hatched areas in the upper spectrum show the energy regions accepted in the gates. The 243 keV line is contaminated with the 245 keV line in the daughter decay ^{189}Ir → ^{189}Os, and therefore two separate gates were set at the composite peak in order to assign the coincidence effect to the right activity. The third gate was set at the background. The coincidence spectra were recorded during two days and show clearly that the 243 and 569 keV lines in ^{189}Ir are coincident.

port for the level scheme proposed in fig. 8 is obtained from two weak transitions fitting energetically from the 1185 keV state to two low-lying positive parity states.

In order to find out the order of the 243 and 569 keV transitions a delayed coincidence experiment was performed using the double lens spectrometer. One lens spectrometer focused the 243.5K c.e. line. For intensity reasons we preferred to detect the 568.9 keV γ-ray in the plastic scintillator mentioned above. Coincidences from the β–γ cascades from ^{60}Co were used to define the position and shape of a prompt decay curve obtained with the same energy settings. A set of delayed and prompt curves (in total 16 spectra) were collected over a period of 7 h. The momentum

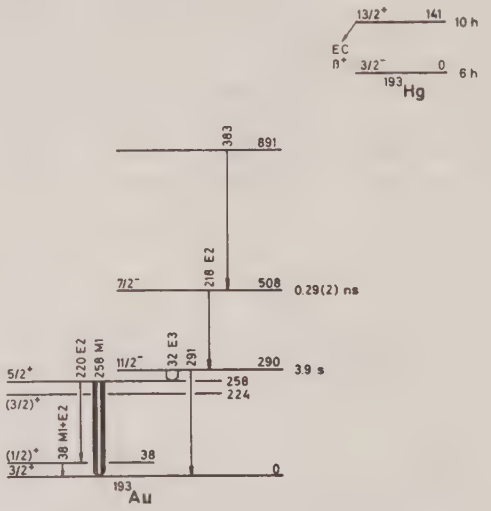

Fig. 10. Partial level scheme of ^{193}Au as obtained from refs. [14,28]). For further explanations see caption of fig. 2.

method clearly showed a systematic time shift between the delayed and prompt curves corresponding to a half-life of 0.14 ± 0.02 nsec for the 243 keV transition. As can be seen in fig. 5a a slight difference in the slope of two consecutive curves is also observed. The data were therefore also analysed with the convolution method [20]), which gave a half-life of 0.178 ± 0.012 nsec together with an indication of a spurious shift of 0.03 nsec in the first momentum of the delay curve. This constant shift is probably due to the different shapes of the energy spectra registered in the γ-channel and has to be corrected for. From our data we thus conclude that the half-life of the 615 keV level in ^{189}Ir is 0.18 ± 0.02 nsec.

Efforts have also been made to measure the half-life of the 1184 keV level in the same nucleus mainly fed in the EC decay of ^{189}Pt. One lens was focused at the 568.9K c.e. line while the other lens was set to accept the KLL Auger line group. Due to the

weak Auger yield in these nuclei the coincidence rate was low ($\approx$ 1 coincidences/min). To determine the shape and position of a prompt distribution we also recorded the β-94.7K cascade in the decay of ^{165}Dy. To be able to use the same energy settings in both measurements, 11 kV was added to the ^{165}Dy source. The result was analysed

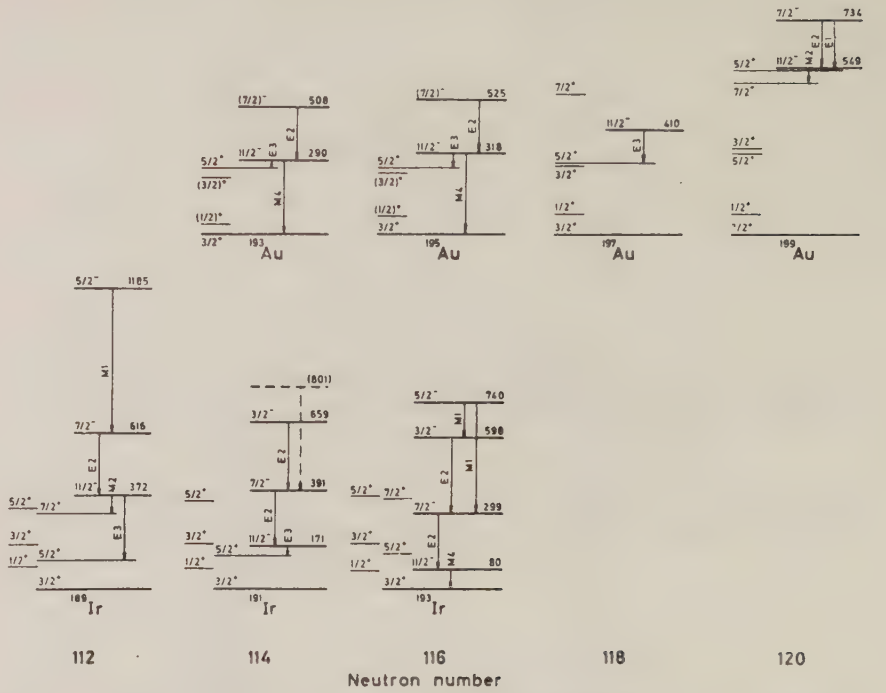

Fig. 11. Survey of negative parity levels in odd-mass Ir and Au nuclei. The data on the Ir nucleides are from the present work. The data on the Au nucleides are taken from refs. [14,28,33,46]).

with the momentum method. Within the statistical errors the prompt and delayed curves have both the same shape and position. From our experimental uncertainties we can set an upper limit for the half-life of the 1185 keV level in ^{189}Ir of < 80 psec.

Regarding the spin values of the 616 and 1185 keV levels the values given in fig. 8 are the only possible making the reasonable assumption that the energy fits of the 1008 and 1184 keV transitions are not accidental and that they are E1 transitions.

3.4. THE ^{193}Au NUCLEUS

Brunner *et al.* [14]) suggest a state at 508 keV in ^{193}Au that is fed by a 383 keV transition and de-excited via a 218 keV E2 transition to the $\frac{11}{2}^-$ isomeric level, see

fig. 10. We have verified the E2 character of the 218 keV transition in an experiment in which the strongest transitions from the decay of $^{193m+193}$Hg have been studied with the $\pi\sqrt{2}$ spectrometer and a Ge(Li) detector. No transitions could be found from the 508 keV level to the lower positive parity states [28]). We suggest that the 508 keV state is analogous to the 734 keV state in ^{199}Au and thus has $I^\pi = \frac{7}{2}^-$.

The half-life of the 508 keV level was determined from the delayed coincidence distribution observed between the feeding 383K and the de-exciting 218K c.e. lines focused in one lens spectrometer each. The β-238.6K cascade in the decay of ^{212}Pb was used to measure the shape and position of the corresponding prompt distribution. To be able to use the same energy settings in both measurements the ^{193}Hg decay electrons were pre-accelerated in a 8 kV electric field. An example of an observed delayed and prompt pair of decay curves is shown in fig. 5d. A difference in the slope of the two curves is evident. Several such pairs were measured and analysed both with the momentum as well as the convolution methods. Good agreement between the different methods was obtained the latter giving the best statistical accuracy. As a mean value we deduce a half-life of 0.29 ± 0.02 nsec for the 508 keV level in ^{193}Au.

A state similar to the 508 keV state in ^{193}Au has been suggested by Brunner *et al.* [ref. [14])] in ^{195}Au at 525 keV. However. no coincidences could be observed in the double lens spectrometer between the proposed 368 keV feeding transition and the 207 keV transition, which may be due to the weak intensity of these transitions. From internal conversion measurements the 207 keV transition was verified to be E2 [ref. [28])].

4. Discussion

A survey of the low-lying levels in odd-mass Au and Ir nuclei including the negative parity states discovered in this work is given in fig. 11. The results on the transition probabilities are given in tables 7 and 8. For simplicity we will discuss the levels in terms of the single-particle models for deformed and spherical nuclei including vibrations in a very qualitative way. However, more refined approaches have been developed for even nuclei in this mass region [29]), which may possibly give a more true description of the properties also of the odd-mass nuclei.

4.1. Au NUCLEI

The lowest positive parity states of the Au nuclei are generally believed to be describable in terms of the spherical shell model including coupling to the quadrupole vibration of the even core [30–33]). The Au nuclei have also on the basis of similarities in M1 and E2 transition rates in Au and Ir nuclei been suggested to be slightly deformed with $\delta \approx 0.09$ [ref. [34])]†. We note that while the energies of the positive parity levels in Ir nuclei fit well into the pattern of rotational bands, this interpreta-

† The large value of 2.94 $e^2 \cdot b^2$ reported [35]) for the 191 keV $\frac{3}{2}^+ \rightarrow \frac{1}{2}^+$ transition in ^{197}Au, which suggests rotational structure, is probably at least a factor of 8 too large [36, 37]).

TABLE 7

Transition probabilities and enhancement factors of E2 transitions in odd-mass Ir and Au nuclei

Nucleus	Level energy (keV)	$T_{\frac{1}{2}}$ level (nsec)	Initial state I^π	Final state I^π	Transition energy (keV)	Branching (%)	Total conversion coefficient [a])	B(E2) ($e^2 \cdot b^2$)	Enhancement factor [b])	B(M1) (μ_N^2)	F_N(M1) [b])
^{199}Au [c])	734.44	0.36 ± 0.04	$\frac{7}{2}^-$	$\frac{11}{2}^-$	185.80	66.7	0.50	0.32 ± 0.04	20		
^{193}Au	508	0.29 ± 0.02	$\frac{7}{2}^-$	$\frac{11}{2}^-$	218.07	100	0.282	0.31 ± 0.02	21		
^{193}Ir	299.45	0.19 ± 0.03	$\frac{5}{2}^-$	$\frac{11}{2}^-$	219.18	100	0.256	0.47 ± 0.08	31		
^{191}Ir	391.14	0.24 ± 0.02	$\frac{7}{2}^-$	$\frac{11}{2}^-$	219.74	100	0.254	0.37 ± 0.04	24		
	659.06	< 0.12	$\frac{9}{2}^-$	$\frac{7}{2}^-$	267.99	100	0.135	> 0.26	> 17		
^{189}Ir	615.70	0.18 ± 0.02	$\frac{7}{2}^-$	$\frac{11}{2}^-$	243.50	100	0.183	0.31 ± 0.03	21	> $2.6 \cdot 10^{-3}$	< $1.2 \cdot 10^3$
	1184.54	< 0.08			568.87	100	0.053				

All experimental data are from the present work except when otherwise stated.

[a]) Ref. [43]). [b]) Calculated relative the Weisskopf estimate [44]) including the statistical factor [45]). [c]) All data for ^{199}Au from ref. [33]).

TABLE 8

Retardation factors of E1 transitions in odd mass Ir and Au nuclei

Nucleus	Level energy (keV)	$T_{\frac{1}{2}}$ level (nsec)	Initial state I^π	Final state I^π	Transition energy (keV)	Branching (%)	Retardation factor F_w [a]	
^{199}Au [b]	734.44	0.36±0.04	$\frac{7}{2}^-$	$\frac{5}{2}^+$	191.59	27	6×10^4	
				$\frac{7}{2}^+$	240.9	< 0.6	$> 2 \times 10^5$	
				$\frac{3}{2}^+$	417.41	4.7	3.6×10^6	
^{193}Au	508	0.29±0.02	$\frac{7}{2}^-$	$\frac{5}{2}^+$	250	< 20 [c]	$> 1.5 \times 10^5$	
^{193}Ir	299.45	0.19±0.03	$\frac{7}{2}^-$	$\frac{5}{2}^+$	160.40	< 1.2	$> 4.1 \times 10^5$	
	598.26	(0.044) [d]	$\frac{3}{2}^-$	$\frac{3}{2}^+$	418.16	< 6	$> 4.0 \times 10^5$	[d]
				$\frac{5}{2}^+$	459.11			[e]
				$\frac{1}{2}^+$	525.3	5.6	$\approx 5.7 \times 10^5$	[d]
				$\frac{3}{2}^+$	598.6	0.3	$\approx 3.4 \times 10^6$	[d]
^{191}Ir	391.14	0.24±0.02	$\frac{7}{2}^-$	$\frac{5}{2}^+$	261.66	< 1.1	$> 1.6 \times 10^6$	
	659.06	< 0.12	$\frac{3}{2}^-$	$\frac{5}{2}^+$	307.8	< 1.1	$> 2.8 \times 10^6$	[f]
				$\frac{3}{2}^+$	479.9	4.8	$< 2.7 \times 10^4$	
				$\frac{5}{2}^+$	529.6	< 0.16	$> 1.0 \times 10^8$	[f]
				$\frac{1}{2}^+$	576.6	13	$< 8.7 \times 10^5$	
				$\frac{3}{2}^+$	659.2	1.6	$< 2.1 \times 10^6$	
^{189}Ir	615.70	0.18±0.02	$\frac{7}{2}^-$	$\frac{5}{2}^+$	308.0	< 0.7	$> 5 \times 10^6$	
				$\frac{7}{2}^+$	315.2	< 1.8	$> 7.3 \times 10^4$	
				$\frac{5}{2}^+$	501.9	< 0.7	$> 2.0 \times 10^7$	

All experimental data are from the present work except when otherwise stated.

[a]) Calculated relative to the Weisskopf estimate [44]) using the statistical factor [45]).

[b]) All data from ref. [33]).

[c]) Ref. [28]). Transition partly masked by strong 255 keV line in daughter decay.

[d]) Calculated value assuming the same enhancement factor of the 299 keV transition as for the 219 keV transition.

[e]) The line coincides with the strong 460 keV transition.

[f]) Although only an upper limit was measured for the 659 keV level the half-life of the level is not expected to be much shorter than the measured limit (0.085 nsec would give the same enhancement factor as found for the 219.7 keV transition). We therefore give the F_w factors of the unobserved 307.8 and 529.6 keV transitions as lower limits.

tion of the Au levels is less convincing. In the following we will assume the low-lying positive parity states in Au nuclei to be spherical.

The shell model predicts the $h_{\frac{11}{2}}$ state as a low-lying state in Au and it is accordingly natural to identify the $\frac{11}{2}^-$ state occurring in all Au nuclei as the $h_{\frac{11}{2}}$ state. (It should however be noted that Kisslinger and Sorensen [30]) predict a strong phonon admixture in the lowest $\frac{11}{2}^-$ state in ^{195}Au and ^{197}Au.)

The $\frac{7}{2}^-$ states in the Au nuclei are then naturally interpreted as the $\frac{7}{2}^-$ member of the multiplet obtained by coupling the $h_{\frac{11}{2}}$ particle to the quadrupole vibration of the even core. This is supported by the B(E2) values of the $\frac{7}{2}^- \rightarrow \frac{11}{2}^-$ transitions, which in fig. 12 are shown to be close to $B(\mathrm{E2}; 2^+ \rightarrow 0^+)$ in the neighbouring even nuclei. In fig. 13 the energies of the $\frac{7}{2}^- \rightarrow \frac{11}{2}^-$ transitions are compared to the 2^+ excitation of

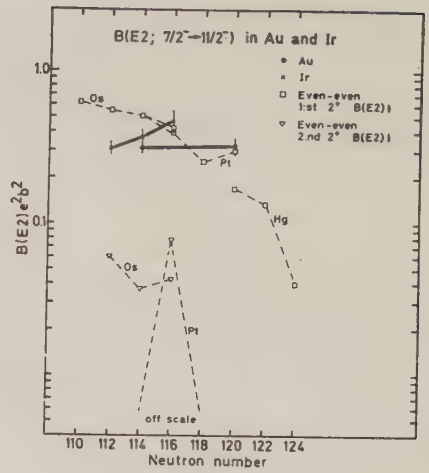

Fig. 12. Experimental values of $B(\mathrm{E2}; \frac{7}{2}^- \rightarrow \frac{11}{2}^-)$ in odd-mass Ir and Au nuclei. For comparison are shown $B(\mathrm{E2}; 2^+ \rightarrow 0^+)$ for the first two excited 2^+ states in the neighbouring even nuclei as taken from refs. [48, 49]).

the neighbouring even nuclei. It is seen that for the Au nuclei the $\frac{7}{2}^- \rightarrow \frac{11}{2}^-$ energy is lower than the 2^+ excitation energy of the core. This may be explained as due to a repulsion effect of higher-lying $\frac{7}{2}^-$ states.

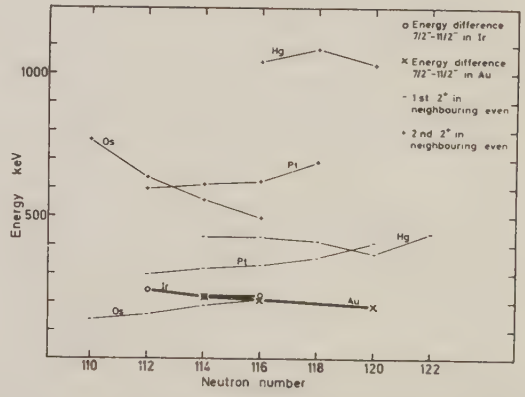

Fig. 13. Excitation energy of the $\frac{7}{2}^-$ state over the $\frac{11}{2}^-$ state in odd-mass Ir and Au nuclei. For comparison are shown the excitation energies of the first and second 2^+ states in the neighbouring even nuclei, ref. [46]).

4.2. Ir NUCLEI

The level structure of the low-lying positive parity states in Ir nuclei differs significantly from that of Au nuclei, since the levels may be arranged into rotational bands, cf. figs. 2, 7, 8. It has been shown [6–8]) that also the transition probabilities and magnetic moments of these states are in decent agreement with the Nilsson model, especially for ^{189}Ir, which in contrast to ^{191}Ir and ^{193}Ir has a well developed deformation of $\delta = 0.23$ [ref. [8])] compared to $\delta = 0.11$ for ^{191}Ir [ref. [7])] and $\delta = 0.13$ for ^{193}Ir [ref. [6])]. In the Nilsson model the $\frac{11}{2}^-$[505] orbital is expected at low excitation energy, and it seems natural to identify the $\frac{11}{2}^-$ state with this orbital.

For the $\frac{7}{2}^-$ state, however, no Nilsson orbital is available at low excitation energy, the lowest being the $\frac{7}{2}^-$[503], which for deformations of 0.12–0.20 is expected 1.5–2 MeV above the $\frac{11}{2}^-$ state [38]). The "compression" of the levels due to the pairing effect may decrease this energy by almost a factor of two [39]), but still this explanation of the $\frac{7}{2}^-$ level seems unlikely. Another possibility to obtain the $\frac{7}{2}^-$ state would be as the K-2γ-vibration based on the $\frac{11}{2}^-$ [505] orbital. We would then empirically expect the $\frac{7}{2}^-$ state to have an excitation energy above the $\frac{11}{2}^-$ state of a few hundred keV less than the γ-vibrational energy of the neighbouring even nuclei and $B(\mathrm{E2}; \frac{7}{2}^- \rightarrow \frac{11}{2}^-)$ to be about equal to $B(\mathrm{E2}; 2^{+\prime} \rightarrow 0^+)$, $2^{+\prime}$ denoting the second 2^+ state in the neighbouring even nuclei. Inspecting figs. 12 and 13 we see that, while the energies may not be unreasonable, the experimental values of $B(\mathrm{E2}; \frac{7}{2}^- \rightarrow \frac{11}{2}^+)$ are an order of magnitude too large to correspond to this interpretation.

Both the B(E2) values and the energies instead suggest that the $\frac{7}{2}^-$ states in the Ir nuclei have the same nature as the $\frac{7}{2}^-$ state in the Au nuclei, i.e. as resulting from a coupling between the $\frac{11}{2}^-$ particle state and the *first* 2^+ *excitation of a spherical even core*, cf. figs. 12 and 13. This implies that while the odd-mass Ir nuclei in their low-spin positive parity states are deformed, they are essentially spherical in the $\frac{11}{2}^-$ and $\frac{7}{2}^-$ states. This may not be unreasonable, since the potential energy minimum calculated for even Os nuclei is rather shallow [29]) and the difference in the specialization energies for different spins may be large enough to shift the equilibrium state from deformed to spherical. Regarding the nature of the $\frac{11}{2}^-$ state, one should also note that according to the Nilsson diagrams the $\frac{11}{2}^-$[505] orbital should be found closer to the $\frac{3}{2}^+$[402] and $\frac{1}{2}^+$[400] orbitals the larger the deformation, while the opposite trend is found experimentally cf. fig. 11.

It is reasonable that the proposed change in equilibrium deformation would give rise to retardation effects in the electromagnetic transitions leading to the positive parity levels. In table 9 we have compiled the available data on the isomeric transitions. It is seen that the M4 transition is an order of magnitude slower in ^{193}Ir than in the Au nuclei. The M2 and E3 transitions can be expected to be retarded also in the spherical Au nuclei. Still the M2 transition is an order of magnitude slower in ^{189}Ir than in ^{199}Au, the former transition being almost the slowest M2 observed [40]). On the other hand the E3 transitions are not particularly retarded in the Ir nuclei, in average they are a factor of 5 faster than in the Au nuclei, so no conclusive

TABLE 9

Isomeric transitions in odd-mass Au and Ir nuclei

Nucleus	$T_{\frac{1}{2}}$ of level (sec) [a])	Initial state I^π	Final state I^π	Transition energy (keV) [a])	Multipolarity	Relative intensity [a])	Total conv. coeff. [b])	F_w [c])
^{199}Au	4.4×10^{-4} [d])	$\frac{11}{2}^-$	$\frac{7}{2}^+$	55.15 [e])	M2	100 [e])	6.0×10^2	220
^{197}Au	7.2	$\frac{11}{2}^-$	$\frac{3}{2}^+$	103.2	E3	100	3.00×10^1	423
^{195}Au	31	$\frac{11}{2}^-$	$\frac{5}{2}^+$	56.7	E3	99 [f])	1.87×10^2	562
			$\frac{3}{2}^+$	318.5	M4	0.93 [f])	1.22×10^5	0.35
^{193}Au	3.9	$\frac{11}{2}^-$	$\frac{5}{2}^+$	32.3	E3	99.5	1.45×10^4	37.5
			$\frac{3}{2}^+$	291	M4	0.5	2.77×10^5	0.05
^{193}Ir	1.03×10^6	$\frac{11}{2}^-$	$\frac{3}{2}^+$	80.27 [g])	M4	100	2.18×10^4	2.53
^{191}Ir	4.9	$\frac{11}{2}^-$	$\frac{5}{2}^+$	41.92 [h])	E3	100	1.69×10^4	53
^{189}Ir	1.4×10^{-2}	$\frac{3}{2}^-$	$\frac{7}{2}^+$	71.69 [i])	M2	93 [i])	7.5×10^1	3450
			$\frac{5}{2}^+$	258.37 [i])	E3	7.0 [i])	8.8×10^{-1}	80

[a]) Taken from ref. [46]) except when otherwise stated.
[b]) Ref. [43]).
[c]) Hindrance factor relative the Weisskopf estimate [44]) including the statistical factor [45]).
[d]) Ref. [47]).
[e]) Ref. [33]).
[f]) Ref. [28]).
[g]) Present work.
[h]) Ref. [25]).
[i]) Ref. [8]).

evidence on "shape isomerism" is obtained from the isomeric transitions.

In general the $\frac{7}{2}^-$ states in both the Ir and Au nuclei may decay also via an E1 transition to the lowest $\frac{5}{2}^+$ state. In table 8 we give the retardation factors F_w for all E1 transitions possible. It is seen that on average F_w is at least one order of magnitude larger in ^{189}Ir than in ^{199}Au, which may be caused by the suggested change in deformation.

Additional negative parity states with spin $\frac{3}{2}$ are found in ^{191}Ir and ^{193}Ir, and $\frac{5}{2}$ states in ^{189}Ir and ^{193}Ir. The $\frac{3}{2}^-$ states have an excitation energy above the $\frac{11}{2}^-$ state of about twice the $\frac{7}{2}^- \rightarrow \frac{11}{2}^-$ energy difference and are de-excited mainly to the $\frac{7}{2}^-$ states via an E2 transition. The measured upper limit of the half-life for this transition in ^{191}Pt corresponds to an enhancement factor > 17, which is almost as large as the value found for the $\frac{7}{2}^- \rightarrow \frac{11}{2}^-$ transition. It therefore seems natural to interpret these states as the $\frac{3}{2}^-$ member of the multiplet obtained by coupling the $\frac{11}{2}^-$ particle to two quanta of the excitation mode of the even core.

One may note the extremely high log ft of > 10 for the allowed β-transition to the $\frac{3}{2}^-$ state in ^{193}Ir. This is larger than any value for allowed transitions found in the compilation by Gleit *et al.* [41]).

The E1 transitions from the $\frac{3}{2}^-$ states in all three Ir nuclei are in general fairly strongly retarded, see table 8, which is not in contradiction to the suggestion of a structure similar to that of the $\frac{7}{2}^-$ states.

Also the $\frac{5}{2}^-$ states observed in ^{189}Ir (fig. 8) and ^{193}Ir (fig. 2) we suggest to have a spherical character, since they prefer the negative parity states in their decay. The nature of these states is not clear but one may conjecture that the $\frac{5}{2}^-$ member of the two-quantum multiplet is a strong component.

Finally we note that both a $\frac{7}{2}^-$ and a $\frac{3}{2}^-$ state are available at fairly low excitation energy if a not too large oblate deformation is assumed. However, in that case it seems difficult to account for the observed level order, but one cannot neglect the possibility that the experimental data could be reproduced if a strong coupling is assumed between the Nilsson orbitals branching off from the $h_{\frac{11}{2}}$ shell-model state.

5. Conclusion

The experimental data on the negative parity states observed in the present work suggest in ^{189}Ir and possible also in ^{191}Ir and ^{193}Ir a definitely smaller deformation for these states than for the positive parity states in these nuclei.

It has been pointed out by Soloviev [50]) that the deformation in an excited state can be smaller than in the ground state if the Nilsson orbital corresponding to the excited particle rises rapidly. This may be the explanation of the situation in the Ir nuclei since the $\frac{11}{2}^-$[505] particle state rises strongly with the deformation.

We are indebted to Dr. Arve Kjelberg and his co-workers in the Nuclear Chemistry Group at CERN for all the trouble they have taken in supplying us with the radioactive sources from ISOLDE.

Note added in proof. Recent coincidence studies [51]) of the decay ^{191}Pt → ^{191}Ir has revealed a 140.5 keV transition in coincidence with both the 220 and 268 keV transitions. This definitely establishes the 800.6 keV level in ^{191}Ir, cf. fig. 7. In fact the 140.5 keV line can be seen in the two coincidence spectra of fig. 6, but it was erroneously interpreted as the very close-lying but weaker Compton scattering lines of the 360 and 410 keV transitions, respectively.

References

1) F. C. Perry and E. S. Murphy, Jr., Nucl. Phys. **A99** (1967) 497
2) R. Avida, J. Burde, A. Molchadzki and Z. Beraut, Nucl. Phys. **A114** (1968) 365
3) Z. Plajner, V. Brabec, L. Maly and M. Vejs, Nucl. Phys. **A121** (1968) 367
4) R. H. Price, M. W. Johns, N. M. Ahmed and E. E. Habib, Can. J. Phys. **47** (1969) 727
5) C. R. Cothern, H. J. Hennecke, J. C. Manthuruthil and R. C. Lange, Phys. Rev. **182** (1969) 1286
6) V. Berg, S. G. Malmskog and A. Bäcklin, Nucl. Phys. **A143** (1970) 177
7) S. G. Malmskog, V. Berg, A. Bäcklin and G. Hedin, Nucl. Phys. **A143** (1970) 160
8) A. Bäcklin, S. G. Malmskog and V. Berg, Nucl. Phys., to be published
9) B. Harmatz, T. H. Handley and J. W. Mihelich, Phys. Rev. **128** (1962) 1186
10) P. H. Blichert-Toft, E. G. Funk and J. W. Mihelich, Nucl. Phys. **77** (1966) 513
11) M. Schumacher, R. Schöneberg and A. Flammersfeld, Z. Phys. **191** (1966) 343
12) M. Schumacher and H. Langhoff, Phys. Rev. **162** (1967) 1152
13) H. R. Lewis, R. A. Naumann, J. M. Prospero and D. Thomas, Phys. Rev. **134** (1964) B322
14) J. Brunner, J. Halter and P. Scherrer, Helv. Phys. Acta **31** (1958) 335
15) G. Bäckström, A. Bäcklin, N. E. Holmberg and K. E. Bergkvist, Nucl. Instr. **16** (1962) 199
16) A. Bäcklin, Nucl. Instr. **53** (1967) 177
17) B. Fogelberg and A. Bäcklin, to be published
18) T. R. Gerholm and J. Lindskog, Ark. Fys. **24** (1963) 171
19) S. G. Malmskog, Ark. Fys. **35** (1967) 255
20) T. Sundström, Nucl. Instr. **16** (1962) 153
21) L. Boström and B. Olsen, Nucl. Instr. **44** (1966) 61
22) A. Kjelberg and G. Rudstam eds., CERN report CERN 70-3 (1970)
23) K. Maack Bisgård and R. J. Hanson, Nucl. Phys. **A125** (1969) 305
24) Nuclear Data Sheets, National Academy of Sciences, Washington, DC
25) S. G. Malmskog and A. Bäcklin, Ark. Fys. **39** (1969) 411
26) B. Svahn, A. Johansson, B. Nyman, G. Malmsten and H. Pettersson, Z. Phys. **210** (1968) 466
27) V. V. Remaev, V. T. Gritsyna and Y. S. Korda, JETP (Sov. Phys.) **17** (1963) 775
28) B. Fogelberg, A. Bäcklin and S. G. Malmskog, unpublished results
29) K. Kumar and M. Baranger, Nucl. Phys. **A122** (1968) 273
30) L. S. Kisslinger and R. A. Sorensen, Rev. Mod. Phys. **35** (1963) 853
31) A. de-Shalit, Phys. Rev. **122** (1961) 1530
32) A. Braunstein and A. de-Shalit, Phys. Lett. **1** (1962) 264
33) A. Bäcklin, B. Fogelberg and S. G. Malmskog, Nucl. Phys. **A103** (1967) 337
34) E. E. Berlovich, Sov. J. Nucl. Phys. **5** (1967) 705
35) K. G. Prasad, R. P. Sharma and B. V. Thosar, Conf. on the properties of nuclear states, Montreal, 1969, contribution 2.62
36) B. Fogelberg and A. Bäcklin, unpublished results
37) R. P. Sharma, private communication
38) S. G. Nilsson, Mat. Fys. Medd. Dan. Vid. Selsk. **29** (1955) nr. 16
39) C. W. Reich and M. E. Bunker, Bull. Acad. Sci. USSR (phys. ser.) **31** (1967) 46
40) M. Goldhaber and A. W. Sunyar, in Alpha-, beta- and gamma-ray spectroscopy, ed. K. Siegbahn (North-Holland, Amsterdam, 1965) ch. 18
41) C. E. Gleit, C. W. Tang and C. E. Coryell, Nuclear Data Sheets 5-5 (1963), National Academy of Sciences, Washington, DC

42) A. Johansson, B. Nyman, G. Malmsten and S. E. Karlsson, Nucl. Phys. **A98** (1967) 278
43) R. S. Hager and E. S. Seltzer, Calt-63-60 (1967)
44) A. H. Wapstra, G. J. Nijgh and R. van Lieshout, Nuclear spectroscopy tables (North-Holland, Amsterdam, 1959)
45) S. Moszkowski, in Alpha-, beta- and gamma-ray spectroscopy, ed. K. Siegbahn (North-Holland, Amsterdam, 1965) ch. 16
46) C. M. Lederer, J. M. Hollander and I. Perlman, Table of isotopes (Wiley, New York, 1967)
47) J. Borggreen and R. A. Naumann, Nucl. Phys. **A115** (1968) 14
48) P. H. Stelson and L. Grodzins, Nuclear Data **A1** (1965) 21
49) A. Marelius, P. Sparrman and T. Sundström, Appendix D in Hyperfine structure and nuclear radiations, ed. E. Matthias and D. Shirley (North-Holland, Amsterdam, 1968)
50) V. G. Soloviev, Phys. Lett. **21** (1966) 311
51) A. Bäcklin, G. Hedin and S. G. Malmskog, to be published

R E F E R E N C E 15

ON THE LOW-ENERGY BAND STRUCTURE IN ^{187}Os

S.G. MALMSKOG and V. BERG

AB Atomenergi, Studsvik, Nyköping, Sweden

and Institute of Physics, University of Stockholm, Sweden

B. FOGELBERG and A. BÄCKLIN

Swedish Research Council's Laboratory, Studsvik, Nyköping, Sweden

1.E.1:
3.A

Nuclear Physics **A166** (1971) 573—593; © *North-Holland Publishing Co., Amsterdam*

Not to be reproduced by photoprint or microfilm without written permission from the publisher

ON THE LOW-ENERGY BAND STRUCTURE IN ^{187}Os

S. G. MALMSKOG and V. BERG
AB Atomenergi, Studsvik, Nyköping, Sweden
and Institute of Physics, University of Stockholm, Sweden

B. FOGELBERG and A. BÄCKLIN
Swedish Research Council's Laboratory, Studsvik, Nyköping, Sweden

Received 26 October 1970
(Revised 22 January 1971)

Abstract: The level structure of ^{187}Os has been investigated in the decay of ^{187}Ir (11 h) produced in 600 MeV proton spallation at CERN and mass-separated in the ISOLDE on-line facility. Special emphasis has been put on the study of absolute transition rates from low-lying levels in ^{187}Os by means of high-resolution electron and γ-ray spectroscopy and half-life measurements using the delayed-coincidence technique. The observed transition rates have been used to assign Nilsson quantum numbers to different levels. The large B(E2) values for some interband transitions have been accounted for through a Coriolis coupling calculation. Through an extensive investigation of the γ-ray spectrum from ^{187}Ir three new levels at 190.70, 332.94 and 586.40 keV have been proposed.

E RADIOACTIVITY ^{187}Ir [from Pb(p, spallation)], measured E_γ, I_γ, E_{ce}, I_{ce}, cece-delay. ^{187}Os deduced levels, $T_{\frac{1}{2}}$, J, π, cc, multipolarities, partial half-lives. Isotope separated sources. Ge(Li) detectors.

1. Introduction

In a recent paper [1]) we have investigated the low-energy level structure of ^{189}Os with special emphasis on determining absolute transition probabilities. From that investigation we concluded that both the electric and magnetic properties for the lowest-lying states could be reasonably well accounted for with the formalism of the Nilsson model [2]), using a deformation parameter $\delta = 0.1$ and a strong mixing of rotational bands.

As a natural extension of that work we have investigated the electric and magnetic properties of the low-lying states in ^{187}Os populated in the decay of ^{187}Ir. The main information on this decay up to now was obtained in the conversion electron studies of Harmatz *et al.* [3]). In the present work, an extensive study has been made of the γ-rays emitted in the same decay. Special attention was given to the transition rates between the low-lying states in order to distinguish between collective and single-particle transitions. With this information, rotational bands similar to those suggested in ^{189}Os could be constructed. The experiments included high-resolution conversion electron measurements to obtain multipole mixing ratios, and half-life measurements

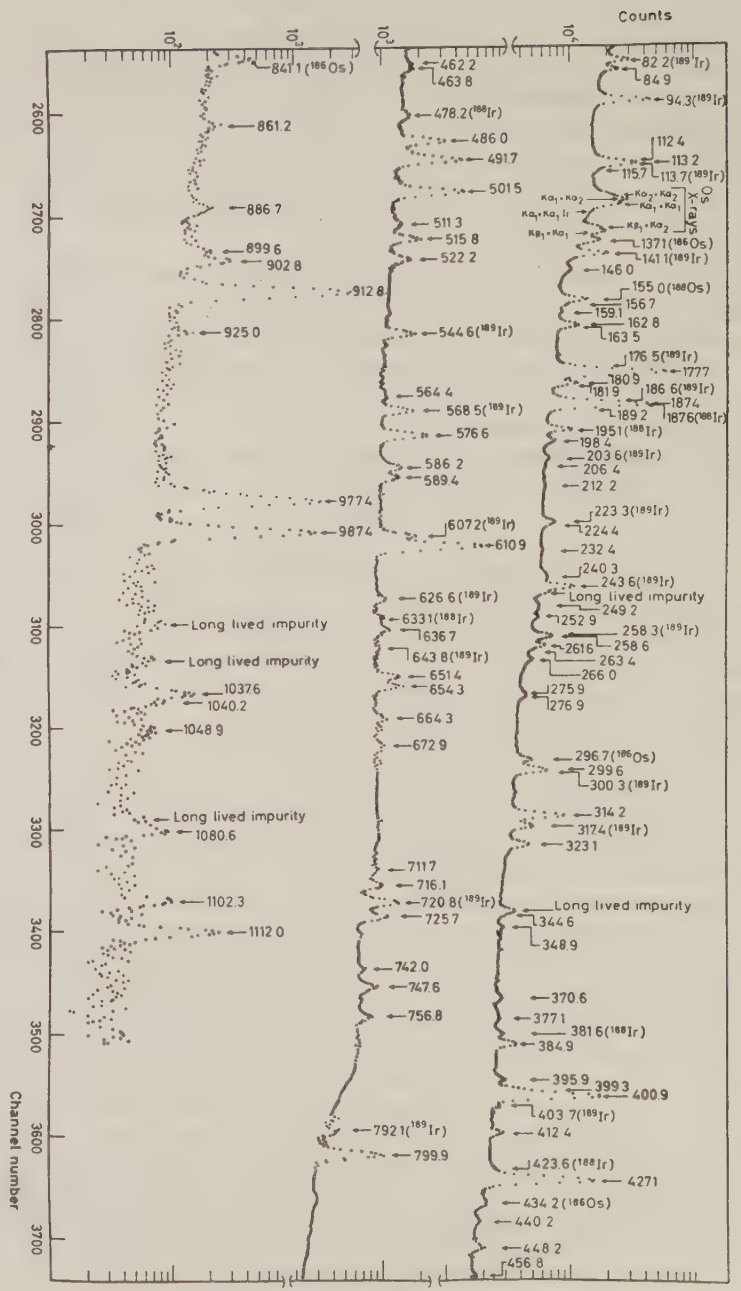

Fig. 1. The γ-ray spectrum of ^{187}Ir as observed with a 2 cm^3 Ge(Li) detector.

using the delayed coincidence technique. The deduced absolute transition probabilities have been compared with the Nilsson model calculations. To account for the strong interband B(E2) values, it is necessary to assume strong Coriolis mixing of the bands [4]).

2. Experimental procedure

2.1. SOURCE PREPARATION

We have investigated ^{187}Os via the decay of ^{187}Ir (11 h). This activity was obtained as a decay product of ^{187}Hg, produced from spallation in a molten lead target at 700 °C when bombarded in the external beam of 600 MeV protons from the synchrocyclotron at CERN. The extracted mercury was isotopically separated in the on-line mass-separator facility ISOLDE [5]) and collected on a 0.9 mg/cm^2 nickel foil, which served as backing in all the measurements described below. The sources were usually collected for 10–15 h, and, due to the transport time between Geneva and Studsvik, measurements were never started before 15 h after the end of irradiation.

2.2. GAMMA-RAY MEASUREMENTS

The γ-ray spectrum in the decay of ^{187}Ir was observed in a 2 cm^3 Ge(Li) detector having an energy resolution of 1.2 keV at 122 keV. A 4096-channel spectrum obtained using this detector is shown in fig. 1. The activity was followed for several half-lives to be able to assign the observed peaks to the ^{187}Ir decay. All of the data were analysed with a computer program [6]) to obtain the positions and areas of the observed peaks. From the analysis it turned out that besides the ^{187}Ir activity the source also contained contributions from the A = 186, 188 and 189 mass chains. The reason for this is that it is rather difficult to have stable conditions on the ISOLDE separator

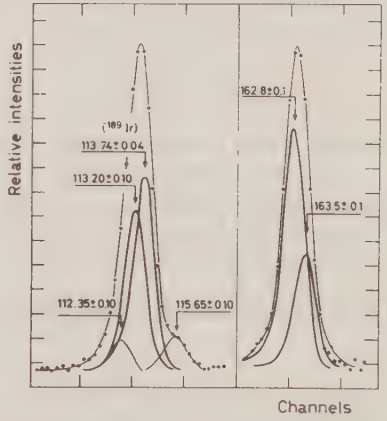

Fig. 2. The complex γ-ray peaks near 113 and 168 keV, resolved into their components using a computer. For further details see subsect. 2.2.

over the comparatively long collection times used in these experiments, especially as other groups were usually working in parallel on the separator, collecting short-lived activities of nearby masses. Of the observed contaminants the ^{186}Ir and ^{189}Pt activities have about the same half-lives as ^{187}Ir. From parallel studies of these former activities [7]) we have, however, been able to subtract the influence from these sources before determining the γ-ray energies and intensities in the decay of ^{187}Ir. The final results are given in table 1. When the broad peaks at about 125 and 131 keV were resolved into their components it was observed that both their energies and intensities were well accounted for by assigning these as sum peaks of the strong X-ray components. This is in agreement with the observation that the relative intensities of these peaks compared to other lines changed with the geometry of the source and detector.

In several other cases lines were so close that they were only partly resolved by the detector. Two such cases are shown in fig. 2. Here the energies of the transitions were known from the electron measurements (see below and ref. [3])). The computer was then used to fit appropriate components, with a given position and shape (taken from nearby single peaks), into the observed curves. As a demonstration of the accuracy of this procedure, we can point to the fact that the intensity ratio between the two contaminant 113.74 and 94.3 keV transitions in ^{189}Ir was obtained correctly to within 5 % of the value observed in a separate investigation of the ^{189}Pt decay [7]). No earlier extensive measurement of the γ-ray intensities in the decay of ^{187}Ir has been reported in the literature. A series of measurements with a small Ge(Li) detector has, however, been performed at CERN [ref. [8])]. In cases where a comparison can be made, their preliminary data are in reasonable agreement with our values.

2.3. CONVERSION ELECTRON MEASUREMENTS

Most of the previous information on the conversion electrons emitted in the decay of ^{187}Ir is from the measurements of Harmatz, Handley and Mihelich [3]) and Emery *et al.* [9]). There seemed, however, to be reasons for a remeasurement of parts of this conversion electron spectrum since the work of ref. [9]) is incomplete, especially below 100 keV, and since the measurements reported by ref. [3]) have been shown to exhibit large systematic intensity errors [1]) in, for instance, the decay of ^{189}Ir. Also, a check of the isotopic identity of earlier-measured lines could be obtained by using the isotope-separated sources from ISOLDE instead of sources separated by chemical means.

The present measurements, which in particular deal with L and M subshell ratios of low-energy transitions in ^{187}Os, were performed with the $\pi\sqrt{2}$ double-focusing beta spectrometer in Studsvik [10,11]). The mass-separated sources were very suitable for conversion electron spectroscopy due to their almost negligible thickness, but the rather large geometrical extension of the sources made it necessary, in order to obtain a high enough resolution, to screen the source with a slit 2 mm wide, through which the electrons had to pass before entering the optical system of the spectrometer. With this arrangement a momentum resolution of 0.2 % could be used.

TABLE 1

Transition energies and intensities in the decay of ^{187}Ir

Transition energies			Intensities		α_K	Multipolarity from α_K
present work	Harmatz *et al.* [3])	Emery *et al.* [9])	γ-lines [a])	K lines [b])		
9.75±0.03	9.8					
25.62±0.05	25.5					
64.59±0.03	64.55					
65.31±0.03	65.3	65.15±0.15				
74.30±0.03	74.35	73.67±0.10				
75.03±0.03	75.05					
84.88±0.05	84.9	85.00±0.07	2.2 ±0.2			
87.62±0.10	87.1		< 0.10	137 [c])	> 0.49	
	90.7		< 0.17	< 135 [c])		
112.35±0.10	112.4		1.1 ± 0.3			
113.20±0.10	113.15		5.8 ± 1.0	167 [c])	1.02	M1+E2
115.65±0.10	115.65		1.2 ± 0.2	40	1.16	M1+E2
146.04±0.20			0.7 ± 0.1			
	150.05		< 0.1			
156.66±0.10	156.6		0.87± 0.10	220 [c])	9.0	M2
159.08±0.20			0.31± 0.05			
162.80±0.15	162.8	162.59±0.21	2.8 ± 0.6	62	0.79	M1
163.50±0.15	163.5		1.4 ± 0.3	36	0.92	M1
	170.4		< 0.1			
177.67±0.10	177.7	177.49±0.11	55.5 ± 3.5	970 [c])	0.62	M1+E2
180.90±0.15	180.9		4.2 ± 0.5	25	0.21	E2
	181.85		< 1.2	10	> 0.30	M1+(E2)
187.44±0.10	187.5	187.08±0.15	35.5 ± 3.0	160 [c])	0.16	E2
	189.2		< 0.8	3	> 0.13	E2 or M1
198.40±0.10	198.7		1.46± 0.16	≈ 22	≈ 0.54	M1
206.4 ±0.3	206.9		0.12± 0.03	2.7	0.80	M1
212.21±0.10			0.29± 0.05			
224.40±0.20	224.4		0.6 ± 0.2	≈ 14	≈ 0.83	M1
232.38±0.15			0.46± 0.08			
240.29±0.25			1.9 ± 0.2			
249.17±0.25			2.0 ± 0.2			
253.10±0.20	252.9		1.9 ± 0.2	11.5	0.22	M1
258.60±0.10	258.45		5.2 ± 0.6	< 64	< 0.43	M1 or E2
261.55±0.10	261.5		4.2 ± 0.4	32	0.27	M1
	263.4		< 0.44	3	> 0.24	M1
265.97±0.10	266.3		1.8 ± 0.2	5.4	0.107	(E2)
275.92±0.25	275.95		0.8 ± 0.2	5.2	0.23	M1
276.89±0.25	276.6		1.3 ± 0.2	weak		(E2)
299.60±0.20	299.5		2.8 ± 0.7	25	0.32	M1
314.19±0.15	313.95	313.83±0.12	19.3 ± 1.5	100	0.185	M1
323.13±0.20			5.7 ± 0.4			
344.6 ±0.2	344.6		0.6 ± 0.2	4.4	0.26	M1
348.87±0.20	348.2		0.8 ± 0.2	5	0.22	M1
370.59±0.20	370.1		1.6 ± 0.2	5.5	0.12	M1
377.12±0.20			1.17± 0.16			
384.91±0.15			6.5 ± 0.5			
395.94±0.15	395.6		2.5 ± 0.3	7.5	0.107	M1
399.30±0.25	398.7	399.22±0.23	5.1 ± 2.0	19	0.13	M1
400.88±0.25	400.7	400.85±0.15	82.7 ± 3.5	67	0.029	E2
412.40±0.15			5.0 ± 0.4			
	426.4			weak		
427.08±0.15	427.1	426.92±0.14	87.5 ± 4.0	≈ 175	≈ 0.072	M1
440.15±0.20			1.21± 0.18			
448.19±0.15	447.6		2.6 ± 0.3	5.4	0.074	M1
456.75±0.20			0.94± 0.13			
462.20±0.40			1.2 ± 0.3			
463.80±0.40			2.3 ± 0.5			
485.96±0.10	486.1		15.7 ± 1.8	9	0.020	E2
491.73±0.10	491.7	491.14±0.25	28.8 ± 2.6	33	0.041	M1
501.53±0.10	501.4	501.50±0.17	31.3 ± 2.7	39	0.045	M1
511.33±0.20			2.4 ± 0.4 [d])			
515.79±0.15	515.5		7.8 ± 0.6	10.5	0.047	M1
522.21±0.15	522.0		5.5 ± 0.5	7.5	0.048	M1
564.42±0.25			1.4 ± 0.2			
576.59±0.10	576.7	576.47±0.39	17.1 ± 1.5	15.5	0.033	M1
586.24±0.15	586.7		6.2 ± 0.5	4.6	0.027	M1
589.42±0.15	588.9		5.9 ± 0.5	3.6	0.022	M1+(E2)
610.88±0.10	610.9	610.59±0.37	79.5 ± 6.5	59	0.027	M1
636.48±0.20	636.8		3.8 ± 0.4	< 5	< 0.047	M1 or E2
651.39±0.15	651.5		8.0 ± 0.7	4	0.018	M1+(E2)
654.31±0.15	654.35		8.5 ± 0.8	5	0.021	M1
664.31±0.15			2.9 ± 0.3			
672.87±0.20			2.5 ± 0.3			
711.67±0.20			1.7 ± 0.2			
716.10±0.15	715.9		4.9 ± 0.4	3	0.022	M1
725.73±0.15	725.65		10.3 ± 0.8	2.6	0.009	E2
742.04±0.20			1.02± 0.14			
747.57±0.15	747.4		5.1 ± 0.4	2.6	0.018	M1
756.81±0.20	757.05		2.9 ± 0.3	2.4	0.029	M1
	760.3		< 0.4	≈ 0.7	> 0.062	(M1, M2)
799.90±0.15	800.2	799.36±0.73	17.8 ± 1.6	6.6	0.013	M1
861.20±0.20			2.0 ± 0.2			
886.67±0.20	886.9		2.6 ± 0.3	weak		
899.60±0.25			2.7 ± 0.3			
902.82±0.15	903.1		6.4 ± 0.5	2.1	0.012	M1
912.82±0.10	912.8	912.59±0.42	100	23	0.0081	M1+(E2)
924.77±0.20			0.86± 0.12			
977.39±0.15	978.0	976.74±0.50	61.2 ± 5.3	10.3	0.0060	M1+E2
987.25±0.15	987.9	987.03±0.43	55.0 ± 5.0	10.7	0.0071	M1+(E2)
1037.6±0.2			4.7 ± 0.6			
1040.2±0.3			1.7 ± 0.3			
1048.9±0.3			0.73± 0.25			
1080.6±0.2			2.7 ± 0.4			
1102.3±0.2	1102.8		2.9 ± 0.4	weak		
1112.0±0.2	1112.1		10.6 ± 1.2	1.5	0.0051	E2

[a]) Present work.
[b]) K conversion line intensities taken from ref. [3]) unless otherwise stated.
[c]) Present work with a normalization to the data of ref. [3]) at 187.44 keV.
[d]) Could also contain contamination from annihilation radiation.

TABLE 2

Low-energy conversion electron data from the decay $^{187}Ir \rightarrow {}^{187}Os$

Transition energy (keV)	Electron intensities (with errors in %)							Multipolarity
	K	L_I	L_{II}	L_{III}	M_I	M_{II}	M_{III}	
9.75±0.03					350 [a])	32 (30) [a])	< 7	M1+ < 0.02 % E2
25.62±0.05		253 (10)	20 (30)	< 4.5	75 (10)	7.5 (30)	< 3	M1+ < 0.05 % E2
64.59±0.03		19.5 (15)	3.2 (30)	1.4 (20)				$M1+(1.7^{+0.6}_{-0.5})$ % E2
65.31±0.03		5.2 (30)	89 (9)	100 [b])				E2+ < 15 % M1
74.30±0.03		26 (15)	2.3 (30)	< 2.0				M1+ < 1.0 % E2
75.03±0.03		< 1.5	29.5 (25)	33 (10)				E2+ < 10 % M1
84.88±0.05 [c])				< 1.0				
87.62±0.10	4.1 (60)	< 0.8	< 0.8	< 0.8				
90.7	< 4.0	< 0.08	< 0.8	< 0.8				
112.35±0.10		< 0.25		0.31 (30)				E2+ < 50 % M1
113.20±0.10	5.0 (60)	1.3 (25)	2.5 (12)	1.8 (15)				$M1+(45^{+6}_{-10})$ % E2
115.65±0.10		0.5 (40)						
156.66±0.10	6.6 (25)	2.3 (15)	0.65 (30)	0.9 (30)				M2
177.67±0.10	29 (10)	5.0 (10)	1.3 (25)	0.9 (25)				M1+(20±5) % E2
187.44±0.10	4.8 (15)							E2+ < 10 % M1

[a]) An additional estimated uncertainty of 30 % should be used when comparing these values with those of other transitions.
[b]) Normalization value.
[c]) Energy from the γ-ray measurement.

The electron detector was a GM counter with a window consisting of 0.6 mg/cm^2 aluminized melinex foil, which had a cut-off energy of about 15 keV and 70 % transmission of 23 keV. A 15 kV pre-acceleration was thus necessary in order to measure the M conversion lines of the 9.75 keV transition, which have electron energies down to 6.7 keV. An acceleration voltage was also applied to the source when L and M conversion lines of the 25.62 keV transition were measured. The high voltage was not found to change the optical properties of the spectrometer. The uncertainty in the intensity measurements due to window absorption is negligibly small.

Broadening and "tailing" of conversion electron lines due to the finite thickness of the sources were observed only for the M lines of the 9.75 keV transition and the L lines of the 25.62 keV transition. It turned out that these effects were serious, with a severe distortion of the 9.75 M line shape in the cases when Al foils were used as

Fig. 3. Some of the measured conversion electron lines in ^{187}Os. The points have not been corrected for the decay. Top: L lines of the 25.62 keV transition measured with a source collected on Al foil, which gave rise to some electron energy losses as seen from the "tail" of the lines. Bottom: L lines of the 64.59 and 65.31 keV transitions. The dashed electron line is the $KL_{II}L_{III}$ Auger line, the intensity of which could be determined by comparison with other members of the KLL group. The insets show theoretical [18]) L subshell ratios as a function of E2 admixture, with the experimental values indicated.

backing. The distortions were reduced to acceptable amounts when the backing material was made of 0.8 mg/cm^2 Ni foil. The greater energy loss in Al is probably due to the great penetrability of the Hg mother in this particular metal. Some of the measured conversion lines in ^{187}Os are shown in fig. 3. The energies were determined

Fig. 4. Ratio of conversion electron intensities reported in ref. [3]) and the presently obtained intensities. Normalization was made on the K shell conversion line of the 177.7 keV transition.

by a calibration relative to the L_{III} line of the 100.107 keV transition [12]) in ^{182}W. The results from the present conversion electron measurements are collected in table 2, where also multipolarities have been deduced from L and M subshell ratios, using the theoretical conversion coefficients of Hager and Seltzer [18]).

As a result of straggling effects, and also of the presence of LMM Auger lines close to the 9.75 M group, an additional uncertainty of 30 % should be added to the values stated in table 2 when the 9.75 M line intensities are compared with conversion lines from other transitions.

It is noted that the conversion electron intensities reported in ref. [3]) agree well with the present results at electron energies above ≈ 100 keV but are significantly lower for the lowest-energy conversion lines (cf. fig. 4, where the ratios between the intensities of ref. [3]) and the present ones are plotted versus energy).

An additional check was made on the intensities of the electron lines above 200 keV as given by Harmatz *et al.* [3]). Lines up to 1 MeV were measured with a Si(Li) detector. Good agreement (within ≈ 20 %) was obtained with the relative intensities of ref. [3]).

2.4. HALF-LIFE MEASUREMENTS

Several half-lives of excited levels in ^{187}Os have been measured using the delayed coincidence technique. The instrumentation was built up around an electron-electron coincidence spectrometer. This equipment has been described in detail earlier [13,14]). The same sources as those used for the conversion electron measurements have been employed in the measurements described below.

TABLE 3

Contributions in the energy channels used for half-life measurements of excited levels in ^{187}Os

Level under investigation (in keV)	Channel 1		Channel 2		Coincidence contributions
	main conversion line	disturbing components	main conversion line	disturbing components	
9.8	9.8 MN	84.9 K 87.6 K 25.6 L_I LMM (LMN) Auger (74.3 K) (75.0 K)	65.3 L_{II}+L_{III}	64.6 L_I (KLL Auger)	9.8 MN → 65.3 L_{II}+L_{III} 9.8 MN → 64.6 L_I 25.6 L_I → 65.3 L_{II}+L_{III} 87.6 K → 65.3 L_{II}+L_{III} LMM (LMN) Auger → 65.3 L_{II}+L_{III} LMM (LMN) Auger → 64.6 L_I
75.0	25.6 L_I	9.8 MN 87.6 K 84.9 K LMM (LMN) Auger	75.0 L_{II}+L_{III}	65.3 M 74.3 L_I 64.6 M	25.6 L_I → 75.0 L_{II}+L_{III} 25.6 L_I → 65.3 M 9.8 MN → 65.3 M 9.8 MN → 64.6 M 87.6 K → 75.0 L_{II}+L_{III} 87.6 K → 65.3 M LMN (LMN) Auger → L converison line

The 9.8 keV *level.* To determine the half-life of the 9.8 keV level the 9.8 N and 65.3 $L_{II}+L_{III}$ conversion electron lines were focused in one spectrometer each. To improve the time resolution of the scintillation system and to shift the 9.8 N lines away from the photomultiplier noise, 20 kV of high tension was applied to the ^{187}Ir source. An

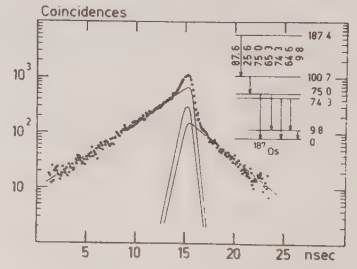

Fig. 5. The delayed time distribution recorded between the 9.8 N and 65.3 L conversion electron lines. After correction for contaminating cascades (see subsect. 2.4) the half-life of the 9.8 keV level in ^{187}Os was found to be $T_{\frac{1}{2}} = 2.38 \pm 0.18$ ns.

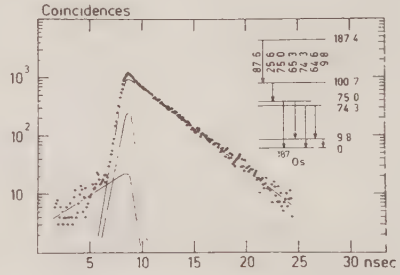

Fig. 6. Time coincidence spectrum obtained by focusing the 25.6 L and 75.0 L lines in one spectrometer each. From the analysis of such curves, the half-life of the 75.0 keV level in ^{187}Os was determined as $T_{\frac{1}{2}} = 2.16 \pm 0.16$ ns.

example of an observed time-coincidence distribution is shown in fig. 5. A time delay in the detection channel for the 9.8 N line introduces a shift to the left in fig. 5. Table 3 gives possible conversion electrons which could give a contribution in one of the selected energy channels. Although both the 74.3 and 75.0 keV transitions convert in the K shell the probability of the 0.4 and 1.1 keV K electrons, respectively, leaving the sources is rather small, and their coincidence rate with the weak KLL Auger group is negligible. The higher-energy channel was also carefully set to avoid as much as possible of the weak KLL Auger group. The main coincidence contributions are shown in the last column in table 3. The first two contributions are responsible for the slope to the left in fig. 5, while the next one introduces the half-life of the 75.0 keV level, which is shown as a slope to the right in the same figure. The next weak cascade

proceeds via the 100.7 keV long-lived level, and its contribution only shows up as a slight increase in the already low random coincidence rate. The weak 84.9 keV transition has not been placed in the decay scheme [3]), but for the present measurement its place is probably irrelevant. The coincidence rate from the cascades involving

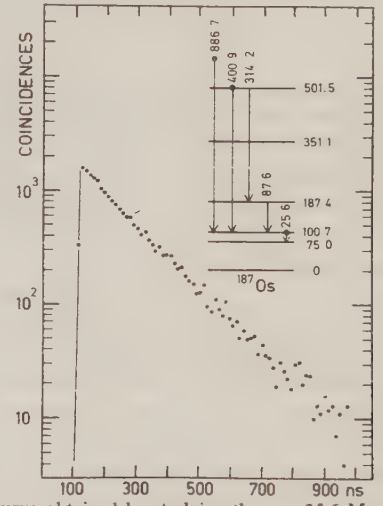

Fig. 7. The coincidence curve obtained by studying the $\gamma \rightarrow 25.6$ M cascade (indicated by dots in the figure). From the slope of such curves the half-life of the 100.7 keV level in ^{187}Os was determined as 112 ± 6 ns.

the LMM (LMN) Auger group is mainly of two types. Coincidences between the relevant L conversion line and its associated LXY Auger electrons are responsible for the main part of the observed prompt time distribution. LXY Auger electrons feeding the 74.3 keV level also give a coincidence contribution to the prompt peak, while those feeding the 75.0 keV level give a slope to the right in fig. 5. Although other weak contributions are also possible they will all give either a prompt distribution or a slope to the right and thus do not significantly influence the half-life measurement of the 9.8 keV level.

The measured time distributions were unfolded into their three main components as is shown in fig. 5, and the half-life of the 9.8 keV level was determined from the slope of the left-hand curve as 2.38 ± 0.18 ns. The slope to the right gives a half-life for the 75.0 keV level of 2.1 ± 0.3 ns. No earlier measurement for the half-life of the 9.8 keV level has been reported [15]).

The 75.0 keV *level.* In this measurement the energy channels were adjusted to detect transitions that involve the 75.0 keV level. The cleanest time spectrum was obtained by focusing the 25.6 L_I line in one spectrometer and the 75.0 L_{III} line in the other spectrometer. As in the previous measurement, 20 kV was applied to the ^{187}Ir source. The observed delayed coincidence time distribution is shown in fig. 6. A

delay in the 75.0 L_{III} channel gives a time shift to the right in this figure. Possible contributions to the observed coincidence rate are shown in the last column in table 3. The first two cascades proceed via the 75.0 keV level, and its half-life is responsible for the slope on the right-hand part of the time distribution in fig. 6. The next two cascades involve the half-life of the 9.8 keV level, giving the weak decay contribution on the left-hand side. As in the earlier measurement the next two weak cascades only give a small contribution to the random-coincidence rate. The contribution to the coincidence rate from cascades involving the LMM (LMN) Auger group gives either a prompt curve or one reflecting the half-life of the 75.0 keV level, as discussed above. The result of unfolding the measured decay curve into its main three components is shown in fig. 6. From the slope of the curve on the right-hand side we find a half-life for the 75.0 keV level in ^{187}Os of 2.16 ± 0.16 ns.

This level has been Coulomb-excited by McGowan *et al.* [16]). In their experiment, they observe a γ-ray line at about 75 keV, which they assume is due to ground-state transitions from both the 75.0 and 74.3 keV levels reported by Harmatz *et al.* [3]). Using arguments based on the total E2 strength expected for ^{187}Os, they somewhat arbitrarily assign 10 % of the observed $\approx$ 75 keV γ-intensity to direct excitation of the 75.0 keV level, and thus obtain B(E2) values of 0.9 $e^2 \cdot b^2$ and 0.68 $e^2 \cdot b^2$ respectively, for the 75.0 and 74.3 keV levels. The deduced B(E2) value for the 75.0 keV state, together with the decay properties of this level reported by Harmatz *et al.* [3]), result in a state half-life of 1.6 ns.

The 100.7 keV *level.* The 100.7 keV level is fed by four transitions (87.6, 400.9, 486.0 and 886.7 keV) which all have low electron intensities. As our source at the time of this measurement was weak, we decided to take advantage of the far stronger γ-radiations from the three high-energy transitions. For this reason one spectrometer lens was replaced by a plastic scintillator mounted on a 56 DVP multiplier, and the channel thus changed was adjusted to admit pulses between 150 and 400 keV. In this way Compton events from the 400.9, 486.0 and 886.7 keV γ-rays were recorded. The other spectrometer lens was focused on electrons from the 25.6 keV transition which de-excites the 100.7 keV level. The 25.6 keV M electron line was chosen because it was well resolved from other lines and had a suitable strength.

The result of a typical measurement is presented in fig. 7. The half-life of the 100.7 keV level in ^{187}Os was obtained from the slope of such curves as 112 ± 6 ns.

In an investigation of the decay properties of a 225 μs isomer in ^{187}Os produced in a (γ, n) reaction, Krehbiel [29]) observed that a 157 keV transition was in delayed coincidence with K X-rays, the delay corresponding to a half-life of 120 ± 20 ns. He explained this by assuming that the 225 μs isomeric level decays via a partially converted 157 keV transition to a level of 120 ns half-life, of unknown energy, which in turn decays via an almost completely converted transition to the ground state. From our measurements this unknown level can be identified with the 100.7 keV level, the coincidence relation measured by Krehbiel presumably being that between the 157 and 75.0 keV (+K X-ray) transitions. The small energy difference between

TABLE 4

Absolute transition probabilities in ^{187}Os

Level (keV)	$T_{\frac{1}{2}}$ (exp) of level (ns)	Transition energy (keV)	Initial state $IK^{\pi}(N\,n_z\Lambda)$	Final state $IK^{\pi}(N\,n_z\Lambda)$	Multi-polarity	Relative N_γ	Relative N_e	$T_{\frac{1}{2}\gamma}$ (exp) (s)	B(M1) $(e\hbar/2Mc)^2$	B(E2) $(e^2 \cdot b^2)$	F_W [a]
9.8	2.38±0.18	9.8	$\frac{3}{2}^-$(512)	$\frac{1}{2}^-$(510)	M1	100	22000	$5.26 \cdot 10^{-7}$	$(8.0\pm0.7) \cdot 10^{-2}$		22
					E2	< 0.02		$> 2.6 \cdot 10^{-3}$		$< 2.4 \cdot 10^{-1}$	$> 2.7 \cdot 10^{-2}$
74.3	< 0.040 [b]	64.6	$\frac{3}{2}^-$(510)	$\frac{3}{2}^-$(512)	M1	7.7 [d]	33.7	$< 1.47 \cdot 10^{-9}$	$> 1.0 \cdot 10^{-1}$		< 1770
					E2	0.13 ± 0.04		$< 1.1 \cdot 10^{-7}$		$> 4.5 \cdot 10^{-1}$	$< 1.4 \cdot 10^{-2}$
		74.3		$\frac{1}{2}^-$(510)	M1	15.6 [d]	226	$7.3 \cdot 10^{-10}$	$> 1.3 \cdot 10^{-1}$		14
					E2	< 0.16		$7.1 \cdot 10^{-8}$		$(3.5\pm1.0) \cdot 10^{-1}$ [b]	$1.8 \cdot 10^{-2}$
75.0	2.16±0.16	65.3	$\frac{5}{2}^-$(512)	$\frac{3}{2}^-$(512)	M1	< 1.4 [d]	266	$> 5.86 \cdot 10^{-7}$	$< 2.4 \cdot 10^{-4}$		> 7300
					E2	9.5 [d]		$8.63 \cdot 10^{-8}$		$(5.6\pm0.8) \cdot 10^{-1}$	$1.2 \cdot 10^{-2}$
		75.0		$\frac{1}{2}^-$(510)	E2	6.6 [d]	98	$1.24 \cdot 10^{-7}$		$(1.9\pm0.3) \cdot 10^{-1}$	$3.4 \cdot 10^{-2}$
100.7	112±6	25.6	$\frac{7}{2}^-$(503)	$\frac{3}{2}^-$(512)	M1	6.9 [d]	400	$6.62 \cdot 10^{-6}$	$(3.58\pm0.22) \cdot 10^{-4}$		4900
					E2	$< 3.6 \cdot 10^{-3}$ [d]		$> 1.2 \cdot 10^{-2}$		$< 4.0 \cdot 10^{-4}$	> 16
		90.7		$\frac{3}{2}^-$(512)	E2	< 0.17 [d]	< 1	$> 2.7 \cdot 10^{-4}$		$< 3.4 \cdot 10^{-5}$	> 190
187.4	0.080 [c]	87.6	$\frac{5}{2}^-$(510)	$\frac{7}{2}^-$(503)	M1	< 0.1		$> 1.5 \cdot 10^{-7}$	$< 4.0 \cdot 10^{-4}$		> 4400
					E2	< 0.1		$> 1.5 \cdot 10^{-7}$		$< 7.5 \cdot 10^{-2}$	$> 8.6 \cdot 10^{-2}$
		112.4		$\frac{5}{2}^-$(512)	M1	< 0.55	≈ 3.6	$> 2.8 \cdot 10^{-8}$	$< 1.0 \cdot 10^{-3}$		> 1780
					E2	< 0.55		$> 2.8 \cdot 10^{-8}$		$< 1.1 \cdot 10^{-1}$	$> 5.7 \cdot 10^{-2}$
		113.2		$\frac{3}{2}^-$(510)	M1	2.6	19.7	$6.00 \cdot 10^{-9}$	$(4.5\pm0.8) \cdot 10^{-3}$		390
					E2	3.2		$4.87 \cdot 10^{-9}$		$(6.3\pm1.6) \cdot 10^{-1}$	$1.03 \cdot 10^{-2}$
		177.7		$\frac{3}{2}^-$(512)	M1	44.4	58.2	$3.50 \cdot 10^{-10}$	$(2.0\pm0.4) \cdot 10^{-2}$		88
					E2	11.1		$1.40 \cdot 10^{-9}$		$(2.2\pm0.7) \cdot 10^{-1}$	$2.8 \cdot 10^{-2}$
		187.4		$\frac{1}{2}^-$(510)	E2	35.5	14.9	$4.35 \cdot 10^{-10}$		$(5.6\pm1.2) \cdot 10^{-1}$ [b]	$1.15 \cdot 10^{-2}$

[a]) Hindrance factor relative to the Weisskopf estimate [17]) with the statistical factor equal to one.
[b]) Obtained from Coulomb-excitation data of McGowan *et al.* [16]) with a correction for the influence from the 75.0 keV level as deduced from our data for this level.
[c]) Calculated from the Coulomb-excitation data of McGowan *et al.* [16]) and our electron and γ-ray intensities.
[d]) Calculated from our electron intensities and multipole mixing ratio and the conversion coefficients of Hager and Seltzer [18]).

the 75.0 keV transition and the K X-rays would explain why Krehbiel could not attribute a γ-transition to the 120 ns decay. A further discussion of both the 225 μs and 120 ns levels is given in sect. 3.2.

From the presently known electron and γ-ray intensities and half-lives of excited levels, the absolute transition probabilities presented in table 4 have been calculated. The last column gives a comparison with the Weisskopf estimate [17]).

3. Level scheme

3.1. THE $\frac{1}{2}^-$(510), $\frac{3}{2}^-$(512) AND $\frac{7}{2}^-$(503) BANDS

The low-energy part of the level scheme (fig. 8), including the 9.8, 74.3, 75.0, 100.7, 187.4 and 351.0 keV levels, can be considered as well established [3,9]). However, there have been some doubts about the assignments of the different levels. Harmatz *et al.* [3]) suggested a $K = \frac{1}{2}$ band with members at 0, 9.8, 75.0 and 100.7 keV and a $K = \frac{3}{2}$ band consisting of levels at 74.3, 187.4 and 351.0 keV. The main objection to these assignments is the abrupt change in systematics of the decoupling parameter ($a_{exp} = -0.60$; $a_{syst} \approx 0$) and of $\hbar^2/2\mathscr{I}$ [$(\hbar^2/2\mathscr{I})_{exp} = 8.2$ keV; $(\hbar^2/2\mathscr{I})_{syst} \approx 24$ keV]. It was then pointed out [19]) that by assigning the 0, 74.3, 187.4 and 351.0 keV levels to a $K = \frac{1}{2}$ band and the 9.8 and 75.0 keV levels to a $K = \frac{3}{2}$ band the values of the parameters a and $\hbar^2/2\mathscr{I}$ come close to the values obtained from systematics. This interpretation is further supported by the transition probabilities obtained in the present work. The 100.7 keV level has been shown to have a half-life of 112 ns, and thus it cannot be the $\frac{7}{2}^-$ member of the $K = \frac{1}{2}$ band but is likely to be the $\frac{7}{2}^-$ (503) state. The comparatively low B(E2) value for the 75.0 keV transition also in-

dicates that this is not a transition within the $K = \frac{1}{2}$ band as suggested by Harmatz *et al.* [3]) but is rather the interband transition $\frac{5}{2}\frac{3}{2} \rightarrow \frac{1}{2}\frac{1}{2}$†. Furthermore, the large B(E2) value of the 187.4 keV transition is characteristic of an intraband transition and not for the $\frac{5}{2}\frac{3}{2} \rightarrow \frac{1}{2}\frac{1}{2}$ transition as suggested in ref. [3]). All the present data thus

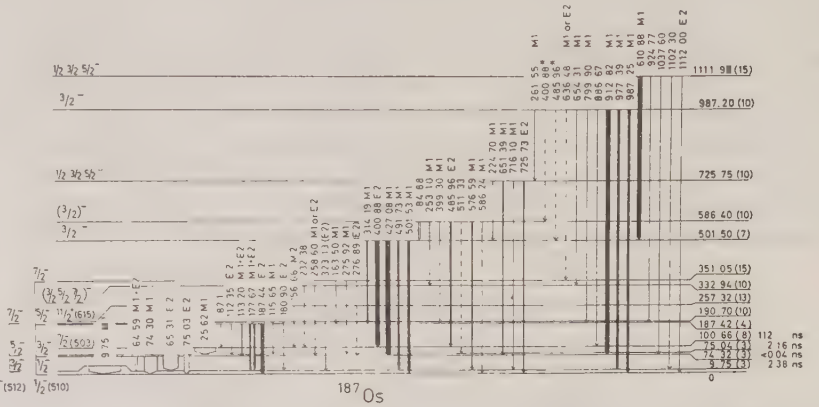

Fig. 8. Decay scheme of ^{187}Os according to the present investigation.

indicate that the low energy level assignments shown in fig. 8 are correct. Our data also contain some additional support for the $\frac{7}{2}\frac{1}{2}^-$ assignment of the 351.0 keV level. The γ-ray intensity of the 276.9 keV line that depopulates this level was measured as 1.6 times the intensity of the 275.9 keV line. From the K line intensity of the latter transition [3]) we have deduced an M1 multipolarity. The fact that the K line for the 276.9 keV transition has been given as weak [3]), i.e., weaker than that of the 275.9 K line, then indicates that this transition could be of E2 multipolarity. Thus the 351.0 keV level probably has a spin and parity of $\frac{7}{2}^-$. The de-excitation of this level to spin $\frac{5}{2}$ states but not to the energetically favourable $\frac{3}{2}\frac{3}{2}^-(512)$ state suggests that the 351.0 keV level should be assigned $\frac{7}{2}\frac{1}{2}^-(510)$.

Since both the $\frac{7}{2}\frac{7}{2}^-(503)$ and $\frac{7}{2}\frac{1}{2}^-(510)$ states are fed in the decay we expect also the $\frac{7}{2}\frac{3}{2}^-(512)$ state to be fed. From the rotational formula we calculate its energy to be 167 keV, but it can be expected to be displaced due to mixing. It should decay mainly to the 75.0 and 9.75 keV levels with M1 + E2 and E2 transitions, respectively. At 190.70 keV we find the only combination of transitions (the 115.65 and 180.90 keV transitions) that fulfill these requirements, and we assign this suggested level as the $\frac{7}{2}\frac{3}{2}^-(512)$ state. Its energy is considerably higher than the calculated energy. Such a deviation is, however, also found for the corresponding level in ^{189}Os [ref. [1])].

† $\frac{5}{2}\frac{3}{2} \rightarrow \frac{1}{2}\frac{1}{2}$ means a transition from the $I = \frac{5}{2}$, $K = \frac{3}{2}$ state to the $I = K = \frac{1}{2}$ state.

3.2. THE $\frac{11}{2}^+$ ISOMERIC LEVEL

By bombarding Re with protons Conlon [20]) found a 156.7 keV M2 transition which was delayed 231 ± 2 μs. He deduced that this transition takes place in ^{187}Os but was not able to place it in the decay scheme. A transition of the same energy and multipolarity has also been observed by us in the decay of ^{187}Ir. To be able to place this transition we have made several electron-electron coincidence measurements, focusing the 156.7 K line in one lens and scanning the low-energy electron spectrum in the other lens. We found definite evidence that the 156.7 K line is in coincidence with lines at 23 and 62 keV. We also observed that both these lines were delayed about 100 ns as compared to the 156.7 K line. These facts are consistent with the interpretation that the two coincident lines are the 25.6 M and 75.0 L lines, and that these two transitions form a cascade from the 100.7 keV level. As no other coincident lines were observed we conclude that the 156.7 keV transition feeds directly the 100.7 keV level, establishing the existence of an isomeric level at 257.3 keV as was suggested in ref. [19]). The M2 multipolarity of the 156.7 keV transition to the $\frac{7}{2}^-$ state at 100.7 keV suggests an $\frac{11}{2}^+$ assignment for the isomeric level.

In terms of the Nilsson model the isomeric state is interpreted as the $\frac{11}{2}\frac{11}{2}^+[615]$ state, which should have a low excitation energy for a moderate deformation. It is interesting to note that a state with such a high I and K value is fed to this extent from the $\frac{3}{2}^+$ Ir mother. In ^{189}Ir, ^{191}Ir and ^{193}Ir there exists a similar situation in that an $\frac{11}{2}^-$ isomer is populated in the decay of Pt or Os nuclei which have $\frac{3}{2}^-$ ground states. It has recently been shown [21]) that this feeding takes place in the Ir nuclei via a system of negative parity states, which are likely to be associated with a considerably smaller deformation than the positive parity states. No spherical $\frac{11}{2}^+$ state is possible in the Os nuclei, so the population mechanism of the isomer is probably not analogous to that in the Ir nuclei. One may conjecture, though, that the feeding of the $\frac{11}{2}^+$ state in ^{187}Os may take place via the $K-2$ γ-vibrational band.

3.3. OTHER LEVELS

A search for additional levels was made using a computer program that systematically investigates energy combinations [22,23]). As a start the 9.8, 74.3, 75.0, 100.7 and 187.4 keV levels were taken as known levels. The first computer run resulted in levels at 501.50, 987.20 and 1111.99 keV, each level having less than 3 % chance of being due to accidental combinations. Feeding these into the computer as known levels and re-running the program resulted in levels at 332.94, 586.40 and 725.75 keV, with less than 3 % chance of these being due to accidental combinations.

The level scheme (fig. 9) agrees well with that of Harmatz *et al.* [3]). New levels are found, in addition to the 190.70 and 257.32 keV levels mentioned above, at 332.94 and 586.40 keV. The decay mode of the former level suggests spin and parity $\frac{3}{2}^-$, $\frac{5}{2}^-$ or $\frac{7}{2}^-$, which may be associated with either the $\frac{3}{2}^-(501)$ or $\frac{5}{2}^-(503)$ orbitals or with a vibration coupled to one of the two lowest orbitals.

The 586.40 keV level has a decay mode compatible only with a $\frac{3}{2}^-$ assignment.

One observes similarities between this level and the $\frac{3}{2}^-$ state at 501.50 keV. The latter is depopulated by a strong E2 transition of 400.88 keV to the $\frac{7}{2}\,\frac{7}{2}^-(503)$ level, which might indicate that the 501.50 keV level is the $K-2$ γ-vibration built on the $\frac{7}{2}^-(503)$ state. It is tempting to assign the 586.40 keV level as the first rotational state built on this $K-2$ vibrational state, especially since these two levels are interconnected with the relatively strong 84.88 keV transition and in addition since the 586.40 keV state de-excites through a strong E2 transition of 485.96 keV to the $\frac{7}{2}\,\frac{7}{2}^-(503)$ state. The only objection in our data against such an interpretation is the observed 586.24 keV M1 transition, which fits energetically as the transition to the $\frac{1}{2}^-$ ground state. The possibility that this fit is accidental cannot be neglected.

The multipolarity data in table 1 imply a negative parity for the 725.75, 987.20 and 1111.99 keV states. The 725.75 keV level was suggested to be $\frac{1}{2}^-$ by Harmatz *et al.* [3]). The fact that no transitions are found to $\frac{5}{2}^-$ and $\frac{7}{2}^-$ levels supports this assignment. On the other hand the E2 character of the ground state transition suggests $\frac{5}{2}^-$.

The 987.20 keV level was suggested to be $\frac{3}{2}^-$ in ref. [3]) and $\frac{5}{2}^-$ in ref. [19]). Our multipolarities support the former value. For the 1111.99 keV level the E2 transition to the ground state suggests an assignment of $\frac{5}{2}^-$ rather than $\frac{1}{2}^-$ as suggested in ref. [19]).

The present level scheme contains only about 50 % of the total number of transitions detected. It is likely that a coincidence experiment would yield many additional levels, which could help to clarify the nature of the higher-lying excitations. A 2048 × 2048 channel $\gamma\gamma$ coincidence spectrum has recently been accumulated at CERN [ref. [8])] and the analysis is now under way. No coincidence work was therefore included in the present work.

4. Transition probabilities

4.1. E2 TRANSITIONS

The 74.3, 75.0 and 187.4 keV levels have been Coulomb-excited in an experiment by McGowan *et al.* [16]). Using that information, together with our measured branching and mixing ratios and half-lives of the 9.8 and 75.0 keV levels, we obtain the reduced E2 transition probabilities given in the first column of table 5. According to the formalism for a deformed nucleus the B(E2) values of the four intraband transitions correspond to an average deformation parameter δ of 0.15±0.02, which is below the values obtained for most nucleides known to have a deformed equilibrium shape. In strongly deformed nuclei the major E2 strength is of a collective nature concentrated within the rotational bands, and the E2 transition probabilities between bands are weaker. This is, however, not the case in ^{187}Os where for instance the interband transition $\frac{3}{2}\,\frac{1}{2} \rightarrow \frac{3}{2}\,\frac{3}{2}$ has a B(E2) value > 0.45 which is of the same magnitude as the B(E2) values for the observed intraband transitions. This is an indication that strong mixing of levels occurs in ^{187}Os.

In order to make a more quantitative comparison of the experimental B(E2) values with the Nilsson model we have made a simple Coriolis coupling calculation where only

TABLE 5

E2 rates for transitions in ^{187}Os

Experimental data [a])		Calculated B(E2) values [b])	Fitted parameters	
$B(\mathrm{E2}, \frac{3}{2}\,\frac{1}{2} \rightarrow \frac{1}{2}\,\frac{1}{2})$ [c])	0.35±0.10	0.36	$E^*\langle\frac{1}{2}\vert j_-\vert\frac{3}{2}\rangle$	90 keV
$B(\mathrm{E2}, \frac{5}{2}\,\frac{1}{2} \rightarrow \frac{3}{2}\,\frac{1}{2})$ [c])	0.63±0.16	0.90	$G_{\mathrm{E2}}(\frac{1}{2} \rightarrow \frac{3}{2})$	5.2 ±4.4
$B(\mathrm{E2}, \frac{5}{2}\,\frac{1}{2} \rightarrow \frac{1}{2}\,\frac{1}{2})$ [c])	0.56±0.12	0.55	$G_{\mathrm{E2}}(\frac{1}{2} \rightarrow \frac{1}{2})$	57.6 ±4.8
$B(\mathrm{E2}, \frac{5}{2}\,\frac{3}{2} \rightarrow \frac{3}{2}\,\frac{3}{2})$ [c])	0.56±0.08	0.58	$G_{\mathrm{E2}}(\frac{3}{2} \rightarrow \frac{3}{2})$	56.7 ±3.4
$B(\mathrm{E2}, \frac{5}{2}\,\frac{3}{2} \rightarrow \frac{1}{2}\,\frac{1}{2})$ [c])	0.19±0.03	0.18	$b_{\mathrm{E2}}G_{\mathrm{E2}}(\frac{1}{2} \rightarrow \frac{3}{2})$	−9.0±3.8
$B(\mathrm{E2}, \frac{5}{2}\,\frac{1}{2} \rightarrow \frac{3}{2}\,\frac{3}{2})$ [c])	0.22±0.07	0.18		
$B(\mathrm{E2}, \frac{3}{2}\,\frac{3}{2} \rightarrow \frac{1}{2}\,\frac{1}{2})$	< 0.24	1.2 ±0.6		
$B(\mathrm{E2}, \frac{3}{2}\,\frac{1}{2} \rightarrow \frac{3}{2}\,\frac{3}{2})$	> 0.45	0.74±0.10		

[a]) B(E2) values given in $e^2 \cdot \mathrm{b}^2$.
[b]) Calculated values using the fitted parameter values shown in the right-hand part of the table.
[c]) Experimental values used in the fitting procedure.

the mixing between the $\frac{1}{2}^-(510)$ and $\frac{3}{2}^-(512)$ orbitals has been taken into account. In this simplified picture the admixed components in the wave functions are only dependent on the energy difference between the two unperturbed states of spin I and the coupling strength parameter $E^*\langle\frac{1}{2}\vert j_-\vert\frac{3}{2}\rangle$ (see ref. [24]) for more details). In the mentioned approximation the observed B(E2) values are determined by the following five parameters [24]) $G_{\mathrm{E2}}(\frac{1}{2} \rightarrow \frac{3}{2})$, $G_{\mathrm{E2}}(\frac{1}{2} \rightarrow \frac{1}{2})$, $G_{\mathrm{E2}}(\frac{3}{2} \rightarrow \frac{3}{2})$, $b_{\mathrm{E2}}G_{\mathrm{E2}}(\frac{1}{2} \rightarrow \frac{3}{2})$ and $E^*\langle\frac{1}{2}\vert j_-\vert\frac{3}{2}\rangle$. As the expression for B(E2) is not a linear function of $E^*\langle\frac{1}{2}\vert j_-\vert\frac{3}{2}\rangle$ we have for simplicity performed the calculations for a few pre-determined values for this quantity. The observed relevant B(E2) values have then, through a least-squares fit, been used to determine the other four parameters. The best fit to the experimental data is obtained at large values of $E^*\langle\frac{1}{2}\vert j_-\vert\frac{3}{2}\rangle$, with a rather flat optimum around 90 keV. The fitted parameters, as well as the experimental and calculated B(E2) values for $E^*\langle\frac{1}{2}\vert j_-\vert\frac{3}{2}\rangle = 90$ keV, are shown in table 5. We see that reasonable agreement is obtained and that the large value for the interband $B(\mathrm{E2}, \frac{3}{2}\,\frac{1}{2} \rightarrow \frac{3}{2}\,\frac{3}{2})$ is accounted for.

The fitted parameters can now be compared with the Nilsson predictions. Using $E^* \approx \hbar^2/2\mathscr{I} \approx 30$ keV, we get $\langle\frac{1}{2}\vert j_-\vert\frac{3}{2}\rangle \approx 3$ which is three times more than predicted. From the fit we get $G_{\mathrm{E2}}(\frac{1}{2} \rightarrow \frac{1}{2}) = G_{\mathrm{E2}}(\frac{3}{2} \rightarrow \frac{3}{2}) = 57 \pm 4$, which corresponds to a quadrupole moment of $Q_0 = 6.5 \pm 0.5$ b or a deformation parameter $\delta = 0.20 \pm 0.02$. The fit is shown to be rather independent of the values of $G_{\mathrm{E2}}(\frac{1}{2} \rightarrow \frac{3}{2})$ and $b_{\mathrm{E2}}G_{\mathrm{E2}}$ $(\frac{1}{2} \rightarrow \frac{3}{2})$, which come out as 5.2±4.4 and −9.0±3.8, respectively, whereas the model predicts 0.05 and −2.0. Although the agreement with theory here is not so good, it turns out that almost as good a fit can be obtained using the latter model values.

With the assignments given above, two E2, $|\Delta K| = 2$ transitions depopulate the 100.7 keV level. From our measurements we are able to set a lower limit for the absolute E2 strength of these transitions. Both E2 components are found to be hindered as compared to the Weisskopf estimate (see table 4). This reflects the fact

222

that these two E2 transitions are asymptotically forbidden in the Nilsson model. Hindrance is also expected due to the pairing effect. If these E2 transitions are compared with the pure Nilsson estimate (hindrance factor F_N) we find that they are actually slightly enhanced. In fig. 9 we show a compilation of E2, $|\Delta K| = 2$ transition

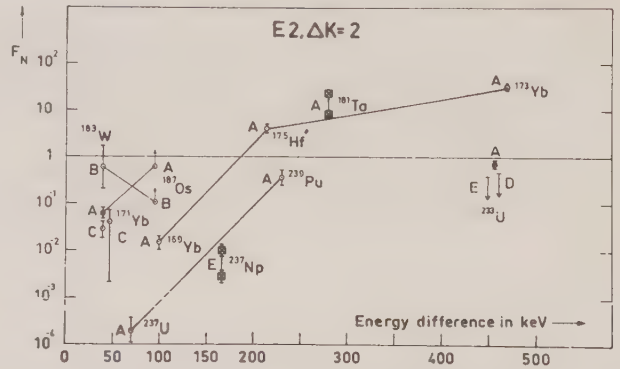

Fig. 9. The hindrance factors F_N (see subsect. 4.1) of E2, $|\Delta K| = 2$ transitions are shown as a function of the energy difference between the decaying state of spin I_i and the member of a final-state band with $|K_i - K_f| = 2$ and $I_f = I_i$. The following symbols are used: ×, proton transitions; ○, neutron transitions; A: transitions from $I_i = K_i$ to $I_f = K_f$; B: $I_i = K$ to $I_f = K_f + 1$; C: $I_i = K_i$ to $I_f = K_f + 2$ and E: $I_i = K_i + 1$ to $I_f = K_f + 1$. Most of the information given in this figure is taken from ref. [25]).

rates. Here the hindrance factor F_N for different transitions has been plotted as a function of the energy difference between the decaying state, of spin I_i, and the member of a final-state band with $|K_i - K_f| = 2$ and $I_f = I_i$ [(e.g., in this case $\frac{7}{2}\frac{3}{2}(512)$]. The figure shows that there is a trend for the F_N factor to increase as the above-mentioned energy difference increases. This can be interpreted as evidence that when this energy difference is small the mixing of states is greater and the introduced collective components speed up the E2 transitions.

4.2. M1 TRANSITIONS

According to the pure rotational model the ratio of transition probabilities between a given level and two rotational members associated with another orbital is given by the ratio of two squared Clebsch-Gordan coefficients. So for instance the ratio $B(\mathrm{M1}, \frac{5}{2}\frac{1}{2} \rightarrow \frac{5}{2}\frac{3}{2})/B(\mathrm{M1}, \frac{5}{2}\frac{1}{2} \rightarrow \frac{3}{2}\frac{3}{2})$ is predicted to be 6.8, while our experiment in ^{187}Os gives < 0.05. This disagreement indicates band mixing.

In the case of ^{189}Os we have made a Coriolis calculation [1]) and from a fitting procedure to the experimental data it was shown that reasonable agreement could be obtained for a coupling strength of roughly $E^*\langle\frac{1}{2}|j_-|\frac{3}{2}\rangle = 30$ keV. The present investigation of ^{187}Os has only provided three B(M1) values (and four limits), and since to our knowledge only the ground state magnetic moment [27,28]) [$\mu = +0.06432$

(3) n.m.] has been measured, we do not have enough experimental data on ^{187}Os to make a similar fit.

A remarkable feature of the band structure is the apparent cancellation of the M1 component in the $\frac{5}{2}\frac{3}{2}^-(512) \rightarrow \frac{3}{2}\frac{3}{2}^-(512)$ 65.3 keV transition. Similar effects have also recently been observed for the M1 component in the $\frac{1}{2}\frac{1}{2}^+(400) \rightarrow \frac{3}{2}\frac{3}{2}^+(402)$ transition in odd-mass Ir isotopes [7]). For instance, in ^{189}Ir this M1 component is hind red about 56000 times [7]) as compared to the Weisskopf estimate [17]). In the Ir nuclei this large hindrance can be accounted for using a simple Coriolis type of mixing calculation, and probably the observed M1 cancellation in ^{187}Os is due to a similar effect. The alternative that $g_K = g_R$ is not possible since the $\frac{7}{2}\frac{3}{2} \rightarrow \frac{5}{2}\frac{3}{2}$ 115.65 keV transition is observed to be M1.

We are greatly indebted to Dr. Arve Kjelberg and co-workers at the Nuclear Chemistry Group at ISOLDE, CERN for the effort they have made to provide us with the separated radioactive sources. This work has been supported by the Swedish Atomic Research Council.

References

1) S. G. Malmskog, V. Berg and A. Bäcklin, Nucl. Phys. **A153** (1970) 316
2) S. G. Nilsson, Mat. Fys. Medd. Dan. Vid. Selsk. **29** (1955) no. 16
3) B. Harmatz, T. H. Handley and J. W. Mihelich. Phys. Rev. **128** (1962) 1186
4) A. K. Kerman, Mat. Fys. Medd. Dan. Vid. Selsk. **30** (1956) no. 15
5) CERN Yellow report No 70–3, The ISOLDE collaboration (ed. A. Kjelberg and G. Rudstam)
6) A. Bäcklin, B. Fogelberg and S. G. Malmskog, Nucl. Phys. **A103** (1967) 337, appendix
7) A. Bäcklin, B. Fogelberg and S. G. Malmskog, to be published
8) The French ISOLDE collaboration, private communication 1970
9) G. T. Emery, W. R. Kane, M. McKeown, M. L. Perlman and G. Scharff-Goldhaber, Phys. Rev. **129** (1963) 2597
10) A. Hedgran, K. Siegbahn and N. Svartholm, Proc. Phys. Soc. **A63** (1950) 960
11) A. Bäcklin, Nucl. Instr. **57** (1967) 261
12) E. J. Seppi, H. Henriksson, F. Boehm and J. W. Dumond, Nucl. Instr. **16** (1962) 17
13) T. R. Gerholm and J. Lindskog Ark. Fys. **24** (1963) 171
14) S. G. Malmskog, Ark. Fys. **35** (1967) 255
15) S. G. Malmskog, Report AE-400 (Studsvik, Sweden, 1970)
16) F. K. McGowan, P. H. Stelson, R. L. Robinson and J. L. C. Ford, ORNL-3425 (1963) p. 26
17) A. H. Wapstra, G. J. Nijgh and R. van Lieshout, Nuclear spectroscopy tables (North-Holland, Amsterdam, 1959)
18) R. S. Hager and E. C. Seltzer, Nucl. Data **4** (1968) part 1 and 2
19) Nuclear Data **1** (1966) no 2, ed. K. Way, compiler W. B. Ewbank
20) T. W. Conlon, Nucl. Phys. **A100** (1967) 545
21) A. Bäcklin, V. Berg and S. G. Malmskog, Nucl. Phys. **A156** (1970) 641
22) A. Bäcklin, Nucl. Instr. **53** (1967) 177
23) R. Helmer and A. Bäcklin, Nucl. Inst. **65** (1968) 31
24) V. Berg, S. G. Malmskog and A. Bäcklin, Nucl. Phys. **A143** (1970) 177
25) K. E. G. Löbner and S. G. Malmskog, Nucl. Phys. **80** (1966) 505
26) G. Alaga, K. Alder, A. Bohr and B. R. Mottelson, Mat. Fys. Medd. Dan. Vid. Selsk. **29** (1955) no. 9
27) K. Murakawa, J. Phys. Soc. Japan **17** (1962) 891
28) A. Schwenk, Z. Phys. **213** (1968) 482
29) H. Krehbiel, Phys. Lett. **13** (1964) 65

REFERENCE 16

TRANSITION PROBABILITIES IN ^{189}Os

S.G. MALMSKOG and V. BERG

AB Atomenergi, Studsvik, Nyköping, Sweden and Institute of Physics, University of Stockholm, Sweden

and

A. BÄCKLIN

The Swedish Research Council's Laboratory, Studsvik, Nyköping, Sweden

1.E.4 *Nuclear Physics* A153 (1970) 316—336; © *North-Holland Publishing Co., Amsterdam*
Not to be reproduced by photoprint or microfilm without written permission from the publisher

TRANSITION PROBABILITIES IN ^{189}Os

S. G. MALMSKOG and V. BERG
AB Atomenergi, Studsvik, Nyköping, Sweden and Institute of Physics, University of Stockholm, Sweden
and
A. BÄCKLIN
The Swedish Research Councils' Laboratory, Studsvik, Nyköping, Sweden

Received 11 February 1970
(Revised 6 April 1970)

Abstract: The level structure of ^{189}Os has been studied from the decay of ^{189}Ir (13.3 d) produced in proton spallation at CERN and mass separated in the ISOLDE on-line facility. The γ-ray spectrum has been recorded both with a high-resolution Si(Li) detector and Ge(Li) detectors. Three previously unreported transitions were observed defining a new level at 438.5 keV. Special attention was given to the low-energy level band structure. Several multipolarity mixing ratios were deduced from measured L-subshell ratios which, together with measured level half-lives, gave absolute transition probabilities. The low-level decay properties are discussed in terms of the Nilsson model with the inclusion of Coriolis coupling.

E RADIOACTIVITY ^{189}Ir[from Pb(p, spallation)]; measured E_γ, I_γ, E_{ce}, I_{ce}, cece-delay; deduced log *ft*. ^{189}Os deduced levels, $T_{\frac{1}{2}}$, J, π, cc, multipolarities, mixing ratios, partial half-lives. Isotope separated sources, Si(Li) and Ge(Li) detectors.

227

1. Introduction

Over a period of several years we have systematically studied nuclei in the transitional regions, where changes between deformed and spherical shapes are expected. Most recently we have studied the low-energy level structure of the odd-proton ^{193}Ir and ^{191}Ir isotopes [1,2]). We were there able to determine the transitions strengths between several of the low-lying excited states indicating that these nuclei are slightly deformed but that particle-rotational couplings and probably also vibrational degrees of freedom are important.

To further investigate the gradual change of deformation in this mass region we have also undertaken a study of the low-energy level properties in odd-neutron Os isotopes and this paper reports on the results from the decay of ^{189}Ir to ^{189}Os. When this work was started the main information on levels in ^{189}Os was obtained from conversion electron [3,4]) and Coulomb excitation [5,6]) measurements. Harmatz *et al.* [3]) proposed from their data on the decay of ^{189}Ir a level scheme of ^{189}Os which was confirmed from decay studies of ^{189}Re by Crasemann *et al.* [7]).

Over the last year a lot of detailed information on the low-energy level properties in ^{189}Os has been obtained mainly through Mössbauer studies [8–11]) from which

magnetic moments and lifetimes of excited states have been deduced. Ref. [11]) also reports for the first time a Ge(Li) detector measurement of the γ-ray spectrum from ^{189}Ir. Very recently a measurement of the half-life of the 69.5 keV level has been reported [12]).

The present work has focused its main interest on the proposed [3]) low-energy rotational bands in ^{189}Os. High-resolution conversion electron (CE) measurements have been performed to obtain mixing ratios, which together with half-life measurements, using the delayed coincidence method, give absolute transition probabilities, which have been compared with predictions from the Nilsson model [13]). Discrepancies with the conversion data from Harmatz *et al.* [3]) have caused some changes in the level scheme proposed by these authors.

2. Experimental procedure

2.1. SOURCE PREPARATION

The ^{189}Ir (13.3 d) activity was obtained as a decay product of ^{189}Hg, produced from spallation in a molten lead target at 700° C when bombarded in an external beam of 600 MeV protons from the synchrocyclotron at CERN. The extracted mercury was isotopically separated in the ISOLDE on-line mass separator facility [14]) at CERN and collected on a 0.9 mg/cm^2 nickel foil, which served as backing in all measurements described below. Typical irradiation times were of the order of 20 hours and at favourable occasions the transport time between Geneva and Studsvik was 12 hours. The 11 h mother activity ^{189}Pt was allowed to decay for one weak before the measurements were started.

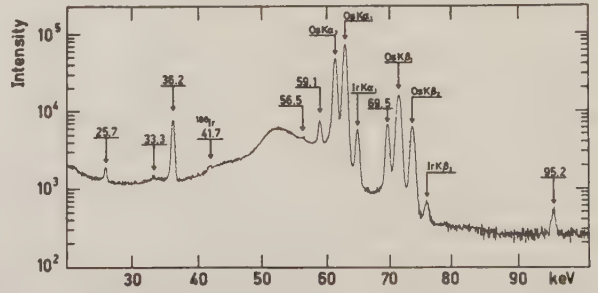

Fig. 1. The low-energy γ-ray spectrum from ^{189}Ir measured with a high-resolution Si(Li) detector.

2.2. GAMMA-RAY MEASUREMENTS

Extensive measurements on the γ-ray spectrum from ^{189}Ir have been performed. The low-energy part was studied with a 2 mm Si(Li) detector having an energy resolution of 0.5 keV at 60 keV. A typical spectrum is shown in fig. 1. As the detection efficiency goes down very fast with energy, no γ-rays above 95.2 keV were observed in this detector. These γ-rays were studied in a 1.5 cm^3 Ge(Li) detector with an energy

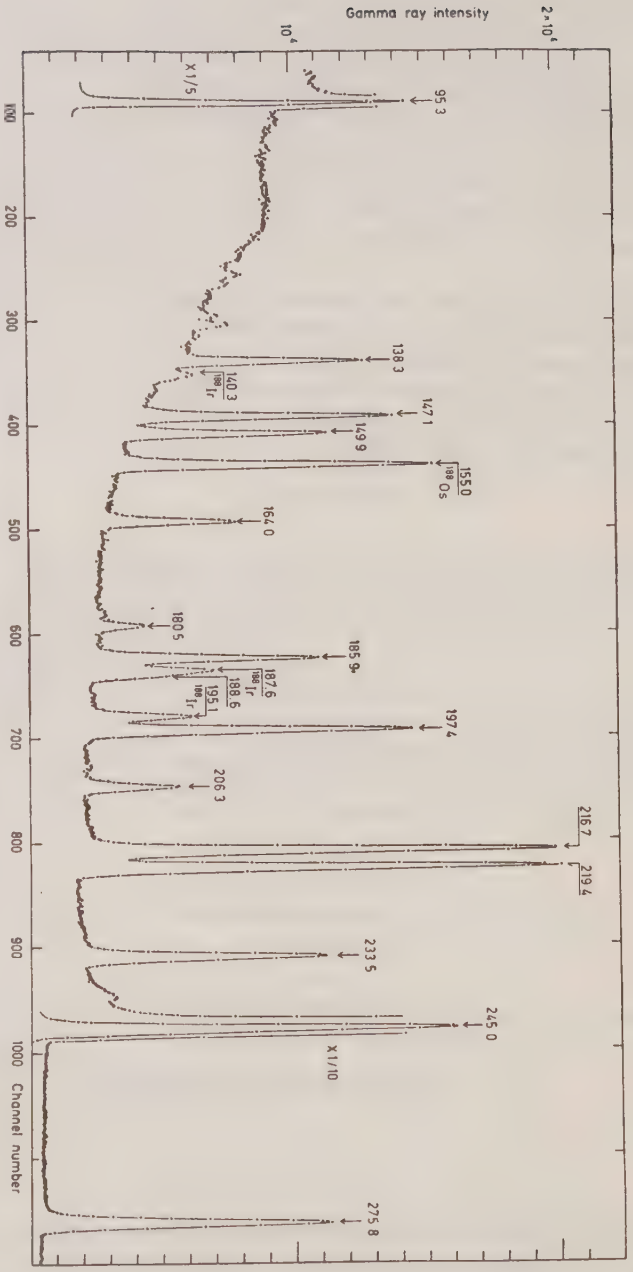

Fig. 2. The γ-ray spectrum from the decay of ^{189}Ir measured with a 1.5 cm^3 Ge(Li) detector.

resolution of 1.2 keV at 122 keV. A spectrum from this detector is shown in fig. 2. All the data were analysed with a computer program [15]) to obtain positions and areas of the observed peaks. All lines were followed for 2 months to assure that they belonged to the ^{189}Ir decay. Besides the investigated ^{189}Ir (13.3 d) activity we also observed the decay of ^{188}Ir (11 d). This contamination gave some problems especially in the energy region around 185-190 keV, where three rather close-lying lines are observed. The decay of the different components was carefully followed and an example of two spectra recorded with a time difference of 65 days is shown in fig. 3. At the positions calculated from the transition energies given by Harmatz *et al.* [3]), lines with predetermined shape were least-square fitted into the observed spectrum and the

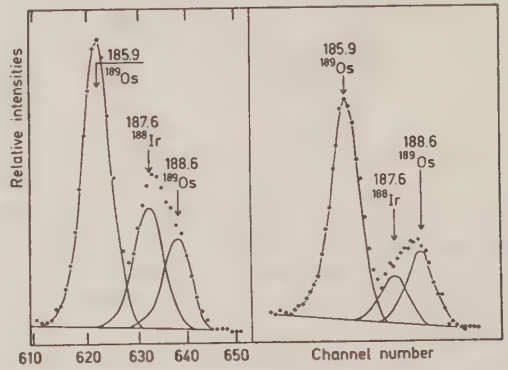

Fig. 3. The same energy region of the γ-ray spectrum measured with a 65 days interval clearly showing the shorter decay time of the 187.6 keV line originating from the decay of ^{188}Pt.

appropriate areas determined. As a check the 187.6 keV line intensity was compared to the 195.1 keV line also belonging to the ^{188}Ir decay and the intensity ratio was in good agreement with the value derived by Hanson *et al.* [16]).

A special search for weak lines above 275.8 keV was also made in a 25 cm^3 Ge(Li) detector with a 2 mm Pb-Cd-Cu absorber. Although several lines were observed in this energy region most of them could be attributed to the $A = 188$ mass chain. Three new weak lines were, however, observed decaying with a 13 d half-life.

All the data from the γ-ray measurements have been collected in table 1. Intensity normalizations between runs with different detectors were made on the 95.2 and 275.8 keV transitions. Our result is compared with the recent findings of Gregory *et al.* [10]) and the values calculated by Harmatz *et al.* [3]) from conversion electron intensities and multipolarity mixing ratios. The poor agreement with the latter at low energies depends on an underestimate of the electron intensities at these energies (see subsect. 2.3). No special effort was made to determine accurate energies of transitions already observed by Harmatz *et al.* [3]).

TABLE 1

Gamma-ray data in the decay of ^{189}Ir

Transition energy [a] (in keV)	Transition intensity		
	Present work	Gregory *et al.* [10]	Harmatz *et al.* [3]
$\Sigma(K_\alpha+K_\beta)$	1270±120		
25.7	0.40±0.05	0.5	0.05 [b]
36.2	11.2 ±1.0	11.8	2.8
56.5	2.5 ±0.5	3.3	1.1
59.1	21 ±2	26.3	12.3
69.5	59 ±6	62.1	36
95.2	6.4 ±0.5	5.1	6.8
97.8	< 0.01		0.2
138.3	1.14±0.13	1.1	0.8
147.1	1.80±0.14	1.4	1.3
149.9	1.41±0.10	0.1 [c]	1.4
164.0	1.23±0.06	0.1 [c]	1.0
180.5	0.49±0.05	0.5	0.37
185.9	3.0 ±0.3	9.2	2.2
188.6	0.86±0.07		1.6
197.4	4.4 ±0.2	3.7	2.1
206.3	1.33±0.05	1.2	2.9
216.7	8.6 ±0.4	6.2	10.4
219.4	8.8 ±0.4	6.4	9.5
233.5	5.0 ±0.2	5.0	6.0
245.0	100	100	100
275.8	9.0 ±0.5	8.8	7.0
343.2±0.1	0.91±0.06		
369.1	< 0.01		
402.8±0.1	0.11±0.01		
438.5±0.1	0.06±0.02		

[a]) Low-energy transition energies are taken from table 2. No special effort was made to accurately determine transition energies on lines given by ref. [3]).
[b]) Calculated by Harmatz *et al.* from their conversion data.
[c]) Probably a misprint in ref. [10]).

2.3. CONVERSION ELECTRON MEASUREMENTS

Internal conversion studies offer the best possibility to obtain information on the relative intensities and multipolarity mixing ratios of transitions within and between the lowest rotational bands in ^{189}Os. Although some studies have been made from the rhenium side [7]) the most extensive data have been obtained from the decay of ^{189}Ir [refs. [3,4])]. However, as can be seen in fig. 4, the electron intensities of Harmatz *et al.* [3]) and Sychikov *et al.* [4]) differ considerably in the low-energy region, where source thickness effects are of importance. We therefore decided to remeasure the low-energy part using a very thin source in order to obtain as accurately as possible the

relative intensities of the L-lines of the transitions within and between the two lowest rotational bands.

The lines were measured with a $\pi\sqrt{2}$ double-focusing beta spectrometer [17]). The detector was a GM tube with a 0.55 mg/cm^2 mylar window with a cut-off energy of about 15 keV. In order to make possible an efficient detection of the L-lines of the transitions in the 25-35 keV region the electrons were pre-accelerated with 10 kV high-voltage. The momentum resolution was 0.3 % at 30 keV and 0.15 % at 70 keV. The same sources as in the γ-ray measurement were used.

All L-groups were measured twice with two different sources, each measurement lasting about 8 days. Some of the recordings are shown in fig. 5. The results are given

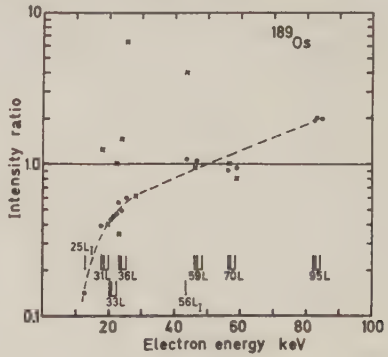

Fig. 4. Comparison between the conversion electron intensities of the present work (=1) and those of Harmatz *et al.* [3]) (dots) and those of Sychikov *et al.* [4]) (crosses). The data of ref. [3]) deviate in a systematic way from the present data as indicated by the dashed line.

in table 2. Energy calibration was made relative to the 47.693 keV [ref. [18])] KL_IL_I Auger line in Os. When comparing intensities of L-lines of transitions in the 30 keV region with lines of higher energy, a 15 % error should be added quadratically to the errors given in columns 2-6 of table 2, since the low-energy transitions showed slight tails, which could not be exactly separated from the background. This effect was larger for the 25.8 L-lines, which when compared to the other lines should be given 30 % extra error.

A number of lines reported by Harmatz *et al.* [3]) were not found in the present work. Although we observed a slight broadening of the 95.23 K-line in comparison with the 33.31 L-lines, cf. fig. 5, which could be interpreted as the K-line of a transition of 0.1 keV lower energy as suggested by Harmatz *et al.* [3]), this broadening is fully accounted for by the larger natural width of the atomic K-shell. The resolution of the present experiment was not sufficient to allow the resolution of the weak transition 0.2 keV higher than the 59.05 keV transition as reported in ref. [3]).

The L_{III} line of the 59.05 keV transition coincides very closely with the stronger KL_IL_{II} Auger line. The latter was subtracted from the composite peak using an in-

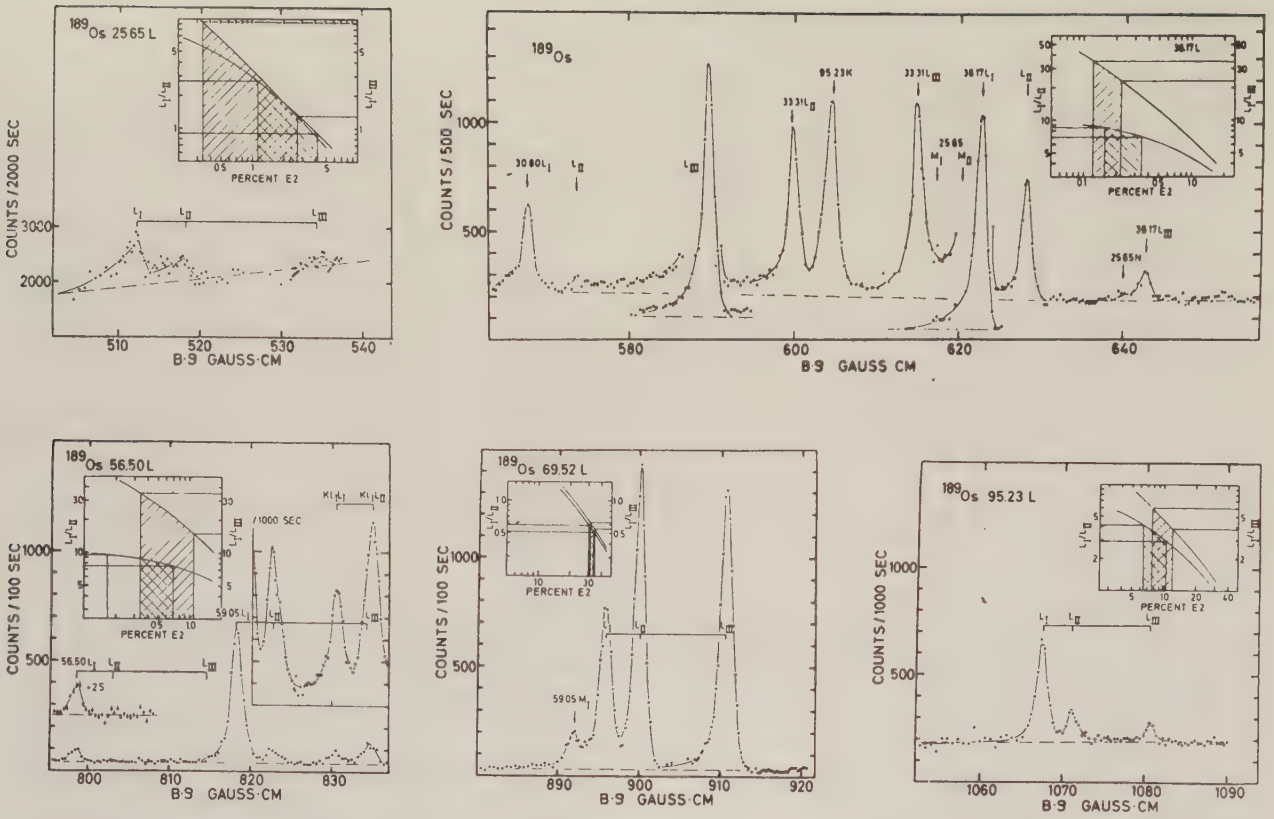

Fig. 5. Low-energy conversion lines from the decay of $^{189}Ir \rightarrow {}^{189}Os$ as recorded with the $\pi\sqrt{2}$ spectrometer. All lines were run with a pre-accelerating voltage of 9.746 kV. The points have not been corrected for decay. The positions of the 25.65 M lines are indicated but these lines could not be resolved from the 33.31 L_{III} and 36.17 L_I lines. The insets show theoretical [21]) L-subshell ratios as functions of the E2 admixture together with their limits obtained from the corresponding experimental data.

TABLE 2

Low-energy conversion electrons from the decay of $^{189}Ir \rightarrow {}^{189}Os$

Transition energy	Electron intensity [a])					Calculated gamma intensity [b])	Multipolarity
	K	L_I	L_{II}	L_{III}	M_I		
25.65±0.10		22 (30)	12.5 (30)	4.2 (70)		0.54 (50)	M1+(1.5$^{+1.5}_{-0.5}$)% E2
30.80±0.04		17.4(10)	1.8 (30)	90 (6)	6.0(15) [c])	$4.9 \cdot 10^{-4}$(12)	M3
33.31±0.04			31 (6)	33 (6)		0.116 (12)	E2
36.17±0.04		135 (6)	21.3 (6)	4.4 (20)		10.1 (12)	M1+(0.20±0.05) % E2
56.50±0.04		7.5(12)	< 1.5			1.8 (20)	M1+< 2 % E2
59.05±0.02		75 (8)	8.8 (10)	3.0 (30)	25 (19)	23.1 (8)	M1+(0.5±0.2) % E2
69.52±0.03		100 (5)	180 (5)	169 (5)		71.3 (5)	M1+(32.0±1.5) % E2
95.23±0.04	33.8(8)	4.8(8)	1.35 (15)	0.97(20)		6.34 (8)	M1+(9.0±2.0) % E2

[a]) Normalized to 100 for 69.52 L_I. The numbers in parentheses give the errors (s. d.) in %.
[b]) Calculated from the conversion intensities using the mixing ratios obtained from the L-intensity ratios and the theoretical conversion coefficients [21]). Normalization to the same intensity scale as table 1 was made on the average of the 36.17, 59.05 and 95.23 keV transitions.
[c]) 30.8 M_{III} = 26(8).

TABLE 3

Disturbing contributions to the half-life measurements

Level under investigation (in keV)	Channel 1		Channel 2		Disturbing coincidence contributions	
	main conversion line	disturbing components	main conversion line	disturbing components		
36.2	36.2 L_I	30.8 L_{III} 33.3 $L_{II}+L_{III}$ 95.2 K 95.3 K	59.1 L_I	56.5 L_I 59.3 L_I KLL Auger	33.3 L →	56.5 L_I 59.3 L_I
					KLL Auger →	33.4 L 95.2 K 95.3 K
69.5	69.5 L	59.1 M KLM Auger	KLL Auger	59.1 L_I	59.1 M → KLL Auger 59.1 L_I → KLM Auger	

tensity ratio $KL_I L_I/KL_I L_{II}$ for Ir of 1.45 as found in the decay of ^{189}Pt [ref. [19])]. This ratio is expected to change less than one percent in going from Ir to Os [ref. [20])].

The relative intensities obtained in the present work are compared to those of Harmatz *et al.* [3]) and Sychikov *et al.* [4]) in fig. 4. A strong systematic deviation as indicated by the dashed curve was found for the work of Harmatz *et al.* [3]), which possibly may be explained as a source thickness effect in the latter work. Very large non-regular deviations were found in comparison with the results of Sychikov *et al.* [4]).

The multipolarities and mixing ratios obtained from the L-subshell ratios and theoretical conversion coefficients [21]) are given in table 2. The mixing ratios are in fair agreement with those of Harmatz *et al.* [3]). This is explained by the fact that although the intensities of ref. [3]) differ very much from those of the present work, when the comparison is made over an extended energy range, the agreement is good when only a very limited region, i.e. an L-group, is considered. cf. fig. 4. The mixing ratio of the 69.52 keV transition has also been measured in Mössbauer experiments [8-10]). The results of 32 ± 6 % E2 [ref. [8])], 33 ± 5 % E2 [ref. [9])] and 36 ± 7 % E2 [ref. [10])]. are in good agreement with the present result.

The electron intensities and mixing ratios were used together with the theoretical conversion coefficients [21]) to calculate the gamma intensities given in table 2. The errors include the possible systematic errors of the electron intensities mentioned above. Normalization to the same scale as the γ-ray intensities given in table 1 was made on the average of the 36.17, 59.05 and 95.23 keV transitions (the 69.52 keV transition was avoided since the gamma line was not completely resolved from the Os K_β X-rays).

2.4. HALF-LIFE MEASUREMENTS

Several half-lives of excited levels in ^{189}Os have been measured with the delayed coincidence method. As the main instrument we have used a long-lens electron-electron coincidence spectrometer described in detail earlier [22,23]). The same sources as in the γ-ray measurements have been used.

The 36.2 keV *level.* The 59.1 L_I and 36.2 L_I conversion electron lines were focused in one spectrometer each and the time coincidence distribution between these lines was registered on a multichannel analyser. To obtain the prompt time resolution function of the system, coincidences from the $\beta \rightarrow$ 94.7 K cascade in the decay of ^{165}Dy were also measured. To be able to use the same energy settings in the two measurements the electrons from the ^{189}Ir source were pre-accelerated in a 16 kV electric field between the source and the spectrometer itself. In table 3 is given a list of possible disturbing coincidence distributions from other cascades in the source. The largest disturbing contribution is expected from cascades containing 33.3 L electrons introducing the half-life of the 69.5 keV level (1.6 nsec, see below). In a preliminary run we were also able to see a weak 1.6 nsec component. In the main runs we therefore set the spectrometer to a somewhat better energy resolution at the same time as we focused on the low-energy side of the 59.1 L_I line. After these adjustments no 1.6

nsec component was observed indicating that coincidence contributions from cascades involving the KLL Auger electrons were now negligible. An example of a delayed and prompt pair is given in fig. 6. Such pairs were analysed with the convolution method [24]). As an average we obtain a half-life of 0.53±0.03 nsec for the 36.2 keV level in ^{189}Os. Recently the 36.2 keV level has been excited in a Mössbauer experiment [11]) and from the width of the observed lines a half-life of 0.50±0.03 nsec was deduced.

The 69.5 keV *level.* According to Harmatz *et al.* [3]) the main feeding to this level is via a strong 245.0 keV transition and EC decay directly from ^{189}Ir. Therefore we first adjusted our lens spectrometers to focus the 245.0 K- and 69.5 L-lines. No coincidences were, however, observed implying that these two conversion lines are not in coincidence. We then re-focused one spectrometer to accept the KLL Auger group instead of the 245.0 K line and recorded the coincidence distribution. As in the previous case the β-94.7 K cascade in the decay of ^{165}Dy was again observed using the same energy settings to get the prompt time distribution. In this case 10 kV was added to the ^{165}Dy source. An example of a pair of delayed and prompt curves is given in fig. 7. The small asymmetry on the left-hand slope is due to the 59.1 $L_1 \rightarrow$ KLM Auger cascade (see table 3) introducing the half-life of the 95.2 keV level (0.23 nsec, see below). Before analysing the data with the convolution method [24]) this disturbing contribution was subtracted. As an average value from several measurements we obtain a half-life of 1.59±0.08 nsec for the 69.5 keV level in ^{189}Os. This value can be compared with the result from several other groups.

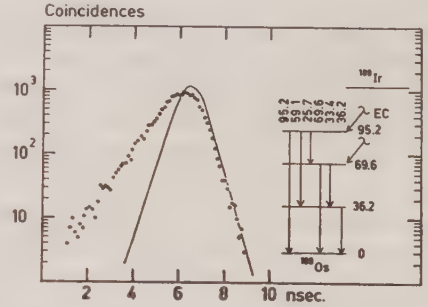

Fig. 6. Observed delayed coincidence curve taken between the 59.1 L_1 and 36.2 L_1 conversion electron lines. The curve drawn in full line is the corresponding prompt distribution. From the analysis we obtain a half-life of 0.53±0.03 nsec for the 36.2 keV level in ^{189}Os.

Andrejtscheff *et al.* [12]) obtain from a very recent delayed coincidence measurement 1.7±0.1 nsec, which is in good agreement with the present result. Persson *et al.* [8]) conclude from their Mössbauer measurements that $T_{\frac{1}{2}}$(69.5 keV) ≧ 1.8±0.2 nsec while Gregory *et al.*[10]) report $T_{\frac{1}{2}}$(69.5 keV) = 1.63±0.05 nsec from a delayed coincidence measurement in good agreement with our value. Using also our conversion electron data in table 2 we can deduce B(E2, 69.5 keV)↑ = (0.98±0.09)$e^2 \cdot b^2$ which can be compared with the corresponding values obtained in Coulomb excitation measurements of 0.63 $e^2 \cdot b^2$ in ref. [5]) and (1.2±0.2)$e^2 \cdot b^2$ in ref. [25]).

The 95.2 keV *level.* This level is mainly fed by direct EC in the decay of ^{189}Ir so the time distribution between the KLL Auger group and the 95.2 L electrons was studied. No disturbing coincidence distribution is expected. An example of the observed time spectrum is given in fig. 8 together with a prompt distribution clearly showing the difference in slope of the two curves. Several such pair of prompt and delayed curves were registered and analysed with the convolution method [24]). As a result we obtain a half-life of 0.23±0.03 nsec for the 95.2 keV level in ^{189}Os. Recently Gregory *et al.* [10]) have made attempts to measure the half-life of the same level. From a delayed coincidence measurement they could set an upper limit for the half-life of < 0.28 nsec while their Mössbauer experiment with the 95.2 keV gamma transition corrected for absorber thickness and internal conversion is compatible with a half-life of 0.13±0.04 nsec. Due to broadening effects such as hyperfine interactions this latter value should be taken as a lower limit and can thus be considered to be in agreement with our result.

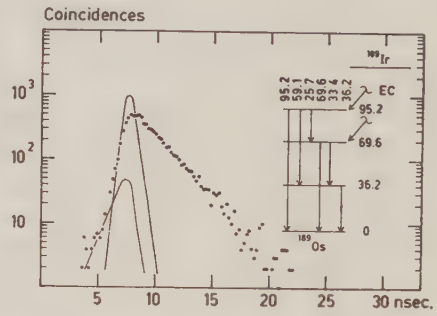

Fig. 7. The delayed time distribution recorded between the 69.5 L-line and the KLL Auger group. From the slope a half-life of 1.59±0.08 nsec was deduced for the 69.5 keV level in ^{189}Os.

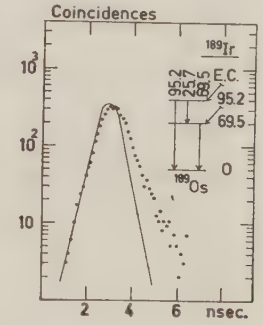

Fig. 8. An observed decay curve from coincidences between the 95.2 L-line and the KLL Auger group. The corresponding prompt curve is shown in full line. From the analysis we obtain a half-life of 0.23±0.03 nsec for 95.2 keV level in ^{189}Os.

The 216.7 *and* 219.4 keV *levels.* Weak K-conversion lines from the 219.4+216.7 and the 188.6+185.9 keV line groups have been observed in the lens spectrometer. Several attempts were made to determine the half-lives of the 216.7 and 219.4 keV levels from the delayed spectra of the 216.7 K → 59.1 L, 185.9 K → 59.1 L, 219.4 K → 56.5 L and 188.6 K → 56.5 L cascades. When compared with prompt spectra

indications of both centroid shifts and shape changes were compatible with half-lives less than 0.25 nsec. The lack of energy resolution and the poor statistics ($\approx$ 25 counts in the peak maximum per day) made it impossible to determine which level (or if both) was responsible for the delay.

The 275.9 keV *level.* The main feeding to this level is via direct electron capture in the decay of ^{189}Ir. The de-excitation strongly favours the intense 245.0 keV E2 transition to the 30.8 keV level. The time distribution between the KLL Auger electron group and the 245 K CE line was recorded using the double lens spectrometer. As the source was rather weak and the Auger yield low each run was continued for about 20 hours after which a prompt curve using the β-238.6 K cascade from a weak ^{212}Pb source was registered. To be able to use the same energy settings in the two measurements, 23 kV of pre-accelerating voltage was applied to the ^{212}Pb source. Several such pairs of delayed and prompt curves were recorded and all of them were analysed by the convolution [24]) method. Although the general form of the delayed curve was not very much different from a prompt curve, the analysis of all the data gave consistently a centroid shift and a shape change of the two curves equivalent to a half-life of 0.17$\pm$0.03 nsec for the 275.9 keV level in ^{189}Os.

3. Discussion

3.1. THE DECAY SCHEME

Our present knowledge of the ^{189}Os decay scheme is mainly obtained from the internal conversion measurements of Harmatz *et al.* [3]) in the decay of ^{189}Ir. Our work does on the whole confirm their proposed level scheme. A few deviations are, however, observed which will be discussed below.

As was pointed out in subsect. 2.3, Harmatz *et al.* [3]) have greatly underestimated the intensities of the low-energy conversion electron lines. This will have some important consequences in the construction of the level scheme. For instance it is rather safe to suppose that the 30.8 keV isomeric level is not directly fed in the decay of ^{189}Ir which means that the intensities of the 185.5, 188.6 and 245.0 keV transitions should balance the 30.8 keV isomeric transition. Using our electron and γ-ray intensities we find this intensity balance to be correct within 10 %. According to Harmatz, however, 83 % of the 245.0 keV transition is de-exciting a 314.6 keV level. If this should be correct, some other strong transitions have to feed the 30.8 keV level. No such transitions have, however, been found in the present work indicating that the 245.0 keV transition is only feeding the 30.8 keV level. This conclusion has also been verified as we did not observe any coincidences between the strong 245.0 K and 69.6 L conversion electron lines (see subsect. 2.4).

Harmatz *et al.* [3]) also report on a weak electron line which they interpret as the 97.8 L_1 line and place between the 314.6 and 216.7 keV levels. Supposing an M1 multipolarity for this transition we get a γ-ray intensity which is 20 times larger than our estimated upper limit for a gamma transition of that energy (see table 1). This means

that if a transition of 97.8 keV exists at all it must have a conversion coefficient of a magnitude at least corresponding to M4 multipolarity. Furthermore we have found no definite evidence that the 95.2 keV line is a doublet (see subsect. 2.3) and the 219.4 keV transition is well accounted for by only de-exciting the 219.4 keV level.

From the above arguments it is very doubtful if the 314.6 keV level exists at all and in any case it is far from being so strongly populated as is proposed by Harmatz *et al.* [3]).

From the energy combinations of a few weak transitions observed in our γ-ray spectrum (see table 1) we propose a new level at 438.5 keV. From its de-excitation

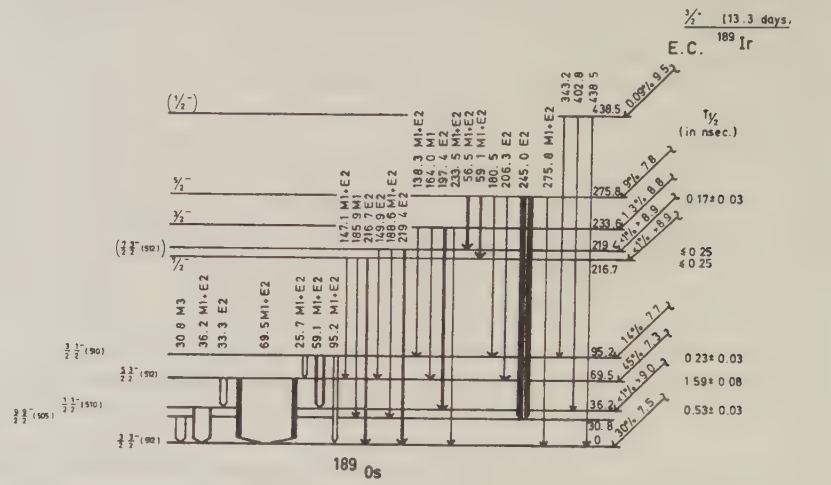

Fig. 9. The level scheme of ^{189}Os as obtained in the decay of ^{189}Ir. The widths of the arrows are approximately proportional to the intensities of the corresponding transitions, the white part indicating the internal conversion intensity. Given further are level energies (in keV), spins, parities and half-lives in nsec together with transition energies (in keV) and multipolarities. From the transition intensity balance appropriate log *ft* values have been calculated using a full decay energy of 800 keV.

to $\frac{1}{2}^-$ and $\frac{3}{2}^-$ levels but not to the 69.5 keV $\frac{5}{2}^-$ level a spin of $\frac{1}{2}$ is suggested for the 438.5 keV level.

Fig. 9 shows the level scheme for ^{189}Os as obtained in the decay of ^{189}Ir. Energies, spins, parities, and half-lives of the levels are given. From the intensity balance of the γ-ray and electron data appropriate log *ft* values have been calculated using a total decay energy of 800 keV [ref. [3])]. Our measured K X-ray intensity was used to determine the direct feeding to the ground state.

3.2. LEVEL ASSIGNMENTS

Recently Himmel [26]) has obtained the nuclear quadrupole moment of the ground state of ^{189}Os from atomic hyperfine structure measurements. His result amounts to

TABLE 4
Absolute transition probabilities in ^{189}Os

Level (keV)	$T_{\frac{1}{2}}$(exp) of level (nsec)	Transition energy (keV)	Initial state $IK^{\pi}(Nn_z\Lambda)$	Final state $IK^{\pi}(Nn_z\Lambda)$	Multipolarity	Relative $N\gamma$ [a]	Relative N_e [b]	$T_{\frac{1}{2}}$(exp) (sec)	B(M1) $(e\hbar/2Mc)^2$	B(E2) $(e^2 \cdot b^2)$	Q_0 (b)	F_W [c]
36.2	0.53±0.03	36.2	$\frac{1}{2}^-$(510)	$\frac{3}{2}^-$(512)	M1	99.8	2080	1.16E−8	(7.1 ±0.6)E−2			25
					E2	0.2		5.78E−6		(1.59±0.42)E−1		4.2E−2
69.5	1.59±0.08	33.3	$\frac{3}{2}^-$(512)	$\frac{1}{2}^-$(510)	E2	0.16	118	1.06E−5		(1.28±0.15)E−1		5.1E−2
		69.5		$\frac{3}{2}^-$(512)	M1	68	840	2.47E−8	(4.72±0.38)E−3			374
					E2	32		5.26E−8		(6.5 ±0.6)E−1	4.36±0.22	1.0E−2
95.2	0.23±0.03	25.7	$\frac{1}{2}^-$(510)	$\frac{3}{2}^-$(512)	M1	1.9	172	1.19E−7	(1.93±0.29)E−2			92
					E2	0.029		7.79E−6		$(6.3^{+6.3}_{-2.1})$E−1		1.1E−2
		59.1		$\frac{1}{2}^-$(510)	M1	99.5	477	2.27E−9	(8.4 ±1.2)E−2			21
					E2	0.5		4.52E−7		(1.7 ±0.7)E−1	3.0 ±0.5	3.8E−2
		95.2		$\frac{3}{2}^-$(512)	M1	27.6	200	8.19E−9	(5.6 ±0.8)E−1			317
					E2	2.9		7.78E−8		(9.2 ±1.6)E−2		7.1E−2
219.4	0.176 [d]	149.9	$\frac{3}{2}^-$(512) [f] $\{\frac{3}{2}^-(512), K+2\}$ γ−vib	$\frac{3}{2}^-$(512)	M1	< 0.3	1.3	>8.8 E−9	< 1.3 E−3			>1300
					E2	1.4		1.88E−9		(3.9 ±0.8)E−1	4.3 ±0.5	1.6E−2
		188.6		$\frac{5}{2}^-$(505)	M1	0.29 [e]	0.51	9.1 E−9	(6.5 ±2.0)E−4			3.7E+4
					E2	0.59		4.62E−9		(5.2 ±1.5)E−2		1.3E−1
		219.4		$\frac{3}{2}^-$(512)	E2	8.8	2.1	3.0 E−10		(3.7 ±0.6)E−1 [d]	5.1 ±0.4	1.8E−2
275.8	0.17±0.03	56.5	$\frac{5}{2}^-$	$\frac{7}{2}^-$	M1	1.8	9.6	1.49E−8	(1.47±0.30)E−2			120
					E2	< 0.04	<2.0	>6.7 E−7		<1.5E−1		>4.5E−2
		59.1		$\frac{7}{2}^-$	M1	< 3 [g]	<13	>9.0 E−9	<2.1E−2			> 84
		180.5		$\frac{1}{2}^-$(510)	M1	0.5	0.5	5.38E−8	(1.24±0.35)E−4			14100
		206.3		$\frac{3}{2}^-$(512)	M1	< 0.27 [h]	0.4	>1.0 E−9	<4.5E−3			>39000
					E2	1.33		2.02E−8		(7.5 ±1.5)E−3		0.88
		245.0		$\frac{5}{2}^-$(505)	E2	100	17.2	2.69E−10		(2.37±0.47)E−1		2.75E−2
		275.8		$\frac{3}{2}^-$(512)	M1	3.4 [i]	17.9	7.91E−9	(2.37±0.60)E−4			7400
					E2	5.6		4.80E−9		(7.3 ±1.5)E−3		0.81

[a]) Normalized for each level.
[b]) $N_e/\Sigma N_\gamma = \alpha$ for each transition.
[c]) Hindrance factor relative to the Weisskopf estimate [27]) with the statistical factor equal to one.
[d]) From the Coulomb excitation measurement of Hrynkiewicz *et al.* [6]).
[e]) M1/E2 ≈ 0.5 from Harmatz *et al.* [3]).
[f]) Only tentative assignments.
[g]) From the intensity balance.
[h]) Given as pure E2 by Harmatz *et al.* [3]).
[i]) M1/E2 ≈ 0.6 from Harmatz *et al.* [3]).

an intrinsic quadrupole moment of 4.55±0.50 b giving a corresponding deformation parameter of $\delta = 0.15 \pm 0.01$. This is a value very similar to the one obtained for the ^{193}Ir and ^{191}Ir isotopes [1,2]) and we would thus expect a similar general structure for all these nuclei with strongly mixed rotational bands together with vibrational excitations.

From their data Harmatz *et al.* [3]) proposed that the ground state of ^{189}Os has a $\frac{3}{2}\frac{3}{2}^-(512)$ configuration with the first rotational state at 69.5 keV. The $\frac{1}{2}^-(510)$ orbital was suggested to have band members at 36.2 and 95.2 keV. Our data on absolute transition probabilities given in table 4 are in general agreement with such an interpretation.

Both McGowan *et al.* [5]) and Hrynkiewicz *et al.* [6]) have shown that the 219.4 keV level is strongly Coulomb excited with a B(E2) corresponding to at least 50 s.p.u. As the spin of this level is unambiguously determined as $\frac{7}{2}$ from its decay characteristics it is tempting to assign this level as $\frac{7}{2}\frac{3}{2}^-(512)$. The fact that the E2 part of the $\frac{7}{2}\frac{3}{2} \rightarrow \frac{5}{2}\frac{3}{2}$ transition of 149.8 keV is also enhanced (62 s.p.u.) speaks in favour of such an interpretation. On the other hand the energy spacing is not consistent with a pure rotational band for which the $[E(\frac{7}{2}) \rightarrow E(\frac{3}{2})]/[E(\frac{7}{2}) - E(\frac{5}{2})]$ ratio is predicted to be 2.4 while we obtain 3.15 in ^{189}Os. In ^{193}Ir and ^{191}Ir for instance [1,2]) we find the corresponding ratio to be 2.58 and 2.68 respectively. As another alternative the $\frac{7}{2}^-$ level can be obtained by coupling a gamma vibration to the $\frac{3}{2}^-(512)$ orbital, but the observed E2 strength is much larger than that usually carried by a pure gamma vibrational phonon. The 219.4 keV level is probably a mixture of several of such excitations where the energy discrepancy depends on interactions with other close-lying $\frac{7}{2}^-$ levels.

No Coulomb excitation of the $\frac{7}{2}^-$ level at 216.7 keV has been reported. This level could therefore be a good candidate for the expected $\frac{7}{2}\frac{7}{2}^-(503)$ single-particle level. Such a state would have to decay by once forbidden M1 transitions to the $K = \frac{3}{2}$ band and could therefore be expected to have a longer half-life. From our upper limit for the 216.7 keV level of < 0.25 nsec we conclude that the hindrance [27]) for the 147.1 keV M1 transition is < 840 which is less than expected for a first-forbidden M1 transition.

The 275.8 keV level with a spin and parity of $\frac{5}{2}^-$ decays mainly by a 245.0 keV E2 transition to the 30.8 keV $\frac{9}{2}^-$ isomeric level. Harmatz *et al.* [3]) have assigned the former as the $\frac{5}{2}\frac{5}{2}^-(503)$ single-particle state. From our limit of the half-life of the 275.8 keV level we find the 245.0 keV E2 transition to be enhanced 36 s.p.u. (see table 4). This value indicates that the 275.8 keV level has a collective nature rather than being the $\frac{5}{2}\frac{5}{2}^-(503$ state). These facts suggest that the 275.8 keV level could be the $(K-2)$ γ-vibrational component built on the $\frac{9}{2}\frac{9}{2}^-(505)$ orbital. We also see that the 56.5 and 59.1 keV M1 transitions are hindered about one hundred times [27]) while the M1 transitions to the ground state and the 95.2 keV levels are much more hindered. The hindrance factor 1.4×10^4 for the 180.5 keV transition is compatible with a first K-forbidden M1 transition while the large hindrance for M1 transitions to the $K = \frac{3}{2}$ band does not have such an obvious explanation. Another origin of the 275.8 keV level is suggested by the excitation energy and the B(E2) value which both have values typical for the first 2^+ state in spherical even nuclei in this mass region. One may accordingly very tentatively propose the 275.8 keV level as formed essentially as a spherical $\frac{5}{2}^-$ state obtained by coupling of a $\frac{9}{2}^-$ particle $(h_{\frac{9}{2}})$ to the 2^+ excitation of the spherical even core. We have recently suggested a similar situation in odd-mass Ir nuclei [28]).

3.3. E2 TRANSITION RATES

From the atomic hyperfine splitting Himmel [26]) has derived the inner quadrupole moment $Q_0 = 4.45 \pm 0.50$ b for the ground state of ^{189}Os. The same quantity can also be derived from Coulomb excitation or half-life measurements. Results from the latter kind of measurements are given in table 4, column 12. The available data for the $K = \frac{3}{2}$ band cluster around $Q_0 = 4.5$ while the only measurement in the $K = \frac{1}{2}$ band gives $Q_0 = 3.0 \pm 0.5$. These values correspond to deformation parameters of $\delta = 0.15 \pm 0.01 (K = \frac{3}{2})$ and $\delta = 0.11 \pm 0.02 (K = \frac{1}{2})$ indicating that ^{189}Os is only a weakly deformed nucleus where both rotational and vibrational degrees of freedom will be of importance together with their coupling to the single-particle states.

An estimate of the effective coupling strength is obtained by studying the interband E2 transition rates which are usually dominated by diagonal contributions obtained via admixtures. The fact that the observed inter- and intraband E2 transitions in ^{189}Os have comparable strengths indicates that strong mixing occurs. Considering only the Coriolis coupling between the $\frac{1}{2}^-(510)$ and $\frac{3}{2}^-(512)$ bands the amplitudes of the different components in the wave functions are only a function of the energy difference between the two states with spin I that mix and the coupling strength parameter $P_+ E^* \langle \frac{1}{2}|j_-|\frac{3}{2}\rangle$ (see ref. [1]) for more details). Here the pairing factor $P_+ \approx 1.0$ and $E^* \approx \hbar^2/2J$ for the actual rotational bands, e.g. about 15 keV. Using the deformed potential parameters recommended by Nilsson [13]) and $\delta = 0.13$ the Nilsson model predicts $\langle \frac{1}{2}|j_-|\frac{3}{2}\rangle = 1.0$.

Predicted B(E2) values for different interband transitions are given in table 5 for three different values of the parameter $E^* \langle \frac{1}{2}|j_-|\frac{3}{2}\rangle$. By comparing these with the experimental values it is generally seen that a much larger effective mixing than predicted by theory ($E^* \langle \frac{1}{2}|j_-|\frac{3}{2}\rangle \approx 15$ keV) is needed to account for the observed strong interband E2 transition rates. On the other hand the ratio of the quadrupole moments $Q(\frac{3}{2}, \frac{5}{2})/Q(\frac{3}{2}, \frac{3}{2})$ as found by Kucheida *et al.* [9]) is reproduced by a value of $E^* \langle \frac{1}{2}|j_-|\frac{3}{2}\rangle = 9$ keV.

3.4. M1 TRANSITION RATES

From the present measurements we can deduce five B(M1) values for transitions going within or between members of the two low-lying rotational bands in ^{189}Os. Other recent papers [8-11]) supply us with three magnetic moments. All this data has been collected in table 6 and can now be compared with the predictions of the Nilsson model [13]). For example this model predicts that $B(\mathrm{M1}, \frac{3}{2}\frac{1}{2} \rightarrow \frac{5}{2}\frac{3}{2})/B(\mathrm{M1}, \frac{3}{2}\frac{1}{2} \rightarrow \frac{3}{2}\frac{3}{2}) = 1.5$ while experiments give 0.034 ± 0.007 which indicates that this model in its simplest form has its clear limitations.

To be able to improve the situation various kinds of admixtures can be taken into account. For simplicity we have confined ourselves to the simple Coriolis mixing between the members of the $\frac{1}{2}^-(510)$ and $\frac{3}{2}^-(512)$ particle states. The fundamental type of expressions for the relevant reduced M1 transition rates and magnetic moments are given in detail in ref. [1]). In the mentioned approximation the magnetic properties of ^{189}Os are determined by the following six parameters [1]) namely $P_+ G_{M1}(\frac{1}{2} \to \frac{3}{2})$, $G_{M1}(\frac{3}{2} \to \frac{3}{2})$, $G_{M1}(\frac{1}{2} \to \frac{1}{2})$, $b_{M1} G_{M1}(\frac{1}{2} \to \frac{1}{2})$, g_R and $E^*\langle\frac{1}{2}|j_-|\frac{3}{2}\rangle$.

Fig. 10. A comparison between fitted and theoretically predicted [13]) values for $G_{M1}(\frac{1}{2} \to \frac{3}{2})$ and $G_{M1}(\frac{3}{2} \to \frac{3}{2})$ as functions of the parameter $K = g_s(\text{effective})/g_s(\text{free})$ (see subsect. 3.4).

As the expressions for B(M1) and μ are not linear in the parameter $E^*\langle\frac{1}{2}|j_-|\frac{1}{2}\rangle$ we have for simplicity preferred to do the calculations for a few pre-determined values for this quantity. The known experimental material in table 6 has then, through a least-squares fit, been used to determine the other five parameters. The fitted values as well as the calculated B(M1) and μ-values are given in the right-hand section of table 6 for some selected values of $E^*\langle\frac{1}{2}|j_-|\frac{3}{2}\rangle$. As can be seen no quantity is particularly sensitive to the coupling strength and only a moderate improvement is achieved by the introduction of the Coriolis coupling.

The fitted parameters which are given in the lower part of table 6 are also seen to be rather independent of the coupling strength but both $G_{M1}(\frac{1}{2} \to \frac{1}{2})$ and $b_{M1} G_{M1}(\frac{1}{2} \to \frac{1}{2})$ are poorly determined. It is now of interest to see how well the fitted parameters can be accounted for by the Nilsson model. The predicted quantities have been deduced for some different values of the model parameters μ, κ, δ, g_s(effective) and g_R (see ref. [1])] to investigate the uncertainty in the model predictions. The results for the two best determined parameters $P_+ G_{M1}(\frac{1}{2} \to \frac{3}{2})$ and $G_{M1}(\frac{3}{2} \to \frac{3}{2})$ are given in fig. 10. Both

TABLE 5
E2 rates for interband transitions in ^{189}Os

	Experimental data ($e^2 \cdot b^2$)	Calculated values [a])		
		$E^*\langle\frac{1}{2}\|j_-\|\frac{3}{2}\rangle = 10$	$E^*\langle\frac{1}{2}\|j_-\|\frac{3}{2}\rangle = 30$	$E^*\langle\frac{1}{2}\|j_-\|\frac{3}{2}\rangle = 90$
$B(E2, \frac{1}{2}\frac{1}{2} \to \frac{3}{2}\frac{3}{2})$	(1.59±0.42)E−1	0.13E−1	0.61E−1	1.26E−1
$B(E2, \frac{5}{2}\frac{5}{2} \to \frac{1}{2}\frac{1}{2})$	(1.28±0.15)E−1	0.22E−1	0.92E−1	1.69E−1
$B(E2, \frac{3}{2}\frac{1}{2} \to \frac{5}{2}\frac{3}{2})$	(6.3 $\pm^{6.3}_{2.1}$)E−1	0.17E−1	0.76E−1	1.21E−1
$B(E2, \frac{3}{2}\frac{3}{2} \to \frac{5}{2}\frac{5}{2})$	(9.2 ±1.6)E−2	4.7 E−2	18.6E−2	25.2 E−2

[a]) We used $G_{E2}(\frac{1}{2}\frac{1}{2}) = 26$ and $G_{E2}(\frac{3}{2} \to \frac{3}{2}) = 39$ corresponding to $= Q_0 = 0.3$ and $Q_0 = 4.5$ b respectively. $E^*\langle\frac{1}{2}|j_-|\frac{3}{2}\rangle$ is given in keV.

TABLE 6
Magnetic properties in ^{189}Os

Experimental data [a])		Calculated B(M1) and μ-values using the fitted parameters given below				
		$E^*\langle\frac{1}{2}\|j_-\|\frac{3}{2}\rangle = 0$	$E^*\langle\frac{1}{2}\|j_-\|\frac{3}{2}\rangle = 10$	$E^*\langle\frac{1}{2}\|j_-\|\frac{3}{2}\rangle = 20$	$E^*\langle\frac{1}{2}\|j_-\|\frac{3}{2}\rangle = 30$	$E^*\langle\frac{1}{2}\|j_-\|\frac{3}{2}\rangle = 50$
$\mu\frac{3}{2}\frac{3}{2}^-(512)$	0.6565±0.0004 [b])	0.6566	0.6565	0.6565	0.6565	0.6565
$\mu\frac{1}{2}\frac{1}{2}^-(510)$	0.266 ±0.013 [c])	0.266	0.254	0.221	0.214	0.292
$\mu\frac{5}{2}\frac{5}{2}^-(512)$	0.977 ±0.010 [d])	0.916	0.963	1.005	1.000	0.979
$B(M1, \frac{1}{2}\frac{1}{2} \to \frac{3}{2}\frac{3}{2})$	(7.1 ±0.6)E−2	5.50E−2	4.93E−2	4.80E−2	5.55E−2	8.29E−2
$B(M1, \frac{5}{2}\frac{5}{2} \to \frac{3}{2}\frac{3}{2})$	(4.72±0.38)E−3	2.61E−3	4.31E−3	5.71E−3	5.48E−3	5.02E−3
$B(M1, \frac{3}{2}\frac{1}{2} \to \frac{5}{2}\frac{3}{2})$	(1.93±0.29)E−2	3.29E−2	3.76E−2	3.16E−2	2.89E−2	1.56E−2
$B(M1, \frac{3}{2}\frac{1}{2} \to \frac{1}{2}\frac{1}{2})$	(8.4 ±1.2)E−2	8.40E−2	8.65E−2	7.78E−2	8.24E−2	7.22E−2
$B(M1, \frac{3}{2}\frac{3}{2} \to \frac{3}{2}\frac{3}{2})$	(5.6 ±0.8)E−1	0.22E−1	0.43E−1	0.44E−1	0.38E−1	0.17E−1
$P_+(\frac{1}{2} \to \frac{3}{2})G_{M1}(\frac{1}{2} \to \frac{3}{2})$		0.97±0.33	1.22±0.30	1.38±0.31	1.59±0.43	1.86±0.48
$G_{M1}(\frac{3}{2} \to \frac{3}{2})$		0.42±0.14	0.41±0.12	0.46±0.13	0.49±0.16	0.68±0.22
$G_{M1}(\frac{1}{2} \to \frac{1}{2})$		1.80±1.25	−1.20±0.82	−1.13±0.81	−1.13±0.79	−1.15±0.66
$G_{M1}(\frac{1}{2} \to \frac{1}{2})b_{M1}$		0.48±1.21	−0.97±0.54	−0.59±0.49	−0.40±0.41	0.29±0.35
g_R		0.32±0.04	0.38±0.04	0.43±0.04	0.48±0.05	0.49±0.05
mean square sum		4.7	2.7	2.9	2.8	3.1

[a]) B(M1) is given in $(e\hbar/2Mc)^2$ and μ in nuclear magnetons. [b]) From ref. [26]). [c]) From ref. [11]). [d]) From ref. [9]).

are reasonably well accounted for using $\mu = 0.45$, $\kappa = 0.06$, $\delta = 0.1$ and g_s(effective) $= 0.8 g_s$(free) where g_s(free) $= 5.585$. Varying g_R by 0.1 units shifts $G_{M1}(\frac{3}{2} \rightarrow \frac{3}{2})$ by 0.3 units and $G_{M1}(\frac{1}{2} \rightarrow \frac{3}{2})$ by 0.1 units. For the same parameters $G_{M1}(\frac{1}{2} \rightarrow \frac{1}{2})$ is predicted to be 1.45 (the right magnitude but wrong sign) and $b_{M1} G_{M1}(\frac{1}{2} \rightarrow \frac{1}{2})$ as 4.1 while experiments in this case give a much smaller value. The same discrepancy has also been observed in both ^{193}Ir and ^{191}Ir [refs. [1,2])]. The gyromagnetic ratio $\gamma_R = 0.38 \pm 0.04$ from the best fit is slightly higher than the recently calculated value 0.31 by Prior *et al.* [29]).

We are greatly indebted to Dr. Arve Kjelberg and co-workers at the Nuclear Chemistry Group at ISOLDE, CERN for the effort they have made to provide us with the separated radioactive sources. The work was supported by the Swedish Atomic Research Council.

References

1) V. Berg, S. G. Malmskog and A. Bäcklin, Nucl. Phys. **A143** (1970) 177
2) S. G. Malmskog, V. Berg, A. Bäcklin and G. Hedin, Nucl. Phys. **A143** (1970) 160
3) B. Harmatz, T. H. Handley and J. W. Mihelich, Phys. Rev. **128** (1962) 1186
4) G. I. Sychikov, O. D. Kovrigin, G. D. Latyshev, G. A. Londarenko and V. N. Novikov, Bull. Akad. Sci. USSR (ser. phys.) **30** (1966) 169
5) F. K. McGowan, P. H. Stelson, R. L. Robinson and J. L. C. Ford, ORNL-3425 (1963) p. 26
6) A. Z. Hrynkiewicz, B. Sawicka, J. Styczén, S. Szymczyk and M. Szawlowski, Acta Phys. Pol. **31** (1967) 437
7) B. Crasemann, G. T. Emery, W. R. Kane and M. L. Perlman, Phys. Rev. **132** (1963) 1681
8) B. Persson, H. Blumberg and M. Bent, Phys. Rev. **174** (1968) 1509
9) D. Kucheida, F. Wagner, G. Kaindl and P. Kienle, Z. Phys. **216** (1968) 346
10) M. C. Gregory, B. L. Robinson and S. Jha, Phys. Rev. **180** (1969) 1158
11) F. Wagner, G. Kaindl, H. Bohn, U. Biebl, H. Schaller and P. Kienle, Phys. Lett. **28B** (1969) 548
12) W. Andrejtscheff, F. Dubbers, K.-D. Schilling and F. Stary, Nucl. Phys. **A137** (1969) 693
13) S. G. Nilsson, Mat. Fys. Medd. Dan. Vid. Selsk. **29**, no. 16 (1955)
14) P. G. Hansen *et al.*, Phys. Lett. **28B** (1969) 415
15) A. Bäcklin, B. Fogelberg and S. G. Malmskog, Nucl. Phys. **A103** (1967) 337 (appendix)
16) R. J. Hanson, P. G. Hansen, H. L. Nielsen and G. Sørensen, Nucl. Phys. **A115** (1968) 641
17) A. Bäcklin, Nucl. Instr. **57** (1967) 261
18) O. Hörnfelt, Ark. Fys. **23** (1963) 235
19) A. Bäcklin, V. Berg and S. G. Malmskog, to be published
20) M. A. Listengarten, Izv. Akad. Nauk SSSR (ser. fiz.) **26** (1962) 182
21) R. S. Hager and E. C. Seltzer, Nucl. Data **A4**, no. 1 and 2 (1968)
22) T. R. Gerholm and J. Lindskog, Ark. Fys. **24** (1963) 171
23) S. G. Malmskog, Ark. Fys. **35** (1968) 255
24) B. Olsen and L. Boström, Nucl. Instr. **44** (1966) 65
25) D. H. Rester, M. S. Moore, F. E. Durham and C. M. Class, Nucl. Phys. **22** (1961) 104
26) G. Himmel, Z. Phys. **211** (1968) 68
27) A. H. Wapstra, G. J. Nijgh and R. van Lieshout, Nuclear spectroscopy tables (North-Holland, Amsterdam, 1959)
28) A. Bäcklin, V. Berg and S. G. Malmskog, Nucl. Phys.. to be published
29) O. Prior, F. Boehm and S. G. Nilsson, Nucl. Phys. **A110** (1968) 257

R E F E R E N C E 17

QUASI-PROLATE AND QUASI-OBLATE BANDS IN SOFT ^{189}Au

V. BERG and R. FOUCHER
Institut de Physique Nucléaire, B.P. nr 1, 91406 Orsay, France
and
A. HOGLUND
Institut of Physics, University of Stockholm, Sweden
(The ISOLDE Collaboration)

1.E.1: 3.A

Nuclear Physics A244 (1975) 462–486; © *North-Holland Publishing Co., Amsterdam*

Not to be reproduced by photoprint or microfilm without written permission from the publisher

QUASI-PROLATE AND QUASI-OBLATE BANDS IN SOFT ^{189}Au

V. BERG and R. FOUCHER

Institut de Physique Nucléaire, BP nr 1, 91406 Orsay, France

and

Å. HÖGLUND

Institute of Physics, University of Stockholm, Sweden

(The ISOLDE Collaboration)

Received 8 August 1974

(Revised 2 December 1974)

Abstract: The decay of ^{189}Hg is studied using mass separated sources. Internal conversion coefficients are determined for 57 transitions and the half-lives of four excited states in ^{189}Au are measured. A decay scheme with 55 states is proposed. It is found that ^{189}Au has many features in common with the heavier gold isotopes. However $\approx \frac{1}{3}$ of the total ^{189}Hg decay proceeds via a new system of negative parity states to the $\frac{11}{2}^-$ isomer. The new states are suggested as resulting from the Coriolis decoupling of a proton in the $h_{\frac{9}{2}}$ orbital. This interpretation implies that a tendency for oblate as well as prolate shapes exists in ^{189}Au.

E RADIOACTIVITY ^{189m,189}Hg [from Pb(p, 3pxn)Hg; mass separated]; measured E_γ, I_γ, E_{ce}, I_{ce}, $T_{\frac{1}{2}}$, ICC, γ-γ coin, ce-γ coin, γ-ce delay. ^{189}Au deduced levels, J, π, $T_{\frac{1}{2}}$, multipolarities, B(M1), B(E1), B(E2). Ge(Li), Si(Li), magnetic spectrometer.

1. Introduction

The study of transitional nuclei in the Os-Hg region has especially been centered on the even nuclei and has shown that these nuclei are soft, with potential energy surfaces characterized by rather shallow minima for both oblate and prolate shapes [1–6]). Odd nuclei, although more difficult to interpret on account of their complexity, should give more detailed information on nuclear shapes, shape fluctuations, and their relations with single particle states. A comparison between the decay properties of the systems of positive and negative parity states in ^{193}Ir [ref. [7])] first led to the proposal of coexistence of different shapes in Ir and Au nuclei [1, 8]). Later experiments gave support to this suggestion [9, 25]). The odd mass Au nuclei, with numbers 191, 193, 195 are very similar and are considered to have an essentially vibrational structure [11–13]). In ^{191}Au, however, signs appear which show that the nucleus is near the critical region of oblate-prolate transition. It then seemed interesting to extend the study to ^{189}Au, so far scarcely known: Gamma rays following the disintegration

of ^{189}Hg were reported by ref. [14]) who also determined two periods in this decay. The half-life of an isomeric state in ^{189}Au and the internal conversion electrons of an intense transition were measured by ref. [15]).

2. Experimental procedures

2.1. SOURCE PREPARATION

Sources of ^{189}Hg were produced at the ISOLDE facility at CERN [16]) by separation of Hg obtained as a spallation product after bombardment of molten lead with 600 MeV protons. All measurements, with the exception of a multipole meter experiment, were made off-line. After collection in the separator on 0.1 mm thick Al strips, the sources were taken out of the vacuum system by an air lock and sent by a pneumatic transport to the detecting area. Typical times for collection, transport, and measurements were 30 s, 5 min, 8 to 10 min. As the decaying levels in ^{189}Hg have half-lives of 7.5 ± 0.2 min and 8.7 ± 0.2 min, the experiments were disturbed by the activity from 4.55 min Au and 28.3 min Au.

2.2. GAMMA-RAY AND INTERNAL CONVERSION ELECTRON MEASUREMENTS

The γ-ray spectrum was measured with Ge(Li) detectors with the following characteristics:

Volume	Energy resolution
35 cm^3	2.3 keV for the 1.33 MeV γ-ray of ^{60}Co
25 cm^3	2.3 keV for the 1.33 MeV γ-ray of ^{60}Co
30 cm^3	3.2 keV for the 1.33 MeV γ-ray of ^{60}Co
1 cm^3	1.0 keV for the 0.12 MeV γ-ray of ^{57}Co

Conversion electrons were recorded with a 1.5 mm thick windowless Si(Li) detector with 3.0 keV resolution for the 570 keV K-line in ^{207}Pb and by using a Gerholm-Lindskog double lens β-spectrometer with a momentum resolution of 3 % [ref. [17])].

The relative efficiencies of the Ge(Li) detectors were obtained by measuring calibrated standard sources (IAEA, Vienna), that of the Si(Li) detector by measuring the electron spectra of ^{133}Ba and ^{207}Bi. The single γ-ray spectra were measured and evaluated in the same way as in ref. [2]).

The γ-γ coincidences were taken with the 35 cm^3 and the 25 cm^3 detectors. The experimental set-up, the measurements and the handling of data are described in ref. [2]).

The e-γ coincidences were obtained using one lens of the magnetic spectrometer and a Ge(Li) detector placed at 180°. Electron lines of low energy transitions (9.9 M,

241

44 L, 78 L) were then focused by the lens and the γ-rays in coincidence selected from the spectrum recorded with the Ge(Li) detector. The 9.9 M electrons became detectable through preacceleration in a potential of 15 kV.

The internal conversion electron spectrum was measured in connection with a multipole meter experiment performed on-line. The Si(Li) electron detector and the 3.2 keV Ge(Li) γ-ray detector then faced each other on either side of the tape of a transport system inside the separator vacuum. The sources were collected during 5 sec on the tape, and then rapidly transported to the detecting position between the detectors which simultaneously recorded the electron and the γ-ray radiation during the following 30 sec. The correlation between e^- and γ intensities was established by measuring bare sources of ^{133}Ba and ^{207}Bi decaying through transitions for which the internal conversion coefficients are very accurately known.

2.3. HALF-LIFE MEASUREMENTS

The half-lives of excited levels were measured with the delayed coincidence technique using the double lens e^--e^- coincidence spectrometer [17]). In some cases, well suited for e^--γ coincidences, one of the lenses was replaced by a plastic scintillator (Pilot B 5 %) for the detection of the photopeaks of low energy γ-rays and X-rays, and the Compton events from high energy γ-rays.

3. Results

3.1. SINGLE GAMMA-RAY MEASUREMENTS

A γ-ray spectrum taken off-line with the 35 cm^3 Ge(Li) detector is shown in fig. 1. The peak density is high and many complex lines remain unresolved. To get more detailed information, the low energy region (20–350 keV) was measured with the small high resolution detector. The γ-ray spectrum recorded on line was mainly due to pure ^{189}Hg, as the cycle of collection, transport and measurement was short compared to the Hg half-lives. To obtain information about the daughter decays, sources were collected to favour the 28 min Au activity. After removing Hg, the Au disintegration was studied [18]), and it was observed that within the resolution of our detectors, many strong γ-transitions appear at the same energy in ^{189}Au and ^{189}Pt. The most intense transition following the ^{189}Hg decay has the energy of 166.5 keV and has been attributed both to the 4.55 min Au and 28.3 min Au disintegration [15]). When seen with the high resolution detector, its γ-ray did not show any broadening, but the electron spectrum revealed that the transition is a doublet with one component in Au and the other in Pt, the K-line being double with the distance between the peaks equal to the difference of the K-binding energies of Au and Pt. The high resolution detector clearly showed the doublet structure of the 320 keV γ-ray [14]), the higher component at 321.0 keV belonging to the Hg, the lower one at 319.8 keV to the 4.55 min Au decay.

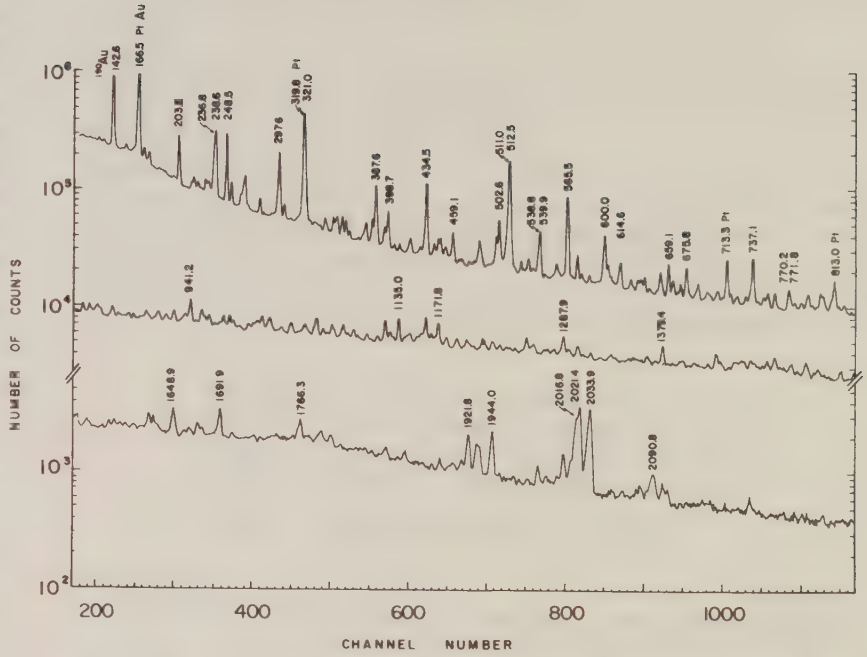

Fig. 1. Gamma-ray spectrum following the decay of ^{189}Hg taken with a 35 cm^3 Ge(Li) detector.

In order to distinguish between transitions fed from the 7.5 ± 0.2 min and 8.7 ± 0.2 min levels in ^{189}Hg the decay of γ-rays were followed during 40 min in multichannel experiments. The result agrees with earlier reported data [14]), with the exception that the 203.8 keV γ-ray is definitely emitted in the 7.5 min decay.

3.2. CONVERSION ELECTRON MEASUREMENTS

In the electron spectrum many peaks were complex on account of the moderate resolution of the Si(Li) detector. In spite of relatively good statistical accuracy, rather large errors had to be accepted at the determination of intensities and at the assignment of multipolarities, obtained by comparing electron and γ-ray intensities. The result is presented in fig. 2 and in table 2. In accordance with other Au nuclei, most transitions show M1, E2 or admixed M1-E2 multipolarities. E1 transitions are scarce and E3 or M4 transitions not observed.

3.3. COINCIDENCES

The result of e-γ and γ-γ coincidences are given in table 1. Transitions placed according to coincidence relations are indicated by full drawn lines in the level scheme, fig. 4.

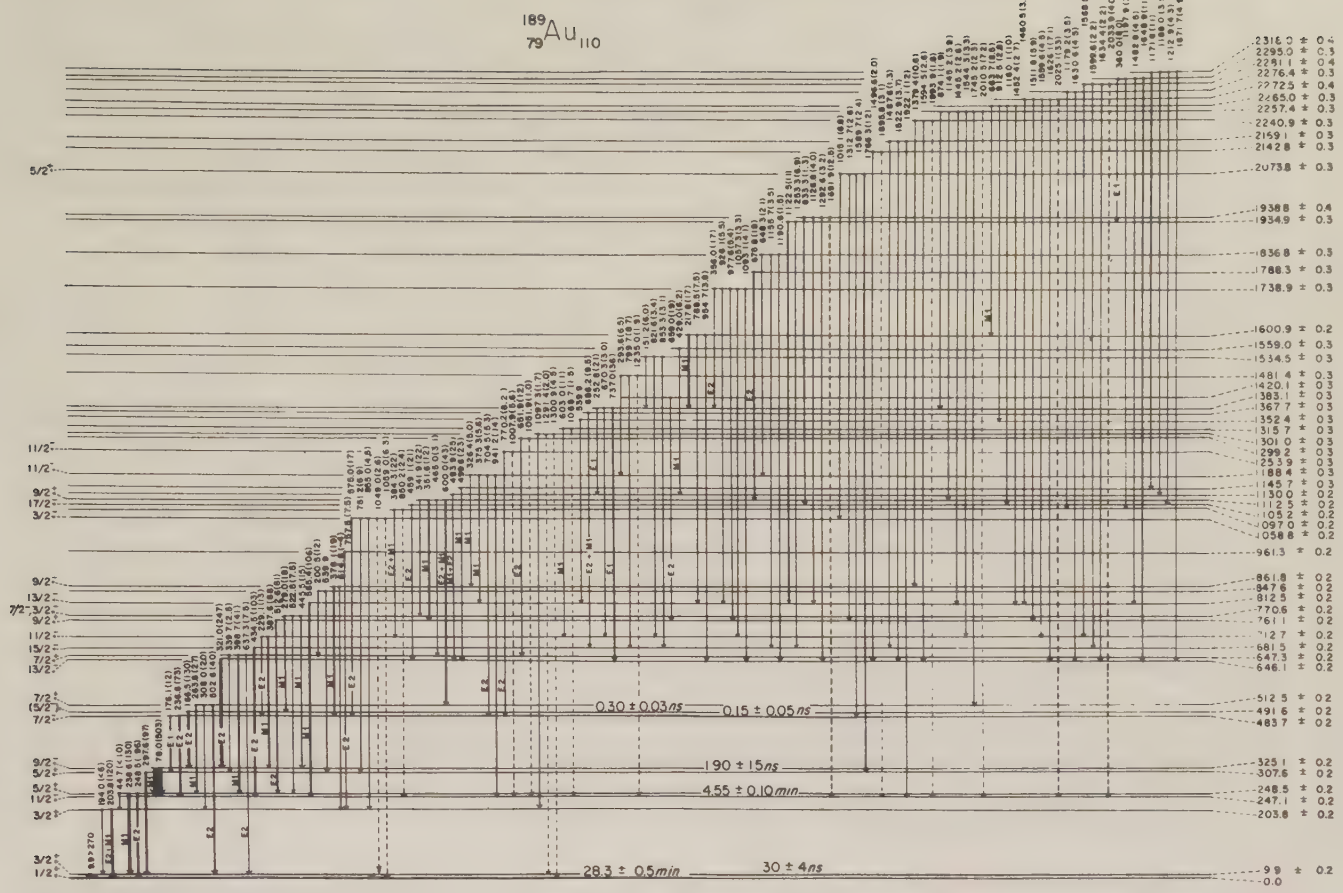

Fig. 4. Level scheme of ^{189}Au. In order to make the figure readable the scale has been extended around 2 MeV, where the level density is high.

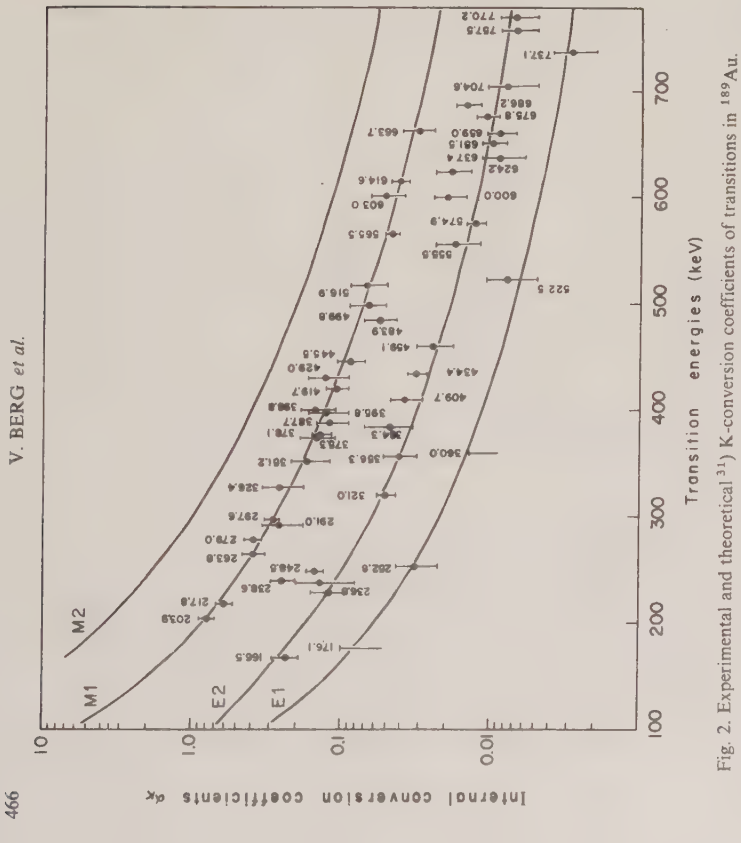

Fig. 2. Experimental and theoretical [31]) K-conversion coefficients of transitions in ^{189}Au.

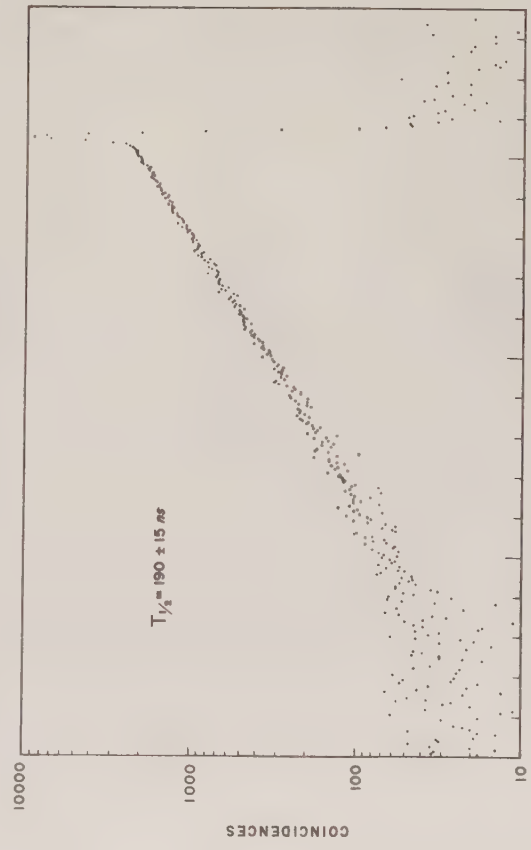

Fig. 3. Time distribution obtained by measuring 78 L-(X-ray plus γ-ray) coincidences. It gives the half-life of the 325.1 keV level as 190 ± 15 ns.

TABLE 1

Gamma-ray data for the decay of ^{189}Hg

E_γ keV	ε keV	I_γ	ε %	$I_{tot.}$	ε %	Coincident transitions	Position
9.9	0.2			> 270		238.6, 297.6	9.9 - 0.0
44.9	0.3			< 10		203.8	248.5 - 203.8
78.0	0.0	133	12	503	12	166.5, 279.0, 321.0, 387.6	325.1 - 247.1
151.2	0.3	1.8	20	6.0	25	252.8, 321.0, 483.9, 737.0	1534.5 - 1383.1
166.5	0.1	75	12	130	15	217.8, 252.8, 279.0, 359.1, 395.7, 419.7, 614.6, 624.2, 936.5	491.6 - 325.1
176.1	0.2	11	8	12	9	229.1, 297.6, 378.1, 575.0, 770.2	483.7 - 247.1
194.0	0.3	< 4		< 6			203.8 - 9.9
200.5	0.2	6.1	12	12	15	238.6, 248.5, 398.7	847.6 - 647.3
203.8	0.2	60	7	120	9	44.7, 398.7, 600.0, 675.8, 757.5, 855.0, 1097.3	203.8 - 0
217.8	0.3	10.5	10	17	12	252.8, 321.0, 418.0, 663.7, 737.0	1600.9 - 1383.2
229.1	0.2	11	20	13	20	176.1, 236.6	712.7 - 483.7
236.6	0.2	60	8	73	9	229.1, 378.1, 575.0, 704.6, 770.2, 1015.1, 1379.4	483.7 - 247.1
238.6	0.2	85	8	130	15	263.8, 351.6, 398.7, 512.6, 600.0, 659.1, 675.8, 1145.2, 1164.6, 1745.2.	248.5 - 9.9
248.5	0.2	81	8	96	8	263.8, 351.6, 398.7, 512.6, 539.9, 600.0, 659.1, 675.1, 675.8, 1145.2, 1164.6, 1745.2	248.5 - 0.0
252.8	0.2	18	15	21	16	151.4, 166.5, 217.8, 279.0, 321.0, 356.0, 359.1	1383.1 - 1130.0
263.8	0.2	18	13	27	15	203.8, 238.6, 248.5, 600.0, 1145.2	512.5 - 248.5
268.4	0.2	3.6	13	5.0	18		
279.0	0.2	13	8	18	10	78.0, 166.5, 217.8, 252.8, 359.1	770.6 - 491.6
291.0	0.3	3.5	15	4.8	20		
293.6	0.3	5.2	16	6.4	22	326.4, 375.3, 941.2	1481.4 - 1188.4
297.6	0.2	72	8	97	10	176.1, 339.7, 378.1, 539.9, 575.0, 751.2, 1015.3, 1766.3,	307.6 - 9.9
308.0	0.4	1.8	15	2.0	20	203.8, 600.0	512.5 - 203.8
321.0	0.2	210	12	247	13	78.0, 151.2, 217.8, 252.8, 356.0, 429.0, 459.1, 483.9, 499.6, 663.7, 737.0, 833.3, 954.7, 1093.1, 1160.1, 1171.8, 1188.0, 1190.6, 1292.6, 1496.6, 1496.6, 1522.9, 1594.5, 1626.1, 1630.6, 1634.4, 1648.9, 1671.7.	646.1 - 325.1
326.0	0.4	4.5	15	5.6	16	236.6, 378.1,	1188.4 - 861.8
330.3	0.4	4.8	15	5.4	20		
339.7	0.3	2.0	18	2.5	20	297.6, 651.9	647.3 - 307.6
351.6	0.2	10	25	12	27	238.6, 248.5, 512.6, 675.8	1112.5 - 761.1
356.2	0.3	16	15	17	18	252.8, 321.0, 483.9, 737.0	1738.9 - 1383.1
360.0	0.4	12	17	12	18	1122.5, 1253.3	2295.0 - 1934.9
363.1	0.3	4.1	17	4.3	19		
375.3	0.2	4.7	16	5.6	19	565.5	1188.4 - 812.5
378.1	0.2	16	10	19	11	176.1, 236.6, 297.6, 326.4, 1379.4	861.8 - 483.7
384.3	0.2	20	9	22	12	387.6, 1179.2, 1197.9, 1212.9	1097.0 - 712.7
387.6	0.2	75	8	10	10	78.0, 384.3, 603.0, 670.0, 821.6, 1057.3, 1544.3, 1568.8	712.7 - 325.1
395.7	0.2	15	9	17.5	12	166.5	
398.7	0.2	35	8	41	11	203.8, 238.6, 248.6, 248.5, 465.0, 651.9, 675.8	647.3 - 248.5

TABLE 1 (continued)

E_γ keV	ε keV	I_γ	ε %	$I_{tot.}$	ε %	Coincident transitions	Position
409.7	0.2	5.4	11	5.6	13		
418.0	0.4	3.4	15	3.9	18		
419.7	0.3	11	17	12	20	166.5	
429.0	0.3	5.0	20	5.7	22	321.0, 483.9	1559.0 - 1130.0
434.5	0.2	99	8	103	9	686.2, 799.7, 853.3, 1155.7, 1253.3, 1487.6, 1559.6	681.5 - 247.1
445.5	0.2	13	10	15	12	252.8, 359.1	770.6 - 325.1
451.9	0.2	9.0	12				
459.1	0.2	21	10	22	11	321.1, 833.3, 1160.1	1105.2 - 646.1
465.0	0.4	2.8	25	3.1	25	637.3	1112.5 - 647.3
467.6	0.4	3.8	20				
474.6	0.4	2.6	20				
483.9	0.4	23	15	25	15	217.8, 252.8, 321.0, 429.0, 1188.0	1130.0 - 646.1
487.1	0.4	4.5	20				
499.6	0.2	21	12	23	15	321.0, 1171.8	1145.7 - 646.1
502.6	0.3	43	12	44	15	600.0, 675.8, 1745.2	512.5 - 9.9
512.4	0.4	80	25	81	25	238.6, 248.5, 351.6, 659.1, 977.6, 1312.7, 1511.8	761.1 - 248.5
516.9	0.3	3.0	20	3.2	20		
522.5	0.2	8.0	15	8.0	15	238.6, 248.5	770.6 - 248.5
538.4	0.3	17					
539.9	0.3	33	25			297.6, 565.5, 912.5	847.6 - 307.5
555.5	0.2	8.1	10	8.1	10		
557.7	0.4	2.1	20				
565.5	0.2	100	7	106	8	375.3, 539.9, 788.5, 926.1, 1122.5, 1126.8, 1445.2, 1452.4, 1460.5	812.5 - 247.1
575.0	0.2	17	10	17	11	176.1, 236.6, 297.5	1058.8 - 483.7
586.1	0.3	4.1	20				
600.0	0.2	46	10	47	11	203.8, 238.6, 248.5, 263.8, 502.6, 675.8, 1145.2	1112.5 - 512.5

E_γ keV	I_γ	ε %	Coincident transitions	Position
603.0 ± 0.3	10.5	13	387.6	1315.7 - 712.7
614.6 ± 0.2	17	10	166.5	
624.2 ± 0.3	5.2	14	166.5	
630.9 ± 0.3	5.8	15		
633.8 ± 0.3	6.5	15		
637.3 ± 0.3	7.0	15	651.9, 651.9	647.3 - 9.9
641.8 ± 0.3	2.5	18		
648.3 ± 0.3	1.9	25	326.4, 941.2	1836.8 - 1188.4
651.9 ± 0.3	12.5	12	203.8, 238.6, 248.5, 398.7, 637.3	1299.2 - 647.3

TABLE 1 (continued)

E_γ keV	I_γ	ε %	Coincident transitions	Position
659.0 ± 0.2	18.5	10	203.8, 238.6, 248.5, 512.6	1420.1 - 761.1
663.7 ± 0.3	8.2	12	217.8, 252.8, 321.0, 737.0	2265.0 - 1600.9
670.4 ± 0.3	4.2	25		1383.1 - 712.7
675.8 ± 0.2	17.5	9	238.6, 248.5, 398.7, 600.0	1788.3 - 1112.5
686.2 ± 0.3	9.4	10	434.5	1367.7 - 681.5
694.7 ± 0.3	4.0	13		
696.9 ± 0.3	2.8	17		
702.6 ± 0.4	2.2	25		
704.5 ± 0.3	4.1	20	176.1, 236.6, 297.6	1188.4 - 483.7
716.4 ± 0.3	3.4	14		
730.5 ± 0.3	3.7	18		
734.8 ± 0.3	5.2	20		
737.0 ± 0.2	36	9	151.2, 217.8, 321.0, 356.0, 874.1	1383.1 - 646.1
746.8 ± 0.3	4.1	12		
749.3 ± 0.3	3.0	20		
751.2 ± 0.2	6.6	15	297.6	1058.8 - 307.6
757.5 ± 0.2	7.2	10	203.8	961.3 - 203.8
770.2 ± 0.3	8.5	12	176.1, 236.6, 297.6	1253.9 - 483.7
771.8 ± 0.3	6.5	15		
775.6 ± 0.3	3.0	17		
781.4 ± 0.4	2.3	25		
782.8 ± 0.4	1.8	25		
786.7 ± 0.3	6.0	30		
788.5 ± 0.3	3.0	30	565.5	1600.9 - 812.5
799.7 ± 0.3	8.5	20	434.4	1481.4 - 681.5
801.9 ± 0.3	6.0	20		
809.6 ± 0.4	4.7	20		
816.4 ± 0.4	1.4	25		
821.6 ± 0.3	3.2	18	387.6	1534.5 - 712.7
833.3 ± 0.4	1.2	30	321.0, 459.1	1938.8 - 1105.2
841.5 ± 0.3	5.1	17		
847.4 ± 0.3	5.1	18		
853.3 ± 0.4	3.0	25	434.5	1534.5 - 681.5
855.0 ± 0.3	4.5	22	203.8	1058.8 - 203.8

TABLE 1 (continued)

E_γ keV	I_γ	ε %	Coincident transitions	Position
857.7 ± 0.4	3.2	20		
868.9 ± 0.3	5.5	20		
874.1 ± 0.3	2.1	20	252.8, 321.0, 737.0	2257.4 - 1383.1
884.3 ± 0.3	1.6	22		
888.3 ± 0.3	1.6	20		
894.7 ± 0.4	1.1	25		
900.5 ± 0.3	4.0	25		
903.1 ± 0.5	1.5	25		
910.7 ± 0.4	3.5	20		
912.5 ± 0.4	2.0	25	539.9, 565.5	2265.0 - 1352.4
918.6 ± 0.3	4.0	20		
926.1 ± 0.3	5.4	15	565.5	173.9 - 812.5
933.1 ± 0.5	2.2	25		
936.5 ± 0.3	5.5	20	166.5	
941.2 ± 0.2	14	15	293.6, 648.3	1188.4 - 247.1
951.8 ± 0.3	7.0	18		
954.7 ± 0.3	3.7	20	321.0	1600.9 - 646.1
958.7 ± 0.3	4.8	15		
968.9 ± 0.4	1.5	25		
972.2 ± 0.3	4.9	15		
977.6 ± 0.3	5.2	15	238.6, 248.5, 512.6	1738.9 - 761.1
981.2 ± 0.3	2.7	20		
995.7 ± 0.4	3.5	25		
999.7 ± 0.4	3.5	25		
1003.7 ± 0.5	4.5	25		
1007.9 ± 0.3	5.6	20		
1015.1 ± 0.4	11	10	176.1, 236.6, 297.6, 575.0	2073.8 - 1058.8
1023.3 ± 0.4	1.2	40		
1026.6 ± 0.3	2.7	20		
1034.9 ± 0.3	6.7	20		
1048.3 ± 0.4	6.0	20		
1051.7 ± 0.4	1.0	35		
1057.3 ± 4.2	3.2	25		
1059.0 ± 0.3	6.8	20		
1064.8 ± 0.3	2.5	22		
1075.0 ± 0.4	3.1	25		
1083.5 ± 0.3	5.2	20		

TABLE 1 (continued)

E_γ keV	I_γ	ε %	Coincident transitions	Position
1087.8 ± 0.3	1.8	25		
1093.1 ± 0.3	4.0	20	321.0	1738.9 -646.1
1097.3 ± 0.3	1.5	25	203.8	1301.0 - 203.8
1105.8 ± 0.3	2.8	20		
1109.6 ± 0.4	0.8	30		
1115.4 ± 0.3	2.4	20		
1122.5 ± 0.2	10	15	565.5	1934.9 - 812.5
1126.8 ± 0.3	4.0	20	565.5	1938.8 - 812.5
1129.6 ± 0.3	1.8	30		
1135.0 ± 0.2	11	13		
1145.4 ± 0.3	3.7	20	236.6, 248.8, 502.6, 600.0	2257.4 - 1112.5
1152.3 ± 0.4	1.8	25		
1155.7 ± 0.3	3.2	25	434.5	1836.8 - 681.5
1160.1 ± 0.3	10	15	321.0, 459.1	2265.0 - 1105.2
1165.0 ± 0.3	4.2	20		
1171.8 ± 0.2	10	12	321.0, 499.6	2318.0 - 1145.7
1179.2 ± 0.4	3.2	20	384.3, 387.6	2276.4 - 1097.0
1188.0 ± 0.4	3.0	25		2318.0 - 1130.0
1190.6 ± 0.4	1.1	30		
1197.9 ± 0.3	3.4	15		2295.0 - 1097.0
1204.1 ± 0.4	1.2	30		
1212.9 ± 0.3	4.2	20	321.0, 459.1	2318.0 - 1105.2
1215.8 ± 0.4	1.2	25		
1221.8 ± 0.3	4.4	20		
1228.6 ± 0.3	2.2	25		
1235.0 ± 0.3	1.8	25		
1238.2 ± 0.4	1.4	30		
1253.3 ± 0.2	6.7	15		
1257.2 ± 0.4	2.4	30		
1260.0 ± 0.3	3.0	20		
1269.6 ± 0.4	2.0	30		
1272.8 ± 0.3	2.4	20		
1276.7 ± 0.4	1.3	30		
1279.3 ± 1.8	30			
1286.4 ± 0.4	2.4	30		

TABLE 1 (continued)

E_γ keV	I_γ	ε %	Coincident transitions	Position
1287.9 ± 0.3	7.7	20		
1291.4 ± 0.4	2.0	30		1301.0 - 9.9
1293.5 ± 0.4	2.0	30		
1300.9 ± 0.3	4.8	20		1301.0 - 0
1312.7 ± 0.3	2.4	25		2073.8 - 761.1
1321.7 ± 0.4	1.3	35		
1331.3 ± 0.3	2.6	20		
1334.9 ± 0.4	1.2	35		
1348.3 ± 0.4	1.4	35		
1352.3 ± 0.3	2.8	30		
1364.6 ± 0.3	2.8	25		
1372.7 ± 0.4	1.3	30		
1379.4 ± 0.2	11	15	176.1, 236.6, 378.1	2240.9 - 861.8
1395.1 ± 0.3	1.4	25		
1397.9 ± 0.3	1.9	25		
1408.4 ± 0.3	1.5	30		
1411.7 ± 0.5	0.7	35		
1421.3 ± 0.4	1.6	30		
1428.3 ± 0.3	6.0	20		
1432.0 ± 0.3	2.8	25		
1434.9 ± 0.4	1.4	40		
1440.5 ± 0.4	1.0	40		
1445.2 ± 0.3	2.7	30	565.5	2257.4 - 812.5
1448.0 ± 0.3	2.4	30		
1452.4 ± 0.3	3.0	30	565.5	2265.0 - 812.5
1460.5 ± 0.4	2.8	30	565.5	2272.5 - 812.5
1463.9 ± 0.5	2.0	30		
1475.8 ± 0.3	3.2	25		
1482.8 ± 0.3	4.4	20	565.5	2295.0 - 812.5
1487.6 ± 0.4	1.0	30	434.5	2169.1 - 681.5
1491.2 ± 0.4	1.3	30		
1496.6 ± 0.4	2.0	30	321.0	2142.8 - 646.1
1498.3 ± 0.4	2.1	30		
1511.8 ± 0.2	15			
1518.9 ± 0.3	1.8	30		
1522.9 ± 0.3	3.7	25	321.0	2169.1 - 646.1
1528.8 ± 0.4	1.4	30		

TABLE 1 (continued)

E_γ keV	I_γ	ε %	Coincident transitions	Position
1533.0 ± 0.4	1.0	35		
1544.3 ± 0.3	3.5	15	387.5	2257.4 - 712.7
1556.1 ± 0.3	2.8	20		
1559.6 ± 0.3	4.1	20	387.5	2272.5 - 712.7
1568.8 ± 0.3	2.4	25	387.5	2281.1 - 712.7
1571.3 ± 0.4	1.4	30		
1582.8 ± 0.4	0.9	30		
1589.7 ± 0.3	2.4	20	176.1, 236.6, 297.6	2073.8 - 483.7
1594.5 ± 0.3	2.6	20	321.0	2240.9 - 646.1
1599.6 ± 0.3	1.9	20	434.5	2281.1 - 681.5
1605.1 ± 0.3	1.8	20		
1626.1 ± 0.2	7.1	20	321.0	2272.5 - 646.1
1630.6 ± 0.2	4.5	20	321.0	2276.4 - 646.1
1634.4 ± 0.4	2.2	25	321.0	2281.1 - 646.1
1648.9 ± 0.2	11	15	321.0	2295.0 - 646.1
1659.1 ± 0.4	1.9	20		
1663.7 ± 0.3	2.5	20		
1671.7 ± 0.3	4.9	20	321.0	2318.0 - 646.1
1675.8 ± 0.3	2.5	20		
1691.9 ± 0.2	13	15		1938.8 - 247.1
1703.5 ± 0.3	1.6	20		
1723.5 ± 0.4	1.4	25		
1745.2 ± 0.3	2.0	25	238.6, 248.5, 502.6	2257.4 - 512.6
1766.3 ± 0.2	10	20	297.6	2073.8 - 307.6
1782.7 ± 0.3	2.9	20		
1786.1 ± 0.3	4.5	20		
1795.1 ± 0.3	4.3	20		
1803.8 ± 0.3	1.2	25		
1826.6 ± 0.3	1.3	25		
1845.7 ± 0.4	2.6	25		
1863.3 ± 0.3	2.7	20		
1895.8 ± 0.3	2.6	20		2142.8 - 247.1
1915.6 ± 0.3	1.9	25		
1922.1 ± 0.2	10	15		
1929.4 ± 0.3	5.6	20		
1932.2 ± 0.3	5.7	20		
1944.2 ± 0.3	12	15		

TABLE 1 (continued)

E_γ keV	I_γ	ε %	Coincident transitions	Position
1951.1 ± 0.4	1.3	25		
1986.8 ± 0.3	3.4	20		
1993.9 ± 0.3	1.5	25		2240.0 - 247.1
2010.1 ± 0.3	7.2	20		2257.4 - 247.1
2016.8 ± 0.4	6.3	25		
2021.4 ± 0.4	23	25		
2025.1 ± 0.4	33	25		2272.5 - 247.1
2033.9 ± 0.3	40	20		2281.1 - 247.1
2081.5 ± 0.4	1.5	25		
2090.8 ± 0.4	3.0	25		
2093.6 ± 0.3	4.0	20		
2102.0 ± 0.4	2.5	25		
2106.1 ± 0.4	1.7	25		
2182.0 ± 0.4	1.5	25		

3.4. HALF-LIFE MEASUREMENTS

The half-life of the 9.9 keV level was obtained from delayed coincidences between the 9.9 keV M-line and X-rays plus Compton events of feeding γ-rays in one measurement, and from coincidences between the 9.9 keV M- and the 297.6 keV K-lines in another. In order to enable the detection of the low energy electrons, they were preaccelerated in a potential of 15 kV. The slope of the delayed time distribution gave the half-life

$$T_{\frac{1}{2}}(9.9 \text{ keV level}) = 30 \pm 4 \text{ ns}.$$

The measurement was hindered by the presence of Auger electrons of approximately the same energy as 9.9 M, and by the small probability of obtaining low energy electrons from samples deeply implanted in the source backing [16]). The thickness of the sources did not permit the measurement of the M-subshell ratios of the 9.9 keV transition, and absolute transition rates could not be determined.

247

TABLE 2

Internal conversion electron data for the decay of ^{189}Hg

Energy keV	Error keV	Relative I_γ	Error %	Electron Line	Relative I_e	Error %	Experiment α_K, K/L, L/M, K/M	Theory E1	α_K, K/L, L/M, K/M [a] E2	M1	Multipolarity
78.0	0.0			L	44000	7	L/M = 4.2 ± 0.4		3.9	4.3	M1 b)
78.0	0.0			M	10500	6					
Pt 166.5	0.1	141	10	K	2600	12	0.24 ± 0.04	0.096	0.27	1.5	E2 b)
Au 166.5	0.1			K	2900	12			0.27	1.5	E2
Pt 166.5	0.1	141	10	L	7100	15	K/L = 0,77 ± 0.13	5.7	0.77	6.0	E2
Au 166.5	0.1										
Pt 166.5	0.1	141	10	M	2100	10	K/M = 2.6 ± 0.4	25	2.9	26	E2
Au 166.5	0.1										
176.1	0.1	11.0	7	K	< 170		< 0.10	0.083	0.24	1.3	E1
200.5	0.2	6.1	12	K	560	30	0.6 ± 0.2	0.059	0.17	0.86	M1 + E2
203.8	0.2	60.0	7	K	7400	7	0.8 ± 0.1	0.057	0.16	0.82	M1
203.8	0.2	60.0	7	L	1410	15	K/L = 5.2 ± 0.9	5.9	1.1	6.0	M1
217.8	0.3	10.5	10	K	980	10	0.61 ± 0.8	0.048	0.14	0.68	M1
229.1	0.2	11.0	20	K	200	25	0.12 ± 0.04	0.043	0.12	0.60	E2
236.8	0.2	60.	8	K	1300	40	0.14 ± 0.06	0.039	0.11	0.54	E2 c)
238.6	0.2	85.	8	K	3200	12	0.25 ± 0.04	0.038	0.11	0.53	E2
236.8	0.2	60	8	L	1750	8	0.079 ±0.009	0.0056	0.0077	0.089	E2 c)
238.6	0.2	85	8	L							E2 + M1
248.5	0.2	81	8	K	1830	8	0.15 ± 0.02	0.035	0.099	0.47	E2+M1 d)
252.8	0.3	18	15	K	100	30	0.036 ±0.012	0.034	0.096	0.45	E1
263.8	0.2	18	13	K	1070	10	0.39 ± 0.07	0.030	0.084	0.39	M1
279.0	0.2	13	8	K	750	12	0.38 ± 0.05	0.026	0.075	0.34	M1
279.0	0.2	13	8	L	150	18	K/L = 5.0 ± 1.2	6.0	1.8	6.0	M1
291.0	0.4	3.5	15	K	140	25	0.26 ± 0.08	0.024	0.068	0.31	M1
297.6	0.2	72	8	K	3200	6	0.29 ± 0.03	0.023	0.064	0.29	M1
297.6	0.2	72	8	L	470	20	K/L = 6.8 ± 1.5	6.1	2.0	6.0	M1
321.0	0.2	210	12	K	1660	10	0.051 ±0.008	0.019	0.053	0.24	E2
326.0	0.4	4.5	15	K	180	25	0.26 ± 0.08	0.019	0.053	0.24	M1

TABLE 2 (continued)

Energy keV	Error keV	Relative I_γ	Error %	Electron Line	Relative I_e	Error %	Experiment α_K, K/M, L/M, K/M	Theory E1	α_K, K/L, L/M, K/M a) E2	M1	Multipolarity
351.6	0.2	10	25	K	210	20	0.14 ± 0.05	0.016	0.043	0.19	M1
356.4	0.2	16	15	K	104	18	0.041 ± 0.010	0.015	0.040	0.17	E2
360.0	0.4	12	17	K	<40		< 0.022	0.014	0.040	0.17	E1
375.3	0.2	4.7	16	K	106	20	0.15 ± 0.04	0.013	0.037	0.16	M1
378.1	0.2	16.5	9	K	360	15	0.14 ± 0.02	0.013	0.037	0.16	M1
384.3	0.2	20	9	K	150	40	0.049 ± 0.020	0.012	0.034	0.15	E2+(M1)
387.6	0.2	75	8	K	1350	20	0.12 ± 0.03	0.012	0.034	0.14	M1
395.8	0.2	15.	9	K	300	25	0.13 ± 0.04	0.012	0.032	0.13	M1
398.7	0.2	35	8	K	910	25	0.15 ± 0.04	0.012	0.032	0.13	M1
409.7	0.3	5.4	11	K	31	20	0.037 ± 0.009	0.011	0.030	0.12	E2
418.0	0.4	3.4	9	K	230	15	0.10 ± 0.02	0.010	0.028	0.11	(M1)
419.7	0.3	11		K							M1
492.0	0.3	5.0	20	K	100	18	0.13 ± 0.04	0.010	0.027	0.11	M1
434.4	0.2	99	8	K	490	12	0.032 ± 0.005	0.010	0.026	0.11	E2 d)
445.5	0.2	13.	10	K	175	25	0.09 ± 0.02	0.009	0.025	0.10	M1
459.1	0.2	21	10	K	85	25	0.026 ± 0.007	0.009	0.023	0.09	E2
				L	22	20	0.007 ± 0.002	0.0014	0.007	0.015	E2
483.9	0.4	23	15	K	200	20	0.057 ± 0.014	0.008	0.021	0.079	M1 + E2
499.6	0.3	21	12	K	224	25	0.069 ± 0.018	0.007	0.019	0.072	M1
502.6	0.3	43	12	K							E2 c)
512.4	0.4	80	25	K	240	15	0.019 ± 0.005	0.007	0.018	0.069	E2
				L	51	12	0.004 ± 0.001	0.001	0.005	0.011	E2
516.9	0.3	3.0	20	K	32	20	0.069 ± 0.019	0.007	0.018	0.065	M1
522.5	0.3	8.0	15	K	10	25	0.008 ± 0.003	0.006	0.017	0.065	E1
555.5	0.3	8.1	11	K	24	30	0.018 ± 0.006	0.006	0.015	0.094	E2

The lifetime of the 325.1 keV level was measured by 78L-(X-ray plus γ-ray) coincidences. The result, shown in fig. 3, is

$$T_{\frac{1}{2}}(325.1 \text{ keV level}) = 190 \pm 15 \text{ ns}.$$

It indicates that the 78 keV transition, being pure M1 [ref. [15])], is hindered by a factor of 15000 compared to the Weisskopf estimate.

The half-life of the 483.9 keV level was measured by recording 236.8 L-(γ-ray) coincidences:

$$T_{\frac{1}{2}}(483.9 \text{ keV level}) = 0.15 \pm 0.05 \text{ ns}.$$

Because of admixture of 238.6 L in the electron channel, the result was not very accurate. A prompt reference curve was obtained by the coincidences from a ^{60}Co source, taken under equal conditions, and the two measurements were analysed with both the momentum and the convolution methods [19]).

The 491.6 keV level also proved to have a measurable half-life. Coincidences between 166.5 K electrons and Compton events in the region 120–300 keV gave

$$T_{\frac{1}{2}}(491.6 \text{ keV level}) = 0.30 \pm 0.03 \text{ ns}.$$

Results of half-life measurements and absolute transition probabilities are summarized in table 3.

4. Level schemes

4.1. LEVELS IN ^{189}Au

The results were used for the construction of the level scheme of ^{189}Au. The coincidences showed that many transitions in ^{189}Au are very closely related to transitions in the heavier gold isotopes. An example is given by the 236.8 keV transition, coincident with transitions at 378.1 (M1), 575.0(E2), 704.6(E2), 770.2(E2) keV. The correspondent transition in ^{193}Au at 218.07 keV [ref. [12])] is fed by transitions at 382.47(M1), 580.97(E2), 706.30(E2), 776.57(E2) keV. Many similar relations led to a level scheme (fig. 4) having many features in common with the level schemes of the heavier gold nuclei. The reasons for spin and parity assignments are the same as given in earlier works [11,12]). Fig. 5 illustrates in a striking way how several levels persist in these nuclei. A small lowering of the levels takes in general place when the neutron number diminishes. Three states with spins and parities $\frac{1}{2}^+$, $\frac{5}{2}^+$, and $\frac{11}{2}^-$ change more rapidly than the others.

The ground state of heavier gold isotopes is $\frac{3}{2}^+$, determined by atomic beam and magnetic moment measurements in ^{197}Au and ^{199}Au [ref. [20])]. In ^{189}Au this assignment is incompatible with the multipolarities of feeding transitions and spins of higher levels. There is consistency if the assignment is $\frac{1}{2}^+$ for the ground state and $\frac{3}{2}^+$ for the first excited state. This is inverse to the traditional order. However, the crossing of the $\frac{1}{2}^+$ and $\frac{3}{2}^+$ levels is anticipated by the systematic trend (fig. 5).

TABLE 2 (continued)

Energy keV	Error %	Relative I	Error %	Electron Line	Relative I_e	Error %	Experiment α_K, K/M, L/M, K/M	Theory E1	α_K, K/L, L/M, K/M a) E2	M1	Multipolarity
565.5	0.2	100	7	K	720	7	0.047 ± 0.005	0.006	0.015	0.052	M1
574.9	0.3	17	10	K	35	15	0.013 ± 0.002	0.005	0.014	0.051	E2
600.0	0.3	46	10	K	130	20	0.018 ± 0.005	0.005	0.013	0.045	E2 + M1
603.0	0.3	10.5	13	K	85	25	0.052 ± 0.014	0.005	0.013	0.045	M1
614.6	0.3	17.2	10	K	110	10	0.042 ± 0.006	0.005	0.012	0.042	M1 d)
624.2	0.3	5.2	14	K	15	25	0.019 ± 0.005	0.005	0.012	0.041	E2 + M1
637.4	0.3	7.4	15	K	9	30	0.008 ± 0.003	0.004	0.011	0.038	E2
651.5	0.3	12.5	12	K	20	17	0.010 ± 0.002	0.004	0.011	0.036	E2
659.0	0.2	18.5	10	K	26	25	0.009 ± 0.002	0.004	0.011	0.035	E2
663.7	0.3	8.2	12	K	40	20	0.032 ± 0.008	0.004	0.011	0.035	M1
675.8	0.2	17.5	9	K	31	20	0.011 ± 0.002	0.004	0.010	0.034	E2
686.2	0.3	9.4	10	K	22	13	0.015 ± 0.003	0.004	0.010	0.032	E2 + M1
704.5	0.3	4.1	20	K	5	30	0.008 ± 0.003	0.004	0.009	0.030	E2
737.1	0.2	36	10	K	16	23	0.003 ± 0.001	0.003	0.009	0.026	E1
757.5	0.2	7.2	10	K	8	25	0.007 ± 0.002	0.003	0.008	0.025	E2
770.2	0.3	8.5	12	K	9	30	0.007 ± 0.002	0.003	0.008	0.023	E2
771.8	0.4	6.5	15	K	18	30	0.018 ± 0.006	0.003	0.008	0.023	M1

a) Ref. [31]).

b) Ref. [15]).

c) assumed to be pure E2 (systematics).

d) shows doublet structure in coincidence experiments.

TABLE 3

Half-lives of excited states and absolute transition probabilities in ^{189}Au

Level (keV)	$T_{\frac{1}{2}}$ level (ns)	Transition energy (keV)	Initial state	Final state	Multi-polarity	B(M1) ($e\hbar/2Mc$) B(E2) ($e^2\cdot b^2$) B(E1) ($e^2\cdot b$)	F_w
9.9	30 ± 4	9.9	$\frac{3}{2}^+$	$\frac{1}{2}^+$			
325.1	190 ±15	78.0	$\frac{9}{2}^-$	$\frac{11}{2}^-$	M1	$(1.2\pm0.1)\times10^{-4}$	15000
483.7	0.15± 0.05	236.6	$\frac{7}{2}^-$	$\frac{11}{2}^-$	E2	$0.36^{+0.18}_{-0.09}$	0.02
		176.1	$\frac{7}{2}^-$	$\frac{5}{2}^+$	E1	$(7\pm3)\times10^{-7}$	3×10^6
491.6	0.30± 0.03	166.5	$\frac{5}{2}^-$	$\frac{9}{2}^-$	E2	0.84 ± 0.08	0.01

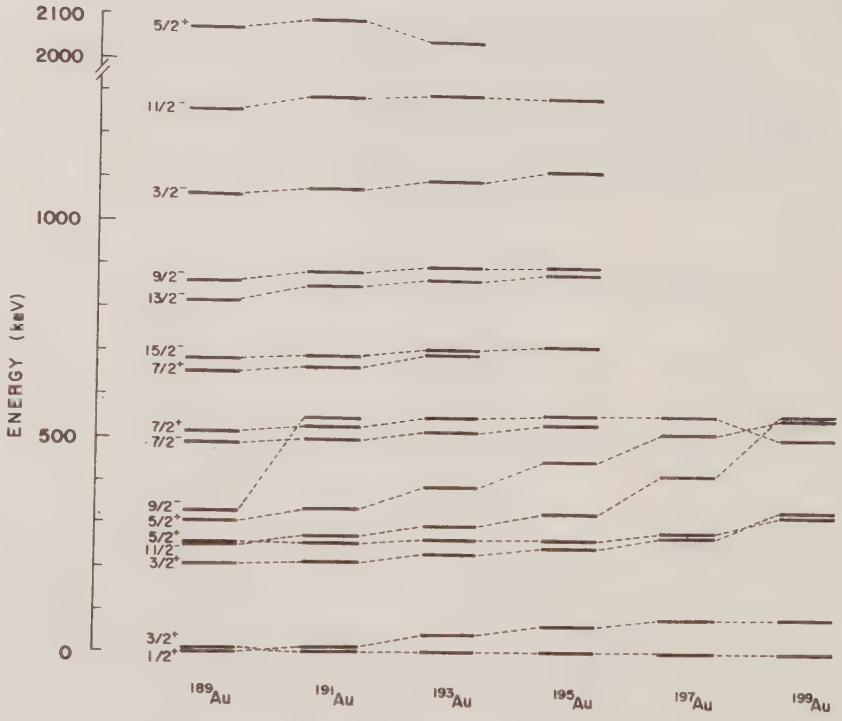

Fig. 5. Comparison of levels in odd mass gold isotopes.

The $\frac{3}{2}^+$ state was located at 9.9 keV through the coincidences between 9.9 M electrons and the 238.6 and 297.6 keV γ-rays. A second $\frac{3}{2}^+$ level at 203.8 keV is fed by a few rather weak transitions from higher states, but mainly through the electron capture and β^+ decay of ^{189}Hg as proved by coincidences between the strong 203.8 keV γ-ray and annihilation radiation. The log $ft \approx 6.5$ agrees with the assumption that the β-decay arises from a level with spin-parity assignment $\frac{3}{2}^-$, attributed to the ground states of neighbouring Hg nuclei. The $\frac{3}{2}^+$ level is fed by the shorter period of the ^{189}Hg decay, 7.5±0.2 min.

The $\frac{11}{2}^-$ isomeric state in ^{189} Au does not reveal itself by high multipole internal transitions as in the other gold isotopes. The coincidences between the 297.6 keV γ-ray, which feeds the first $\frac{3}{2}^+$ state, and an E1 transition of 176.3 keV determines a negative parity level at 483.9 keV. Moderately strong transitions of 378, 575, 705, and 770 keV (already mentioned), also seen in coincidence with the 297.6 keV line, feed this level, which decays predominantly by an E2 transition of 236.8 keV, identified through the feeding γ-rays as the $\frac{7}{2}^-$ to $\frac{11}{2}^-$ transition observed in most Au nuclei. Other levels feeding both the ground state and the isomeric state, located at 247.1 keV, are found at 1058.8, 2073.8, and 2272.5 keV.

The isomeric state has slightly lower energy than the first $\frac{5}{2}^+$ state. This explains the absence of an $\frac{11}{2}^-$ to $\frac{5}{2}^+$ E3 transition in ^{189}Au. One could expect to find an M4 transition of 237.2 keV between $\frac{11}{2}^-$ and $\frac{3}{2}^+$, but it was not observed. This may be explained by the fact that it nearly coincides in energy with the intense 236.8 keV $\frac{7}{2}^-$ to $\frac{11}{2}^-$ and the 238.6 keV $\frac{5}{2}^+$ to $\frac{3}{2}^+$ transitions. According to the Weisskopf estimate an M4 of this energy has $T_{\frac{1}{2}} \approx 14$ h. Comparing this half-life with the period 4.55 min of the isomer, one concludes that approximately 0.6% of the Hg decay should proceed by this internal transition. The strength would be ≈ 6 according to the intensity scale used in table 1. From the 236.8 L and 238.6 L electron intensities, we find that the M4 strength is < 5. The corresponding M4 transition in ^{193}Au is hindered by a factor of 8 [ref. [12])].

In parallel with the traditional gold structure, new features manifest themselves in the lighter isotopes. A system of negative parity states becomes visible in ^{191}Au [ref. [13])], and its importance gets more accentuated in ^{189}Au. About 10% of the total Hg decay proceeds via these levels in the former nucleus, about 30% in the latter one. In both nuclei, the levels are fed in a similar way from the ground state as well as from the isomeric state in Hg. Only few transitions connect them with earlier established states, and their feeding the $\frac{11}{2}^-$ isomer is based on intensity considerations. In ^{189}Au the strength of the 166.5 keV transition, which follows the isomer decay, cannot be explained without taking into consideration their contribution. The connection with the $\frac{11}{2}^-$ state is made by strong M1 transitions, at 274 keV in ^{191}Au and at 78 keV in ^{189}Au, both hindered by factors of 15000. We have adopted $\frac{9}{2}$ as spin for the band head of the new levels and tentatively proposed spins for some of the higher lying states, (figs. 4, 6): $\frac{11}{2}^-$ for the 712.7 keV state because of its E2 connection with $\frac{7}{2}^-$ at 483.7 keV, and $\frac{3}{2}^-$, $\frac{7}{2}^-$ for the 770.6 keV level on account of its decay by

an E1 transition to $\frac{5}{2}^+$ at 248.5 keV. The 491.6 and 646.1 keV states have been assigned $\frac{5}{2}^-$ and $\frac{13}{2}^-$ respectively. They both decay to the $\frac{9}{2}^-$ state by E2 transitions, and the 646.1 keV level is fed from a high spin state in ^{189}Hg.

4.2. LEVELS IN ^{189}Hg

The comparison in fig. 5 shows that a great many levels in ^{189}Au have common properties with states in other Au isotopes, and a closer study proves that they are fed in a similar way. This suggests that the decaying states in ^{189}Hg have the same spin-parity assignments as those of the heavier Hg isotopes, that is $\frac{3}{2}^-$ and $\frac{13}{2}^+$. The multianalysis of γ-rays in ^{189}Au proves that the low spin state has $T_{\frac{1}{2}} = 7.5 \pm 0.2$ min and the high spin state $T_{\frac{1}{2}} = 8.7 \pm 0.2$ min. No internal transition has been observed.

5. Discussion

The study of ^{189}Au has shown that it has many properties in common with the heavier gold isotopes ^{193,195}Au (fig. 5), recently interpreted in the frames of the pairing plus quadrupole [12]) and the three-hole cluster models [28]).

The structure of the negative parity states of ^{195}Au has been described with the rotational aligned coupling scheme [34]), and in the following this macroscopic approach is applied to the low lying, high spin states observed in ^{189}Au. In gold the Fermi level lies above the $h_{\frac{11}{2}}$ orbital. On account of small deformation the rotational frequencies are high and the Coriolis force on an $\frac{11}{2}^-$ hole so strong, that it may decouple it and align its angular momentum with the direction of the rotation. The low Ω-states issued from the $h_{\frac{11}{2}}$ orbital are especially influenced. They approach the Fermi level on the oblate side, and the existence of a decoupled $\frac{11}{2}^-$ band should be a sign of negative deformation. The rotation aligned coupling predicts that yrast states with spins $(\frac{11}{2}+2n)$ will be separated by approximately the energies in the ground state bands of neighbouring even nuclei. In ^{189}Au the $\frac{15}{2}^-$ to $\frac{11}{2}^-$ spacing, 434 keV, is much larger than the 2^+ energy, 265 keV, in ^{188}Pt, but agrees well with that of ^{190}Hg, 416 keV [refs. [2,35])]. Analogous relations exist between other odd Au and corresponding even Hg isotopes. This suggests that the core of an Au nucleus in the $\frac{11}{2}^-$ state much resembles the Hg core. According to ref. [22]) B(E2) values in decoupled bands correspond closely to B(E2) values calculated using the strong coupling formalism, with the assumption that $K = \frac{1}{2}, \frac{3}{2}$, or $\frac{5}{2}$, and that for the odd nucleus the value of Q_0 is the average of the Q_0 values of the neighbouring even isotopes. Referring to the observed energy spacing between the $\frac{15}{2}^-$ and $\frac{11}{2}^-$ states we use $Q_0 = 3.1$ b, deduced from the 2^+ energy in ^{190}Hg [ref. [23])] and find the strong coupling value $B(\mathrm{E2};\ \frac{7}{2}^-$ to $\frac{11}{2}^-) = 0.47\, e^2 \cdot \mathrm{b}^2$. It falls within the limits of our experimental result $0.38^{+0.18}_{-0.09}\, e^2 \cdot \mathrm{b}^2$.

When seeking for the explanation of the new system of negative parity levels, the $\frac{9}{2}(505)$ and $\frac{9}{2}(514)$ states have been considered as possible basis states. Both require

that the feeding levels form a normal rotational band. The $\frac{9}{2}$ system in ^{189}Au does not show such features but resembles much the decoupled $\frac{11}{2}^-$ band (fig. 6), although the spins are shifted by one unit and the energy spacings are smaller. Thanks to the lower spins, the band is more developed and can show two members, at 321 and 459 keV, in the yrast cascade. It seems far-fetched to assume the decoupling of a particle in the $h_{\frac{9}{2}}$ orbital outside the 82 shell closure, but experiments have shown that states issued from this orbital appear in Tl, Ir and Re nuclei at astonishingly low energies [30]).

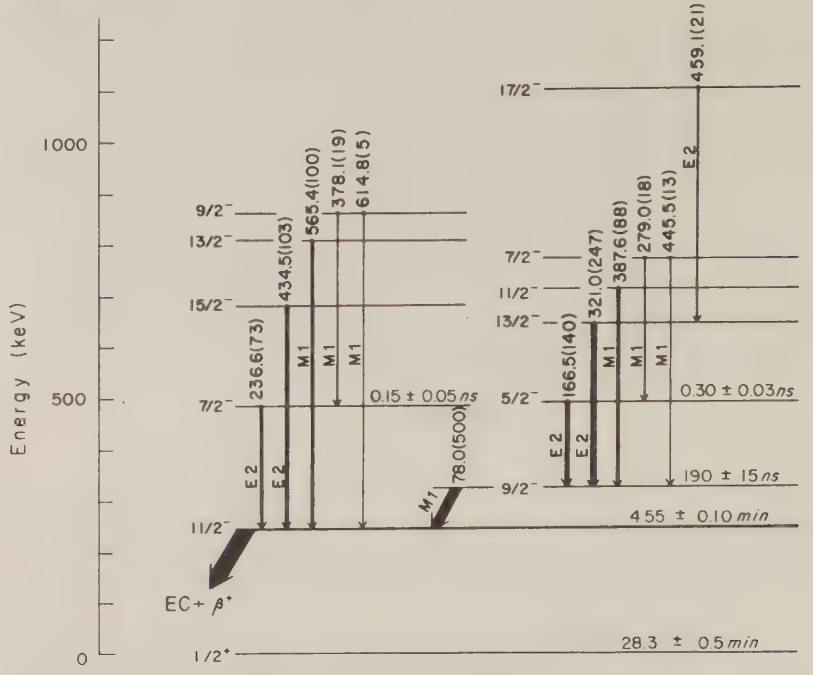

Fig. 6. The low energy parts of the $\frac{11}{2}^-$ and $\frac{9}{2}^-$ level systems.

The $\frac{1}{2}(541)$ state, most easily decoupled, lowers towards the Fermi level at positive deformation, and the interpretation of the new system as a decoupled band implies that in these states the nucleus has prolate shape. The $\frac{13}{2}^-$ to $\frac{9}{2}^-$ difference, 321 keV, does not agree with the 2^+ energies in either ^{188}Pt or ^{190}Hg, but corresponds approximately to their mean value, 340 keV. The $\frac{17}{2}^-$ to $\frac{13}{2}^-$ spacing, 459 keV, is also somewhat smaller than the average of the 4^+ to 2^+ spacings, 515 keV. The value $B(\mathrm{E2};\ \frac{5}{2}^-$ to $\frac{9}{2}^-) = 0.8 \pm 0.1\ e^2 \cdot \mathrm{b}^2$ deduced from the half-life of the $\frac{5}{2}^-$, 491.6 keV level, suggests, when compared with $B(\mathrm{E2};\ \frac{7}{2}^-$ to $\frac{11}{2}^-) = 0.38^{+0.18}_{-0.09}\, e^2 \cdot \mathrm{b}^2$, that the $\frac{9}{2}^-$ band is more deformed than the $\frac{11}{2}^-$ one. An estimate of the deformation is given

by the formula [36])

$$\beta = \left(\frac{1225}{6(\hbar^2/2\mathcal{I})A^{\frac{7}{3}}}\right)^{\frac{1}{4}},$$

where $6\hbar^2/2\mathcal{I}$ corresponds to the $\frac{13}{2}^-$ to $\frac{11}{2}^-$ distance of 0.434 MeV for the $\frac{11}{2}^-$ band, and to the $\frac{13}{2}^-$ to $\frac{9}{2}^-$ spacing of 0.321 MeV for the $\frac{9}{2}^-$ one. The calculation gives $\beta_{\frac{11}{2}^-} = 0.11$ and $\beta_{\frac{9}{2}^-} = 0.14$. The result agrees with the observation that the change from oblate to prolate shapes generally implies an increase in $|\beta|$ of $\approx 50\%$ [ref. [24])]. Both β-values fall within the limits where the rotation aligned coupling is preferred to the deformed one [10]). When comparing the experimental $B(\mathrm{E2}; \frac{5}{2}^-$ to $\frac{9}{2}^-) = 0.8 \pm 0.1\, e^2 \cdot \mathrm{b}^2$ with the strong coupling value, we use the average value of Q_0 for ^{188}Pt and ^{190}Hg and find the theoretical $B(\mathrm{E2}) = 0.82\, e^2 \cdot \mathrm{b}^2$.

The interpretation in terms of decoupled bands makes it possible to explain the hindrance ($F_\mathrm{W} = 15000$) of the $\frac{9}{2}^-$ to $\frac{11}{2}^-$ M1 transition, as the change from prolate to oblate shapes reduces the overlap between the initial and final states. The existence of decoupled band should also imply that the $\frac{9}{2}^-$ and the $\frac{11}{2}^-$ states are pure particle and hole configurations respectively and a transition between them has to be retarded. In ^{187}Ir the retardation of the corresponding $\frac{11}{2}^-$ to $\frac{9}{2}^-$ transition is larger ($F_\mathrm{W} = 5 \times 10^5$) [ref. [9])] and seems to be due mainly to the small overlap between rotation aligned ($\frac{9}{2}^-$) and strong coupling ($\frac{11}{2}^-$) wave functions [33]).

To confirm the interpretation of the $\frac{11}{2}^-$ and $\frac{9}{2}^-$ systems as decoupled bands, heavy ion experiments, ^{181}Ta(^{12}C, 4n)^{189}Au, have been made at the Orsay variable cyclotron [26]). In the $\frac{11}{2}^-$ band yrast states were observed with spins up to $\frac{23}{2}$, in the $\frac{9}{2}^-$ band up to $\frac{25}{2}$. New experiments with the aim to study high spin isomeric states in ^{189}Au are now going on [27]).

For the decoupled $\frac{11}{2}^-$ band in ^{195}Au, Meyer ter Vehn *et al.* [21]) recently obtained better agreement between experimental and theoretical level positions, when asymmetric nuclear shape was assumed, and deformation parameters $\beta = 0.131$ and $\gamma = 37.4°$ were taken from the neighbouring ^{196}Hg. As on the one hand the parameters β and γ vary very little from ^{196}Hg to ^{190}Hg, and on the other hand the $\frac{11}{2}^-$ band changes insignificantly from ^{195}Au to ^{189}Au (fig. 5), the good agreement is valid even for the lighter nucleus.

The same procedure seems difficult to apply for the $\frac{9}{2}^-$ band, as both ^{190}Hg and ^{188}Pt are considered to be oblate [4]) with $\gamma = 36.1°$ and $36.5°$, respectively. A comparison of the level order and spacings in the $\frac{9}{2}^-$ band with the calculations for an asymmetric rotor [21]) shows that the best fit is for $\gamma \approx 25°$ which gives support for prolate shape. As ^{188}Pt is very soft [2, 3]), it is possible that the addition of a $h_{\frac{9}{2}}$ particle to the core induces a tendency to prolate shape.

The nucleus ^{197}Au has been found to be essentially prolate in the $\frac{3}{2}^+$ ground state [32]). Experiments on the lighter gold isotopes show that the E2 deexcitation of the low energy, positive parity states increases with diminishing mass number. This is a sign of collective contributions and suggests a development towards a more pronounced deformation.

6. Conclusion

Even if semi-microscopic models seem to be necessary for a more general interpretation of ^{189}Au, the macroscopic approach of Stephens and Diamond [34]) leads to a good and simple explanation of the high spin states of negative parity. It implies that states with essentially prolate shape and states with essentially oblate shape coexist in this nucleus. The model description becomes especially good, when the asymmetry parameter γ is taken into account as in the even nuclei. Our results on even Pt nuclei [2, 29]) support the hypothesis, that γ is an effective parameter, representing the mean value of the fluctuations ($\gamma = \gamma_{\mathrm{rms}}$). If ^{188}Pt is oblate, γ for the $\frac{9}{2}^-$ band cannot be taken from the neighbouring even nuclei, and one is led to conclude that the $h_{\frac{9}{2}}$ particle gives rise to the quasi prolate shape. A more detailed discussion on the shape of ^{189}Au and neighbouring nuclei is made in forthcoming papers [37, 27]).

We are indebted to the separator group at ISOLDE, CERN for the production of sources. We also thank the members of the french ISOLDE group for helping us during the on-line e^--γ measurements. One of us (V.B.) is grateful to the Joliot-Curie Foundation for financial support.

References

1) Proc. Colloque sur les noyaux de transition, Orsay, France (1971)
2) M. Finger, R. Foucher, J. P. Husson, J. Jastrzebski, A. Johnson, G. Astner, B. R. Erdal, A. Kjellberg, P. Patzelt, Å. Höglund, S. G. Malmskog and R. Henck, Nucl. Phys. **A188** (1972) 369
3) M. Cailliau, Thesis, Orsay, France, 1974
4) K. Kumar and M. Baranger, Nucl. Phys. **A110** (1968) 529
5) U. Götz, H. C. Pauli, K. Alder and K. Junker, Nucl. Phys. **A192** (1972) 579
6) S. G. Nilsson, J. R. Nix, P. Möller and J. Ragnarsson, to be published
7) V. Berg, S. G. Malmskog and A. Bäcklin, Nucl. Phys. **A143** (1970) 177
8) A. Bäcklin, V. Berg and S. G. Malmskog, Nucl. Phys. **A156** (1970) 647
9) C. Sebille-Schück, M. Finger, R. Foucher, J. P. Husson, J. Jastrzebski, V. Berg, S. G. Malmskog, G. Astner, B. R. Erdal, P. Patzelt and P. Siffert, Nucl. Phys. **A212** (1973) 45
10) F. S. Stephens, R. M. Diamond and S. G. Nilsson, Phys. Lett. **44B** (1973) 429
11) Ch. Vieu, A. Peghaire and J. S. Dionisio, Rev. Phys. Appl. **8** (1973) 231
12) Ch. Vieu, Thesis, Orsay, France, 1974
13) Å. Höglund, V. Berg, P. Kilcher, J. Jastrzebski, B. R. Erdal and S. G. Malmskog, to be published
14) M. Finger *et al.*, CERN 70–29 (1970)
15) J. Jastrzebski and P. Kilcher, J. of Phys. **34** (1973) 755
16) The ISOLDE isotope separator on-line facility at CERN, ed. A. Kjelberg and G. Rudstam, CERN 70–3 (1970)
17) T. R. Gerholm and J. Lindskog, Ark. Fys. **24** (1963) 171
18) V. Berg, R. Foucher and Å. Höglund, to be published
19) B. Olsen and L. Bostrom, Nucl. Instr. **44** (1966) 65
20) G. H. Fuller and V. W. Cohen, Nucl. Data Tables **A5** (1969) 433
21) J. Meyer ter Vehn, F. S. Stephens and R. M. Diamond, Phys. Rev. Lett. **32** (1974) 1383
22) K. Nakai, D. Proetel, R. M. Diamond and F. S. Stephens, Phys. Rev. Lett. **32** (1974) 1380
23) L. Grodzins, Phys. Lett. **2** (1962) 88
24) M. Cailliau, J. Letessier, H. Flocard and P. Quentin, Phys. Lett. **46B** (1973) 11

25) S. André, J. Boutet, J. Jastrzebski, J. Lukasiak, J. Rivier, C. Sebille-Schück, Z. Swikowski and J. Treherne, Int. Conf. on nuclear physics, Munich, 1973, p. 196
26) V. Berg, M. A. Deleplanque, C. Gerschel and N. Perrin, Proc. Int. Conf. on nuclear structure and spectroscopy, Amsterdam, 1974, p. 113
27) M. A. Deleplanque, C. Gerschel, N. Perrin and V. Berg, Nucl. Phys., submitted
28) G. Alaga and V. Paar, private communication
29) M. Cailliau, R. Foucher, J. P. Husson and J. Letessier, J. de Phys. **35** (1974) 470
30) J. R. Leigh, J. O. Newton, L. A. Ellis, M. C. Evans and M. J. Emmot, Nucl. Phys. **A183** (1972) 477
31) S. Hager and E. C. Seltzer, Nucl. Data **A4** (1968) no. 1, 2
32) A. Veyssière, H. Beil, R. Bergère, P. Carlos and A. Leprêtre, Nucl. Phys. **A159** (1970) 561
33) S. André, J. Boudet, J. Jastrzebski, R. Kaczarowski, J. Lukasiak, J. Rivier, C. Sebille-Schück, Z. Sujkowski and J. Treherne, Nashville Conf. on reactions between complex nuclei (1974) p. 192
34) F. S. Stephens, R. M. Diamond, D. Benson, Jr. and M. R. Maier, LBL Annual Report (1972) p. 15
35) C. R. Bingham *et al.*, Proc. Int. Conf. on reactions between complex nuclei (1974) p. 180
36) F. S. Stephens, R. M. Diamond, J. R. Leigh, T. Kammuri and K. Nakai, Phys. Rev. Lett. **29** (1972) 438
37) V. Berg, C. Bourgeois and R. Foucher, J. de Phys., July 1975

R E F E R E N C E 18

SOME FEATURES OF ODD Au NUCLEI REVEALED BY HALF-LIFE MEASUREMENTS

V. BERG, C. BOURGEOIS (*) and R. FOUCHER
Institut de Physique Nucléaire, BP 1, 91406 Orsay, France

LE JOURNAL DE PHYSIQUE TOME 36, JUILLET-AOÛT 1975, PAGE 613

Classification
Physics Abstracts
4.162

SOME FEATURES OF ODD Au NUCLEI REVEALED BY HALF-LIFE MEASUREMENTS

V. BERG, C. BOURGEOIS (*) and R. FOUCHER

Institut de Physique Nucléaire, BP 1, 91406 Orsay, France

(*Reçu le 17 mars 1975, accepté le 21 mars 1975*)

Résumé. — L'identité de structure des premiers niveaux $9/2^-$ dans les noyaux d'or de nombre de masse impair de 187 à 193 ainsi que cette structure elle-même, sont révélées par le mode de population et désexcitation de ces niveaux et leurs vies moyennes. Ceci montre l'importance de la prise en compte du paramètre d'asymétrie γ dans les noyaux impairs d'or comme cela a déjà été montré pour les noyaux de platine. Ceci montre également la nécessité de tenir compte dans ces noyaux d'états appartenant à la couche majeure suivante.

Abstract. — The half-life (1.2 ± 0.1 ns) of the 789.9 keV $9/2^-$ level in ^{193}Au is measured. The retardation of the deexciting M 1 and E 2 transitions suggests that this $9/2^-$ state, as well as those found in 187, 189, 191 gold nuclei, issues from the $h_{9/2}$ orbit. The average shape of the Au nuclei in these states and of their even Pt cores is interpreted with the particle + asymmetric rotor model.

The great interest focused on transitional nuclei in the Os to Pb region is connected with observations made precedently :

— Signs of a prolate to oblate shaped transition revealed by the study of level positions in even Pt nuclei [1, 2].

— Establishment of $9/2^-$ states issued from the $h_{9/2}$ orbital in Tl nuclei [3].

— The discovery and interpretation of negative parity states in Ir nuclei [4].

— The existence of unexpectedly large retardations of transitions in Ir and Pt nuclei [5].

— The large isotopic shift measured between ^{185}Hg and ^{187}Hg [6].

Most of the above information was obtained at ISOLDE, CERN and studies of odd Au and Pt nuclei are actually continued at ISOCELE, Orsay.

Half-life measurements of excited states [7] and heavy ion reaction experiments [8, 9] have led to the proposal of two decoupled bands in ^{189}Au. They are based on $9/2^-$ and $11/2^-$ levels, joined as in ^{187}Ir [4] by a very retarded M 1 transition (78 keV, $F_W \sim 15\,000$).

The $11/2^-$ band is supposed to result from the coupling of an $h_{11/2}$ proton hole to the « rotation » of a Hg core and has, in fact, « rotation » energies similar to those of even Hg isotopes. In these states the deformation of the nucleus should be oblate as in Hg nuclei. The band appears in all odd Au isotopes and is observed to have a very stable structure [7-14]. As seen in figure 2 the band head lowers slowly, when the neutron number decreases.

The $9/2^-$ state is proposed to arise from the coupling of a proton in the $h_{9/2}$ shell to the « rotation » of a Pt core and has, according to this interpretation, a prolate shape. States issued from the high lying $h_{9/2}$ orbital, have already been observed in Tl nuclei and their appearance at low excitation energy is explained by the gain in pairing energy [3]. In Tl, and, as shown below, in Au these states lower rapidly with decreasing mass number.

In ^{187}Au the $9/2^-$ state is placed below the $11/2^-$ isomer (Fig. 2) and the decoupled character of the band is well developed [13]. The half-life of the $11/2^-$ state has been measured, but the retardation factors for the $11/2^-$ to $9/2^-$ transition cannot be given, as the M 1 to E 2 mixing ratio has not yet been determined. (The experimental results on ^{185}Au are now being analysed.) In ^{195}Au the $9/2^-$ level is proposed as lying at 1 068 keV [15]. More information is available in ^{191}Au : Höglund *et al.* [14] have found the $9/2^-$ band at about 200 keV higher excitation energy than in ^{189}Au (Fig. 2), and measured a similar hindrance as in the latter nucleus for the $9/2^-$ to $11/2^-$ M 1 transition (Table I). For the identification of the $9/2^-$ state in ^{193}Au, the extensive studies by Vieu and Dionisio [11] give aid. Their table of analogue states in ^{193}Au and ^{195}Au, i.e. states with the same spin and parity, nearly same excitation energy and identical depopulation mode, shows that the 789.9 keV $9/2^-$ level in ^{193}Au has no equivalence in the 195 iso-

(*) And University Paris VII.

TABLE I

Half-lives of $9/2^-$ *levels, and absolute transition probabilities of* $9/2^-$ *to* $11/2^-$ $(7/2^-)$ *transitions in* 189, 191, 193 Au *isotopes*

Nucleus	Level keV	$T_{1/2}$ level ns	Transition keV	Initial state	Final state	Multipole	F_W	B (M 1) $(e\hbar/2Mc)^2$	B (E 2) $e^2 b^2$
^{193}Au	789.9	1.2 ± 0.1	499.65	$9/2^-$	$11/2^-$	M 1 (a)	17 000	$(1.0 \pm 0.3) \times 10^{-4}$	
						E 2	11		$(6.0 \pm 2.0) \times 10^{-4}$
			281.76	$9/2^-$	$7/2^-$	M 1	14 000	$(1.3 \pm 0.3) \times 10^{-4}$	
						E 2	6.3		$(11 \pm 3) \times 10^{-4}$
^{191}Au	541.3	12 ± 1 (b)	274.1	$9/2^-$	$11/2^-$	M 1 (b)	16 000	$(1.1 \pm 0.2) \times 10^{-4}$	
^{189}Au	325.1	190 ± 15 (c)	78.0	$9/2^-$	$11/2^-$	M 1 (d)	15 000	$(1.2 \pm 0.1) \times 10^{-4}$	
						E 2	> 20		$< 3.2 \times 10^{-4}$

(a) Référence [11].
(b) Référence [14].
(c) Référence [7].
(d) Référence [25].

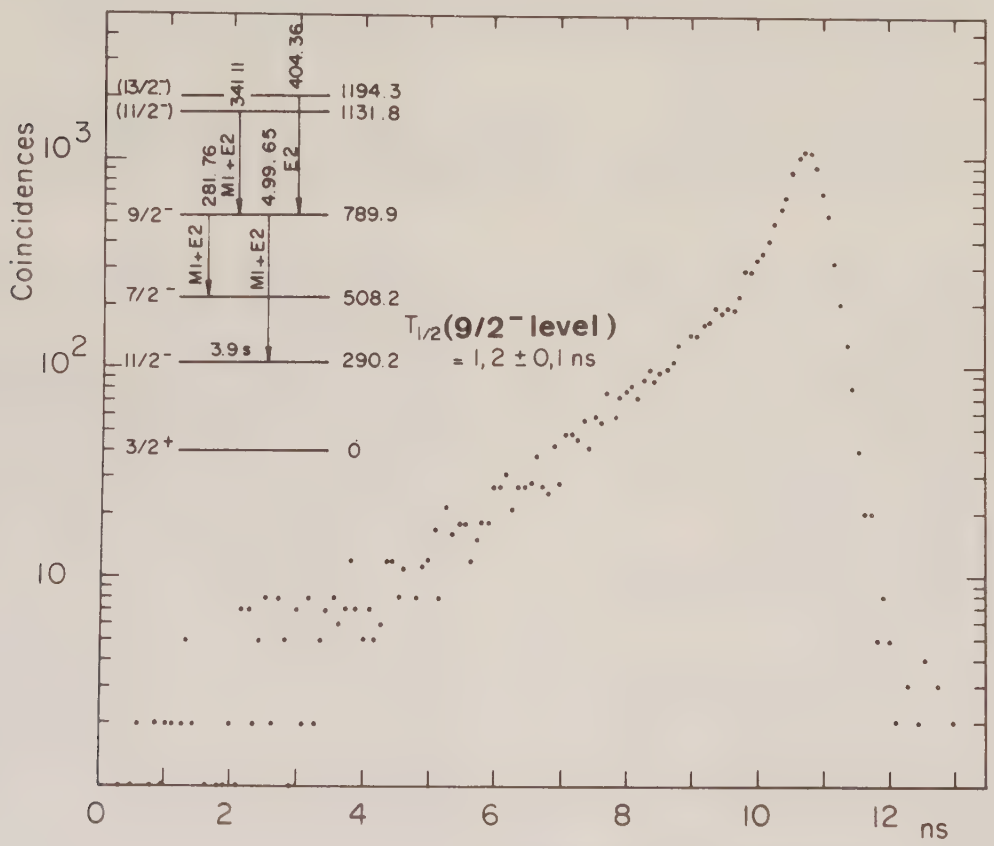

FIG. 1. — Time distribution obtained by measuring 499.65 K − γ coincidences in ^{193}Au.

tope. The level lies about 200 keV higher than the $9/2^-$ state in ^{191}Au. It decays to the $11/2^-$ isomer and is fed as the $9/2^-$ states in ^{189}Au and ^{191}Au by a pure E 2 and a mixed M 1 + E 2 transition (Fig. 1). However, calculations of transition rates performed within the frame of the Alaga Paar 3-hole cluster model [16] (using parameters fitting best the positive parity states and without octupole coupling), do not give the large retardation factors expected for the deexciting transitions [11]. A state with the required properties was placed at 500 keV higher energy. It therefore seemed necessary to make a half-life measurement in order to check the character of the state. The experiment was performed according to the delayed coincidence method, with an isotopically pure ^{193}Hg source, using a Gerholm

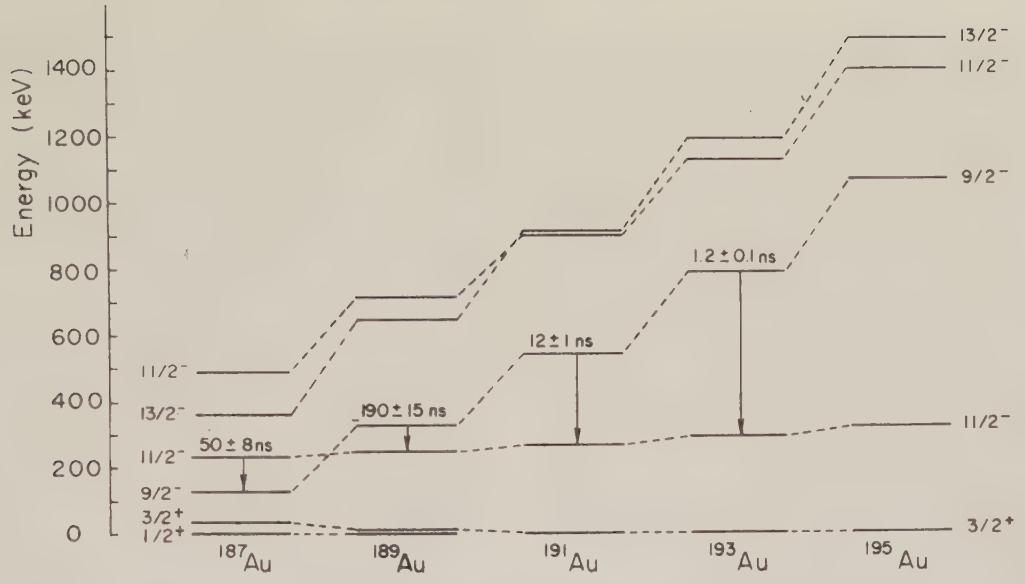

FIG. 2. — Ground state, $11/2^-$, and $9/2^-$ levels in odd Au isotopes. The two highest levels are the first two excited states of the $9/2^-$ band. Their relative positions indicate that, in this band, rotation aligned coupling and prolate shape dominate in ^{187}Au and ^{189}Au, strong coupling and oblate shape in the heavier gold nuclei.

coincidence spectrometer [17]. The K-line of the 499.7 keV transition, which depopulates the 789.9 keV level, was then selected by one lens and the feeding γ-rays were detected with a plastic scintillator.

Figure 1 shows the time distribution of the e-γ coincidences and the relevant part of the decay scheme. The slope of the curve gives

$$T_{1/2}\,(789.9\text{ keV level}) = 1.2 \pm 0.1\text{ ns}\,.$$

The retardation factors of the depopulating M 1 transitions (Table I) resemble those obtained for the correspondent transitions in ^{189}Au and ^{191}Au. Even the E 2 transitions are hindered compared to the Weisskopf estimate. The measurement provides good support to the assumption that the 789.9 keV $9/2^-$ state in ^{193}Au has the same structure as the $9/2^-$ levels in ^{189}Au and ^{191}Au.

The study of even Pt [1, 2] and Hg [18] nuclei has shown the necessity of taking into account, not only the variation of the deformation parameter β from one state to another and the fluctuations of it within each state, but also the variations and the fluctuations of the shape asymmetry parameter γ. In a recent interpretation of the $11/2^-$ band of ^{195}Au, Meyer *et al.* [19] assume a triaxial nuclear shape and investigate, as a first step, the band structure of a single j-nucleon coupled to a rigid asymmetric rotor. For $\gamma = 0°$, they find a pure rotation aligned level order with strongly populated I, $I+2$, $I+4$. ... states; for $\gamma = 60°$ the band structure becomes typically strong coupled with an I, $I+1$, $I+2$, ... spin sequence. A continuous transition from decoupled to strong coupled structure takes place by changing γ from 0° to 60°. The strong coupling level order dominates in the interval $30° < \gamma < 60°$.

The model allows a comparison between even Pt nuclei and the $9/2^-$ states in Au, interpreted as formed by the coupling of an $h_{9/2}$ proton to the rotation of the neighbouring Pt core. The measurement of the static quadrupole moment in ^{194}Pt has proved that this nucleus has an oblate shape [20], but a change to the prolate form is expected in lighter Pt nuclei [1, 21] (around mass 188).

In accordance with the negative deformation of ^{194}Pt and its γ parameter > 30°, the $9/2^-$ band in ^{195}Au shows the strong coupling level sequence (Fig. 2). This is also the case for the bands in ^{193}Au and ^{191}Au, thus suggesting an oblate shape for ^{192}Pt and ^{190}Pt. In ^{189}Au, the $13/2^-$ member of the $9/2^-$ band is found at a lower energy than the $11/2^-$ one, and the band is decoupled, which corresponds to $\gamma < 30°$ and a *prolate* shape for the ^{188}Pt core. The assumption of positive deformation of ^{188}Pt, is supported by the fact that the $11/2^-$ isomeric state in ^{187}Ir, interpreted as a hole in the ^{188}Pt core, has been shown to be prolate [15]. The decoupled character of the $9/2^-$ band becomes more pronounced in ^{187}Au, in agreement with the prolate shape proposed for ^{186}Pt [21].

According to this simple comparison, the oblate-prolate shape transition in even Pt nuclei, i.e. the transfer of the total energy minimum from the oblate to prolate side, should occur in the step between the isotopes 190 and 188. The change of the potential

minimum takes place between ^{188}Pt and ^{186}Pt [21], which seems to demonstrate the influence of the β and γ dependent mass parameters on the location of the shape transition [1, 21]. In the above comparison, no attention was given to the influence of the particle-core interaction, which may be strong enough to shift the shape transition [7, 9, 24]. Admixtures in the $9/2^-$ state were not considered either. The most important contribution is expected to come from the 9/2 (514) state. It should give rise to a tendancy for a strong coupling level pattern in the lighter, more deformed isotopes. This effect is not observed.

It is interesting to notice that the shape transition, which arises as a function of neutron number N in Pt and Au nuclei, also takes place as a function of Z. In 191 to 199 Tl isotopes the $9/2^-$ band is found to be oblate [3], in ^{187}Ir and ^{189}Ir it is prolate [22]. These observations support the suggestion that the shape transition of the even cores occurs near a line joining ^{182}Hg, ^{188}Pt, and ^{194}Os [21].

It remains now to discuss the cause of the large retardations of the interband transitions. Several reasons can be suggested. In the lighter nuclei, a certain hindrance may be due to the change from prolate to oblate shape. According to the simple rotation aligned and strong coupling models, the $9/2^-$ and the $11/2^-$ states are respectively a pure particle state coupled to a Pt core and a pure hole state coupled to a Hg core. A transition between them is a two step process. In ^{187}Ir [5] the $11/2^-$ to $9/2^-$ transition is about 30 times more retarded than in the Au isotopes. In this case, the $11/2^-$ state is essentially strong coupled, while the $9/2^-$ one is rotation aligned and their wave functions have a very small overlap. In Au nuclei, the overlap is expected to be larger, as the difference in structure between the initial and final states are less pronounced. The retardation in ^{187}Ir can also be explained by K-forbiddeness; the states involved being $11/2^-$ (505) and a strongly perturbed $1/2^-$ (541).

The study of the $9/2^-$ states in odd Au nuclei has shown that, to a first approximation, the approach of Meyer *et al.* [19] can explain their characteristics. This indicates that a new type of coupling between particle and a collective state can appear in soft nuclei, and that γ asymmetry has to be taken into account in odd as well as in even nuclei. It must be noticed that this successful model for high angular momentum states has, necessarily, the limitations of the Davydov model [23], which identifies β with β_{rms} and γ with γ_{rms}, and thus neglects the shape and pairing fluctuations shown to be large in the even nuclei of this region [21]. Our result seems also to show the limitations of models which take into account the shape fluctuations, but neglect states belonging to the next higher shell.

We are indebted to M. Jacques Obert for the preparation of the ^{193}Hg source and to the ISOCELE collaboration for on line measured sources.

References

[1] Kumar, K., Baranger, M., *Nucl. Phys.* A **122** (1968) 273.
[2] Finger, M., Foucher, R., Husson, J. P., Jastrzebski, J., Johnson, A., Astner, G., Erdal, B. R., Kjelberg, A., Patzelt, P., Höglund, A., Malmskog, S. G., Henck, R., *Proc. Int. Conf. Leysin* (1970) 1031, and *Nucl. Phys.* A **188** (1972) 369.
[3] Newton, J. O., Cirilov, S. D., Stephens, F. S. and Diamond, R. M., *Nucl. Phys.* A **148** (1970) 593.
[4] Bäcklin, A., Berg, V., Malmskog, S. G., *Nucl. Phys.* A **156** (1970) 647.
[5] Sebille-Schück, C., Finger, M., Foucher, R., Husson, J. P., Jastrzebski, J., Berg, V., Malmskog, S. G., Astner, G., Erdal, B. R., Patzelt, P., Siffert, P., *Proc. Int. Conf. Leysin* (1970) 1045, and *Nucl. Phys.* A **212** (1973) 45.
[6] Bonn, J., Huber, G., Kluge, H. J., Kugler, L., Otten, E. W., *Phys. Lett.* **38B** (1972) 308.
[7] Berg, V., Foucher, R., Höglund, A., *Proc. Int. Conf. Amsterdam* (1974) 112, and *Nucl. Phys.*, in print.
[8] Berg, V., Deleplanque, M. A., Gerschel, C., Perrin, N., *Proc. Int. Conf. on Nuclear Structure and Spectroscopy*, Amsterdam (1974) 113 and IPNO-Ph. N-74-12.
[9] Deleplanque, M. A., Gerschel, C., Perrin, N., Berg, V., *Nucl. Phys.* à paraître.
[10] Vieu, Ch., Peghaire, A. et Dionisio, J. S., *Revue Phys. Appl.* **8** (1973) 231.
[11] Vieu, Ch., Dionisio, J. S., *Proc. of the topical Conference on problems of vibrational nuclei*, Zagreb (1974).
[12] Tjöm, P. O., Maier, M. R., Benson, D. Jr, Stephens, F. S. and Diamond, R. M., *Nucl. Phys.* A **231** (1974) 397.
[13] Deleplanque, M. A., Gerschel, C., Ishihara, M., Perrin, N., Berg, V., Bourgeois, C., Desthuilliers, M. G., Husson, J. P., Kilcher, P., Letessier, Jocelyne, *J. Physique Lett.* à paraître.
[14] Höglund, A., Berg, V., Erdal, B. R., Jastrzebski, J., Kilcher, P., Malmskog, S. G., Annuaire IPNO (1975) 5, and to be published.
[15] Meyer ter Vehn, J., LBL-3416 (1974).
[16] Paar, V., *Nucl. Phys.* A **211** (1973) 29.
[17] Gerholm, T. R. and Lindskog, J., *Ark. Fys.* **24** (1963) 171.
[18] Proetel, D., Diamond, R. M. and Stephens, F. S., *Phys. Lett.* **48B** (1974).
[19] Meyer ter Vehn, J., Stephens, F. S. and Diamond, R. M., *Phys. Rev. Lett.* **32** (1974) 1383.
[20] Pryor, R. J. and Saladin, J. X., *Phys. Rev.* **1C** (1970) 1573.
[21] Cailliau, M., Thesis, IPN Orsay (1974).
[22] André, S., Boutet, J., Jastrzebski, J., Kaczarowski, R., Lukasiak, J., Rivier, J., Sebille-Schück, C., Sujkowski, Z., Treherne, J., Nashville Conference on Reaction Between Complex Nuclei (1974) 192.
[23] Davidov, A. S., Filipov, G. F., *Nucl. Phys.* **8** (1958) 237.
[24] Dickman, F., Dietrich, K., *Z. Phys.* **271** (1974) 417.
[25] Jastrzebski, J., Kilcher, P., *J. Physique* **34** (1973) 755.

R E F E R E N C E 19

COEXISTENCE DE FORME DANS LE NOYAU ^{187}Au

(1) M.A. DELEPLANQUE, C. GHERSCHEL, M. ISHIHARA (*), N. PERRIN

(2) V. BERG, C. BOURGEOIS (**), M.G. DESTHUILLIERS (***), J.P. HUSSON (****)

P. KILCHER et J. LETESSIER

Division de Physique Nucléaire, Institut de Physique Nucléaire, 91406 Orsay, France

Classification
Physics Abstracts
4.470

COEXISTENCE DE FORME DANS LE NOYAU ^{187}Au

(1) M. A. DELEPLANQUE, C. GERSCHEL, M. ISHIHARA (*), N. PERRIN
(2) V. BERG, C. BOURGEOIS (**), M. G. DESTHUILLIERS (***), J. P. HUSSON (****), P. KILCHER et J. LETESSIER

Division de Physique Nucléaire, Institut de Physique Nucléaire, 91406 Orsay, France

(*Reçu le 23 avril 1975, révisé le 28 mai 1975, accepté le 4 juin 1975*)

Résumé. — L'or a été formé dans la désintégration de ^{187}Hg et dans la réaction ^{175}Lu(^{16}O, 4 nγ)^{187}Au. Les deux bandes découplées construites sur les états intrinsèques $h_{9/2}$ et $h_{11/2}$ impliquent la coexistence de déformations respectivement *prolate* et *oblate*. Le comportement des états de haut spin est discuté par rapport au platine 186.

Abstract. — In ^{187}Au, studied by radioactivity and by the ^{175}Lu(^{16}O, 4 nγ) ^{187}Au reaction at 95 MeV, two decoupled bands are built on $h_{9/2}$ and $h_{11/2}$ intrinsic states, implying, as in ^{189}Au, the coexistence of prolate and oblate deformations. The behavior of high spin states is analysed and compared to ^{186}Pt.

Récemment, des résultats sur les ors impairs obtenus par réaction (ions lourds, *x*n) ont permis d'attribuer une déformation aplatie (oblate) aux ors les plus lourds (A = 195 à 191) [1] ; de plus, dans le noyau ^{189}Au [2, 3], la coexistence de déformations allongée (prolate) et aplatie a été mise en évidence. En effet, pour les noyaux d'or, le niveau de Fermi en protons se trouve situé entre les couches $h_{11/2}$ et $h_{9/2}$. L'observation de bandes découplées, par effet de Coriolis, pour une orbitale $h_{11/2}$, indique [4, 5] une déformation aplatie ; pour le noyau ^{189}Au, où apparaît en plus une bande découplée sur l'état 9/2$^-$, les deux formes

(1) Réactions (ions lourds, *x*n).
(2) Radioactivité (séparateur ISOCELE).
(*) Institute of Nuclear Study, Tokyo, Japon.
(**) Université Paris VII.
(***) Centre de Spectroscopie Nucléaire et de Spectrométrie de masse, 91406 Orsay.
(****) Université Paris VI.

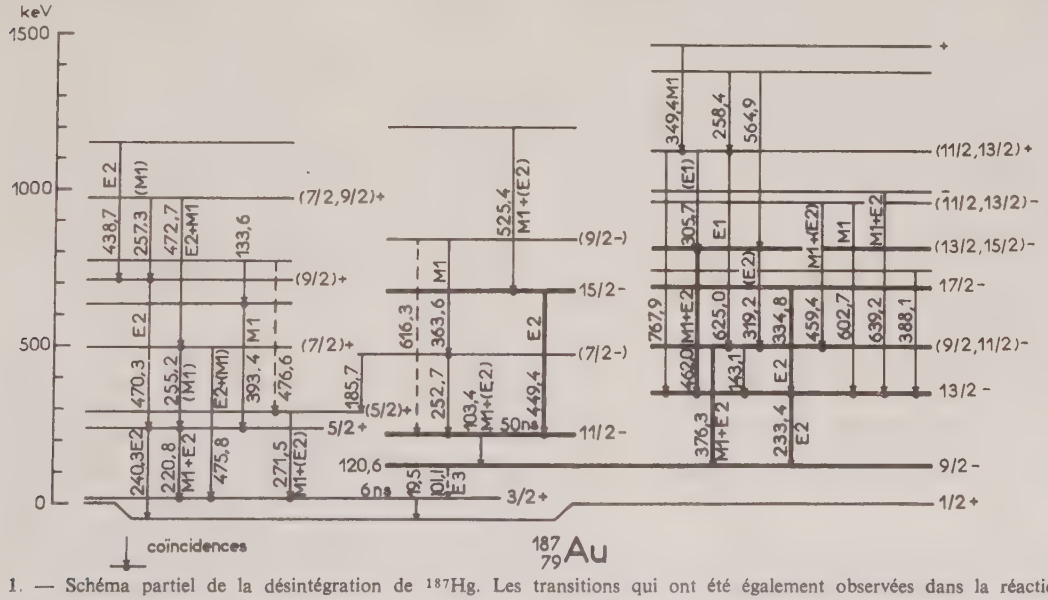

FIG. 1. — Schéma partiel de la désintégration de ^{187}Hg. Les transitions qui ont été également observées dans la réaction ^{175}Lu(^{16}O, 4n)^{187}Au ainsi que les niveaux qui en découlent sont en traits épais.

aplatie et allongée coexistent, le paramètre de déformation ayant une valeur plus grande pour la forme allongée. De plus, dans ce noyau, la *bande* $h_{11/2}$ est plus alimentée que la *bande* $h_{9/2}$ [3].

L'étude de ^{187}Au a été entreprise par la réaction ^{175}Lu(^{16}O, 4n)^{187}Au et par la décroissance radioactive de ^{187}Hg ($T_{1/2} = 133 \pm 13$ s). La réaction par ions lourds a été effectuée à 95 MeV au cyclotron à énergie variable d'Orsay. La cible ^{175}Lu de 1 mg/cm^2 est autosupportée. Les mesures comprennent des spectres gamma directs, des distributions angulaires et des coïncidences tridimensionnelles (E_{γ_1}-E_{γ_2}, temps entre γ_1 et γ_2). Les expériences de radioactivité ont été réalisées auprès du séparateur d'isotopes ISOCELE [6] en ligne sur le faisceau du synchrocyclotron d'Orsay. Une cible d'or fondu est bombardée par des protons de 157 MeV, les produits de réaction (p, xn) sont ionisés, accélérés, puis séparés isotopiquement. Le faisceau d'ions séparés est focalisé sur une bande de mylar aluminisé ; la source ainsi obtenue est transportée devant les détecteurs (γ et e^-) à l'aide d'un dérouleur de bande. Dans la deuxième ligne du séparateur, le faisceau est recueilli sur des pastilles, un système automatique permet d'envoyer régulièrement ces pastilles dans un spectromètre β de type Gerholm [7]. Nous avons effectué des spectres directs (γ, e^-), des coïncidences (γ-γ-t et e^--γ), des mesures de vies moyennes (coïncidences e^--e^- et e^--γ). Les premiers spectres directs d'électrons de conversion et gamma avaient été obtenus auprès du séparateur ISOLDE du C. E. R. N. L'analyse des expériences a été effectuée avec l'ordinateur IBM 370-135 du laboratoire (A. R. I. E. L.).

Le schéma de niveaux partiel de ^{187}Au obtenu par radioactivité est présenté sur la figure 1. Les coefficients de conversion tirés des spectres directs d'électrons et gamma nous donnent les multipolarités des principales transitions. Nous ne parlerons ici que des points délicats de ce schéma :

1) la transition de 19,5 keV a été mise en évidence sur le spectre d'électrons obtenu avec le spectromètre Gerholm (Fig. 2). Le spectre gamma observé en coïncidence avec la raie de conversion M de la transition de 19,5 keV permet, par l'intermédiaire des raies de 271,5 et 185,7 keV, de proposer l'état isomérique à 120,6 keV. La période du niveau de 19,5 keV est $T_{1/2} = (6 \pm 1)$ ns.

2) les résultats concernant les énergies et les conversions des transitions de 101,1 et 103,4 keV sont tout à fait compatibles avec une transition de 101,1 keV de nature E3($\alpha_L = 75 \pm 20$) et une transition de 103,4 keV de nature essentiellement M1. C'est ce qui permet de proposer la transition de 101,1 keV comme désexcitant l'état isomérique de 120,6 keV vers l'état de 19,5 keV.

3) l'ensemble des résultats obtenus nous conduit à supposer que la transition de 103,4 keV est double ; en effet, la transition de 103,4 keV présente exactement les mêmes caractéristiques que la transition de 78 keV

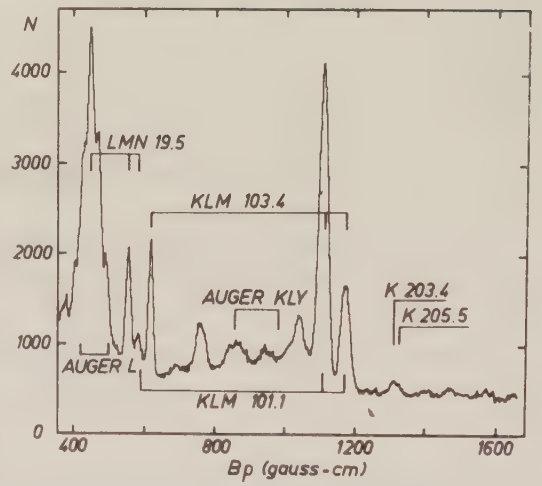

FIG. 2. — Spectre d'électrons de basse énergie de ^{187}Au obtenu avec une préaccélération de 9,7 kV.

dans ^{189}Au : nature essentiellement M1, retard ($T_{1/2} = 50 \pm 8$ ns) par rapport à la transition E2 de 449,4 keV. Bien que située entre deux états isomériques, elle est observée en coïncidence rapide avec les transitions de 271,5 et 153,7 keV (non placée). Une étude systématique des noyaux d'or voisins [8, 9] (1), ainsi que les résultats obtenus par ions lourds dans le noyau ^{187}Au nous font attribuer le spin $9/2^-$ au niveau de 120,6 keV. Les autres spins sont déduits à l'aide des multipolarités des transitions. Comme dans l'or 189, il existe une transition M1 retardée entre les niveaux $11/2^-$ et $9/2^-$, mais leur position relative est l'inverse de celle des ors plus lourds. Dans ces deux noyaux les transitions sont retardées d'un facteur $F_{SP} \simeq 2 \times 10^4$ par rapport au modèle à une particule.

Les principaux résultats obtenus par la réaction ^{175}Lu(^{16}O, 4n)^{187}Au sont présentés dans le tableau I. On observe deux bandes découplées (Fig. 3) construites sur les états $11/2^-$ et $9/2^-$, la *bande* $h_{9/2}$ étant la plus alimentée conformément à l'évolution du niveau de Fermi entre ^{189}Au et ^{187}Au. Les coïncidences énergie-temps ont permis d'établir que les transitions de la *bande* $h_{9/2}$ dépeuplent un niveau isomérique de période $T_{1/2} \simeq 100$ ns, et que celles de la *bande* $h_{11/2}$ dépeuplent un niveau isomérique de période environ 25 ns.

L'ensemble des résultats obtenus indique donc la coexistence des formes allongée et aplatie dans le noyau ^{187}Au. Lorsque les noyaux d'or deviennent de plus en plus déficients en neutrons, on constate que la déformation de la forme allongée augmente ($E(j+2 \rightarrow j) = 321$ keV pour ^{189}Au et 233 keV pour ^{187}Au) alors que celle de la forme aplatie est stationnaire jusqu'à ^{187}Au puisque de ^{195}Au à ^{187}Au l'énergie

(1) Berg, V., Hoglund, A., communication privée.

TABLEAU I

^{187}Au

E_γ (keV)	A_2 %	I_γ	Multipolarité	Remarques
233,5 ± 0,2	0,10 ± 0,04	100 ± 13	E2	(c), (e)
334,7 ± 0,2	0,13 ± 0,04	74 ± 10	E2	(c), (e)
413,8 ± 0,3		63 ± 12	(E2)	(a), (c)
449,5 ± 0,3	0,15 ± 0,09	51 ± 8	E2	(d), (e)
491,4 ± 0,2	0,24 ± 0,07	73 ± 11	E2	(c)
509,2 ± 0,5		40 ± 20		(a), (b), (c)
566,5 ± 0,3		57 ± 10	(E2)	(a), (c)
709,6 ± 0,4	0,23 ± 0,18	22 ± 5	(E2)	(d)
731,6 ± 0,4	0,06 ± 0,17	25 ± 5	(M1 + E2, E2)	(d)

(a) Ces raies sont doubles et à cause du déplacement Doppler à 26°, la détermination de l'anisotropie est très imprécise.
(b) L'énergie et l'intensité de cette transition sont très approximatives à cause de la présence de la raie de 511 keV.
(c) Ces transitions sont alimentées en majorité par un état isomérique de période ≃ 100 ns, ce qui atténue leur anisotropie et permet entre autres d'isoler la raie de 509,2 keV de la raie d'annihilation.
(d) Ces transitions sont alimentées en majorité par un état isomérique de période ≃ 25 ns.
(e) La multipolarité de ces raies a été confirmée par les mesures de coefficient de conversion en radioactivité.

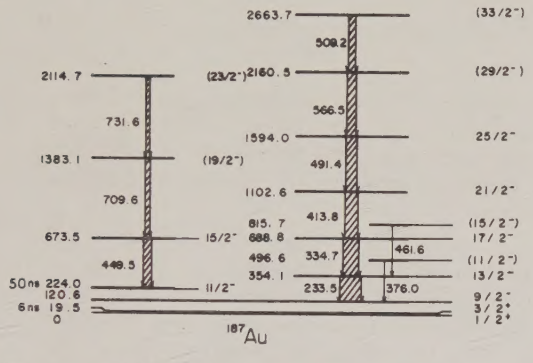

FIG. 3. — Schéma partiel du noyau ^{187}Au. Les niveaux en traits fins ont été observés par radioactivité. Les niveaux en traits épais ont été observés dans l'expérience ^{175}Lu(^{16}O, 4n)^{187}Au. La transition de 103,4 keV entre les niveaux 11/2⁻ à 224,0 keV et 9/2⁻ à 120,6 keV a été aussi observée dans cette réaction, mais son intensité n'a pu être déterminée.

des transitions de cette bande reste à peu près constante [3].

La situation des états de spin $j + 1$ (où j est le moment angulaire de la particule impaire) à l'intérieur des deux bandes indique comme dans les ors plus lourds l'existence d'asymétrie γ [5]. Mais le rapport

$$R = \frac{E(j+1) - E(j)}{E(j+2) - E(j)} = 1{,}6 \text{ (bande } h_{9/2})$$

et

$$2{,}2 \text{ (bande } h_{11/2})$$

manifeste des déformations non axiales moins importantes que dans les ors plus lourds où R reste compris entre 1,3 et 1,4.

Comme dans $^{189}_{79}$Au [2] et dans les noyaux $^{189}_{77}$Ir et ^{187}Ir [10], la *bande* $h_{9/2}$ présente une analogie avec la bande quasi-rotationnelle fondamentale des cœurs pairs-pairs voisins. En particulier, la réaction

$$^{174}\text{Yb}(^{16}\text{O}, 4n)^{186}\text{Pt à 95 MeV}$$

nous a permis d'observer les états de la bande quasi-rotationnelle fondamentale jusqu'au spin 14^+ : en plus des transitions de 191,5, 298,6, 387,0, 464,3 et 514,6 keV placées par Burde *et al.* [11], nous avons observé (voir Tabl. II) deux transitions de 478,0 keV

TABLEAU II

^{186}Pt

E_γ (keV)	Transition	I_γ	A_2 exp %	Remarques
191,5 ± 0,2	$2^+ \rightarrow 0^+$	100 ± 7	0,07 ± 0,05	
298,6 ± 0,3	$4^+ \rightarrow 2^+$	100 ± 7	0,10 ± 0,05	
387,0 ± 0,3	$6^+ \rightarrow 4^+$	80 ± 6	0,12 ± 0,05	
464,3 ± 0,4	$8^+ \rightarrow 6^+$	68 ± 7		(b)
478,0 ± 0,8	$12^+ \rightarrow 10^+$	46 ± 14	(0,22 ± 0,09)	(a)
488,9 ± 0,5	$(14^+ \rightarrow 12^+)$	24 ± 2	0,29 ± 0,10	
514,6 ± 0,6	$10^+ \rightarrow 8^+$	56 ± 6		(b)

(a) Cette raie est un doublet et correspond à deux transitions, l'une dans ^{185}Pt et l'autre dans ^{186}Pt. Le coefficient A_2 correspond à l'anisotropie du doublet. Dans ^{185}Pt cette transition est de caractère E2, ce qui implique une nature E2 pour la transition de ^{186}Pt.
(b) Le déplacement Doppler (à 26°) dans ces groupes complexes de raies rend impossible la détermination du coefficient A_2.

et 488,9 keV, de multipolarité probable E2, en coïncidence avec l'ensemble de ces raies, alors que la raie de 551 keV proposée par ces auteurs comme désexcitant l'état 12^+ n'est pas observée en coïncidence avec l'ensemble de la bande. Nous suggérons donc que ces transitions de 478,0 keV et 488,9 keV désexcitent respectivement les niveaux 12^+ et 14^+ du platine 186. Sur la figure 4, nous avons porté les courbes donnant

$$\frac{2\,\mathfrak{J}(I)}{\hbar^2} = \frac{4\,I - 2}{E\gamma(I \to I - 2)}$$

en fonction du carré de la fréquence de rotation

$$(\hbar\omega)^2 = \frac{E\gamma^2(I \to I - 2)}{4}$$

pour la bande yrast du platine 186 et pour la *bande* $h_{9/2}$ du noyau ^{187}Au (I est le moment angulaire total pour le niveau considéré, $\mathfrak{J}(I)$ le moment d'inertie pour le niveau de spin I). Des résultats récents [12, 13] ont montré l'importance de l'étude des noyaux impairs dans l'interprétation du *backbending*. Dans les noyaux ^{186}Pt et ^{184}Pt, le *backbending* observé à partir du spin 10^+ peut être interprété par l'alignement d'une paire de protons $h_{11/2}$ sur le moment angulaire de rotation. Ceci est cohérent avec l'observation du *backbending* dans la *bande* $h_{9/2}$ du noyau ^{187}Au (Fig. 4).

Ces résultats sont en accord avec ce que l'on connaît des déformations des noyaux de cette région [10, 14, 15, 16]. Ils permettent de souligner le rôle de l'orbitale $1/2^-$ [541] qui, fortement descendante, tend à augmenter la déformation. Au contraire l'orbitale $1/2^-$ [501] ascendante favorise la symétrie sphérique. On peut en particulier conclure que l'influence des paires de protons $h_{11/2}$ est importante pour définir la forme aplatie et peu déformée des mercures et des platines

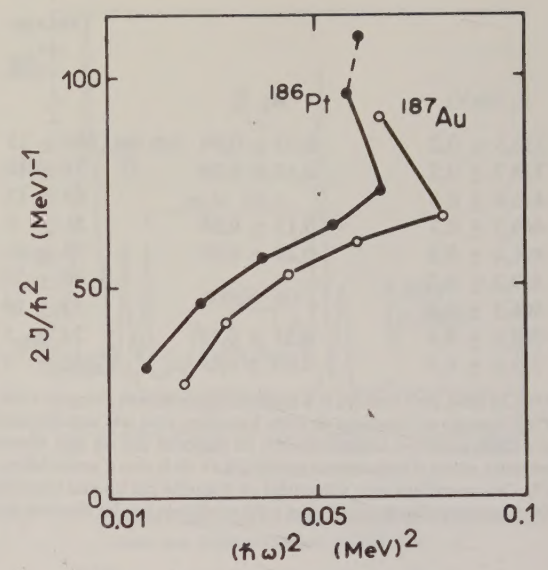

FIG. 4. — $2\,\mathfrak{J}/\hbar^2$ en fonction de $(\hbar\omega)^2$ pour ^{186}Pt et ^{187}Au.

plus lourds [16, 17]. C'est sans doute en partie à cause de la participation de plus en plus prépondérante des paires de protons $h_{9/2}$ que les platines les plus déficients [16] et les osmiums [18] deviennent déformés et allongés.

Remerciements. — Nous remercions très vivement l'équipe d'ISOCELE qui a assuré la mise au point et le fonctionnement du séparateur pour ces expériences. Nous remercions également les équipes qui assurent le fonctionnement du synchrocyclotron et du cyclotron à énergie variable.

Bibliographie

[1] TJOM, P. O., MAIER, M. R., BENSON, D., STEPHENS, F. S. and DIAMOND, R. M., *Nucl. Phys.* A **231** (1974) 397.

[2] BERG, V., DELEPLANQUE, M. A., GERSCHEL, C. and PERRIN, N., *Proceedings of the International Conference on Nuclear Structure and Spectroscopy* (Amsterdam, North Holland) **1** (1974) 113.

[3] DELEPLANQUE, M. A., GERSCHEL, C., PERRIN, N. et BERG, V. (à paraître dans *Nucl. Phys.*).

[4] STEPHENS, F. S., DIAMOND, R. M., LEIGH, J. R., KAMMURI, T. and NAKAI, K., *Phys. Rev. Lett.* **29** (1972) 438.

[5] MEYER TER VEHN, J., STEPHENS, F. S. and DIAMOND, R. M., *Phys. Rev. Lett.* **32** (1974) 1383.

[6] The Orsay on-line separator : ISOCELE (à paraître).

[7] GERHOLM, T. R. and LINDSKOG, J., *Ark. Fys.* **24** (1963) 171.

[8] BERG, V. et BOURGEOIS, C., *J. Physique* **36** (1975) 613.

[9] VIEU, C., thèse Orsay (1974).

[10] ANDRÉ, S. *et al.*, *Int. Conf. on Reactions between complex nuclei* (Nashville, North Holland) **1** (1974) 192.

[11] BURDE, J., DIAMOND, R. M. and STEPHENS, F. S., *Nucl. Phys.* A **92** (1967) 306.

[12] WARD, D., *Int. Conf. on Reactions between complex nuclei* (Nashville, North Holland) **2** (1974) 417.

[13] LIEDER, R. M., *Proceedings of the International Conference on Nuclear Structure and Spectroscopy* (Amsterdam, North Holland) **2** (1974) 212.

[14] HAMILTON, J. H. *et al.*, *Int. Conf. on Reactions between complex nuclei* (Nashville, North Holland) **1** (1974) 178.

[15] NEWTON, J. O., STEPHENS, F. S. and DIAMOND, R. M., *Nucl. Phys.* A **236** (1974) 225.

[16] FINGER, M. *et al.*, *Nucl. Phys.* A **188** (1972) 369.

[17] BEUSCHER, H., DAVIDSON, W. F., LIEDER, R. M., NESKAKIS, A. and MAYER-BORICKE, C., *Phys. Rev. Lett.* **32** (1974) 843.

[18] SODAN, H. *et al.*, *Nucl. Phys.* A **237** (1975) 333.